AD-772 717

THE LOW-G ACCELEROMETER CALIBRATION SYSTEM ORBITAL ACCELEROMETER EXPERIMENT. VOLUME 1. EXPERIMENT DESCRIPTION AND METHODOLOGY

J. A. Pearson, et al

Aerospace Corporation

Prepared for:

Space and Missile Systems Organization

1 July 1973

DISTRIBUTED BY:

NTIS

National Technical Information Service
U. S. DEPARTMENT OF COMMERCE
5285 Port Royal Road, Springfield Va. 22151

DISCLAIMER NOTICE

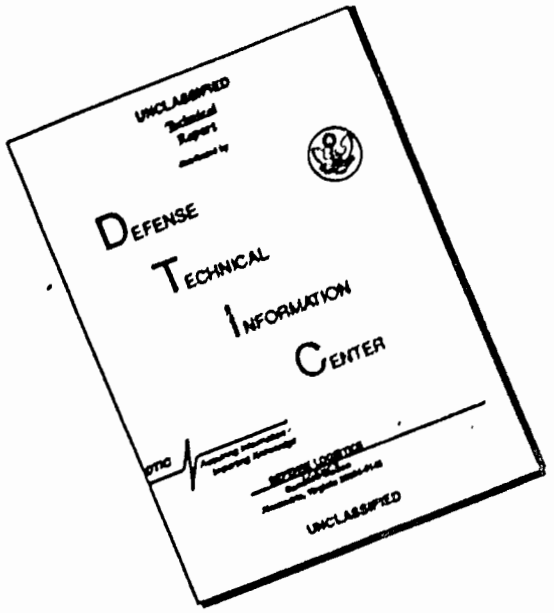

THIS DOCUMENT IS BEST QUALITY AVAILABLE. THE COPY FURNISHED TO DTIC CONTAINED A SIGNIFICANT NUMBER OF PAGES WHICH DO NOT REPRODUCE LEGIBLY.

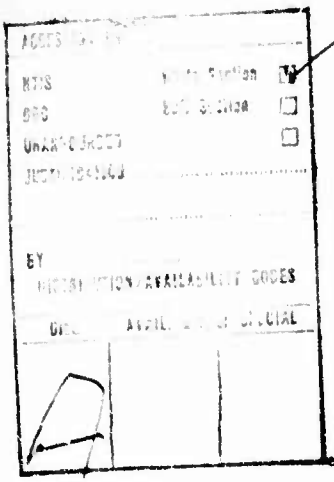

LABORATORY OPERATIONS

The Laboratory Operations of The Aerospace Corporation is conducting experimental and theoretical investigations necessary for the evaluation and application of scientific advances to new military concepts and systems. Versatility and flexibility have been developed to a high degree by the laboratory personnel in dealing with the many problems encountered in the nation's rapidly developing space and missile systems. Expertise in the latest scientific developments is vital to the accomplishment of tasks related to these problems. The laboratories that contribute to this research are:

Aerophysics Laboratory: Launch and reentry aerodynamics, heat transfer, reentry physics, chemical kinetics, structural mechanics, flight dynamics, atmospheric pollution, and high-power gas lasers.

Chemistry and Physics Laboratory: Atmospheric reactions and atmospheric optics, chemical reactions in polluted atmospheres, chemical reactions of excited species in rocket plumes, chemical thermodynamics, plasma and laser-induced reactions, laser chemistry, propulsion chemistry, space vacuum and radiation effects on materials, lubrication and surface phenomena, photosensitive materials and sensors, high precision laser ranging, and the application of physics and chemistry to problems of law enforcement and biomedicine.

Electronics Research Laboratory: Electromagnetic theory, devices, and propagation phenomena, including plasma electromagnetics; quantum electronics, lasers, and electro-optics; communication sciences, applied electronics, semiconducting, superconducting, and crystal device physics, optical and acoustical imaging; atmospheric pollution; millimeter wave and far-infrared technology.

Materials Sciences Laboratory: Development of new materials; metal matrix composites and new forms of carbon; test and evaluation of graphite and ceramics in reentry; spacecraft materials and electronic components in nuclear weapons environment; application of fracture mechanics to stress corrosion and fatigue-induced fractures in structural metals.

Space Physics Laboratory: Atmospheric and ionospheric physics, radiation from the atmosphere, density and composition of the atmosphere, aurorae and airglow; magnetospheric physics, cosmic rays, generation and propagation of plasma waves in the magnetosphere; solar physics, studies of solar magnetic fields; space astronomy, x-ray astronomy; the effects of nuclear explosions, magnetic storms, and solar activity on the earth's atmosphere, ionosphere, and magnetosphere; the effects of optical, electromagnetic, and particulate radiations in space on space systems.

THE AEROSPACE CORPORATION
El Segundo, California

UNCLASSIFIED
Security Classification

AD-772 717

DOCUMENT CONTROL DATA - R & D
(Security classification of title, body of abstract and indexing annotation must be entered when the overall report is classified)

1 ORIGINATING ACTIVITY (Corporate author)
The Aerospace Corporation
El Segundo, California

2a REPORT SECURITY CLASSIFICATION
Unclassified

2b GROUP

3 REPORT TITLE
THE LOW-G ACCELEROMETER CALIBRATION SYSTEM ORBITAL ACCELEROMETER EXPERIMENT, Volume I: Experiment Description and Methodology

4 DESCRIPTIVE NOTES (Type of report and inclusive dates)

5 AUTHOR(S) (First name, middle initial, last name)
J. A. Pearson, Editor, and R. W. Bruce, Y. T. Chiu, W. A. Feess, E. G. Fotou, J. A. Pearson, A. B. Prag, and K. R. Young, Authors

6 REPORT DATE	7a TOTAL NO. OF PAGES	7b NO. OF REFS
1 July 1973	~~284~~ 344	6

8a CONTRACT OR GRANT NO.	9a ORIGINATOR'S REPORT NUMBER(S)
F04701-73-C-0074	TR-0074(4260-10)-1, Vol I
b PROJECT NO.	
c	9b OTHER REPORT NO(S) (Any other numbers that may be assigned this report)
d	SAMSO-TR-73-355, Vol I

10 DISTRIBUTION STATEMENT
Approved for public release; distribution unlimited

11 SUPPLEMENTARY NOTES	12 SPONSORING MILITARY ACTIVITY
	Space and Missile Systems Organization Air Force Systems Command Los Angeles, California

13 ABSTRACT

The LOGACS (Low-G Accelerometer Calibration System) experiment, which contained a miniature electrostatic accelerometer (MESA), was placed in a low-altitude polar orbit on 22 May 1967. The experiment provided approximately 100 hours of acceleration data from which the accelerometer scale factor, accelerometer null bias, and atmospheric drag on the satellite were calculated.

The mission description, the characteristics of the accelerometer, the instrumentation used in the experiment, and a summary of the results of the inflight accelerometer calibration are presented in this volume. The accelerometer's sensing environment is discussed, as are the data reduction methods used to extract the scale factor and bias of the accelerometer and the methods of determining the acceleration due to aerodynamic drag.

DD FORM 1473 (FACSIMILE)

UNCLASSIFIED
Security Classification

344

14

KEY WORDS

Accelerometers
Atmospheric Drag
Data Reduction

Distribution Statement (Continued)

Abstract (Continued)

Air Force Report No.
SAMSO-TR-73-355, Vol I

Aerospace Report No.
TR-0074(4260-10)-1, Vol I

THE LOW-G ACCELEROMETER CALIBRATION SYSTEM
ORBITAL ACCELEROMETER EXPERIMENT

Volume I

Experiment Description and Methodology

Prepared by

J. A. Pearson
Electronics and Optics Division
Engineering Science Operations

73 JUL 01

Laboratory Operations
THE AEROSPACE CORPORATION

Prepared for

SPACE AND MISSILE SYSTEMS ORGANIZATION
AIR FORCE SYSTEMS COMMAND
LOS ANGELES AIR FORCE STATION
Los Angeles, California

Approved for public release;
distribution unlimited.

ic

FOREWORD

This report is published by The Aerospace Corporation, El Segundo, California, under Air Force Contract No. F04701-73-C-0074. The document was compiled and edited by J. A. Pearson; the authors include R. W. Bruce, W. A. Feess, E. G. Fotou, J. A. Pearson, and K. R. Young, Engineering Science Operations, and Y. T. Chiu and A. B. Prag, Laboratory Operations.

This report documents experimental work carried out from June 1966 through June 1970. The present compilation, published in the interests of wider dissemination of this technical information, was completed in March 1973 and submitted on 1 July 1973 to Lt. E. L. Lockwood, SAMSO (DYAE) for review and approval.

This work gathers together under one cover a complete description of the LOGACS orbital accelerometer experiment and the results obtained from that experiment. The editor gratefully acknowledges the assistance and support of members of both the Upper Atmosphere Physics Department of the Space Physics Laboratory, Laboratory Operations, and the Satellite Navigation Department of the Electronics and Optics Division, Engineering Science Operations, in the preparation of this document. The editor also thanks the authors of the individual papers included in these volumes for permitting their work to be included and for their valuable technical assistance. A list of the LOGACS documents is included in the bibliography of this volume.

Approved by

A. J. Boardman, Director
Navigation and Sensor Subdivision
Electronics and Optics Division
Engineering Science Operations

G. A. Paulikas, Director
Space Physics Laboratory
Laboratory Operations

Publication of this report does not constitute Air Force approval of the report's findings or conclusions. It is published only for the exchange and stimulation of ideas.

Ernest L Lockwood

E. L. Lockwood, 1st Lt., USAF
Technology Development Division
Deputy for Technology

ABSTRACT

The LOGACS (LOw-G Accelerometer Calibration System) experiment, which contained a miniature electrostatic accelerometer (MESA), was placed in a low-altitude polar orbit on 22 May 1967. The experiment provided approximately 100 hr of acceleration data from which the accelerometer scale factor, accelerometer null bias, and atmospheric drag on the satellite were calculated.

Many reports were written during 1967 and 1968 on the LOGACS experiment and on the analyses that were performed on the data. These reports have been combined into this document, which will be the definitive report on the LOGACS experiment by The Aerospace Corporation.

The mission description, the characteristics of the accelerometer, the instrumentation used in the experiment, and a summary of the results of the inflight accelerometer calibration are presented in Volume I. The accelerometer's sensing environment is discussed, as are the data reduction methods used to extract the scale factor and bias of the accelerometer and the methods of determining the acceleration due to aerodynamic drag.

Volume II contains data plots of the reduced accelerometer time histories and of the deduced atmospheric densities over the flight. Peculiarities of the density data are examined in some detail and extensive comparisons of the data to various model atmospheres are made. These analyses are the more interesting because of the intense solar and geomagnetic activity during the latter part of the LOGACS flight, which enormously affected the atmosphere.

Models of atmospheric density have been developed over the altitudes for which LOGACS data were available. Both midlatitude models and polar and auroral models are formulated and presented.

An analysis was also performed on the LOGACS data to determine the wind magnitude and characteristics normal to the orbit plane of the experiment. The results confirm that the earth's atmosphere (up to the altitude of

100 nmi) have high-velocity winds that are present in high-latitude regions as a result of the great magnetic storm. An analysis of these wind data shows they can be described as convective motion due to excessive heating of the polar thermosphere.

VOLUME I

CONTENTS

FOREWORD ii

ABSTRACT iii

I. LOGACS EXPERIMENT . . . . . (E. G. Fotou) 1-1

A. Historical Background 1-1

B. Experiment Design 1-2

C. Description of MESA 1-6

D. Equipment Design 1-13

E. Preflight Checkout 1-21

F. Flight Operations 1-25

G. Equipment Problems During Flight 1-26

H. Data Acquisition 1-27

I. Data Processing 1-28

J. Discussion of Results 1-30

1. Instrument Results 1-30

II. LOGACS DATA REDUCTION . . . . . (W. A. Feess) 2-1

A. LOGACS Sensing Environment 2-1

1. Agena Configuration 2-1

2. Acceleration Algorithms 2-4

3. Agena Rigid Body Equations of Motion 2-6

4. Agena Control System Response Characteristics . . 2-9

5. Aerodynamic Forces and Moments 2-17

6. Order of Magnitude Estimates 2-18

7. Time Average Responses 2-21

B. LOGACS Data Processing Methods 2-23

1. Accelerometer Calibrations - Apogee 2-25

2. Accelerometer Rotating Modes - Perigee 2-26

3. Fixed Mode Data Processing 2-27

4. Control System Functions 2-28

C. Data Processing Results 2-30

D. Response Anomalies 2-32

VOLUME I

CONTENTS (continued)

REFERENCES 3-1

BIBLIOGRAPHY 4-1

APPENDIXES

A. EXPERIMENTAL CLOCK ERROR A-1

B. LOGACS DRAWINGS AND DOCUMENTS B-1

C. SPECIFICATION FOR LOGACS DATA ANALYSIS PROGRAM C-1

D. LOGACS DATA ANALYSIS PROGRAM D-1

E. LOGACS SENSED ACCELERATION ALGORITHM E-1

F. SAMPLE RAW DATA PLOTS F-1

G. REDUCED DATA PLOTS G-1

VOLUME II

CONTENTS

FOREWORD ii

ABSTRACT iii

I. UPPER ATMOSPHERE DENSITY DETERMINATION FROM LOGACS . . . . . (R. W. Bruce) 1-1

A. The Orbit 1-1

1. Orbital Parameters 1-1

2. Tracking and Orbit Determination 1-2

B. Aerodynamic Coefficients 1-2

C. Solar Activity 1-4

D. Atmosphere Density Data 1-7

1. Atmosphere Density Between 75 and 120 nmi Before Great Magnetic Storm 1-9

2. Atmosphere Density Between 75 and 120 nmi During Great Magnetic Storm 1-21

3. Variation in Density at 90 nmi During Intense 25 May Proton Shower 1-32

4. Relative Density vs Time for Specific Altitudes 1-33

5. Atmosphere Density Amplitude and Phase Reponse Due to Great Magnetic Storm 1-35

6. Comparison of LOGACS Measured Density with Density Obtained from Orbital Decay of LOGACS Spacecraft, Satellite 1967 50B 1-39

7. Comparison of LOGACS Measured Density with Prevalent Model Atmospheres 1-42

II. ANALYSIS OF UPPER ATMOSPHERE DENSITY (J. A. Pearson) 2-1

A. Comparisons of LOGACS Densities with Models 2-1

B. Internal Comparisons of LOGACS Densities 2-7

1. Sorting by Time 2-7

2. Sorting by Altitude 2-19

III. ATMOSPHERIC PREDICTABILITY . . . . . (J. A. Pearson) 3-1

A. Density Prediction 3-1

B. Discussion 3-1

C. Conclusion 3-2

VOLUME II

CONTENTS (continued)

IV. MIDLATITUDE DENSITY MODEL ATMOSPHERE BETWEEN 120 AND 175 km . . . . . (A. B. Prag) 4-1

A. Introduction 4-1
B. Data Reduction 4-1
C. Results 4-3
1. Forms of g and Z 4-3
2. Density Coefficients 4-4
D. Discussion 4-8
1. Limitations of Model 4-9
2. Extensions of Model 4-10
3. Examples of Model 4-11

V. ALTERNATE FORMULATION OF MIDLATITUDE MODEL . . . . . (A. B. Prag) 5-1

A. Introduction 5-1
B. Temperature/Density Profile 5-1
C. Method of Analysis 5-3
D. Results 5-4
1. Discussion 5-10
2. Energy Considerations 5-27

VI. AURORAL AND POLAR ATMOSPHERE DENSITY MODEL BETWEEN 120 AND 175 km . . . . . (A. B. Prag) 6-1

A. Introduction 6-1
B. Data Reduction 6-1
C. Polar Model 6-4
1. Symbols List 6-4
2. Region of Validity 6-4

VOLUME II

CONTENTS (continued)

3. Bulge Model 6-5
4. Bulgeless Model 6-7

D. Discussion 6-8

VII. LOGACS WIND ANALYSIS . . . . . (W A. Feess) 7-1

A. Introduction 7-1
B. Force and Moment Algorithms 7-1
C. Aerodynamic Coefficients 7-5
D. LOGACS Side Force Processing 7-10
E. Parameter Calibration 7-14
F. Mission Pitch and Yaw Angle-of-Attack Time Histories 7-27
G. Yaw Winds in Geographical Coordination 7-28
H. Wind Analysis Conclusions 7-39

VIII. THERMOSPHERIC CONVECTIVE INSTABILITY (Y. T. Chiu) 8-1

A. Introduction 8-1
B. Observation 8-1
C. Convective Instability 8-3
D. Thermohydrodynamic Instability in Rotating Thermosphere 8-22
E. Characteristic Features and Observation 8-28
F. Fully Developed Convective Instability 8-30

REFERENCES 9-1

BIBLIOGRAPHY 10-1

APPENDIXES

A. ACCELEROMETER DATA A-1

B. DENSITY DATA B-1

C. LOGACS WIND DATA C-1

VOLUME I

FIGURES

1.	Bias and Scale Factor Calibration Concept	1-4
2.	Exterior View of MESA Accelerometer	1-7
3.	MESA Without Insulating Cover	1-8
4.	Exploded View of MESA	1-9
5.	Cross Section of MESA	1-10
6.	Characteristic Accelerometer Output (Constant Drag Case)	1-14
7.	LOGACS Centrifuge	1-15
8.	Block and Signal Flow Diagram for LOGACS Experiment	1-18
9.	Relay Closure Logic Pulse	1-21
10.	Location of LOGACS Equipment on Agena	1-22
11.	LOGACS Side Panel	1-23
12.	LOGACS Bottom Panel	1-24
13.	Data Analysis with No Thruster Edit	1-35
14.	Data Analysis with Thruster Edit	1-36
15.	Alternate Data Analysis	1-39
16.	Nonsymmetrical Proof Mass	1-42
17.	Relationship of Scale Factor to Pickoff Null	1-47
18.	Typical Curve from MESA Saturation Tests	1-51
19.	Configuration of Vehicle and LOGACS	2-2
20.	Static Performance Characteristics	2-10
21.	Idealized Time History	2-12

VOLUME I

FIGURES (continued)

22.	Time History Assuming a Small Constant Torque	2-13
23.	Density and Drag Accelerations	2-20
A-1.	Experiment Clock Error	A-3
A-2.	Experiment Clock Error as a Function of Temperature	A-4
E-1.	Force Vector Diagram	E-1
F-1.	Sample Raw Data (revolution 52.7 to 53.8)	F-2
F-2.	Acceleration Profile from Revolution 52 Apogee Calibration	F-3
F-3.	Corrected Raw Accelerometer Data (revolution 52.7 to 53.8)	F-4
F-4.	Corrected Raw Accelerometer Data (modes 1 and 2, revolution 54 perigee)	F-5
G-1(a)	Acceleration Profile and Ephemeris Data (23 May)	G-2
G-1(b)	Acceleration Profile and Ephemeris Data (24 May)	G-3
G-1(c)	Acceleration Profile and Ephemeris Data (25 May)	G-4
G-1(d)	Acceleration Profile and Ephemeris Data (26 May)	G-5
G-2(a)	Agena Control System Functions (23 May)	G-6
G-2(b)	Agena Control System Functions (24 May)	G-7
G-2(c)	Agena Control System Functions (25 May)	G-8
G-2(d)	Agena Control System Functions (26 May)	G-9

VOLUME II

FIGURES

1. Apogee and Perigee, and Latitude of Perigee vs Time 1-3

2. Agena Configuration Used to Determine Aerodynamic Coefficients 1-5

3. Drag Coefficient at Zero Angle of Attack vs Altitude for Agena 1-6

4. Solar Indices Observed During LOGACS Experiment 1-8

5. LOGACS Satellite Ground Traces for Revs. 26, 27, 28, and 31 1-10

6. Density vs Altitude for Rev. 26 1-11

7. Density vs Altitude for Rev. 27 1-12

8. Density vs Altitude for Rev. 28 1-13

9. Density vs Altitude for Rev. 31 1-15

10. Normalized Density vs Latitude for Rev. 26 1-16

11. Normalized Density vs Latitude for Rev. 27 1-17

12. Normalized Density vs Latitude for Rev. 28 1-18

13. Normalized Density vs Latitude for Rev. 31 1-19

14. Reference Model Density vs Altitude 1-20

15. LOGACS Satellite Ground Traces for Revs. 46, 47, 48, and 57 1-22

16. Density vs Altitude for Rev. 46 1-23

17. Density vs Altitude for Rev. 47 1-24

18. Density vs Altitude for Rev. 47 (Toward Perigee) 1-25

19. Density vs Altitude for Rev. 47 (Away from Perigee) 1-26

20. Density vs Altitude for Rev. 48 1-27

VOLUME II

FIGURES (continued)

21. Density vs Altitude for Rev. 57 1-28

22. Normalized Density vs Latitude for Rev. 46 1-29

23. Normalized Density vs Latitude for Rev. 47 1-30

24. Normalized Density vs Latitude for Rev. 48 1-31

25. Normalized Density vs Latitude for Rev. 57 1-33

26. Density vs Altitude During Proton Shower 1-34

27. Normalized Density vs Time (Toward Perigee) 1-36

28. Normalized Density vs Time (Away from Perigee) 1-37

29. Phase Response of Atmosphere Density to Great Magnetic Storm vs Altitude and Latitude 1-38

30. Amplitude Response of Atmosphere Density to Great Magnetic Storm vs Altitude and Latitude 1-40

31. Density Comparison: Orbital Decay vs LOGACS 1-41

32. Comparison of LOGACS Data (Rev. 5, Leaving Perigee) with Jacchia Static Diffusion Model 2-2

33. Comparison of LOGACS Data (Rev. 59, Leaving Perigee) with Jacchia Static Diffusion Model 2-4

34. Ratio of LOGACS-Derived Density to Walker-Bruce Model Density for a Portion of 23 May 1967; Vehicle Altitude Included for Reference 2-5

35. Ratio of LOGACS-Derived Density to Walker-Bruce Model Density for a Portion of 25 May 1967; Vehicle Altitude Included for Reference 2-6

36. Ratio of LOGACS-Derived Density to 1962 U.S. Standard Atmosphere Density for a Portion of 23 May 1967; Vehicle Altitude Included for Reference 2-8

37. Ratio of LOGACS-Derived Density to 1962 U.S. Standard Atmosphere Density for a Portion of 25 May 1967; Vehicle Altitude Included for Reference 2-9

VOLUME II

FIGURES (continued)

38. The Density Ratio LOGACS/Jacchia-Walker-Bruce Model for High Latitude (Toward Perigee) Data at Various Altitudes 2-10

39. The Density Ratio LOGACS/Jacchia-Walker-Bruce Model for High Latitude (Away from Perigee) Data at Various Altitudes 2-11

40. Density vs Altitude for Vector 1 2-12

41. Density vs Altitude for Vector 2 2-13

42. Density vs Altitude for Vector 3 2-14

43. Density vs Altitude for Vector 4 2-15

44. Density vs Altitude for Vector 5 2-16

45. Density vs Altitude for Vector 6 2-17

46. Density vs Altitude for Vector 7 2-18

47. Mean and RMS of Density Values at 148 km (80 nmi) During LOGACS Flight 2-20

48. Mean and RMS of Density Values at 150 km (81 nmi) During LOGACS Flight 2-21

49. Mean and RMS of Density Values at 166 km (90 nmi) During LOGACS Flight 2-22

50. Mean and RMS of Density Values at 185 km (100 nmi) During LOGACS Flight 2-23

51. Mean and RMS of Density Values at 200 km (108 nmi) During LOGACS Flight 2-24

52. Mean and RMS of Density Values at 203 km (110 nmi) During LOGACS Flight 2-25

53. Mean and RMS of Density Values at 222 km (120 nmi) During LOGACS Flight 2-26

VOLUME II

FIGURES (continued)

54. Mean and RMS of Density Values at 250 km (135 nmi) During LOGACS Flight 2-27

55. Ratio of Measured Densities to Those Predicted by Present Model for Entire Flight at Low Latitudes 4-6

56. Comparison Between Steady-State Density Prediction of Present Model and That of CIRA 1965 4-12

57. Variation of Present Model with $\bar{F}$ 4-13

58. Response of Present Model to a 30 min Impulsive Disturbance with Maximum Amplitude $a_p = 100$ 4-14

59. Response of Present Model to Realistic Moderate Magnetic Storm 4-16

60. Mass Density vs Altitude for $a_p = 0$, 5, 10, and 20 5-5

61. Mass Density vs Altitude for $a_p = 40$, 59, 60, and 100 5-6

62. Mass Density vs Altitude for $a_p = 200$, 300, and 400 5-7

63. Temperature Distribution Parameters H_T, T_0, and a 5-8

64. Mass Densities of N_2, O_2, and O at 120 km 5-9

65. Temperature Profiles for $a_p = 0$, 10, 40, 60, and 400 5-12

66. Number Density Profiles of Atomic Oxygen for $a_p = 0$, 10, 40, 60, and 400 5-13

67. Number Density Profiles of Molecular Nitrogen for $a_p = 0$, 10, 40, 60, and 400 5-14

68. Number Density Profiles of Molecular Oxygen for $a_p = 0$, 10, 40, 60, and 400 5-15

69. Left Ordinate: Energy Content of Atmosphere Above 120 km. Right Ordinate: Minimum Energy Deposition Rate Above 120 km 5-28

70. Average Density of Polar Atmosphere 6-11

VOLUME II

FIGURES (continued)

71. Fractional Density Between 270° and 30° E, 50° to 90° N 6-13

72. Force/Moment Diagram (Yaw Plane) 7-2

73. Aerodynamic Coefficients as a Function of Molecular Speed 7-7

74. Molecular Speed Ratio vs Altitude and Temperature 7-8

75. Aerodynamic Coefficients as a Function of Altitude 7-9

76. LOGACS Side Force Processing 7-13

77. Revolution 38 (TRGO = 202490) 7-15

78. Revolution 39 (TRGO = 208640) 7-16

79. Revolution 41 (TRGO = 218880) 7-17

80. Revolution 43 (TRGO = 229120) 7-18

81. Revolution 53 (TRGO = 282240) 7-19

82. Revolution 54 (TRGO = 288384) 7-20

83. Revolution 56 (TRGO = 298624) 7-21

84. Parameter Calibration Results (Revs. 38, 39, 41, 43) 7-25

85. Parameter Calibration Results (Revs. 53, 54, 56) 7-26

86. Orbit Geometry 7-29

87. Wind Components in Geographical Coordinates (Revs. 38, 39, 41, 43) 7-31

88. Wind Components in Geographical Coordinates (Revs. 53, 54, 56) 7-32

89. Wind Components in Geographical Coordinates for 23 May 1968 7-33

90. Wind Components in Geographical Coordinates for 24 May 1968 7-34

VOLUME II

FIGURES (continued)

91. Wind Components in Geographical Coordinates for 25 May 1968 7-35

92. Wind Components in Geographical Coordinates for 26 May 1968 7-36

93. Expanded View of Fig. 92 (Trajectory Toward Pole) 7-37

94. Expanded View of Fig. 92 (Trajectory Away from Pole) 7-38

95. Thomas-Ching Model Temperature Profile of CIRA 2 Atmosphere Heated by Sheet Source at 150 km Depositing 3×10^5 erg/cm^2 Spread over Polar Caps, Equivalent to 7×10^{18} erg/sec Energy Deposition Rate over 8 hr 8-5

96. Ring Current Energy Dissipation Rate of 26 May 1967 Storm 8-6

97. Thomas-Ching Model Temperature Profile of CIRA 2 Atmosphere Heated by Sheet Source at 150 km depositing 3×10^4 erg/cm^2 Spread over Polar Caps, Equivalent to 1.17×10^{18} erg/sec Energy Deposition Rate over 8 hr 8-8

98. Thomas-Ching Model Temperature Profile of CIRA 2 Atmosphere Heated by Sheet Source at 150 km Depositing 1×10^5 erg/cm^2 Spread over Polar Caps, Equivalent to 2.34×10^{18} erg/sec Energy Deposition Rate over 8 hr 8-9

99. Thomas-Ching Model Temperature Profile of CIRA 2 Atmosphere Heated by Sheet Source at 150 km Depositing 2×10^5 erg/cm^2 Spread over Polar Caps, Equivalent to 4.67×10^{18} erg/sec Energy Deposition Rate over 8 hr 8-10

100. Effect of Increasing Heat Source Thickness 8-11

101. Relation Between Rayleigh Number R and Horizontal Characteristic Length η in Units of Layer Depth h 8-18

102. Solution of $G(\lambda) = 0$ for λ Near Zero and $m = 1$ 8-21

VOLUME II

FIGURES (continued)

103. Relation Between Rayleigh Number R and Characteristic Length η Showing Effects of Coriolis Force in Case of Vanishing Growth Rate 8-27

A-1. LOGACS Accelerometer Data for Rev. 5 . . . . . A-3

A-2. LOGACS Accelerometer Data for Rev. 6 . . . . . A-4

A-3. LOGACS Accelerometer Data for Rev. 7 . . . . . A-5

A-4. LOGACS Accelerometer Data for Rev. 8 . . . . . A-6

A-5. LOGACS Accelerometer Data for Rev. 9 . . . . . A-7

A-6. LOGACS Accelerometer Data for Rev. 10 . . . . . A-8

A-7. LOGACS Accelerometer Data for Rev. 11 . . . . . A-9

A-8. LOGACS Accelerometer Data for Rev. 12 . . . . . A-10

A-9. LOGACS Accelerometer Data for Rev. 13 . . . . . A-11

A-10. LOGACS Accelerometer Data for Rev. 14 . . . . . A-12

A-11. LOGACS Accelerometer Data for Rev. 15 . . . . . A-13

A-12. LOGACS Accelerometer Data for Rev. 16 . . . . . A-14

A-13. LOGACS Accelerometer Data for Rev. 17 . . . . . A-15

A-14. LOGACS Accelerometer Data for Rev. 18 . . . . . A-16

A-15. LOGACS Accelerometer Data for Rev. 19 . . . . . A-17

A-16. LOGACS Accelerometer Data for Rev. 20 . . . . . A-18

A-17. LOGACS Accelerometer Data for Rev. 21 . . . . . A-19

A-18. LOGACS Accelerometer Data for Rev. 22 . . . . . A-20

A-19. LOGACS Accelerometer Data for Rev. 23 . . . . . A-21

A-20. LOGACS Accelerometer Data for Rev. 24 . . . . . A-22

VOLUME II

FIGURES (continued)

A-21. LOGACS Accelerometer Data for Rev. 25 . . . . . A-23

A-22. LOGACS Accelerometer Data for Rev. 26 . . . . . A-24

A-23. LOGACS Accelerometer Data for Rev. 27 . . . . . A-25

A-24. LOGACS Accelerometer Data for Rev. 28 . . . . . A-26

A-25. LOGACS Accelerometer Data for Rev. 29 . . . . . A-27

A-26. LOGACS Accelerometer Data for Rev. 30 . . . . . A-28

A-27. LOGACS Accelerometer Data for Rev. 31 . . . . . A-29

A-28. LOGACS Accelerometer Data for Rev. 32 . . . . . A-30

A-29. LOGACS Accelerometer Data for Rev. 33 . . . . . A-31

A-30. LOGACS Accelerometer Data for Rev. 34 . . . . . A-32

A-31. LOGACS Accelerometer Data for Rev. 35 . . . . . A-33

A-32. LOGACS Accelerometer Data for Rev. 36 . . . . . A-34

A-33. LOGACS Accelerometer Data for Rev. 37 . . . . . A-35

A-34. LOGACS Accelerometer Data for Rev. 38 . . . . . A-36

A-35. LOGACS Accelerometer Data for Rev. 39 . . . . . A-37

A-36. LOGACS Accelerometer Data for Rev. 40 . . . . . A-38

A-37. LOGACS Accelerometer Data for Rev. 41 . . . . . A-39

A-38. LOGACS Accelerometer Data for Rev. 42 . . . . . A-40

A-39. LOGACS Accelerometer Data for Rev. 43 . . . . . A-41

A-40. LOGACS Accelerometer Data for Rev. 44 . . . . . A-42

A-41. LOGACS Accelerometer Data for Rev. 45 . . . . . A-43

A-42. LOGACS Accelerometer Data for Rev. 46 . . . . . A-44

VOLUME II

FIGURES (continued)

A-43. LOGACS Accelerometer Data for Rev. 47 . . . . . A-45

A-44. LOGACS Accelerometer Data for Rev. 48 . . . . . A-46

A-45. LOGACS Accelerometer Data for Rev. 49 . . . . . A-47

A-46. LOGACS Accelerometer Data for Rev. 50 . . . . . A-48

A-47. LOGACS Accelerometer Data for Rev. 51 . . . . . A-49

A-48. LOGACS Accelerometer Data for Rev. 52 . . . . . A-50

A-49. LOGACS Accelerometer Data for Rev. 53 . . . . . A-51

A-50. LOGACS Accelerometer Data for Rev. 54 . . . . . A-52

A-51. LOGACS Accelerometer Data for Rev. 55 . . . . . A-53

A-52. LOGACS Accelerometer Data for Rev. 56 . . . . . A-54

A-53. LOGACS Accelerometer Data for Rev. 57 . . . . . A-55

A-54. LOGACS Accelerometer Data for Rev. 58 . . . . . A-56

A-55. LOGACS Accelerometer Data for Rev. 59 . . . . . A-57

A-56. LOGACS Accelerometer Data for Rev. 60 . . . . . A-58

A-57. LOGACS Accelerometer Data for Rev. 61 . . . . . A-59

A-58. LOGACS Accelerometer Data for Rev. 62 . . . . . A-60

A-59. LOGACS Accelerometer Data for Rev. 63 . . . . . A-61

A-60. LOGACS Accelerometer Data for Rev. 64 . . . . . A-62

A-61. LOGACS Accelerometer Data for Rev. 65 . . . . . A-63

A-62. LOGACS Accelerometer Data for Rev. 66 . . . . . A-64

A-63. LOGACS Accelerometer Data for Rev. 67 . . . . . A-65

B-1. LOGACS Density Data for Rev. 5, Toward Perigee B-2

VOLUME II

FIGURES (continued)

B-2. LOGACS Density Data for Rev. 5, Away from Perigee B-3

B-3. LOGACS Density Data for Rev. 6, Toward Perigee B-4

B-4. LOGACS Density Data for Rev. 6, Away from Perigee B-5

B-5. LOGACS Density Data for Rev. 7, Toward Perigee B-6

B-6. LOGACS Density Data for Rev. 7, Away from Perigee B-7

B-7. LOGACS Density Data for Rev. 9, Toward Perigee B-8

B-8. LOGACS Density Data for Rev. 9, Away from Perigee B-9

B-9. LOGACS Density Data for Rev. 10, Toward Perigee B-10

B-10. LOGACS Density Data for Rev. 10, Away from Perigee B-11

B-11. LOGACS Density Data for Rev. 11, Toward Perigee B-12

B-12. LOGACS Density Data for Rev. 11, Away from Perigee B-13

B-13. LOGACS Density Data for Rev. 12, Toward Perigee B-14

B-14. LOGACS Density Data for Rev. 12, Away from Perigee B-15

B-15. LOGACS Density Data for Rev. 13, Toward Perigee B-16

B-16. LOGACS Density Data for Rev. 13, Away from Perigee B-17

B-17. LOGACS Density Data for Rev. 14, Away from Perigee B-18

B-18. LOGACS Density Data for Rev. 18, Toward Perigee B-19

B-19. LOGACS Density Data for Rev. 18, Away from Perigee B-20

B-20. LOGACS Density Data for Rev. 20, Away from Perigee ... B-21

B-21. LOGACS Density Data for Rev. 21, Toward Perigee B-22

B-22. LOGACS Density Data for Rev. 21, Away from Perigee B-23

B-23. LOGACS Density Data for Rev. 22, Toward Perigee B-24

VOLUME II

FIGURES (continued)

B-24. LOGACS Density Data for Rev. 24, Toward Perigee B-25

B-25. LOGACS Density Data for Rev. 24, Away from Perigee B-26

B-26. LOGACS Density Data for Rev. 25, Toward Perigee B-27

B-27. LOGACS Density Data for Rev. 25, Away from Perigee B-28

B-28. LOGACS Density Data for Rev. 26, Toward Perigee B-29

B-29. LOGACS Density Data for Rev. 26, Away from Perigee B-30

B-30. LOGACS Density Data for Rev. 27, Toward Perigee B-31

B-31. LOGACS Density Data for Rev. 27, Away from Perigee B-32

B-32. LOGACS Density Data for Rev. 28, Toward Perigee B-33

B-33. LOGACS Density Data for Rev. 29, Toward Perigee B-34

B-34. LOGACS Density Data for Rev. 29, Away from Perigee B-35

B-35. LOGACS Density Data for Rev. 30, Toward Perigee B-36

B-36. LOGACS Density Data for Rev. 30, Away from Perigee B-37

B-37. LOGACS Density Data for Rev. 31, Toward Perigee B-38

B-38. LOGACS Density Data for Rev. 31, Away from Perigee B-39

B-39. LOGACS Density Data for Rev. 32, Toward Perigee B-40

B-40. LOGACS Density Data for Rev. 32, Away from Perigee B-41

B-41. LOGACS Density Data for Rev. 33, Toward Perigee B-42

B-42. LOGACS Density Data for Rev. 33, Away from Perigee B-43

B-43. LOGACS Density Data for Rev. 34, Toward Perigee B-44

B-44. LOGACS Density Data for Rev. 34, Away from Perigee B-45

B-45. LOGACS Density Data for Rev. 35, Toward Perigee B-46

VOLUME II

FIGURES (continued)

B-46. LOGACS Density Data for Rev. 35, Away from Perigee B-47

B-47. LOGACS Density Data for Rev. 36, Away from Perigee B-48

B-48. LOGACS Density Data for Rev. 37, Toward Perigee B-49

B-49. LOGACS Density Data for Rev. 37, Away from Perigee B-50

B-50. LOGACS Density Data for Rev. 38, Toward Perigee B-51

B-51. LOGACS Density Data for Rev. 38, Away from Perigee B-52

B-52. LOGACS Density Data for Rev. 39, Toward Perigee B-53

B-53. LOGACS Density Data for Rev. 39, Away from Perigee B-54

B-54. LOGACS Density Data for Rev. 40, Toward Perigee B-55

B-55. LOGACS Density Data for Rev. 40, Away from Perigee B-56

B-56. LOGACS Density Data for Rev. 41, Toward Perigee B-57

B-57. LOGACS Density Data for Rev. 41, Away from Perigee B-58

B-58. LOGACS Density Data for Rev. 43, Toward Perigee B-59

B-59. LOGACS Density Data for Rev. 43, Away from Perigee B-60

B-60. LOGACS Density Data for Rev. 44, Toward Perigee B-61

B-61. LOGACS Density Data for Rev. 45, Toward Perigee B-62

B-62. LOGACS Density Data for Rev. 45, Away from Perigee B-63

B-63. LOGACS Density Data for Rev. 46, Toward Perigee B-64

B-64. LOGACS Density Data for Rev. 46, Away from Perigee B-65

B-65. LOGACS Density Data for Rev. 47, Toward Perigee B-66

B-66. LOGACS Density Data for Rev. 47, Away from Perigee B-67

B-67. LOGACS Density Data for Rev. 48, Toward Perigee B-68

VOLUME II

FIGURES (continued)

B-68. LOGACS Density Data for Rev. 48, Away from Perigee B-69

B-69. LOGACS Density Data for Rev. 49, Toward Perigee B-70

B-70. LOGACS Density Data for Rev. 50, Away from Perigee B-71

B-71. LOGACS Density Data for Rev. 51, Toward Perigee B-72

B-72. LOGACS Density Data for Rev. 51, Away from Perigee B-73

B-73. LOGACS Density Data for Rev. 52, Toward Perigee B-74

B-74. LOGACS Density Data for Rev. 52, Away from Perigee B-75

B-75. LOGACS Density Data for Rev. 53, Toward Perigee B-76

B-76. LOGACS Density Data for Rev. 53, Away from Perigee B-77

B-77. LOGACS Density Data for Rev. 54, Toward Perigee B-78

B-78. LOGACS Density Data for Rev. 54, Away from Perigee B-79

B-79. LOGACS Density Data for Rev. 55, Toward Perigee B-80

B-80. LOGACS Density Data for Rev. 55, Away from Perigee B-81

B-81. LOGACS Density Data for Rev. 56, Toward Perigee B-82

B-82. LOGACS Density Data for Rev. 56, Away from Perigee B-83

B-83. LOGACS Density Data for Rev. 57, Toward Perigee B-84

B-84. LOGACS Density Data for Rev. 57, Away from Perigee B-85

B-85. LOGACS Density Data for Rev. 58, Away from Perigee B-86

B-86. LOGACS Density Data for Rev. 59, Toward Perigee B-87

B-87. LOGACS Density Data for Rev. 59, Away from Perigee B-88

B-88. LOGACS Density Data for Rev. 61, Away from Perigee B-89

B-89. LOGACS Density Data for Rev. 62, Toward Perigee B-90

VOLUME II

FIGURES (continued)

B-90. LOGACS Density Data for Rev. 62, Away from Perigee B-91

B-91. LOGACS Density Data for Rev. 63, Toward Perigee B-92

B-92. LOGACS Density Data for Rev. 63, Away from Perigee B-93

B-93. LOGACS Density Data for Rev. 64, Toward Perigee B-94

B-94. LOGACS Density Data for Rev. 64, Away from Perigee B-95

B-95. LOGACS Density Data for Rev. 65, Toward Perigee B-96

B-96. LOGACS Density Data for Rev. 65, Away from Perigee B-97

B-97. LOGACS Density Data for Rev. 66, Toward Perigee B-98

B-98. LOGACS Density Data for Rev. 66, Away from Perigee B-99

C-1. Revolution 56, Corrected Data C-3

C-2. Revolution 56, Residuals C-5

C-3. Pitch and Yaw Angle-of-Attack Time Histories C-7

VOLUME I

TABLES

1.	LOGACS Centrifuge Modes	1-13
2.	Typical Data Page from LOGACS Flight	1-29
3.	MESA Instrument Bias and Scale Factor (No edit of data acquired during thrust valve firings)	1-31
4.	MESA Instrument Bias and Scale Factor (Edit of all data acquired during thrust valve firings)	1-33
5.	MESA Instrument Bias and Scale Factor (Data reduced by means of alternate analysis program)	1-37
6.	Bias and Scale Factor	1-40
7.	Expected Relationship of Bias and Scale Factor	1-41
8.	Bias Determination at Bell Aerosystems Company	1-41
9.	Configuration Data	2-3
10.	Accelerations During Gas Valve Firing	2-16
11.	Aerodynamic Coefficients	2-17
12.	Aerodynamic Forces and Accelerations	2-19
13.	Order of Magnitude Estimates	2-22

VOLUME II

TABLES

1. Orbital Parameters for LOGACS 1-1
2. Representative LOGACS Density Measurements 1-43
3. Comparison of LOGACS Data with Density Models 1-43
4. Mean and RMS Density for All 12-Rev. Groups 3-2
5. First Rev After 12-Rev. Mean, Relative Difference 3-3
6. Second Rev. After 12-Rev. Mean, Relative Difference 3-3
7. Third Rev. After 12-Rev. Mean, Relative Difference 3-3
8. Fourth Rev. After 12-Rev. Mean, Relative Difference 3-4
9. Values of Adopted Parameters for Present Model 4-5
10. Comparison of Present Model with Four Others During LOGACS Flight 4-7
11. Atmospheric Parameters for $\bar{F} = 183$, $a_p = 0$ 5-16
12. Atmospheric Parameters for $\bar{F} = 183$, $a_p = 5$ 5-17
13. Atmospheric Parameters for $\bar{F} = 183$, $a_p = 10$ 5-18
14. Atmospheric Parameters for $\bar{F} = 183$, $a_p = 20$ 5-19
15. Atmospheric Parameters for $\bar{F} = 183$, $a_p = 40$ 5-20
16. Atmospheric Parameters for $\bar{F} = 183$, $a_p = 59$ 5-21
17. Atmospheric Parameters for $\bar{F} = 183$, $a_p = 60$ 5-22
18. Atmospheric Parameters for $\bar{F} = 183$, $a_p = 100$ 5-23
19. Atmospheric Parameters for $\bar{F} = 183$, $a_p = 200$ 5-24
20. Atmospheric Parameters for $\bar{F} = 183$, $a_p = 300$ 5-25
21. Atmospheric Parameters for $\bar{F} = 183$, $a_p = 400$ 5-26
22. Comparison of Density Models 6-9

SECTION I

LOGACS EXPERIMENT

A. HISTORICAL BACKGROUND

It has long been recognized that accurate acceleration measurements aboard satellite vehicles in near-earth orbits would improve on-orbit navigation, would allow the determination of a more accurate atmosphere model, and would enhance orbit prediction capability. Unfortunately, it has also been recognized that the accelerations that must be sensed are generally several orders of magnitude below those which can be measured accurately on earth. As a result, even though an accelerometer might be capable of sensing the extremely low accelerations encountered aboard a satellite vehicle, the calibration of the accelerometer prior to launch could not be accomplished except at levels several orders of magnitude above those which would be experienced on-orbit. This impasse led directly to the formulation of a plan to calibrate an extremely sensitive accelerometer in the orbital environment. The result of this plan was the LOGACS (LOw-G Accelerometer Calibration System) experiment.

Briefly, the plan called for an orbital experiment wherein it would be demonstrated that the bias and scale factor coefficients of the accelerometer could be determined while on-orbit and, further, that the accelerometer would measure (along the accelerometer's sensitive axis) the nonconservative forces acting on the satellite vehicle. Measurements would be made nearly continuously while on-orbit.

Selection of a suitable accelerometer did not prove to be a difficult task. Schedule and limited funding demanded that the instrument already be developed. A brief survey revealed that a device that promised the required sensitivity had already been developed and produced in prototype quantity by Bell Aerosystems Company.

Bell Aerosystems Company had initiated in 1959, under Contract AF 33(616)-6637, a program to develop a single axis, force rebalance, digital, electrostatic accelerometer (ESA) for extremely low acceleration measurements. The force rebalance was to be accomplished by sensing the displacement of a proof mass and using that displacement signal to close the loop to an electrostatic force generator to null the displacement signal. The feasibility of the design was demonstrated after four years of development effort. Under sponsorship of the NASA Lewis Research Center, a contract (NAS-3-4102) was initiated in 1963 to develop two miniature versions of the electrostatic accelerometer (MESA IA and MESA IB). The MESA IA was successfully qualified to the Thor-Delta launch environment. The MESA IB was a low power version which was successfully qualified to the Atlas-Agena launch environment.

Since it was recognized that a ride as a noninterfering passenger aboard an orbiting Agena vehicle could be arranged, it was decided to proceed with the plan. The preliminary design of the experiment was performed by The Aerospace Corporation. Discussions were held with Lockheed Missiles and Space Company (LMSC) and Bell Aerosystems Company, and subsequently, LMSC was authorized to proceed with the acquisition of the necessary equipment to fly two LOGACS experiments aboard separate Agena vehicles to be designated by the Space Systems Division of the USAF.

B. EXPERIMENT DESIGN

The fundamental experiment design problem was the provision of a means to calibrate the accelerometer bias and scale factor while on-orbit. Let us define bias and scale factor as follows*

$$A_m = K(B + A_s)$$

* See Section C for a detailed description of the instrument and its operation.

where

A_m = accelerometer output (pulses/sec)

K = scale factor (pulses/sec-g)

B = bias (g)

A_s = sensed acceleration (g)

The calibration of accelerometer bias can best be illustrated by a simple example. Let us fix the accelerometer such that the sensitive axis is aligned with the drag vector (call this Mode 3). Next, reorient the sensitive axis by turning it end over end so that it is again aligned with the drag vector but with the opposite sense (call this Mode 4). Let us further assume that the drag vector is constant during the measurement interval; then the equations for the accelerometer output for Mode 3 and Mode 4 are

$$\text{Mode 3: } A_{m3} = K(B + A_{drag}) \tag{1}$$

$$\text{Mode 4: } A_{m4} = K(B - A_{drag}) \tag{2}$$

Adding Eqs. (1) and (2), we obtain

$$B = \frac{A_{m3} + A_{m4}}{2K} \tag{3}$$

Thus, if we know K (scale factor), we can solve for bias.

To solve for K, we must create a standard linear acceleration. A centrifuge is a common solution to the problem of creating a linear acceleration standard. While a centrifuge is normally employed to create a large acceleration, there is no conceptual reason for not employing it to create small accelerations.

It was decided to employ a small centrifuge which could be programmed to run at a fixed speed (and hence generate a fixed centripetal acceleration of magnitude $R\omega^2$, where R is the distance from the center of

mass of the sensitive element to the center of rotation and ω is the fixed angular velocity of the centrifuge). The centrifuge also could be programmed to stop at specified locations. Thus a single device could be employed to calibrate for bias and scale factor. The bias and scale factor calibration concept is summarized in Fig. 1.

The manner in which the scale factor can be extracted from the accelerometer output data can be illustrated by the following. Define Mode 1 as the condition wherein the centrifuge rotates at a fixed speed ω and Mode 2 as the condition wherein the centrifuge rotates at a fixed speed 2ω. Then

BIAS

ACCELEROMETER OUTPUT (1) = SCALE FACTOR $|$BIAS + DRAG$|$ BY REVERSING THE SENSITIVE AXIS

ACCELEROMETER OUTPUT (2) = SCALE FACTOR $|$BIAS - DRAG$|$

SCALE FACTOR

MESA MOUNTED A KNOWN DISTANCE R FROM TABLE CENTER

TABLE ROTATION RATE (ω) CONTROLLED

$R\omega^2$ BECOMES ACCELERATION STANDARD

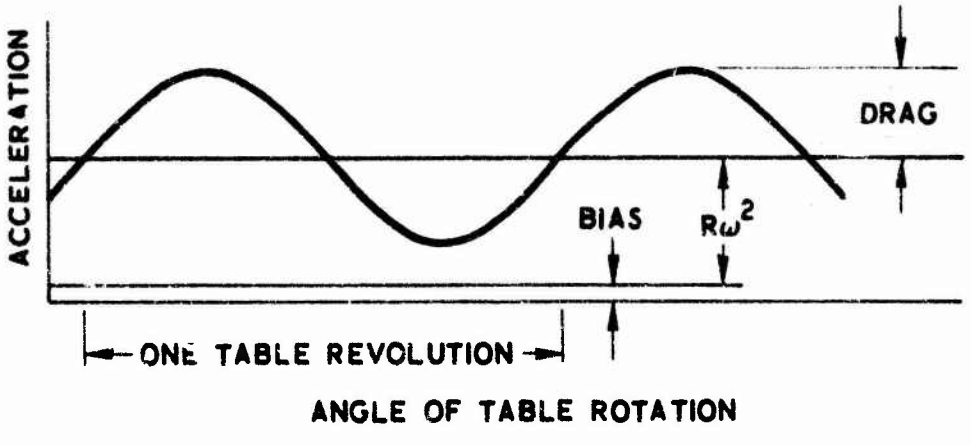

Fig. 1. Bias and Scale Factor Calibration Concept

the equations which describe the accelerometer output for Mode 1 and Mode 2 are

$$\text{Mode 1: } A_{m1} = K\left[B + A_{drag}\cos\omega t + R\omega^2\right] \tag{4}$$

$$\text{Mode 2: } A_{m2} = K\left[B + A_{drag}\cos 2\omega t + 4R\omega^2\right] \tag{5}$$

For the simple case where drag is essentially constant, as at apogee, we can imagine integrating the accelerometer output for one rev. of the centrifuge and then dividing the result by the time over which the rev. occurred. Since A_{drag} would average to zero over one rev., the average accelerometer output over one rev. for Mode 1 and Mode 2 can be expressed as

$$\dot{A}_{m1} = \frac{1}{2\pi}\int_0^{2\pi} \dot{A}_{m1}\, d\theta = K\left[B + R\omega^2\right] \tag{6}$$

$$\dot{A}_{m2} = \frac{1}{2\pi}\int_0^{2\pi} \dot{A}_{m2}\, d\theta = K\left[B + 4R\omega^2\right] \tag{7}$$

If we subtract Eq. (7) from Eq. (6), we find

$$K = \frac{\dot{A}_{m2} - \dot{A}_{m1}}{3R\omega^2} \tag{8}$$

We also find, if we multiply Eq. (6) by four and then subtract the Eq. (7) from it, that

$$B = \left[\frac{4\dot{A}_{m1} - \dot{A}_{m2}}{\dot{A}_{m2} - \dot{A}_{m1}}\right] R\omega^2 \tag{9}$$

It should be noted that Eq. (9) does not provide the same accuracy in determination of instrument bias as would Eq. (3). This is because Eq. (9) is dependent on a small difference of two large numbers for its determination of bias. In the actual determination of the instrument parameters, the drag is not constant and the simplified expressions shown above do not apply. The actual case is covered by representing the drag by a second-order polynomial with unknown coefficients. Such a polynomial representation permits the development of equations which are equivalent to but more complex than Eqs. (1) through (9).

When the initial calibration concept outlined above had been established, it was necessary to generate a preliminary design to the level of a block diagram and signal flow diagram as well as a preliminary estimate of the experiment parameters. A schedule and cost estimate were also made.

It was decided to proceed with the design and fabrication of three LOGACS assemblies. One was to be used for qualification testing; the other two were to be scheduled for flight. The Agena vehicle on which the LOGACS would be mounted would be stabilized with respect to the local vertical and the orbit plane. The location of the equipment would be the aft equipment racks. The vehicle would fly a near earth orbit with a small eccentricity ($\epsilon = 0.014$).

At this point, a contract was let to LMSC to acquire, test, integrate with the Agena, and support two LOGACS flights. LMSC was directed to subcontract to Bell Aerosystems Company the key subsystem of the LOGACS, which would consist of the centrifuge on which would be mounted a single miniature electrostatic accelerometer (MESA) and its electronics.

C. DESCRIPTION OF MESA

The basic MESA instrument consists of an electrostatically supported proof mass that is electrostatically pulse rebalanced along a preferred or sensitive axis. Figure 2 shows the complete MESA instrument while Fig. 3 shows the instrument without the insulating cover. The exploded view of the MESA shown in Fig. 4 and the cross section shown in Fig. 5 will be useful in the description of the MESA which follows.

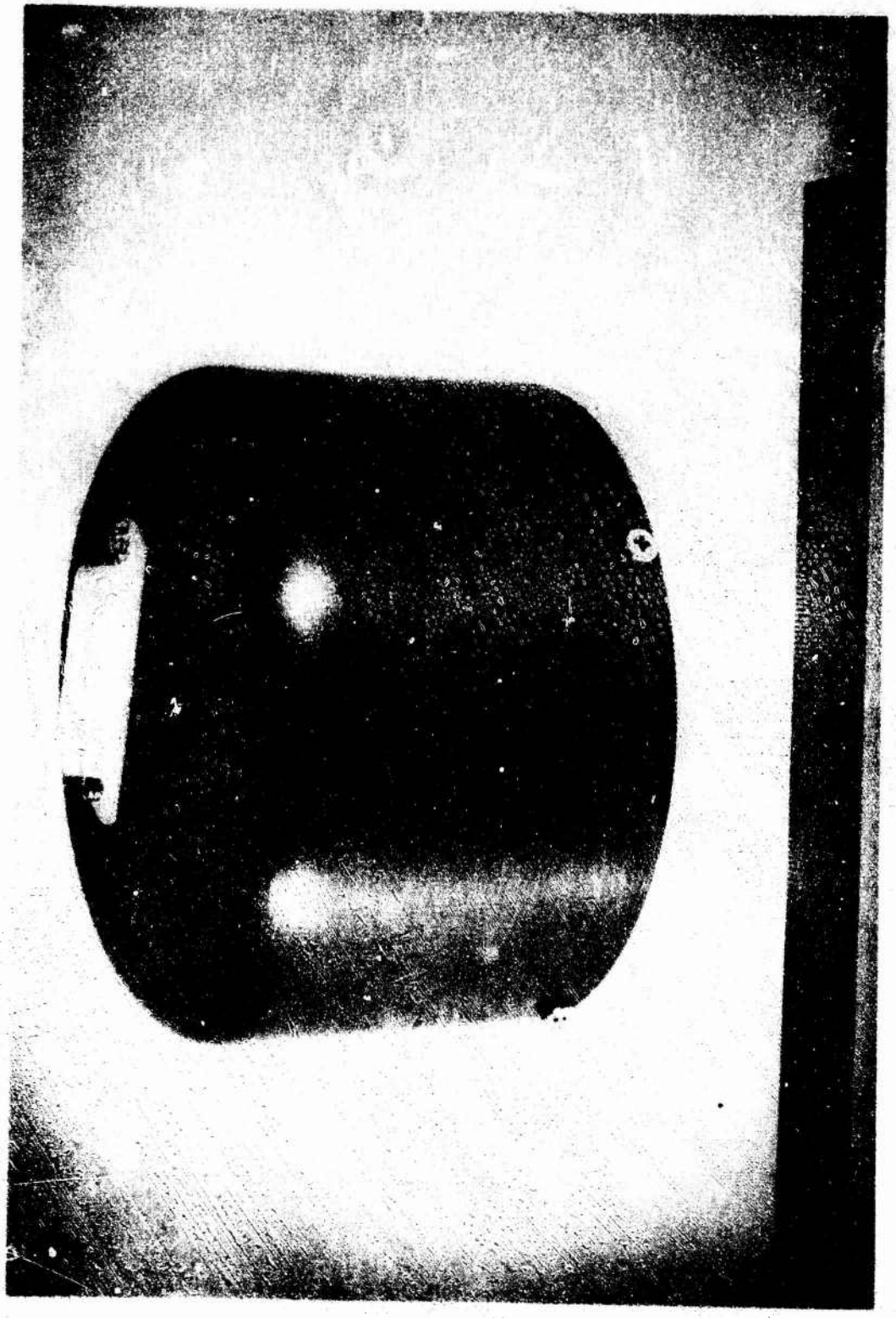

Fig. 2. Exterior View of MESA Accelerometer

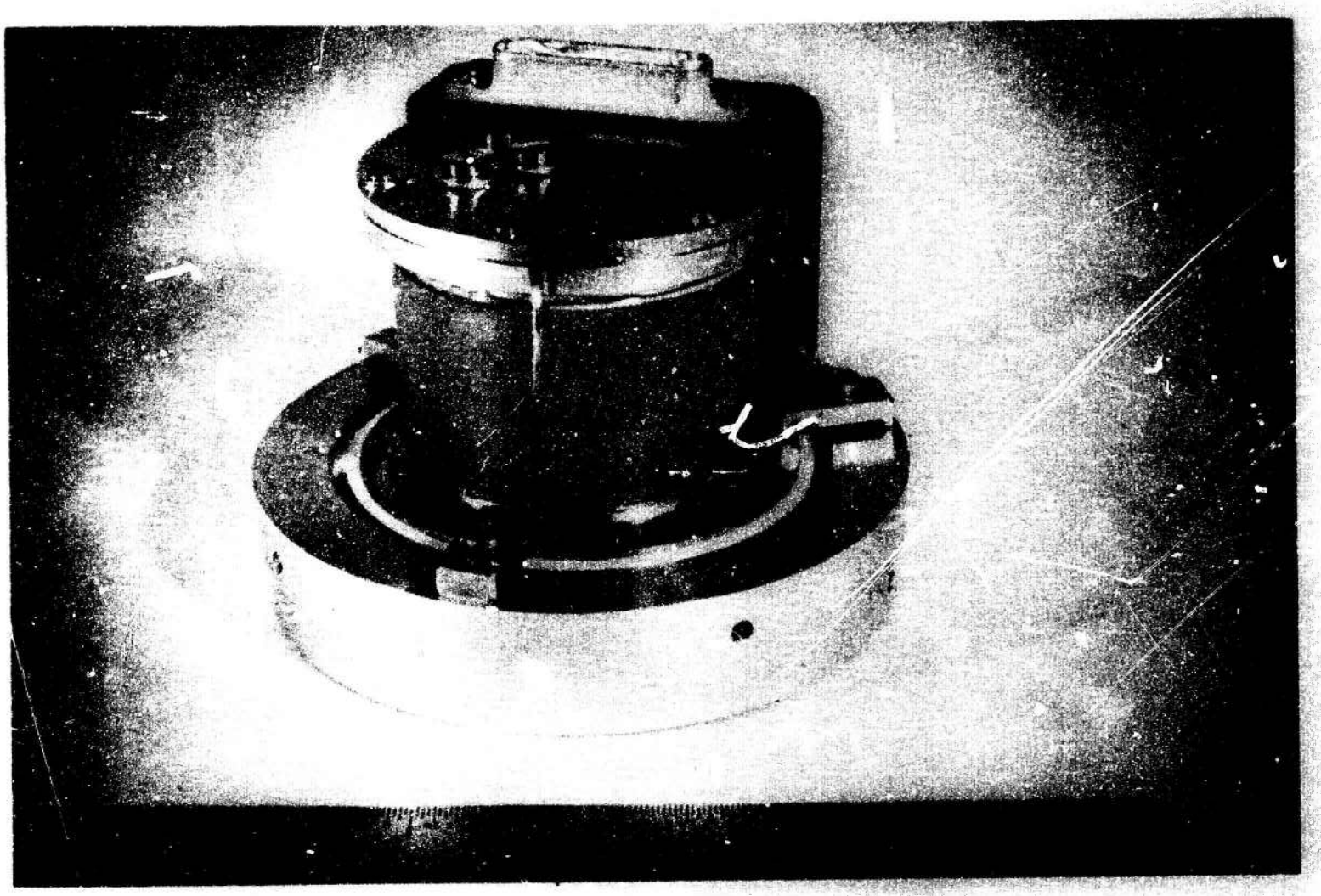

Fig. 3. MESA Without Insulating Cover

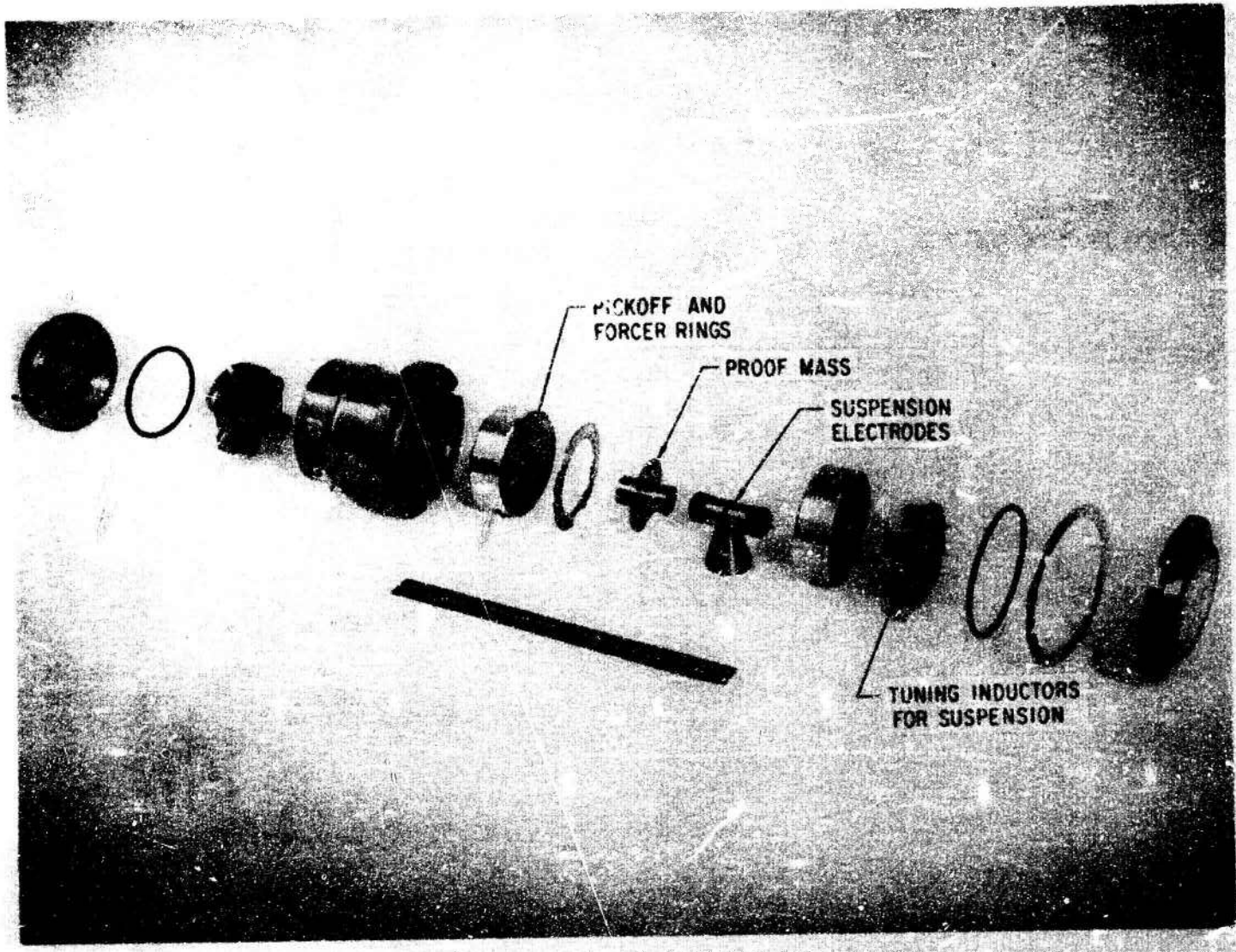

Fig. 4. Exploded View of MESA

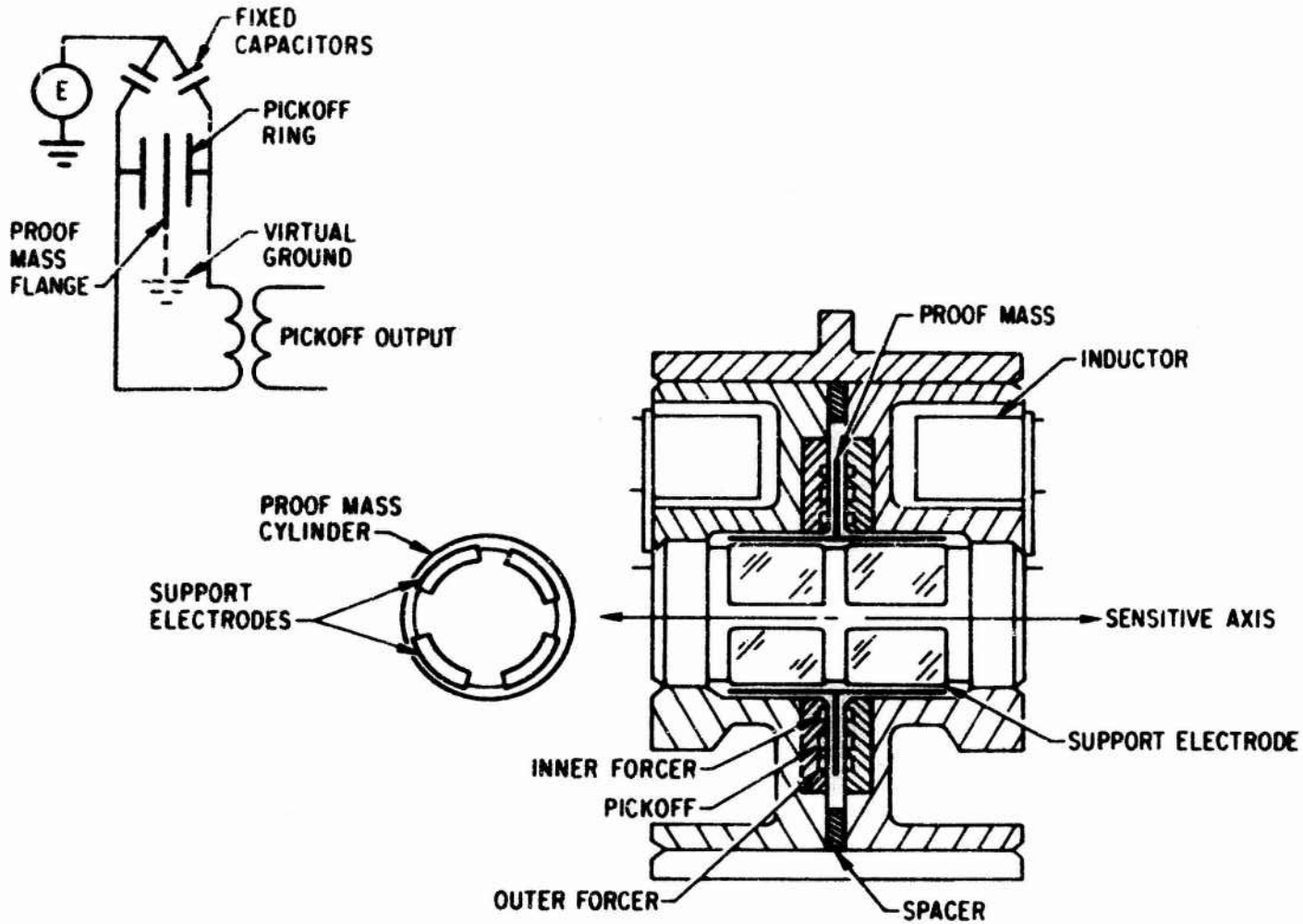

Fig. 5. Cross Section of MESA

The proof mass consists of a hollow cylinder with a centrally located flange. The proof mass is supported by electric fields generated by the eight support electrodes, each of which is in series with a tuning inductor. The capacitance in each series tuned circuit changes as a function of the relative displacement of the proof mass from the support electrode. Since each resonant circuit is tuned to operate on the high-frequency side of the resonance curve, each electrode-to-proof-mass voltage varies directly as the electrode-to-proof-mass displacement. As a result, the attractive force between each electrode and the proof mass increases as the electrode-to-proof-mass distance increases, thus producing a stable support. This cross-axis support system for the proof mass constrains the proof mass translationally along the two axes perpendicular to the sensitive axis and rotationally about the same two axes. The proof mass remains rotationally unconstrained about the sensitive axis. The remaining degree of freedom of the proof mass is translation along the sensitive axis, which is constrained by the pulse rebalance system.

The proof mass support capability provided by the cross-axis support system can be changed by simply changing the voltage applied to the electrodes. Since the support capability varies as the square of the electrode-to-proof-mass voltage, it is apparent that orders of magnitude change in the support capability can easily be achieved.

The particular support capabilities that were chosen for the MESA employed in LOGACS were (a) 1.5 g for use during ground test and on-orbit by command and (b) 7.5×10^{-3} g for on-orbit use.

The displacement of the proof mass along the sensitive axis is detected by an extremely sensitive capacitance bridge which, in simple form, is illustrated in the upper left corner of Fig. 5. The flange of the proof mass serves as the moving plate of the capacitance bridge while the pickoff ring in each housing is the fixed plate. Each pickoff-ring-to-flange capacitance forms a leg of the bridge while the other two legs can be assumed fixed and equal.

Displacement of the proof mass causes unbalance in the bridge, and the bridge output, when amplified and phase-sensitive demodulated, provides a signal whose amplitude is proportional to displacement from center and whose polarity indicates sense.

When the demodulated output of the capacitance bridge reaches a fixed trigger level (E_T or $-E_T$), the logic within the instrument gates a precisely controlled pulse from the pulse generator to the forcer rings. A pulse always goes to a pair (inner and outer) of forcer rings in one housing or the other.

When a pulse is directed to a forcer ring pair, the pulse polarity is such that a positive pulse is sent to one ring and a negative (i.e., inverted) pulse is sent to the other ring. Since the force on the proof mass is proportional to the square of the pulse voltage, the force resulting from the positive and negative pulses will be the same for equal area rings. More importantly, the technique of using opposite polarities for the pulse on each forcer ring prevents the buildup of charge on the proof mass.

As described above, the simultaneous application of positive and negative (i.e., inverted) pulses to the inner and outer forcer rings on the same side of the proof mass provides a restoring force that attracts the proof mass to the forcer rings to which the pulses were applied. The application of the same pulses to the forcer ring pair on the opposite side of the instrument provides a restoring force in the opposite direction. Thus, knowledge of which pair of forcer rings is being pulsed is the only information required to establish direction of the sensed acceleration. The logic that directs the pulses to one forcer ring pair or the other is set by the polarity of the demodulated capacitance bridge output.

The rate at which pulses are demanded is directly proportional to the net force on the proof mass and hence to acceleration applied along the sensitive axis.

A more detailed description and analysis of the instrument operation is given in Ref. 1.

D. EQUIPMENT DESIGN

The longest lead time items in the LOGACS equipment were the centrifuge and the MESA. Thus, the design constraints for these items had to be established first. The Aerospace Corporation, in conjunction with the two contractors, determined the design constraints for the centrifuge and the MESA. It was decided that the MESA would have a full scale range of 5×10^{-4} g, which would correspond to an output of 5000 pulses/sec. It was also decided that the centrifuge should be programmed to have four modes, each of 512 sec duration. The four modes were to be as defined in Table 1. The accelerometer output would be as shown in Fig. 6.

Table 1. LOGACS Centrifuge Modes

Mode	Description	Accelerometer Output
1	Rotation at fixed angular speed ω	$A_1 = K(B + A_{drag} \cos \omega t + R\omega^2)$
2	Rotation at fixed angular speed 2ω	$A_2 = K(B + A_{drag} \cos 2\omega t + 4R\omega^2)$
3	No rotation ($\omega = 0$), sensitive axis forward	$A_3 = K(B + A_{drag})$
4	No rotation ($\omega = 0$), sensitive axis aft	$A_4 = K(B - A_{drag})$

The centrifuge itself is shown in Fig. 7. The rotating member housed the MESA and the MESA electronics. The distance from the center of mass of the MESA proof mass to the center of rotation of the centrifuge was 3.9701 ± 0.0024 in. The large bull gear shown in Fig. 7 was part of the rotating member. The power to drive the rotating member was provided by a hysteresis synchronous motor. The motor was basically a 400-Hz machine, but it was driven at 300 Hz and 600 Hz with appropriate voltages to provide the two speeds for Mode 1 and Mode 2, respectively. The power and signal leads from the frame of the centrifuge assembly to the rotating member

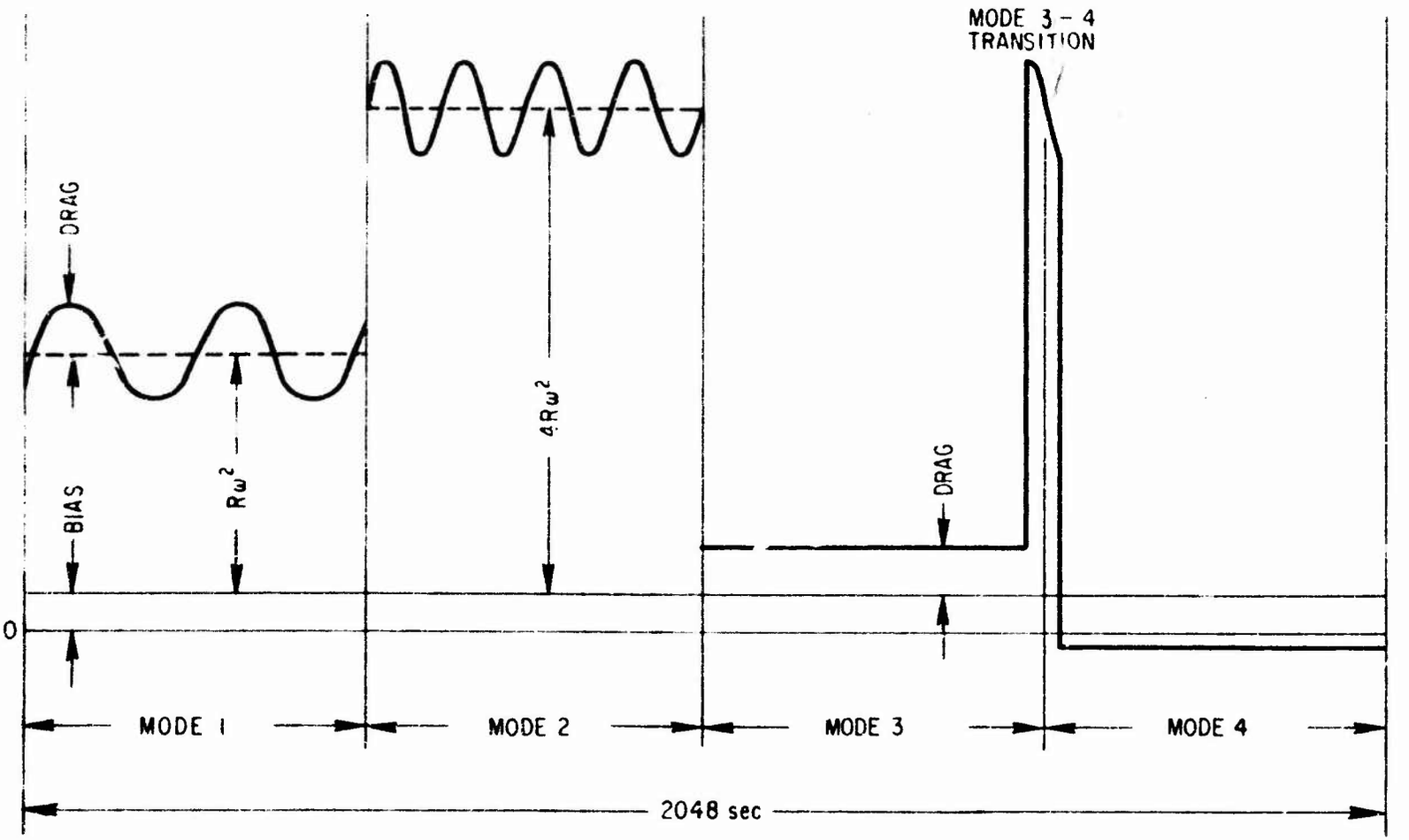

Fig. 6. Characteristic Accelerometer Output (constant drag case)

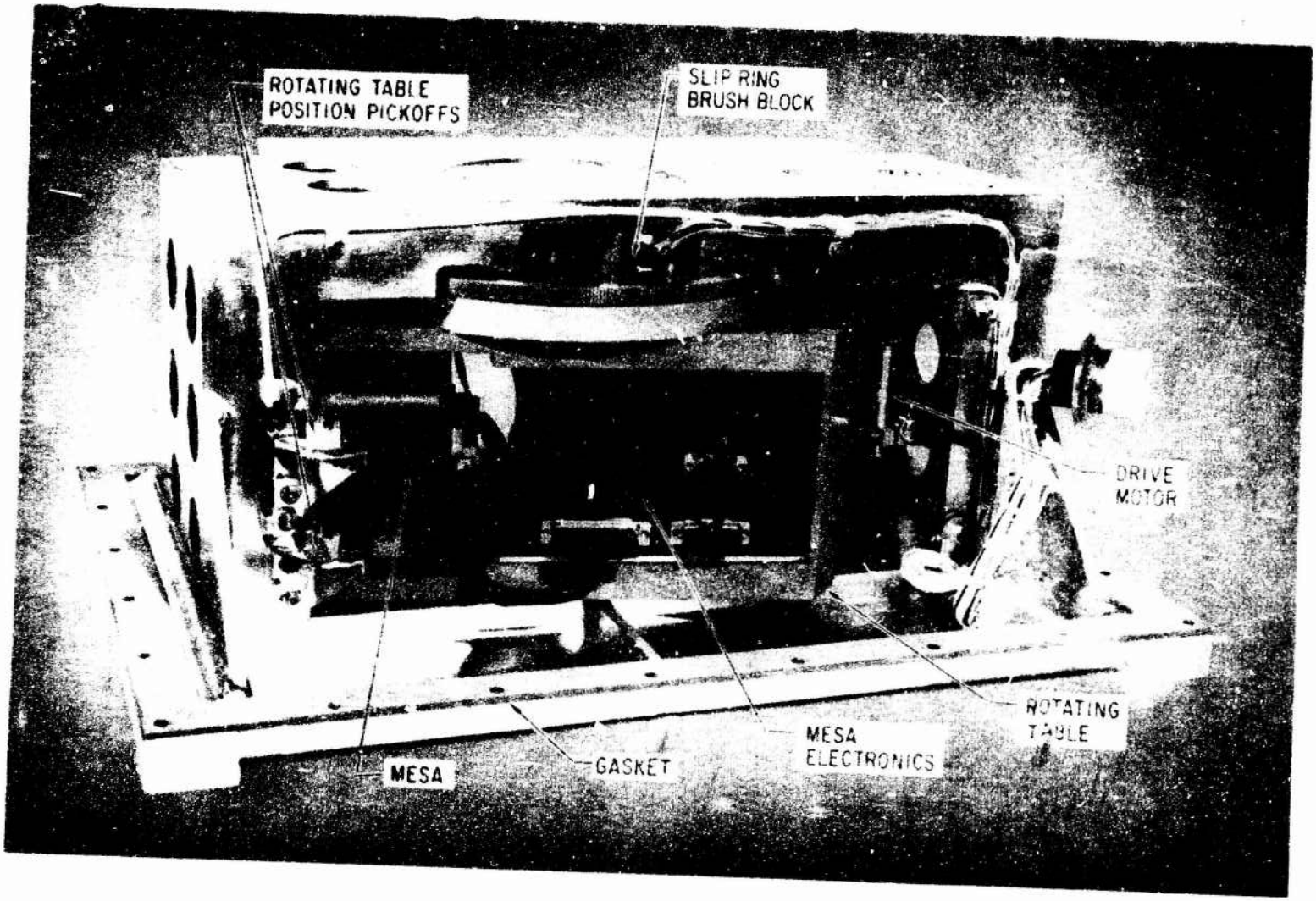

Fig. 7. LOGACS Centrifuge

were conveyed through a slip ring assembly mounted adjacent to the bull gear. The brush block of the slip ring assembly can be seen in Fig. 7. The position pickoffs indicated when the rotating member was positioned such that the MESA sensitive axis was fore or aft. These were simply reed relays actuated by a small magnet inset into the periphery of the rotating member. The reed relays can be seen fastened to the framework of the centrifuge in Fig. 7. The problem of lubrication for the slip rings while in the orbital environment was avoided by maintaining a partial atmosphere of dry air in the centrifuge assembly. The cover that enclosed the basic centrifuge shown in Fig. 7 contained a relief valve that maintained 4 psi gauge pressure within the centrifuge assembly. The seal between the cover and the baseplate of the centrifuge was effected with the gasket shown in Fig. 7.

One can calculate the two rotation rates (ω) and (2ω) of the rotating member using the known gear ratio of the gear train and the motor excitation frequencies of 300 Hz and 600 Hz. The values are

$$\omega = 0.4449445 \text{ rpm}$$

and

$$2\omega = 0.8898890 \text{ rpm}$$

Since the experiment clock was the reference for the motor supply frequencies, and it is known that the experiment clock ran fast by one part in 50,000 (see Appendix A), the above values should be multiplied by 1.00002 to obtain the actual values. Performing the multiplication and rounding off to five significant figures yields the following values for (ω) and (2ω):

$$\omega = 0.44495$$

and

$$2\omega = 0.88990$$

Use of the corrected values rather than the ideal values results in no discernible difference in the parameters reduced by the data analysis program.

As time progressed, the remainder of the LOGACS subsystems were defined and design or acquisition of these elements began to take place. The final block and signal flow diagram which evolved is shown in Fig. 8.

It will be helpful if a few explanatory comments are made about Fig. 8. Note that the centrifuge (which contains the MESA and its electronics) and the LOGACS IFU (interface unit) have a clean interface with the remainder of the elements. These two blocks comprised the portion furnished to LMSC by Bell Aerosystems Company. The remainder of the LOGACS equipment was acquired and integrated with the Agena vehicle by LMSC.

The primary channel of information which was to be recovered from LOGACS was the accelerometer output. As indicated in Fig. 8, the accelerometer output was formatted on two lines. One line contained the output pulses while the other line carried a binary signal that provided the sense or polarity to be associated with each output pulse. Thus the polarity of the input acceleration could be recovered for each output pulse.

The "pulse line" and the "polarity line" were fed to logic that was composed of two up-down counters and a register. The two counters were interrogated on alternate 1-sec intervals. Thus, the first counter would count for a 1-sec interval; then, while the second counter was counting for the next succeeding second, the count magnitude and polarity of the first counter would be transferred to the register and subsequently to the commutator and tape recorder. The 1-sec counts were transmitted as an octal number. Each integer of the octal number was represented as a voltage on an octal ladder. The least significant integer in the octal number represented one accelerometer output pulse.

Since the tape recorder had two channels and only one channel was required for the commutated information, the second channel was devoted to recording accelerometer output but in a different format than was employed with the commutator. The output pulse line and the polarity line were made

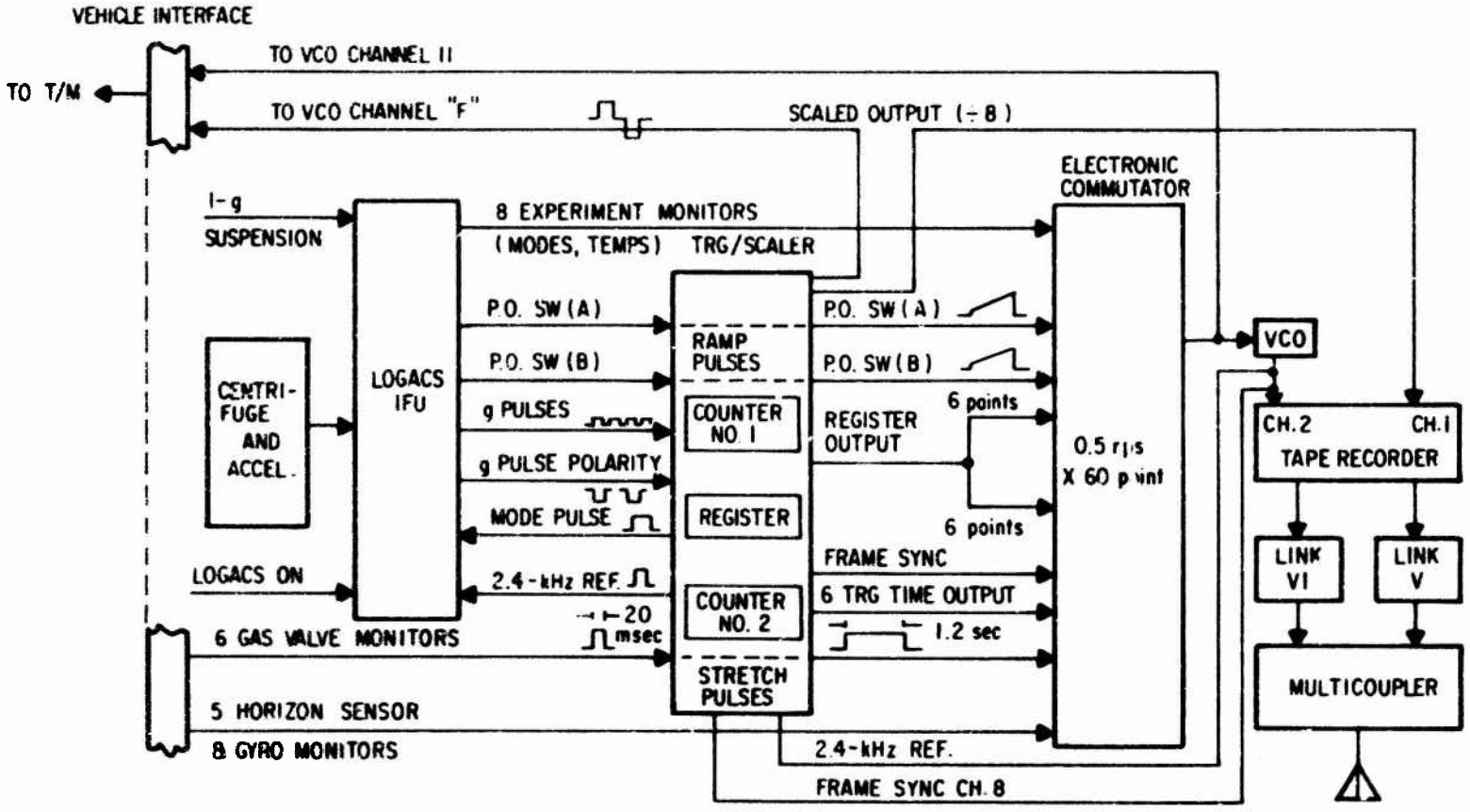

Fig. 8. Block and Signal Flow Diagram for LOGACS Experiment

available to logic consisting of an up-down counter that overflowed at a count of eight and set a flip-flop to trigger either a plus pulse or a negative pulse depending on the direction of the overflow of the counter. The same flip-flop also reset the counter. This reformatted pulse train was directly recorded on the second channel of the tape recorder. The utility of this second channel was twofold: (a) it offered a degree of redundancy and (b) it offered data with finer time resolution than the 1-sec pulse counts that were placed on the commutated channel.

The entire LOGACS equipment was synchronized from the airborne clock. This clock was a high accuracy 8-day clock with an octal ladder output format. The least significant octal count corresponded to 4 sec. The increment on the second octal ladder was 32 sec; on the third, 256 sec; on the fourth, 2048 sec; and on the fifth, 16,384 sec. A sixth octal ladder was reserved for count days (i.e., increments of 86,400 sec). Each 24 hr after turn-on of the clock, each of the first five octal ladders was reset to zero. The several additional functions provided by the clock were:

a. Providing a mode change pulse every 512 sec. The logic for the mode change was related to even steps in the ladder which had an increment size of 256 sec. Since each of the first five ladders was reset to zero at the end of each 24-hr period, the logic would issue a mode change pulse at 86,400 sec. Since 86,400 lacks 128 of being an integral multiple of 512, the last mode of each 24-hr period was not of 512 sec duration but was 512 minus 128, or 384 sec long

b. Providing a 2400-Hz square wave as a reference frequency

c. Providing a commutator synchronizing pulse each 2 sec (the commutator was a 0.5 rps × 60 point electronic commutator)

The clock package also contained the 1-sec counters and their accompanying register as well as the up-down eight counter plus circuits to format several miscellaneous signals.

The measured drift of the airborne clock was established from post-flight data analysis. The drift was found to be approximately 1 sec every 50,000 sec. The details of this determination can be found in Appendix A.

The two-channel tape recorder had approximately 163 min of storage. The recorder had a 26/1 reproduce/record speed ratio so that the information acquired during each orbital rev. could be transmitted to the ground station during a single station acquisition.

The LOGACS experiment included its own telemetry transmitters and attendant antennas as well as an S-band transponder for accurate tracking of the vehicle. The LOGACS experiment also included a complete command receiving system so that commands could be issued by the ground stations for purposes of controlling the LOGACS equipment while on-orbit.

The information contained on the commutator consisted of:

a. Accelerometer pulse counts per second
b. Experiment clock time in seconds since turn-on
c. Mode status
d. Two centrifuge table position pickoff signals
e. Monitor of Agena attitude control jet firings
f. Agena gyro output signals
g. Agena horizon scanner output signals
h. MESA instrument temperature
i. MESA electronics temperature
j. 28-V unregulated voltage
k. MESA proof mass position signal
l. MESA proof mass suspension signal
m. Necessary synch and calibration values

The manner in which the Agena attitude control jet firings [item (e) above] were recovered is not obvious when it is recognized that the typical duration of each firing is only 0.020 sec. Since the commutator scanned 60 points each second, some formating of the relay closure that activated each jet firing was needed. Each relay closure was routed to logic that generated a pulse as shown in Fig. 9.

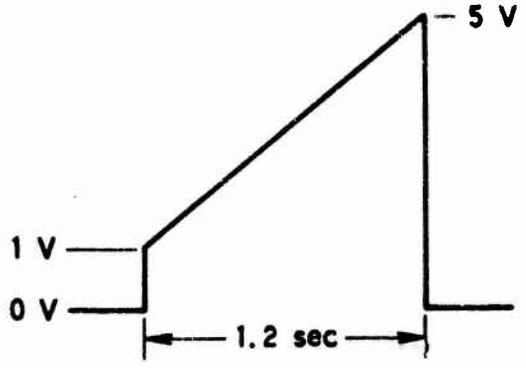

Fig. 9. Relay Closure Logic Pulse

Each of the six jets was scanned twice on the commutator, and the spacing between the first and second placement of each jet on the commutator was approximately 30 spaces. Since the commutator was synchronized with the experiment clock, the time at which the leading edge of the commutated segment occurred would be known. Knowledge of the voltage that existed during the scan of the commutator segment concerned with a particular jet, combined with the known starting time of that particular segment, makes it possible to determine the time for the beginning of each jet firing.

The attitude control monitor described above would not be adequate if the attitude control jet firing rate exceeded 1 firing per second for a particular jet. Postflight analysis has shown that firing rates did not exceed 1 firing per second for a particular jet except for an occasional occurrence during extremely high drag regions late in the LOGACS flight. Further discussion of the attitude control jet firing rate is contained in Section III.

A list of the drawings and documents that describe the LOGACS equipment is presented in Appendix B.

E. PREFLIGHT CHECKOUT

The entire LOGACS equipment array was accommodated on the bottom panel and the right side panel of the Agena aft equipment rack (see Fig. 10). The side panel is shown in Fig. 11, and the bottom panel is shown in Fig. 12. As can be seen in these photographs, reflective tape was applied

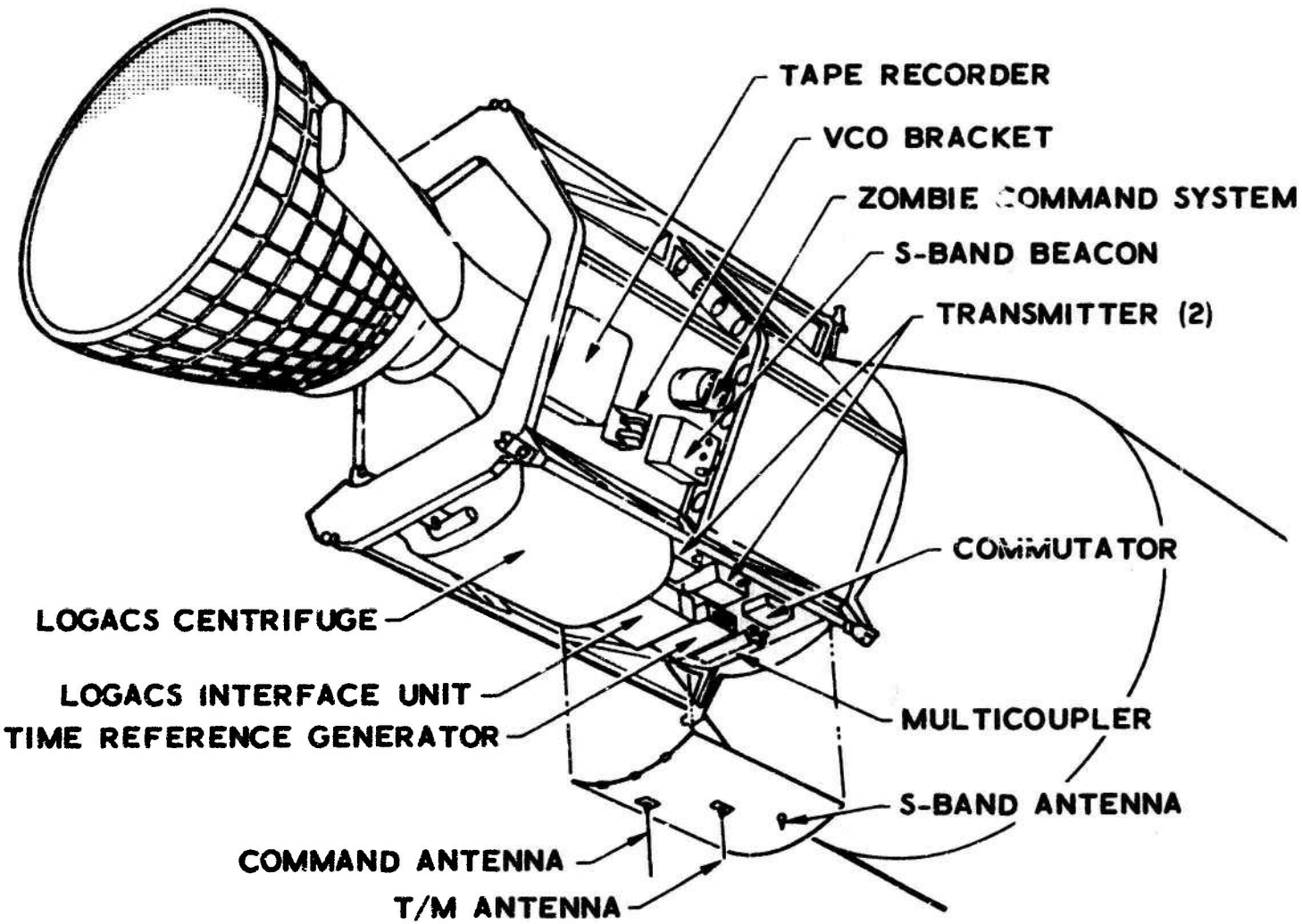

Fig. 10. Location of LOGACS Equipment on Agena

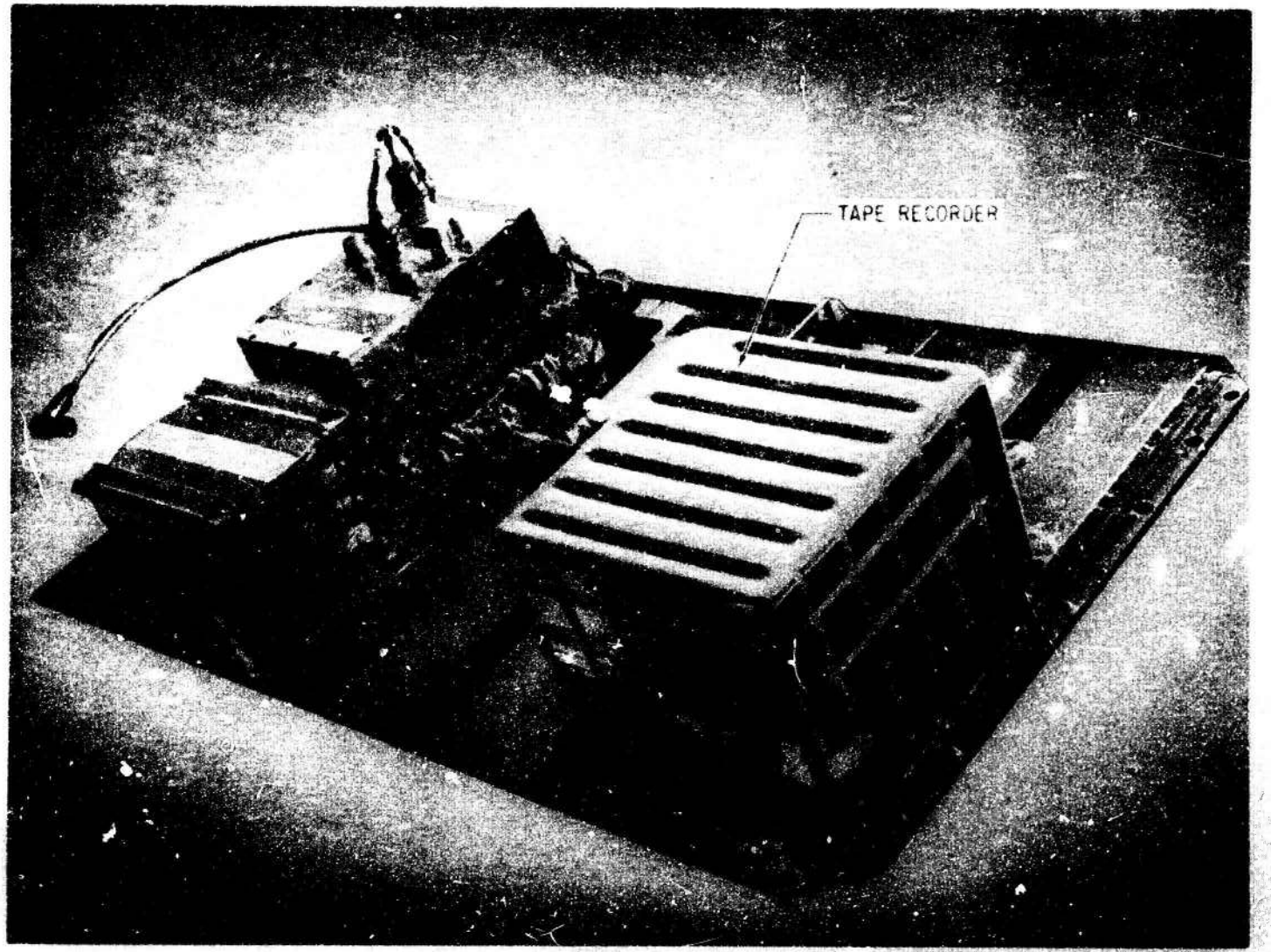

Fig. 11. LOGACS Side Panel

Reproduced from best available copy.

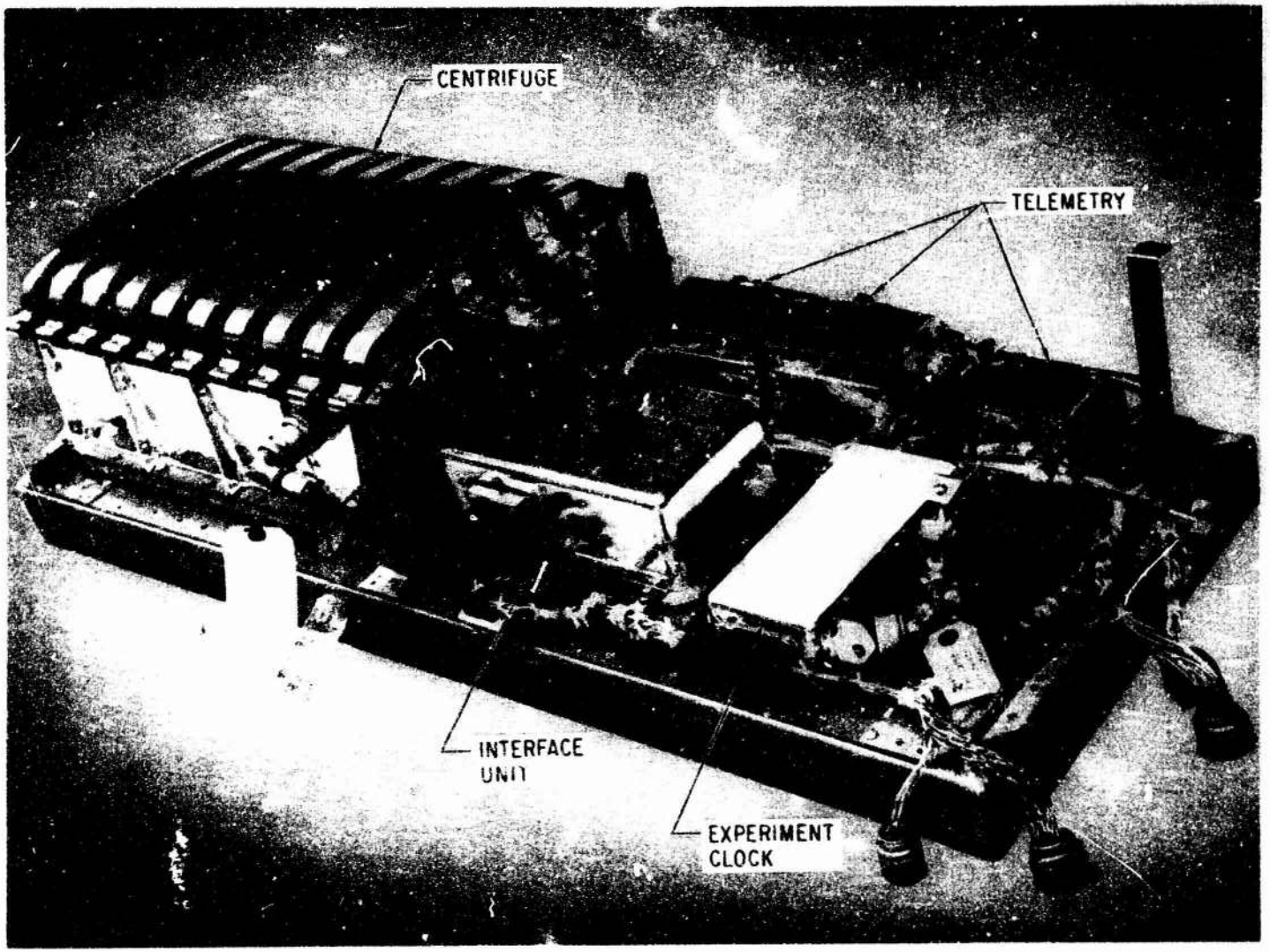

Fig. 12. LOGACS Bottom Panel

to the surfaces of much of the equipment to provide the thermal conditioning of the experiment for orbital use. The antennas and the antenna ground plane have not yet been installed on the bottom panel shown in Fig. 12.

After the panels were checked out as an integrated system at the LMSC facility at Sunnyvale, California, they were shipped to the LMSC facility at Vandenberg AFB. At Vandenberg the panels were subjected to a complete sequence of tests prior to integration with the Agena. The test sequence included testing of the command equipment by sending actual commands from the Vandenberg launch complex. After satisfactory completion of the testing, the panels were mated with the Agena and the testing sequence was essentially repeated. At the conclusion of this last set of tests, the LOGACS equipment was to remain dormant until the power turn-on command was sent after injection of the Agena into orbit. Subsequent to the final LOGACS tests, the Agena was mated to the Atlas launch vehicle and the normal preparations for launch proceeded.

F. FLIGHT OPERATIONS

After the Agena was successfully injected into orbit, power was applied to the LOGACS equipment by means of a switch actuated by the Agena "D" timer.

The USAF Satellite Control Facility provided the means whereby the LOGACS equipment could be controlled via real-time commands issued from the ground stations in the satellite control network. These same stations provided radar tracking of the Agena on which the LOGACS equipment resided.

Continuous monitoring of the LOGACS experiment was required, since at each ground station acquisition it was necessary to command the telemetry on and the tape recorder to switch from record to reproduce. The telemetry data transmitted from the LOGACS experiment were recorded on magnetic tape at the ground stations. In addition, the real-time LOGACS data transmitted at each station acquisition were decommutated and printed out at the USAF Satellite Test Center in Sunnyvale, California. Thus, a real-time monitor of the status of the LOGACS experiment was maintained and some

preliminary calculations of accelerometer instrument bias and scale factor as well as atmospheric drag were made during the 100-hr lifetime of the LOGACS experiment.

In addition to the normal commands issued at each station acquisition, several special command situations were planned during the LOGACS flight. An orbit adjust rocket firing was commanded at the Rev. 18.4 station acquisition so that the orbital lifetime of the Agena vehicle could be extended. At the Rev. 48.4 station acquisition, a command was issued to switch to the higher cross-axis support voltages for the MESA. The higher support voltages were left on until the Rev. 56.1 station acquisition, at which time a command was issued to return the cross-axis support voltages to the normal level used on-orbit. The purpose of leaving the higher support voltages on for several revs. was to calibrate for instrument bias and scale factor with the higher support voltages as well as the same quantities when the normal support voltages used on-orbit were employed. The values so obtained were intended to be used for comparison with the ground measurements obtained prior to flight.

G. EQUIPMENT PROBLEMS DURING THE FLIGHT

At the Rev. 1.3 station acquisition, the real-time data were decommutated, and a printout was provided subsequent to the acquisition. It was found that all the LOGACS equipment appeared to be operating properly but that the MESA output was saturated; i.e., a full scale output was present constantly. It had not been anticipated that the instrument would remain saturated for so long after launch, but it was decided to simply wait for the next acquisition and see what existed at that time. At the Rev. 2.4 station acquisition, the LOGACS data printout was obtained and the MESA output was again found to be at full scale. Since it had been anticipated that the MESA output would remain saturated for just a few hundred seconds after injection into orbit, there was a good deal of anxiety among the experimenters at this time. Though not planned for this purpose, the 1.5 g support voltage was commanded on for a brief period at the next station acquisition (Rev. 5.2)

on the presumption that if the test mass were somehow "stuck," this would serve to free it. The data available following the acquisition showed that this action was unnecessary because the instrument was operating properly at the beginning of the Rev. 5.2 acquisition. Further discussion of the long saturation period appears in Section J.

Another instance of saturation for a long period of time occurred immediately after the orbit adjust rockets were fired at the Rev. 18.4 station acquisition. The orbit adjust rockets consisted of two small solid propellant charges whose net thrust was directed along the longitudinal axis of the Agena. The result of firing the rockets was to increase the height of apogee by a few miles and thereby extend the orbital lifetime of the Agena vehicle. The sensitive axis of the MESA was fixed pointing aft with respect to the Agena during the orbit adjust rocket firing, and hence the output of the MESA saturated at this time. Again the MESA output remained saturated for an extended period of time. At the Rev. 20.5 station acquisition, the MESA output was found to be on scale. No further instances of a saturated output occurred during the LOGACS flight.

It was anticipated that the MESA instrument bias would change in accordance with the ratio of the support voltages. But when the MESA cross-axis support voltages were changed to the higher level at the Rev. 48.4 station acquisition, the instrument bias only changed in magnitude by about a factor of 10 compared to the change in the ratio of the support voltages of 200. Thus, the bias did not change as expected. Further discussion of this problem will be left to Section J.

H. DATA ACQUISITION

The LOGACS data were tape recorded on-orbit and then, at the ground station acquisitions, the tape recorder was commanded to reproduce. The playback of the orbital data was recorded at the ground station. It should be made clear that while the spacecraft tape recorder was in reproduce mode, the LOGACS data were also being transmitted in real time on another telemetry channel. Thus, no information was lost during the tape recorder

reproduce sequence. The real-time data were decommutated and printed out subsequent to each station acquisition. Analog records of much of the real-time data were also made during many station acquisitions.

After the LOGACS flight, all the recordings made at the ground stations were collected. These included both the real-time data and the tape recorder playback data. All of this information was decommutated, changed to desired format, ordered with respect to the experiment clock time, and encoded on a floating point binary tape suitable for computer processing. Listings of the final merged tape were made, as were plots of the MESA output pulse rate. The attitude control jet firing occurrences were plotted on the same graph as the MESA output pulse rate, as were the Agena attitude control system gyro signals. A sample of these plots and typical data pages are shown in Fig. F-1 and Table 2.

The second channel of the tape recorder contained the formated accelerometer output pulses. The information from this channel has not been exploited because the accelerometer output pulses per second were available on the pair of counters that were on the commutated channel. While the pulse information on the second channel generally duplicates the counter information, it does contain some fine grain information which is not apparent from the accelerometer output pulse counters.

I. DATA PROCESSING

The objective of the LOGACS data processing was to determine values of MESA instrument bias, instrument scale factor, and drag on the vehicle. The specifications for the LOGACS data analysis program are delineated in Appendix C. A listing of the LOGACS data analysis program is presented in Appendix D.

The essence of the LOGACS data processing was to fit, in a least squares sense, the data to the following simple model

$$A_m = K\left[B + R\omega^2 + \left(A_{drag} + \dot{A}_{drag}t + \ddot{A}_{drag}\frac{t^2}{2}\right)\cos(\omega t + \phi)\right]$$

where

A_m = accelerometer output (pulses/sec)

B = instrument bias (g)

K = instrument scale factor (pulses/sec-g)

R = distance from centrifuge center of rotation to center of mass of the MESA proof mass

ω = centrifuge rotation speed (rad/sec)

ϕ = phase angle of centrifuge (rad)

A_{drag} = vehicle acceleration due to nonconservative forces acting on the vehicle (g)

The values of B, K, A_{drag}, and ϕ are solved for during each mode sequence; that is, a solution for the above parameters is accomplished for every 2048-sec period during which no large data gap occurs.

An alternate data processing routine was also employed to independently solve for the same parameters. The alternate scheme was conceptually almost identical to the above scheme but did differ in detail. A comprehensive description of the alternate processing scheme is contained in Section II.

J. DISCUSSION OF RESULTS

1. INSTRUMENT RESULTS

The MESA instrument data obtained from the data analysis program that made use of a second-order fit to the LOGACS Mode 1 and Mode 2 data (see Appendix D) are presented in Tables 3 and 4 and Figs. 13 and 14. Table 3 shows the instrument bias and scale factor where no edit was made of thrust valve firings; Fig. 13 is a plot of the data in Table 3. Table 4 shows the bias and scale factor for which an edit was made of all data periods containing thrust valve firings; Fig. 14 is a plot of the data in Table 4.

Table 5. MESA Instrument Bias and Scale Factor (no edit of data acquired during thrust valve firings)

Experiment Clock Time, sec	Bias, g × 10^{-7}	Scale Factor, pulses/sec-g × 10^{7}
12288	- 3.8	0.9860
26624	- 3.0	0.9863
28672	- 3.9	0.9833
30720	+ 0.5	0.9840
45056	- 6.6	0.9856
47104	- 2.8	0.9891
49152	- 5.9	0.9848
51200	- 6.7	0.9857
53248	- 2.3	0.9815
55296	- 6.5	0.9853
57344	- 8.8	0.9919
59392	- 7.3	0.9845
63488	+ 2.7	0.9795
65538	- 6.3	0.9853
67584	- 5.3	0.9825
69632	- 5.3	0.9836
71680	- 7.7	0.9853
108416	- 7.3	0.9843
110464	- 6.7	0.9852
112512	- 7.7	0.9843
114560	- 8.4	0.9852
126848	-10.8	0.9891
128896	- 8.4	0.9836
130944	- 7.5	0.9835
132992	- 5.1	0.9838
155520	- 7.7	0.9833
1575.0	- 7.9	0.9830
161664	- 7.9	0.9834
163712	- 7.3	0.9824
173824	- 7.2	0.9851
175872	- 4.9	0.9853
177920	- 8.5	0.9846
179968	- 7.2	0.9825
186112	-10.9	0.9972
188160	- 7.8	0.9842
194304	- 8.4	0.9843

Table 3. MESA Instrument Bias and Scale Factor (no edit of data acquired during thrust valve firings) (continued)

Experiment Clock Time, sec	Bias, $g \times 10^{-7}$	Scale Factor, pulses/sec-g $\times 10^{7}$
196352	- 6.3	0.9799
198400	- 9.4	0.9859
204544	- 6.9	0.9827
208640	- 0.2	0.9776
210688	- 8.1	0.9841
214784	- 7.7	0.9837
218880	- 9.1	0.9904
220928	- 8.3	0.9825
229120	-12.6	0.9899
231168	- 9.4	0.9850
241408	- 8.3	0.9821
243456	- 8.8	0.9837
247552	- 9.2	0.9842
249600	- 8.1	0.9798
251648	0.0	0.9743
253696	- 8.5	0.9821
257792	+73.4	0.9849
259712	+72.8	0.9848
269952	+73.0	0.9847
272000	+75.6	0.9913
274048	+73.9	0.9835
280192	+72.2	0.9846
284288	+71.7	0.9868
286336	+71.6	0.9846
288384	+66.8	0.9940
290434	+72.6	0.9838
294528	+72.5	0.9842
296576	+71.3	0.9866
298624	-12.5	1.0193
300672	- 6.4	0.9840
302720	- 6.9	0.9830
304768	+21.8	0.9563
306816	- 6.8	0.9828
317056	- 7.4	0.9843
337536	- 6.1	0.9815
339584	- 8.3	0.9835
349696	- 8.6	0.9836
355840	- 8.5	0.9821

NOTE: The value of 1 g $\triangleq$ 32.145 ft/sec^2 was used to calculate the above data.

Table 4. MESA Instrument Bias and Scale Factor (edit of all data acquired during thrust valve firings)

Experiment Clock Time,* sec	Bias, $g \times 10^{-7}$	Scale Factor, pulses/sec-$g \times 10^{7}$
12288	- 4.0	0.9861
26624	- 9.1	0.9897
28672	- 4.6	0.9836
45056	- 6.5	0.9854
49152	- 5.5	0.9838
51200	- 7.0	0.9840
53248	-24.9	1.0061
55296	- 7.0	0.9861
65538	- 7.4	0.9858
67584	- 7.3	0.9871
69632	- 7.1	0.9838
71680	- 6.2	0.9836
108416	- 7.8	0.9841
110464	- 7.8	0.9814
112512	- 8.4	0.9849
114560	- 8.2	0.9853
126848	- 8.4	0.9812
128896	- 8.0	0.9830
130944	- 9.1	0.9852
155520	- 8.4	0.9849
157570	- 8.4	0.9838
161664	- 8.2	0.9841
163712	- 7.6	0.9820
173824	- 8.7	0.9849
177920	- 8.7	0.9849
179968	- 6.9	0.9815
188160	- 9.0	0.9857
194304	- 8.0	0.9830
196352	- 7.7	0.9803
198400	-16.3	0.9928
204544	- 7.1	0.9827
210688	- 8.7	0.9847
214784	- 9.0	0.9854
220928	- 8.1	0.9820
231168	-10.3	0.9858
241408	- 8.2	0.9815
243456	- 9.6	0.9844

*The time sequence in this table differs from that of Table 3; points missing here were edited because of thrust valve firings.

Table 4. MESA Instrument Bias and Scale Factor (edit of all data acquired during thrust valve firings) (continued)

Experiment Clock Time,* sec	Bias, g × 10^{-7}	Scale Factor, pulses/sec-g × 10^{7}
247552	- 9.2	0.9835
249600	- 7.1	0.9759
253696	- 9.2	0.9824
257792	+73.0	0.9851
259712	+74.5	0.9827
269952	+72.5	0.9850
274048	+71.7	0.9851
280192	+71.8	0.9848
284288	+67.4	0.9908
286336	+71.9	0.9843
290434	+71.4	0.9848
296576	+70.9	0.9867
300672	- 8.2	0.9858
302720	- 6.6	0.9799
306816	- 7.0	0.9831
317056	- 8.7	0.9860
337536	-15.7	0.9907
339584	- 8.4	0.9834
349696	- 8.7	0.9835
355840	-10.7	0.9834

*The time sequence in this table differs from that of Table 3; points missing here were edited because of thrust valve firings.

NOTE: The value of 1 g $\triangleq$ 32.145 ft/sec^2 was used to calculate the above data.

The MESA instrument data obtained from the alternate data analysis technique differed from the second-order fit data analysis in that the editing was done by hand and, therefore, involved judgment. Table 5 shows the bias and scale factor values determined by this aiternate method, and Fig. 15 is a plot of the data in Table 5.

A summary of the mean values and the standard deviation about the mean for the MESA instrument bias and scale factor is presented in Table 6. The values of bias and scale factor presented in Table 6 are derived from that set of data points which was common to the three different analysis programs.

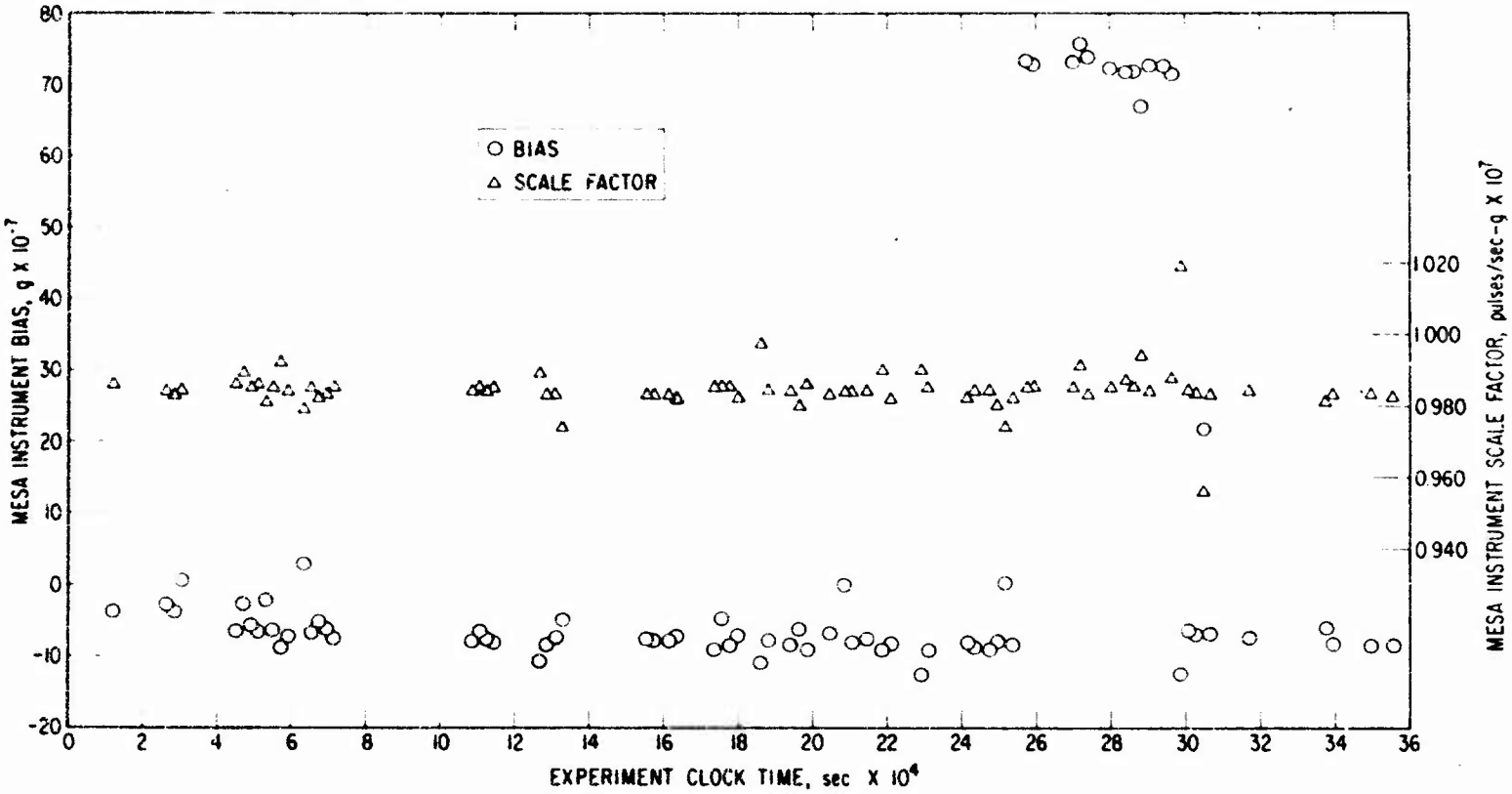

Fig. 13. Data Analysis with No Thruster Edit

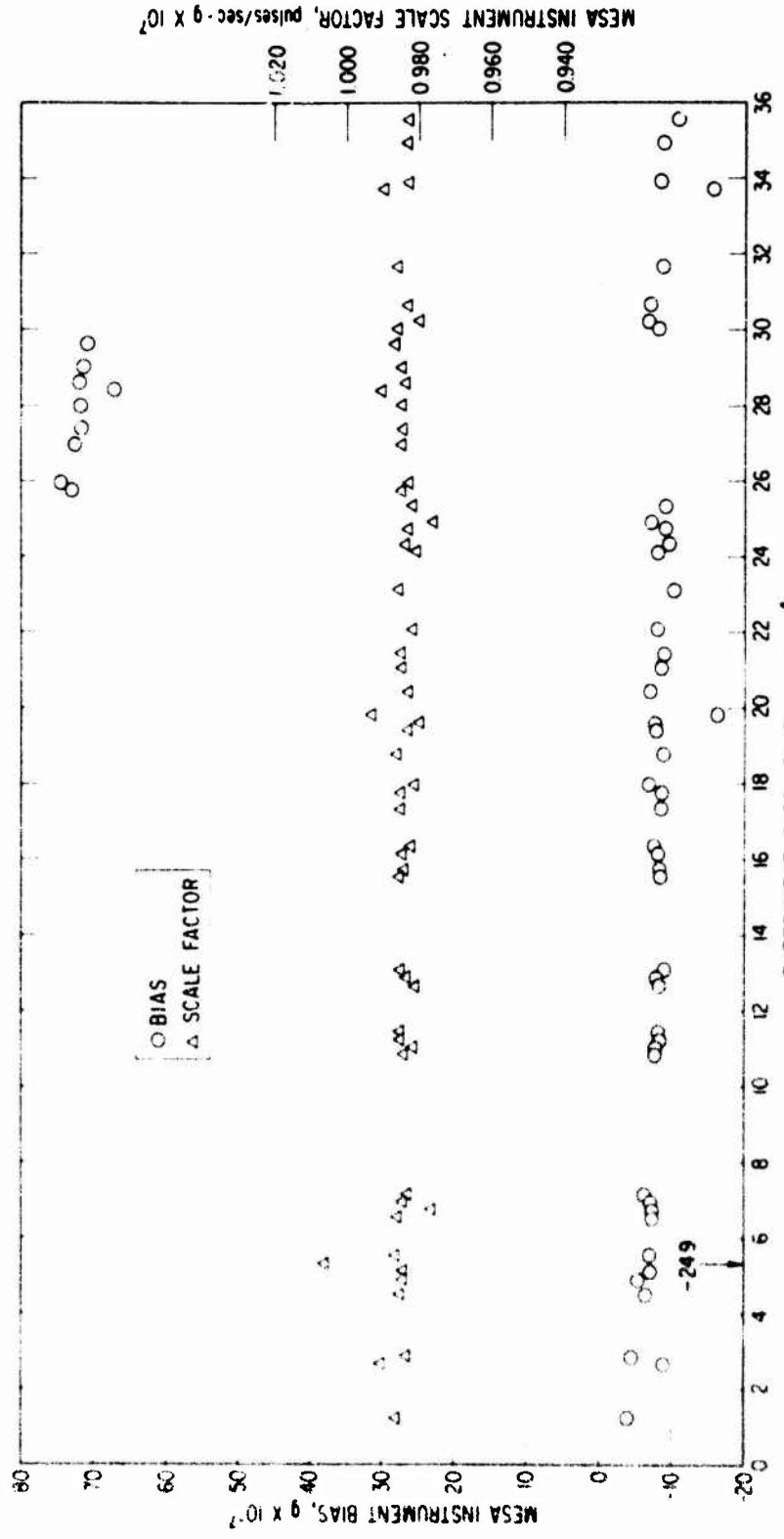

Fig. 14. Data Analysis with Thruster Edit

Table 5. MESA Instrument Bias and Scale Factor (data reduced by means of alternate analysis program)

Experiment Clock Time,* sec	Bias, g $\times 10^{-7}$	Scale Factor, pulses/sec-g $\times 10^{7}$
12288	- 4.1	0.9861
28672	- 4.2	0.9834
32768	- 5.0	0.9840
45056	- 6.5	0.9855
49152	- 6.6	0.9852
51200	- 6.4	0.9843
55296	- 6.9	0.9861
59392	- 6.9	0.9853
65536	- 7.2	0.9853
71680	- 7.0	0.9844
108416	- 7.8	0.9841
114560	- 8.0	0.9849
124800	- 8.9	0.9840
128896	- 8.6	0.9838
130944	- 8.4	0.9848
135040	- 8.1	0.9832
157568	- 8.3	0.9838
161664	- 8.0	0.9832
163712	- 7.5	0.9817
173824	- 8.8	0.9847
177920	- 8.4	0.9845
179968	- 7.8	0.9828
188160	- 8.4	0.9844
190208	- 7.7	0.9842
194304	- 8.0	0.9833
196352	- 8.0	0.9815
200448	- 8.6	0.9850
204544	- 7.9	0.9834
210688	- 8.6	0.9846
214784	- 9.1	0.9852
216832	- 7.4	0.9824
220928	- 8.3	0.9823
227072	- 8.8	0.9837
231168	- 9.7	0.9847
233216	- 8.7	0.9828
243456	- 9.0	0.9837

* The time sequence in this table is different from that of Table 3; points missing here were edited because of thrust valve firings.

Table 5. MESA Instrument Bias and Scale Factor (data reduced by means of alternate analysis program) (continued)

Experiment Clock Time,* sec	Bias, g × 10-7	Scale Factor, pulses/sec-g × 10^7
247552	- 9.2	0.9838
249600	- 8.0	0.9802
253696	- 8.8	0.9829
257792	+73.4	0.9847
259712	+74.1	0.9836
274048	+72.9	0.9846
276096	+71.9	0.9848
280192	+72.2	0.9844
286336	+72.2	0.9839
290432	+72.1	0.9841
296576	+70.8	0.9869
300672	- 7.5	0.9848
302720	- 7.6	0.9842
306816	- 7.4	0.9835
312960	- 8.0	0.9850
317056	- 8.6	0.9856
329344	- 8.0	0.9830
333440	- 8.1	0.9835
339584	- 8.5	0.9841
343680	- 8.5	0.9835
349696	- 8.3	0.9831
355840	- 8.7	0.9821

*The time sequence in this table differs from that of Table 3; points missing here were edited because of thrust valve firings.

NOTE: The value of 1 g $\triangleq$ 32.145 ft/sec^2 was used to calculate the above data.

The decision to employ only the common data points was made in an effort to avoid the errors introduced by the computational procedures. While the raw input data to the three analysis programs were identical, the degree and specific manner in which the edit of the data was performed did influence some of the bias and scale factor determinations in unique ways.

The stability of the bias and scale factor during the nearly 100-hr orbital calibration is evident from the small values of standard deviation shown in Table 6 as well as from the data plots shown in Figs. 13 through 15.

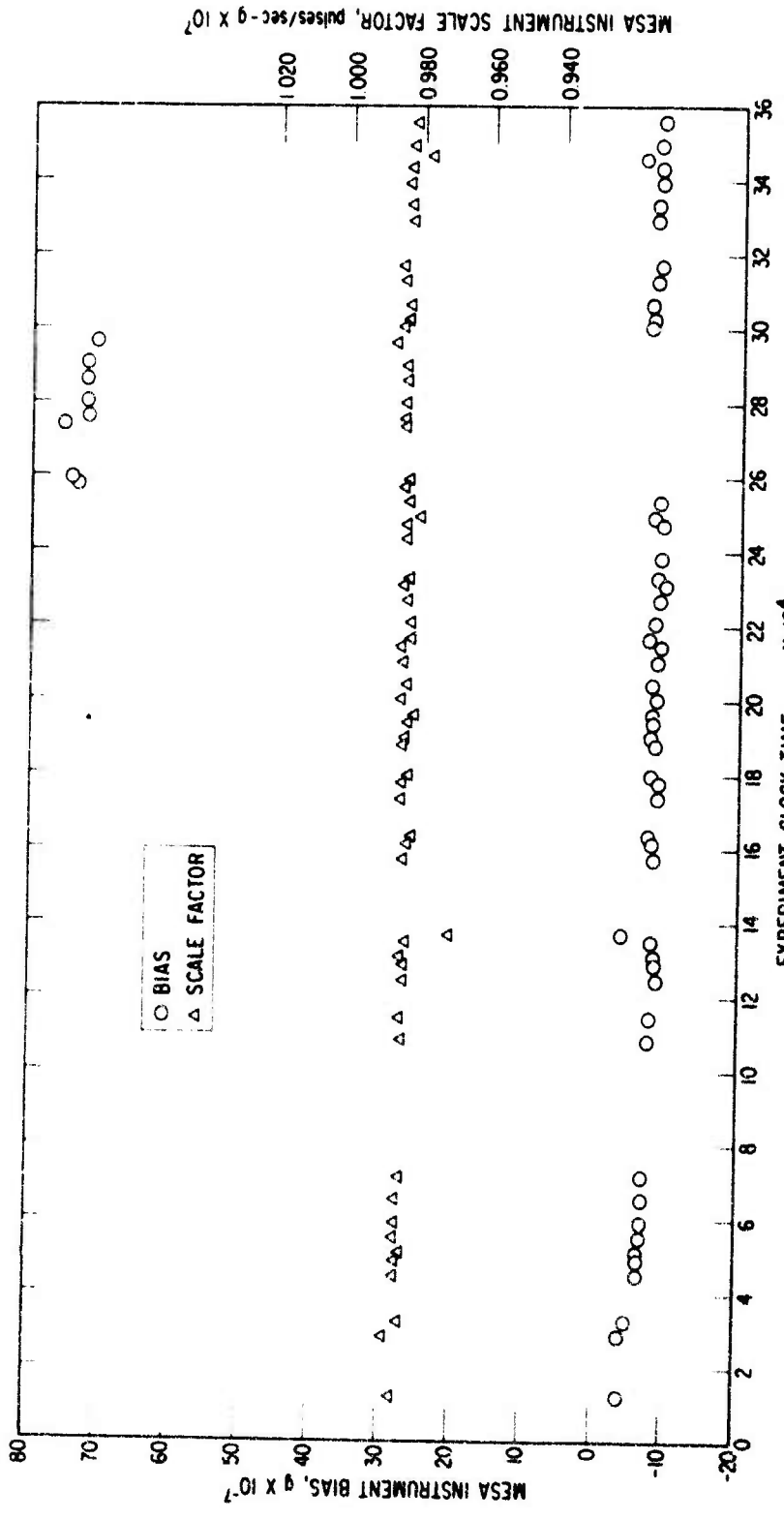

Fig. 15. Alternate Data Analysis

Table 6. Bias and Scale Factor

a. Determinations made from data periods when the 7.5×10^{-3} g cross-axis support capability prevailed:

	Bias, g $\times 10^{-7}$		Scale Factor, pulses/sec-g $\times 10^{7}$	
	Mean	Std. Dev.	Mean	Std. Dev.
Data analysis without edit	-7.5	1.3	0.9837	0.0014
Data analysis with edit	-7.9	1.4	0.9837	0.0011
Alternate data analysis	-7.8	1.2	0.9839	0.0013

b. Determinations made from data periods when the 1.5 g cross-axis support capability prevailed:

	Bias, g $\times 10^{-7}$		Scale Factor, pulses/sec-g $\times 10^{7}$	
	Mean	Std. Dev.	Mean	Std. Dev.
Data analysis without edit	+72.3	1.9	0.9846	0.0009
Data analysis with edit	+71.7	2.1	0.9848	0.0011
Alternate data analysis	+72.5	1.0	0.9846	0.0010

NOTE: The value of 1 g $\triangleq$ 32.145 ft/sec^2 was employed for all computations.

The relationship between the values of bias and scale factor determined prior to flight, on-orbit with the 7.5×10^{-3} g cross-axis support, and on-orbit with the 1.5 g cross-axis support are presented in Table 7.

Table 7. Expected Relationship of Bias and Scale Factor

	Preflight	On-Orbit 7.5×10^{-3} g Support	On-Orbit 1.5 g Support
Scale factor	X	X	X
Bias	Y	(1/200) Y	Y

The bias and scale factor coefficients for the MESA instrument were determined by Bell Aerosystems Company prior to installation of the MESA in the centrifuge assembly. The uncertainty in the value of bias as measured at Bell was on the order $\pm 50 \times 10^{-7}$ g. The uncertainty in the value of scale factor as measured at Bell was on the order ±0.5 percent.

The bias was measured at Bell on three separate occasions. The result of the three determinations is presented in Table 8.

Table 8. Bias Determination at Bell Aerosystems Company

Determination No. 1	$0 \pm 50 \times 10^{-7}$ g
Determination No. 2	$0 \pm 50 \times 10^{-7}$ g
Determination No. 3	$+50 \pm 50 \times 10^{-7}$ g

The scale factor was measured once at Bell and the value was found to be $1.031 \pm 0.005 \times 10^{7}$ pulses/sec-g.

If the values of bias and scale factor obtained prior to the flight are compared to those obtained on-orbit, we find two startling facts. The first is that the scale factor changed by about 4.7 percent, although no change was expected. The second is that the preflight bias value correlates reasonably

well with the on-orbit value when the 1.5 g cross-axis support was used, but when the cross-axis support voltages were reduced by a factor of 200, the bias changed polarity from positive to negative and became a factor of 10 smaller.

Since the LOGACS flight, the above anomalies in bias and scale factor have been given a considerable amount of attention. In the case of the bias changing in a manner not linearly correlated with the cross-axis support voltage, a clear explanation has evolved as to why the bias should in general never be expected to correlate linearly with the cross-axis support voltages.

Consider the cross-axis support forces that act upon the proof mass of the accelerometer. For ease of illustration let us confine our examination to a single plane. The forces on the proof mass when the proof mass does not possess symmetry would be as in Fig. 16.

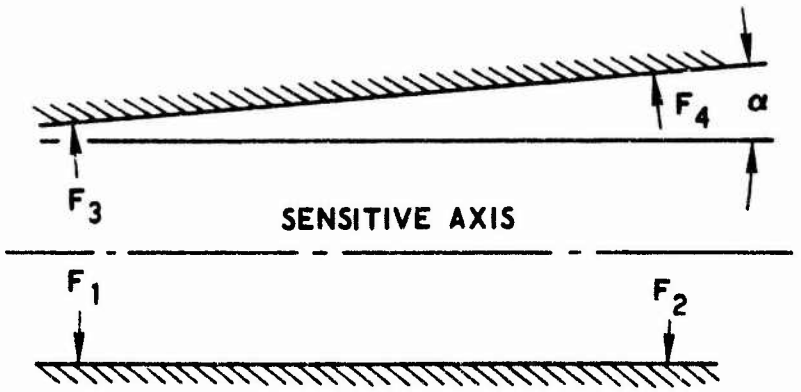

Fig. 16. Nonsymmetrical Proof Mass

The individual forces on the proof mass are the results of the electrostatic force associated with each of the eight support electrodes. Each support force acts normal to the region of the proof mass which it is intended to support. Thus, the forces F_1 and F_2 are acting normal to the sensitive axis direction for the geometry shown in Fig. 16, while forces F_3 and F_4 are

acting at an angle α away from such a normal. Clearly then, the force on the proof mass in the direction of the sensitive axis is the instrument bias. The bias can be expressed as

$$\text{Bias} = F_3 \sin \alpha + F_4 \sin \alpha \tag{10}$$

or

$$\text{Bias} = (F_3 + F_4) \sin \alpha \tag{11}$$

Also, the support forces must satisfy the relationship

$$F_1 + F_2 = (F_3 + F_4) \cos \alpha \tag{12}$$

if static equilibrium is to be maintained in the vertical direction. So far, we have not taken into account the proof mass itself and the alterations in the support forces that occur as a function of the acceleration in the cross-axis direction; that is, the relationships above are only valid for a zero cross-axis acceleration condition.

Now, imagine that the conditions imposed above for Fig. 16 are changed such that a cross-axis acceleration, a, exists and is directed vertically upward. The imposition of the cross-axis acceleration changes the equilibrium in the vertical direction by the force ma. Thus, we have

$$F_1' + F_2' = F_1 + F_2 - ma \tag{13}$$

and

$$(F_3' + F_4') \cos \alpha = (F_3 + F_4) \cos \alpha + ma \tag{14}$$

where the prime notation signifies the condition existing with the cross-axis acceleration. For this condition, we find that

$$\text{Bias} = (F_3' + F_4') \sin \alpha \tag{15}$$

Substituting Eq. (14) into Eq. (15), we have

$$\text{Bias} = (F_3 + F_4) \sin \alpha + ma \tan \alpha \tag{16}$$

Thus, the bias has changed from the value shown in Eq. (11) by the simple expedient of changing the cross-axis acceleration. The same general argument can be extended to show that any asymmetry in the proof mass or support electrode geometry will lead to a cross-axis acceleration sensitivity of the bias.

The net cross-axis acceleration sensitivity for the MESA used in LOGACS was on the order of 50 μg/cross-axis g. Recent analysis by the MESA manufacturer (Bell Aerosystems Company) suggests that the sensitivity can be reduced to the order of 5 μg/cross-axis g.

The reason for the scale factor change of 4.7 percent is not specifically known. The source of a change in scale factor can be generally separated into electrical or mechanical categories.

The mechanical category includes: (a) the length of the radius arm of the centrifuge being different from that used to compute the orbital scale factor values, (b) the angular velocity of the centrifuge being different from that used to compute the orbital scale factor values, and (c) the internal geometry of the MESA shifting after the ground calibration.

The radius arm length computations were carefully rechecked after the flight to ascertain whether an error could have been made. Since the nominal length of the radius arms is 4 in., the necessary change in radius arm length to produce a 4.7 percent change in scale factor would have to be about 0.2 in. Such a gross error could only result from something like a

transposition of numbers or a computational oversight. The rechecking of the radius arm computations failed to uncover any such error; hence we can discard a change in radius arm length as the source of the scale factor shift.

In the course of the meticulous rechecking of the radius arm length, no reason was found to doubt the measured value of R of 3.9701 ± 0.0024 in. The uncertainty in centrifuge rotational speed (ω) was less than 20 parts per million as judged by the demonstrated accuracy of the experiment clock, and therefore it can be neglected insofar as its contribution to uncertainty in $R\omega^2$ is concerned. Thus, the uncertainty in scale factor due to uncertainties in R and ω is due almost completely to the uncertainty in R, which leads to ±0.06 percent uncertainty in the absolute scale factor. This means that the mean value of scale factor determined from the flight data is uncertain in absolute value by ±0.06 percent.

The rotational speed of the centrifuge was independently checked by means of the telemetry data. Each rev. of the rotating arms of the centrifuge tripped a pair of reed relay position pickoffs located 180 deg apart. Thus, obtaining the time between the tripping of the reed relays from the real time telemetry data made it possible to show that the rotational speed was at the design speed with an error not exceeding 0.1 percent and not at the speed required to produce a 4.7 percent scale factor error.

The possibility of a mechanical shift of elements within the MESA exists but is considered to be an unlikely source. The demonstrated stability of scale factor during the 100-hr flight serves to testify that a gradual shift of the mechanical elements of the MESA did not occur. The remaining possibility is that a shift of the mechanical elements occurred as a step change and that thereafter the elements remained fixed. The latter does exist as a finite possibility, but it appears contrived and is not considered to be a likely explanation for the 4.7 percent scale factor shift.

Another possible explanation for the scale factor shift is that it does not exist at all but is simply the result of an erroneous ground determination. This possibility fails because independent sources have examined the data

and calculated the scale factor only to verify that a 4.7 percent shift in scale factor actually does exist.

The possible sources of scale factor shift which fall into the electrical category involve two basic circuits: (a) the temperature controller for the magnetic core that supplies the precision rebalance pulses and (b) the capacitance pickoff which detects the proof mass displacement along the sensitive axis and which is used to trigger the rebalance pulses.

The change in set point or control temperature which would produce a change in pulse size (i.e., scale factor) of 4.7 percent is approximately 94°F. Such a change is considered extremely unlikely because the orbital data are stable during the entire 100-hr flight. Again the possibility exists that a step change in set point of the temperature controller occurred after the ground test but remained stable afterwards. This latter possibility again appears contrived and is not considered to be a likely explanation for the 4.7 percent scale factor shift.

A change in scale factor will result from a shift in the electrical null of the capacitance bridge pickoff. Figure 17 illustrates how the scale factor changes as a function of shifts in the electrical null of the pickoff. The figure is not to scale but is used to illustrate the principles involved. As the proof mass moves along the sensitive axis, the capacitance bridge becomes unbalanced and the amplified and phase-demodulated output of the bridge is directly proportional to its displacement. The bridge output voltage is represented as E in Fig. 17. Imagine that the pickoff electrical null is represented by E_0 and that E_T and $-E_T$ represent, respectively, the positive and negative thresholds that are used to gate the voltage pulses to the forcer rings and thus apply force to the proof mass. Assume that the scale factor for each sense is identical for this case. The force on the proof mass during each application of voltage to the forcer rings is

$$\text{force in positive sense} \propto 1/\Delta^2$$

$$\text{force in negative sense} \propto 1/\Delta^2$$

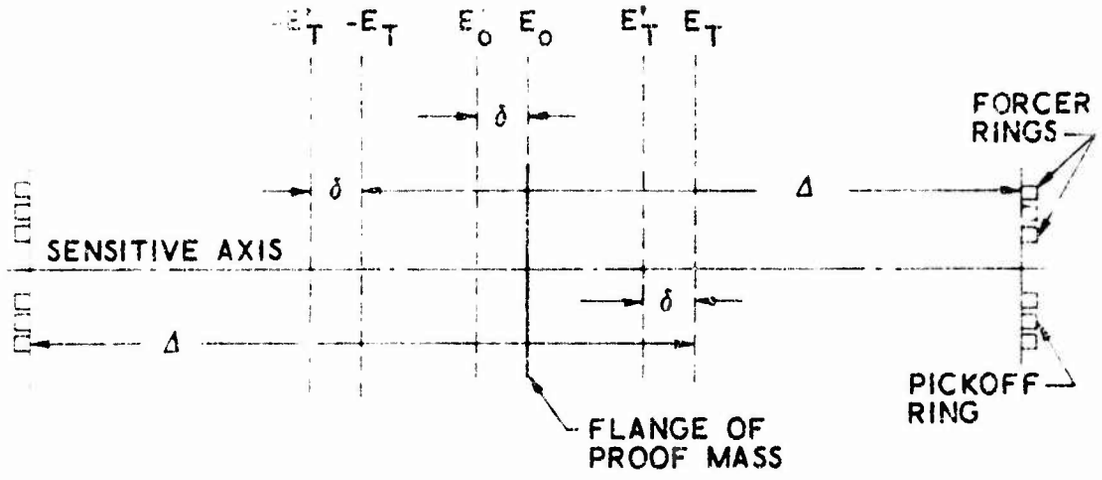

Fig. 17. Relationship of Scale Factor to Pickoff Null

Now imagine that the electrical null of the bridge shifts (i.e., one leg of the bridge changes in capacitance). Then the proof mass must move to a new position in order for the bridge to be balanced. The new null position of the proof mass is represented in Fig. 17 as E'_0. The proof mass displacement corresponding to the shift in electrical null is represented as δ. Due to the shift in balance of the capacitance bridge, we find that the proof mass positions corresponding to the positive and negative thresholds have changed. The new threshold positions are represented by E'_T and $-E'_T$. It should be noted that E'_T and $-E'_T$ have the same magnitude as E_T and $-E_T$. The prime notation is used as an expedient to denote the change in position which is due to the change in balance of the bridge. In this case, the force on the proof mass during each application of voltage to the forcer rings is

$$(\text{force})' \text{ in positive sense} \propto \frac{1}{(\Delta - \delta)^2} = \frac{1}{\Delta^2 - 2\delta\Delta} = \frac{1}{\Delta^2}\left(1 + \frac{2\delta}{\Delta}\right)$$

$$(\text{force})' \text{ in negative sense} \propto \frac{1}{(\Delta + \delta)^2} = \frac{1}{\Delta^2 + 2\delta\Delta} = \frac{1}{\Delta^2}\left(1 - \frac{2\delta}{\Delta}\right)$$

Since the force applied to the proof mass during the application of a voltage pulse to the forcer rings is different when the bridge balance is changed, the pulse rate that must be supplied to the forcer rings to rebalance the proof mass for a given acceleration will change in the same manner.

The capacitance bridge unbalance necessary to produce a scale factor change of 4.7 percent is very small -- on the order of 0.070 pF. (Since the pickoff gain is on the order of 1000 pF/cm, the displacement δ that corresponds to the 0.070-pF bridge unbalance is about 7×10^{-5} cm.)

While the precise mechanism for a shift in the capacitance bridge balance is not known, it appears to be the most likely explanation for a large change in scale factor.

The expressions developed above for the force applied to the proof mass when the pickoff null has been displaced reveal that a scale factor shift caused in this manner would exhibit a differential behavior; that is, the scale factor in one sense would increase by $1 + 2\delta/\Delta$ whereas the scale factor for the opposite sense would decrease by $1 - 2\delta/\Delta$. Recognition of this led to the hope that such a behavior could be recognized in the LOGACS flight data and hence lend support to the conjecture that a shift in the capacitance bridge balance caused the scale factor shift.

The portion of the data that lends itself to testing for a different scale factor in the two senses is where mode 3 (MESA pointing forward) ends. The centrifuge then rotates 180 deg and mode 4 (MESA pointing aft) begins. Two things interfere with any attempt to examine the data for differences in scale factor which are associated with sense. Clearly a large drag value is desirable to test for the scale factor change, but it is also true that the drag value changes more rapidly as the drag value gets large. Another associated difficulty is that the vehicle attitude control firings become significantly more frequent as drag increases and hence the "noise" in the data induced by the attitude control firings increases. Thus, we find ourselves faced with the unfortunate conflict wherein the drag and the "noise" on the drag signal increase substantially together. As a result, the attempts to date to show that a differential relationship exists for the scale factor for each sense have failed.

The MESA manufacturer also produces a line of accelerometers that employ a hinged pendulum as the proof mass. These accelerometers make use of a very sensitive capacitance bridge pickoff (≈600 pF/cm) which is similar in both concept and design to that of the MESA. Due to the mechanization of the pendulous accelerometers, a shift in the balance of the capacitance bridge pickoff results in a shift in the null bias of the instrument. A change of 0.07 pF in the balance of the capacitance bridge of the pendulous accelerometer would result in a null bias change of 350 μg. Such a shift would be abnormally large for these devices. The similarity in the capacitance pickoffs would suggest that if a shift of 0.07 pF is unusual in the hinged pendulum accelerometers, it would also be unusual in the MESA. Furthermore, since the MESA scale factor demonstrated approximately 0.1 percent stability during 100 hr on-orbit, the shift would have had to be a step change rather than a random wander.

The facts above do not prove but do lend support to the following conjecture: if the scale factor shift observed in the LOGACS MESA was due to a shift in the balance of the capacitance bridge, then that shift was an anomalous one and should not be considered typical of the MESA instrument.

In Section G it was noted that the accelerometer remained saturated for a long period of time after launch and again after the orbit adjust was accomplished. The reason for the long saturation time has not been conclusively proved, but a plausible explanation has evolved.

When the MESA proof mass is driven over against one side of the instrument, the force which can be applied to restore the proof mass to the centered position is only 1/4 that which can be applied when the instrument is centered. Thus, with a 1-gram proof mass and a 5×10^{-4} g constrainment capability along the sensitive axis, the force that can be applied to the centered proof mass is about 5×10^{-1} dyne. If the proof mass moves against the inactive forcer ring set (and hence is twice as far away from the operating forcer rings), the force that can be applied is about 1.25×10^{-1} dyne. Now, if the average force on the proof mass approaches 1.25×10^{-1} dyne and if the proof mass is already over against the stop, then the proof mass will take

longer and longer to return to the centered position. In fact, if the force that can be applied exactly equals or is less than the average force on the proof mass, then the proof mass will remain against the stop indefinitely. Laboratory tests with a MESA instrument have demonstrated that long saturation times can be easily produced by the technique described above. A typical curve generated in the course of such tests is shown in Fig. 18. While the tests do not show conclusively that this phenomenon explains the observed behavior, they lend strong support to this hypothesis.

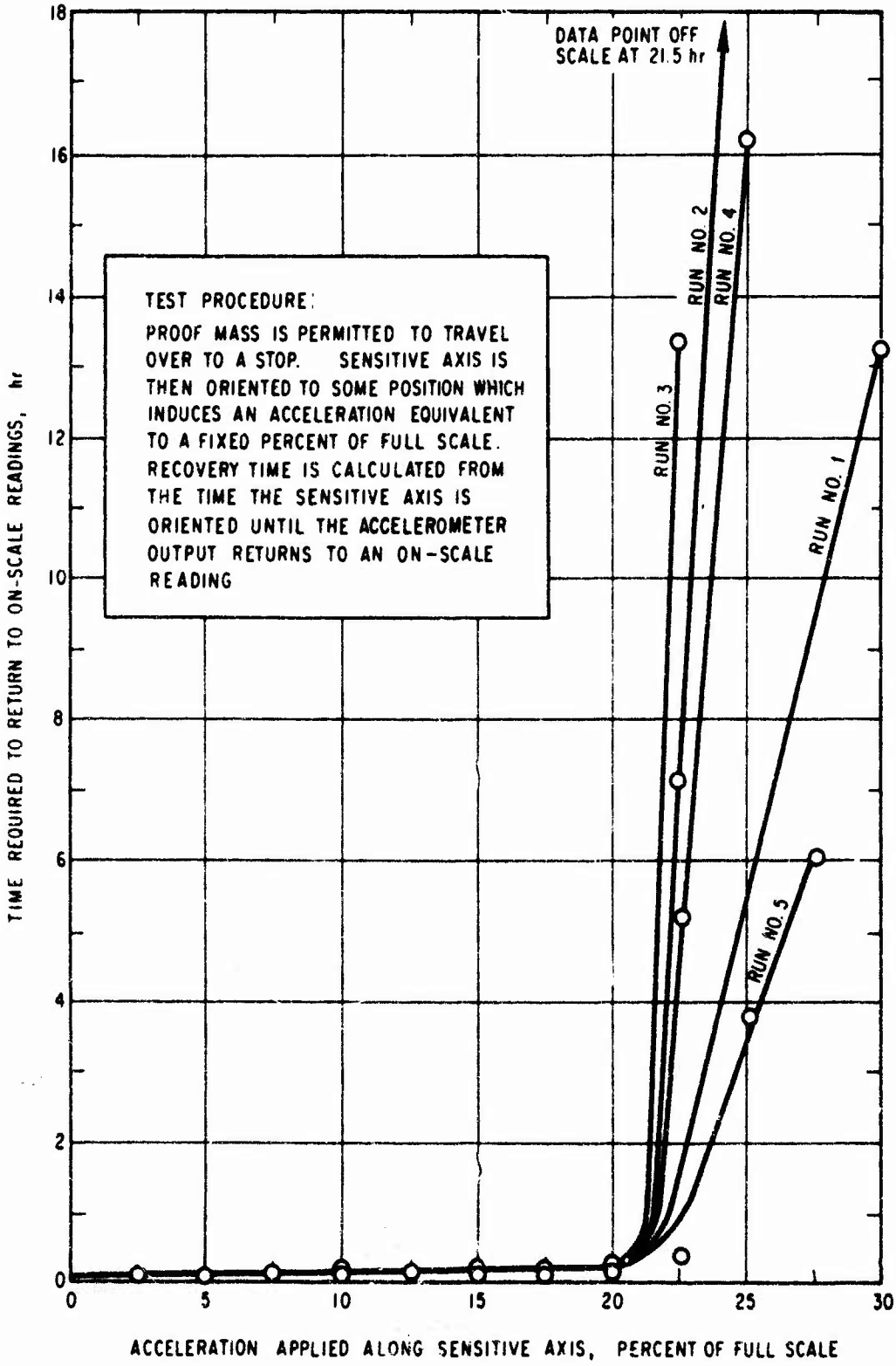

Fig. 18. Typical Curve from MESA Saturation Tests

SECTION II

LOGACS DATA REDUCTION

A. LOGACS SENSING ENVIRONMENT

Since it is desired to calibrate the accelerometer in a drag-free environment while it is desired to measure drag with the accelerometer in a fixed orientation, the environment for either objective was not ideal. In addition, during rotating modes the lateral forces and moments induced by aerodynamics and the Agena control system contribute to the measured acceleration. For these reasons it was necessary to perform an analysis of the sensing environment. This section presents this analysis and develops the algorithm for the acceleration sensed by the LOGACS accelerometer. The terms in this equation are then analyzed and their order of magnitude established. Based on this analysis, simplifications are made to the algorithm used for processing the accelerometer data.

1. AGENA CONFIGURATION

Figure 19 presents a schematic configuration diagram of the vehicle and the LOGACS instrument. A body-fixed coordinate system is used as a reference for defining the terms to be used in the analysis which follows. The x (roll) axis lies on the geometric center line of the vehicle pointing forward, the y (pitch) axis points out the right side of vehicle, and the z (yaw) axis is down. The center of this coordinate system is defined to lie on the vehicle center line at the reported Agena cg station (251.4 in.). Based on these definitions and those in Fig. 19, the data pertinent to the configuration used in this analysis are presented in Table 9.

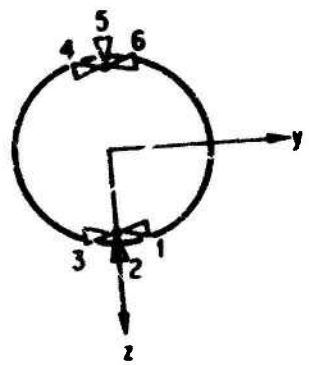

GAS VALVE ARRANGEMENT LOOKING FORWARD

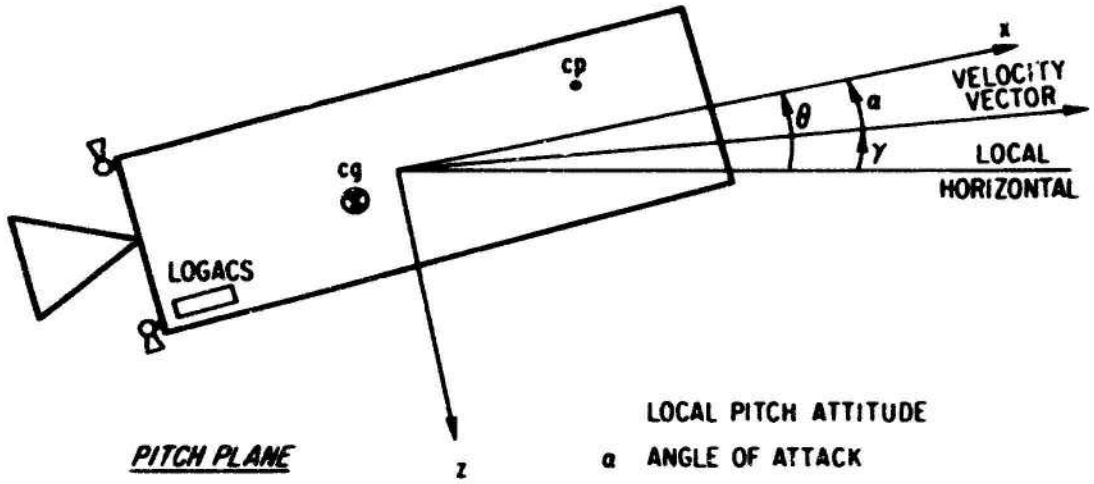

PITCH PLANE

θ LOCAL PITCH ATTITUDE
α ANGLE OF ATTACK
γ FLIGHT PATH ANGLE
cp EFFECTIVE AERODYNAMIC CENTER OF PRESSURE
cg CENTER OF GRAVITY

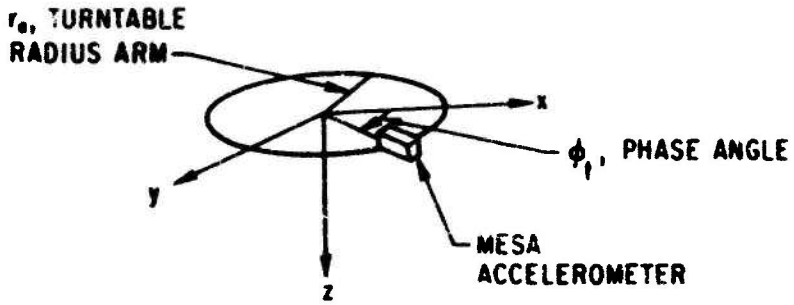

LOGACS TURNTABLE

Fig. 19. Configuration of Vehicle and LOGACS

Table 9. Configuration Data

Term	Symbol	Value	Units	Remarks
Mass	m	59.5	slug	1912 lb
Inertia	I_x	172	slug-ft^2	
	I_y	2560	slug-ft^2	
	I_z	2560	slug-ft^2	
Center of gravity	X_{cg}	0	ft	Station 351.4 in.
	Y_{cg}	0.1915	ft	2.3 in.
	Z_{cg}	0.125	ft	1.5 in.
LOGACS location	X_{ac}	-.9	ft	
	Y_{ac}	0	ft	
	Z_{ac}	1.5	ft	
Gas valve locations	X_{gv}	-.9	ft	
	Y_{gv}	0	ft	
	Z_{gv}	±2.166	ft	
Aerodynamic center	X_{cp}	See Section 2.5		
	Y_{cp}	0	ft	
	Z_{cp}	0	ft	
Reference area	S	19.6	ft^2	
Reference length	L_r	5	ft	
Gas valve force	F_i	0.5	lb	(i = 1, 2, ..., 6)
LOGACS radius arm	r_a	1/3	ft	
Turntable phase angle	ϕ_t	$-180 \leq \phi_t \leq 180$	deg	
Turntable rates	$\dot{\phi}_t$	0	rpm	Mode 3(ϕ_t = 0), Mode 4(ϕ_t = π)
		0.445	rpm	Mode 1 (2.67 deg/sec)
		0.890	rpm	Mode 2 (5.34 deg/sec)
Accelerometer scale factor	K	10^7	counts/g-sec	

2. ACCELERATION ALGORITHMS

Appendix E presents the development of the algorithm for the input axis acceleration sensed by the LOGACS accelerometer. The final result is

$$A_{si} = A_{xcg} \cos \phi_t + A_{ycg} \sin \varphi_t - r_a \left[(\dot{\phi}_t + \omega_z)^2 + (\cos \varphi_t \omega_y - \sin \phi_t \omega_x)^2 - \omega_o^2 \right]$$

$$+ X_{ag} \left[\sin \phi_t (\dot{\omega}_z + \omega_x \omega_y) - \cos \phi_t (\omega_y^2 + \omega_z^2 - \omega_o^2) \right]$$

$$+ Y_{ag} \left[\cos \phi_t (-\dot{\omega}_z + \omega_x \omega_z) - \sin \phi_t (\omega_x^2 + \omega_z^2 - \omega_o^2) \right]$$

$$+ Z_{ag} \left[\cos \phi_t (\omega_x \omega_z + \dot{\omega}_y + 3\omega_o^2 \theta) - \sin \phi_t (\dot{\omega}_x - \omega_y \omega_z + 3\omega_o^2 \varphi) \right] \qquad (17)$$

where

A_{si} = total sensed acceleration along accelerometer input axis

A_{xcg} = component of sensed acceleration along x due to external forces

A_{ycg} = component of sensed acceleration along y due to external forces

r_a = radius arm of LOGACS

$\dot{\phi}_t$ = turntable rotational rate

ϕ_t = turntable phase angle

$\omega_x, \omega_y, \omega_z$ = inertial rotational rates about x, y, and z, respectively

ω_o = instantaneous orbital rate = $(\mu/R^3)^{1/2}$

$\dot{\omega}_x, \dot{\omega}_y, \dot{\omega}_z$ = inertial rotational accelerations about x, y, and z, respectively

X_{ag}, Y_{ag}, Z_{ag} = coordinates of LOGACS with respect to Agena cg

$= (X_{ac} - X_{cg}), (Y_{ac} - Y_{cg}), (Z_{ac} - A_{cg})$

θ = Agena pitch attitude with respect to local horizontal

φ = Agena roll attitude with respect to local horizontal

Excluding the dynamics of the LOGACS accelerometer, the truncated output in units of counts each second is

$$V_s(t+1) = -K \int_t^{t+1} (A_{si} + A_b + \cdots)\, dt + R \tag{18}$$

where

K = instrument scale factor in counts/g-sec

A_{si} = sensed acceleration along instrument input axis

A_b = instrument bias

$+ \cdots$ = represents nonlinear terms, cross-axis acceleration sensitivity, etc., which are assumed zero for this analysis

R = remainder term of fractional counts from previous cycle

This incremental integration is performed and recorded each second; therefore, the number of counts recorded represents an average input g level over the 1-sec interval. Denoting this as N, it is desired to determine the acceleration due to drag from the measurement(s) N. Using Eq. (17), one can determine the drag acceleration over each 1-sec interval from (positive drag equals $-A_{xcg}$)

$$A_d = \frac{1}{\cos \phi_t}\left\{\frac{N}{K} + A_b + A_{ycg} \sin \phi_t - r_a \left[(\dot{\phi}_t + \omega_z)^2 + (\cos \phi_t \omega_y - \sin \phi_t \omega_x)^2 - \omega_o^2\right]\right\}$$

$$+ X_{ag}\left[\tan \phi_t(\dot{\omega}_z + \omega_x\omega_y) - (\omega_y^2 + \omega_z^2 - \omega_o^2)\right]$$

$$+ Y_{ag}\left[(-\dot{\omega}_z + \omega_x\omega_z) - \tan \phi_t(\omega_x^2 + \omega_z^2 - \omega_o^2)\right]$$

$$+ Z_{ag}\left[(\omega_x\omega_z + \dot{\omega}_y + 3\omega_o^2\theta) - \tan \phi_t(\dot{\omega}_x - \omega_y\omega_z + 3\omega_o^2\varphi)\right] \qquad (19)$$

where all terms on the right side of Eq. (19) are considered averaged values over the 1-sec interval. It is apparent that singularities exist in this equation at $\phi_t = \pm 90$ deg. Since only N, ϕ_t, θ, and φ are explicitly measured, it is necessary to determine the other terms implicitly. The remainder of this section derives the order of magnitude of each term and presents the approximations made to these algorithms for the purpose of data processing.

3. AGENA RIGID BODY EQUATIONS OF MOTION

It is assumed that:

a. The configuration is a rigid body (excludes propellant motions inside the tanks)

b. The principal axes are parallel to the reference axes

c. The only external forces and moments are caused by aerodynamics and control system gas valve thrusts

d. There are no internally generated forces or moments

e. The gravity gradient torques are negligible

On the basis of these assumptions, the equations can be written as follows:

a. Moments

$$I_x\dot{\omega}_x = (Z_{gv} - Z_{cg})(T_1 - T_3) + (Z_{gv} + Z_{cg})(T_4 - T_6)$$

$$+ Y_{cg}(T_2 - T_5)$$

$$I_y\dot{\omega}_y = (I_z - I_x)\omega_x\omega_z + (X_{gv} - X_{cg})(T_2 - T_5) \qquad (20)$$

$$+ F_{az}(X_{cg} - X_{cp}) - F_{ax}(Z_{cg} - Z_{cp})$$

$$I_z\dot{\omega}_z = (I_x - I_y)\omega_x\omega_y + (X_{gv} - X_{cg})(T_3 + T_4 - T_1 - T_6)$$

$$- F_{ay}(X_{cg} - X_{cp}) + F_{ax}(Y_{cg} - Y_{cp})$$

where

I_i = moments of inertia about principal axes (i = x, y, z)

$\dot{\omega}_i$ = angular accelerations about principal axes (i = x, y, z)

ω_i = angular rates about principal axes (i = x, y, z)

T_i = gas valve forces (i = 1, 2, ··· 6)

i_{gv} = coordinates of gas valve (i = X, Y, Z)

i_{cg} = coordinates of center of gravity (i = X, Y, Z)

i_{cp} = coordinates of aerodynamic center (i = X, Y, Z)

F_{ai} = aerodynamic forces along reference axes (i = x, y, z)

Note that the moment of inertia coupling term drops out of the $I_x \dot{\omega}_x$ equation of Eqs. (20) because $I_y = I_z$. The aerodynamic forces are determined from

$$F_{ax} = -C_D QS$$

$$F_{ay} = C_{N\beta} QS\beta \qquad (21)$$

$$F_{az} = -C_{N\alpha} QS\alpha$$

where

S = reference area

C_D = drag coefficient (assumed equal to axial coefficient)

C_{Ni} = normal force coefficients ($i = \alpha, \beta$)

α, β = angle of attack and side slip angle, respectively

Q = dynamic pressure = $(1/2)\rho V_a^2$ (ρ is atmospheric density and V_a is relative velocity)

b. Sensed cg Accelerations

$$A_{xcg} = \frac{F_{ax}}{m}$$

$$A_{ycg} = \frac{F_{ay} + (T_3 + T_4 - T_1 - T_6)}{m} \qquad (22)$$

$$A_{zcg} = \frac{F_{az} + (T_5 - T_2)}{m}$$

where m is the vehicle mass and the other terms are defined above.

4. AGENA CONTROL SYSTEM RESPONSE CHARACTERISTICS

This section presents a tutorial discussion of the Agena control system responses under the influence of torques, and develops the order of magnitude of the angular rates and the angular and translational accelerations induced by the control system. Reference 3 presents a more detailed description of the control system and its characteristics than is given here. The basic elements of the control system are:

a. Horizon sensor for detecting vehicle pitch and roll attitude with respect to the local horizontal

b. Pitch, yaw, and roll integrating gyros for detecting vehicle attitude displacements from the gyros' reference axes

c. Six cold gas control valves for producing control moments about the pitch, yaw, and roll axes (see Fig. 19)

d. Cold gas supply and associated pressure regulators

e. Associated electronics including a programmer

The gas valve with electronics represents a nonlinear element in the control loop in that the valve mode is either on or off. Figure 20 presents the static performance characteristic in which a given error voltage (derived from the gyro error signals) produces a given pulsewidth and pulse repetition rate. The mod factor is a product of the two curves. It is seen that for rather large input voltages the pulsewidth remains relatively constant whereas the pulse repetition rate increases rapidly with applied voltage. Preceding this circuit is a deadband circuit in which the voltage must exceed a given value before it will be detected by the control valve circuits. It should be noted that the minimum valve firing duration is 20 msec. Also, the error voltage is a composite signal derived from passing the gyro error signal through a lead circuit; therefore, the voltage contains error rate components as well. The deadband is set such that a nominal ±1 deg error at zero rate will cause a minimum firing rate of the appropriate valve.

The pitch valves (2 and 5) respond to the pitch gyro error, where a pitch-up error will cause valve 2 to fire to produce a nose-down moment. Conversely, a pitch-down error will cause valve 5 to fire to produce a nose-up

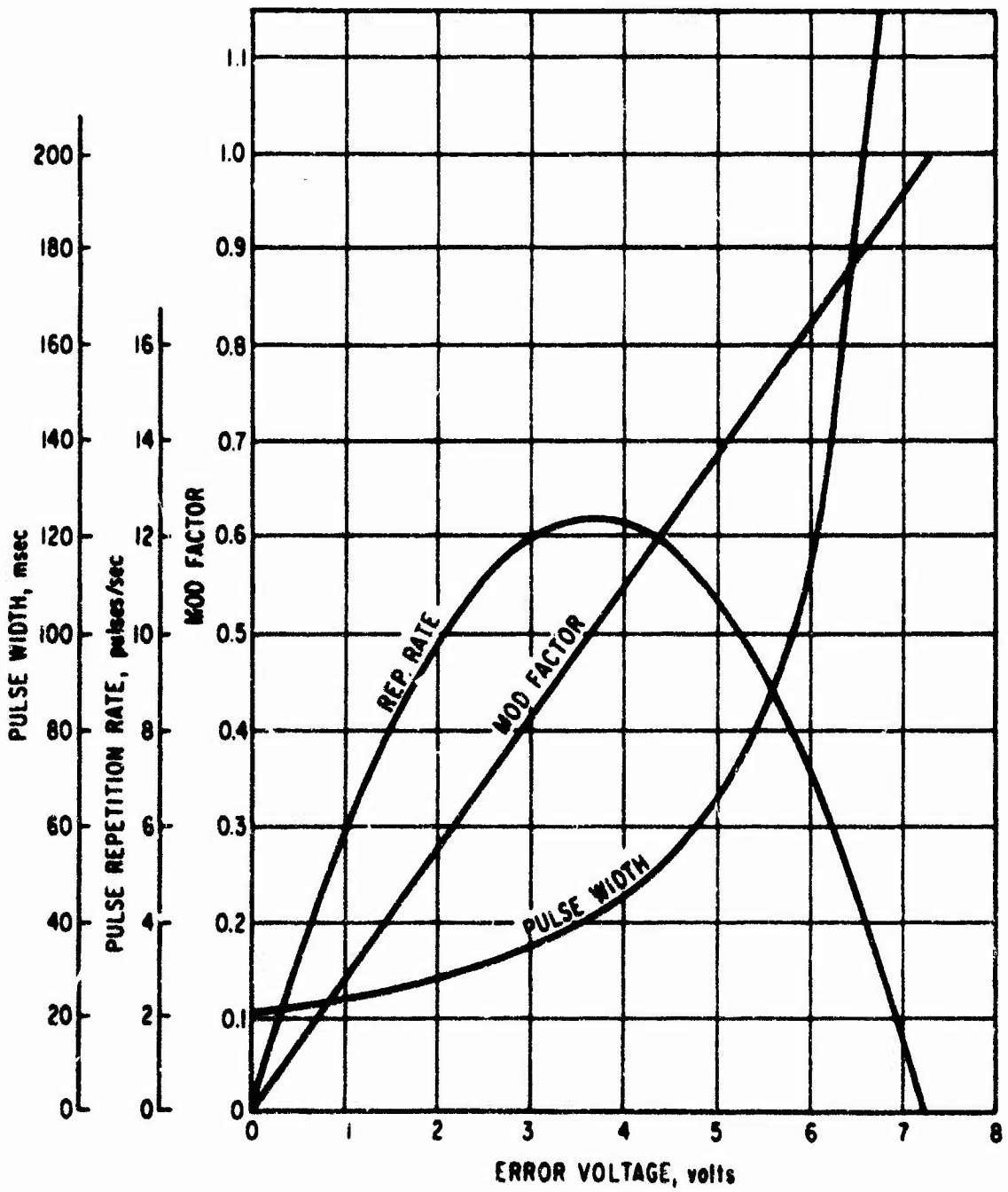

Fig. 20. Static Performance Characteristics

moment. Valves 1, 3, 4, and 6 respond to roll and yaw gyro error signals in the following manner: for a yaw right error, valves 3 and 4 will attempt to fire to produce a yaw left moment, whereas for a roll clockwise error, valves 3 and 6 will attempt to fire to produce a counterclockwise moment; similarly for a yaw left error, valves 1 and 6 will attempt to fire, whereas for a roll counterclockwise error, valves 1 and 4 will attempt to fire. That is, valves 1 and 3 respond to the sum of the roll and yaw errors whereas valves 4 and 6 respond to the difference of these errors. As a result of this summing (and differencing), the probability that two valves will fire simultaneously is very small because it occurs only when one gyro error (plus rate component) is zero when the other reaches the voltage level to cause a commanded firing. Under the most ideal conditions of no cross-axis coupling, no cg offsets, and no aerodynamic torques, the pitch moment equations can be written as

$$I_y \dot{\omega}_y = (X_{gv} - X_{cg})(T_2 - T_5)$$

An idealized time history assuming perfect electronics and ideal initial conditions would be depicted as shown in Fig. 21. During the interval of a gas valve firing, one finds

$$\dot{\omega}_y = \frac{T_i(X_{gv} - X_{cg})}{I_y} = \frac{0.5 \times 8.85}{2550} = 1.76 \times 10^{-3} \text{ rad/sec}^2 = 0.1 \text{ deg/sec}^2$$

$$\omega_y^+ = \omega_y^- = \frac{1}{2} \int_t^{t+\Delta t} \dot{\omega}_y \, dt = \frac{\omega_y}{2} \Delta t$$

For a control valve firing duration (Δt) of 20 msec, ω_y equals 0.001 deg/sec. Under these conditions there would be a gas valve firing every 2000 sec.

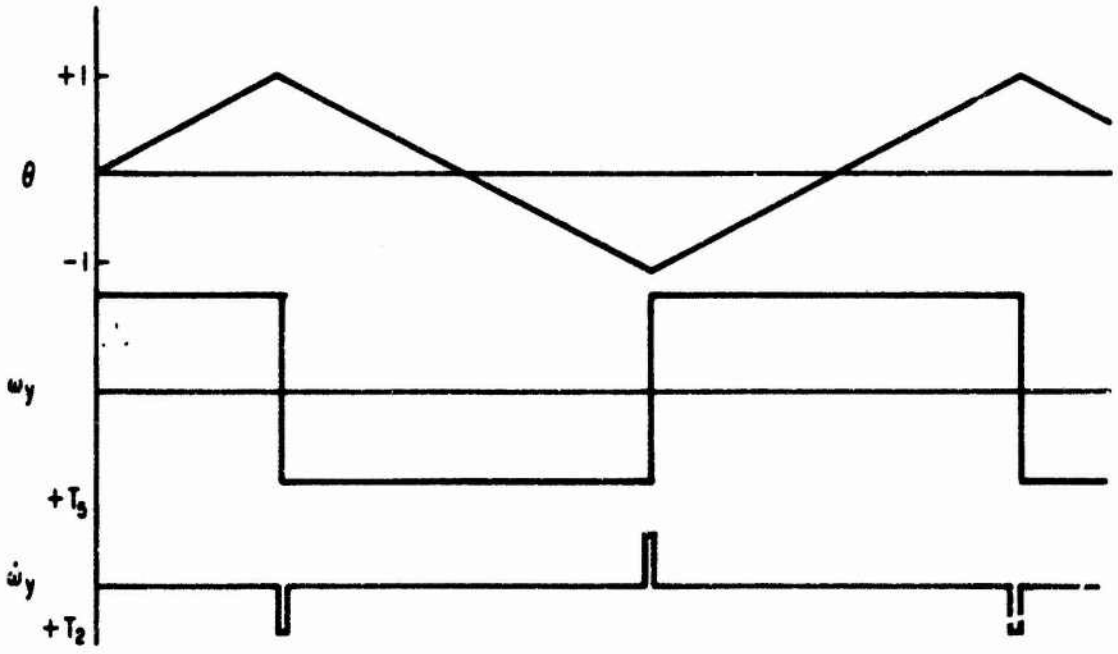

Fig. 21. Idealized Time History

When it is assumed that there is a small constant torque applied (maintaining the same characteristic of minimum pulsewidth and symmetrical rate change at the occurrence of the pulse), the time history characteristics change to those shown in Fig. 22.

For the case where the attitude just reaches the deadband, but does not cause a gas valve firing, the period between firings would be 8000 sec. Increasing the applied torque decreases the period between firings and decreases the attitude excursion. For example, a torque large enough to cause a firing once per second (holding all assumptions including $\Delta t = 0.02$) would result in an attitude excursion of 0.00025 deg.

The roll and yaw responses are coupled and cannot be treated on a single-axis basis, but the order of magnitude of the terms can be established. Since the lever arm and inertia are the same for yaw as for pitch, the rate change and acceleration due to a roll/yaw valve firing is the same for yaw as

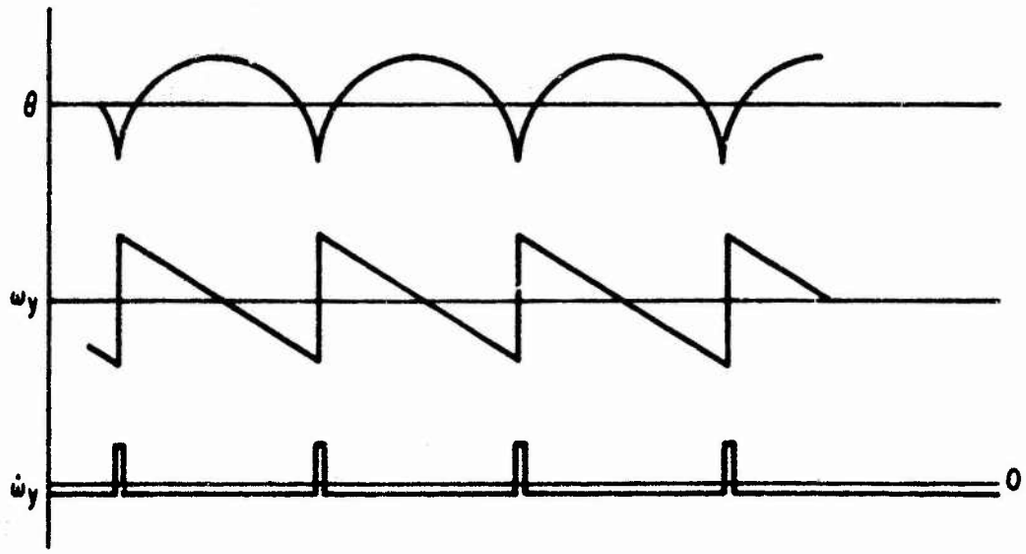

Fig. 22. Time History Assuming a Small Constant Torque

for pitch. The roll response for a roll/yaw valve firing is larger due to the small roll inertia. The minimum roll acceleration is

$$\dot{\omega}_x = \frac{0.5 \times 2.166}{172} = 6.3 \times 10^{-3} \text{ rad/sec}^2 = 0.36 \text{ deg/sec}^2$$

and the corresponding roll rate is

$$\omega_x^+ = \omega_x^- = \frac{1}{2}\dot{\omega}_x \Delta t = 0.0036 \text{ deg/sec}$$

The conditions and assumptions applied in the above analysis are not generally met under flight conditions; however, the results serve to illustrate the response characteristics and to establish approximate values for angular rates and accelerations of the vehicle. The telemetric data were used to establish the bounds on the angular rate terms, and to verify the magnitude of angular accelerations induced by control gas valve firings.

Two sources of telemetric data are available: that which was directly associated with the LOGACS experiment and the normal Agena telemetric data. The LOGACS data, which were tape recorded and played back during real-time acquisitions, include gyro error data (pitch, yaw, and roll) and control system gas valve firing data. The gyro error data are recorded at a 2-sec sample interval. For each of the control valves the data recorded indicated whether one (or more) firing(s) of the valve had occurred in a 1-sec interval. The number of firings and the duration of each over the 1-sec interval are not recorded with the LOGACS data. The Agena data, available only during real-time acquisitions, include a continuous gas valve time history so that the on-off state of each valve can be determined. These data can be used to establish the number of firings and the time duration of each for the periods of real-time acquisition.

A rigorous analysis of the control system data has not been made; however, from a cursory examination, various response characteristics have been established. LMSC analyzed the real-time Agena control valve data (Ref. 4). In this analysis, data from Revs. 20, 25, 38, 54, and 66 were used. It was found that each valve firing observed was of a minimum duration (20 msec). The data available on Rev. 66 were also analyzed for pulse repetition rate. Initiation of the real-time acquisition on this pass occurred approximately 200 sec after perigee. Thus, the control torques required to compensate for the aerodynamic moments are typical of the maximum required over the complete mission. The analysis of this data set showed the average period between firings for each valve (1, 2, and 6 were the only valves firing) was greater than 1 sec. There was only one occurrence in this data set where the period between firings was less than 1 sec. Based on this analysis, it is assumed for this report that all indicated valve firings by the LOGACS data set represent a single firing of 20 msec duration.

The LOGACS gyro error data were analyzed in regions where the control system was not operating on its deadband (see Appendix G, Fig. G-2, which includes plots of the attitude error time histories). At selected apogee regions (minimum disturbing torques), the attitude error rate change when a

gas valve fired was determined. Within the accuracy of the telemetric data and method, the rate changes agreed with that predicted by the idealized analysis, confirming the magnitudes of the angular accelerations.

The rate deduced from analysis of the attitude error data reflects the difference between the vehicle rate (ω_i, i = x, v, z) and the gyro reference rate. This rate is defined as a limit cycle rate, and the gyro error data were examined to determine the maximum limit cycle rate. Relatively large limit cycle rates occurred when the vehicle entered the perigee region. Here the build-up of aerodynamic torque drives the attitude toward the control deadband. Until the deadband is reached, there is no compensating control torque. The maximum rate achieved depends on the initial conditions when entering this region. Also, for the later revs. (Revs. 47 and up), relatively large rates are observed in the perigee regions when anomalies occur in the yaw/roll responses (see Section D). In either of the above mentioned regions, the limit cycle rates did not exceed 0.01 deg/sec and in general were much smaller.

In the perigee regions where the aerodynamic torques are sufficient to cause the control system to operate continuously at the pitch and yaw deadbands, vehicle rates cannot be observed in the telemetric data. However, from the character of the pulse repetition rate observed in the LMSC analysis, it is concluded that the system is operating as described for the torqued ideal system; i.e., the maximum pitch and yaw limit cycle rates are 0.001 deg/sec and the maximum roll rate is 0.004 deg/sec.

The gyro references are controlled by the horizon sensor in a gyrocompassing mode (see Ref. 3) so that gyro drifts are compensated by signals from the horizon sensor and/or yaw attitude misalignment with respect to the orbital plane. The pitch gyro is programmed at a constant rate to compensate for the orbital rate. Differences between the instantaneous orbital rate and the programmed rate are also compensated by the horizon sensor. Thus, the limit cycle rates deduced from telemetry for roll and yaw are, to first

order, the vehicle rates ω_x, ω_z. Also, to first order, the pitch vehicle rate is the sum of the orbital rate and the limit cycle rate, i.e.

$$\omega_y = \omega_o + \dot{\theta}$$

The translational acceleration during a gas valve firing is

$$A_{icg} = \frac{T_j}{m} = \frac{0.5}{59.5} = 0.0835 \text{ ft/sec}^2$$

Summarizing, the roll and yaw vehicle rates do not exceed 0.01 deg/sec and the vehicle pitch rate is bounded within the limits of orbital rate plus or minus 0.01 deg/sec. The accelerations experienced during a gas valve firing are summarized in Table 10.

Table 10. Accelerations During Gas Valve Firing

	1	2	3	4	5	6
A_{xcg}, ft/sec^2	0	0	0	0	0	0
A_{ycg}, ft/sec^2	-0.835×10^{-2}	0	0.835×10^{-2}	0.835×10^{-2}	0	-0.835×10^{-2}
A_{zcg}, ft/sec^2	0	-0.835×10^{-2}	0	0	0.835×10^{-2}	0
ω_x, rad/sec^2	5.7×10^{-3}	0	-5.7×10^{-3}	5.7×10^{-3}	0	-5.7×10^{-3}
ω_y, rad/sec^2	0	1.76×10^{-3}	0	0	1.76×10^{-3}	0
ω_z, rad/sec^2	1.76×10^{-3}	0	-1.76×10^{-3}	-1.76×10^{-3}	0	1.76×10^{-3}

5. AERODYNAMIC FORCES AND MOMENTS

Reference 5 presents aerodynamic data for the Agena configuration flown on this mission. In preparing the data, a flat-plate front end configuration was assumed. The data are presented in terms of lift, drag, and moment coefficients. For this analysis it is more convenient to deal with body axis coefficients (normal and axial force) and a center of pressure distance for determining moments. The equations used for this transformation are:

$$C_N = C_L \cos \alpha + C_D \sin \alpha \qquad \text{(normal force coefficient)}$$

$$C_A = C_D \cos \alpha - C_L \sin \alpha = C_D \qquad \text{(axial force coefficient)}$$

$$L_{cp} = (-C_m/C_N)L_r \qquad \text{(center-of-pressure distance from Station 247)}$$

$$C_{N\alpha} = C_N(\alpha)/\alpha \qquad \text{(normal force coefficient slope)}$$

The data of Ref. 5 for an exospheric temperature of 1500°K were used to prepare the set of aerodynamic terms shown in Table 11.

Table 11. Aerodynamic Coefficients

h, nmi	$C_A = C_D$ ($\alpha = 0$)	$C_{N\alpha}$ (per deg)	L_{cp}, ft	X_{cp}, ft
60	2.3	0.0275	- 6.7	2.0
80	2.56	0.048	- 7.6	1.1
100	2.68	0.052	- 9.4	-0.7
150	2.83	0.056	-11.5	-2.8
200	2.95	0.059	-11.5	-2.8

Above 95 nmi, the x axis location of the aerodynamic center of pressure is predicted to be behind the cg, providing aerodynamic stability. The flat-plate front end configuration places the aerodynamic center for axial force

on the x axis. Lateral cg offset provides a lever arm for the axial force, resulting in a moment. The combination of off-axis cg and stable aerodynamic normal forces results in a shift of the trim angle of attack from zero to

$$\alpha = \frac{C_A Z_{cg}}{C_{N\alpha} X_{cp}}$$

provided X_{cp} is negative. For the aerodynamic and cg data given, the trim angle of attack exceeds the control system deadband for all altitudes so that a control torque is necessary to compensate the total induced aerodynamic moment.

Using the aerodynamic coefficients of Table 11 and density data from the 1962 standard atmosphere tables, we calculated the aerodynamic forces and accelerations predicted as a function of altitude; they are presented in Table 12. The density data and the drag acceleration in units of accelerometer counts are plotted in Fig. 23.

6. ORDER OF MAGNITUDE ESTIMATES

Based on the data presented in Sections 4 and 5, an order of magnitude estimate can be made for the individual terms of the sensed acceleration given in Eq. (17). Before a term-by-term estimate is made, certain terms are eliminated from Eq. (17) based on their order of magnitude as follows:

a. Limit cycle rate terms: Using the maximum value of 0.01 deg/sec (or 2×10^{-4} rad/sec), products of limit cycle rates ($\omega_i\omega_j$, $\omega_i\dot{\theta}$; i, j = x, z) are less than 4×10^{-8} rad/sec^2. With lever arms less than 10 ft, the resulting accelerations are less than 4×10^{-7} ft/sec^2 (1.25×10^{-8} g = 0.125 accelerometer counts). Thus, products of limit cycle rates are eliminated from further consideration.

b. Orbital rate terms: Using a maximum value for the orbital rate term (ω_o) of 4.35 deg/min (1.3×10^{-3} rad/sec), products of orbital rate and limit cycle rates are less than 2.5×10^{-7} rad/sec^2. With lever arms less than 10 ft, the resulting accelerations are less than 2.5×10^{-6} ft/sec^2 (8×10^{-8} g = 0.8 accelerometer counts). The square of the orbital rate term

Table 12. Aerodynamic Forces and Accelerations

h, nmi	ρ, slug/ft^3	x axis					y axis/deg β			
		Q, lb/ft^2	lb	ft/sec^2	g	LOGACS Counts Φ_t = 0	lb	ft/sec^2	g	LOGACS Counts Φ_t = 90 deg
65	4.0×10^{-11}	1.31×10^{-2}	6.2×10^{-1}	1.04×10^{-2}	3.23×10^{-4}	3230	9.0×10^{-3}	1.51×10^{-4}	4.7×10^{-6}	47
80	4.0×10^{-12}	1.31×10^{-3}	6.54×10^{-2}	1.1×10^{-3}	3.42×10^{-5}	342	1.24×10^{-3}	2.08×10^{-5}	6.45×10^{-7}	6.5
100	1.0×10^{-12}	3.28×10^{-4}	1.72×10^{-2}	2.9×10^{-4}	9.00×10^{-6}	90	3.34×10^{-4}	5.61×10^{-6}	1.74×10^{-7}	1.7
150	1.1×10^{-13}	3.61×10^{-5}	2.00×10^{-3}	3.36×10^{-5}	1.04×10^{-6}	10	3.95×10^{-5}	6.63×10^{-7}	2.06×10^{-7}	---
200	2.0×10^{-14}	6.55×10^{-6}	3.75×10^{-4}	6.35×10^{-6}	1.97×10^{-7}	2	7.55×10^{-6}	1.27×10^{-7}	3.95×10^{-9}	---

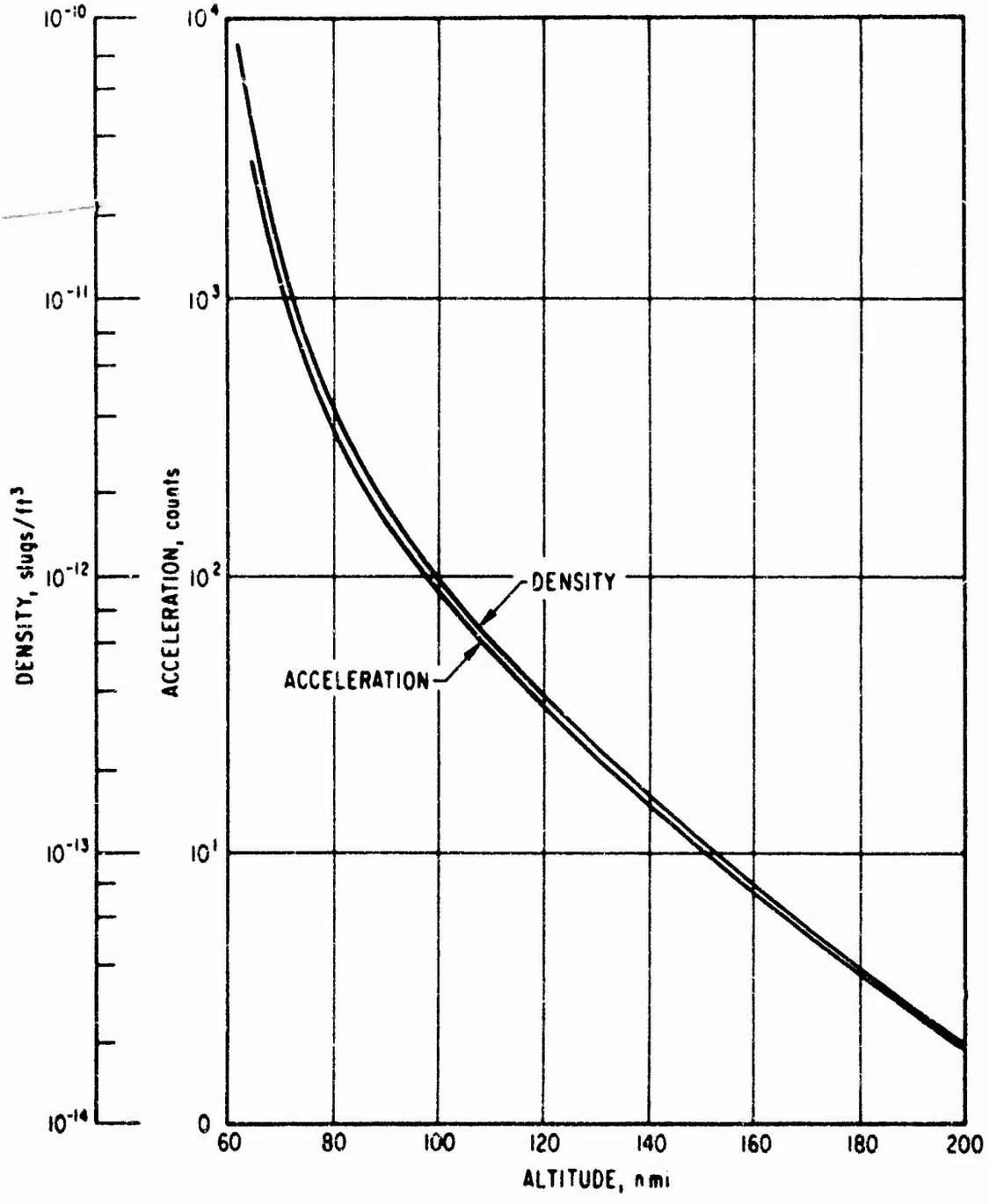

Fig. 23. Density and Drag Accelerations

times the turntable radius (r_a), or the y-axis lever arm (Y_{ag}), is less than 6×10^{-7} ft/sec^2 (2×10^{-8} g = 0.2 accelerometer counts). The term $(\omega_y^2 - \omega_o^2)$ reduces to $2\omega_o\dot{\theta} + \dot{\theta}^2$), and by (a) above reduces further to $2\omega_o\dot{\theta}$. This term has a maximum magnitude of ±1.6 accelerometer counts. None of the above terms is considered large enough for further consideration.

c. Coupling of yaw rate and turntable rate: The coupling term ($2r_a\dot{\phi}_t\omega_z$) can result in an acceleration of 9.2×10^{-6} ft/sec^2 (3×10^{-7} g = 3 accelerometer counts). Although this magnitude is detectable, it occurs only for mode 2 of the calibration cycle when the yaw rate is maximum. Both the probability of occurrence and the magnitude are small so that it too is eliminated from further consideration.

d. Gravity gradient terms: The terms associated with attitude ($3Z_{ag}\omega_o^2\theta$ and $3Z_{ag}\omega_o^2\phi$) are of order $\pm 1.69 \times 10^{-7}$ ft/sec^2 (0.05 accelerometer counts) and are eliminated from further consideration.

As a result of the above considerations, all vehicle rate terms in Eq. (17) can be eliminated and the sensed acceleration equation reduces to

$$A_{si} = -r_a\dot{\phi}_t^2 + \cos\phi_t(A_{xcg} - Y_{ag}\dot{\omega}_z + Z_{ag}\dot{\omega}_y)$$

$$+ \sin\phi_t(A_{ycg} + X_{ag}\dot{\omega}_z - Z_{ag}\dot{\omega}_x) \qquad (23)$$

Based on an accelerometer scale factor of 10^7 counts/g-sec, and with contributions of aerodynamic moments neglected (see Section 7), the order of magnitude estimates for the terms in Eq. (23) are presented in Table 13.

7. TIME AVERAGE RESPONSES

As discussed in Section 4, the control system responds to limit the amplitude of attitude excursion. Under the relatively high aerodynamic torque experienced below 130 nmi altitude, the attitude error is nearly constant (well within 0.05 deg of its deadband limit), and the limit cycle rates (integral of $\dot{\omega}$) are bounded at approximately their threshold values. Thus, the time

Table 13. Order of Magnitude Estimates

Term	Source	Magnitude, ft/sec^2	Accelerometer Counts			
			Φ_t = 0	Φ_t = 90 deg	Φ_t = 180 deg	Φ_t = 270 deg
$A_{xg} \sin \Phi_t$	Aerodynamic drag (76.2 nmi)	1.97×10^{-3} / 6.45×10^{-6}	+10 / 2	0	-10 / -2	0
$A_{yg} \sin \Phi_t$	Yaw-left aerodynamic sideforce (76.2 nmi) deg	4.7×10^{-5} / 1.2×10^{-7}	0	12 / 0	0	12 / 0
	Yaw gas valve firing (1 or 4, 20 msec)	1.67×10^{-4}	0	54	0	54
$r_t \dot{\Phi}_t^2$	Table entry (0.44 and 3.88 rpm)	7.15×10^{-4} / 2.86×10^{-3}	←		225 / 893	→
$X_{xg} \dot{r}_t \sin \Phi_t$	Yaw gas valve firing (1 or 4, 20 msec)	2.28×10^{-4}	0	88	0	-88
$Y_{xg} \dot{r}_t \cos \Phi_t$	Yaw gas valve firing (1 or 4, 20 msec)	6.7×10^{-6}	2	0	-2	0
$A_{zg} \sin \Phi_t$	Pitch gas valve firing (2, 20 msec)	9.55×10^{-5}	24	0	-24	0
$A_{xg} \sin \Phi_t$	Roll gas valve firing (3 or 6, 20 msec)	2.46×10^{-4} / 2.46×10^{-4}	0	76 / 76	0	-76 / -76

NOTE: When gas valve 1 fires, the total contribution to counts for a 20-msec duration and Φ_t = 90 deg is the sum of 54 + 88 + 76 = 218.

When gas valve 4 fires, the total contribution to counts for a 20 msec duration and Φ_t = 90 deg is the sum of 54 + 88 - 76 = 62.

Gas valve 3 has same magnitude and opposite polarity of 1.

Gas valve 4 has same magnitude and opposite polarity of 6.

Gas valve 5 has same magnitude and opposite polarity of 2.

average of $\dot{\bar{\omega}}$ has a mean (expected) value of zero. The integral of $\dot{\bar{r}} \times \dot{\bar{\omega}}$ terms (components of which are sensed by the LOGACS accelerometer) would also have zero mean. In essence, the mean of the gas control torque is equal in magnitude and opposite in polarity to the mean of the aerodynamic torque.

If the pneumatic control system was a linear system (proportional instead of pulsed valves), the $\dot{\bar{r}} \times \dot{\bar{\omega}}$ terms would be negligible. With the pulse system, however, the accelerometer output at each second will be related to the difference of the torque sources over the interval. Over a given interval the probability is negligible that the integrated magnitudes of each are exactly equal; therefore, there is a variance associated with each accelerometer output. This variance is also associated with the magnitude of the aerodynamic torque as well as the orientation phase angle during the rotating calibration modes. The accelerometer's dynamic response to pulsed accelerations also contributes to the variance of the accelerometer's output. Consequently, a given numerical value cannot be established for the variance; however, Table 13 does give the order of magnitude of a maximum error value. Filtering techniques are employed to minimize the variance associated with the processed output data.

B. LOGACS DATA PROCESSING METHODS

The telemetered functions which were processed and their results included in this report are:

a. Accelerometer counts (N)
b. Control valve firing occurrences (T_i)
c. Pitch, yaw, and roll gyro error (θ_e, ψ_e, ϕ_e)
d. Pitch and roll horizon sensor (θ, ϕ)

The data rate for the first two was once per second while the latter two had a data rate of once every other second. The time base used for processing and presenting the data is the LOGACS clock data designated

TRG. For purposes of this report the relationship between system time (SYST) and TRG is

$$SYST = 67,507 - m(86,400) + TRG$$

where

$m = 0, 1, 2, 3, 4$ (m = 0 on 22 May)

A complete list of the telemetered functions and also the accuracy of the TRG clock is given in Section I.

There were a number of obvious errors in the accelerometer data displayed as a 512 or 4096 count deviation from the mean of the surrounding data points due to transmission, receiving, or decoding problems. Most probably there are an equal number of 1, 8, and 64 (and multiples of) count errors which are not recognizable. The larger errors were edited from the source data tape. The frequency of occurrence of this type error is such that the smaller errors would not contribute significantly to the final results.

Figure F-1 of Appendix F contains an example of the raw data plots (excluding horizon sensor data) covering the data span from 280,000 to 286,300 TRG sec. This time span includes the apogee regions of Revs. 52 and 53 and the perigee of Rev. 53. The control valve data are displayed by an X in the appropriate row for each valve when the data indicated the occurrence of a valve firing. The accelerometer and gyro functions are plotted at their respective amplitudes and data rates. The initiation of each accelerometer calibration cycle mode is indicated on the plot. Gaps in the data reflect missing data points either in data transmission, source processing, or from the editing procedure described above.

There were a number of approaches investigated for processing the accelerometer data to meet the objectives of accelerometer calibration and determination of drag acceleration. The methods adopted for this report were in the interest of expediency with some loss in accuracy. Three separate methods were used which are described below.

1. ACCELEROMETER CALIBRATIONS, APOGEE

The calibration of the accelerometer's scale factor and bias was performed using modes 1 and 2 data from apogee regions only. This was done because a minimum of external disturbing accelerations occur in this region. The data set used for these calibrations were edited for observed responses due to gas valve firings and any accelerometer count anomalies that exceeded 50 counts from the surrounding data mean. The editing of data due to gas valve firings allowed the elimination of $\dot{\omega}_i$ from Eq. (23) as well as the contribution of gas valve firings to A_{ycg}. Also, the aerodynamic normal forces are negligible in the apogee region so that under these conditions the sensed acceleration equation reduces to

$$A_{si} = -r_a \dot{\phi}_t^2 + A_{xcg} \cos \phi_t \tag{24}$$

The corresponding accelerometer output each second is

$$N_i = K \int_t^{t+1} \left(r_a \dot{\phi}_t^2 + a_d \cos \phi_t \right) dt + B \tag{25}$$

With the initiation of the first calibration cycle known, ϕ_t and $\dot{\phi}_t$ are deterministic functions of time. The value for the turntable radius arm r_a is that determined from ground calibrations. Therefore, the unknowns in the above equation are the scale factor K, the accelerometer bias B, and the drag acceleration A_d. To determine these quantities, we assumed that the drag acceleration behaved as a quadratic in time over the mode 1 and 2 calibration cycle interval (1024 sec). Using this approximation for drag results in a set of overdetermined linear equations for the unknown parameters. These equations were mechanized in a computer program and the solutions for the unknowns were obtained using a least squares formulation.

Having determined the scale factor and bias, one can compute the measured drag acceleration from

$$A_d = \frac{1}{\cos \phi_t} \left(\frac{N - B}{K} - r_a \dot{\phi}_t^2 \right) \tag{26}$$

Since this equation has a singularity at $\phi_t = \pm 90$ deg, calculations using Eq. (26) were not performed for phase angles $\phi_t = \pm |90 \pm 12 \text{ deg}|$. Figure F-2 of Appendix F presents the results from the Rev. 52 apogee calibration. Both the quadratic-derived acceleration profile and the one calculated using Eq. (26) are plotted. In the interval of ±12 deg from the singularity, A_d is plotted as a zero value. This plot demonstrates the residual noise on the raw data. It should be noted that in this presentation form, the noise is amplified by the factor $1/\cos \phi_t$.

A total of 59 data sets were processed using the procedure described above. The scale factor and bias values determined from these calibrations are presented in Section I. The acceleration profiles derived from the polynomial are presented in Section C.

2. ACCELEROMETER ROTATING MODES, PERIGEE

In the perigee regions, at least one control valve was firing each second; therefore, the transients induced by the valve firings cannot be edited without deleting the complete data set. As discussed in Section 7, the angular accelerations induced by aerodynamics and control valve firings average to zero in the perigee region. Deleting the angular acceleration terms ($\dot{\omega}_i$) from Eq. (23) results in the following sensed acceleration equation

$$A_{si} = -r_a \dot{\phi}_t^2 + A_{xcg} \cos \phi_t + A_{ycg} \sin \phi_t \tag{27}$$

The corresponding accelerometer output each second is

$$N_i = K \int_t^{t+\Delta t} \left(r_a \dot{\phi}_t^2 + A_d \cos \phi_t - A_{ycg} \sin \phi_t \right) dt + B \tag{28}$$

Since estimates of K and B are known from the apogee calibration, the unknowns in Eq. (28) are the drag and normal acceleration components. Various approaches can be used to determine these by appropriate modeling of the acceleration components and least squares fitting of the data.

Since the primary objective was the determination of the drag acceleration component, it was decided to solve Eq. (28) for the drag component assuming the normal acceleration component was zero. With this assumption, the drag acceleration component becomes Eq. (26) with an error term of $A_{ycg} \tan \phi_t$. The error term is zero or negligibly small in the immediate region of $\phi_t = 0$ or 180 deg. All the raw data were processed using Eq. (26) and plotted. For the mode 1 and 2 data, an inverted triangular symbol was placed on the plot when the phase angle was 0 or 180 deg. A typical plot is shown in Fig. F-3 of Appendix F which covers the same time interval as the raw data set of Fig. F-1. The data are corrected for bias, and the amplitude is normalized in units of accelerometer counts using a normalizing scale factor of 10^7 counts/g-sec. These plots were then used to hand-reduce the perigee rotating mode data. The eyeball average around the indicated phase angles of 0 or 180 deg was recorded and the results of this processing are presented in Section C. These plots were also useful for processing the fixed mode (3 and 4) data, which is described in Section 3.

For the data set presented in Fig. F-3, the mode 1 and 2 results appear well behaved ($282,240 < TRG < 283,270$ sec). This is due to a response anomaly experienced during this time interval in which the normal acceleration component (A_{ycg}) was near zero (see Section D). Figure F-4 of Appendix F presents a more typical time history plot of the perigee mode 1 and 2 corrected data. The influence of the normal acceleration component is immediately apparent as well as the difficulty in extracting the drag acceleration component.

3. FIXED MODE DATA PROCESSING

For the fixed orientation modes, Eq. (26) also holds where $\cos \phi_t = \pm 1$ and $\dot{\phi}_t = 0$. A linear least squares filter was used to process

these data sets. The filter time interval was chosen as 20 sec in the regions where the drag acceleration exceeded 60 accelerometer counts, and 60 sec when it was less than 60 counts. The data plots of corrected acceleration were used to set up the processing intervals and to edit data points or intervals which exhibited questionable data.

One notable data time interval when the accelerometer readings did not indicate the acceleration level was the interval immediately following the mode transitions from rotating to fixed orientation (Modes 2 to 3 and 3 to 4) in the apogee regions. The time required to traverse the instrument dead zone for a change in polarity of the total force on the proof mass (acceleration plus bias) is inversely proportional to the square root of the force level. Knowing the bias term, we could calculate the acceleration from the time interval. For this report, these intervals were edited from the data processing.

The results from the fixed mode processing are also presented in Section C.

4. CONTROL SYSTEM FUNCTIONS

The control functions of gyro error data (pitch, yaw, and roll) and horizon sensor data (pitch and roll) were processed using a linear least squares filter and a 30-sec processing interval. No attempt was made to edit extraneous data points. The differences between the filtered pitch gyro and pitch horizon sensor data, and the corresponding roll differences, were also determined and plotted.

The control valve firing data were processed making the assumption that each indicated valve firing was representative of a single firing for a minimum 20-msec duration (see Section 4). The accumulated number of firings over a 100-sec time interval was determined for each valve (N_i). Also, the data duty cycle, i.e., the number of recorded data times (M) in the 100-sec interval, was determined. Using the predicted values for the gas valve thrust(s) level and the vehicle mass, we determined the average

accelerations due to control firings along the vehicle y and z axes in units of accelerometer counts as follows

$$A_{ycg} = K_c \left[\frac{N_3 + N_4 - (N_1 + N_6)}{M}\right]$$

$$A_{zcg} = K_c\left(\frac{N_5 - N_2}{M}\right) \qquad (29)$$

where

$$K_c = K\left(\frac{T\Delta t}{mg}\right) = 10^7\left(\frac{0.5 \quad 0.02}{1912}\right) = 52.3$$

The time associated with each processed interval was computed as the time average for the data set, i.e.,

$$TRG_a = \frac{\Sigma TRG_i}{M}$$

Since the processed valve firing counts N_i cannot exceed M, the above relationships have a saturation level of ±52.3 for A_{zcg} and ±104.6 for A_{ycg}.

The average roll control moment was calculated based on the predicted vehicle cg data and the assumed value for control valve thrust(s) as follows

$$M_r = \frac{T\Delta t}{M}\left[(Z_{gv} - Z_{cg})(N_1 - N_3) + Z_{gv} + Z_{cg})(N_4 - N_6)\right.$$

$$\left. + (Y_{cg})(N_2 - N_5)\right]$$

$$= \frac{0.01}{M}\left[2.041\,(N_1 - N_3) + 2.291\,(N_4 - N_6) + 0.1915\,(N_2 - N_5)\right] \qquad (30)$$

A bias in the reduced data would indicate an error in the assumed cg data. Systematic trends in the perigee region would be indicative of aerodynamic roll moments.

The results of the control system data processing are presented in Section C.

C. DATA PROCESSING RESULTS

The drag acceleration profile reduced from the data is plotted in Fig. G-1 of Appendix G. The acceleration is normalized into units of counts where one count represents 10^{-7} g. A different symbol is used dependent on the processing method (see Section B) as follows:

Method	Plot Symbol
Perigee rotating Modes 1 & 2	Δ
Fixed Modes 3 & 4	+
Apogee rotating Modes 1 & 2	∇

Included in this plot are data from the best-fit ephemeris (Ref. 2) of latitude, longitude, and altitude, and the drag acceleration determined from the model atmosphere used.

There are some redundant regions of processed data where the hand-reduction method was used to read data from the fixed orientation modes and from the apogee calibration modes. The gaps in the data reflect data voids. The discontinuities of ephemeris data reflect the differences between the independent vector solutions (see Ref. 2).

The data associated with the control system are plotted in Fig. G-2 of Appendix G. The drag acceleration is also plotted so that the characteristics of response anomalies can be observed more easily. Plotted are the data duty cycle, gyro errors (pitch, yaw, and roll), differences between gyro error and horizon sensor (pitch and roll), roll moment, negative z and y axis acceleration due to control valve firings, and the drag acceleration profile.

With respect to the results obtained for the normal acceleration components, nowhere in the processed data set did the results produce a saturated value for these components. This result lends credence to the premise stated in Section 4 that the minimum average control valve firing period was greater than 1 sec.

The accuracy of the derived normal accelerations degrades with reduced data duty cycle. For example, if the duty cycle were 1 percent [M = 1 in Eq. (29)] for a 100-sec processing interval, then the indicated occurrence (or nonoccurrence) of a firing would produce a saturated (or null) result. For this example, the probability that the result is correct (assuming no other contributing factors) is 0.01, since nothing is known about the control valve firing state for the other 99 sec. For duty cycles between 1 and 100 percent, the probability that the reduced data represent an accurate estimate is also dependent on the duty cycle data sequence. The associated probabilities with a given duty cycle have not been calculated here, but this accuracy degradation is pointed out so that caution is exercised about interpretations placed on the reduced normal acceleration data for regions of low data duty cycle. To a lesser degree, low duty cycles also affect the results for the accelerometer data, particularly if the cause of the low duty cycle was a low telemetering signal strength.

The accumulated number of valve firings for the data set processed is

$$N_1 = 18,684$$

$$N_2 = 21,648$$

$$N_3 = 620$$

$$N_4 = 145$$

$$N_5 = 79$$

$$N_6 = 16,469$$

$$N_T = 57,645$$

The accumulated data duty cycle is 63.666 percent. Assuming the characteristics of valve firings were the same for the time intervals not recorded, the estimated total number of firings for the mission from injection is 90,500. Assuming a specific impulse of 50 sec for the gas mixture used, the control gas weight expended was

$$W = N_T \frac{T\Delta t}{I_{sp}} = 18 \text{ lb}$$

D. RESPONSE ANOMALIES

The data processing performed for this report was intended to establish gross trends from which regions of particular interest could be isolated for detailed analysis. One region that exhibits a pronounced anomaly, observed as a large reduction in drag from that expected on Rev. 47 and following, is when the vehicle is approaching perigee. This phenomenon is most clearly displayed in the perigee data of Rev. 53 [see Fig. G-1(c)]. The raw data for this pass are included in Fig. F-1 and the corrected accelerometer data are presented in Fig. F-3.

Correlated with the reduction in drag acceleration is a change in polarity of yaw control force (see Fig. G-2), and consequently a corresponding polarity change of yaw control moment. From this response characteristic, and the assumption that it is externally caused, it must be concluded that during this interval the yaw aerodynamic moment had changed polarity. The equation for yaw aerodynamic moment is [see Section 3, Eq. (20)]

$$M_{az} = -F_{ay}(X_{cg} - X_{cp}) + F_{ax}(Y_{cg} - Y_{cp}) \tag{31}$$

where

$$F_{ay} = C_{N\beta} Q S \beta$$

$$F_{ax} = C_D Q S$$

$$Q = 1/2 \rho V_a^2$$

Since the second term in the moment equation did not change sign, the change in polarity must be attributed to the aerodynamic side force term (F_{ay}). This in turn leads to the conclusion that there occurred a large change in the yaw angle of attack (β) caused by a large horizontal wind component. A similar phenomenon of lesser degree is observed in the pitch axis immediately following perigee of Rev. 53. By the same analogies, it is conjectured that a vertical component of wind was encountered. Accepting the existance of large wind components, the effect of winds on the dynamic pressure term (Q) must also be investigated to fully evaluate the drag acceleration reduction and the inferred atmospheric density.

Before the anomalous regions can be analyzed comprehensively, a more precise data reduction procedure will be required in which the total lateral acceleration is determined from the calibration rotating mode data. Accompanying this is the requirement for a more precise determination of aerodynamic coefficients in which the open front end configuration is used as the model instead of the assumption of a flat plate. Also, calculations for larger angles of attack than considered for the data of Ref. 5 will be required. With this information and assuming aerodynamic symmetry in pitch and yaw, the magnitude of Q and the vertical and horizontal components of V_a can be determined (at least in principle). The remaining unknowns then relate to density (ρ) and the in-track component of V_a. Unfortunately, there was no vehicleborne instrumentation which could be used to determine either; however, a bounded functional relationship is established. With reduced time histories of the functional relationship in conjunction with analysis of atmospheric dynamics, the atmospheric properties sought can be determined.

Another response anomaly observed in the data is associated with the reduced difference between the roll gyro and roll horizon sensor data (see Fig. G-2). A cursory examination leads to the conclusion that a scale factor of approximately 20 percent exists, either in the control system or the telemetry of the respective functions. To isolate the source would require a dynamic analysis of the gyrocompassing loop under the influence of the

observed response. The utility of this function is to determine yaw gyro drift and its effect on the yaw reference of the control system (see Ref. 3 for a description and analysis of the gyrocompass loop and sources of yaw reference error). The anomaly is not of sufficient magnitude to cause great concern, and the function magnitude implies the yaw gyro drift was well within its tolerance bounds.

REFERENCES

1. Summary Report - Development of a Miniature *Electrostatic* Accelerometer (MESA) for Low-G Applications, NASA CR-54137, Bell Aerosystems Company, Buffalo, New York.

2. M. Nakamura, Postflight Ephemeris for Vehicle 4838, TOR-0158(3110-01)-15, The Aerospace Corporation, El Segundo, California (15 February 1968).

3. Classified reference.

4. T. Davis, private communication, Lockheed Missiles and Space Company, Sunnyvale, California.

5. J. H. Kainer, Estimated Variation of Aerodynamic Coefficients with Altitude for an Agena Configuration, The Aerospace Corporation, El Segundo, California (January 1968), Report No. TOR-0158(3110-01)-14.

6. P. G. Blandin, Computer Programs for LOGACS Data Reduction, TOR-0158(3110-01)-28, The Aerospace Corporation, El Segundo, California, July 1, 1969.

BIBLIOGRAPHY

Bruce, R. W., Upper Atmosphere Density Determined from a Low-G Accelerometer on Satellite 1967 50B, TOR-0158(3110-01)-16, The Aerospace Corporation, El Segundo, California (15 February 1968).

Chiu, Y. T., Thermospheric Convective Instability, TR-0066(9260-02)-3, The Aerospace Corporation, El Segundo, California (1 July 1969).

Feess, W. A., Reduced Data from the LOGACS Experiment, TOR-0158(3110-01)-17, The Aerospace Corporation, El Segundo, California (15 February 1968).

Feess, W. A., LOGACS Wind Analysis, TOR-0200(9990)-1, The Aerospace Corporation, El Segundo, California (August 1968).

Fotou, E. G., LOGACS - An Orbital Accelerometer Calibration Experiment, TOR-0158(3110-01)-21, The Aerospace Corporation, El Segundo, California (February 1968).

Pearson, J. A., Analysis of Atmosphere Density Obtained from Low-G Accelerometer Data on Satellite 1967 50B, TOR-0066(5306)-3, The Aerospace Corporation, El Segundo, California (7 July 1969).

Pearson, J. A., Predictability of Upper Atmosphere Density Based on LOGACS Data, ATM 69(4110-01)-60, The Aerospace Corporation, El Segundo, California (28 October 1968) (Internal correspondence only; not available outside The Aerospace Corporation).

Pearson, J. A., Computer Reduced Atmospheric Density Obtained from Low-G Accelerometer Data on Satellite 1967 50B, TOR-0200(9990)-2, The Aerospace Corporation, El Segundo, California (16 December 1968).

Prag, A. B., Alternate Formulation of the Midlatitude Model of the Upper Atmosphere, TOR-0200(4110-01)-22, The Aerospace Corporation, El Segundo, California (11 March 1969).

Prag, A. B., Density Model of the Aurural and Polar Atmosphere Between 120 and 175 km, TOR-0066(5260-10)-1, The Aerospace Corporation, El Segundo, California (15 September 1969).

Prag, A. B., Density Model of the Midlatitude Atmosphere Between 120 and 220 km, TOR-0200(4110-01)-9, The Aerospace Corporation, El Segundo, California (26 December 1968).

Young, K. R., LOGACS Accelerometer Data, TOR-0200(4113-04)-1, The Aerospace Corporation, El Segundo, California (August 1968).

APPENDIX A

EXPERIMENT CLOCK ERROR

The experiment clock was a model 11477 Time Reference Generator made by Adcole Corporation. The clock played a key role in the LOGACS experiment because the centrifuge mode change pulses and the centrifuge motor supply frequency were derived from the clock circuitry.

After the LOGACS flight, the local time of each station acquisition was correlated with the experiment clock time acquired during each station acquisition. A plot of the relationship between the local station time and experiment clock time is shown in Fig. A. 1. As can be quickly seen from the figure, the experiment clock steadily gained time (i.e., was fast) by about one part in 50,000.

The clock accuracy as a function of temperature was measured during the acceptance testing. The experiment clock was about 65°F at the time of turn-on of the clock and then slowly approached a temperature of 50 ± 5°F. The experiment clock error as a function of temperature is shown in Fig. A. 2. As can be seen, the clock error over the 45°F to 75°F region is almost exactly one part in 50,000 fast (i.e., the experiment clock was indicating a larger value of time than had actually transpired).

The correlation between the laboratory tests on the experiment clock and the data obtained from the clock while on-orbit certainly provide graphic evidence of the stability of the time reference during the 100 hr of orbital operation.

Since all data processing was accomplished with respect to the experiment clock time, the clock error did not really propagate as an error in the calculations that were made. The known clock error results in a scale factor error of one part in 25,000, or 0.004 percent, which is significantly below the LOGACS experimental error. It is only when one desires to

correlate the drag information derived from the LOGACS data with the ephemeris of the satellite vehicle that one must reckon with the clock error at all. For most such purposes, the known clock error of one part in 50,000 is small enough to ignore.

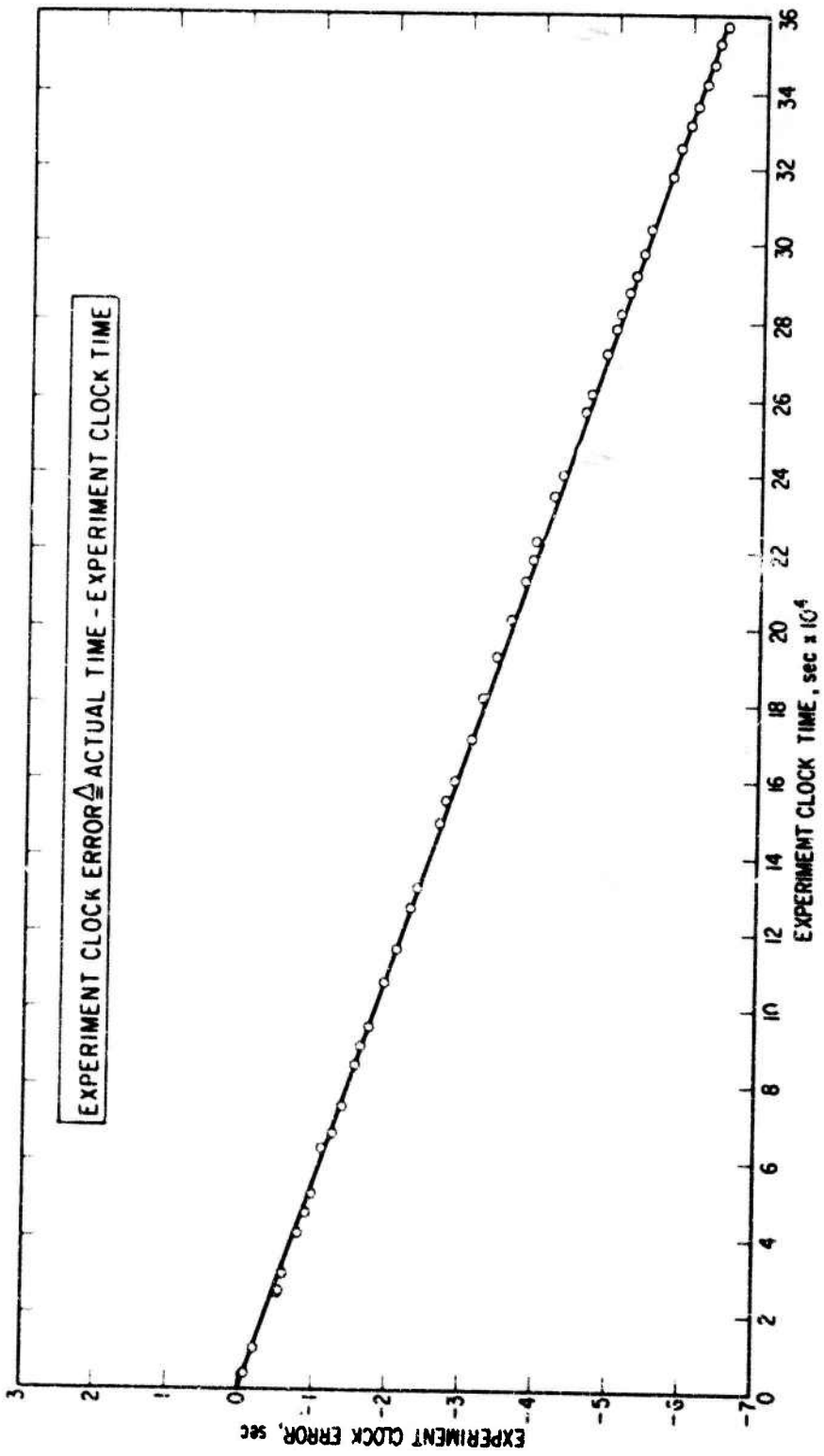

Fig. A. 1. Experiment Clock Error

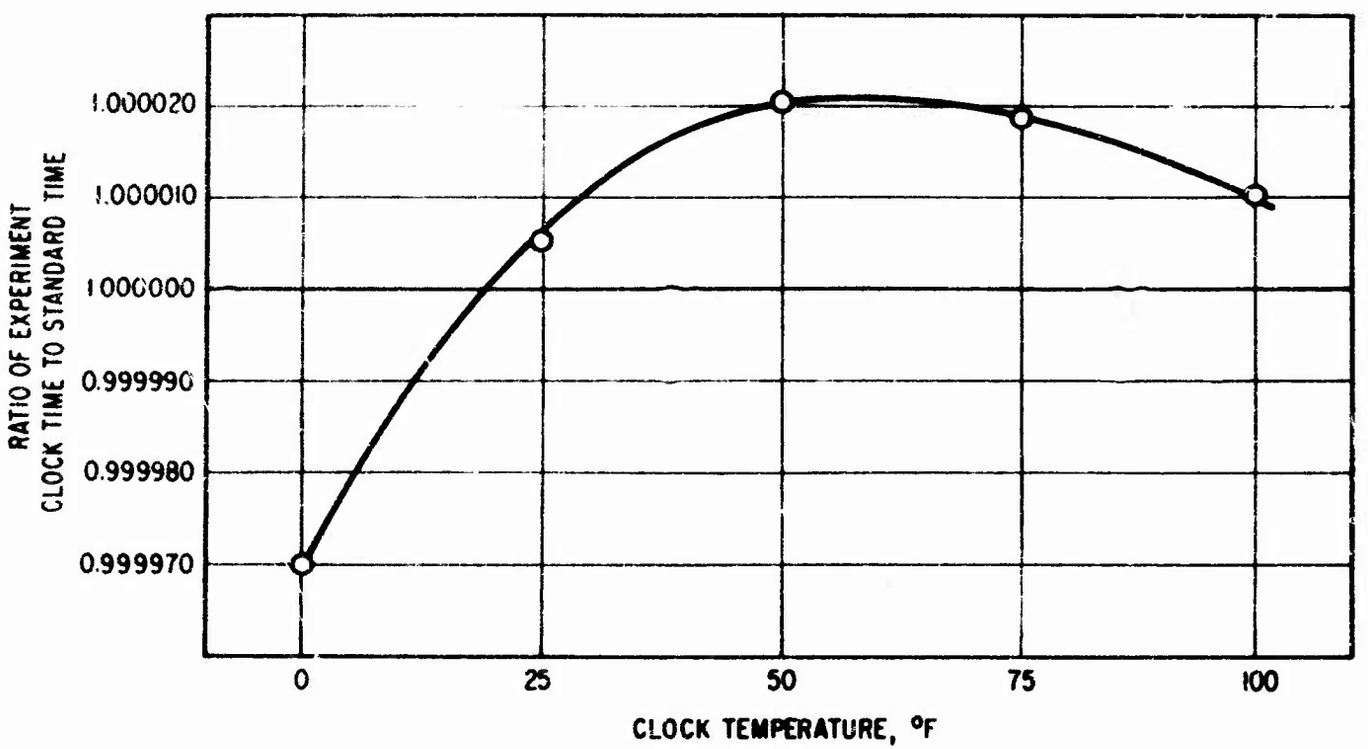

Fig. A. 2. Experiment Clock Error as a Function of Temperature

APPENDIX B

LOGACS DRAWINGS AND DOCUMENTS

B.1 BELL AEROSYSTEMS COMPANY

A. DRAWINGS

1.	Centrifuge, LOGACS Outline	E 6087-300300
2.	Centrifuge, LOGACS	E 14-11501
3.	Cover, Centrifuge LOGACS	J 14-11512
4.	Seal, Centrifuge, LOGACS	D 14-11550
5.	Table, Centrifuge	J 14-11554
6.	Mount, Table, Centrifuge	J 14-11555
7.	System Cable Diagram, LOGACS	J 6087-300002
8.	Pinion, Drive Motor, LOGACS	D 14-11553
9.	Gear, Rotation, LOGACS	E 14-11552

B. DOCUMENTS

1.	Preliminary Design Report - LOGACS	
2.	Structural Analysis of LOGACS Centrifuge	6087-941001
3.	Qualification Test Procedure for Centrifuge	60004-591
4.	Qualification Test Procedure for MESA System	60004-592
5.	Acceptance Test Procedure for LOGACS	60004-594
6.	Summary Report - Development of a Miniature Electrostatic Accelerometer (MESA) for Low-G Applications	60009-509 (NASA CR-54137)

B.2 LOCKHEED MISSILES AND SPACE COMPANY (LMSC)

A. DRAWINGS

1.	Module 464-5 Schematic Diagram	SK2P 17804

B. DOCUMENTS

1.	Conceptual Design Review Audit	LMSC/A838724
2.	Detail Design Review Audit	LMSC/A841150
3.	Instrumentation Schedule, Vehicle 4838, Module 464	LMSC/2P14611
4.	Detail Specification, Time Reference Generator, Type II	LMSC/2P14314
5.	Integrated Systems Test Procedure, Module 464	LMSC/2P19515
6.	Test Plan, Module 464	LMSC/TP464
7.	Operations Plan and Requirements for Module 464	LMSC/0P464
8.	LOGACS Data Processing Specification	LMSC/DPA-1063
9.	Flight Report, LOGACS	LMSC/A876880

B.3 AEROSPACE CORPORATION DOCUMENTS

1.	Orbital Requirements Document for Low "G" Accelerometer Calibration System (LOGACS) Experiment	TOR-1001(2101-01)-16
2.	Orbital Support Plan Program LOGACS	
3.	Upper Atmosphere Density Determined from a Low-G Accelerometer on Satellite 1967 50B	TOR-0158(3110-01)-16
4.	Reduced Data from the LOGACS Experiment	TOR-0158(3110-01)-17
5.	Computer Programs for LOGACS Data Reduction	TOR-0158(3110-01)-28
6.	Postflight Ephemeris for Vehicle 4838	TOR-0158(3110-01)-15

7.	LOGACS Wind Analysis	TOR-0200(9990)-1
8.	Computer-Reduced Atmospheric Density Obtained from Low-G Accelerometer Data on Satellite 1967-50B	TOR-0200(9900)-2
9.	Analysis of Atmosphere Density Obtained from a Low-G Accelerometer on Satellite 1967-50B	TOR-0066(5306)-3
10.	LOGACS Accelerometer Data	TOR-0200(4113-04)-1
11.	Predictability of Upper Atmosphere Density Based on LOGACS Data	ATM-69(4110-01)-60
12.	Density Model of the Mid-latitude Atmosphere Between 120 and 220 km	TOR-0200(4110-01)-9
13.	Alternate Formulation of the Midlatitude Model of the Upper Atmosphere	TOR-0200(4110-01)-22
14.	Density Model of the Auroral and Polar Atmosphere Between 120 and 175 km	TOR-0066(5620-10)-1
15.	Thermospheric Convective Instability	TOR-0066(9260-02)-3

B.4 AIR FORCE DOCUMENTS

1.	Test Operations Order 67-2	USAF Report No. 67-2

APPENDIX C

SPECIFICATION FOR LOGACS DATA ANALYSIS PROGRAM

C.1 INTRODUCTION

The purpose of the LOGACS experiment is to calibrate a low-g accelerometer aboard a satellite vehicle and use it to measure the acceleration of the vehicle due to nongravitational forces, primarily aerodynamic drag.

The accelerometer is calibrated by rotating it at two different known angular rates, thereby inducing known centripetal accelerations. The accelerometer is also stopped at two fixed points so that its input axis is parallel to the satellite longitudinal axis pointing either forward or aft.

The input to this data analysis program is a floating binary digital tape. The output will be values of accelerometer scale factor and bias and a time history of the vehicle acceleration due to drag.

C.2 SYMBOLS

i	experiment clock time expressed as an integral number of seconds
t_0	mode starting time (sec)
$\sigma(j)$	corrected total of accelerometer pulses accumulated over 20R sec from $t_0 + 300 + 20(j-10)$ to $t_0 + 300 + 20(j-9)R$ or over 20 sec from $t_0 + 20(j+4)$ to $t_0 + 20(j+5)$
$\sigma'(i)$	corrected total of accelerometer pulses accumulated over 4 sec from i - 2 to i + 2
$\sigma''(i)$	corrected total of accelerometer pulses accumulated over 1 sec from i - 1 to i
$\sigma'''(i)$	original total of accelerometer pulses accumulated over 1 sec from i - 1 to i
$g(j)$	weighting factor applied to $\sigma(j)$ for interpolation
R	ratio between nominal and actual turntable rates (R = 184,798,313/164,450,000)

m(i)	calibration cycle mode number (m = 1, 2, 3, 4, or 5)
S(m, 1)	weighted summation of $\sigma(j)$ for mode m
A	centripetal acceleration induced by turntable in mode 1 (ft/sec^2)
f	accelerometer scale factor (pulses/ft/sec)
b	accelerometer bias (ft/sec^2)
d(j)	computed values of drag acceleration (ft/sec^2)
D(m)	average value of drag acceleration (ft/sec^2)
$\dot{D}(m)$	average rate of change of drag acceleration (ft/sec^3)
$\phi(m)$	turntable angle at start of mode m (deg)
Δ	*dif*ference between bias determined in modes 3 and 4 and bias determined in modes 1 and 2 (ft/sec^2)

C.3 PROGRAM INPUT

The general format for the input tape will be as shown in Section C.4. Selected values from each 2-sec cycle of a 60-position commutator are recorded in digital form on the input tape. Each commutator cycle constitutes one data frame.

The signals of primary interest to the data analysis program are:

a. Time: A nonrepeating time signal from an 8-day clock aboard the satellite sampled once every 2 sec

b. Pulse count: Signed accelerometer pulses accumulated for 1 sec in an up-down counter aboard the satellite and recorded twice every 2 sec

c. Mode: The experiment continuously cycles through four primary modes and a transitional mode. The length of each primary mode including the appropriate transitional mode is 512 sec. The total calibration cycle is thus 2048 sec

d. Pickoff switch: The time at which the turntable reaches point A (forward) and B (aft) is recorded on the digital tape

e. Thruster signal: A signal indicating which, if any, of the six attitude control thrusters has fired in the last 1.2 sec is given twice every 2 sec

The calibration cycle is divided as shown in Table C.1. The cycle is repeated every 2048 sec.

Table C.1. Calibration Cycle Modes

Mode	Position	Start Time, sec	Stop Time, sec	Elapsed Time, sec
1	Low Speed	0.00	512.00	512.00
2	High Speed	512.00	1024.00	512.00
5	High Speed	1024.00	1031.38	7.38
3	Stop A	1031.38	1536.00	504.62
5	High Speed	1536.00	1569.71	33.71
4	Stop B	1569.71	2048.00	478.29

Time gaps in the telemetered data will occur due to difficulties in transfering the data recorded on board the satellite to various ground locations.

Other inputs are the Mode 1 centripetal acceleration (A), and the ground calibrated values of scale factor (f) and bias (b).

C.4 FLOATING BINARY FORMAT

Mode: Binary

Density: 800 bits per inch

Record Length: Data records are variable but are set at 117 sets of time and quantity (quantities) per record

Indicative records may contain up to 19 three-word indicatives

- The first record of a file is the indicative record. All the rest are data records
- Each time-word of a data record is followed by N ($1 \leq N \leq 19$) quantity words
- Number of words per record = $42 [T + N(Q)]$
- Each quantity word is associated with the indicative that has the same numerical position
- The last data record may have less than 42 sets of time and quantity
- There may be any number of files per tape
- One (1) end-of-file indicates the end of the data channel
- Three (3) consecutive end-of-files indicate the end of the data tape

INDICATIVE FORMAT

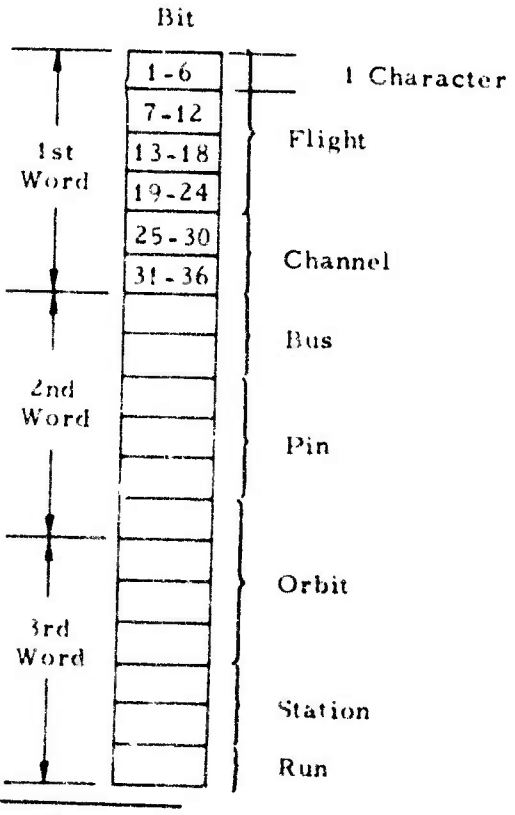

DATA WORD FORMAT

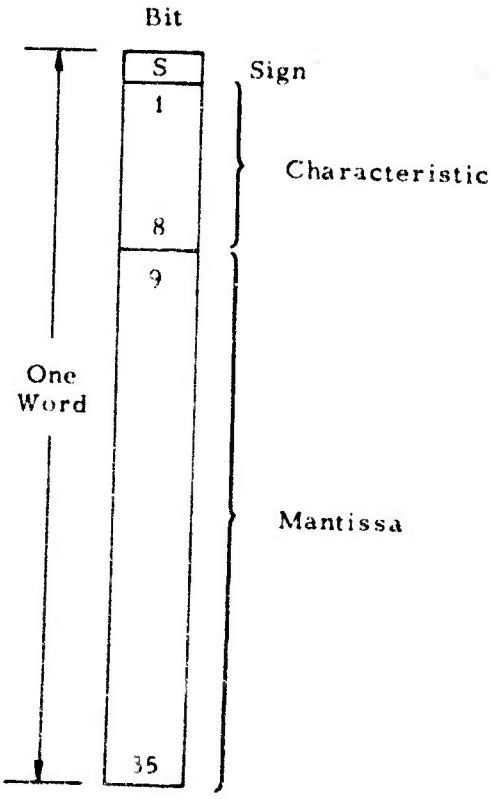

A negative number will have a "1" in the sign bit. A positive number will have a "0" in the sign bit.

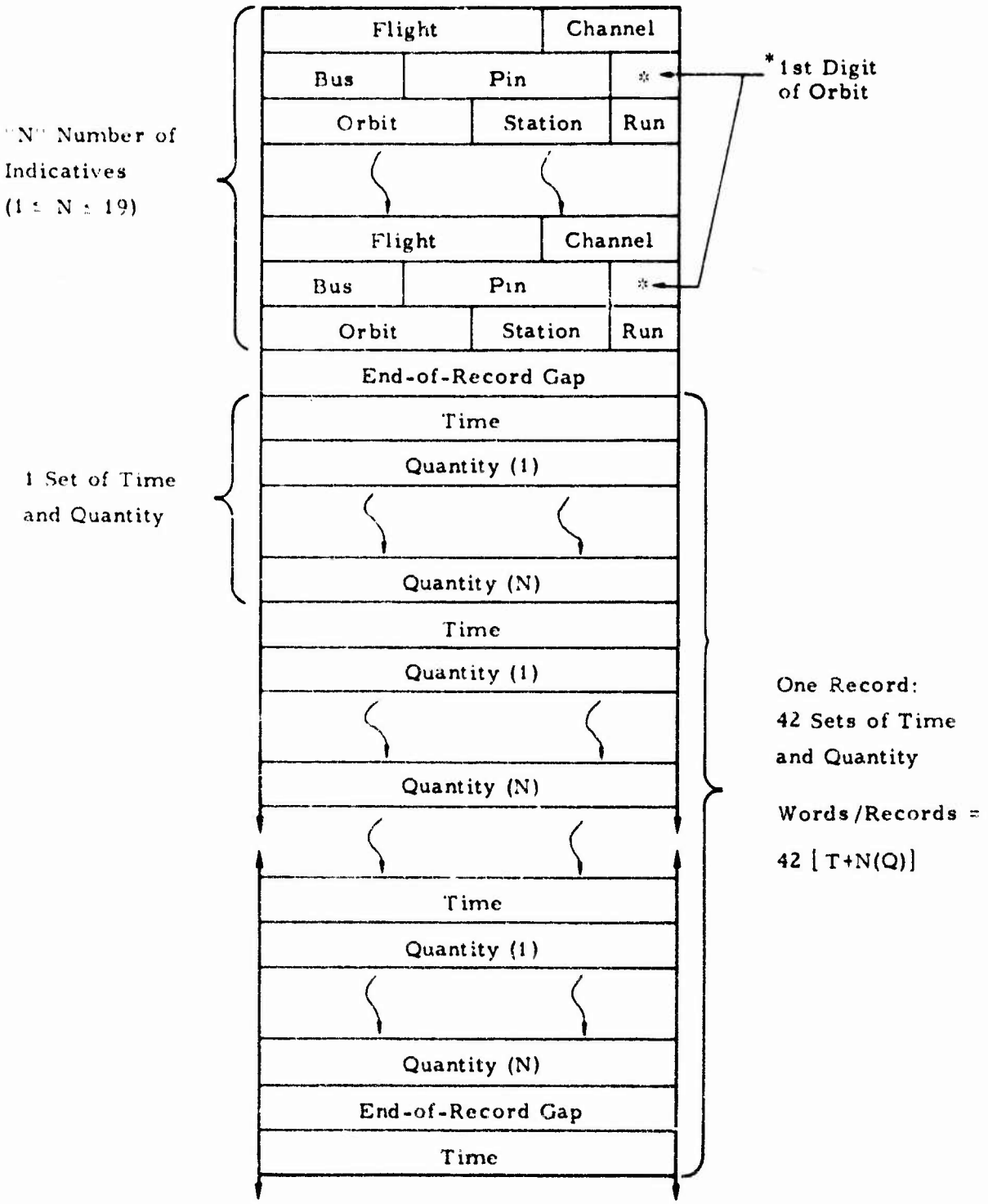
Flight
Channel
Bus
Pin
*
Orbit
Station
Run
"N" Number of Indicatives (1 ≤ N ≤ 19)
*1st Digit of Orbit
End-of-Record Gap
Time
Quantity (1)
Quantity (N)
1 Set of Time and Quantity
One Record: 42 Sets of Time and Quantity
Words/Records = 42 [T+N(Q)]

C.5 BLOCK A

The 1-sec accumulations from the input digital tape are processed in the following manner. If there is a thruster firing signal in the first half of the commutator cycle, then a value of 2048 is substituted for the original value of the pulse count for both the first half of the commutator cycle and the second half of the previous cycle. If there is a thruster firing signal in the second half of the commutator cycle, then 2048 is substituted for both halves of the commutator cycle. This is outlined in Table C-2.

Table C-2. Accelerometer Pulse Corrections

Thruster Signal		Corrected Time of Accelerometer Pulses			
1st Half of Cycle	2nd Half of Cycle	$\sigma''(i-2)$	$\sigma''(i-1)$	$\sigma''(i)$	$\sigma''(i+1)$
No	No	$\sigma'''(i-2)$	$\sigma'''(i-1)$	$\sigma'''(i)$	$\sigma'''(i+1)$
Yes	No	$\sigma'''(i-2)$	2048	2048	$\sigma'''(i+1)$
No	Yes	$\sigma'''(i-2)$	$\sigma'''(i-1)$	2048	2048
Yes	Yes	$\sigma'''(i-2)$	2048	2048	2048

Next a 4-sec accumulation of accelerometer pulses is made by summing the pulse count for four consecutive 1-sec intervals, substituting an average value for those 1-sec counts whose magnitude exceeds 2000. In case all of the four exceed 2000, an extrapolation is made from previous 4-sec counts.

If n = number of 1-sec counts where $|\sigma''(i+k-2)| \geq 2000$, then for $n < 4$, one finds

$$\sigma'(i) = \frac{4}{4-n}\sum_{k=1}^{4}\sigma''(i+k-2) \qquad \text{for} \qquad |\sigma''(i+k-2)| < 2000$$

For n = 4, one finds

$$\sigma'(i) = \frac{\sigma'(i-4) + \sigma'(i-8)}{2}$$

The above equation should also be used to bridge short (<20 sec) breaks in the data.

The printout from Block A should consist of every fifteenth value of $\sigma'(i)$ along with the corresponding time and mode:

Time, sec	Mode	Accelerometer Count
i	m(i)	$\sigma'(i)$

There will be one sample per minute of experiment time. An asterisk (*) should be used to indicate those accelerometer counts for which n = 4 and the extrapolation formula is used.

C.6 DEVELOPMENT OF MODE 1 EQUATIONS

If it is assumed that the drag during a 400-sec period may be represented by a second-order polynomial, then the accelerometer counts accumulated in 20R sec is given by

$$\sigma = f \int_{t-10R}^{t+10R} \left[A + b + \left(D + \dot{D}t + \frac{1}{2}\ddot{D}t^2 \right) \cos(\omega t + \phi) \right] dt$$

where

$$\omega = \frac{\pi}{60R} \text{ sec}^{-1}$$

Integrating the above equation results in

$$\frac{\omega\sigma}{f} = \frac{\pi}{3}(A + b) + \left[D + \left(\frac{1}{72}\pi^2 + \frac{\pi}{6}\sqrt{3} - 1\right)\frac{\ddot{D}}{\omega^2}\right]\cos(\omega t + \phi) - \left(1 - \frac{\pi}{6}\sqrt{3}\right)\frac{\dot{D}}{\omega}\sin(\omega t + \phi)$$

$$+ \dot{D}t\cos(\omega t + \phi) - \left(1 - \frac{\pi}{6}\sqrt{3}\right)\frac{\ddot{D}t}{\omega}\sin(\omega t + \phi) + \frac{1}{2}\ddot{D}t^2\cos(\omega t + \phi)$$

This may be further reduced by trigonometric identities to

$$\frac{\omega\sigma}{f} = \frac{\pi}{3}(A + b) + \left[D\cos\phi - \left(1 - \frac{\pi}{6}\sqrt{3}\right)\frac{\dot{D}\sin\phi}{\omega} + \left(\frac{1}{72}\pi^2 + \frac{\pi}{6}\sqrt{3} - 1\right)\frac{\ddot{D}\cos\phi}{\omega^2}\right]\cos\omega t$$

$$- \left[D\sin\phi + \left(1 - \frac{\pi}{6}\sqrt{3}\right)\frac{\dot{D}\cos\phi}{\omega} + \left(\frac{1}{72}\pi^2 + \frac{\pi}{6}\sqrt{3} - 1\right)\frac{\ddot{D}\sin\phi}{\omega^2}\right]\sin\omega t$$

$$+ \left[\dot{D}\cos\phi - \left(1 - \frac{\pi}{6}\sqrt{3}\right)\frac{\ddot{D}\sin\phi}{\omega}\right]t\cos\omega t - \left[\dot{D}\sin\phi + \left(1 - \frac{\pi}{6}\sqrt{3}\right)\frac{\ddot{D}\cos\phi}{\omega}\right]t\sin\omega t$$

$$+ \frac{1}{2}\ddot{D}\cos\phi\, t^2\cos\omega t - \frac{1}{2}\ddot{D}\sin\phi\, t^2\sin\omega t$$

In matrix form,

$$\frac{\omega\sigma}{f} = \frac{\pi}{3}(A + b) + \frac{1}{72}\left[\cos\omega t \;\; \omega t\sin\omega t \;\; \frac{1}{2}(\omega t)^2\cos\omega t\right]\begin{bmatrix} 72 & -72 + 12\pi\sqrt{3} & \pi^2 + 12\pi\sqrt{3} - 72 \\ 0 & -72 & -72 + 12\pi\sqrt{3} \\ 0 & 0 & 72 \end{bmatrix}\begin{bmatrix} D\cos\phi \\ (\dot{D}/\omega)\sin\phi \\ (\ddot{D}/\omega^2)\cos\phi \end{bmatrix}$$

$$+ \frac{1}{72}\left[\sin\omega t \;\; \omega t\cos\omega t \;\; \frac{1}{2}(\omega t)^2\sin\omega t\right]\begin{bmatrix} -72 & -72 + 12\pi\sqrt{3} & -\pi^2 - 12\pi\sqrt{3} + 72 \\ 0 & 72 & -72 + 12\pi\sqrt{3} \\ 0 & 0 & -72 \end{bmatrix}\begin{bmatrix} D\sin\phi \\ (\dot{D}/\omega)\cos\phi \\ (\ddot{D}/\omega^2)\sin\phi \end{bmatrix}$$

Allowing t to take on the values

$$t(j) = 10(2j - 19)R \qquad 1 \le j \le 18$$

yields

$$\omega t(j) = \frac{\pi}{6}(2j - 19)$$

When the values of t(j) are substituted into the above matrix equation and odd and even components are separated, the even matrix equation becomes

$$\begin{bmatrix} \sigma(18) + \sigma(1) \\ \sigma(17) + \sigma(2) \\ \sigma(16) + \sigma(3) \\ \sigma(15) + \sigma(4) \\ \sigma(14) + \sigma(5) \\ \sigma(13) + \sigma(6) \\ \sigma(12) + \sigma(7) \\ \sigma(11) + \sigma(8) \\ \sigma(10) + \sigma(9) \end{bmatrix} = \frac{\sqrt{3}}{72} \begin{bmatrix} 1 & -1 & -17 & \cdots \\ 1 & 0 & -30 & 0 \\ 1 & 1 & -13 & 169 \\ 1 & 1 & 11 & 121 \\ 1 & 0 & 18 & 0 \\ 1 & -1 & 7 & -49 \\ 1 & -1 & -5 & -25 \\ 1 & 0 & -6 & 0 \\ 1 & 1 & -1 & 1 \end{bmatrix} \begin{bmatrix} 16\pi\sqrt{3} & 0 & 0 & 0 \\ 0 & 72 & -72 + 12\pi\sqrt{3} & \pi^2 + 12\pi\sqrt{3} - 72 \\ 0 & 0 & 4\pi\sqrt{3} & 4\pi\sqrt{3} - 2\pi^2 \\ 0 & 0 & 0 & \pi^2 \end{bmatrix} \begin{bmatrix} A + b \\ D\cos\phi \\ (\dot{D}/\omega)\sin\phi \\ (\dot{D}/\omega^2)\cos\phi \end{bmatrix}$$

This may be solved in a least-squares sense by first premultiplying by a matrix with orthogonal rows

$$\begin{bmatrix} 1 & 1 & 1 & 1 & 1 & 1 & 1 & 1 & 1 \\ -1 & 0 & 1 & 1 & 0 & -1 & -1 & 0 & 1 \\ -11 & -26 & -11 & 13 & 22 & 13 & 1 & -2 & 1 \\ -1915 & 500 & 995 & 41 & -244 & 623 & 1100 & 128 & -1228 \end{bmatrix} \begin{bmatrix} \sigma(18) + \sigma(1) \\ \sigma(17) + \sigma(2) \\ \sigma(16) + \sigma(3) \\ \sigma(15) + \sigma(4) \\ \sigma(14) + \sigma(5) \\ \sigma(13) + \sigma(6) \\ \sigma(12) + \sigma(7) \\ \sigma(11) + \sigma(8) \\ \sigma(10) + \sigma(9) \end{bmatrix} \frac{\pi}{1}$$

$$\begin{bmatrix} 6\pi & 0 & 0 & 0 \\ 0 & \frac{1}{6}\sqrt{3} & 0 & 0 \\ 0 & 0 & \frac{\pi}{2}\sqrt{3} & 0 \\ 0 & 0 & 0 & 9268\pi^2\sqrt{3} \end{bmatrix} \begin{bmatrix} 1 & 0 & -1 & -1 \\ 0 & 36 & -36 + 10\pi\sqrt{3} & -36 + 10\pi\sqrt{3} + 53\pi^2 \\ 0 & 0 & 194\sqrt{3} & 194\sqrt{3} - 35\pi \\ 0 & 0 & 0 & 1 \end{bmatrix} \begin{bmatrix} A + b \\ D\cos\phi \\ (\dot{D}/\omega)\sin\phi \\ (\dot{D}/\omega^2)\cos\phi \end{bmatrix}$$

Inverting the square m trices yields

$$f\begin{bmatrix} A+b \\ D\cos\phi \\ (\dot{D}/\omega)\sin\phi \\ (\ddot{D}/\omega^2)\cos\phi \end{bmatrix} = \frac{\pi}{60R}\begin{bmatrix} 1 & 0 & 6\sqrt{3} & 35\pi\sqrt{3} \\ 0 & 1 & 6\sqrt{3}-5\pi & 35\pi\sqrt{3}-886\pi^2 \\ 0 & 0 & 6\sqrt{3} & -582+35\pi\sqrt{3} \\ 0 & 0 & 0 & 582 \end{bmatrix}\begin{bmatrix} 6\pi & 0 & 0 & 0 \\ 0 & 6\sqrt{3} & 0 & 0 \\ 0 & 0 & 1746\pi\sqrt{3} & 0 \\ 0 & 0 & 0 & 5393976\pi^2\sqrt{3} \end{bmatrix}^{-1}$$

$$\times\begin{bmatrix} 1 & 1 & 1 & 1 & 1 & 1 & 1 & 1 & 1 \\ -1 & 0 & 1 & 1 & 0 & -1 & -1 & 0 & 1 \\ -11 & -26 & -11 & 13 & 22 & 13 & 1 & -2 & 1 \\ -1913 & 500 & 995 & 41 & -244 & 623 & 1100 & 128 & -1228 \end{bmatrix}\begin{bmatrix} \sigma(18)+\sigma(1) \\ \sigma(17)+\sigma(2) \\ \sigma(16)+\sigma(3) \\ \sigma(15)+\sigma(4) \\ \sigma(14)+\sigma(5) \\ \sigma(13)+\sigma(6) \\ \sigma(12)+\sigma(7) \\ \sigma(11)+\sigma(8) \\ \sigma(10)+\sigma(9) \end{bmatrix}$$

Similarly the odd matrix equation becomes

$$\begin{bmatrix} \sigma(18)-\sigma(1) \\ \sigma(17)-\sigma(2) \\ \sigma(16)-\sigma(3) \\ \sigma(15)-\sigma(4) \\ \sigma(14)-\sigma(5) \\ \sigma(13)-\sigma(6) \\ \sigma(12)-\sigma(7) \\ \sigma(11)-\sigma(8) \\ \sigma(10)-\sigma(9) \end{bmatrix} = \frac{1}{72}\begin{bmatrix} -1 & -17 & -289 \\ -2 & 0 & -450 \\ -1 & 13 & -169 \\ 1 & 11 & 121 \\ 2 & 0 & 162 \\ 1 & -7 & 49 \\ -1 & -5 & -25 \\ -2 & 0 & -18 \\ -1 & 1 & -1 \end{bmatrix}\begin{bmatrix} 72 & 72-12\pi\sqrt{3} & \pi^2+12\pi\sqrt{3}-72 \\ 0 & 12\pi\sqrt{3} & -12\pi\sqrt{3}+6\pi^2 \\ 0 & 0 & \pi^2 \end{bmatrix}\begin{bmatrix} D\sin\phi \\ (\dot{D}/\omega)\cos\phi \\ (\ddot{D}/\omega^2)\sin\phi \end{bmatrix}$$

Premultiplying to get the least-squares solution yields

$$\begin{bmatrix} 1 & -2 & -1 & 1 & 2 & 1 & -1 & -2 & -1 \\ -49 & 4 & 41 & 31 & -4 & -23 & -13 & 4 & 5 \\ -1590 & -3265 & -1570 & -352 & -611 & -364 & 1325 & 2549 & 1329 \end{bmatrix} \begin{bmatrix} \sigma(18) - \sigma(1) \\ \sigma(17) - \sigma(2) \\ \sigma(16) - \sigma(3) \\ \sigma(15) - \sigma(4) \\ \sigma(14) - \sigma(5) \\ \sigma(13) - \sigma(6) \\ \sigma(12) - \sigma(7) \\ \sigma(11) - \sigma(8) \\ \sigma(10) - \sigma(9) \end{bmatrix} \quad (3-7)$$

$$= \begin{bmatrix} \frac{1}{6} & 0 & 0 \\ 0 & \frac{\pi}{6} & 0 \\ 0 & 0 & \frac{81431}{3}\pi \end{bmatrix} \begin{bmatrix} 108 & 108 - 6\pi\sqrt{3} & 167\pi^2 + 6\pi\sqrt{3} - 108 \\ 0 & 1938\sqrt{3} & -1938\sqrt{3} + 1607\pi \\ 0 & 0 & 1 \end{bmatrix} \begin{bmatrix} D \sin\phi \\ (\dot{D}/\omega)\cos\phi \\ (\ddot{D}/\omega^2)\sin\phi \end{bmatrix}$$

Inverting the square matrices yields

$$\begin{bmatrix} D \sin\phi \\ (\dot{D}/\omega)\cos\phi \\ (\ddot{D}/\omega^2)\sin\phi \end{bmatrix} = \frac{\pi}{60R} \begin{bmatrix} 1 & -6\sqrt{3} + \pi & 1607\pi - 3086\pi^2\sqrt{3} \\ 0 & 6\sqrt{3} & 1938\sqrt{3} - 1607\pi \\ 0 & 0 & 1938\sqrt{3} \end{bmatrix} \begin{bmatrix} 18 & 0 & 0 \\ 0 & 5814\pi & 0 \\ 0 & 0 & 52604426\pi^2\sqrt{3} \end{bmatrix}^{-1}$$

$$\times \begin{bmatrix} -1 & -2 & -1 & 1 & 2 & 1 & -1 & -2 & -1 \\ -49 & 4 & 41 & 31 & -4 & -23 & -13 & 4 & 5 \\ -1590 & -3265 & -1570 & -352 & -611 & -364 & 1325 & 2549 & 1329 \end{bmatrix} \begin{bmatrix} \sigma(18) - \sigma(1) \\ \sigma(17) - \sigma(2) \\ \sigma(16) - \sigma(3) \\ \sigma(15) - \sigma(4) \\ \sigma(14) - \sigma(5) \\ \sigma(13) - \sigma(6) \\ \sigma(12) - \sigma(7) \\ \sigma(11) - \sigma(8) \\ \sigma(10) - \sigma(9) \end{bmatrix}$$

C.7 DEVELOPMENT OF MODE 2 EQUATIONS

If it is assumed that the drag during a 400-sec period may be represented by a second-order polynomial, then the number of accelerometer counts accumulated in 20R sec is given by

$$\sigma = f\int_{t-10R}^{t+10R}\left[4A + b + \left(D + \dot{D}t + \frac{1}{2}\ddot{D}t^2\right)\cos(\omega t + \phi)\right]dt$$

where $\omega = (\pi/30R)\ \text{sec}^{-1}$. Integrating the above equation results in

$$\frac{\omega\sigma}{f} = \frac{2\pi}{3}(4A + b) + \left[\sqrt{3}D + \left(\frac{1}{18}\pi^2\sqrt{3} + \frac{\pi}{3} - \sqrt{3}\right)\frac{\ddot{D}}{\omega^2}\right]\cos(\omega t + \phi)$$

$$-\left(\sqrt{3} - \frac{\pi}{3}\right)\frac{\dot{D}}{\omega}\sin(\omega t + \phi) + \sqrt{3}\,\dot{D}t\cos(\omega t + \phi)$$

$$-\left(\sqrt{3} - \frac{\pi}{3}\right)\frac{\ddot{D}t}{\omega}\sin(\omega t + \phi) + \sqrt{3}\,\frac{1}{2}\ddot{D}t^2\cos(\omega t + \phi)$$

This may be further transformed by trigonometric identities to

$$\frac{\omega\sigma}{f} = \frac{2\pi}{3}(4A + b) + \left[\sqrt{3}D\cos\phi - \left(\sqrt{3} - \frac{\pi}{3}\right)\frac{\dot{D}\sin\phi}{\omega} + \left(\frac{1}{18}\pi^2\sqrt{3} + \frac{\pi}{3} - \sqrt{3}\right)\frac{\ddot{D}\cos\phi}{\omega^2}\right]\cos\omega t$$

$$-\left[\sqrt{3}D\sin\phi + \left(\sqrt{3} - \frac{\pi}{3}\right)\frac{\dot{D}\cos\phi}{\omega} + \left(\frac{1}{18}\pi^2\sqrt{3} + \frac{\pi}{3} - \sqrt{3}\right)\frac{\ddot{D}\sin\phi}{\omega^2}\right]\sin\omega t$$

$$+\left[\sqrt{3}\dot{D}\cos\phi - \left(\sqrt{3} - \frac{\pi}{3}\right)\frac{\ddot{D}\sin\phi}{\omega}\right]t\cos\omega t - \left[\sqrt{3}\,\dot{D}\sin\phi + \left(\sqrt{3} - \frac{\pi}{3}\right)\frac{\ddot{D}\cos\phi}{\omega}\right]t\sin\omega t$$

$$+\sqrt{3}\,\frac{1}{2}\ddot{D}\cos\phi t^2\cos\omega t - \sqrt{3}\,\frac{1}{2}\ddot{D}\sin\phi t^2\sin\omega t$$

The matrix form is

$$\frac{\omega\sigma}{\ell} = \frac{2\pi}{3}(4A + b)$$

$$+ \frac{1}{18}\sqrt{3}\left[\cos\omega t \;\; \omega t \sin\omega t \;\; \frac{1}{2}(\omega t)^2 \cos\omega t\right]\begin{bmatrix} 18 & -18 + 2\pi\sqrt{3} & \pi^2\sqrt{3} - 18 \\ 0 & -18 & -18 + 2\pi\sqrt{3} \\ 0 & 0 & 18 \end{bmatrix}\begin{bmatrix} D\cos\phi \\ (\dot{D}/\omega)\sin\phi \\ (\ddot{D}/\omega^2)\cos\phi \end{bmatrix}$$

$$+ \frac{1}{18}\sqrt{3}\left[\sin\omega t \;\; \omega t \cos\omega t \;\; \frac{1}{2}(\omega t)^2 \sin\omega t\right]\begin{bmatrix} -18 & -18 + 2\pi\sqrt{3} & -\pi^2 - 2\pi\sqrt{3} + 18 \\ 0 & 18 & -18 + 2\pi\sqrt{3} \\ 0 & 0 & -18 \end{bmatrix}\begin{bmatrix} D\sin\phi \\ (\dot{D}/\omega)\cos\phi \\ (\ddot{D}/\omega^2)\sin\phi \end{bmatrix}$$

Allowing t to take on the values

$$t(j) = 10(2j - 19)R \qquad 1 \le j \le 18$$

gives

$$\omega t(j) = \frac{\pi}{3}(2j - 19)$$

When the values of t(j) are substituted into the above matrix equation and odd and even components are separated, the even matrix equation becomes

$$\frac{\pi}{18}\begin{bmatrix} \sigma(18) + \sigma(1) \\ \sigma(17) + \sigma(2) \\ \sigma(16) + \sigma(3) \\ \sigma(15) + \sigma(4) \\ \sigma(14) + \sigma(5) \\ \sigma(13) + \sigma(6) \\ \sigma(12) + \sigma(7) \\ \sigma(11) + \sigma(8) \\ \sigma(10) + \sigma(9) \end{bmatrix} - \frac{\sqrt{3}}{18}\begin{bmatrix} 1 & 1 & 17 & 289 \\ 1 & -2 & 0 & -450 \\ 1 & 1 & -13 & 169 \\ 1 & 1 & 11 & 121 \\ 1 & -2 & 0 & -162 \\ 1 & 1 & -7 & 49 \\ 1 & 1 & 5 & 25 \\ 1 & -2 & 0 & -18 \\ 1 & 1 & -1 & 1 \end{bmatrix}\begin{bmatrix} 8\pi\sqrt{3} & 0 & 0 & 0 \\ 0 & 18 & -18 + 2\pi\sqrt{3} & \pi^2 + 2\pi\sqrt{3} - 18 \\ 0 & 0 & 6\pi\sqrt{3} & 6\pi\sqrt{3} - 2\pi^2 \\ 0 & 0 & 0 & \pi^2 \end{bmatrix}\begin{bmatrix} 4A + b \\ D\cos\phi \\ (\dot{D}/\omega)\sin\phi \\ (\ddot{D}/\omega^2)\cos\phi \end{bmatrix}$$

This may be solved in a least-squares sense by first premultiplying by a matrix with orthogonal rows:

$$\begin{bmatrix} 1 & 1 & 1 & 1 & 1 & 1 & 1 & 1 & 1 \\ 1 & -2 & 1 & 1 & -2 & 1 & 1 & -2 & 1 \\ 5 & 0 & -5 & 3 & 0 & -3 & 1 & 0 & -1 \\ 5 & -10 & 5 & -1 & 2 & -1 & -4 & 8 & -4 \end{bmatrix} \begin{bmatrix} \sigma(18) + \sigma(1) \\ \sigma(17) + \sigma(2) \\ \sigma(16) + \sigma(3) \\ \sigma(15) + \sigma(4) \\ \sigma(14) + \sigma(5) \\ \sigma(13) + \sigma(6) \\ \sigma(12) + \sigma(7) \\ \sigma(11) + \sigma(8) \\ \sigma(10) + \sigma(9) \end{bmatrix} \frac{\omega}{\Gamma}$$

$$= \begin{bmatrix} 12\pi & 0 & 0 & 0 \\ 0 & 2\sqrt{3} & 0 & 0 \\ 0 & 0 & 70\pi\sqrt{3}/3 & 0 \\ 0 & 0 & 0 & 336\pi^2\sqrt{3} \end{bmatrix} \begin{bmatrix} 1 & 0 & 1 & 1 \\ 0 & 9 & 3\pi\sqrt{3} - 9 & 53\pi^2 + 3\pi\sqrt{3} - 9 \\ 0 & 0 & 3\sqrt{3} & 3\sqrt{3} + \pi \\ 0 & 0 & 0 & 1 \end{bmatrix} \begin{bmatrix} 4A + b \\ D \cos\phi \\ (\dot{D}/\omega) \sin\phi \\ (\ddot{D}/\omega^2) \cos\phi \end{bmatrix}$$

Inverting the square matrices yield

$$\begin{bmatrix} 4A + b \\ D \cos\phi \\ (\dot{D}/\omega) \sin\phi \\ (\ddot{D}/\omega^2) \cos\phi \end{bmatrix} = \frac{\pi}{30R} \begin{bmatrix} 1 & 0 & -\sqrt{3} & \pi\sqrt{3} \\ 0 & 1 & -\pi + \sqrt{3} & -52\pi^2 - \pi\sqrt{3} \\ 0 & 0 & \sqrt{3} & -9 - \pi\sqrt{3} \\ 0 & 0 & 0 & 9 \end{bmatrix} \begin{bmatrix} 12\pi & 0 & 0 & 0 \\ 0 & 18\sqrt{3} & 0 & 0 \\ 0 & 0 & 210\pi\sqrt{3} & 0 \\ 0 & 0 & 0 & 3024\pi^2\sqrt{3} \end{bmatrix}^{-1}$$

$$\times \begin{bmatrix} 1 & 1 & 1 & 1 & 1 & 1 & 1 & 1 & 1 \\ 1 & -2 & 1 & 1 & -2 & 1 & 1 & -2 & 1 \\ 5 & 0 & -5 & 3 & 0 & -3 & 1 & 0 & -1 \\ 5 & -10 & 5 & -1 & 2 & -1 & -4 & 8 & -4 \end{bmatrix} \begin{bmatrix} \sigma(18) + \sigma(1) \\ \sigma(17) + \sigma(2) \\ \sigma(16) + \sigma(3) \\ \sigma(15) + \sigma(4) \\ \sigma(14) + \sigma(5) \\ \sigma(13) + \sigma(6) \\ \sigma(12) + \sigma(7) \\ \sigma(11) + \sigma(8) \\ \sigma(10) + \sigma(9) \end{bmatrix}$$

Similarly, the odd matrix equation becomes

$$\begin{bmatrix} \sigma(18) - \sigma(1) \\ \sigma(17) - \sigma(2) \\ \sigma(16) - \sigma(3) \\ \sigma(15) - \sigma(4) \\ \sigma(14) - \sigma(5) \\ \sigma(13) - \sigma(6) \\ \sigma(12) - \sigma(7) \\ \sigma(11) - \sigma(8) \\ \sigma(10) - \sigma(9) \end{bmatrix} = \frac{1}{18} \begin{bmatrix} 1 & 17 & 289 \\ 0 & -30 & 0 \\ -1 & 13 & -169 \\ 1 & 11 & 121 \\ 0 & -18 & 0 \\ -1 & 7 & -49 \\ 1 & 5 & 25 \\ 0 & -6 & 0 \\ -1 & 1 & -1 \end{bmatrix} \begin{bmatrix} 54 & 54 - 6\pi\sqrt{3} & 3\pi^2 + 6\pi\sqrt{3} - 54 \\ 0 & 6\pi\sqrt{3} & -6\pi\sqrt{3} + 2\pi^2 \\ 0 & 0 & 3\pi^2 \end{bmatrix} \begin{bmatrix} D \sin\phi \\ (\dot{D}/\omega)\cos\phi \\ (\ddot{D}/\omega^2)\sin\phi \end{bmatrix}$$

Premultiplying to get the least-squares solution gives

$$\begin{bmatrix} 1 & 0 & -1 & 1 & 0 & -1 & 1 & 0 & -1 \\ 5 & -10 & 5 & 3 & -6 & 3 & 1 & -2 & 1 \\ 20 & 5 & -10 & 0 & 3 & 6 & -11 & 1 & 13 \end{bmatrix} \begin{bmatrix} \sigma(18) - \sigma(1) \\ \sigma(17) - \sigma(2) \\ \sigma(16) - \sigma(3) \\ \sigma(15) - \sigma(4) \\ \sigma(14) - \sigma(5) \\ \sigma(13) - \sigma(6) \\ \sigma(12) - \sigma(7) \\ \sigma(11) - \sigma(8) \\ \sigma(10) - \sigma(9) \end{bmatrix} \frac{\omega}{\pi}$$

$$= \begin{bmatrix} \frac{1}{3} & 0 & 0 \\ 0 & 210\pi & 0 \\ 0 & 0 & 1148\pi^2 \end{bmatrix} \begin{bmatrix} 54 & 54 + 6\pi\sqrt{3} & 334\pi^2 - 6\pi\sqrt{3} - 54 \\ 0 & \sqrt{3} & \pi - \sqrt{3} \\ 0 & 0 & 1 \end{bmatrix} \begin{bmatrix} D \sin\phi \\ (\dot{D}/\omega)\cos\phi \\ (\ddot{D}/\omega^2)\sin\phi \end{bmatrix}$$

Inverting the square matrices gives

$$f \begin{bmatrix} D \sin\phi \\ (\dot{D}/\omega)\cos\phi \\ (\ddot{D}/\omega^2)\sin\phi \end{bmatrix} = \frac{\pi}{30R} \begin{bmatrix} 1 & -3\sqrt{3} - \pi & -328\pi^2 + 18\pi\sqrt{3} \\ 0 & 3\sqrt{3} & -18\pi\sqrt{3} + 54 \\ 0 & 0 & 54 \end{bmatrix} \begin{bmatrix} 18 & 0 & 0 \\ 0 & 1890\pi & 0 \\ 0 & 0 & 61992\pi^2 \end{bmatrix}^{-1}$$

C.8 BLOCK B NUMERICAL COMPUTATION

The calculations of Block B are performed whenever there is a complete mode or a beginning fragment of Mode 3 or 4. The start of each mode is determined by a change in the mode signal. For Modes 3 and 4, the starting time is considered to be the start of the previous transitional mode (Mode 5). The starting time can be determined either by the change from the previous mode to the transitional mode, or by the change from Mode 5 to Mode 3 or 4 minus a known correction. The time corrections are outlined in Table C-3.

Table C-3. Mode Time Correction

Start of Mode	Mode Change		Time Correction, sec
	from	to	
1	4	1	0
2	1	2	0
3	2	5	0
	5	3	8
4	3	5	0
	5	4	34

The starting time (t_0) is determined by subtracting the time correction from the time a change in mode is detected. If a determination has been made at the start of Mode 5, the redundant determination at the end of Mode 5 should be omitted.

For Modes 1 and 2, the 4-sec accumulations of accelerometer counts are combined into 18 accumulations in the 20R - sec intervals from $t_0 + 300 - 180R$ to $t_0 + 300 + 180R$; therefore,

$$\sigma(j) = \sum_{k=1}^{17} g(k)\, \sigma'(t_0 + 74 + 20j + 4k) \qquad 1 \le j \le 18$$

where

$g(k) = 1$ for $5(j-9)R + 56 \ge 5j + k \ge 5(j-10)R + 57$

$g(k) = 5(j-9)R + 57 - 5j - k$ for $5(j-9)R + 57 > 5j + k > 5(j-9)R + 56$

$g(k) = 5j + k - 56 - 5(j-10)R$ for $5(j-10)R + 57 > 5j + k > 5(j-10)R + 56$

$g(k) = 0$ for $5(j-10)R + 56 \ge 5j + k$
$5(j-9)R + 57 \le 5j + k$

Numerical calculations can best be performed by first forming auxiliary summations as indicated by the following matrix equations. For data from Mode 1

$$\begin{bmatrix} SS(1,0) \\ SS(1,2) \\ SS(1,4) \\ SS(1,6) \end{bmatrix} = \begin{bmatrix} 6\pi & 0 & 0 & 0 \\ 0 & 6\sqrt{3} & 0 & 0 \\ 0 & 0 & 1746\pi\sqrt{3} & 0 \\ 0 & 0 & 0 & 5393976\pi^2\sqrt{3} \end{bmatrix}^{-1}$$

$$\times \begin{bmatrix} 1 & 1 & 1 & 1 & 1 & 1 & 1 & 1 & 1 \\ -1 & 0 & 1 & 1 & 0 & -1 & -1 & 0 & 1 \\ -11 & -26 & -11 & 13 & 22 & 13 & 1 & -2 & 1 \\ -1915 & 500 & 995 & 41 & -244 & 623 & 1100 & 128 & -1228 \end{bmatrix} \begin{bmatrix} \sigma(18) + \sigma(1) \\ \sigma(17) + \sigma(2) \\ \sigma(16) + \sigma(3) \\ \sigma(15) + \sigma(4) \\ \sigma(14) + \sigma(5) \\ \sigma(13) + \sigma(6) \\ \sigma(12) + \sigma(7) \\ \sigma(11) + \sigma(8) \\ \sigma(10) + \sigma(9) \end{bmatrix}$$

$$\begin{bmatrix} SS(1,1) \\ SS(1,3) \\ SS(1,5) \end{bmatrix} = \begin{bmatrix} 18 & 0 & 0 \\ 0 & 5814\pi & 0 \\ 0 & 0 & 52604426\pi^2\sqrt{3} \end{bmatrix}^{-1}$$

$$\times \begin{bmatrix} -1 & -2 & -1 & 1 & 2 & 1 & -1 & -2 & -1 \\ -49 & 4 & 41 & 31 & -4 & -23 & -13 & 4 & 5 \\ -1590 & -3265 & -1570 & -352 & -611 & -364 & 1325 & 2549 & 1329 \end{bmatrix} \begin{bmatrix} \sigma(18) - \sigma(1) \\ \sigma(17) - \sigma(2) \\ \sigma(16) - \sigma(3) \\ \sigma(15) - \sigma(4) \\ \sigma(14) - \sigma(5) \\ \sigma(13) - \sigma(6) \\ \sigma(12) - \sigma(7) \\ \sigma(11) - \sigma(8) \\ \sigma(10) - \sigma(9) \end{bmatrix}$$

For data from Mode 2

$$\begin{bmatrix} SS(2,0) \\ SS(2,2) \\ SS(2,4) \\ SS(2,6) \end{bmatrix} = \begin{bmatrix} 12\pi & 0 & 0 & 0 \\ 0 & 18\sqrt{3} & 0 & 0 \\ 0 & 0 & 210\pi\sqrt{3} & 0 \\ 0 & 0 & 0 & 3024\pi^2\sqrt{3} \end{bmatrix}^{-1}$$

$$\times \begin{bmatrix} 1 & 1 & 1 & 1 & 1 & 1 & 1 & 1 & 1 \\ 1 & -2 & 1 & 1 & -2 & 1 & 1 & -2 & 1 \\ 5 & 0 & -5 & 3 & 0 & -3 & 1 & 0 & -1 \\ 5 & -10 & 5 & -1 & 2 & -1 & -4 & 8 & -4 \end{bmatrix} \begin{bmatrix} \sigma(18) + \sigma(1) \\ \sigma(17) + \sigma(2) \\ \sigma(16) + \sigma(3) \\ \sigma(15) + \sigma(4) \\ \sigma(14) + \sigma(5) \\ \sigma(13) + \sigma(6) \\ \sigma(12) + \sigma(7) \\ \sigma(11) + \sigma(8) \\ \sigma(10) + \sigma(9) \end{bmatrix}$$

$$\begin{bmatrix} SS(2,1) \\ SS(2,3) \\ SS(2,5) \end{bmatrix} = \begin{bmatrix} 18 & 0 & 0 \\ 0 & 1890\pi & 0 \\ 0 & 0 & 61992\pi^2 \end{bmatrix}^{-1}$$

$$\times \begin{bmatrix} 1 & 0 & -1 & 1 & 0 & -1 & 1 & 0 & -1 \\ 5 & -10 & 5 & 3 & -6 & 3 & 1 & -2 & 1 \\ 20 & 5 & -10 & 0 & 3 & 6 & -11 & 1 & 13 \end{bmatrix} \begin{bmatrix} \sigma(18) - \sigma(1) \\ \sigma(17) - \sigma(2) \\ \sigma(16) - \sigma(3) \\ \sigma(15) - \sigma(4) \\ \sigma(14) - \sigma(5) \\ \sigma(13) - \sigma(6) \\ \sigma(12) - \sigma(7) \\ \sigma(11) - \sigma(8) \\ \sigma(10) - \sigma(9) \end{bmatrix}$$

If data are available to compute the summations for consecutive Modes 1 and 2, then calibration calculations are performed to update the values for accelerometer scale factor (f) and bias (b)

$$f = \frac{\pi}{180RA}\Big\{2SS(2,0) - SS(1,0) - 2\sqrt{3}[SS(2,4) + 3SS(1,4)] + \pi\sqrt{3}[2SS(2,6) - 35SS(1,6)]\Big\}$$

$$b = \frac{\pi}{90Rf}\Big\{2SS(1,0) - SS(2,0) + \sqrt{3}[12SS(1,4) + SS(2,4)] + \pi\sqrt{3}[70SS(1,6) - SS(2,6)]\Big\}$$

If either Mode 1 or 2 is not complete, then the previous values of scale factor and bias are used to compute drag acceleration and phase angle.

For Mode 1

$$D(1) = \frac{\pi}{60R}\,\frac{1}{f}\left[SS(1,1) - (6\sqrt{3}-\pi)SS(1,3) - \pi(3086\pi\sqrt{3}-1607)SS(1,5)\right]$$

$$\times\left\{1 + \left[\frac{SS(1,2) - (5\pi - 6\sqrt{3})SS(1,4) - \pi(886\pi - 35\sqrt{3})SS(1,6)}{SS(1,1) - (6\sqrt{3}-\pi)SS(1,3) - \pi(3086\pi\sqrt{3}-1607)SS(1,5)}\right]^2\right\}^{1/2}$$

$$\dot{D}(1) = \left(\frac{\pi}{60R}\right)^2 \frac{1}{f}\left[6SS(1,4) - (194\sqrt{3} - 35\pi)SS(1,6)\right]$$

$$\times\left\{3 + \left[\frac{6\sqrt{3}\,SS(1,3) - (1607\pi - 1938\sqrt{3})SS(1,5)}{6SS(1,4) - (194\sqrt{3} - 35\pi)SS(1,6)}\right]^2\right\}^{1/2}$$

$$\ddot{D}(1) = \left(\frac{\pi}{60R}\right)^3 \frac{1938}{f}\,SS(1,5)\left\{3 + \left[\frac{97SS(1,6)}{323SS(1,5)}\right]^2\right\}^{1/2}$$

$$\phi(1) = \arctan\left[\frac{SS(1,1) - (6\sqrt{3}-\pi)SS(1,3) - \pi(3086\pi\sqrt{3}-1607)SS(1,5)}{SS(1,2) - (5\pi - 6\sqrt{3})SS(1,4) - \pi(886\pi - 35\sqrt{3})SS(1,6)}\right]$$

For Mode 2

$$D(2) = \frac{\pi}{30R}\,\frac{1}{f}\left[SS(2,1) - (3\sqrt{3}+\pi)SS(2,3) - 2\pi(164\pi - 9\sqrt{3})SS(2,5)\right]$$

$$\times\left\{1 + \left[\frac{SS(2,2) - (\pi - \sqrt{3})SS(2,4) - \pi(52\pi + \sqrt{3})SS(2,6)}{SS(2,1) - (3\sqrt{3}+\pi)SS(2,3) - 2\pi(164\pi - 9\sqrt{3})SS(2,5)}\right]^2\right\}^{1/2}$$

$$\dot{D}(2) = \left(\frac{\pi}{30R}\right)^2 \frac{\sqrt{3}}{f}\left[SS(2,4) - (3\sqrt{3}+\pi)SS(2,6)\right]$$

$$\times\left\{1 + 9\left[\frac{SS(2,3) - 6(\pi - \sqrt{3})SS(2,5)}{SS(2,4) - (3\sqrt{3}+\pi)SS(2,6)}\right]^2\right\}^{1/2}$$

$$\ddot{D}(2) = \left(\frac{\pi}{30R}\right)^3 \frac{9}{f} SS(2,5)\left\{36 + \left[\frac{SS(2,6)}{SS(2,5)}\right]^2\right\}^{1/2}$$

$$\phi(2) = \arctan\left[\frac{SS(2,1) - (3\sqrt{3} + \pi)SS(2,3) - 2\pi(164\pi - 9\sqrt{3})SS(2,5)}{SS(2,2) - (\pi - \sqrt{3})SS(2,4) - \pi(52\pi + \sqrt{3})SS(2,6)}\right]^2\Bigg\}^{1/2}$$

For both Modes 1 and 2

$$d(j) = D + 10(2j - 21)\dot{D} + 50(2j - 21)^2\ddot{D} \qquad 1 \le j \le 20$$

For both Modes 3 and 4

$$\sigma(j) = \sum_{k=1}^{5} \sigma'(t_0 + 78 + 20j + 4k) \qquad 1 \le j \le 20$$

For Mode 3

$$d(j) = \frac{\sigma(j)}{20f} - b$$

$$D(3) = -b + \frac{1}{46,816,000f} \sum_{j=1}^{20} (738,507 - 24,519j + 13,663j^2)\sigma(j)$$

For Mode 4

$$d(j) = b - \frac{\sigma(j)}{20f}$$

$$D(4) = b - \frac{1}{46,816,000f} \sum_{j=1}^{20} (-168,245 + 85,349j - 4,257j^2)\sigma(j)$$

For Modes 1, 2, 3, and 4, the time of each drag value is

$$i(j) = t_0 + 90 + 20j$$

The values of d(j) should be computed even for partial Mode 3 or 4. Whenever consecutive Modes 3 and 4 are complete, the bias check Δ should be computed as follows

$$\Delta = \frac{1}{2}\left[D(3) - D(4)\right]$$

A printout should be made for each four-mode calibration cycle of scale factor, bias, phase angles, and bias check. For incomplete cycles not all of these quantities will be available. The format of the printout shall be as shown below:

Time, sec	Scale Factor, pulses/ft/sec	Bias, ft/sec^2	Bias Check, ft/sec^2	Phase 1, deg	Phase 2, deg
t_0 (Mode 1) or t_0 (Mode 3) - 1024	f	b	Δ	$\phi(1)$	$\phi(2)$

In addition, a printout of the 20 values of drag acceleration should be made for each mode. Less than 20 values may be present for partial Mode 3 or 4. The format is shown below:

Time, sec	ft/sec^2	g
i(j)	d(j)	d(j)/32.145

The values of time and acceleration should also be preserved in a form which can be used as the input to a subsequent computer program.

C.9 FLOW CHART

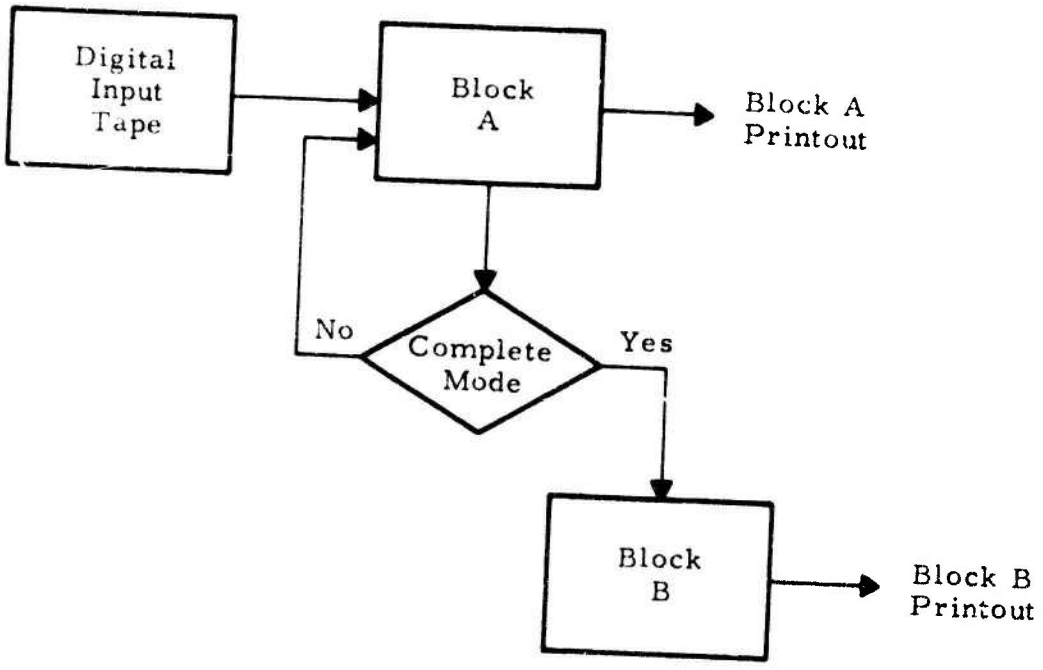

APPENDIX D

LOGACS DATA ANALYSIS PROGRAM

NOTE: A complete development of the computer program and subroutines used for the LOGACS data analysis is presented.

```
      PROGRAM ACCORD (INPUT=1001,OUTPUT=1001,TAPE 61=OUTPUT,
     *                TAPE10=1001,TAPE11=1001,TAPE62=1001)

C     ACCELEROMETER COUNT REDUCTION    DR037A    PROGRAMMER  P.G.BLANDIN
C     THIS PROGRAM PERFORMS THE LOGACS ACCELEROMETER CALIBRATIONS
C     SPECIFIED BY J.T.EPHGRAVE IN AIM-68(3113-02)-6
C     SECOND ORDER FITTING * * * *

      INSERT
      COMMON /BCYCLE/ FRAME(16), TBIAS(4), L, KMANY, TAU1, TAU2, TAU3
      DATA TBIAS,L,KMANY,TAU1,TAU2,TAU3/2*0.,.5,.34,.5,10,3*3./
      COMMON /FLAGWD/ FLAG
      DATA  FLAG/ 999999999./
      COMMON /LOCATE/ TIMEWD,ASWTCH,BSWTCH,MODEWD,KOUNT1,KOUNT2,THRUST
      INTEGER         TIMEWD,ASWTCH,BSWTCH,                   THRUST
      DATA            TIMEWD,ASWTCH,BSWTCH,MODEWD,KOUNT1,KOUNT2,THRUST
     *              /      1,     2,     3,     4,     5,     6,     7 /
      COMMON /OPTION/ IEDIT,IVENT
      DATA IEDIT,IVENT/2*2HNO/
      COMMON KRAY(1027)
      DIMENSION  BCNSTS(4),ITAB(15),DATA(256,7,4),SIG(128,4),T0(5),MS(4)
      DIMENSION LABELS(16), FLABEL(16)
      EQUIVALENCE (LABELS,FLABEL)
      DATA START,STOPD/-1.E5,1.E9/, IX/3/
      DATA BCNSTS /1.123735561,0.0007,400000.0,0.0/
      DATA LABELS/6HTIME  ,6HSWTCHA,6HSWTCHB,6HMODE  ,6HCOUNT1,6HCOUNT2
     *           ,6HTHRUST,6H      /

      DATA ITAB/6HSTART ,6HSTOP  ,6HLABELS,6HRATIO ,6HACCENT,6HSCALE
     *         ,6HBIAS  ,6HTAU1  ,6HTAU2  ,6HTAU3  ,6HTBIAS ,6HTHNSNT
     *         ,6HKMANY ,6HEDIT  ,6HEVENTS/

      CALL CARDS(15,
     *           START,STOPD,LABELS,BCNSTS(1),BCNSTS(2),BCNSTS(3),
     *           BCNSTS(4),TAU1,TAU2,TAU3,TBIAS,L,KMANY,IEDIT,IVENT,
     *           ITAB,I)
      IF(I.NE.1) STOP
C
      CALL OUTAPE(1)

      DIMENSION IN(512)
      REWIND 1
```

```
      CALL RDTR(11,IN,6HACCEPT,I)
      J=IN+2
      WRITE(61,100) (IN(I),I=1,J)
  100 FORMAT(33H1  INPUT TAPE IDENTIFICATION FILE,3I5,      /
     .       (9X10A10)//)
      CALL RDTR(11,IN,6HACCEPT,I)
      IF(I.NE.2) STOP 100

      CALL BLOCKB(BCNSTS)

      DO 2 I=1,16
    2 FRAME(I)=FLABEL(I)
    5 CALL LOADER(FRAME,IX)
      IF(IX.EQ.1) GO TO 20
      WRITE(61,200)   $STOP200
  200 FORMAT(31H0*** CANNOT FIND START TIME *** )
   20 IF(FRAME(TIMEWD).LT.START) GO TO 5
   50 CALL CYCLE(DATA,T0)

      WRITE(61,40)
   40 FORMAT(1H0,9X36HTIME(SEC)  MODE  ACCELEROMETER COUNT/;
      DO 10 K=1,4
   10 CALL BLOCKA(DATA(1,1,K),SIG(1,K))
      IF(IVENT.EQ.3HYES) CALL EVENTS(DATA(1,1,1))
      CALL BLOCKB(T0,SIG)
      IF(T0.GE.STOPD) STOP 77
      GO TO 50

      END ACCORD
```

```
      SUBROUTINE BLOCKA (DATA,SIG)
*     THIS SUBROUTINE PERFORMS THE BLOCK-A CALCULATIONS FOR EACH MODE.
*       DATA IS THE ARRAY OF FRAMES FOR ONE MODE.
*       SIG  IS THE ARRAY SIGMA PRIME.  - THE CORRECTED TOTAL OF
*            ACCELEROMETER PULSES ACCUMULATED OVER 4-SECOND INTERVALS.
      INSERT,LOCATE,FLAGWD,OPTION.
      EQUIVALENCE (NTYM,TIMEWD),(MODE,MODEWD),(K1,KOUNT1),(K2,KOUNT2)
     .          ,(KJ,THRUST),(IF,TIMEWD)
      DIMENSION DATA(256,7), SIG(128)
*       CHECK DATA FOR THRUSTER ACTIVITY
      J=JET(DATA(1,KJ))
      IF(IEDIT.EQ.2HNO) J=0
      IF(J.NE.0) DATA(1,K1)=FLAG
      IF(J.GE.2) DATA(1,K2)=FLAG

      DO 2 I=2,256
      IF(DATA(I,IF).EQ.FLAG) GO TO 2
      J=JET(DATA(I,KJ))
      IF(IEDIT.EQ.2HNO) J=0
      IF(J.EQ.0) GO TO 2
                 DATA(I,K1)=FLAG
      IF(J.GE.2) DATA(I,K2)=FLAG
      IF(J.A.1)DATA(I-1,K2)=FLAG
    2 CONTINUE
*
*       DO FIRST PAIR OF ACCUMULATIONS
      SIG(1)=SUM(DATA(1,K1),DATA(1,K2),DATA(2,K1),DATA(2,K2))
      SIG(2)=SUM(DATA(3,K1),DATA(3,K2),DATA(4,K1),DATA(4,K2))

      MISS=0
      MPRYNT=1

      WRITE(61,70) DATA(2,NTYM), DATA(2,MODE), SIG(1)
*       PROCESS REST OF DATA SET
```

```
      DO 6 I=1,126
      L=I+1
      MPHYNT(I)=MPHYNT+1
      SIG(I)=SUM(DATA(L-1,K1),DATA(L-1,K2),DATA(L,K1),DATA(L,K2))
      IF(SIG(I).NE.FLAG) MISS=0
      IF(SIG(I).NE.FLAG) GO TO 7
*
*       EXTRAPOLATE UP TO 20 SECONDS
      IF(MISS.GE.5) GO TO 7
      MISS=MISS+1
      SIG(I)=.5*(SIG(I-1)+SIG(I-2))
      IF(ABS(SIG(I)).GT.8000.) SIG(I)=FLAG
*
*       PRINT OUT SAMPLE AT ONE MINUTE
    7 IF(MPHYNT.LT.15) GO TO 8
      MPHYNT=0
                    MYS=1H*
      IF(MISS.EQ.0) MYS=1H
      WRITE(61,70) DATA(L,NTYM),DATA(L,MODE),SIG(I),MYS
   70 FORMAT(1OXF7.5AF2.7XF5.2XA1)
    8 CONTINUE

      RETURN

      END BLOCKA
```

```
      SUBROUTINE BLOCKB(T0,SIG)

*     THIS SUBROUTINE PERFORMS THE BLOCK-B CALCULATIONS FOR THE 4 MODES
*     OF A CALIBRATION CYCLE.
*     THE PROGRAM MUST BE CALLED ONCE (FIRST) TO LOAD INITIAL VALUES.
*       MS  IS A 4-VECTOR GIVING THE STATUS OF EACH MODE.
*           .EQ.0 - INCOMPLETE MODE - NO CALCULATIONS WILL BE MADE
*           .GT.0 - MODE DATA IS COMPLETE
*           .LT.0 - PARTIAL FRAGMENT OF MODE DATA   (MODES 3 AND 4 ONLY)
*       T0  IS A 4-VECTOR GIVING THE START TIMES OF EACH MODE.
*           (THIS ARRAY CONTAINS CONSTANTS ON THE FIRST CALL)
*       SIG IS THE ARRAY SIGMA PRIME. - THE CORRECTED TOTAL OF
*           ACCELEROMETER PULSES ACCUMULATED OVER 4-SECOND INTERVALS.


      INSERT,FLAGWD.
      COMMON KRAY(1027)
      DIMENSION  MS(4), T0(4), SIG(128,4)
      DIMENSION  SS(2,7), SAG(20,4), DRAG(20,4), QUANT(6), TRIX(9,3,4)
      DIMENSION  VECT(9,2), SPUR(4,3)
      EQUIVALENCE (VECT,SPUR)
      REAL  KB, KB4, KB6, KF, KF4, KF6

      DATA EXFLAG/1777000000000000000B/
      DATA PI/3.1415926536/, CDEG/57.29578/
      DATA TRIX /   -1,    0,    1,    1,    0,   -1,   -1,    0,    1,
     .             -11,  -26,  -11,   13,   22,   13,    1,   -2,    1,
     .           -1915,  500,  995,   41, -244,  623, 1100,  128,-1228,
     .              -1,   -2,   -1,    1,    2,    1,   -1,   -2,   -1,
     .             -49,    4,   41,   31,   -4,  -23,  -13,    4,    5,
     .           -1590,-3265,-1570, -352, -611, -364, 1325, 2549, 1329,
     .               1,   -2,    1,    1,   -2,    1,    1,   -2,    1,
     .               5,    0,   -5,    3,    0,   -3,    1,    0,   -1,
     .               5,  -10,    5,   -1,    2,   -1,   -4,    8,   -4,
     .               1,    0,   -1,    1,    0,   -1,    1,    0,   -1,
     .               5,  -10,    5,    3,   -6,    3,    1,   -2,    1,
     .              20,    5,  -10,    0,    3,    6,  -11,    1,   13 /
*
*       HAVE INITIAL CALCULATIONS BEEN MADE
      IF(INITAL.EQ.1) GO TO 10

*** INITIALIZE ROUTINE ***
```

```
      INITAL=1
*       LOAD CONSTANTS FROM THE ARRAY TO
      RAT=TO(1)    $ACCENT=TO(2)    $SCAL=TO(3)    $BIAS=TO(4)
      RAT5=RAT*5.      $RSCAL=1./SCAL
      SQRT3=SQRT(3.)

*     SET MATRIX ELEMENTS
      SPUR(1,1)=1./ 6./SQRT3  $SPUR(1,2)=1./(1746.*PI*SQRT3)
      SPUR(2,1)=1./18.        $SPUR(2,2)=1./(5814.*PI)
      SPUR(3,1)=1./18./SQRT3  $SPUR(3,2)=1./( 210.*PI*SQRT3)
      SPUR(4,1)=1./18.        $SPUR(4,2)=1./(1890.*PI)
      SPUR(1,3)=1./( 5393976.*PI*PI*SQRT3)
      SPUR(2,3)=1./(52604426.*PI*PI*SQRT3)
      SPUR(3,3)=1./(    3024.*PI*PI*SQRT3)
      SPUR(4,3)=1./(   61992.*PI*PI)
      DO 2 K=1,4
      DO 2 J=1,3
      DO 2 I=1,9
   2  TRIX(I,J,K)=FLOAT(TRIX(I,J,K))*SPUR(K,J)

*       SET COEFFICIENTS FOR BLOCK-B EQUATIONS
      KF=PI/(180.*RAT*ACCENT) $KF4=-2.*SQRT3  $KF6=PI*SQRT3
      KB=PI/(90.*RAT)         $KB4=SQRT3      $KB6=PI*SQRT3
      CD1 = PI/60./RAT        $CD2 = PI/30./RAT
      CD13=-(6.*SQRT3-PI)     $CD15=-PI*(3086.*PI*SQRT3-1607.)
      CD14=-(5.*PI-6.*SQRT3)  $CD16=-PI*(886.*PI-35.*SQRT3)
      CD23=-(3.*SQRT3-PI)     $CD25=-2.*PI*(164.*PI-9.*SQRT3)
      CD24=-(PI-SQRT3)        $CD26=-PI*(52.*PI-SQRT3)
      CDD13=6.*SQRT3          $CDD15=-(1607.*PI-1938.*SQRT3)
      CDD14=6.                $CDD16=-(194.*SQRT3-35.*PI)
      CDD23=3.                $CDD25=-18.*(PI-SQRT3)
      CDD24=1.                $CDD26=-(3.*SQRT3-PI)
      CGRAV=1./32.145
      RETURN
*
  1(  M=1
*** ESTABLISH MODE STATUS ***
      MS(1)=1    $MS(2)=2    $MS(3)=0    $MS(4)=0
      DO 4 I=25,126
      IF(SIG(I,1).EQ.FLAG) MS(1)=0
      IF(SIG(I,2).EQ.FLAG) MS(2)=0
   4  CONTINUE
```

```
      DO 6 I=26,125
      IF(SIG(I,3).NE.FLAG) MS(3)=MS(3)+1
      IF(SIG(I,4).NE.FLAG) MS(4)=MS(4)+1
    6 CONTINUE
      IF(MS(3).LT.100) MS(3)=-MS(3)
      IF(MS(4).LT.100) MS(4)=-MS(4)
      DO 8 I=1,80
    8 DRAG(I)=EXFLAG

*** COMPUTE THE BLOCK-8 EQUATIONS ***
   11 IF(MS(M).EQ.0) GO TO 14

*       THE FOUR-SECOND ACCUMULATIONS ARE COMBINED INTO 18 ACCUMULATIONS
*       IN THE 20R-SECOND INTERVALS FROM  T0+300-180R  TO  T0+300+180R.
      DO 13 J=1,18
      RJ=J-10
      SAG(J,M)=0.
      DO 13 K=1,17
      L= J*5+K
      RJL=RJ*RAT5 + FLOAT(56-L)
      L= L + 19
                              G=0.0
      IF(RJL.GT.-RAT5-1.)G=RJL+RAT5+1.0
      IF(RJL.GE.-RAT5)    G=1.0
      IF(RJL.GT.-1.0)     G=-RJL
      IF(RJL.GE.0.0)      G=0.0
   13 SAG(J,M)=SAG(J,M) + G*SIG(L,M)

   14 IF(M.EQ.2) GO TO 15
      M=2    $GO TO 11
*
   15 IF(MS(1).EQ.0) GO TO 20

*       WEIGHTED SUMS FOR MODE 1
      DO 16 I=1,9
      VECT(I,1)=SAG(19-I,1)+SAG(I,1)
   16 VECT(I,2)=SAG(19-I,1)-SAG(I,1)


      SS(1,1)=VDOT(TRIX(1,1,2),VECT(1,2))
      S(1,2)=VDOT(TRIX(1,1,1),VECT(1,1))
```

```
      SS(1,3)=VDOT(TRIX(1,2,2),VECT(1,2))
      SS(1,4)=VDOT(TRIX(1,2,1),VECT(1,1))
      SS(1,5)=VDOT(TRIX(1,3,2),VECT(1,2))
      SS(1,6)=VDOT(TRIX(1,3,1),VECT(1,1))

*     THE AUXILARY SUMMATION TERM INDEXED AS 0 IN EQUATIONS IS 7 HERE.
      SS(1,7)=0.
      DO 18 I=1,9
   18 SS(1,7)=SS(1,7)+VECT(I,1)
      SS(1,7)=SS(1,7)/6./PI
*
   20 IF(MS(2).EQ.0) GO TO 30

*       WEIGHTED SUMS FOR MODE 2
      DO 22 I=1,9
      VECT(I,1)=SAG(19-I,2)+SAG(I,2)
   22 VECT(I,2)=SAG(19-I,2)-SAG(I,2)

      SS(2,1)=VDOT(TRIX(1,1,4),VECT(1,2))
      SS(2,2)=VDOT(TRIX(1,1,3),VECT(1,1))
      SS(2,3)=VDOT(TRIX(1,2,4),VECT(1,2))
      SS(2,4)=VDOT(TRIX(1,2,3),VECT(1,1))
      SS(2,5)=VDOT(TRIX(1,3,4),VECT(1,2))
      SS(2,6)=VDOT(TRIX(1,3,3),VECT(1,1))

      SS(2,7)=0.
      DO 24 I=1,9
   24 SS(2,7)=SS(2,7)+VECT(I,1)
      SS(2,7)=SS(2,7)/12./PI



      IF(MS(1).EQ.0) GO TO 35

*       UPDATE ACCELEROMETER BIAS AND SCALE FACTOR
      SCAL=(SS(2,7)+SS(2,7)-SS(1,7)+KF4*(SS(2,4)+3.*SS(1,4))
     .     +KF6*(SS(2,6)+SS(2,6)-35.*SS(1,6)))*KF

      RSCAL=1./SCAL

      BIAS=(SS(1,7)+SS(1,7)-SS(2,7)+KB4*(SS(1,4)*12.+SS(2,4))
```

```
     .      *FMAX(7.*SS(1,6)-SS(2,6)))*KB*RSCAL
     .
    3   IF(MS(1).EQ.0) GO TO 35
     .
     .        COMPUTE DRAG VALUES AND TURNTABLE PHASE ANGLE FOR MOVE 1
          DX = SS(1,1) + CD13*SS(1,3) + CD15*SS(1,5)
          DY = SS(1,2) + CD14*SS(1,4) + CD16*SS(1,6)
          DRGAV= CD1*RSCAL*DX*SQRT(1.+DY*DY/(DX*DX))
          DDX= CDD14*SS(1,4) + CDD16*SS(1,6)
          DDY= CDD13*SS(1,3) + CDD15*SS(1,5)
          DDRGAV=CD1*CD1*RSCAL*DDX*SQRT(3.+DDY*DDY/(DDX*DDX))
          DDDRAG=CD1*CD1*CD1*RSCAL*1938.*SS(1,5)
         .      *SQRT(3.+9409.*SS(1,6)*SS(1,6)/(104329.*SS(1,5)*SS(1,5)))
          PHI1 = .5*PI-ATAN2(DY,DX)

          DO 32 J=1,20
          FLJ=FLOAT(2*J-21)
    32    DRAG(J,1)=-(DRGAV+DDRGAV*FLJ*10.+DDDRAG*FLJ*FLJ*50.)



    35    IF(MS(2).EQ.0) GO TO 40
     .
     .        COMPUTE DRAG VALUES AND TURNTABLE PHASE ANGLE FOR MOVE 2
          DX = SS(2,1) + CD23*SS(2,3) + CD25*SS(2,5)
          DY = SS(2,2) + CD24*SS(2,4) + CD26*SS(2,6)
          DRGAV= CD2*RSCAL*DX*SQRT(1.+DY*DY/(DX*DX))
          DDX= CDD24*SS(2,4) + CDD26*SS(2,6)
          DDY= CDD23*SS(2,3) + CDD25*SS(2,5)
          DDRGAV=CD2*CD2*RSCAL*SQRT3*DDX*SQRT(1.+DDY*DDY/(DDX*DDX))
          DDDRAG=CD2*CD2*CD2*RSCAL*9.*SS(2,5)
         .      *SQRT(36.+SS(2,6)*SS(2,6)/(SS(2,5)*SS(2,5)))
          PHI2 = .5*PI-ATAN2(DY,DX)

          DO 37 J=1,20
          FLJ=FLOAT(2*J-21)
    37    DRAG(J,2)=-(DRGAV+DDRGAV*FLJ*10.+DDDRAG*FLJ*FLJ*50.)
     .
    40    IF(MS(3).EQ.0) GO TO 45
     .
     .        THE FOUR-SECOND ACCUMULATIONS ARE COMBINED INTO 20 ACCUMULATIONS
```

```
C       IN THE 20-SECOND INTERVALS FROM  T0+100  TO  T0+500  FOR MODE 3

      DO 42 J=1,20
      SAG(J,3)=0.0
      DO 41 K=1,5
      L= J*5+K + 20
   41 SAG(J,3)=SAG(J,3) + SIG(L,3)

C       DRAG VALUES COMPUTED FOR MODE 3
      DRAG(J,3)=FLAG
      IF(SAG(J,3).GE.+0000.) GO TO 42
      DRAG(J,3)=SAG(J,3)/(20.*SCAL) -BIAS
   42 CONTINUE



      IF(MS(3).LT.0) GO TO 45

      DRGAV3=0.0
      DO 43 J=1,20
      FLJ=FLOAT(J)
   43 DRGAV3=DRGAV3+SAG(J,3)*(738507.-24519.*FLJ+1363.*FLJ*FLJ)
      DRGAV3=DRGAV3/40816000.*RSCAL-BIAS
C
   45 IF(MS(4).EQ.0) GO TO 50

C       THE FOUR-SECOND ACCUMULATIONS ARE COMBINED INTO 20 ACCUMULATIONS
C       IN THE 20-SECOND INTERVALS FROM  T0+100  TO  T0+500  FOR MODE 4

      DO 47 J=1,20
      SAG(J,4)=0.0
      DO 46 K=1,5
      L= J*5+K + 20
   46 SAG(J,4)=SAG(J,4) + SIG(L,4)

C       DRAG VALUES COMPUTED FOR MODE 4
      DRAG(J,4)=FLAG
      IF(SAG(J,4).GE.40000.) GO TO 47
      DRAG(J,4)=BIAS - SAG(J,4)/(20.*SCAL)
   47 CONTINUE
```

```
      IF(MS(4).LT.0) GO TO 50

      DRGAV4=0.0
      DO 40 J=1,20
      FLJ=FLOAT(J)
   40 DRGAV4=DRGAV4+SAG(J,4)*(-168245.+85349.*FLJ-4257.*FLJ*FLJ)
      DRGAV4=-145-RSCAL*DRGAV4/46816000.


      IF(MS(3).LE.0) GO TO 50

*       BIAS CHECK COMPUTED IF MODES 3 AND 4 ARE COMPLETE
      BIASCK=.5*(DRGAV3-DRGAV4)
*
*** OUTPUT DRAG VALUES AND CYCLE SUMMARY ***


   50 DO 52 I=1,6
   52 QUANT(I)=EXPLAG

*       LOAD CYCLE SUMMARY QUANTITIES
                      QUANT(1)=T0(1)
      IF(MS(1).NE.0) QUANT(5)=PHI1*CUEG
      IF(MS(2).NE.0) QUANT(6)=PHI2*CUEG
      IF((MS(1).EQ.0).OR. (MS(2).EQ.0)) GO TO 55
                      QUANT(2)=SCAL
                      QUANT(3)=BIAS
   55 IF((MS(3).NE.0).AND.(MS(4).NE.0)) QUANT(4)=BIASCK

      WRITE(61,560)
      WRITE(61,561) QUANT
      WRITE(62,561) QUANT


*       OUTPUT DRAG VALUES
      DO 68 I=1,4
      IF(MS(I).EQ.0) GO TO 68
      WRITE(61,601) I
      DO 65 J=1,20
      QUANT(2)=EXPLAG    $QUANT(3)=EXPLAG
```

```
      QUANT=T0(I)+FLOAT(J-20+90)
      IF(IDRAG(J,I).EQ.FLAG) GO TO 65
      QUANT(2)=DRAG(J,I)    $QUANT(3)=DRAG(J,I)*CGRAV
      CALL ADVR(2,ARAY,1,QUANT,K)
      IF(K.EQ.2) CALL OUTAPE(2)
   65 WRITE(61,650)(QUANT(K),K=1,3)

   66 CONTINUE

      RETURN

C
  560 FORMAT(75H1    TIME      SCALE FACTOR          BIAS          BIAS CHECK
     +     PHASE1    PHASE2
     +       /75H    (SEC)      (PULSE/FT/SEC)       (FT/SEC2)       (FT/SEC2)
     +     (DEGS)    (DEGS)   )
  561 FORMAT(      2X  F6.     5X     E11.4,      6X     E11.4,  3X     E11.4,
     +   4X F7.2, 2X F7.2 //)

  631 FORMAT(/13X32HTIME  MODE      DRAG ACCELERATION/12X5H(SEC)I5,2X
     +         11H  (FT/SEC2)  7X 3H(G) /)

  650 FORMAT(10XF7.8AE11.4,2XE11.4)

      END BLOCKH
```

```
      SUBROUTINE CYCLE(DATA,T0)

      INSERT,=CYCLE,LOCATE,FLAGWD.
      DIMENSION  DATA(256,7,4), T0(5), LTIME(4)

*     THIS SUBROUTINE FILLS THE CYCLE DATA BLOCK WITH INPUT FRAMES.
*     MODE AND MODE CHANGES ARE MATCHED AGAINST TIME TO DEFINE CYCLE.

*       DATA   - DATA BLOCK FOR THE CYCLE
*       FLAG   - THE (DEFINITE) REAL MISSING POINT FLAG
*       FRAME  - INPUT AREA FOR DATA FROM TAPE11
*       L      - TRANSIENT MODE INDICATOR
*       LTIME  - FLAG FOR MODE START TIMES (HOW DETERMINED)
*       K      - MODE OF PRESENT FRAME
*       KMANY  - MAXIMUM KOUNT ALLOWABLE
*       KOUNT  - COUNTER FOR ABNORMAL FRAMES
*       M      - MODE OF LAST FRAME USED
*       MODE   - EFFECTIVE MODE OF DATA
*       MODEWD - RELATIVE LOCATION OF MODE WORD IN DATA FRAME
*       NDATA  - END OF DATA FLAG
*       S      - TIME OF PRESENT FRAME
*       T      - TIME OF LAST FRAME USED
*       T0(M)  - START TIME FOR THE MTH MODE  (T0(5) IS CYCLE-END TIME)
*       TAU1   - TIME TOLERENCE FOR MODE TRANSITION IN SYNC-SEARCH
*       TAU2   - TIME TOLERENCE FOR NEXT CYCLE DEFINITION
*       TAU3   - TIME TOLERENCE FOR MODE TRANSITION IN CYCLE LOADING
*       THIAS  - AN ARRAY OF CORRECTIONS FOR THE CYCLE START TIME
*       TIMEWD - RELATIVE LOCATION OF TIME WORD IN DATA FRAME
*
      IF(NDATA.NE.0) GO TO 90

*** SEARCH FOR CYCLE SYNC-TIME DEFINED BY FIRST-ORDER MODE TRANSITION **

   10 J=1    $KOUNT=0
   12 IF(FRAME(MODEWD).EQ.M)          GO TO 20
      IF(FRAME(TIMEWD).GT.(T+TAU1)) GO TO 20

*       IS THIS A FIRST-ORDER MODE TRANSITION
      K=FRAME(MODEWD)              $ MODE=0
      IF((M.EQ.4).AND.(K.EQ.1)) MODE=1
      IF((M.EQ.1).AND.(K.EQ.2)) MODE=2
      IF((M.EQ.2).AND.(K.EQ.L)) MODE=3
```

```
      IF ((MODE.EQ.L).AND.(K.EQ.3)) MODE=3
      IF ((MODE.EQ.3).AND.(K.EQ.L)) MODE=4
      IF ((MODE.EQ.L).AND.(K.EQ.4)) MODE=4
      IF(MODE.NE.0) GO TO 30

C       STORE CURRENT MODE-TIME AND READ A NEW FRAME
   20 M=FRAME(MODEWD)    ST=FRAME(TIMEWD)
      CALL LOADER(FRAME,J)
      FRAME(MODEWD)=ABS(FRAME(MODEWD))
      IF(J.EQ.1) GO TO 12
      GO TO 99

C       SYNC-TIME HAS BEEN FOUND
   30 S=FRAME(TIMEWD)
      T0(1)=S-FLOAT((MODE-1)*512)
      IF(M.EQ.L) T0(1)=T0(1)-TBIAS(K)
      DO 31 I=1,4
      LTIME(I)=0
   31 T0(I+1)=T0(1)+FLOAT(I*512)
      LTIME(MODE)=1
      WRITE(61,370) M,K,S
   37 FORMAT(46H1 CYCLE SYNC-TIME HAS BEEN FOUND WITH A I1,1H= I1,
     .       32H MODE TRANSITION AT TIME(SECS) =F7)

C       CLEAR DATA AREA
      DO 35 I=1,7168
   35 DATA(I)=FLAG
C
C*** LOAD CYCLE DATA ***
   40 J=(S-T0(MODE))*.5 + 1.2
      IF(J.GT.256) GO TO 49

C       LOAD THIS FRAME
      M=F    ST=S

      DO 42 I=1,7
   42 DATA(J,I,MODE)=FRAME(I)


C       READ ANOTHER FRAME
   45 I=1     CALL LOADER(FRAME,I)
```

```
      FRAME(MODEWD)=ABS(FRAME(MODEWD))
      IF(I.EQ.1) GO TO 47
      NDATA=1    $RETURN

   47 K=FRAME(MODEWD)    $S=FRAME(TIMEWD)
      IF(S.GE.T0(5)) RETURN
      IF(K.NE.M) GO TO 50
      IF(S.LT.T0(MODE+1))GO TO 40
      IF(K.EQ.L) GO TO 54

*       ABNORMAL MODE-TIME BEHAVIOR
   49 KOUNT=KOUNT+1
      IF(KOUNT.LT.KMANY) GO TO 45
*       ABORT THIS CYCLE - RESUME SEARCH
      WRITE(61,490) KMANY
  490 FORMAT(4H0***I3,46H ABNORMAL FRAMES HAVE BEEN READ - RESETTING **)
      GO TO 10

*** MODE TRANSITION ***

   50 IF(K.NE.1) GO TO 52
      IF(S.GE.(T0(5)-TAU2)) RETURN
      GO TO 49

   52 IF(M.EQ.4) GO TO 49
      IF((K.EQ.2).A.(M.NE.1)) GO TO 49

      I=K
      IF(K.NE.L) GO TO 56
   54                                                          I=0
      IF((S.GT.(T0(3)-TAU3)).AND.(S.LE.(T0(3)+TBIAS(3)))) I=3
      IF((S.GT.(T0(4)-TAU3)).AND.(S.LE.(T0(4)+TBIAS(4)))) I=4
      IF(I.NE.0) GO TO 58
      GO TO 49

   56 IF((S.LE.(T0(I)-TAU3)).OR.(S.GT.T0(I+1))) GO TO 49
   58 IF((LTIME(I).NE.0).OR.(S.GT.(T+TAU1))) GO TO 60

      T0(I)=S
      LTIME(I)=1
      IF(M.EQ.L) T0(I)=T0(I)-TBIAS(I)
```

```
      GO TO 40

C
C     TERMINATE PROCESSING
   40 CONTINUE
      REWIND 11
      WRITE(61,900)
  900 FORMAT(12H1 END OF JOB)
      CALL OUTAPE(3)

      END CYCLE
```

```
      SUBROUTINE EVENTS(DATA)
*     THIS SUBROUTINE REVIEWS THE CYCLE DATA AND PRINTS OUT A HISTORY
*     OF THE PICKOFF SWITCH SIGNALS AND THE THRUST VALVE FIRINGS.
      INTEGER,LOCATE,FLAGWD.
      EQUIVALENCE (NTYM,TIMEWD),(NSWA,ASWTCH),(NSWB,BSWTCH),(KJ,THRUST)
      DIMENSION DATA(256,7,4)
      DIMENSION T(14),KEY(6)

      WRITE(61,1)
      WRITE(61,10)
      DO 3 I=1,14
    3 T(I)=0.
      DO 8 K=1,4
      DO 8 J=1,256
      TYM=DATA(J,NTYM,K)
      IF(TYM.EQ.FLAG) GO TO 8
*       LOAD PICKOFF SWITCH TIMES
      T(1)=DATA(J,NSWA,K)
      T(2)=DATA(J,NSWB,K)
*       CHECK FOR OCCURRENCE OF ANY EVENT
      IF((DATA(J,KJ,K)+T(1)+T(2)).EQ.0.) GO TO 8
*       LOAD THRUSTER SIGNAL TIMES
      CALL FIRINGS(DATA(J,KJ,K),KEY)
      DO 6 I=1,6
      T(2*I+1)=0.     $ T(2*I+2)=0.
      IF (KEY(I).GE.2) T(2*I+2)=TYM+1.
      IF(KEY(I).AND.1) T(2*I+1)=TYM
    6 CONTINUE
      WRITE(61,20) T
    8 CONTINUE
      RETURN

    1 FORMAT(1H1)
   10 FORMAT(1X10HH TIME SWA  TIME SWB     THRUSTER 1      THRUSTER 2
     .THRUSTER 3      THRUSTER 4      THRUSTER 5      THRUSTER 6/)
   20 FORMAT(2(1XF9.2),6(2XF6.1XF6))
      END EVENTS
```

```
      SUBROUTINE FIRINGS(WORD,KEY)
      INSERT,FLAGWD.
      DIMENSION KEY(6)

*     THIS SUBROUTINE EXAMINES THE THRUST VALVE WORD TO DETERMINE THE
*     STATUS OF EACH OF THE SIX(6) THRUSTERS AND RETURNS IN KEY A
*        0 = NO THRUSTER FIRING
*        1 = FIRING IN FIRST HALF OF FRAME
*        2 = FIRING IN LAST  HALF OF FRAME
*        3 = FIRING IN EACH  HALF OF FRAME

      DO 1 I=1,6
    1 KEY(I)=0
      IF(WORD.EQ.0.) RETURN
      IF(WORD.EQ.FLAG) RETURN

*       ADD SEVENTH DIGIT TO GET LEADING ZEROS
      DROW=WORD+1000000.
      ENCODE(10,10,I) DROW
   10 FORMAT(F10)
      DECODE(10,20,I) KEY(6),KEY(5),KEY(4),KEY(3),KEY(2),KEY(1)
   20 FORMAT(4X6I1)

      RETURN
      END OF FIRINGS
```

```
      FUNCTION JET(THRUST)
      DIMENSION KEY(6)

*     THIS FUNCTION EXAMINES THE THRUST VALVE WORD AND RETURNS A
*        0 - NO THRUSTER FIRINGS
*        1 - FIRING IN FIRST HALF OF FRAME
*        2 - FIRING IN LAST  HALF OF FRAME
*        3 - FIRING IN EACH  HALF OF FRAME


      CALL FIRINGS(THRUST,KEY)
      JET= KEY(1).OR.KEY(2).OR.KEY(3).OR.KEY(4).OR.KEY(5).OR.KEY(6)
      RETURN

      END JET
```

```
      SUBROUTINE LOADER(FRAME,IX)
*     THIS SUBROUTINE READS A STANDARD DATA TAPE AND RETURNS ONE FRAME.
*     THE FRAME IS EDITED TO THE SPECIFIED ELEMENTS WHICH ARE ENTERED ON
*     THE FIRST DATA CALL.  (IX SHOULD BE SET TO 3 AND THE ARRAY -FRAME-
*     CONTAINS UP TO 16 6-CHARACTER ELEMENT-IDENTIFIERS.  A BLANK LABEL
*     WILL TERMINATE THE FRAME DEFINITION.  A LABEL OF -ZERO  - WILL PUT
*     A ZERO IN THAT POSITION OF THE FRAME FOR ALL DATA FRAMES RETURNED)
*       IX IS AN EXIT STATUS INDICATOR WITH THE FOLLOWING MEANINGS
*         =1 NORMAL DATA RETURN
*         =2 END OF DATA FILE HAS BEEN READ
*         =3 ESTABLISH FRAME DEFINITION (SET ON FIRST ENTRY)
*         =4 INPUT TAPE HAS BEEN CONTINUED ON NEW REEL (INTERNAL)
*         =5 END OF INPUT TAPE HAS BEEN REACHED
      DIMENSION  FRAME(16),IRAY(1027),NDEX(16),TEMP(16),ZERO(2)
      EQUIVALENCE  (TEMP,ZERO(2)), (RK,K)
      DATA ZERO/0./


      IF(IX.GT.1) GO TO 40
*       LOAD DATA FRAME
   10 CALL RDVR(2,IRAY,6HACCEPT,1,TEMP,I,IX)
      IF(IX.EQ.2) GO TO 20
      DO 15 I=1,N
      J=NDEX(I)
   15 FRAME(I)=TEMP(J)
      RETURN
*       CHECK FOR CONTINUED REEL
   20 CALL RDTR(11,IRAY,6HACCEPT,I)
      IF((I.EQ.1).AND.(IRAY(2).EQ.-5)) GO TO 22
      IF(IRAY(2).EQ.5) IX=5    $BACKSPACE 11    $RETURN
   22 CALL RUNTP(11)    $CALL REMARK(32HEND OF TAPE 11 - MOUNT NEXT REEL)
      REWIND 11    $CALL RDTR(11,IRAY,6HACCEPT,J)
      I=IRAY*2     $WRITE(61,200) (IRAY(K),K=1,I)
      CALL RDTR(11,IRAY,6HACCEPT,I)    $IX=4
      IF((I.EQ.2).AND.(J.EQ.1)) GO TO 40
      WRITE(61,220)    $STOP 220
*
*       READ DATA FILE IDENTIFICATION RECORD
    4 CALL RDTR(11,IRAY,6HACCEPT,I)
      IF(I.NE.1) STOP 400
      J=IRAY*2     $WRITE(61,400) (IRAY(I),I=1,J)
      K=IRAY(2)    $IF(IABS(K).NE.2) STOP 401
```

```
      IF ((K.EQ.2).A.(IX.EQ.3)) GO TO 50
      IF ((K.EQ.2).A.(IX.EQ.2)).OR.((K.EQ.-2).A.(IX.EQ.4))) GO TO 60
      IF ((K.EQ.2).A.(IX.EQ.4)) GO TO 70
      WRITE(61,410)    $STOP 410

*       FIND WORD POSITIONS FOR SPECIFIED ELEMENT IDENTIFIERS
   50 DO 53 I=1,16
      K=FRAME(I)
      IF(K.EQ.1H ) GO TO 55
      ENCODE(10,500,IRAY(I+512)) K
   53 N=I
   55 CALL USET(IRAY,N,IRAY(513),NDEX,6HUNUSED,I)
      DO 58 I=1,N
      IF((INDEX(I).EQ.0).AND.(IRAY(I+512).NE.5HRZERO)) GO TO 59
   58 CONTINUE
      GO TO 60
   59 WRITE(61,590) IRAY(I+512)    $STOP 500

*       INITIALIZE DATA BUFFERS
   60 CALL RDVH(1,IRAY,11,IRAY(4))    $IX=1    $GO TO 10

*       CONTINUATION REEL STARTS WITH NEW DATA FILE
   70 IX=2    $BACKSPACE 11    $RETURN


  200 FORMAT(33H1  INPUT TAPE IDENTIFICATION FILE,3I5,       /
     .        (9X10A10)//)
  220 FORMAT(28H0*** INPUT TAPE UNACCEPTABLE)
  400 FORMAT(33H0  INPUT TAPE DATA FILE ID RECORD,2I5,4XA10,I5,/
     .        (9X10A10)//)
  410 FORMAT(30H0*** INVALID RECORD IDENTIFIER)
  500 FORMAT(1HRA6)
  590 FORMAT(28H0*** UNABLE TO LOCATE LABEL ,A7)
      END LOADER
```

```
      SUBROUTINE OUTAPE(NTRY)
*     THIS SUBROUTINE DOES ALL OF THE OUTPUT TAPE HANDLING EXCEPT WDVR-2
      COMMON KRAY(1027)

      IF(NTRY.GT.1) GO TO 10
      N=1
      CALL WTIF(10,1,1,10HACCORD OUT,KRAY)
      CALL WDF1(10,2,10HDRAG FT/S2,2,2,20HRTIME  001HDRAG  001,KRAY,K)
      CALL WDVR(1,KRAY,10,2,250)
      WRITE(62,560)
      RETURN

   10 IF(NTRY.EQ.2) GO TO 20
      CALL WDVR(3,KRAY)
      CALL WEOT(10,5,N,KRAY)
      END FILE 62
      STOP 7777

   20 CALL WDVR(3,KRAY)
      CALL WEOT(10,-5,N,KRAY)
      N=N+1
      CALL KUNTP(10)    $CALL REMARK(32HEND OF TAPE 10 - MOUNT NEW REEL.)
      CALL WTIF(10,N+1,10HACCORD OUT,KRAY)
      CALL WDF1(10,-2,10HDRAG FT/S2,2,2,20HRTIME  001HDRAG  001,KRAY,K)
      CALL WDVR(1,KRAY,10,2,250)
      RETURN

   56 FORMAT(/5H1    TIME      SCALE FACTOR          BIAS          BIAS CHECK
     .     PHASE1    PHASE2
     .       /7SH    (SEC)      (PULSE/FT/SEC)       (FT/SEC2)       (FT/SEC2)
     .     (DEGS)    (DEGS)   )
      END OUTAPE
```

```
      FUNCTION SUM(A1,A2,A3,A4)
C     THIS FUNCTION PERFORMS THE FOUR COUNT SUMMATION FOR COUNTS LESS
C     THAN 2000.   IF ALL COUNTS ARE BAD THE MISSING POINT FLAG IS SET.
      INSERT,FLAG=0.
      DIMENSION B(4)

      N=0
      B(1)=A1  $B(2)=A2  $B(3)=A3  $B(4)=A4

      DO 3 II=1,4
      IF(ABS(B(II)).LT.2000.) GO TO 3
      B(II)=0.
      N=N+1
    3 CONTINUE

      SUM=FLAG
      IF(N.GE.4) RETURN
      SUM = (B(1)+B(2)+B(3)+B(4))*4./FLOAT(4-N)
      RETURN

      END SUM
```

```
      FUNCTION VDOT(A,B)
*     THIS FUNCTION FORMS THE DOT PRODUCT OF TWO 9-VECTORS
      DIMENSION  A(9),B(9)

      VDOT=0.
      DO 1 I=1,9
    1 VDOT=VDOT+A(I)*B(I)
      RETURN
      END VDOT
```

```
      PROGRAM LOGJAM(INPUT=1001,OUTPUT=1001,TAPE1=1001,TAPE2=1001,
     .               TAPE11=1001)
*     LOGACS JOGGLE AND MERGE    DR037H    PROGRAMMER  P.G.BLANDIN
*
*     THIS PROGRAM MERGES TWO LOGICAL TAPES (64-FLOATING-POINT FORMAT)
*     TO FORM ONE (6000 STANDARD DATA TAPE FORMAT) WITH MONOTONICALLY
*     INCREASING TIME.  TIME EDITING CAN ALSO BE DONE.
*     PARAMETERS ENTERED IN CARDS-II FORMAT                          (CODE)
*        FIRST1 -  FIRST FILE TO BE MERGED FROM TAPE 1               (I)
*        FIRST2 -  FIRST FILE TO BE MERGED FROM TAPE 2               (I)
*        LAST1  -  LAST  FILE TO BE MERGED FROM TAPE 1               (I)
*        LAST2  -  LAST  FILE TO BE MERGED FROM TAPE 2               (I)
*        START1 -  START TIME TAPE 1                                 (R)
*        START2 -  START TIME TAPE 2                                 (R)
*        STOP1  -  STOP  TIME TAPE 1                                 (R)
*        STOP2  -  STOP  TIME TAPE 2                                 (R)
*        TYM1   -  ARRAY OF TIMES TO BE EDITED FROM TAPE 1           (R)
*        TYM2   -  ARRAY OF TIMES TO BE EDITED FROM TAPE 2           (R)
*        NAUATA -  TIMES OF FRAMES TO EDIT EVEN THOUGH THE
*                  TIME BEHAVIOR IS REASONABLE (MONOTONIC)           (R)
*        IDENTIFICATION (UP TO 600 CHARACTERS) FOR OUTPUT TAPE  (T)-TITLE

      COMMON /NAUBLK/ BAD(1536),L
      COMMON /BLOCK/ TYM(64,2), JA(2)
      DIMENSION  KF(2),KF1(2),KF2(2),START(2),STOP(2),ITAB(10)
      DIMENSION  ARRAY(1032), FRAME(15,2), IDENT(15), KDENT(10), NUM(2)
      DATA  TYM(1,1),TYM(1,2),BAD(1) / 3*999999./
      DATA  KF1,KF2,START,STOP/ 2*1, 2*99, 2*0., 2*999999. /
      DATA ENDTYM,NREEL,IDWDS,NUM / 1.E10,1,10,1,0 /
      DATA KDENT/ 35HLOGACS MERGE TAPE FOR TEST ORBIT 38/
      DATA  IDENT / 10HRTIME  001, 10HRGMTIME001, 10HRSWTCHA001
     .            , 10HRSWTCHB001, 10HRMODE  001, 10HRCOUNT1001
     .            , 10HRCOUNT2001, 10HRTHRUST001, 10HRFMONIT001
     .            , 10HRSMONIT001, 10HRROLLGY001, 10HRROLLHS001
     .            , 10HRPTCHGY001, 10HRPTCHHS001, 10HRYAWGY 001 /
      DATA ITAB /6HFIRST1,6HFIRST2,5HLAST1,5HLAST2,6HSTART1,6HSTART2,
     .           5HSTOP1,5HSTOP2,4HTYM1,4HTYM2/
*
*     DECK IDENTIFICATION
      IDATE=8H25SEP70
      PRINT 2,IDATE
    2 FORMAT(1H1////2H   LOGJAM  DR037H  -  LOGACS JOGGLE AND MERGE  -
```

```
      .DECK COMPILATION DATE A8)

       CALL CARDS(1,BAD,6HBADATA,K)    $IF(K.NE.1) STOP 1

    1  CALL CARDS(11,KF1(1),KF1(2),KF2(1),KF2(2),START(1),START(2),
     .                 STOP(1),STOP(2),TYM(1,1),TYM(1,2),KDENT,ITAB,K)
       IF(K.EQ.2) GO TO 90
       IF(K.EQ.3) KK=1  $IF(KK.EQ.1) GO TO 1
       IF(IOFILE.EQ.0) CALL WTIF(11,NREEL,IDWDS,KDENT,ARRAY)    $IOFILE=1
       JA(1)=1  $JA(2)=1

*        POSITION INPUT TAPES
       DO 10 N=1,2
       REWIND N
       KF(N)=1
    6  IF(KF(N).GE.KF1(N)) GO TO 10
    8  CALL HEADER(N,I,ARRAY,K)
       IF(K.NE.2) GO TO 8
       KF(N)=KF(N)+1   $GO TO 6
   10  CALL INDICTV(N,K)

*        INITIALIZE BADATA
       T=AMIN1(START(1),START(2))
       DO 15 I=1,100000
       IF(T.LT.BAD(1)) GO TO 16
   15  CONTINUE
   16  L=I     $T=-1.

*        INITIALIZE OUTPUT TAPE
       CALL WDFI(11, 2,10HLOGJAM OUT,15,15,IDENT,ARRAY,K)
       CALL WDVR(1,ARRAY,11,15,33)
*
*        INITIALIZE MERGE ROUTINE
       DO 25 N=1,2
       FRAME(1,N)=ENDTYM
       IF(KF1(N).EQ.0) GO TO 25
   21  CALL SINGLE(N,FRAME(1,N))
       IF(FRAME(1,N).GE.ENDTYM) GO TO 28
       IF(FRAME(1,N).LT.START(N)) GO TO 21
       CALL EDITYM(N,FRAME(1,N),K)
       IF(K.EQ.2) GO TO 21
   25  CONTINUE
```

```
      GO TO 40
   28 PRINT 280    $GO TO 1
  280 FORMAT(29H0***CANNOT FIND START TIME***)


   30 CALL SINGLE(N,FRAME(1,N))
      K=1
      IF(FRAME(1,N).NE.ENDTYM)  CALL EDITYM(N,FRAME(1,N),K)
      IF(K.NE.1) GO TO 30
      IF(FRAME(1,N).GT.STOP(N)) FRAME(1,N)=ENDTYM
      IF(FRAME(1,N).EQ.ENDTYM) GO TO 50

   40 N=1
      IF(FRAME(1,1).GT.FRAME(1,2)) N=2
      IF(FRAME(1,N).EQ.T) GO TO 60
      CALL BADATA(FRAME(1,N),K)  $IF(K.NE.1) GO TO 30
      T=FRAME(1,N)
      CALL #DVR(2,ARRAY,1,FRAME(1,N),K)
      IF(K.EQ.1) GO TO 30
*
*       END OF OUTPUT TAPE REEL - INITIALIZE NEW REEL
      CALL #DVR(3,ARRAY)
      CALL #EOT(11,-5,NREEL,ARRAY)
      CALL RUNTP(11)    $CALL REMARK(32HEND OF TAPE 11 - MOUNT NEW  REEL)
      NREEL=NREEL+1     $CALL WTIF(11,NREEL,IDWDS,KDENT,ARRAY)
      CALL #DFI(11,-2,10HLOGJAM OUT,15,15,IDENT,ARRAY,K)
      CALL #DVR(1,ARRAY,11,15,33)    $GO TO 30


   50 KF(N)=KF(N)+1
      IF(KF(N).GT.KF2(N)) GO TO 55
      CALL INDICTV(N,K)    $IF(K.EQ.1) GO TO 30
      CALL RUNTP(N)
      IF(N.EQ.1)  CALL REMARK(33HEND OF TAPE 1  -  MOUNT NEXT REEL)
      IF(N.EQ.2)  CALL REMARK(33HEND OF TAPE 2  -  MOUNT NEXT REEL)
      REWIND N
      CALL INDICTV(N,K)
      GO TO 30

   55 FRAME(1,N)=ENDTYM
```

```
      K=K+1  $IF(K.EQ.3) K=1  $IF(FRAME(1,K).EQ.ENDTYM) GO TO 80
      GO TO 40
*
*       TIME FRAME PRESENT ON BOTH TAPES
   60 PRINT 600,T  $GO TO 30
  600 FORMAT(4X3H1-2,F7)
*       CLOSE CASE
   80 CALL WOVR(3,ARRAY)
      REWIND 1
      REWIND 2
      GO TO 1
   90 CALL WEOT(11, 5,NKEEL,ARRAY)
      STOP 77
      END LOGJAM
```

```
      SUBROUTINE BADDATA(T,K)

C     THIS SUBROUTINE PERFORMS EDITING FOR FRAMES WITH GOOD TIME
C     BUT BAD DATA.  IT ASSUMES MONOTONIC EDITING HAS BEEN DONE.

      COMMON /BADBLK/ BAD(1536),L


      K=1
    1 IF(T.LT.BAD(L)) RETURN
      IF(T.GT.BAD(L)) GO TO 2
      PRINT 100, BAD(L)     $L=L+1     $K=2        $RETURN
    2 PRINT 200, BAD(L)     $L=L-1     $GO TO 1

  100 FORMAT(25XF8)
  200 FORMAT(40X5HMISS F8)

      END BADATA
```

```
      SUBROUTINE EDITYM(N,T,K)
*     THIS SUBROUTINE MONITORS THE TIME WORD AND PRINTS EACH BAD TIME.
*     THE TIMES TO BE EDITED FROM EACH TAPE ARE LOADED IN TYM(J,N).
*     EACH EDIT LIST SHOULD BE TERMINATED WITH TIME LATER THAN STOP TIME
*     ALL REGRESSIVE TIMES ARE REJECTED
*       N IS THE TAPE NUMBER  (1 OR 2)
*       T IS THE TIME WORD
*       K IS A FLAG RETURNED 1=ACCEPT 2=REJECT
      COMMON /BLOCK/ TYM(64,2), JA(2)
      DIMENSION S(2)
      DATA S /-1.E-10,-1.E-10/

      IF(T.LE.S(N)) GO TO 3
    1 J=JA(N)    $IF(T.GE.TYM(J,N)) GO TO 2
*       ACCEPTABLE TIME
      S(N)=T    $K=1    $RETURN

    2 JA(N)=JA(N)+1
      IF(T.GT.TYM(J,N)) GO TO 1
    3 K=2    $PRINT 30,N,T    $RETURN
   30 FORMAT(5X11,F8)

      END EDITYM
```

```
      SU ROUTINE INDICTV(II,K)
*     THIS SUBROUTINE READS AND PRINTS THE INDICITIVE RECORD ON THE
*     24-FORMAT INPUT TAPE. (TAPE IT)  (K IS FLAG 1-NORMAL  2-EOF)
*     THE ROUTINE ALSO INITIALIZES READER AND SINGLE
      INTEGER ARAY(512),LIST(64)
      DATA  LIST / 33B,34B,35B,36B,37B,40B,41B,42B,43B,44B,45B,54B,64B,
     .             74B,63B,61B,55B,01B,02B,03B,04B,05B,06B,07B,10B,11B,
     .             72B,57B,52B,65B,60B,67B,46B,12B,13B,14B,15B,16B,17B,
     .             20B,21B,22B,66B,53B,47B,70B,71B,73B,45B,50B,23B,24B,
     .             25B,26B,27B,30B,31B,32B,62B,56B,51B,75B,76B,77B /


      BUFFER IN(II,1) (ARAY,ARAY(512))
    1 IF(UNIT,IT) 1,2,3,2
    2 PRINT 20,IT
   20 FORMAT(32H0 INDICITIVE RECORD FROM TAPE NO,I2)
      DO 5 I=1,26
      DO 5 K=1,5
      J=32*K+5*(I-1)
    5 ARAY(J)=MBYTE(ARAY(I),K)
      DO 7 I=1,14
    7 CALL ACODE(6,ARAY(33+9*(I-1)),LIST)
      PRINT 80,(ARAY(I),I=33,158)
   80 FORMAT(4(2X6R2,1X30A))
      CALL READER(IT,1,ARAY,K)
      CALL SINGLE(-II)
      RETURN

    3 K=2    $RETURN

      END INDICTV
```

```
      SUBROUTINE  READER (IT,NBYTS,ARRAY,IFLAG)
      DIMENSION  ARRAY(512), BUF(512,2,2), NDEX(2)
      DATA NDEX/1,1/

*     THIS SUBROUTINE READS TWO TAPES (DOUBLE-BUFFERING) AND RETURNS
*     ONE RECORD AT A TIME ALONG WITH THE NUMBER OF BYTES READ.
*       IT     IS TAPE NUMBER (1 OR 2)
*       NBYTS IS NUMBER OF BYTES READ
*       ARRAY IS LOCATION TO LOAD RECORD JUST READ
*       IFLAG IS EXIT INDICATOR  (1 NORMAL, 2 EOF, 3 PARITY)

      IFLAG=1
    1 IF(UNIT,IT) 1,4,2,3
    2 IFLAG=2    $RETURN
    3 IFLAG=3

    4 NBYTS=NBYTE(IT)
      NWDS=NBYTS/5+1
      N=NDEX(IT)
      BUFFER IN (IT,1) (BUF(1,N,IT),BUF(512,N,IT))

      N=N+1    $IF(N.GT.2) N=1    $NDEX(IT)=N
      DO 6 I=1,NWDS
    6 ARRAY(I)=BUF(I,N,IT)
      RETURN

      END READER
```

```
      SUBROUTINE SINGLE(IT,FRAME)
*     THIS SUBROUTINE RETURNS (IN 6000 FORMAT) A SINGLE FRAME PER CALL
*     FROM TAPE IT.  (USES READER AND FL948)

      DIMENSION ARAY(512,2),BRAY(15,42,2),NDEX(2),MANY(2),FRAME(15)
      DATA NDEX, MANY, ENDTYM / 4*0,1.E10 /


      IF(IT.LT.0) GO TO 70
    1 N=NDEX(IT)
      IF(N.GE.MANY(IT)) GO TO 50
      DO 10 I=1,15
   10 FRAME(I)=BRAY(I,N,IT)
      NDEX(IT)=NDEX(IT)+1     $RETURN

*       RELOAD DATA BLOCK
   50 CONTINUE
      NDEX(IT)=1
      CALL READER(IT,MANY(IT),ARAY(1,IT),I)
      MANY(IT)=MANY(IT)/45
      IF((I.NE.2).AND.(MANY(IT).GT.0)) GO TO 60
      FRAME=ENDTYM    $RETURN

   60 CALL FL948(MANY(IT)*15,ARAY(1,IT),BRAY(1,1,IT),I)
      GO TO 1

   70 NDEX(-IT)=0    $MANY(-IT)=0    $RETURN
      END SINGLE
```

```
      ASCENT SUBROUTINE XCODE (N,ARG,LIST)
* CONVERTS N 10-CHARACTER WORDS (LOCATED IN A BLOCK BEGINNING AT ARG)
* FROM ONE CODE FORMAT TO ANOTHER ACCORDING TO A TABLE (BEGINNING AT
* LIST) WHICH MUST BE SUPPLIED BY THE USER (SEE WRITE-UP)
          BSS       5
RET       BSS       1
          SA5       B1
LOOP1     SA1       B2          .CURRENT WORD
          SA6       B0
          MX2       54          .MASK
          SB4       10          .CHARACTER COUNTER
LOOP2     LX1       6
          BX3       -X2*X1      .CURRENT CHARACTER
          SA4       B3+X3       .TABLE LOOKUP
          LX6       6
          BX6       X6+X4       .CONVERTED CHARACTER
          SB4       B4-1
          NZ        B4,LOOP2    .TO NEXT CHARACTER
          SA6       B2          .CONVERTED WORD
          SB2       B2+1
          SX5       X5-1
          NZ        X5,LOOP1    .TO NEXT WORD
          JP        RET
          END
```

```
      PROGRAM SPLINTR(INPUT=1001,OUTPUT=1001,TAPE11=1001,
     .                ITAPEA=1001,TAPE10=ITAPEA)

*     SPECIAL LINK TO REFORMAT LOGAJS DATA FOR PLOTTING    DR037C
*       P.G.BLANDIN     (EXTENSION OF EXISTING PROGRAM *STDUMP*)
*     THIS PROGRAM READS THE STANDARD DATA TAPE WRITTEN BY LOGJAM
*     AND WRITES A STANDARD DATA TAPE WHICH IS PLOTTED WITH UI900
*     THE OUTPUT TAPE HAS DUMMY TIME FRAMES ADDED TO PROVIDE EACH
*     COUNTER WORD WITH ITS DECOMMUTATED TIME VALUE (1-SEC STEPS)
*     THE THRUST VALVE STATUS WORD IS DECODED TO YIELD ONE STATUS
*     WORD FOR EACH THRUSTER IN EACH HALF OF THE COMMUTATOR FRAME

      DIMENSION ARAY(1027),FRAME(512),IN(512),LAB(16),NDEX(16),ITAB(9)
      DIMENSION IDENT(19),IRAY(1030),FOUT(19,2),KEY(6),TV(6)
      EQUIVALENCE (IN,FRAME)
      DATA ITAB /6HNUMBER,6HLABELS,6HFORMAT,4HHEAD,5HSTART,4HSTOP
     .          ,6HFILENO,5HOFTEN,5HLINES/ , IER,L/0,0/ , JMAX/38/
      DATA TV / 1.,2.,3.,4.,5.,6. /
      DATA M,N,T1,T2 /2*1,-1.E20,+1.E20/
      DATA FOUT/ 38*17770000000000000000B /
      DATA IDENT / 10HRTIME  001, 10HRGMTIME001, 10HRSWTCHA001,
     .             10HRSWTCHB001, 10HRMODE  001, 10HRYAWGY 001,
     .             10HRFMONIT001, 10HRSMONIT001, 10HRROLLGY001,
     .             10HRROLLHS001, 10HRPTCHGY001, 10HRPTCHHS001,
     .             10HRCOUNTR001,
     .             10HRTHRST1001, 10HRTHRST2001, 10HRTHRST3001,
     .             10HRTHRST4001, 10HRTHRST5001, 10HRTHRST6001/
      DATA NUM,LAB/15, 7HRTIME  , 7HRGMTIME, 7HRSWTCHA, 7HRSWTCHB,
     .                 7HRMODE  , 7HRYAWGY , 7HRFMONIT, 7HRSMONIT,
     .                 7HRROLLGY, 7HRROLLHS, 7HRPTCHGY, 7HRPTCHHS,
     .                 7HRCOUNT1, 7HRCOUNT2, 7HRTHRUST/ , NNN/0/
*
*       READ ID FILE
      REWIND 10
      REWIND 11
      CALL RDTR(11,IN,6HACCEPT,K)
      IF((K.NE.1).OR.(IN(2).NE.1)) STOP 1
      I=IN+2   $PRINT 100, (IN(K),K=1,I)
  100 FORMAT(33H1  INPUT TAPE IDENTIFICATION FILE,3I5,      /
     .       (9X10A10)//)
      BUFFER OUT (10,1) (IN,IN(I))
   41 IF(UNIT,10) 41,42,42,42
```

```
   42 END FILE 10
    1 IF(NNN.NE.0) GO TO 90     $NNN=1

*       POSITION TAPE TO SELECTED DATA FILE
      IF(L.LT.N) GO TO 3
      L=0    $REWIND 11
    3 CALL RDTR(11,IN,6HACCEPT,K)
      IF(IN(2).EQ.5) STOP 5
      IF(K.NE.2) GO TO 3
      L=L+1    $IF(L.LT.N) GO TO 3

*       PROCESS DATA ID RECORD - INITIALIZE BUFFERS
      CALL RDTR(11,IN,6HACCEPT,K)
      IF((IN(2).NE.2).OR.(K.NE.1)) STOP 2
      I=IN+2    $PRINT 102, (IN(K),K=1,I)
  102 FORMAT(33H0  INPUT TAPE DATA FILE ID RECORD,2I5,4XA10,I5,/
     .       (9X10A10)//)
      CALL USEI(IN,NUM,LAB,NDEX,6HUNUSED,K)    $IF(K.NE.1) STOP 3
      CALL RDVR(1,ARAY,11,IN(4))
      CALL WDFI(10,2,10HPLOT TAPE ,19,19,IDENT,IRAY,K)
      CALL WDVR(1,IRAY,10,19,26)
*
    7 CALL RDVR(2,ARAY,6HACCEPT,1,FRAME,1,K)
      IF(K.EQ.2) BACKSPACE 11    $IF(K.EQ.2) GO TO 1
      IF(FRAME.LT.T1) GO TO 7
      IF(FRAME.GT.T2) GO TO 1
      MM=MM+1    $IF(MM.LT.M) GO TO 7    $MM=0
      DO 9 I=1,NUM
      K=NDEX(I)
    9 FOUT(I)=FRAME(K)

      FOUT(1,2)=FOUT(1,1)+1.
      FOUT(13,2)=FOUT(14,1)
      CALL FIRINGS(FOUT(15,1),KEY)
      DO 10 I=1,6
      K=I+13
      FOUT(K,1)=FOUT(2,2)    $FOUT(K,2)=FOUT(2,2)
      IF(KEY(I).EQ.0) GO TO 10
      IF(KEY(I).A .1) FOUT(K,1)=TV(I)
      IF(KEY(I).GE.2) FOUT(K,2)=TV(I)
   10 CONTINUE
      CALL WDVR(2,IRAY,2,FOUT,K)
```

```
      GO TO 7

9     REWIND 11
      CALL #OVR(3,IRAY)
      CALL #EXT(10,5,1,IRAY)
      STOP
      END SPLINTER
```

APPENDIX E

LOGACS SENSED ACCELERATION ALGORITHM

The LOGACS accelerometer's proof mass is connected to the Agena vehicle through a force suspension system in which one component (defined as the input axis component) is measured explicitly. This appendix develops the algorithm for this measured acceleration component.

Assuming the Agena vehicle is a rigid body, a force vector diagram of the vehicle/accelerometer system in a fixed reference frame can be constructed as shown in Fig. E-1.

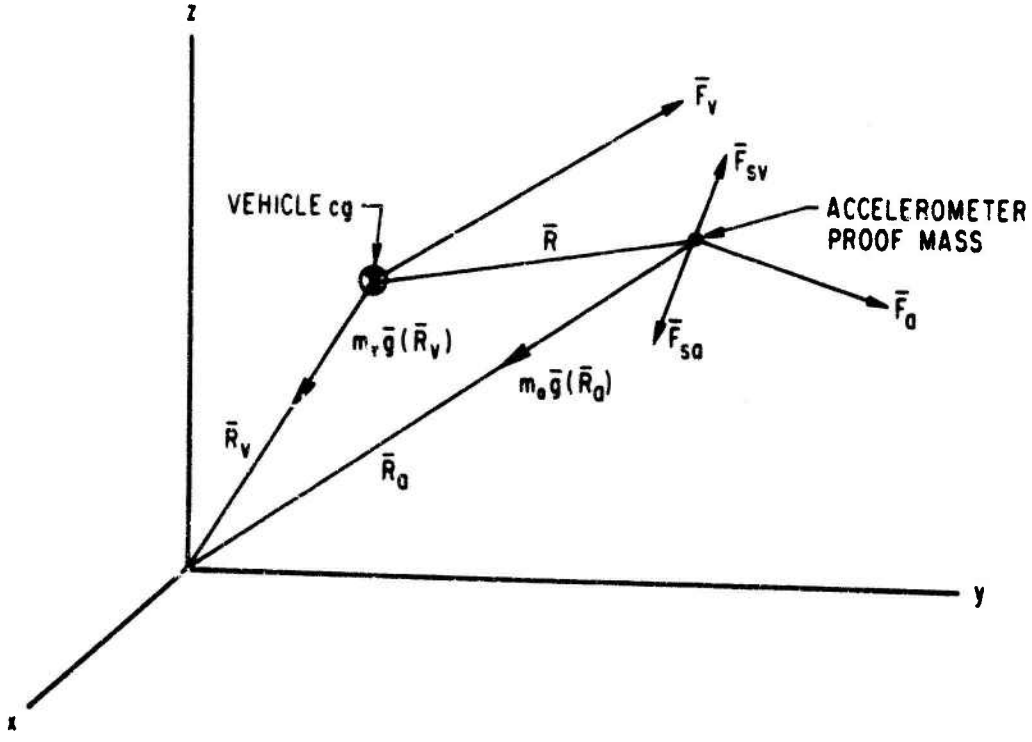

Fig. E-1. Force Vector Diagram

The symbols in Fig. E-1 are defined as follows:

$\overline{R}_i$ = radius vector from the earth center to i (i = v, a)

$\overline{F}_i$ = vector sum of external forces applied to i (i = v, a; $\overline{F}_a$ represents accelerometer bias term)

$\overline{F}_{si}$ = suspension force vector (i = v, a)

$m_i\overline{g}(\overline{R}_i)$ = gravity force vector (i = v, a)

From these definitions, the acceleration equation for each mass is

$$\ddot{\overline{R}}_v = \frac{\overline{F}_v + \overline{F}_{sv}}{m_v} + \overline{g}(\overline{R}_v) \qquad \text{(E-1)}$$

$$\ddot{\overline{R}}_a = \frac{\overline{F}_a + \overline{F}_{sa}}{m_a} + \overline{g}(\overline{R}_a) \qquad \text{(E-2)}$$

Using the relationships

$$\overline{R} = \overline{R}_a - \overline{R}_v$$

$$\ddot{\overline{R}} = \ddot{\overline{R}}_a - \ddot{\overline{R}}_v$$

$$\overline{F}_{sv} + \overline{F}_{sa} = 0$$

and substracting Eq. (E-1) from (E-2) results in

$$\ddot{\overline{R}} = \frac{\overline{F}_a + \overline{F}_{sa}}{m_a} - \frac{\overline{F}_v + \overline{F}_{sa}}{m_v} + \overline{g}(\overline{R}_a) - \overline{g}(\overline{R}_v) \qquad \text{(E-3)}$$

Assuming the accelerometer mass is negligible with respect to the vehicle mass, the acceleration sensed by the accelerometer's force suspension system is

$$\frac{\overline{F}_{sa}}{m_a} = \frac{\overline{F}_v}{m_v} + \ddot{\overline{R}} - \left[\overline{g}(\overline{R}_a) - \overline{g}(\overline{R}_v)\right] - \frac{\overline{F}_a}{m_a} \qquad \text{(E-4)}$$

The acceleration vector $\ddot{\overline{R}}$ expressed in the rotating vehicle axis frame is

$$\ddot{\overline{R}} = \ddot{\overline{r}} + \overline{\omega} \times (\overline{\omega} \times \overline{r}) + \dot{\overline{\omega}} \times \overline{r} + 2\overline{\omega} \times \dot{\overline{r}} \qquad \text{(E-5)}$$

where $\overline{\omega}$ and $\dot{\overline{\omega}}$ are the inertial angular rate and acceleration vectors, respectively, of the vehicle axes and $\overline{r}$ is the displacement vector expressed in body axes coordinates. Neglecting the bias term $(\overline{F}_a/m_a)$, changing the symbols of the force to mass terms, and using the symbol $\overline{g}(\overline{r})$ for the gravity gradient term results in the following equation for the sensed acceleration vector expressed in body axis coordinates

$$\overline{A}_s = \overline{A}_{cg} + \ddot{\overline{r}} + \overline{\omega} \times (\overline{\omega} \times \overline{r}) + \dot{\overline{\omega}} \times \overline{r} + 2\overline{\omega} \times \dot{\overline{r}} - \overline{g}(\overline{r}) \qquad \text{(E-6)}$$

where

$$\overline{r} = \begin{pmatrix} X_{ag} + r_a \cos \phi_t \\ Y_{ag} + r_a \sin \phi_t \\ Z_{ag} \end{pmatrix}$$

instantaneous coordinates of proof mass with respect to the vehicle cg (see Fig. 19)

$$\overline{\omega} = \begin{pmatrix} \omega_x \\ \omega_y \\ \omega_z \end{pmatrix}$$

Inertial body rates

$\overline{g}(\overline{r})$ = gravity gradient term (see below)

Since the coordinates of the LOGACS package with respect to the cg (X_{ag}, Y_{ag}, Z_{ag}) and the turntable radius arm r_a are assumed constant, the relative velocity and acceleration of the proof mass are

$$\dot{\bar{r}} = r_a \dot{\phi}_t \begin{pmatrix} -\sin \phi_t \\ \cos \phi_t \\ 0 \end{pmatrix} \tag{E-7}$$

$$\ddot{\bar{r}} = - r_a \dot{\phi}_t^2 \begin{pmatrix} \cos \phi_t \\ \sin \phi_t \\ 0 \end{pmatrix} + r_a \ddot{\phi}_t \begin{pmatrix} -\sin \phi_t \\ \cos \phi_t \\ 0 \end{pmatrix} \tag{E-8}$$

and

$$\dot{\bar{\omega}} = \begin{pmatrix} \dot{\omega}_x \\ \dot{\omega}_y \\ \dot{\omega}_z \end{pmatrix} \tag{E-9}$$

The gravity gradient term is developed assuming a spherical earth as follows:

$$\bar{g}(\bar{R}_v) = - \frac{\mu}{R_v^3} \bar{R}_v$$

$$\bar{g}(\delta \bar{R}) = \frac{\mu}{R_v^3} \left[\frac{3 \bar{R}_v \bar{R}_v^T}{R_v^2} - I \right] \delta \bar{R} = \omega_o^2 \begin{bmatrix} -1 & 0 & 0 \\ 0 & -1 & 0 \\ 0 & 0 & 2 \end{bmatrix} \delta \bar{R}$$

where

$$\bar{R}_v = \begin{pmatrix} 0 \\ 0 \\ -Z \end{pmatrix}$$ radius vector from the earth center to the Agena cg expressed in orbit plane coordinates*

$$\delta\bar{R} = \begin{pmatrix} \delta X \\ \delta Y \\ \delta Z \end{pmatrix}$$ displacement coordinates from the cg expressed in orbit plane coordinates

$\omega_o = -(\mu/R_v^3)^{1/2}$ instantaneous orbital rate

The body axis system is related to the orbit axis system by

$$\begin{pmatrix} x \\ y \\ z \end{pmatrix}_b = \begin{bmatrix} 1 & 0 & 0 \\ 0 & \cos\varphi & \sin\varphi \\ 0 & -\sin\varphi & \cos\varphi \end{bmatrix} \begin{bmatrix} \cos\psi & \sin\psi & 0 \\ -\sin\psi & \cos\psi & 0 \\ 0 & 0 & 1 \end{bmatrix} \begin{bmatrix} \cos\theta & 0 & -\sin\theta \\ 0 & 1 & 0 \\ \sin\theta & 0 & \cos\theta \end{bmatrix} \begin{pmatrix} x \\ y \\ z \end{pmatrix}_c$$

where

θ,ψ,φ = ordered rotations (pitch, yaw, roll) of the Agena vehicle axis with respect to the orbit plane axis.

When it is assumed that the angles (θ,ψ,φ) are small (cos = 1, sin = angle, sin products = 0), the order of rotations is immaterial and the transformation reduces to a skew symmetric matrix

$$\begin{pmatrix} x \\ y \\ z \end{pmatrix}_b = \begin{bmatrix} 1 & \psi & -\theta \\ -\psi & 1 & \varphi \\ \theta & -\varphi & 1 \end{bmatrix} \begin{pmatrix} x \\ y \\ z \end{pmatrix}_c = M_{bo} \begin{bmatrix} x \\ y \\ z \end{bmatrix}_o$$

*In the orbit plane coordinate system, the z axis is directed along the negative radius vector, the y axis is directed normal to the orbit plane, and the x axis is directed forward, formating a right-hand system.

With the above definitions, the gravity gradient term is

$$\bar{g}(\bar{r}) = M_{bo}\bar{g}(\delta\bar{R})$$

$$= \omega_o^2 M_{bo}\begin{bmatrix} -1 & 0 & 0 \\ 0 & -1 & 0 \\ 0 & 0 & 2 \end{bmatrix} M_{bo}^T \bar{r}$$

$$= \omega_o^2\begin{bmatrix} -1 & 0 & -3\theta \\ 0 & -1 & 3\varphi \\ -3\theta & 3\varphi & 2 \end{bmatrix} \bar{r} \qquad \text{(E-10)}$$

Substituting Eqs. (E-7), (E-8), (E-9), and (E-10) into Eq. (E-6) and collecting terms results in the following x and y components

$$A_{sx} = A_{xcg} - r_a\{\cos\phi_t[(\dot{\phi}_t + \omega_z)^2 + \omega_y^2 - \omega_o^2] + \sin\phi_t(\ddot{\phi}_t + \dot{\omega}_z - \omega_x\omega_y)\}$$

$$-X_{ag}(\omega_y^2 + \omega_z^2 - \omega_o^2) - Y_{ag}(\dot{\omega}_z - \omega_x\omega_y) + Z_{ag}(\omega_x\omega_z + \dot{\omega}_y + 3\omega_o^2\theta)$$

$$A_{sy} = A_{ycg} - r_a\{\sin\phi_t[(\dot{\phi}_t + \omega_z)^2 + \omega_x^2 - \omega_o^2] + \cos\phi_t(-\ddot{\phi}_t - \dot{\omega}_z - \omega_x\omega_y)\}$$

$$-X_{ag}(\omega_x\omega_y - \dot{\omega}_z) - Y_{ag}(\omega_x^2 + \omega_z^2 - \omega_o^2) - Z_{ag}(\dot{\omega}_x - \omega_y\omega_z + 3\omega_o^2\varphi)$$

The input axis acceleration to the LOGACS accelerometer is

$$A_{si} = A_{sx}\cos\phi_t + A_{sy}\sin\phi_t$$

Performing the above transformation and collecting terms results in

$$A_{si} = A_{xcg} \cos \phi_t + A_{ycg} \sin \phi_t - r_a[(\dot{\phi}_t + \omega_z)^2 + (\cos \phi_t \omega_y - \sin \phi_t \omega_x)^2 - \omega_o^2]$$

$$+ X_{ag}[\sin \phi_t(\dot{\omega}_z + \omega_x \omega_y) - \cos \phi_t(\omega_y^2 + \omega_z^2 - \omega_o^2)]$$

$$+ Y_{ag}[\cos \phi_t(\omega_x \omega_y - \dot{\omega}_z) - \sin \phi_t(\omega_x^2 + \omega_z^2 - \omega_o^2)]$$

$$+ Z_{ag}[\cos \phi_t(\omega_x \omega_z + \dot{\omega}_y + 3\omega_o^2 \theta) - \sin \phi_t(\dot{\omega}_x - \omega_y \omega_z + 3\omega_o^2 \varphi)] \qquad \text{(E-11)}$$

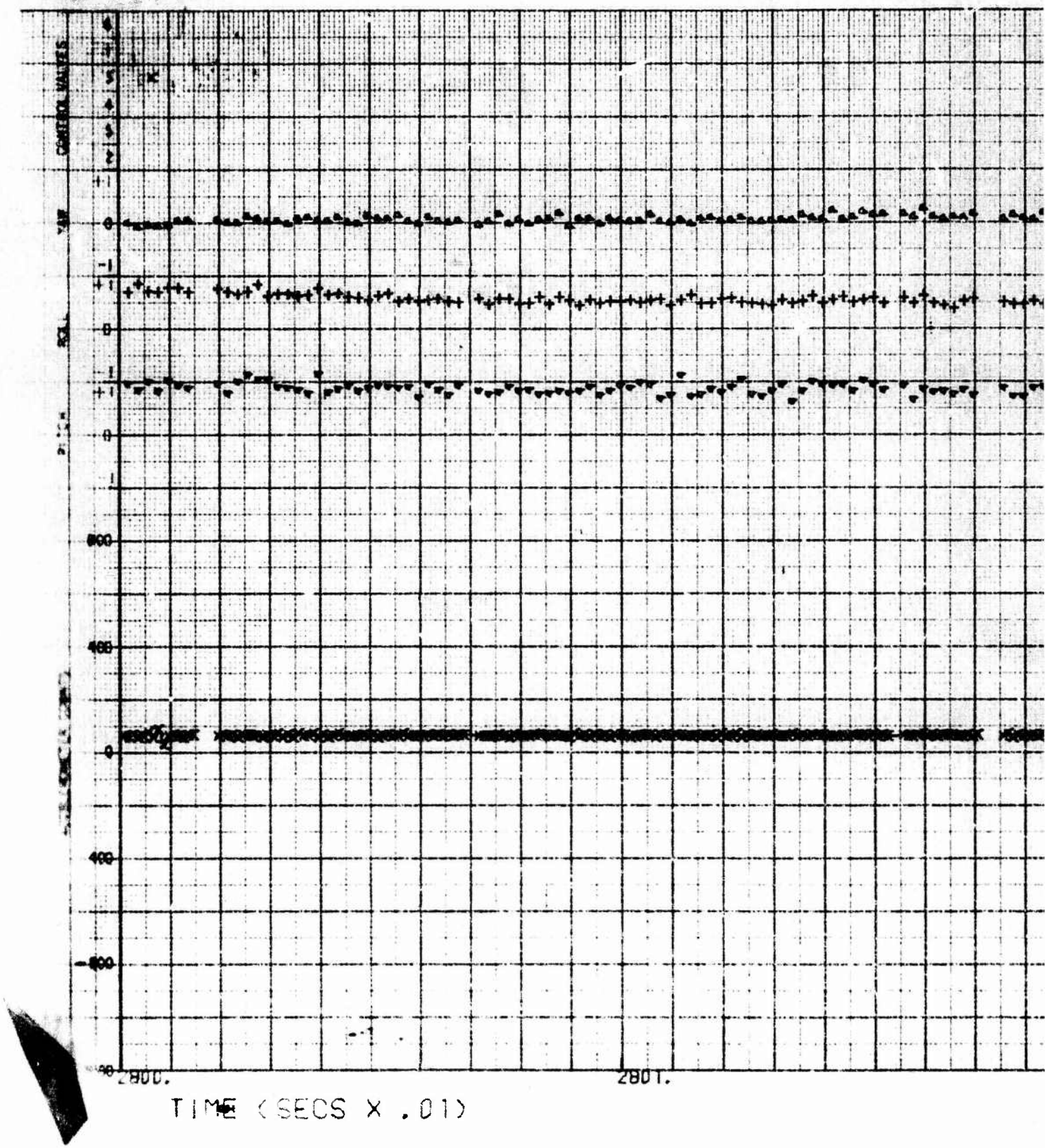
CONTROL VALVES
YAW
ROLL
800
400
0
400
800
2800.
2801.
TIME (SECS X .01)

B

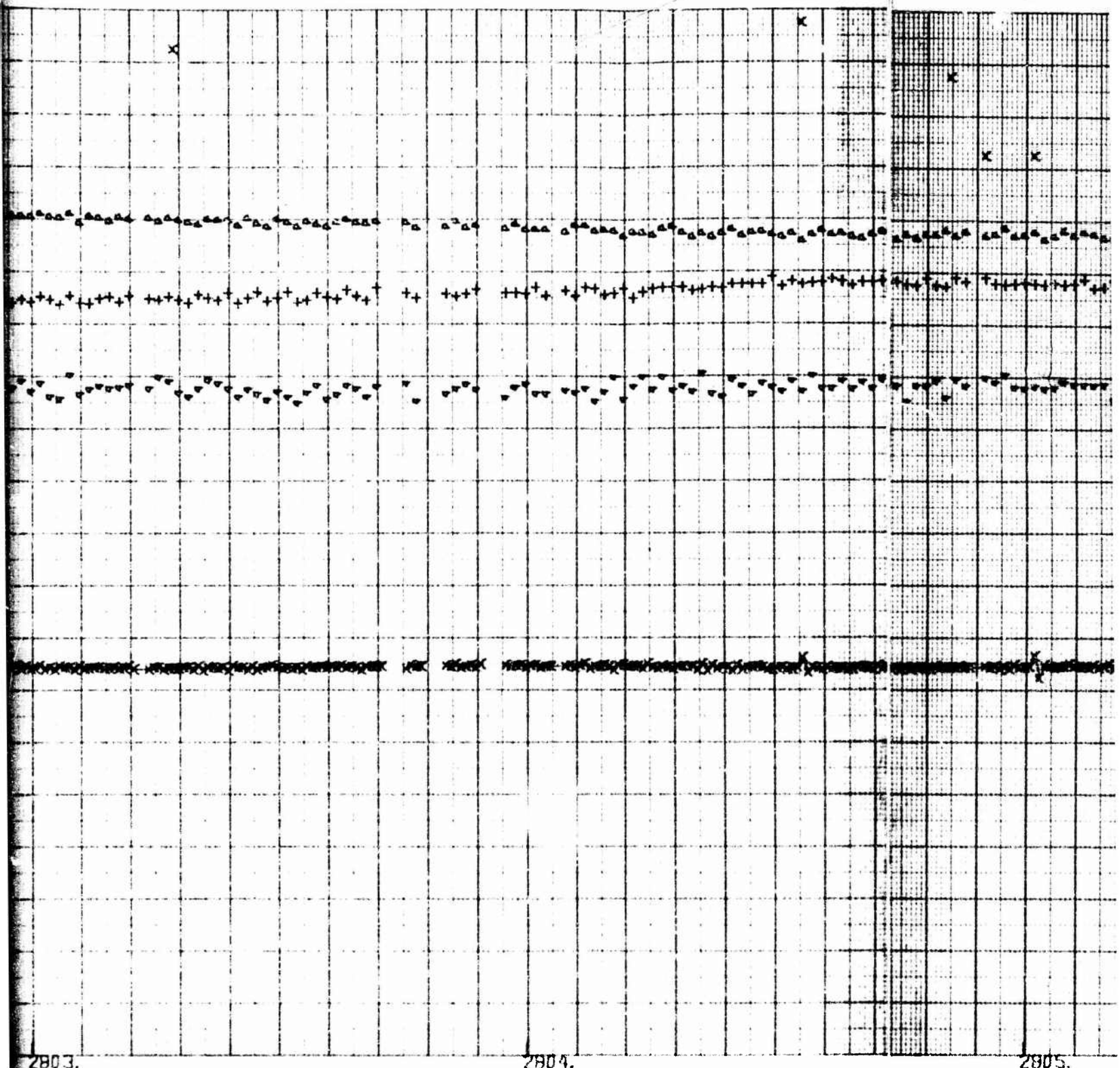
2803.
2804.
2805.

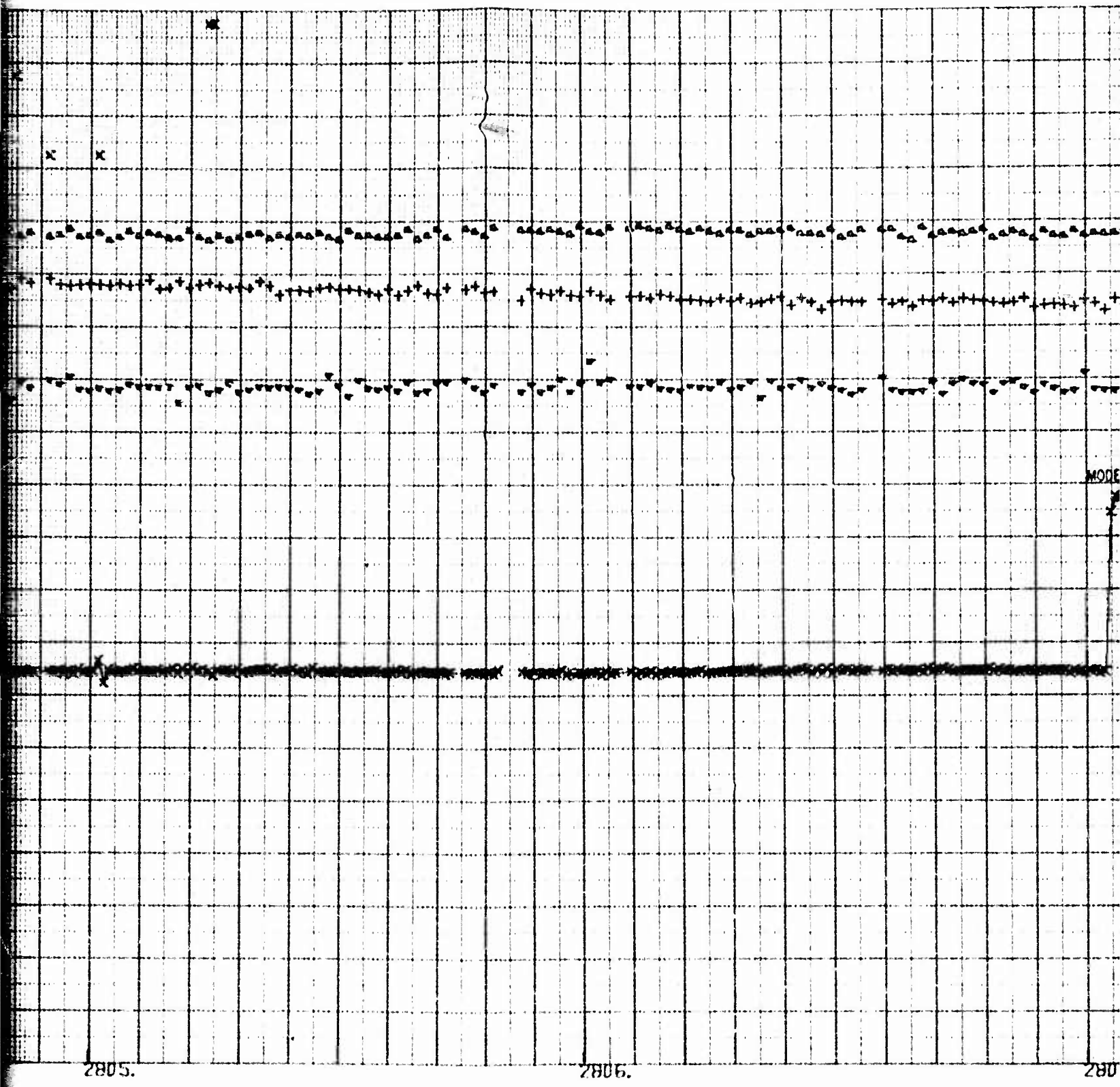

D

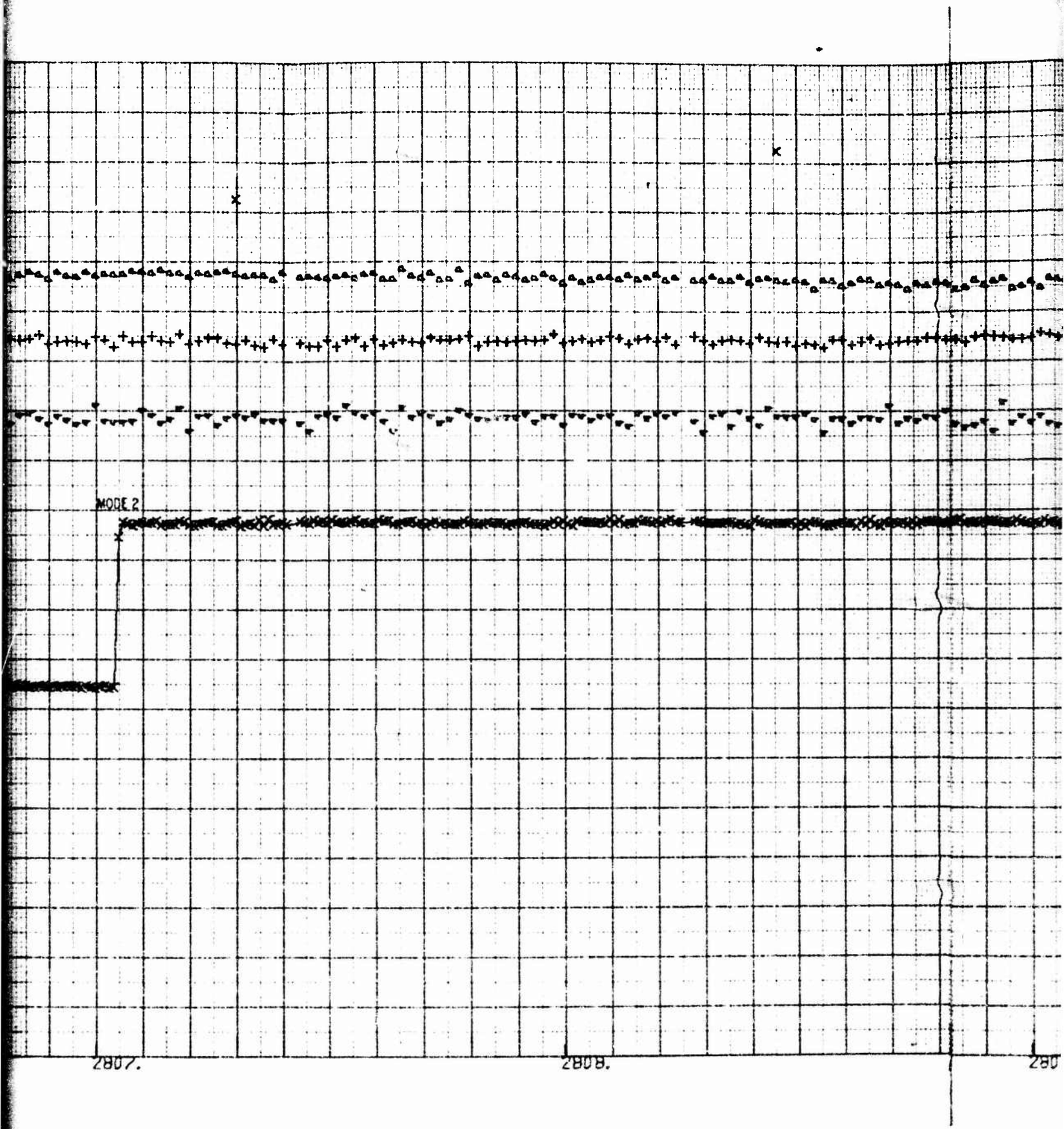
MODE 2
2807.
2808.
280

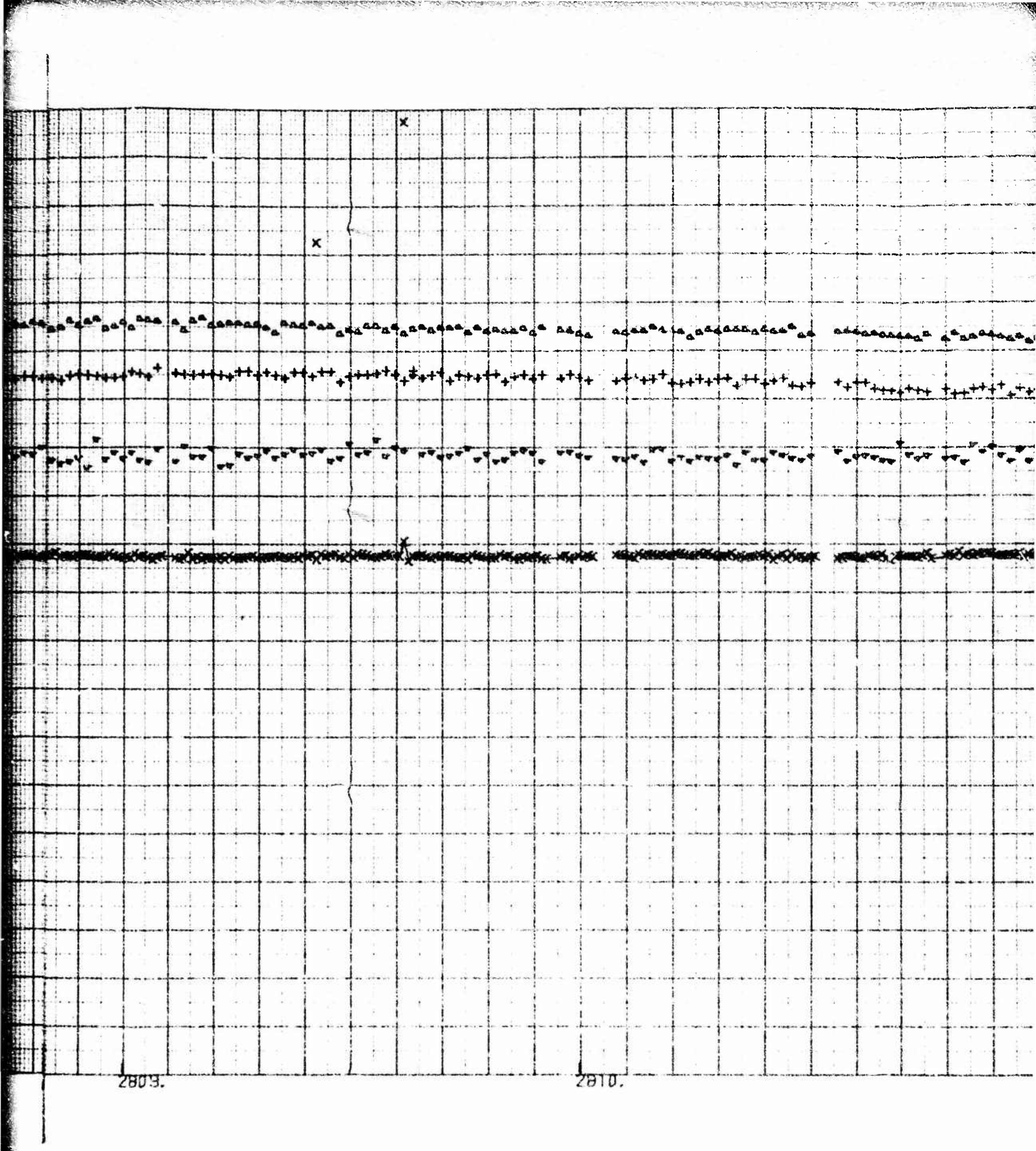
2803.
2810.

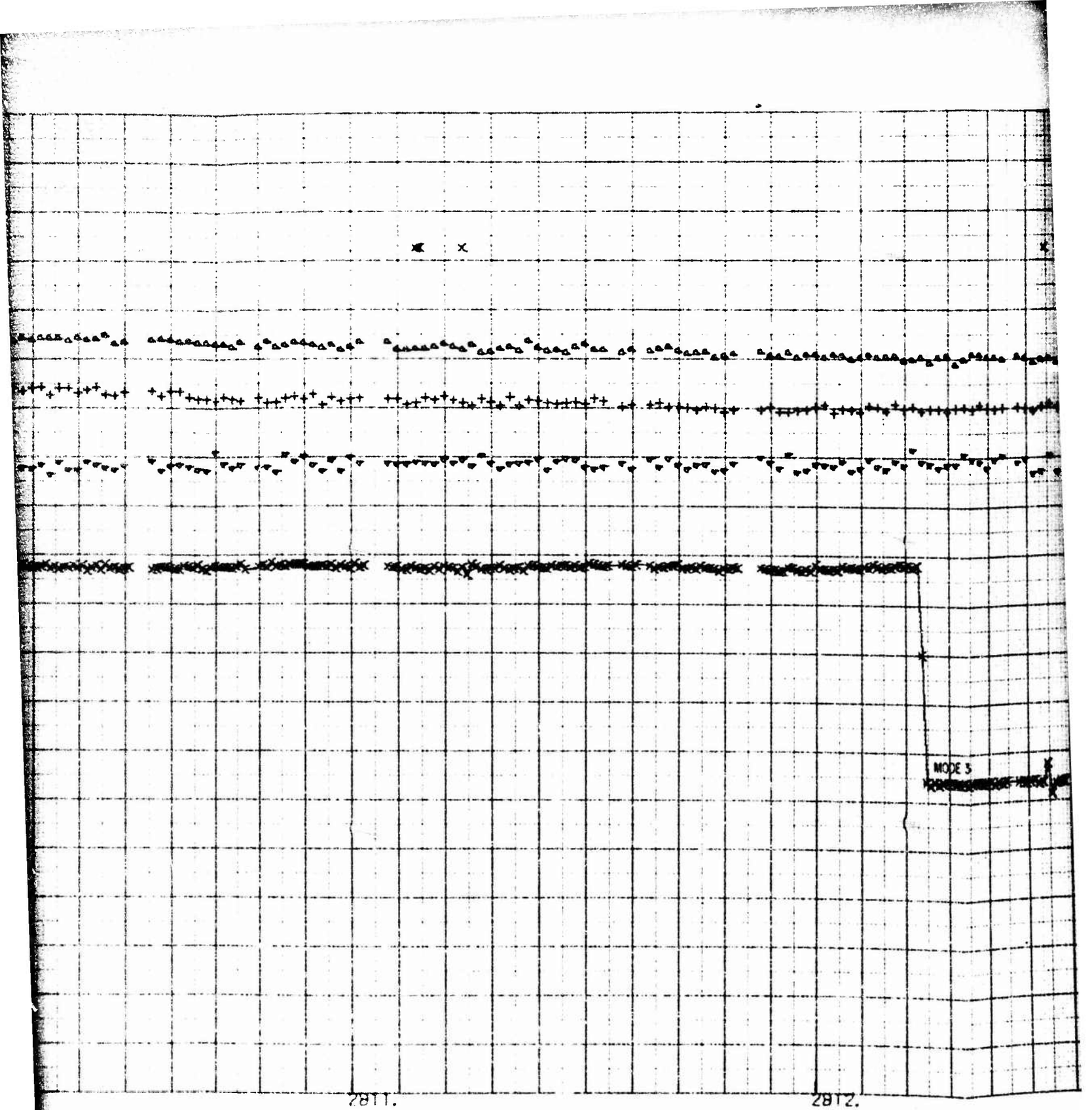

2811.

2812.

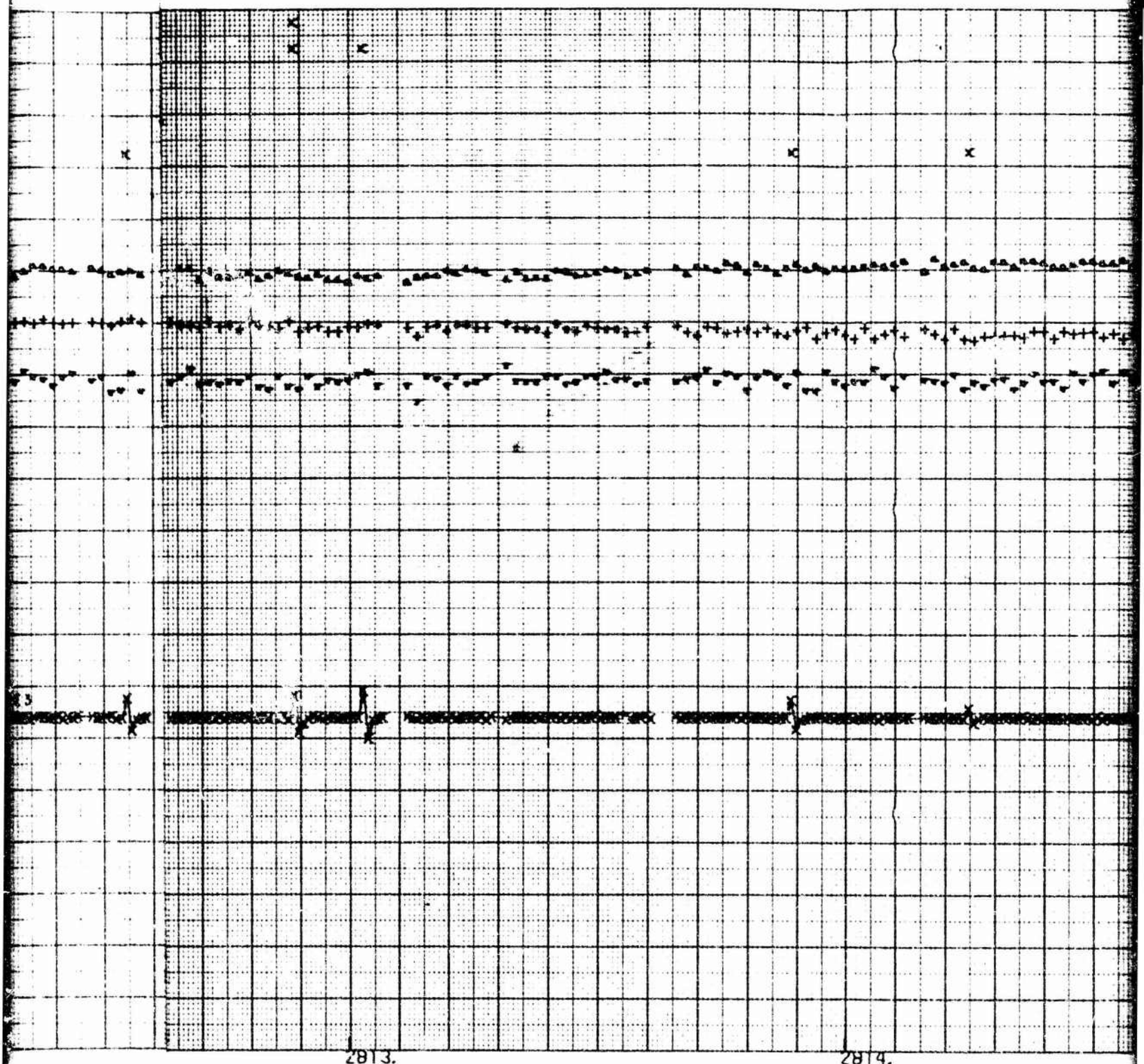
2813.
2814.

MODE 4

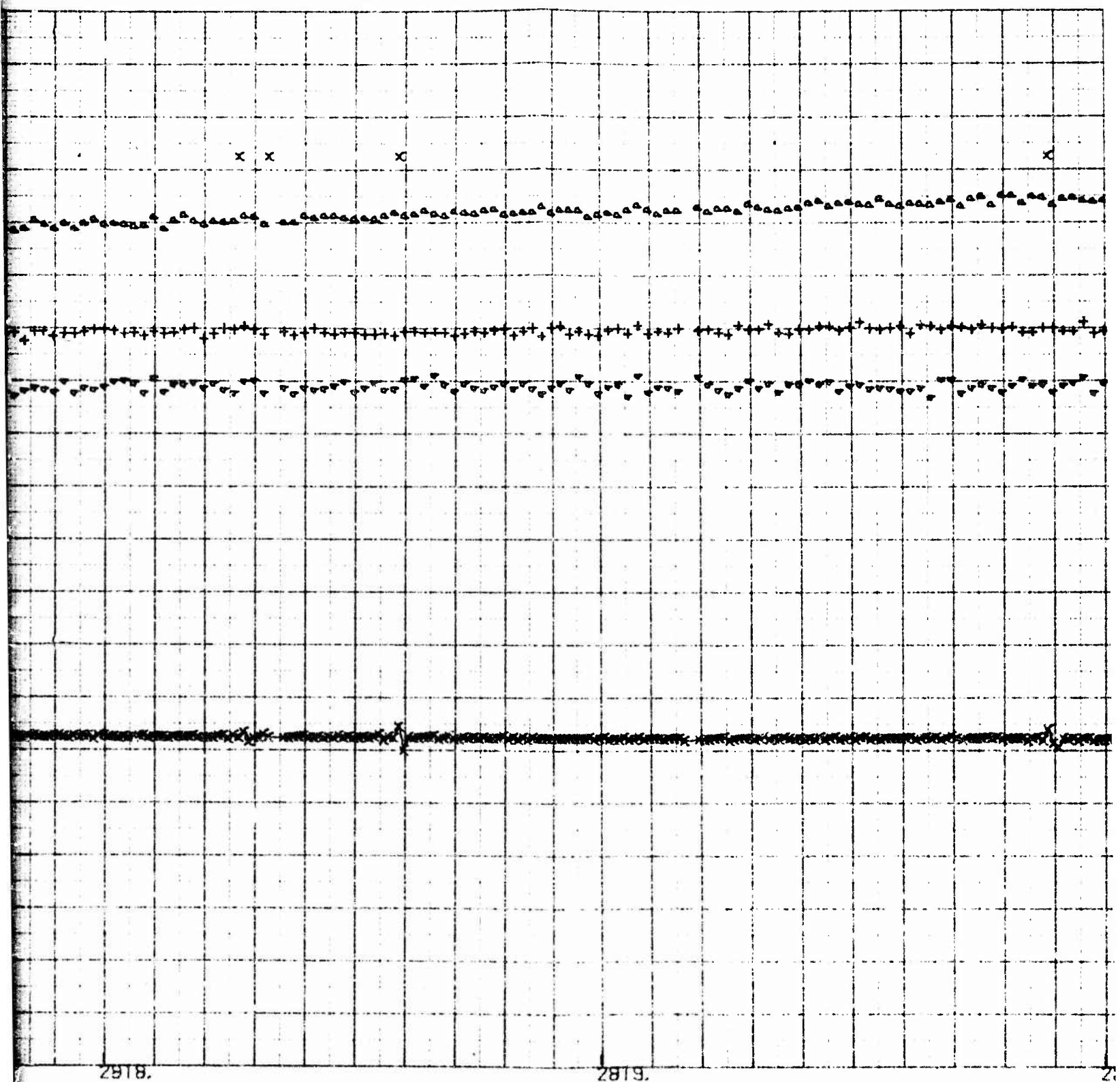
2818.
2819.

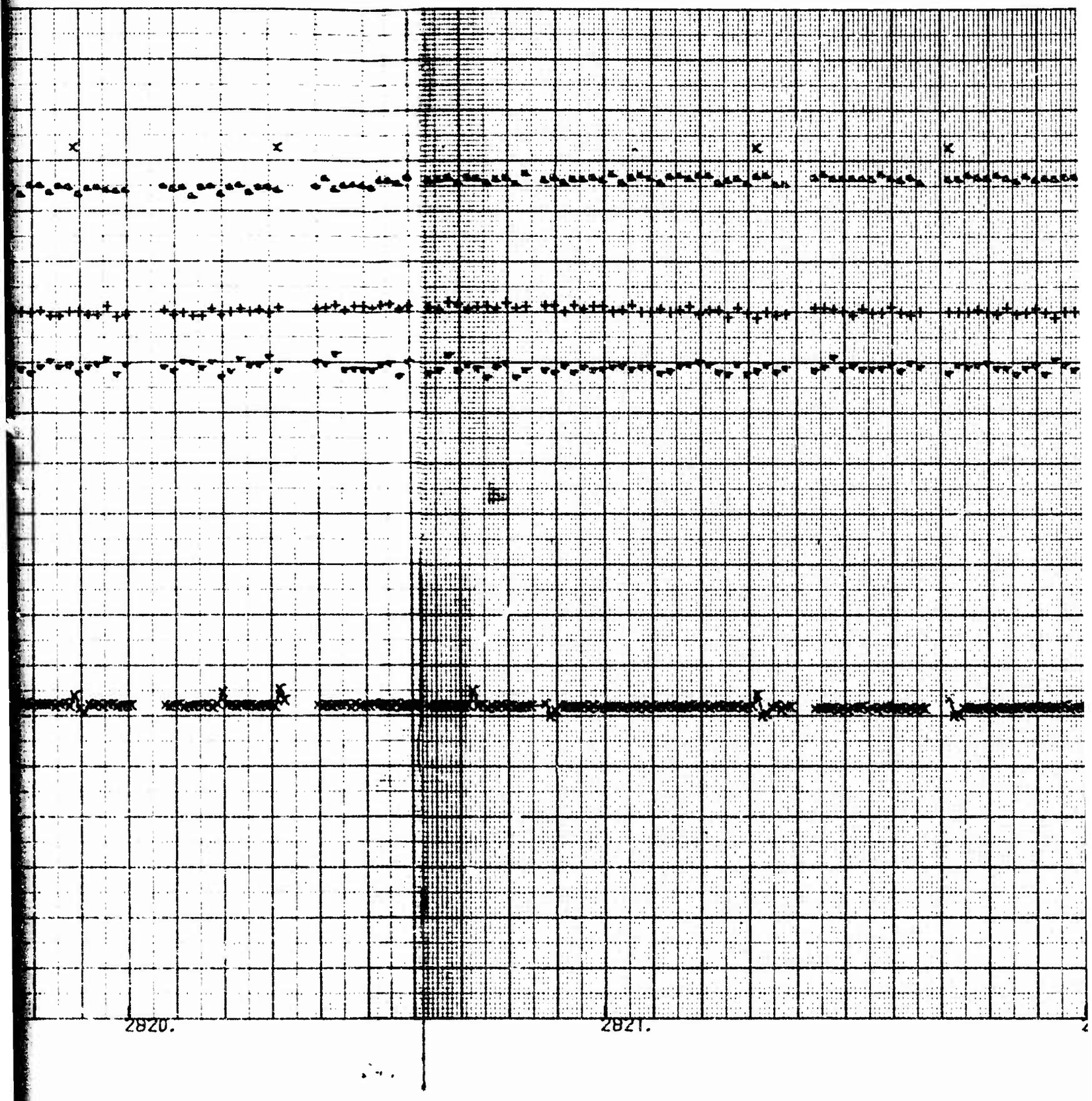
2820.
2821.

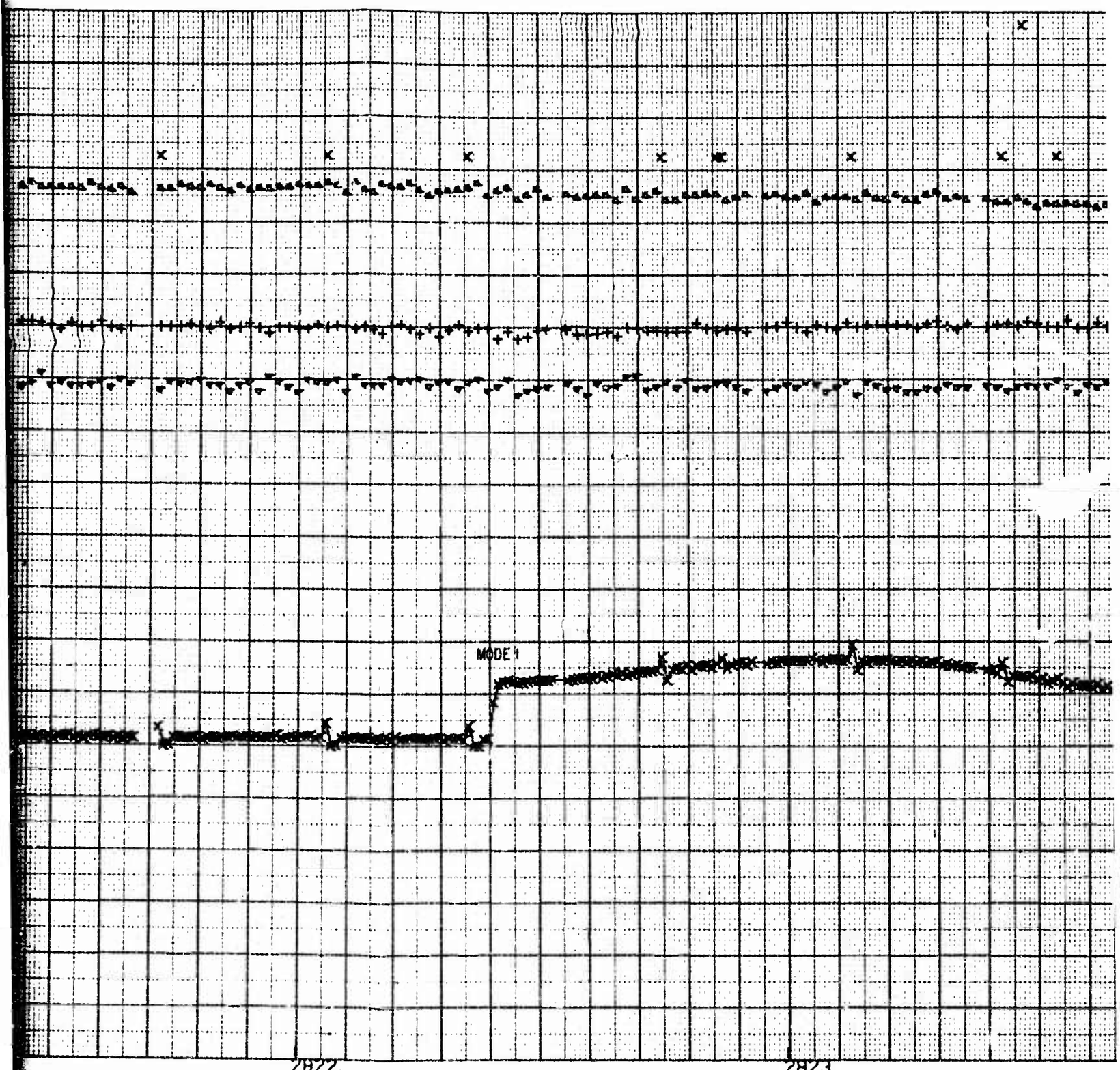

2822. 2823.

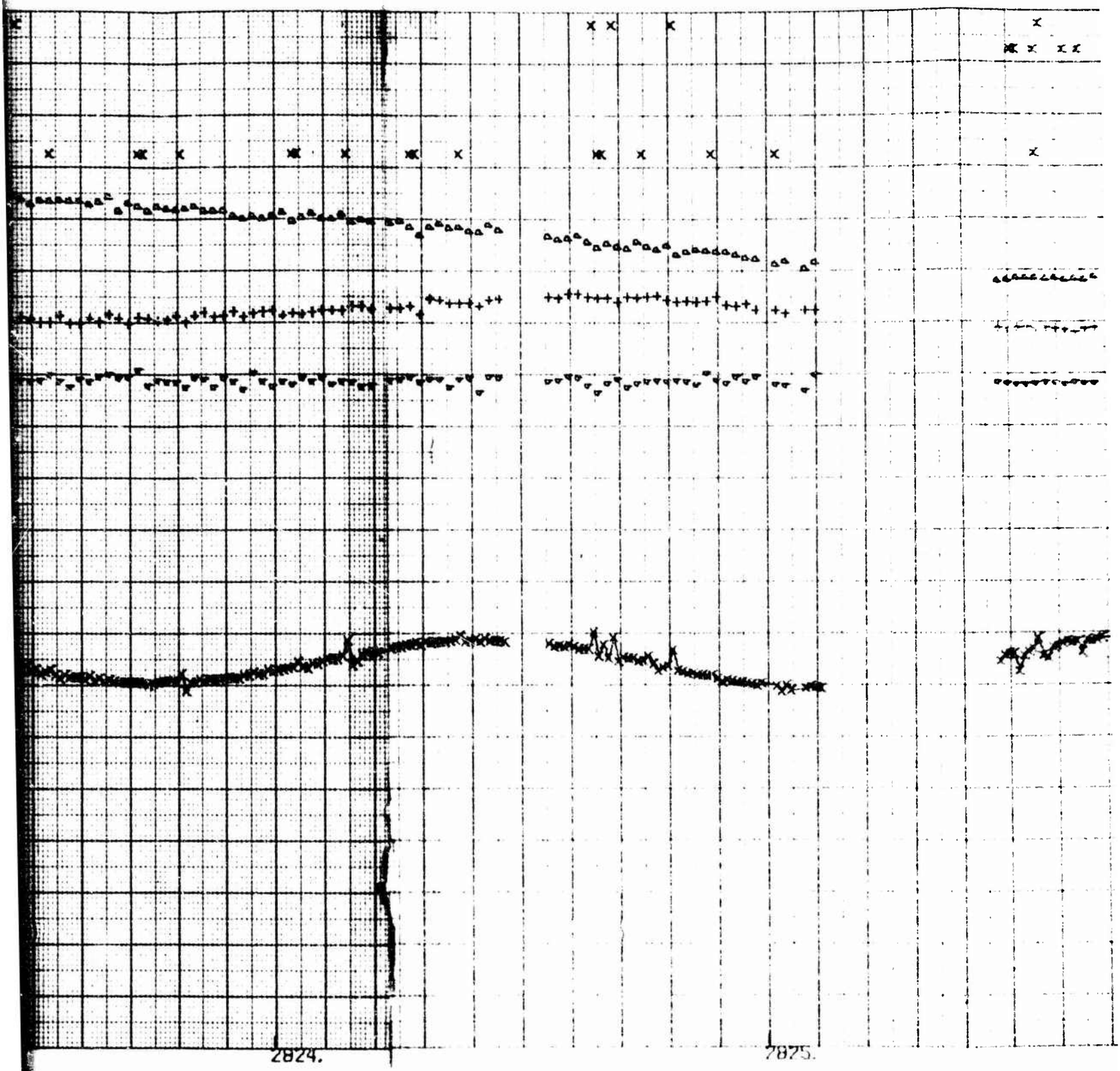
2824.
2825.

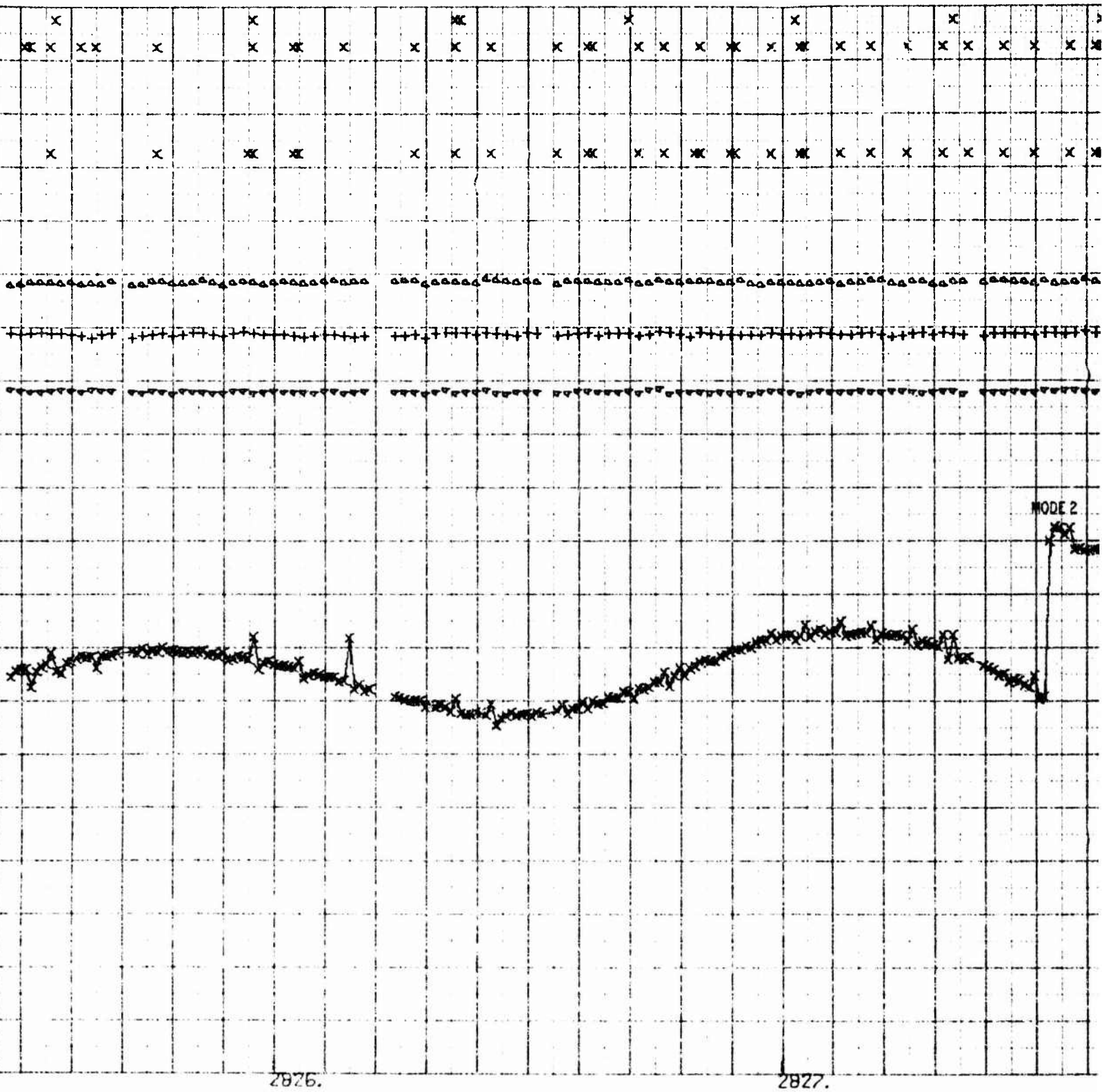

2826.

2827.

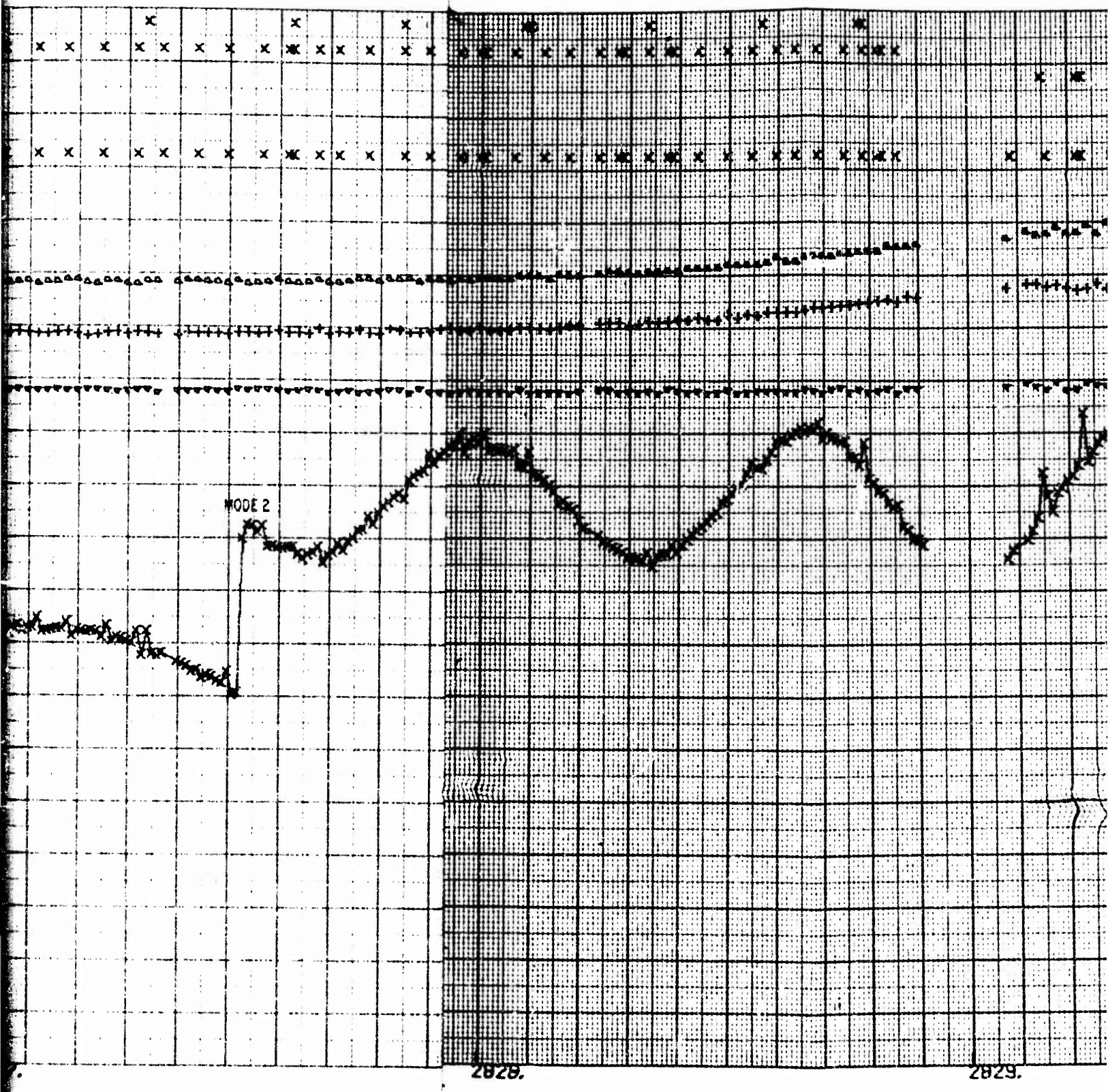
MODE 2
2828.
2829.

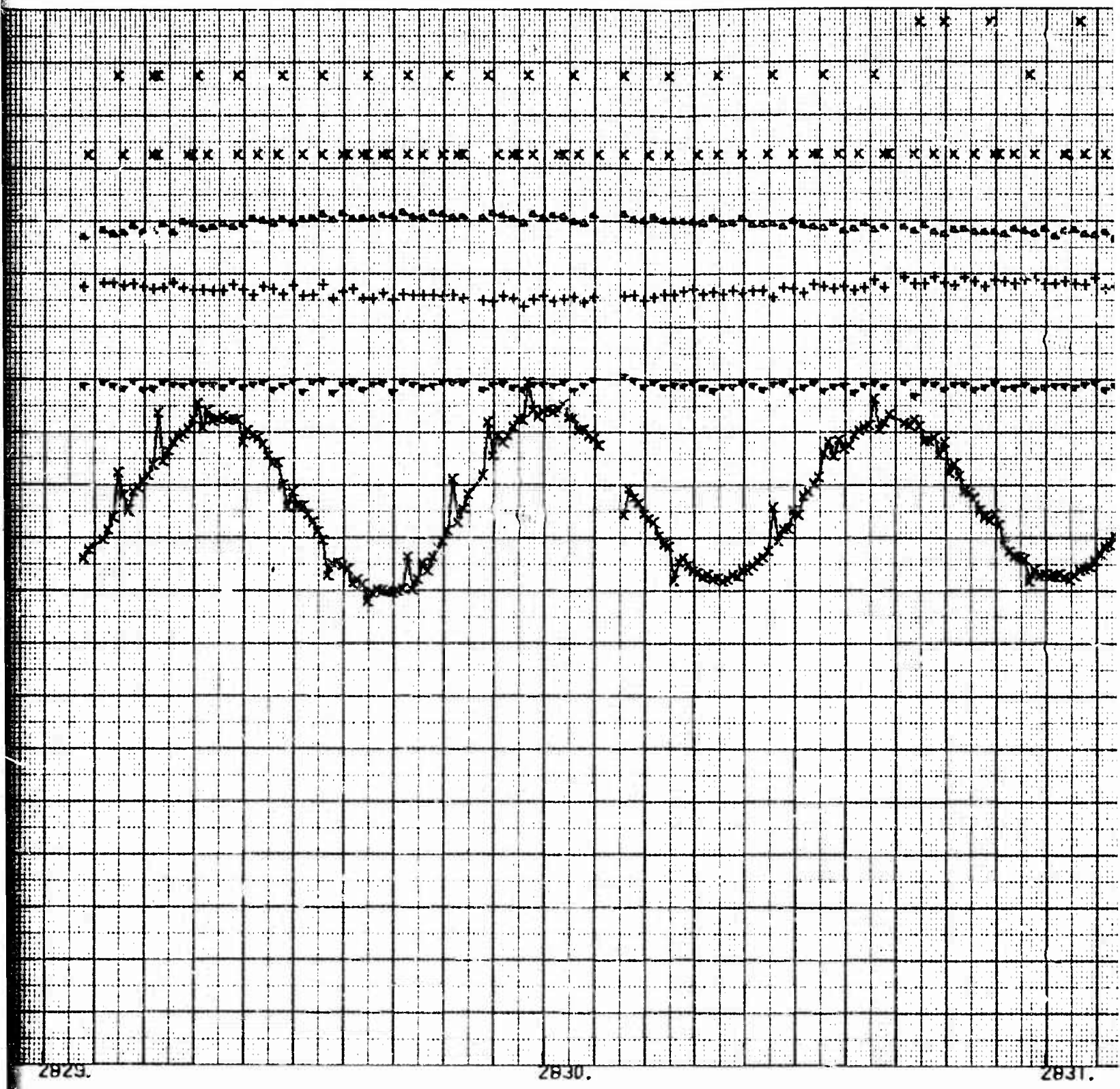
2829.
2830.
2831.

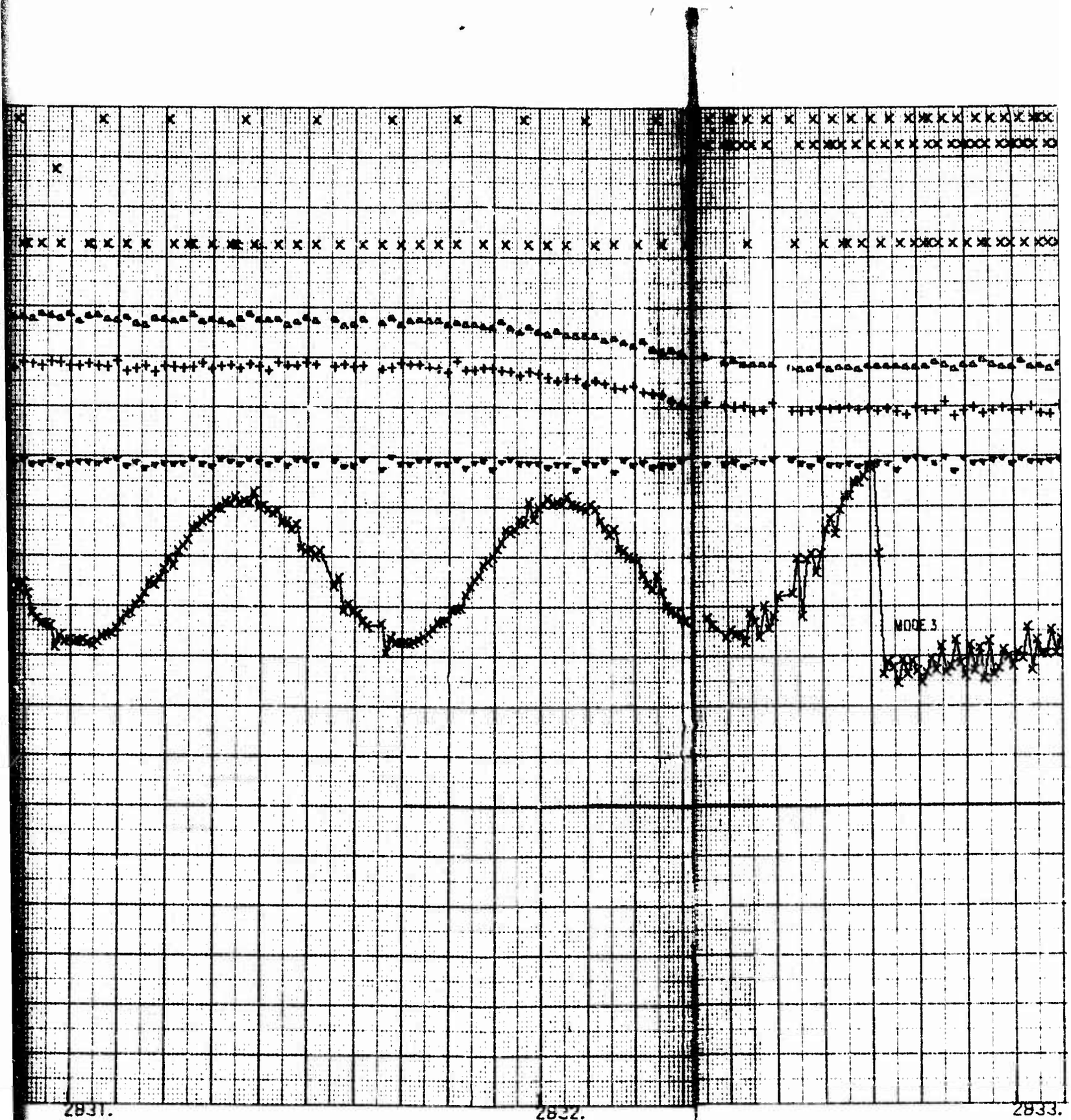
MODE 3
2831.
2832.
2833.

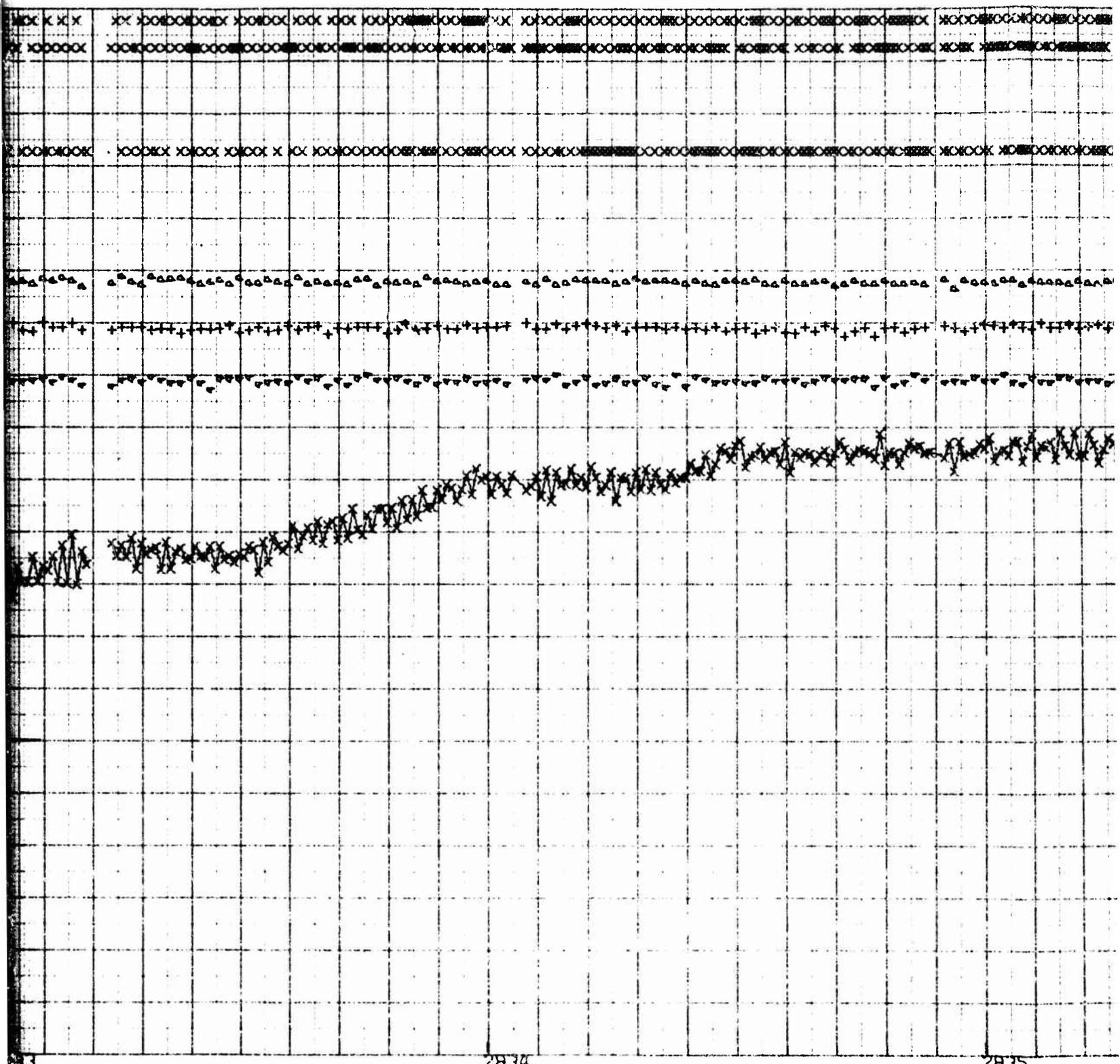

2833. 2834. 2835.

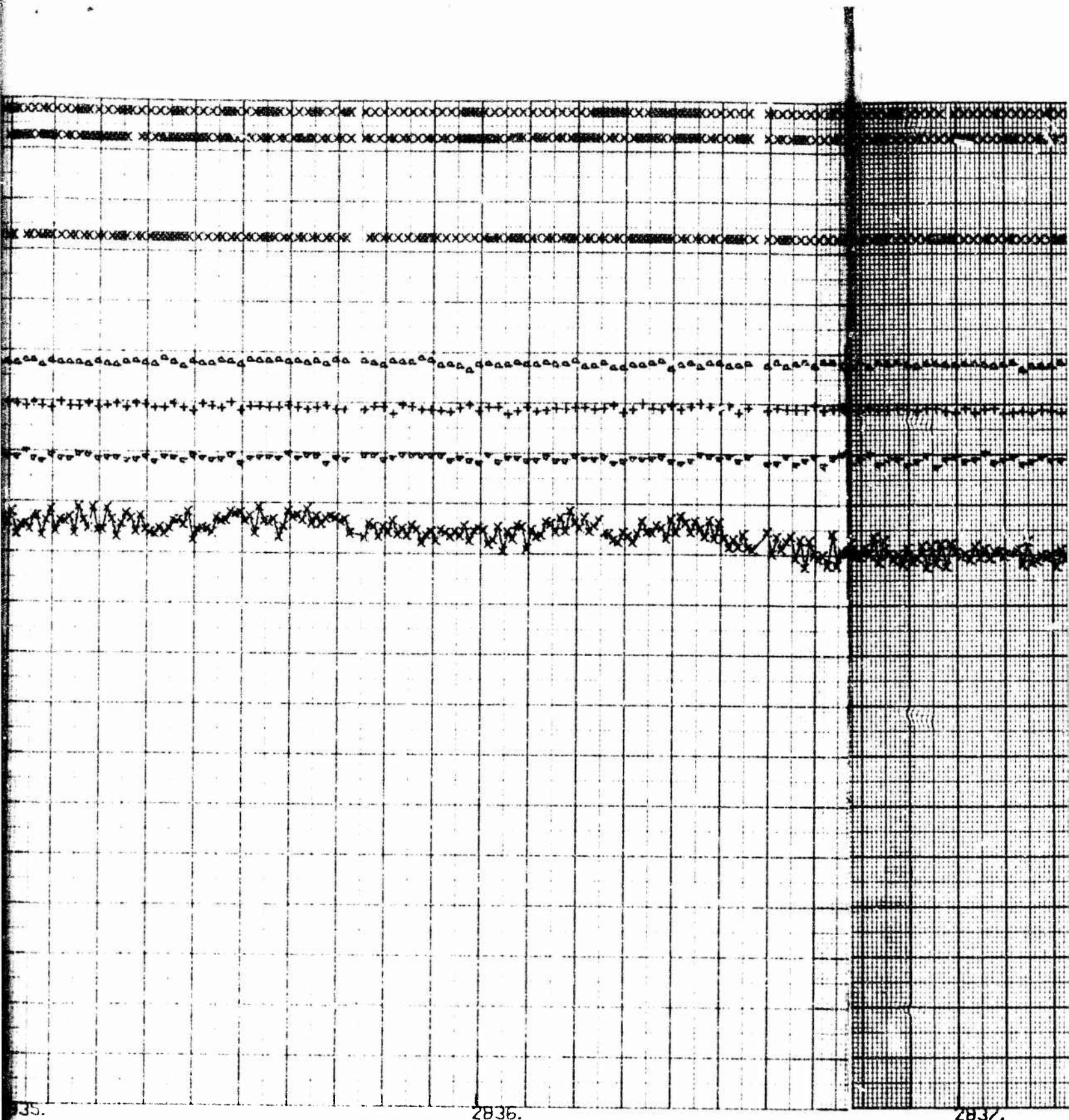

2835.

2836.

2837.

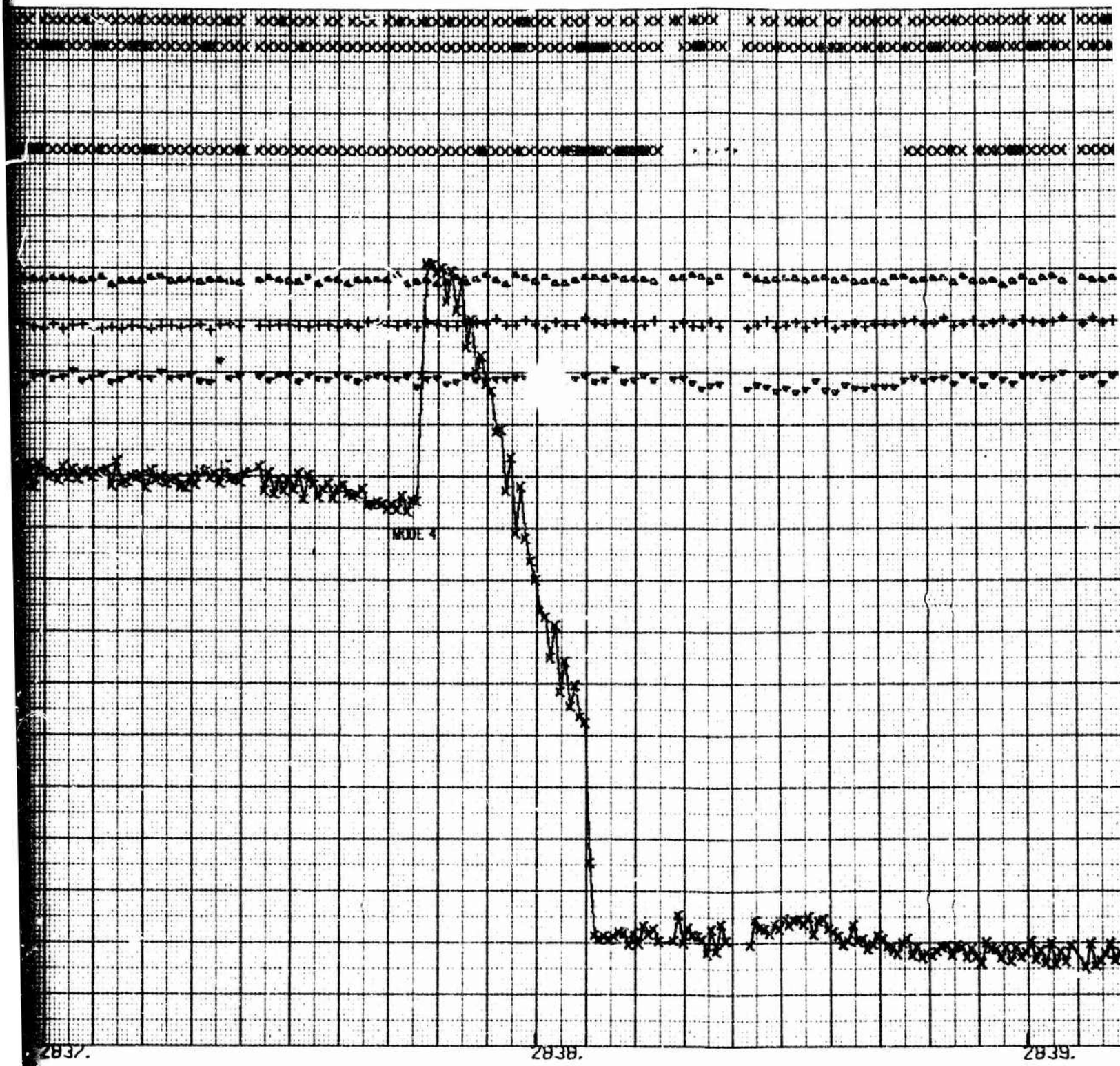
MODE 4
2837.
2838.
2839.

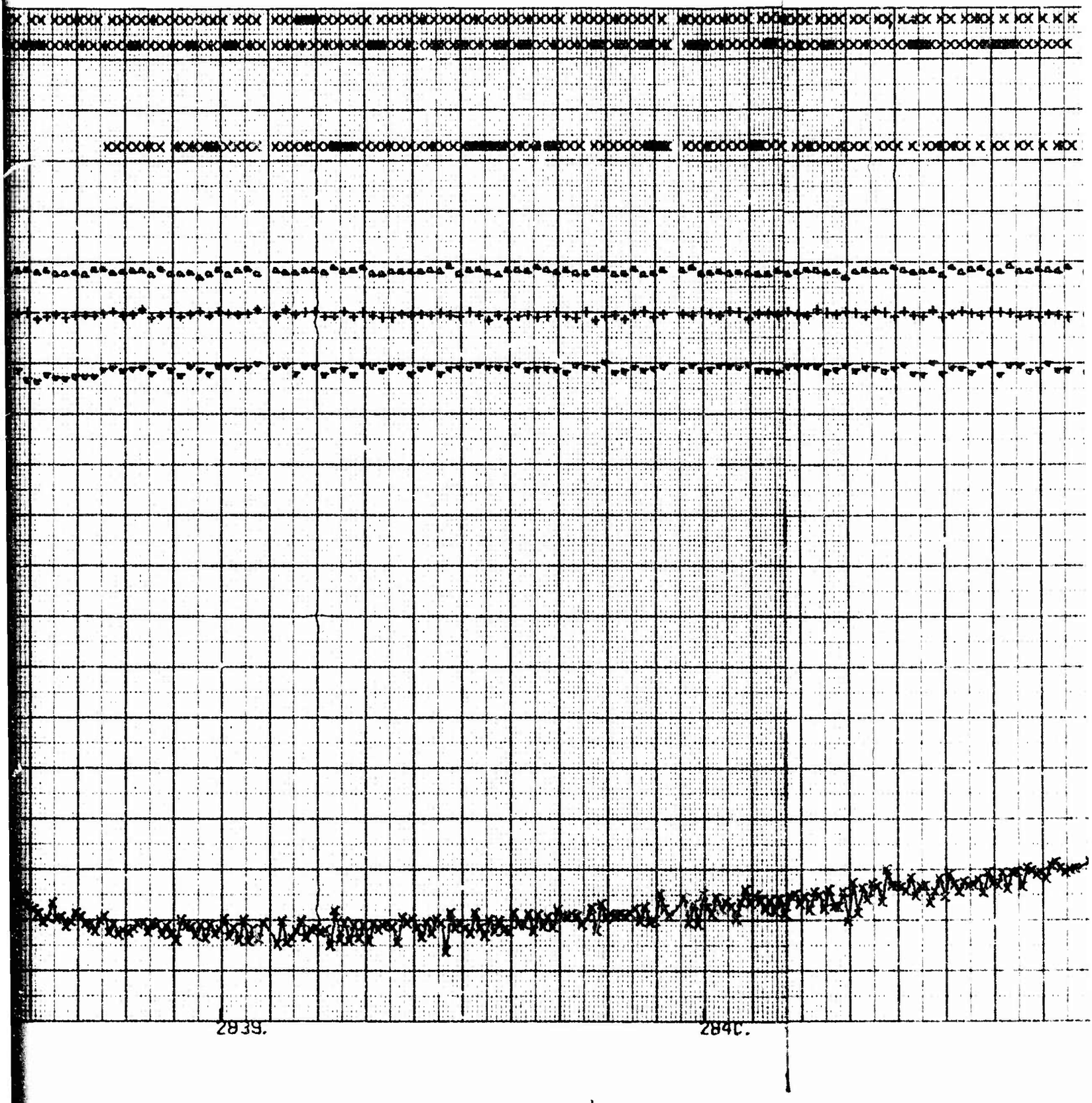
2839.
2840.

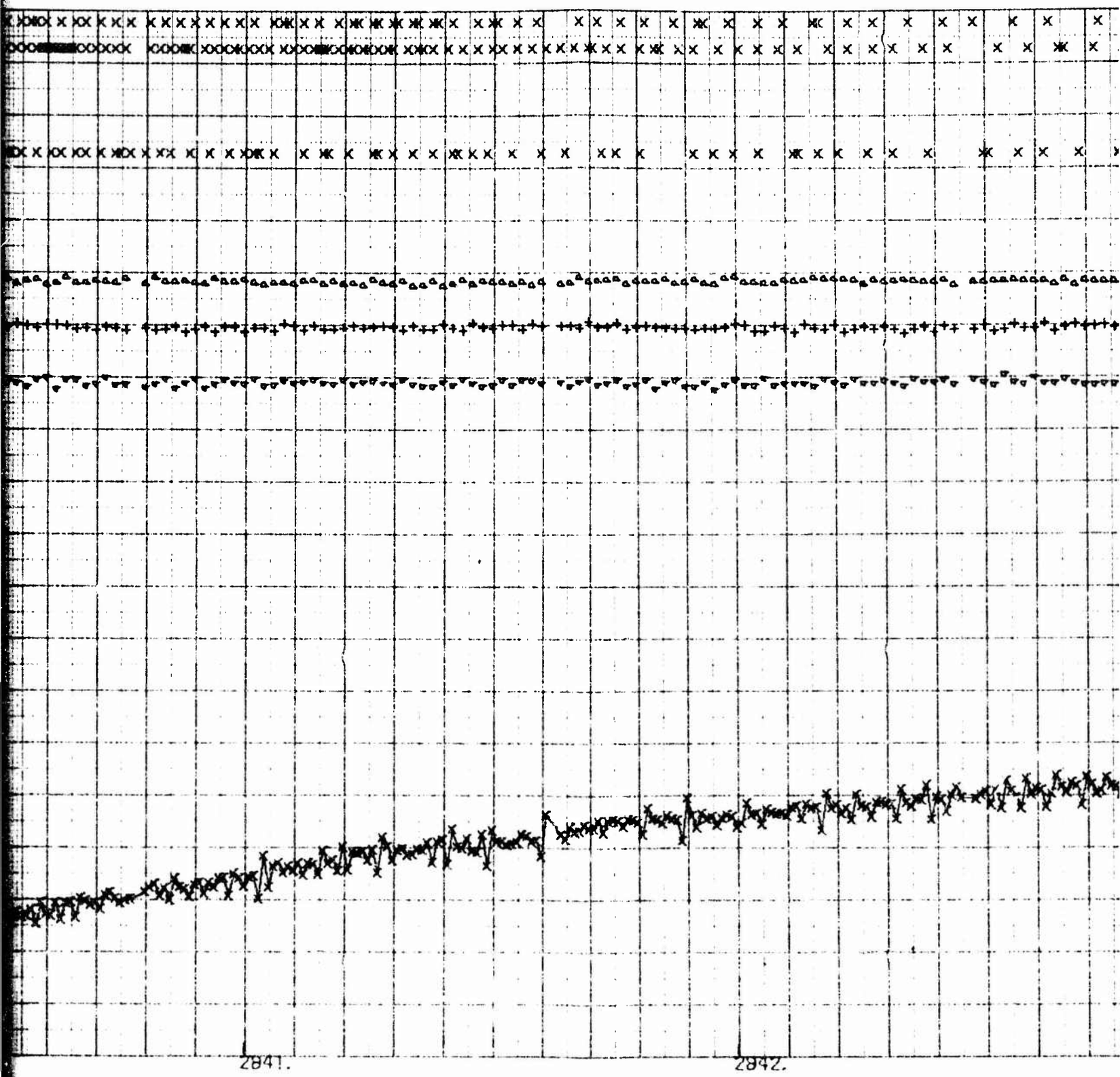
2841.
2842.

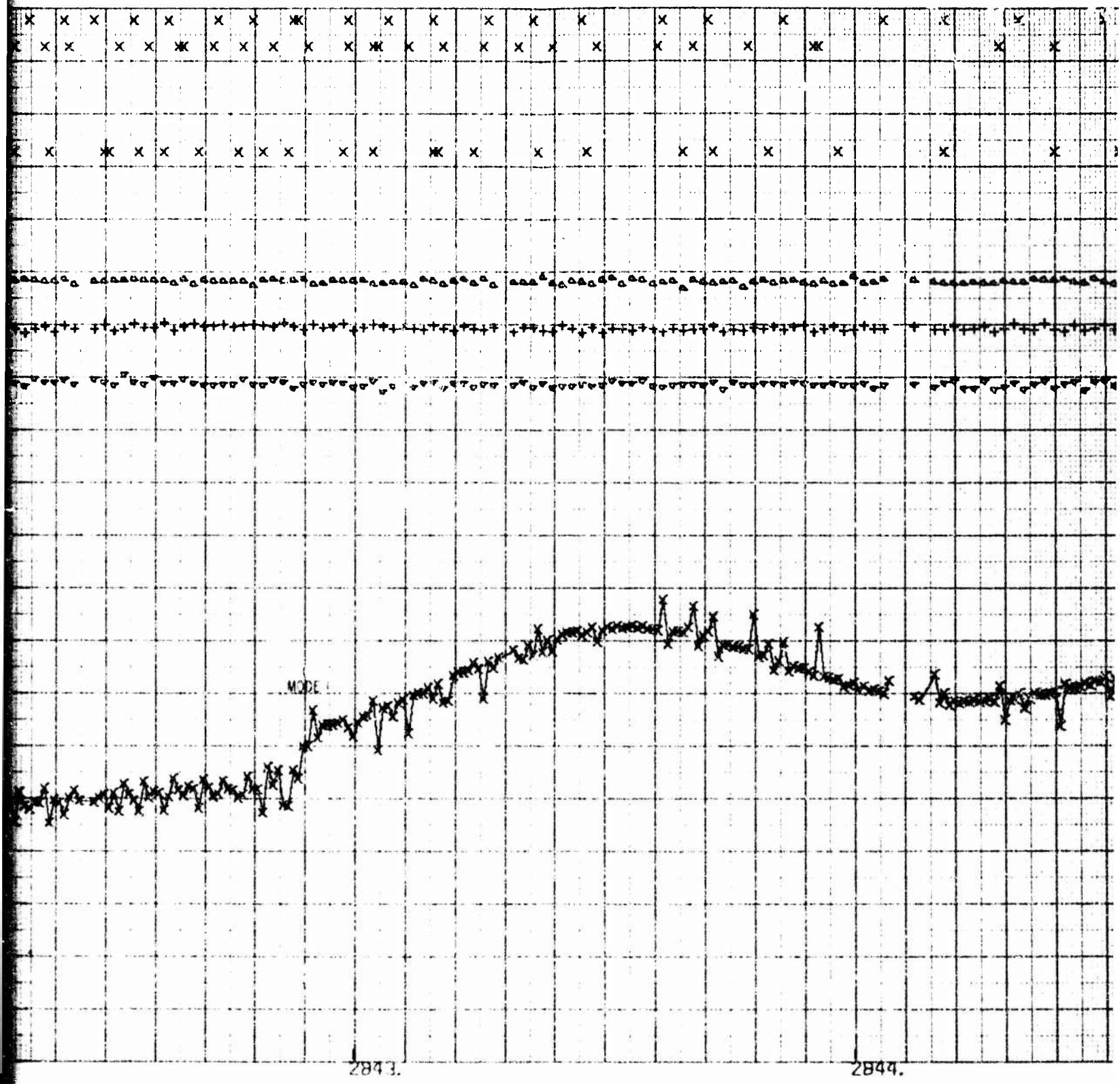
MODE
2843.
2844.

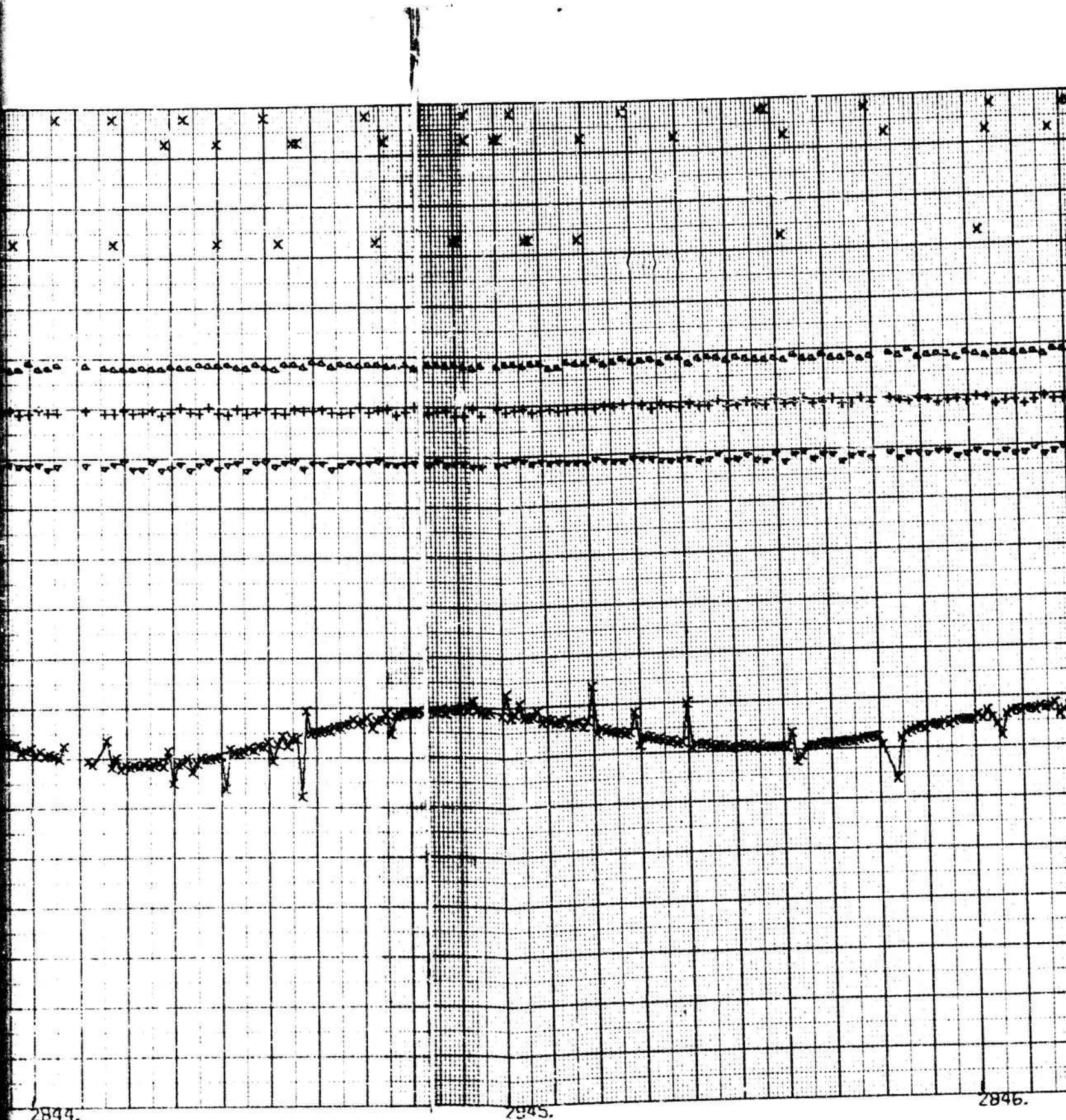
2844.
2845.
2846.

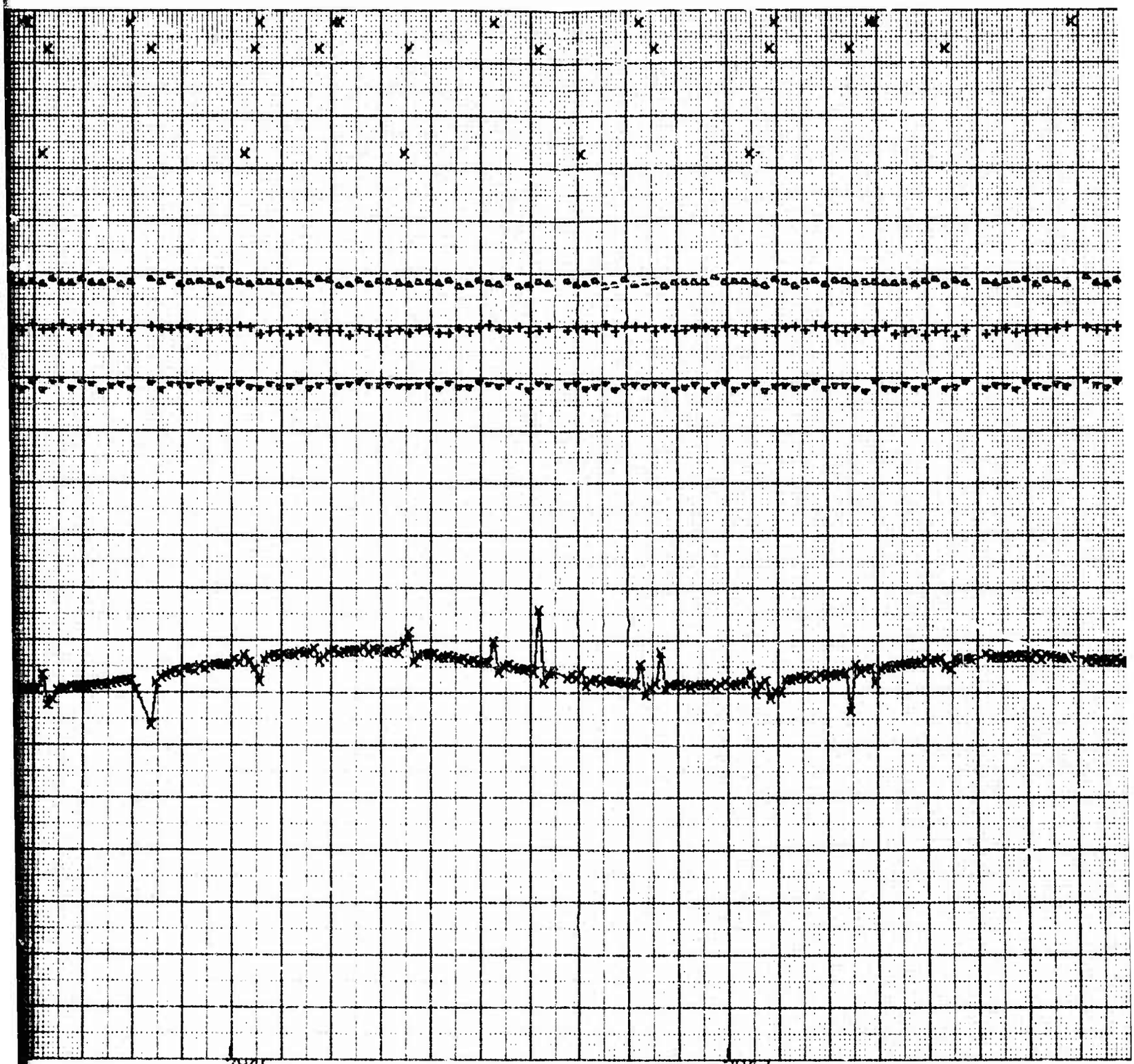

2846. 2847.

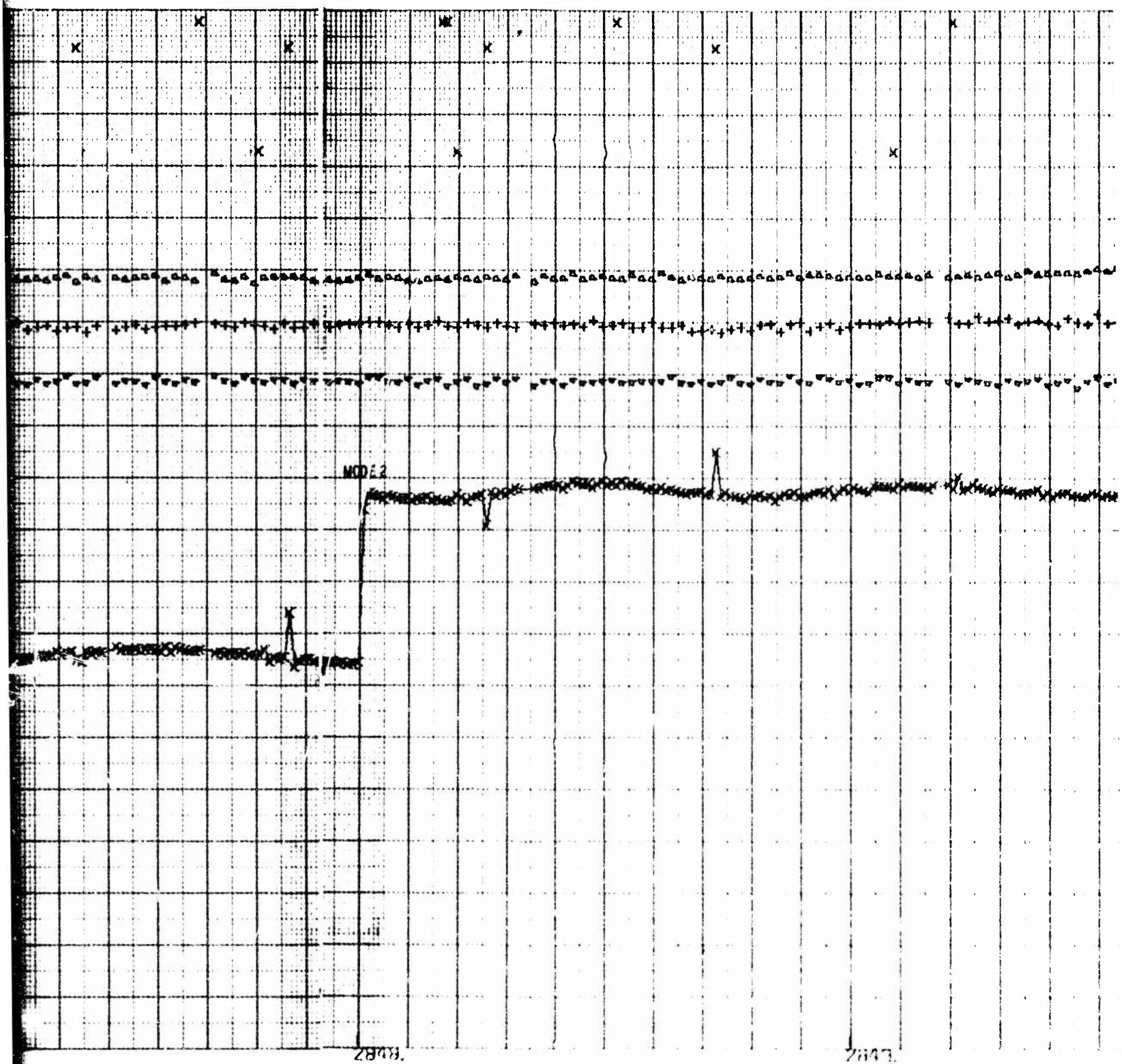
MODE 2

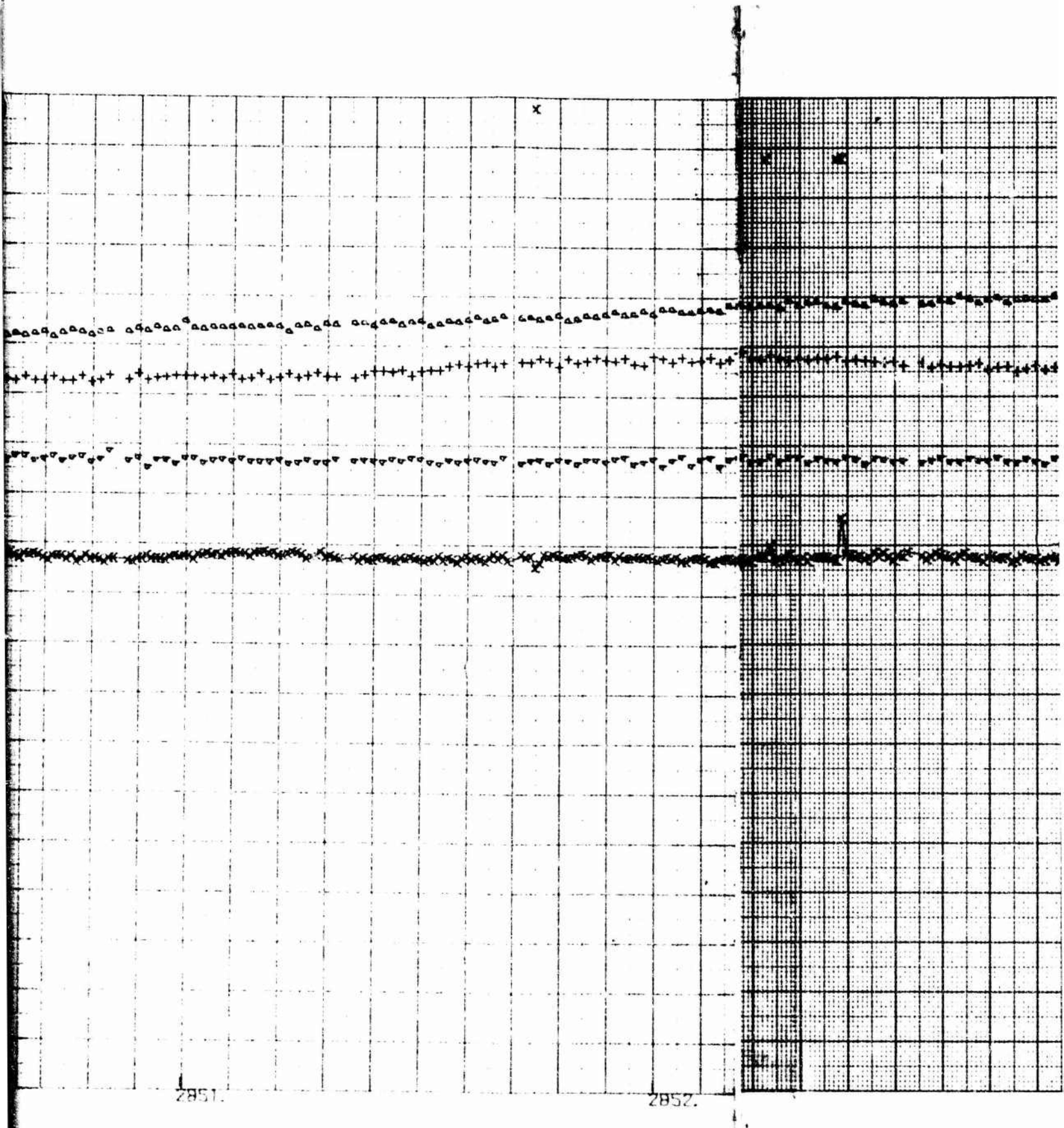
2851.
2852.

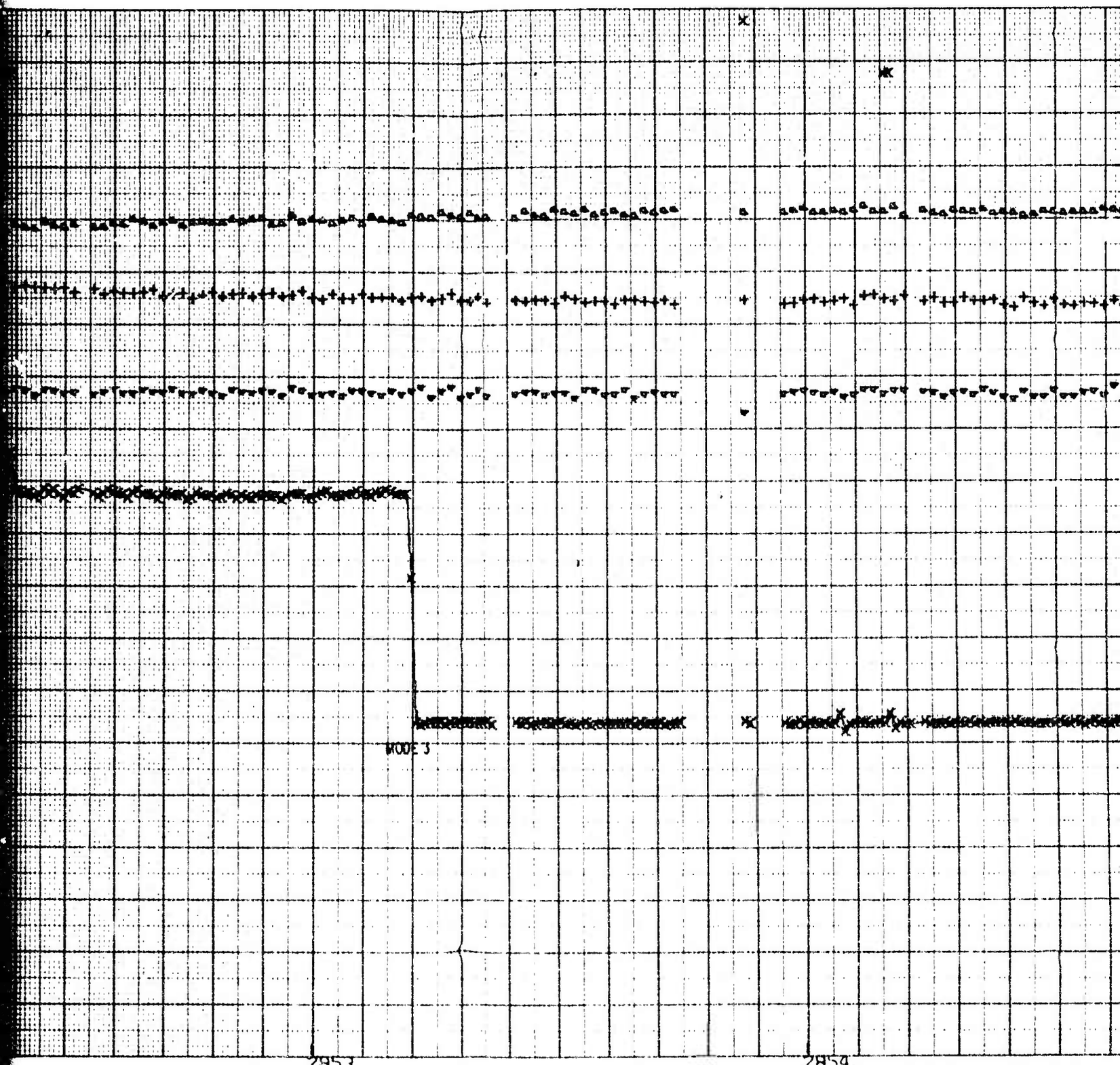

2853. 2854.

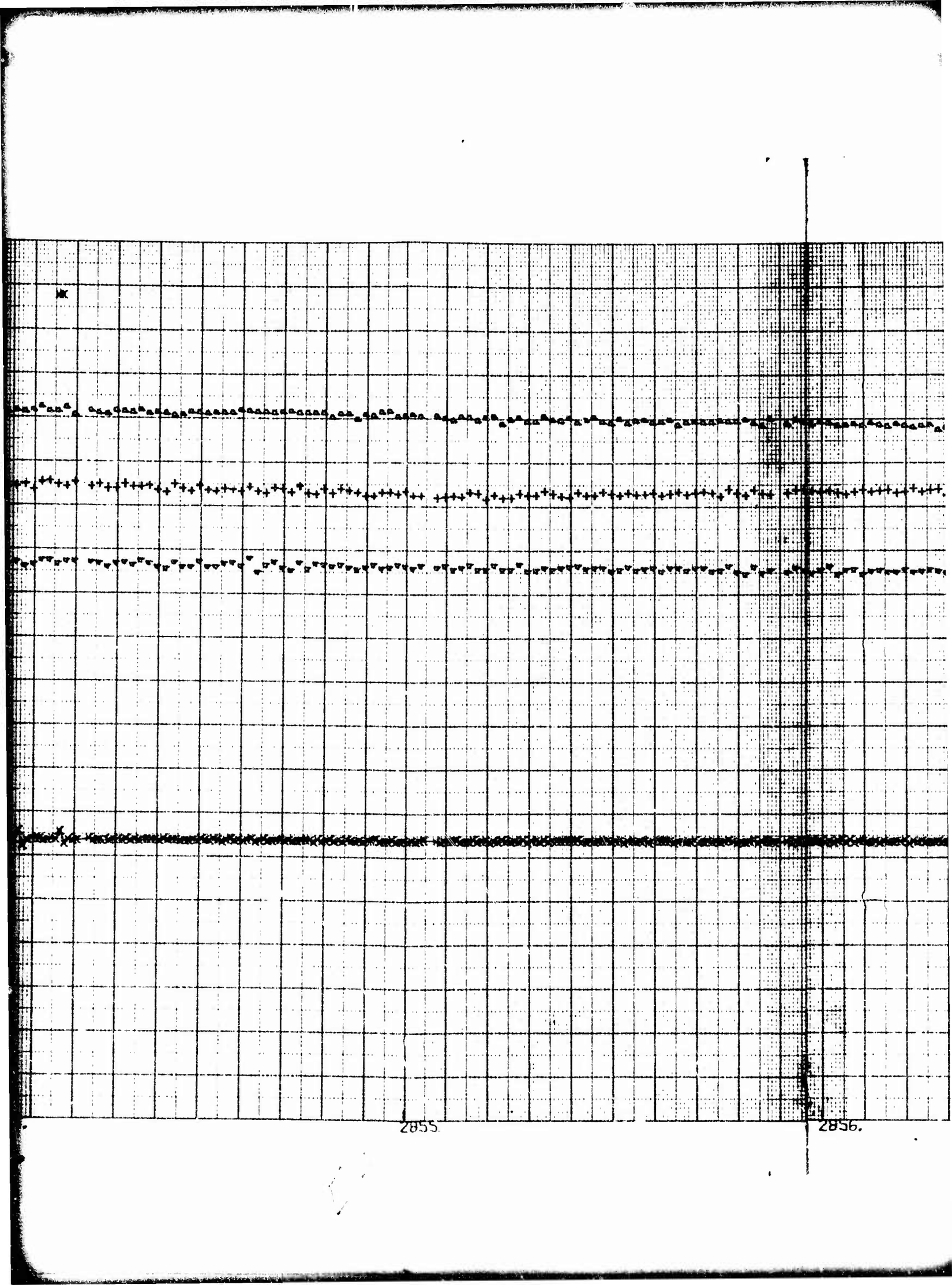
2855.
2856.

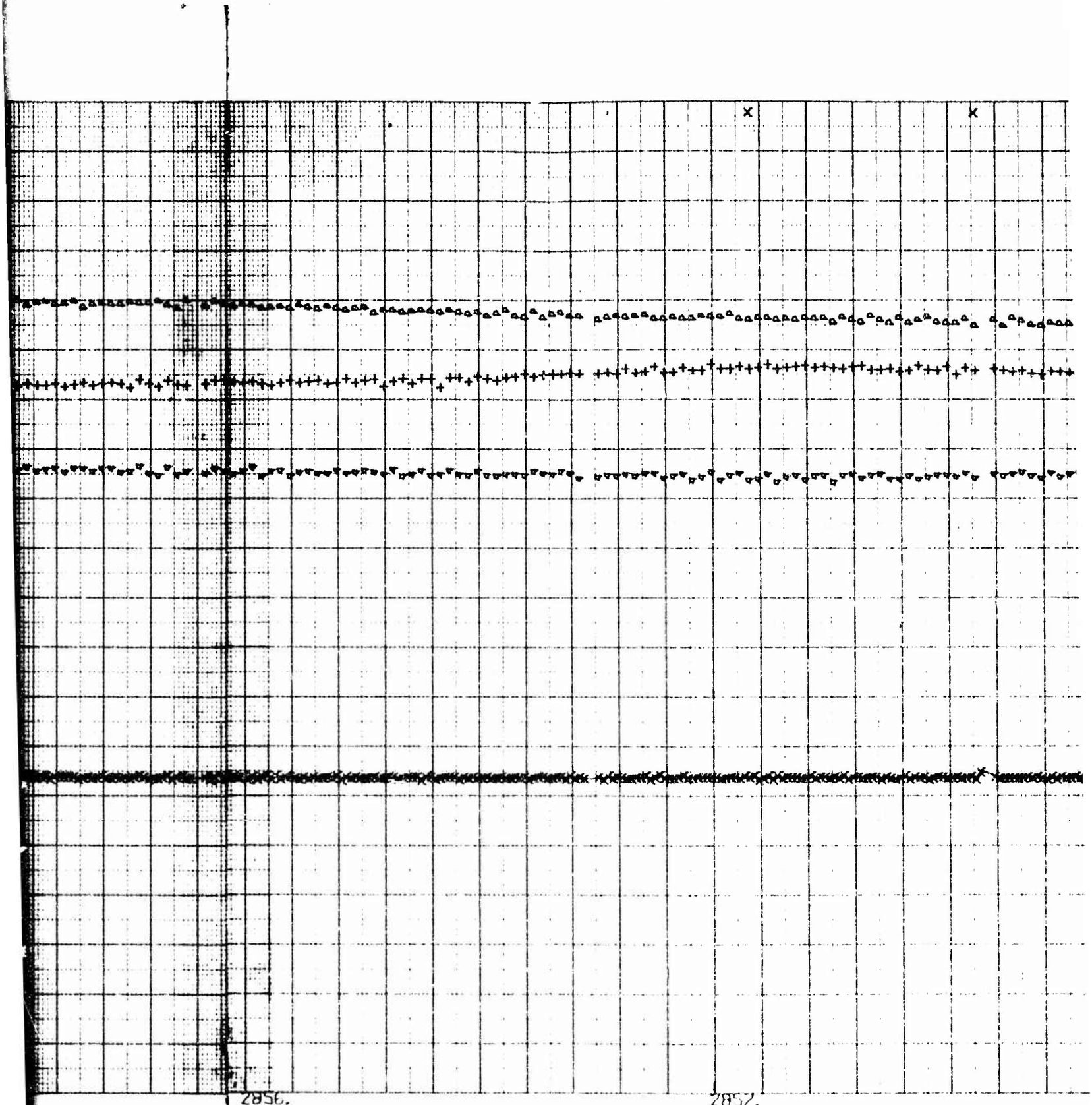
2856.
2852.

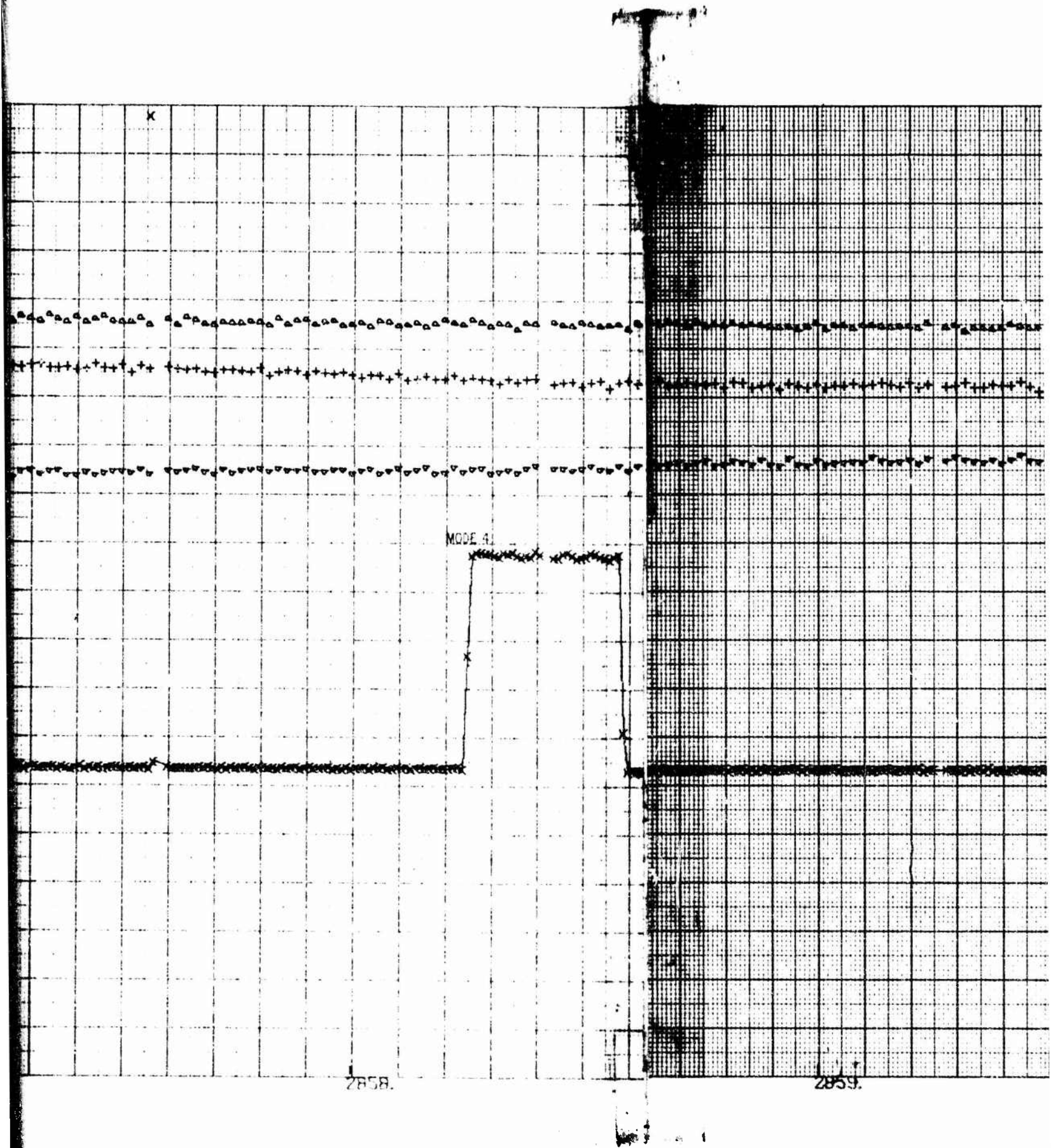
MODE 4
2858.
2859.

2860.

2861.

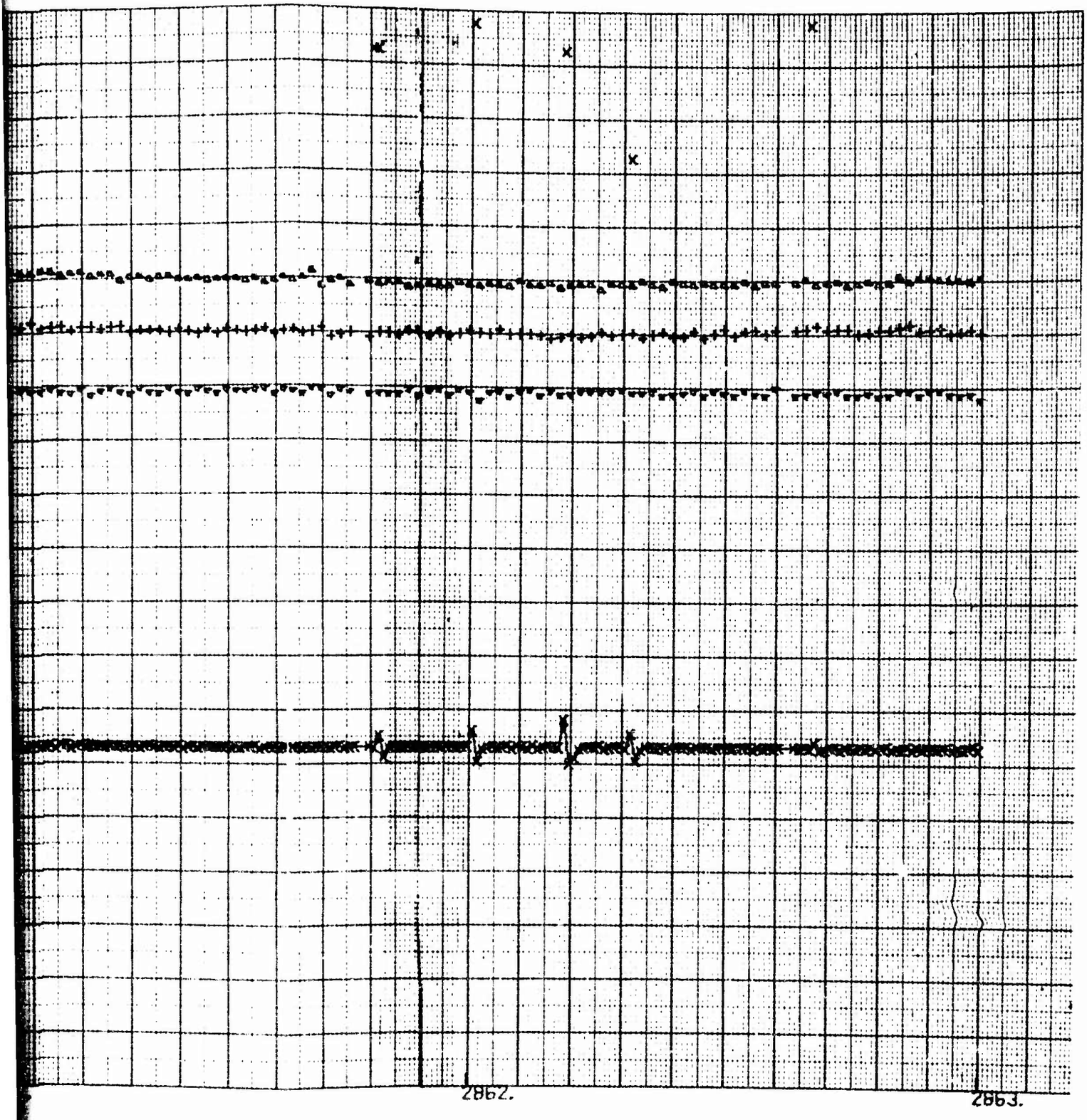

Fig. F-1. Sample Raw Data (Revolution 52.7 to 53.8)

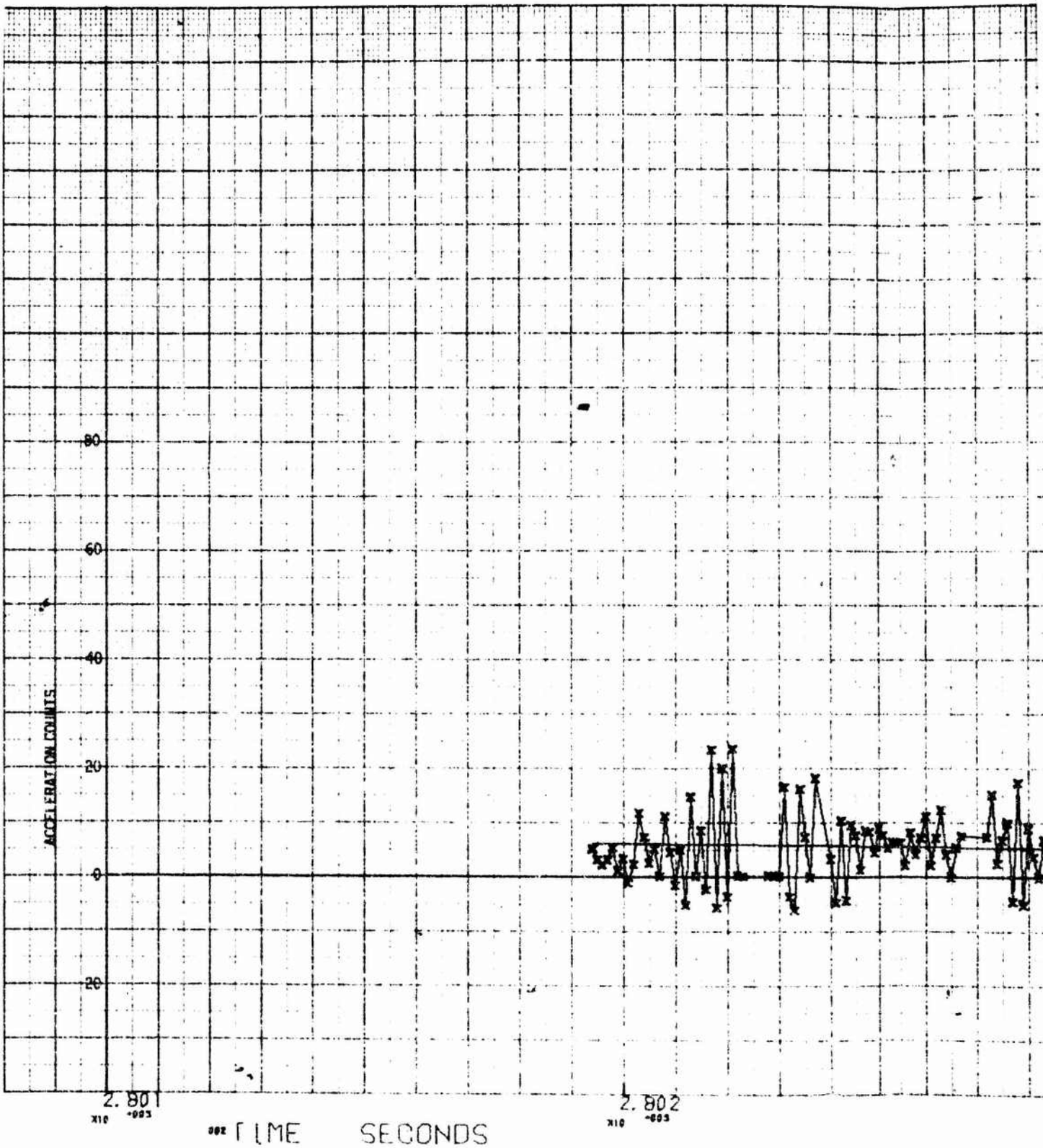
80
60
40
20
0
20
ACCELERATION COUNTS
2.801
X10 +003
2.802
X10 +003
TIME SECONDS

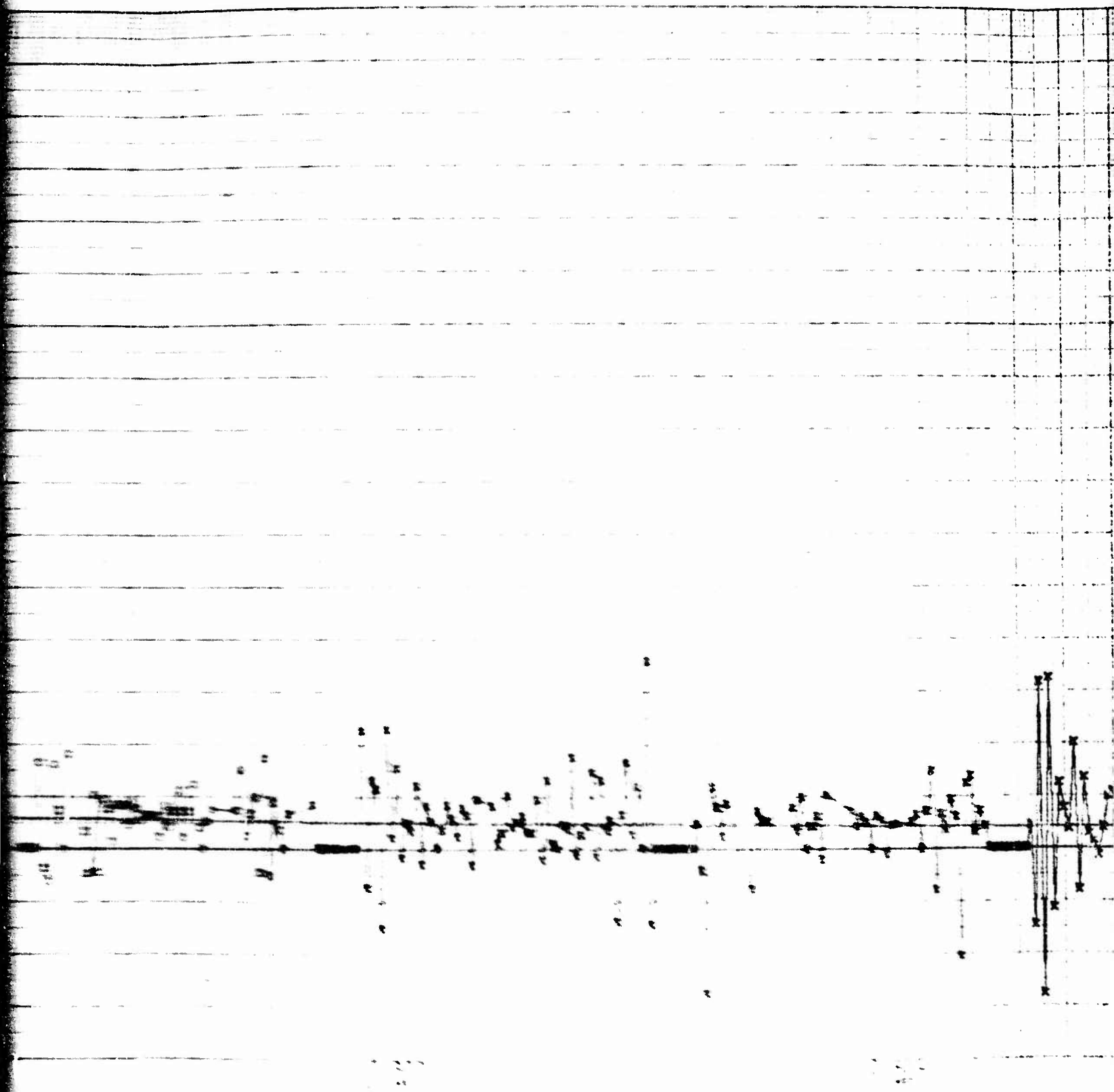

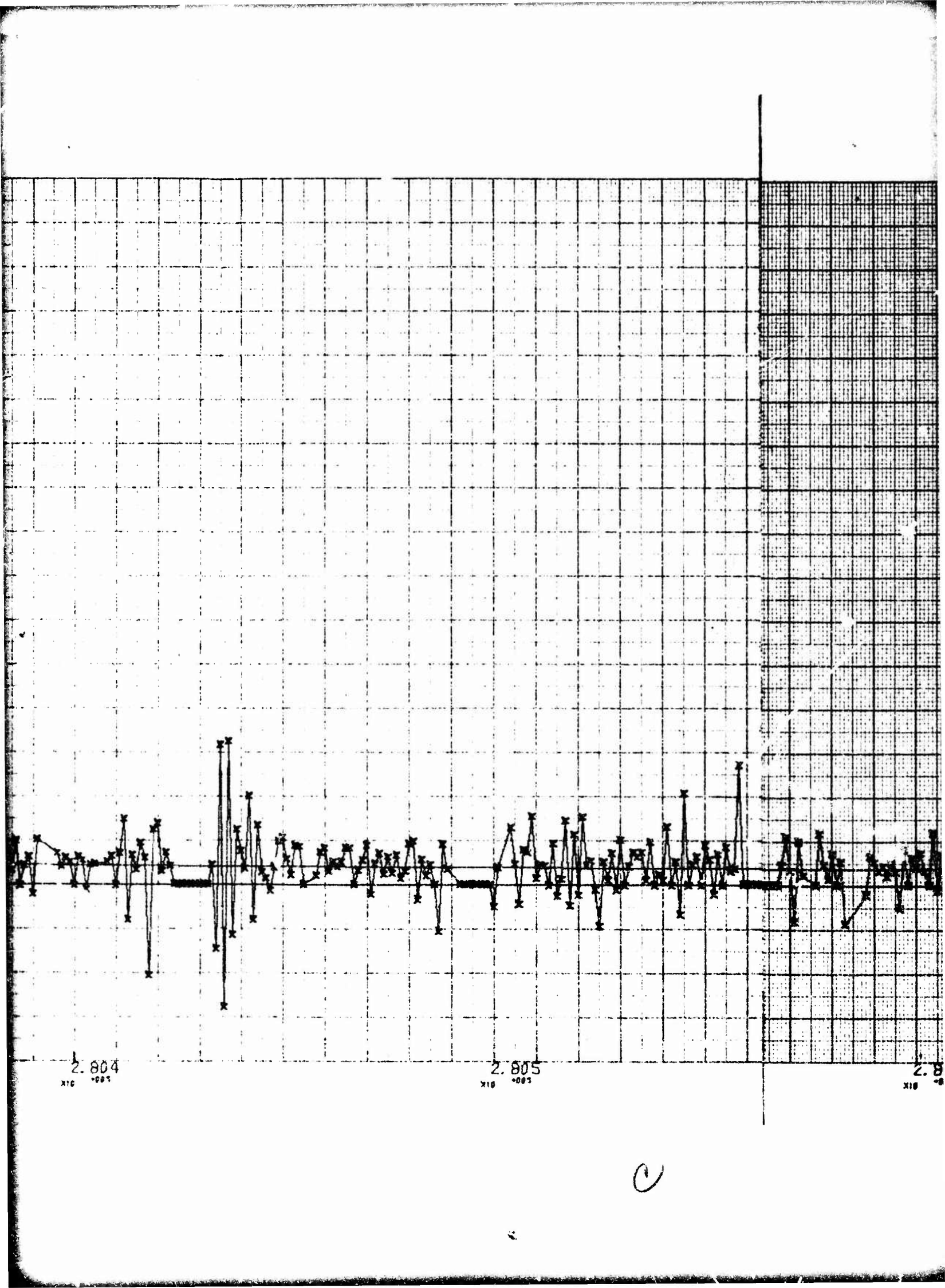
2.804
2.805

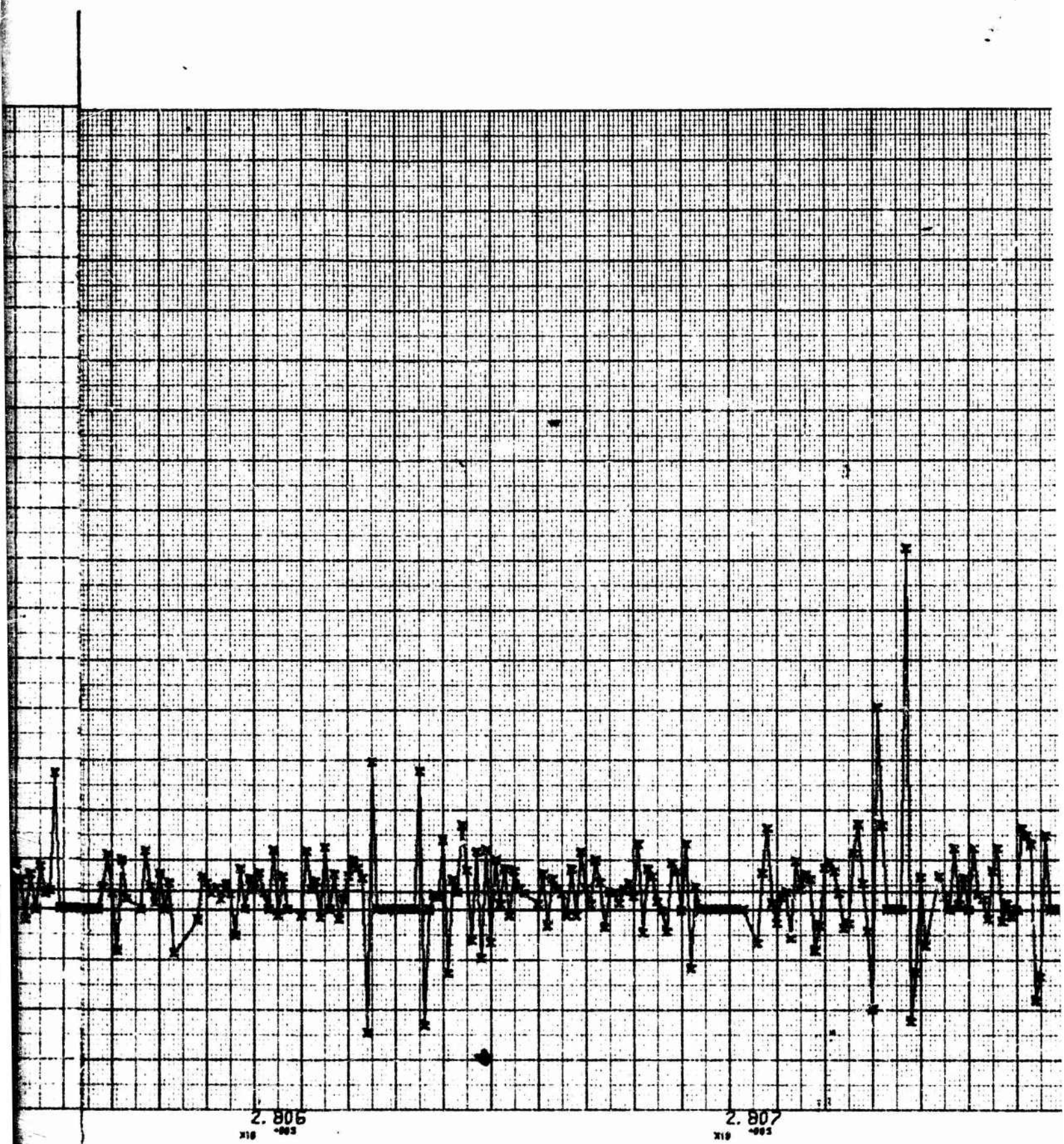
2.806
X18 +003
2.807
X19 +003

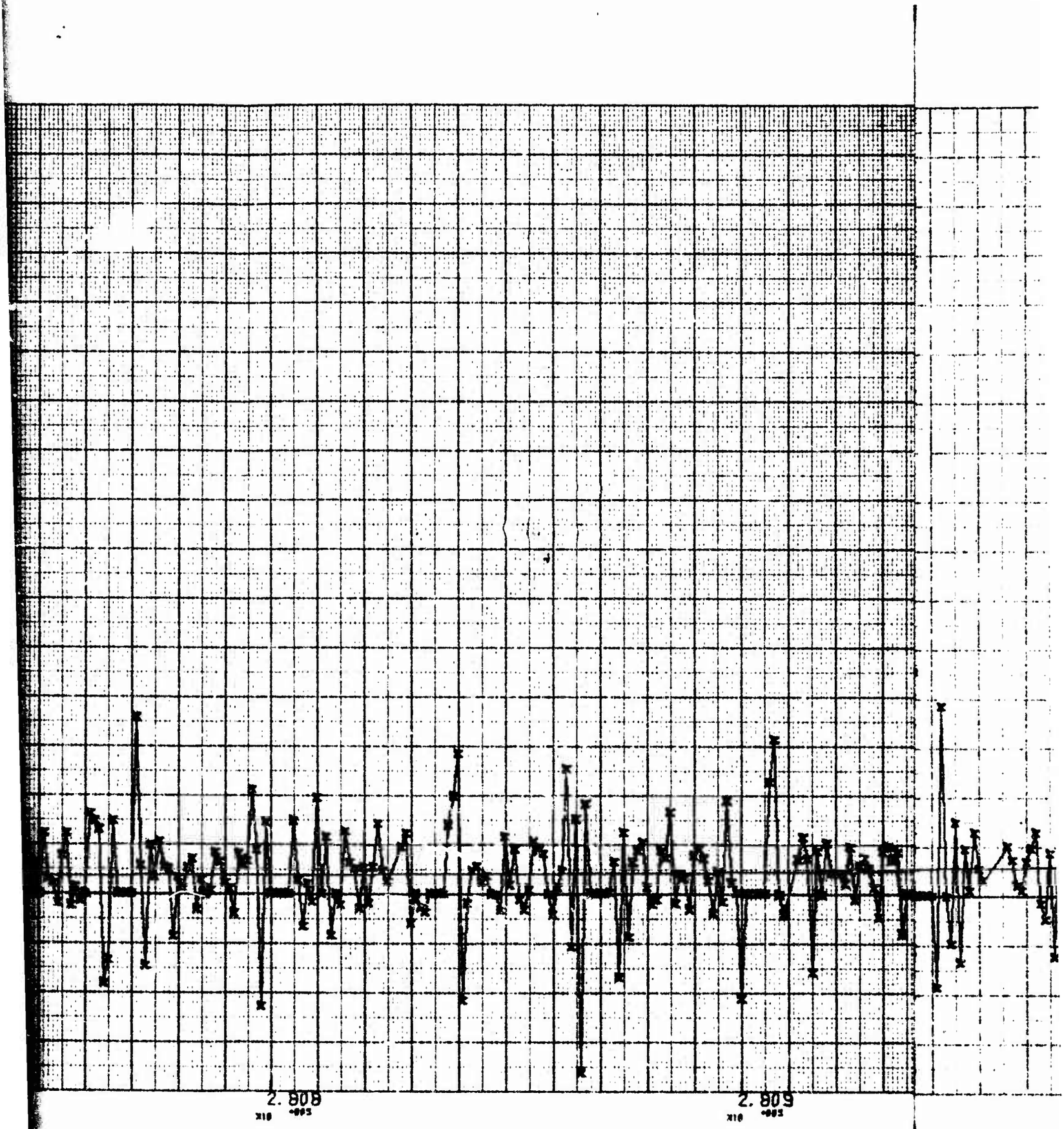
2.808
X10 +003
2.809
X10 +003

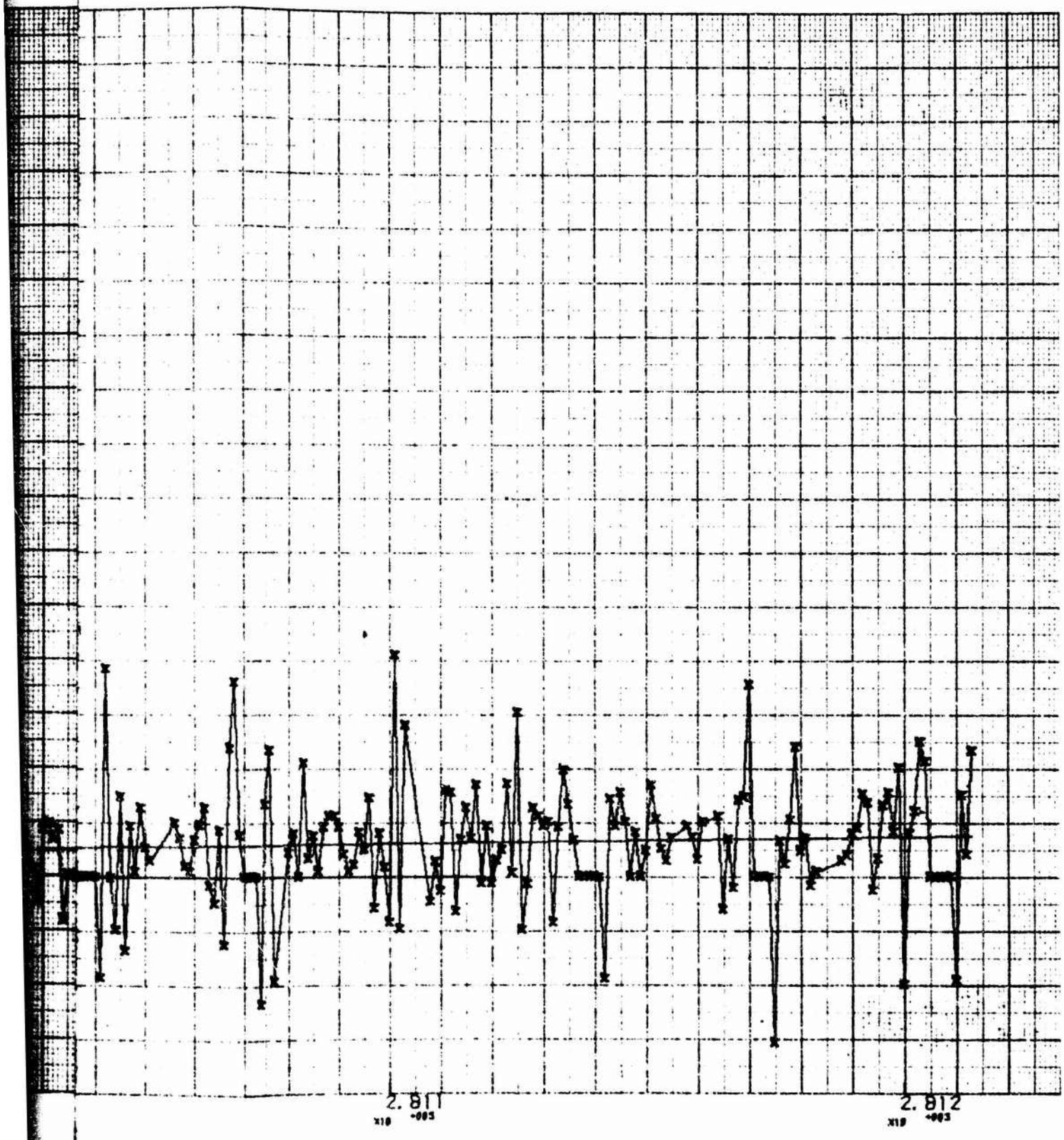

Fig. F-2. Acceleration Profile from Revolution 52 Apogee Calibration

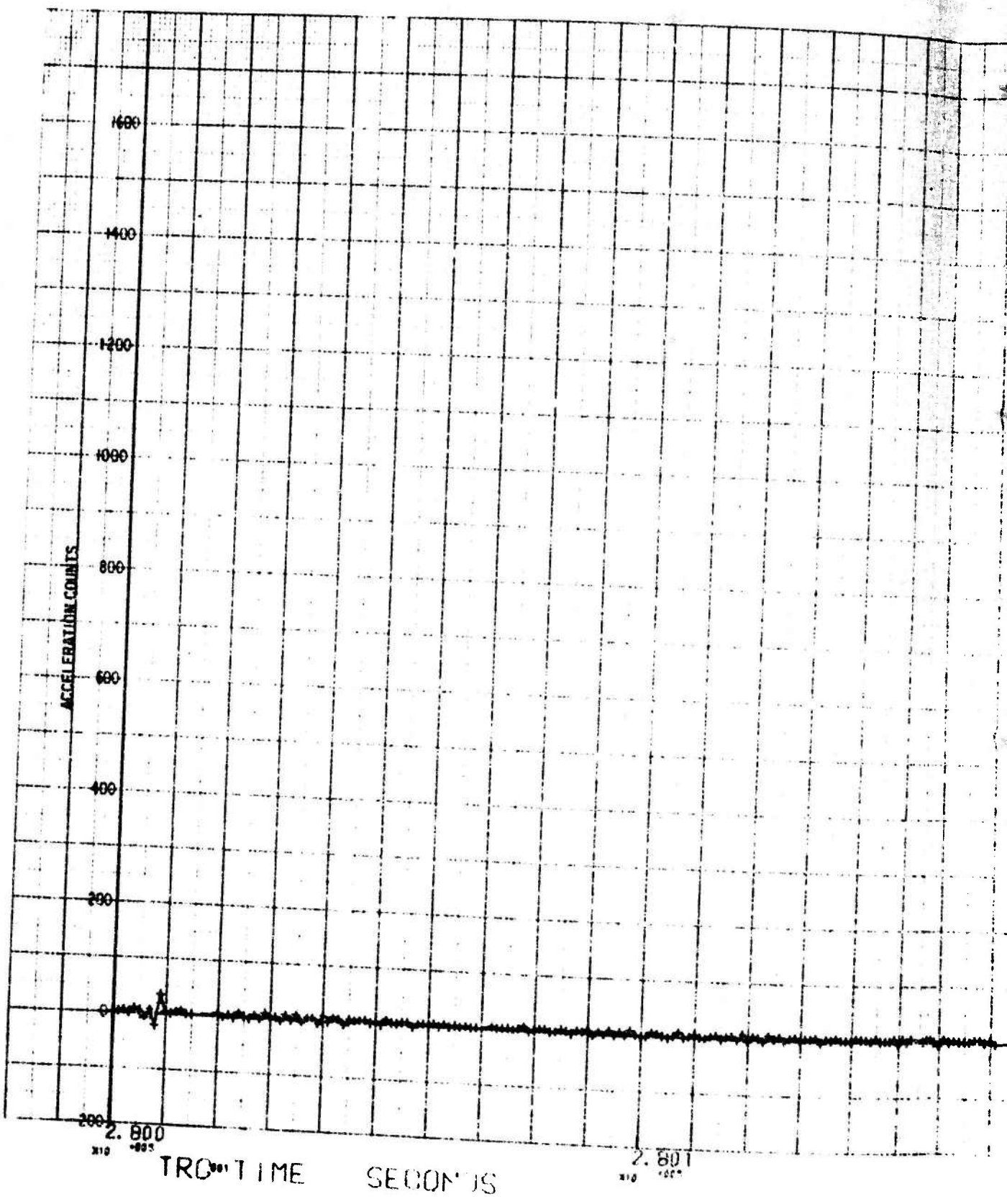
1600
1400
1200
1000
800
600
400
200
0
200
ACCELERATION COUNTS
2.800
2.801
TRO TIME SECONDS

A

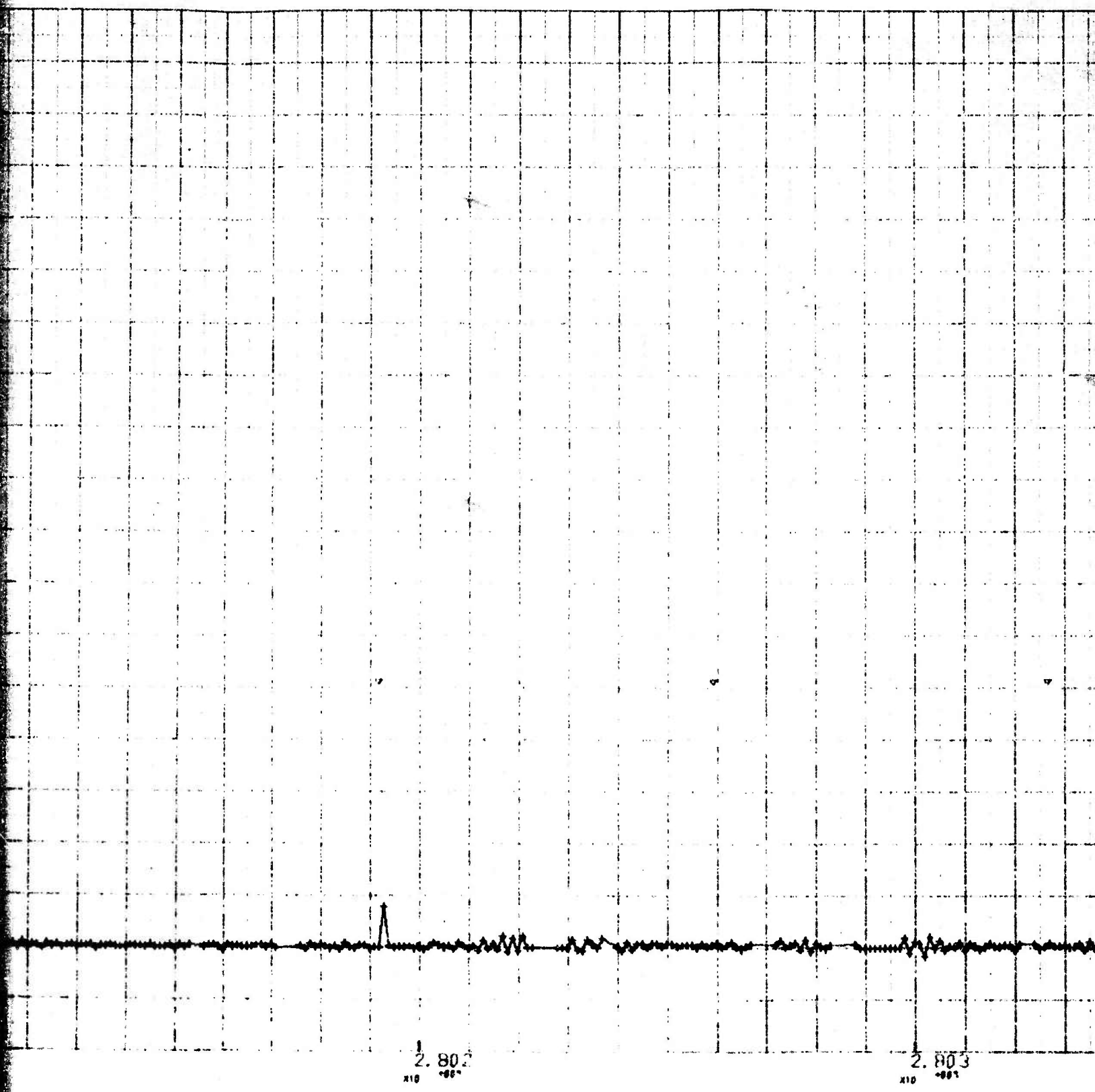

B

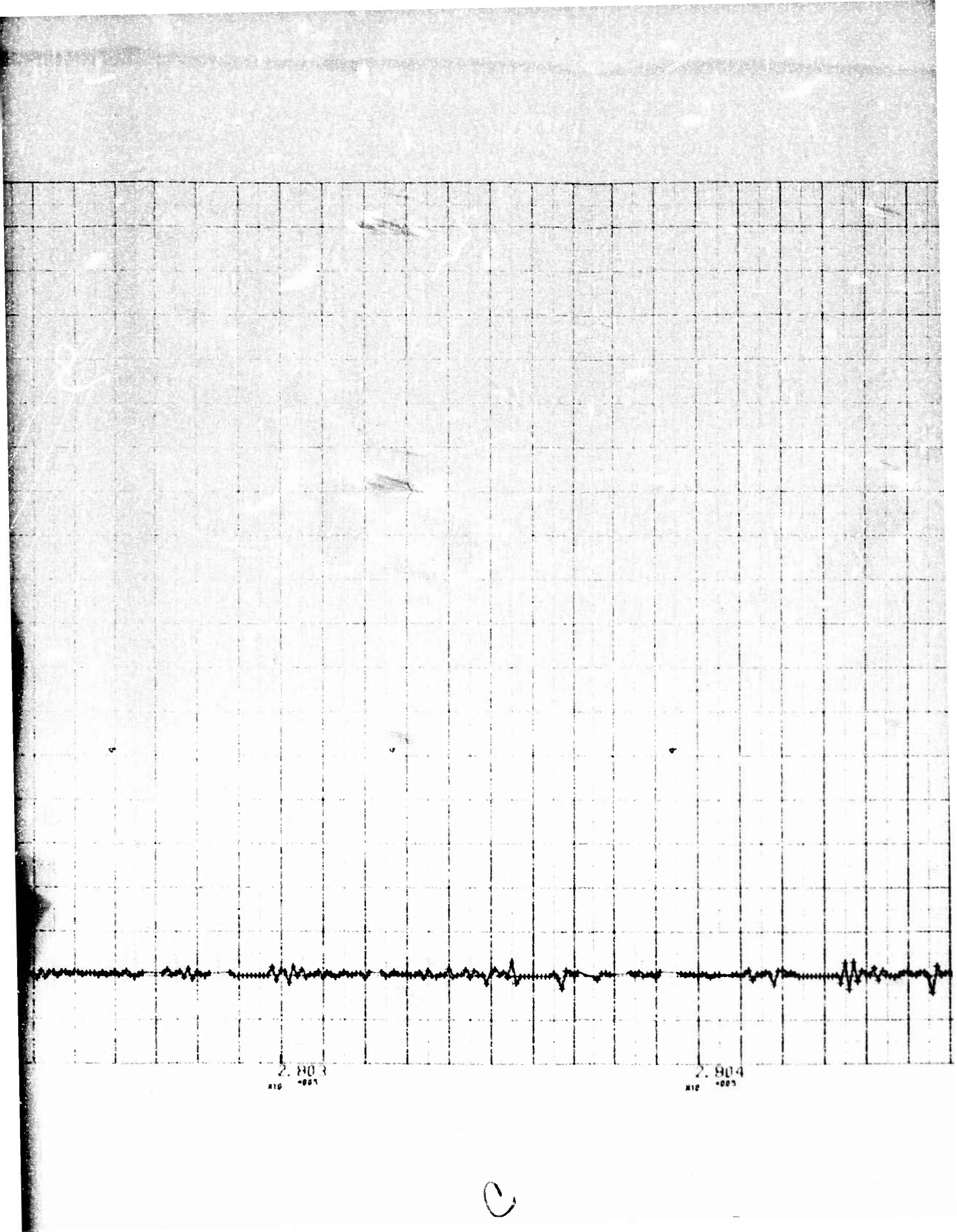
2.803
2.904

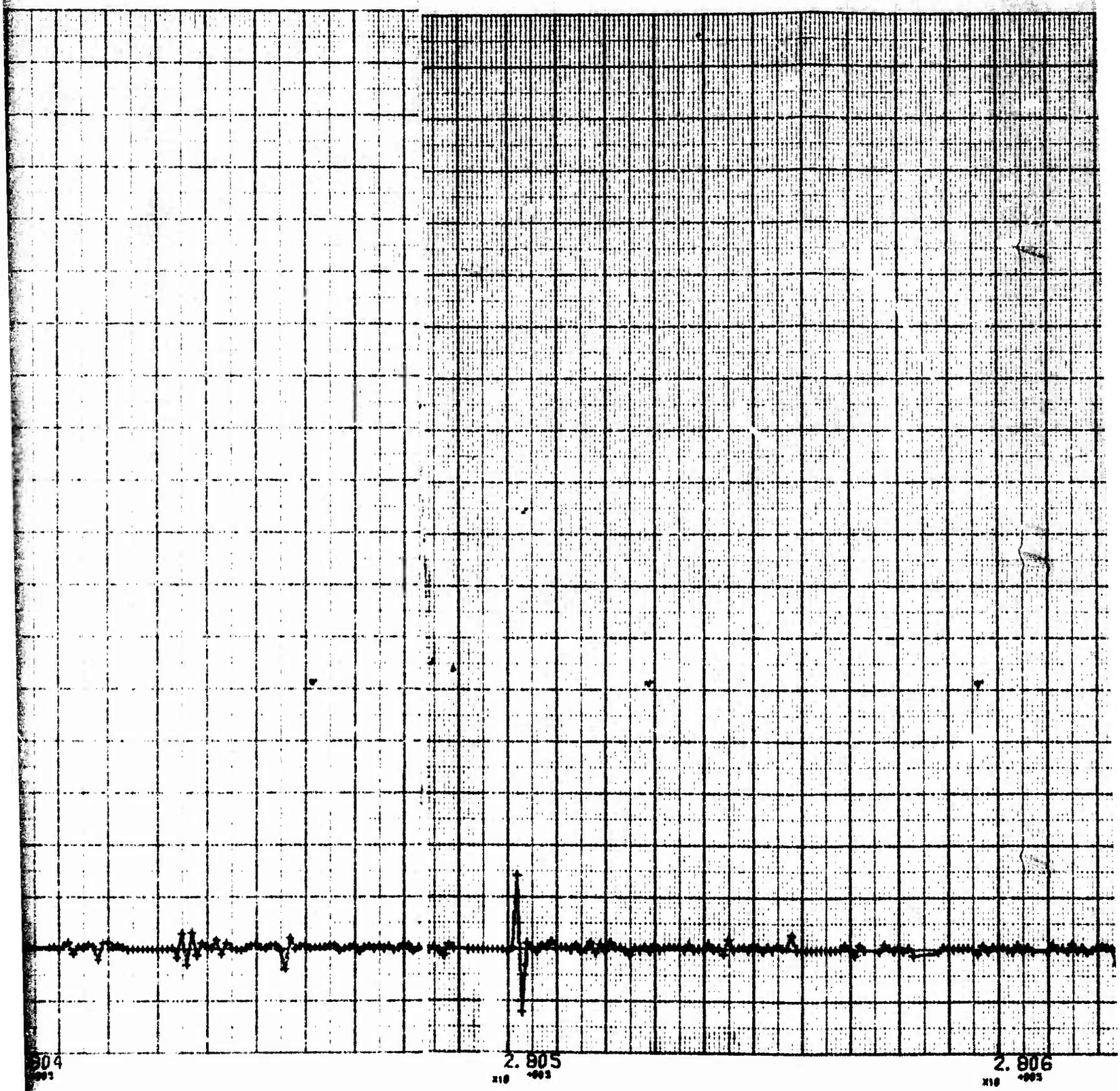
2.805
2.806

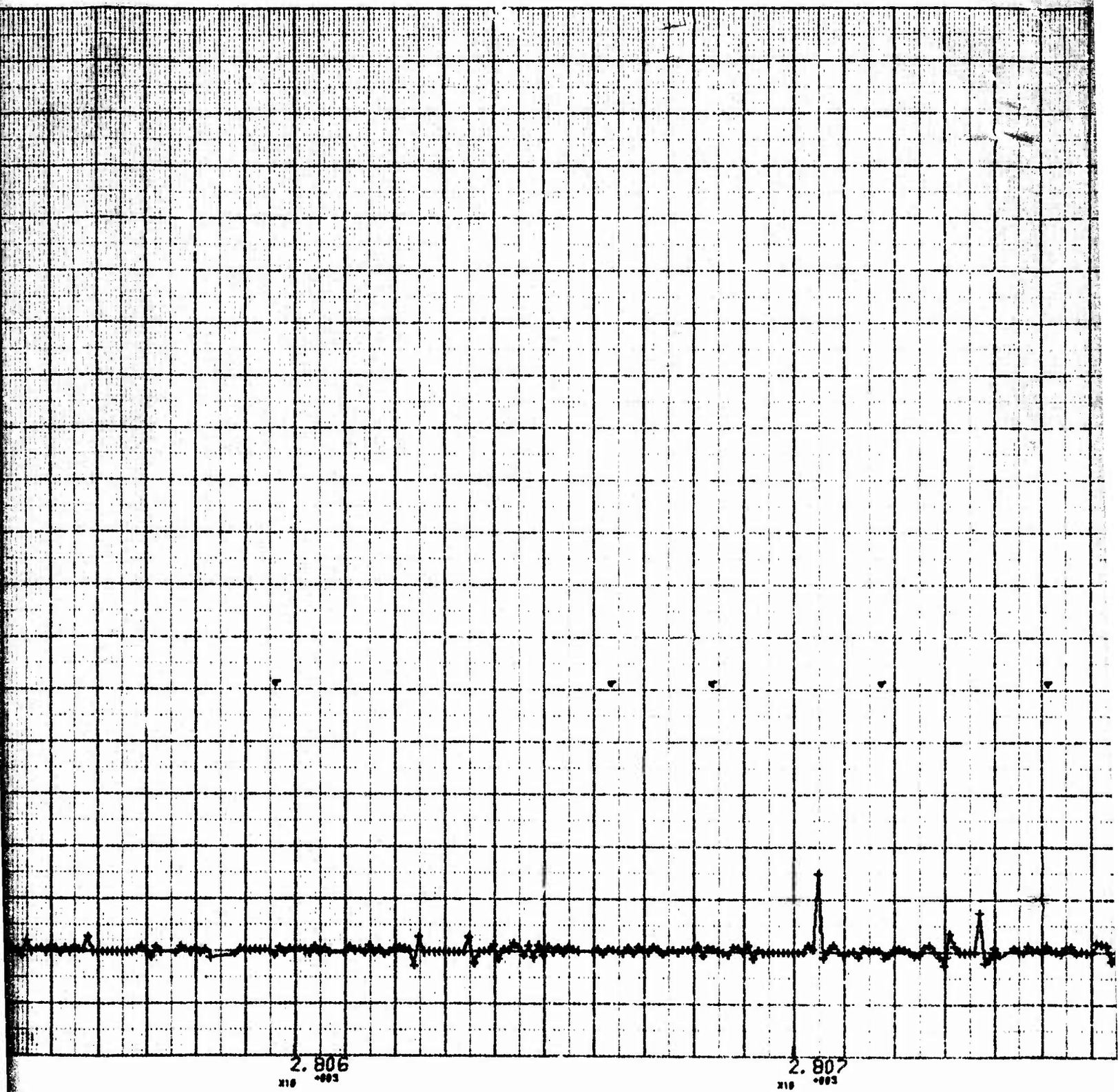
2.806
X10 +003
2.807
X10 +003

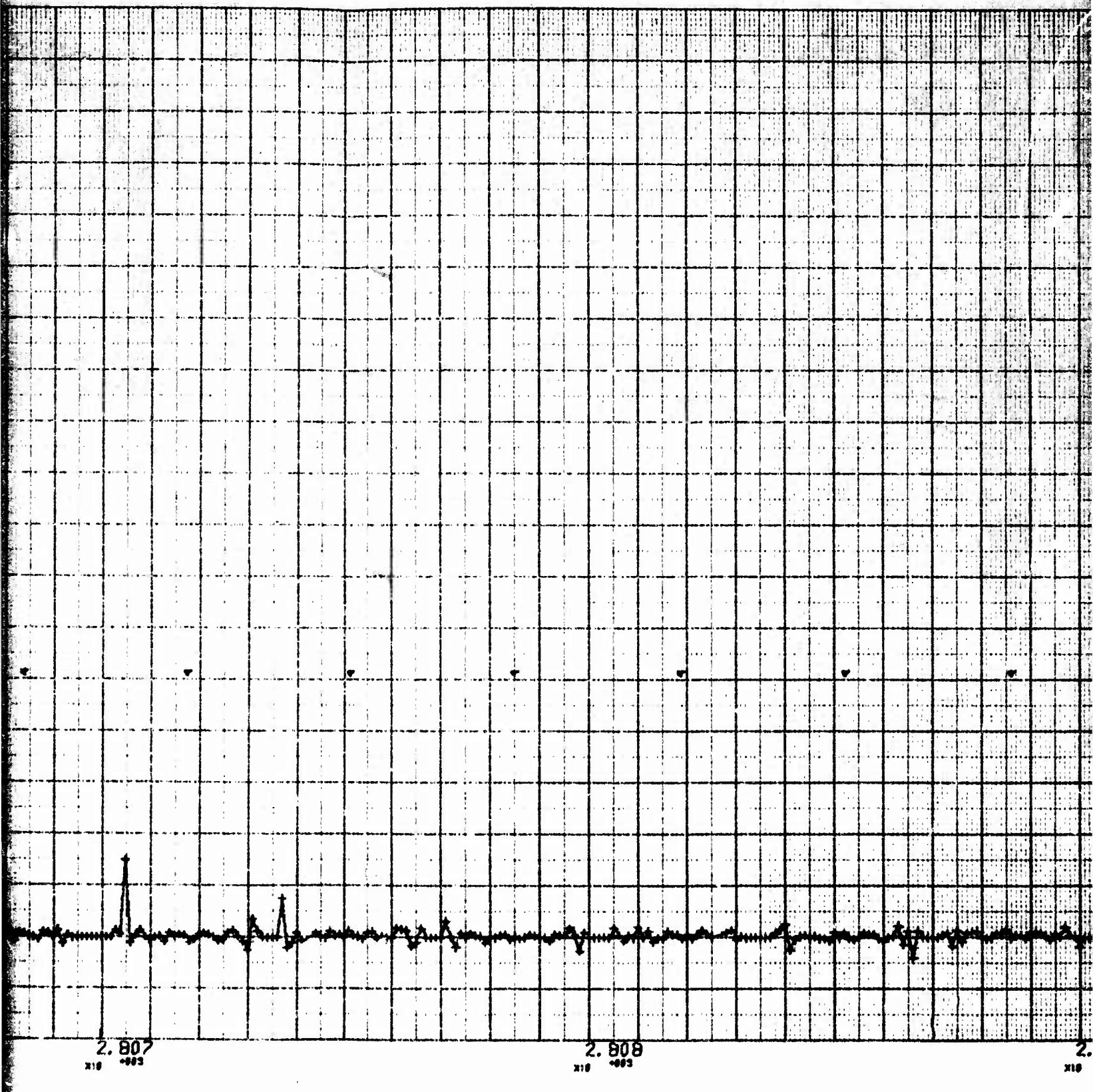
2.807
X10 +003
2.808
X10 +003
2.
X10

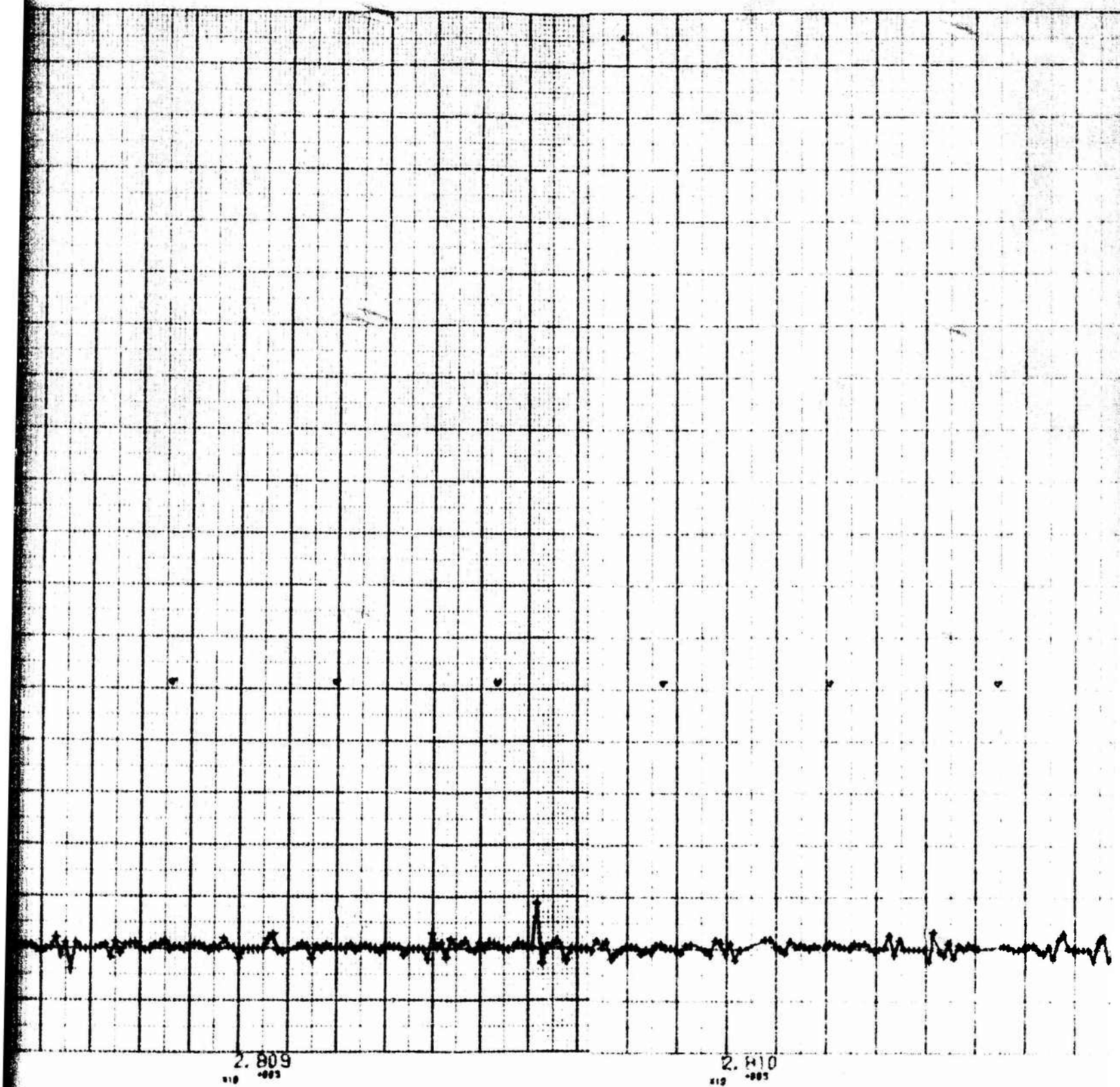
2. 809
2. 810

2.811
2.812

2.813
X10 +003
2.814
X10 +003

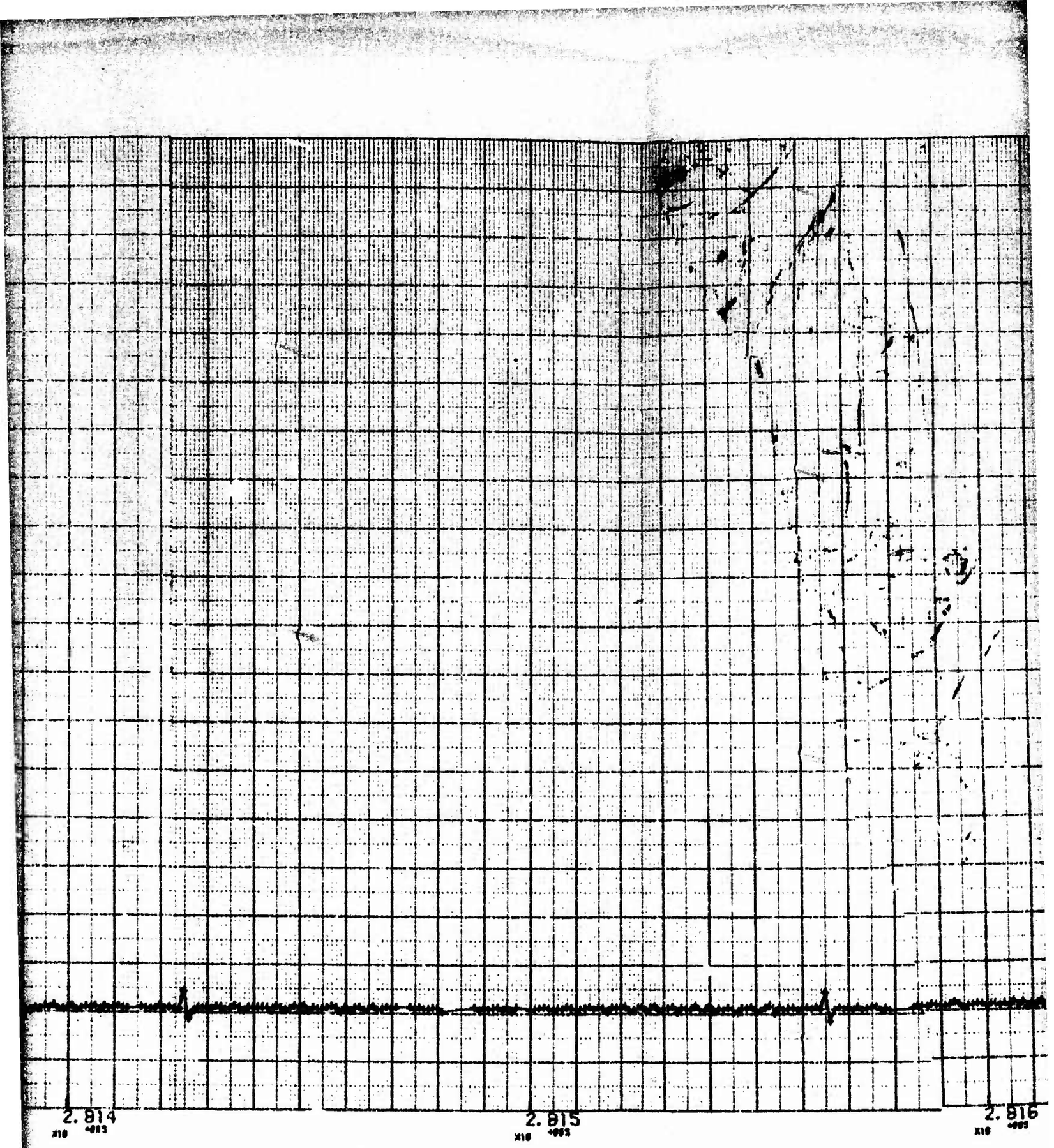
2.814
X10 +003
2.815
X10 +003
2.816
X10 +003

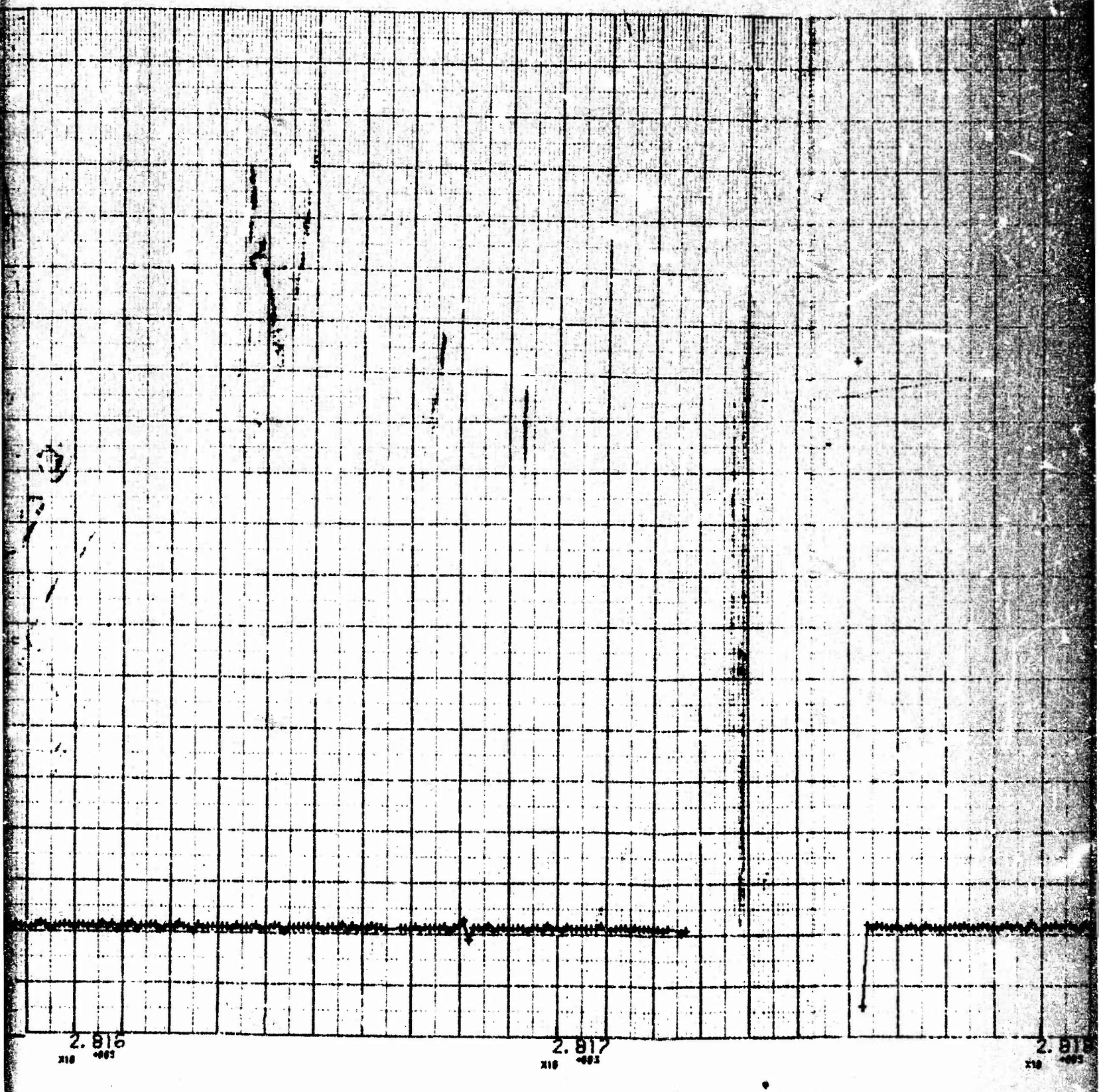

K

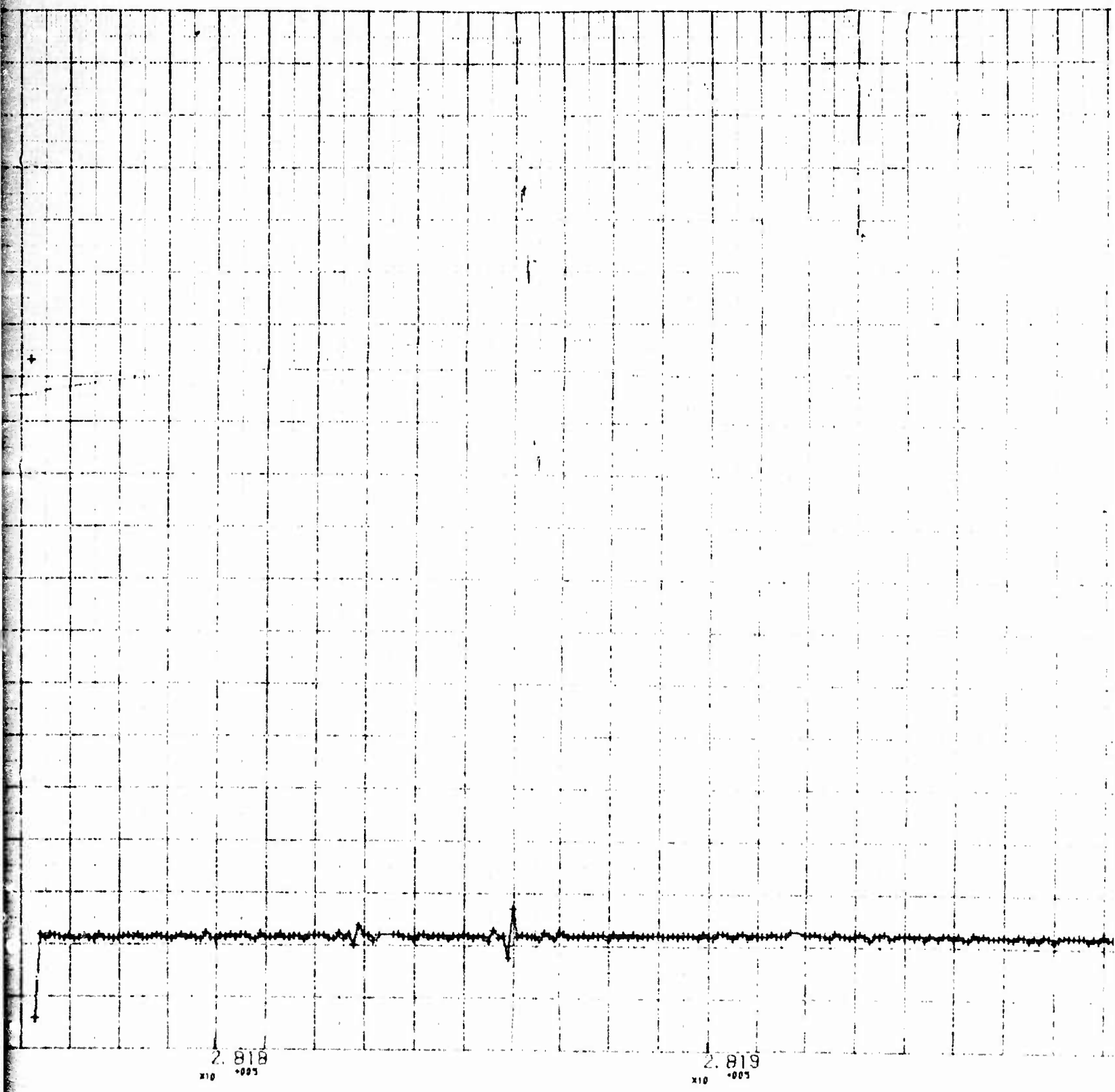
2.818
X10 +005
2.819
X10 +005

2.820
2.821

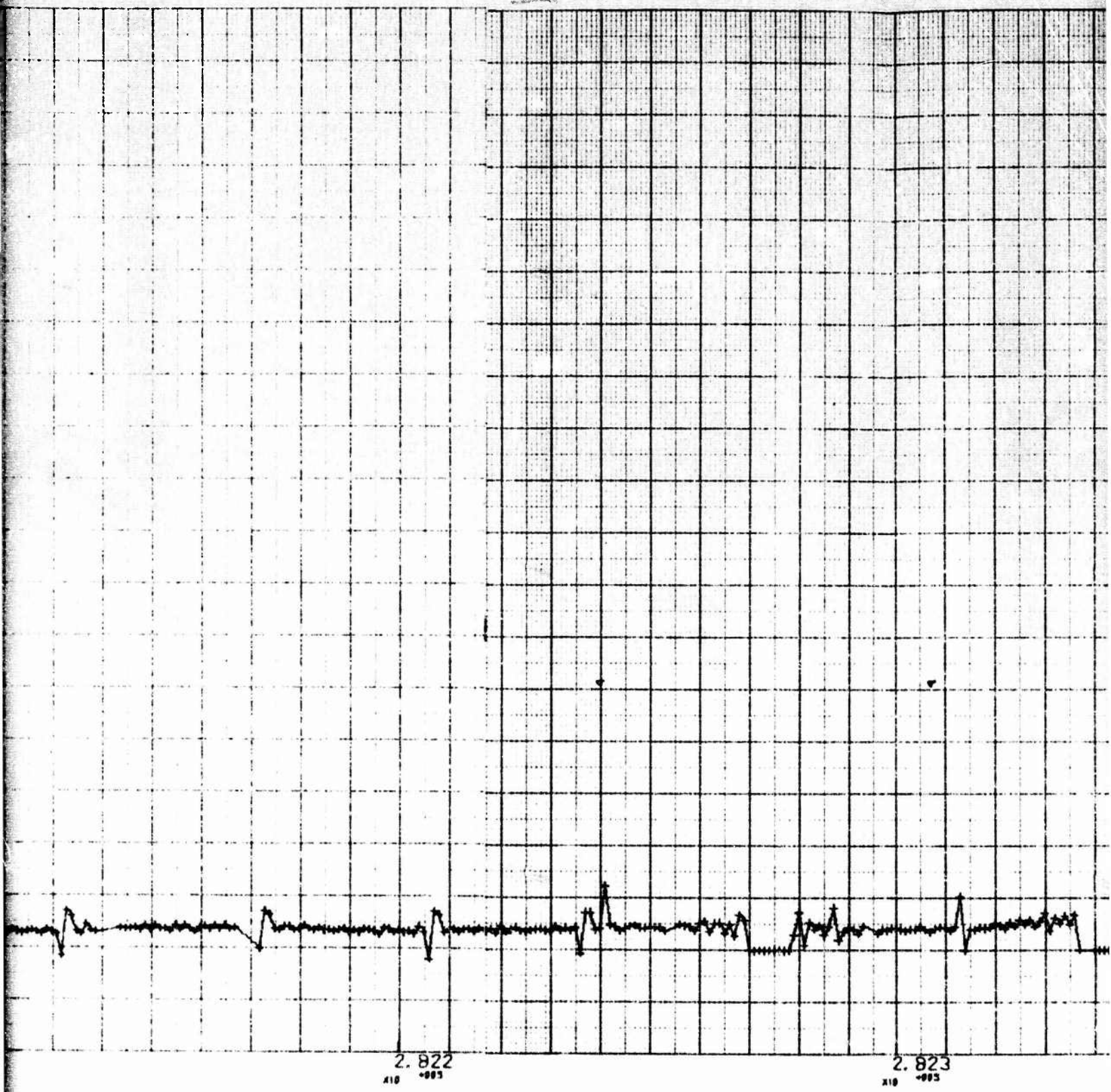
2.822
X10 +003
2.823
X10 +003

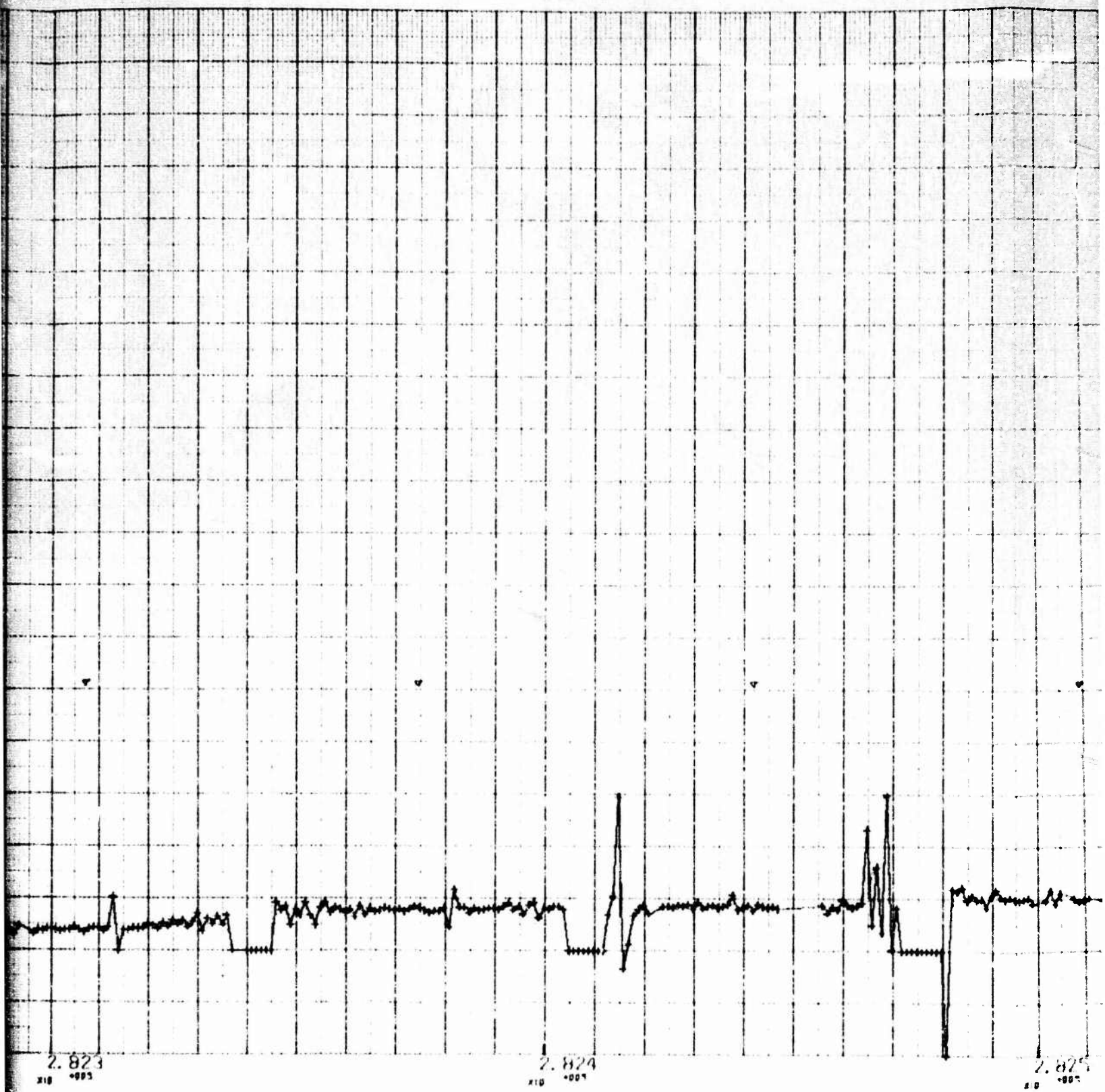
2.823
2.824

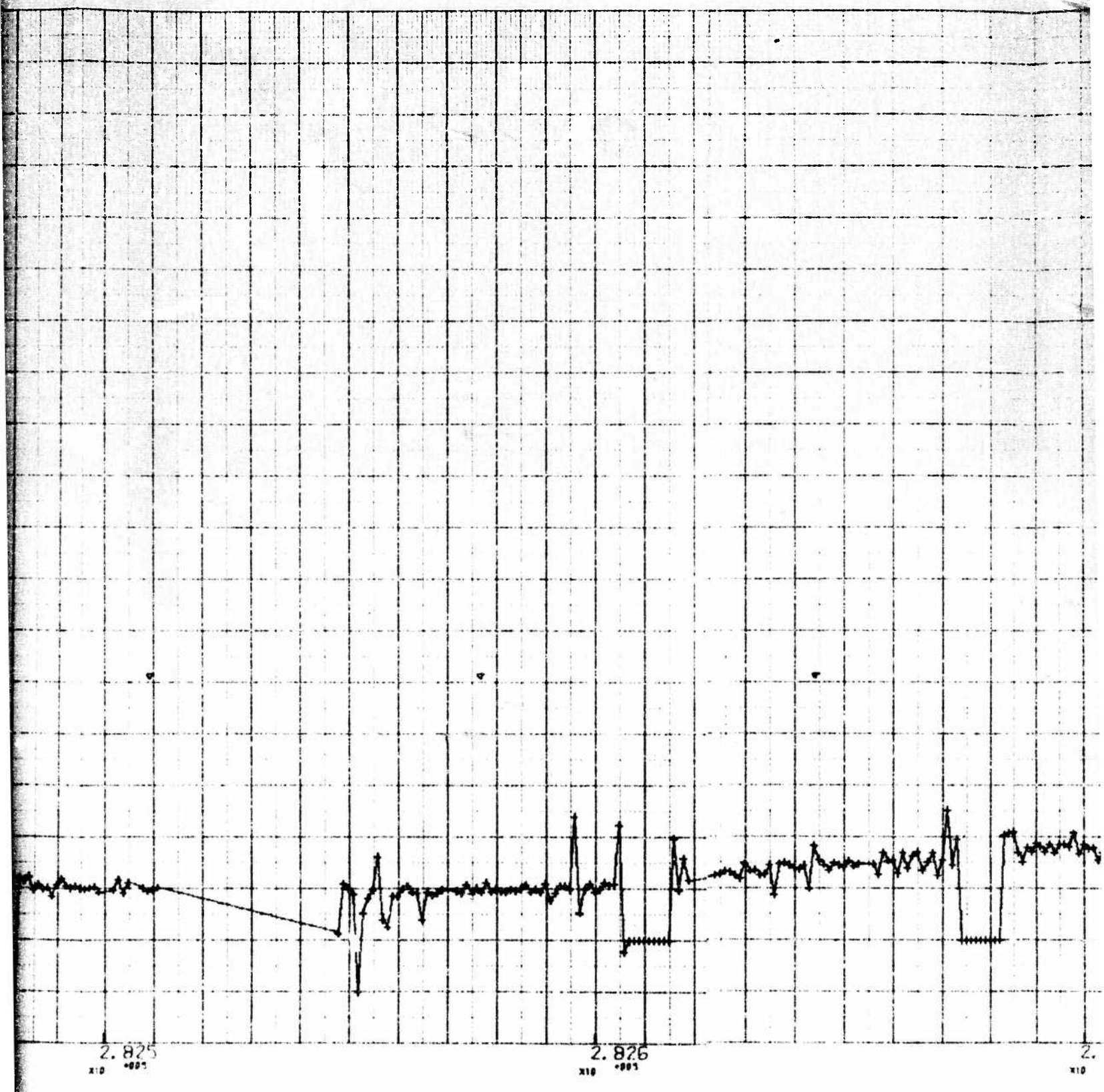

P

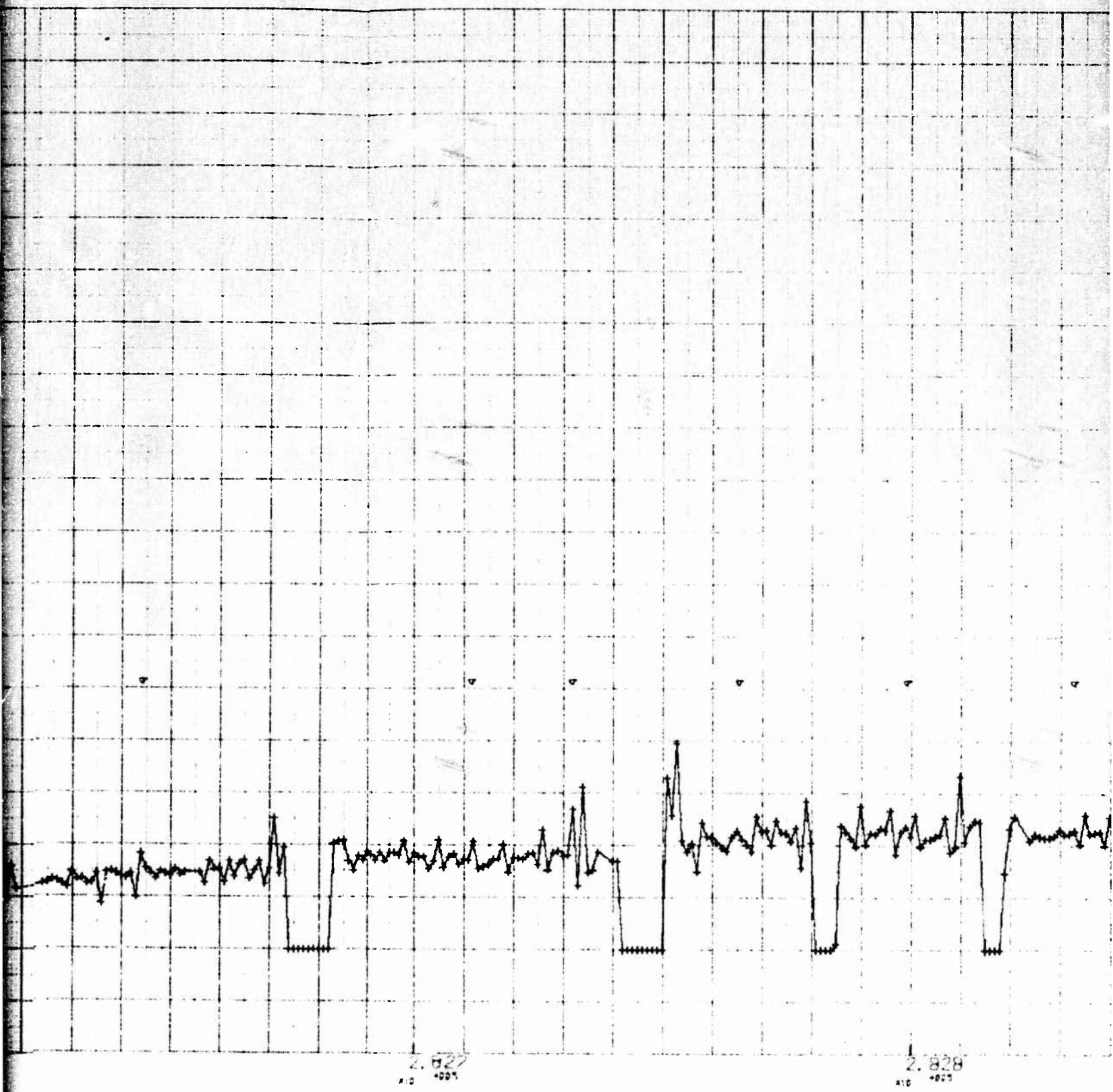
2.827
2.828

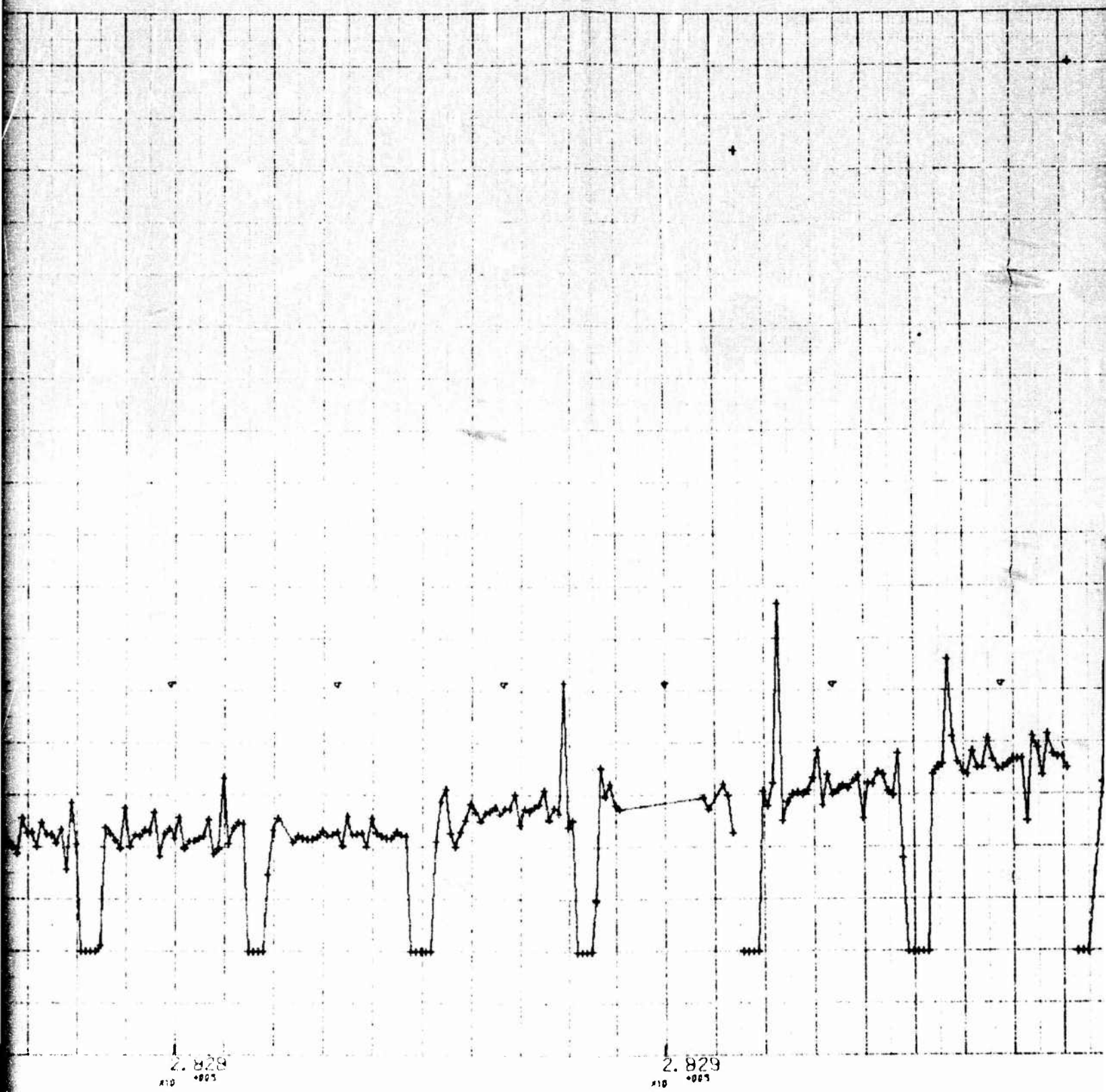

R

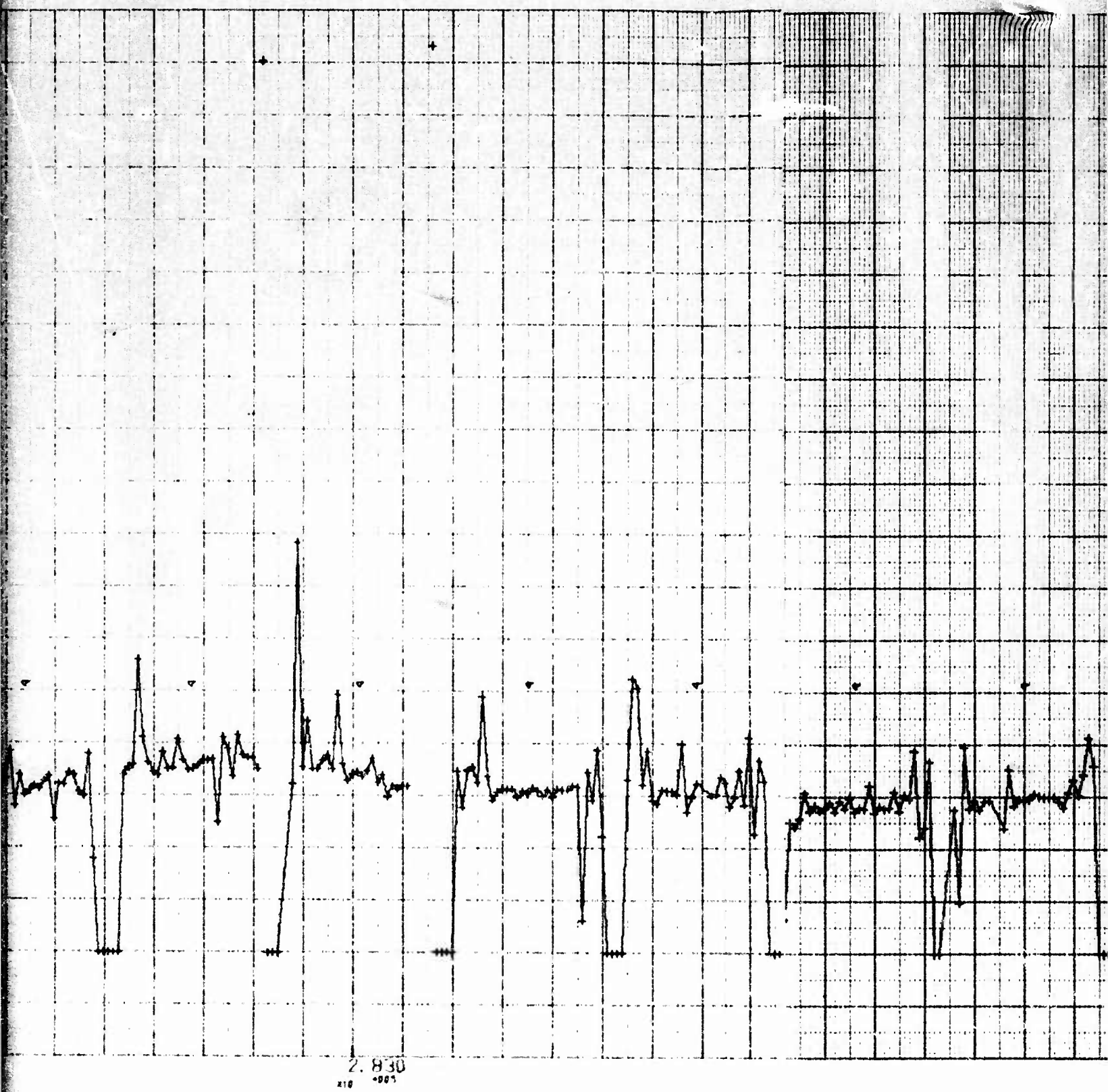
2.830

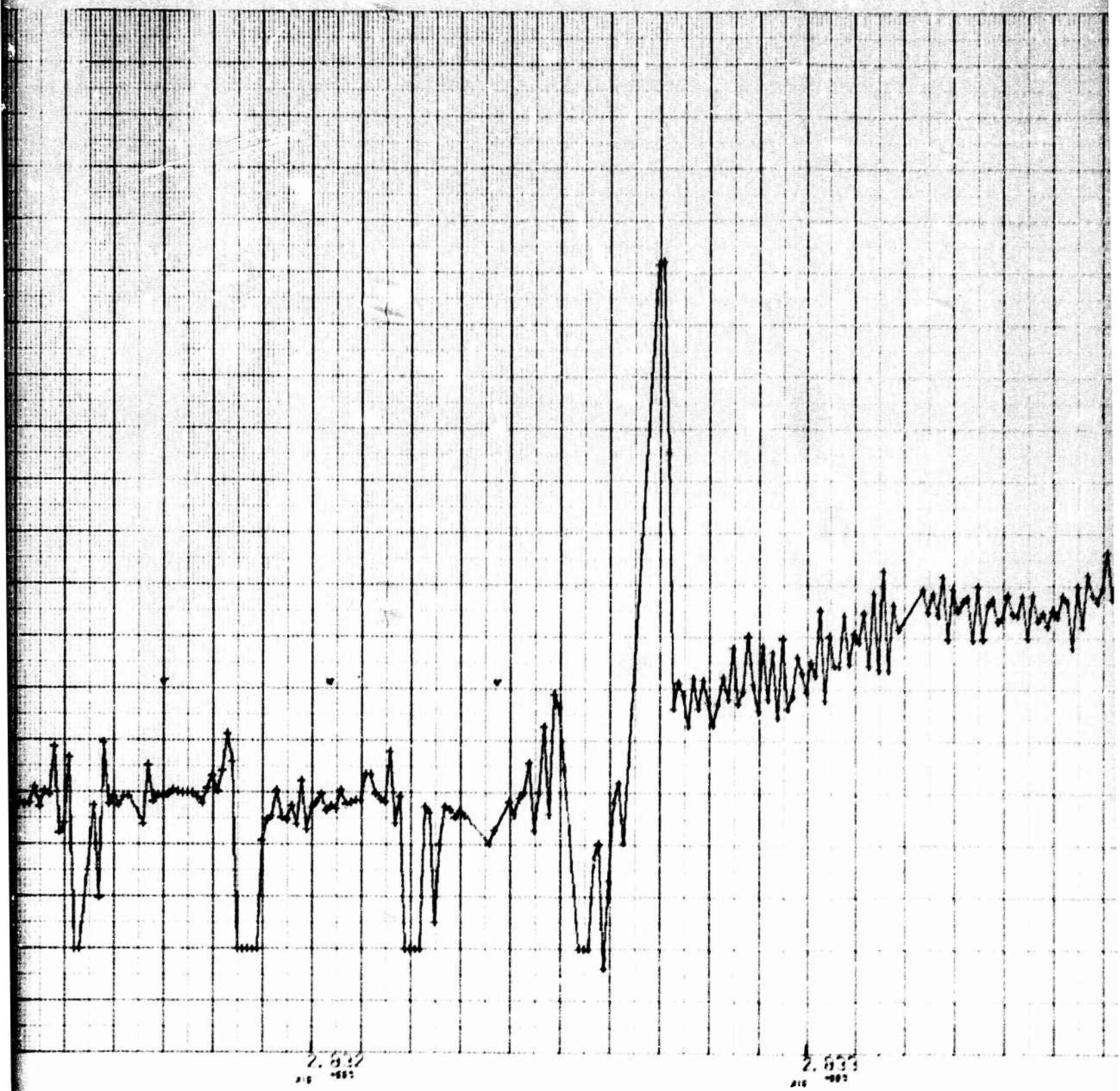

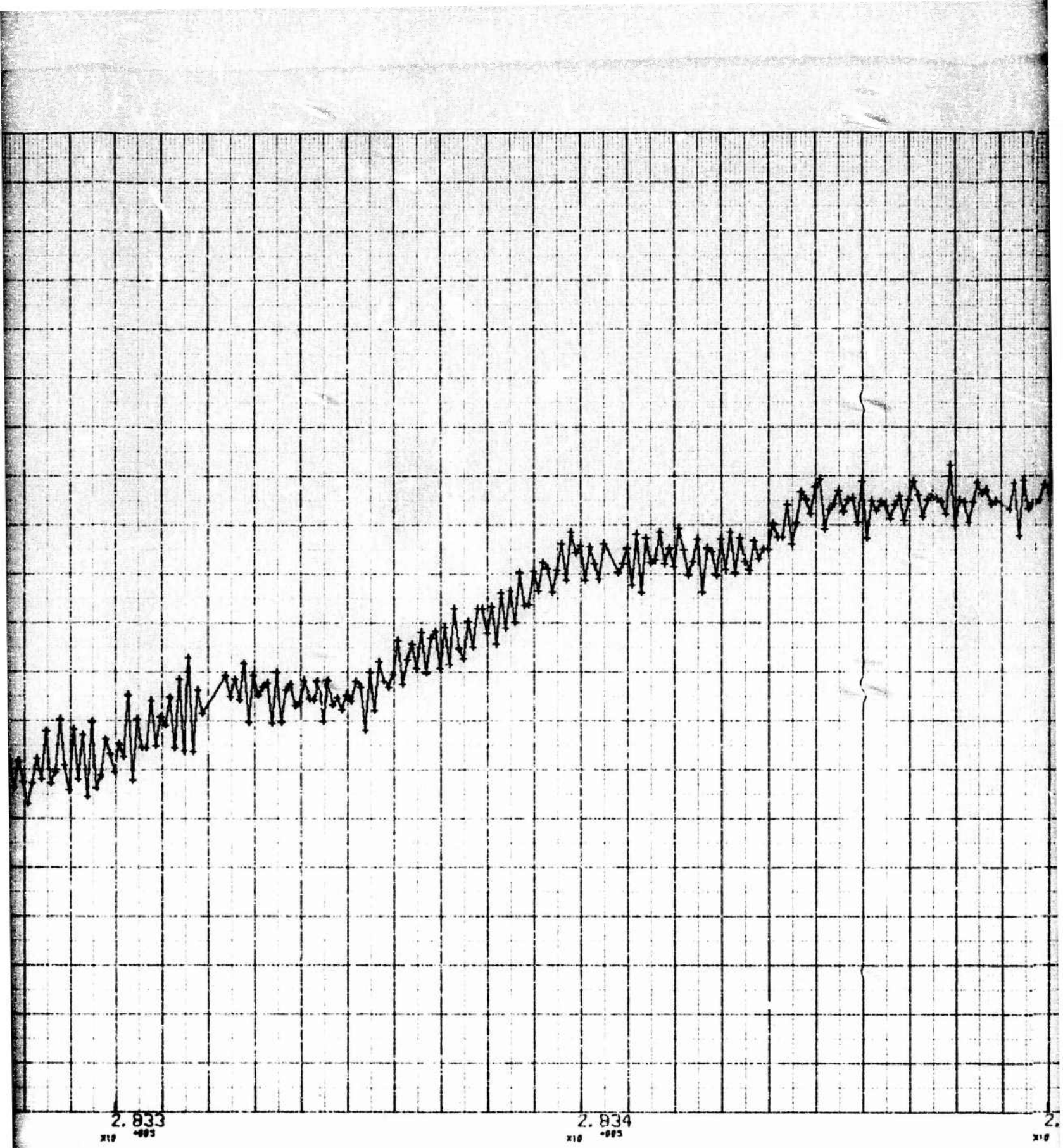

4

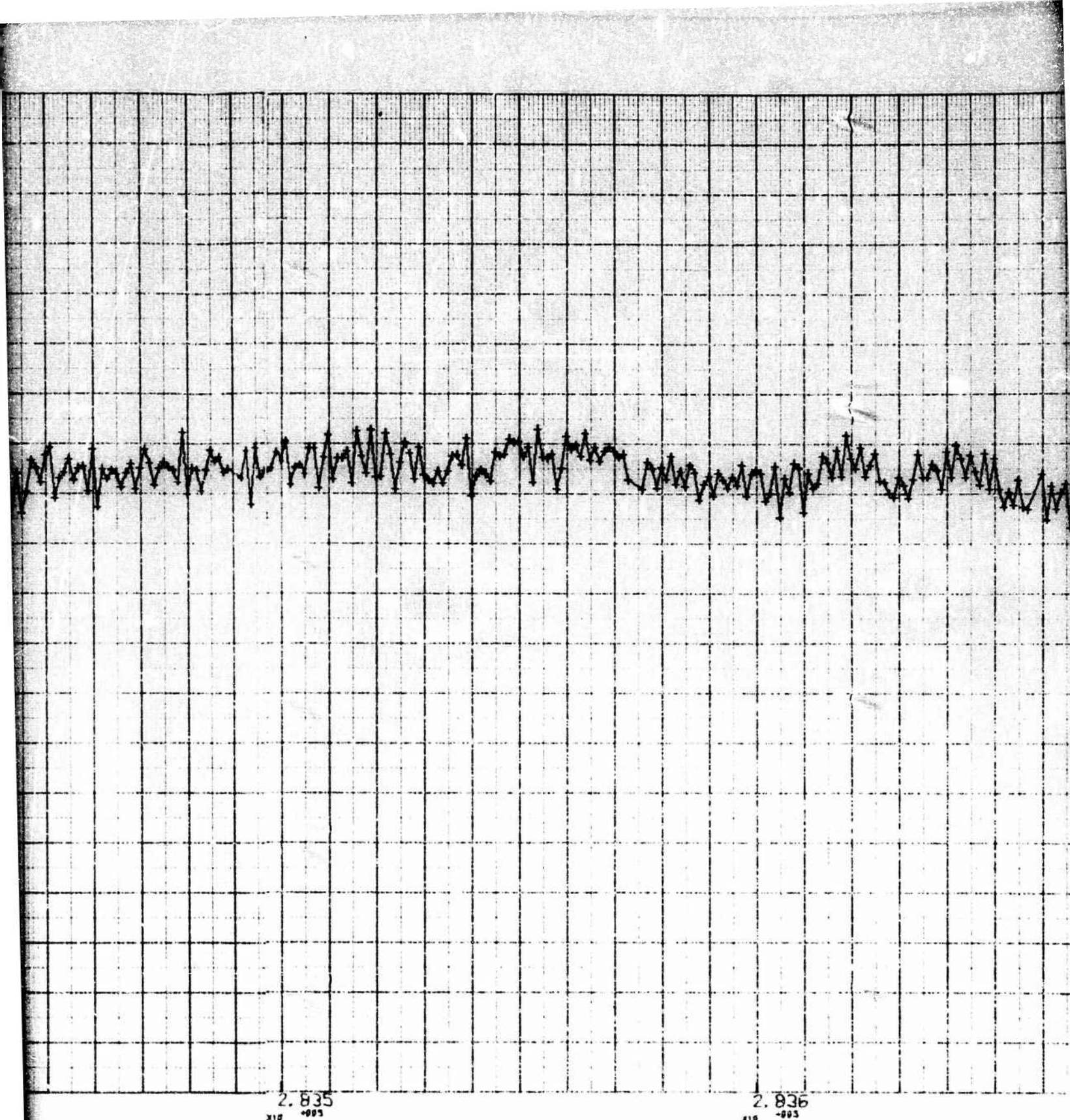
2.835
X10 +003
2.836
X10 +003

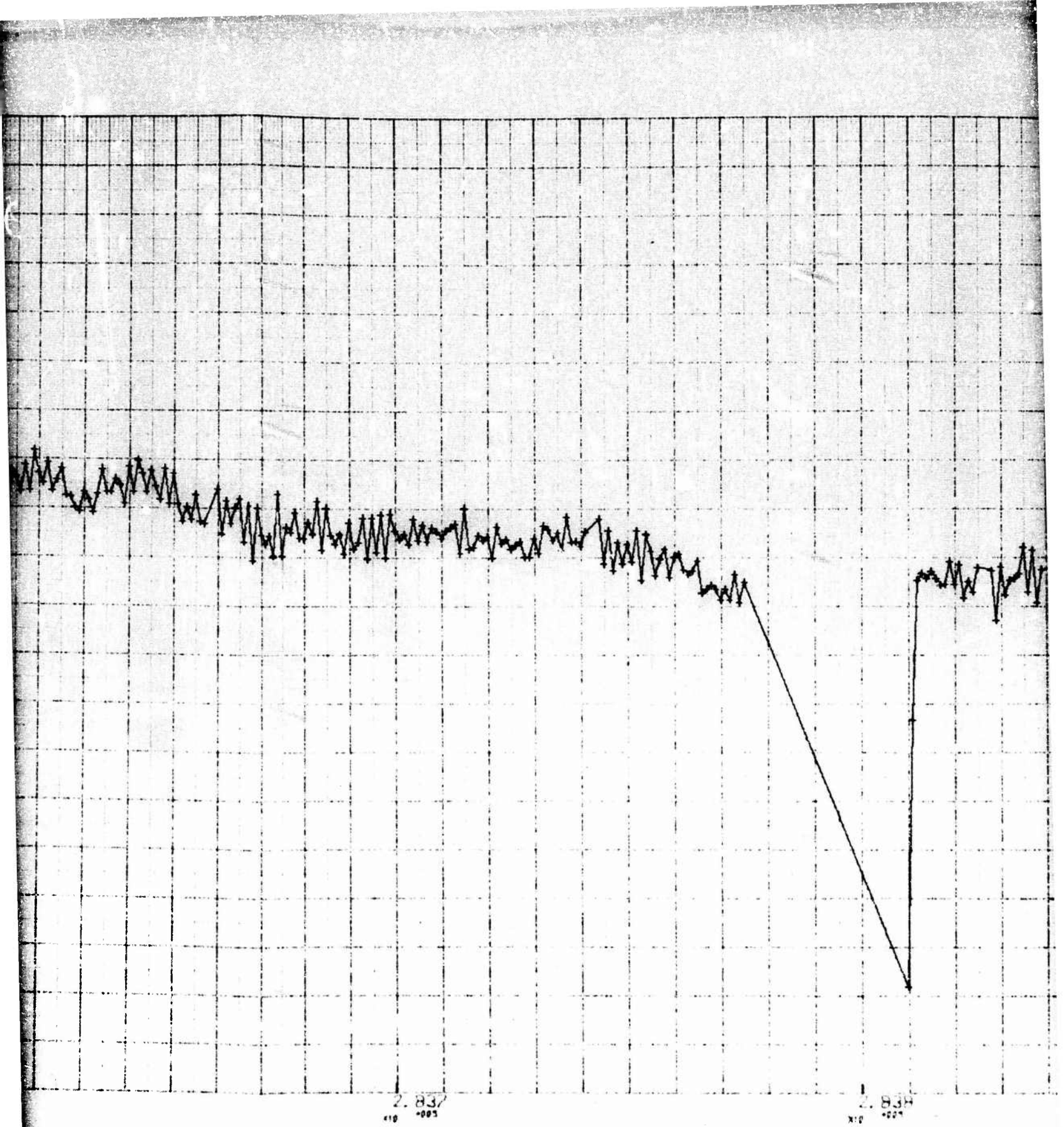
2.837
2.838

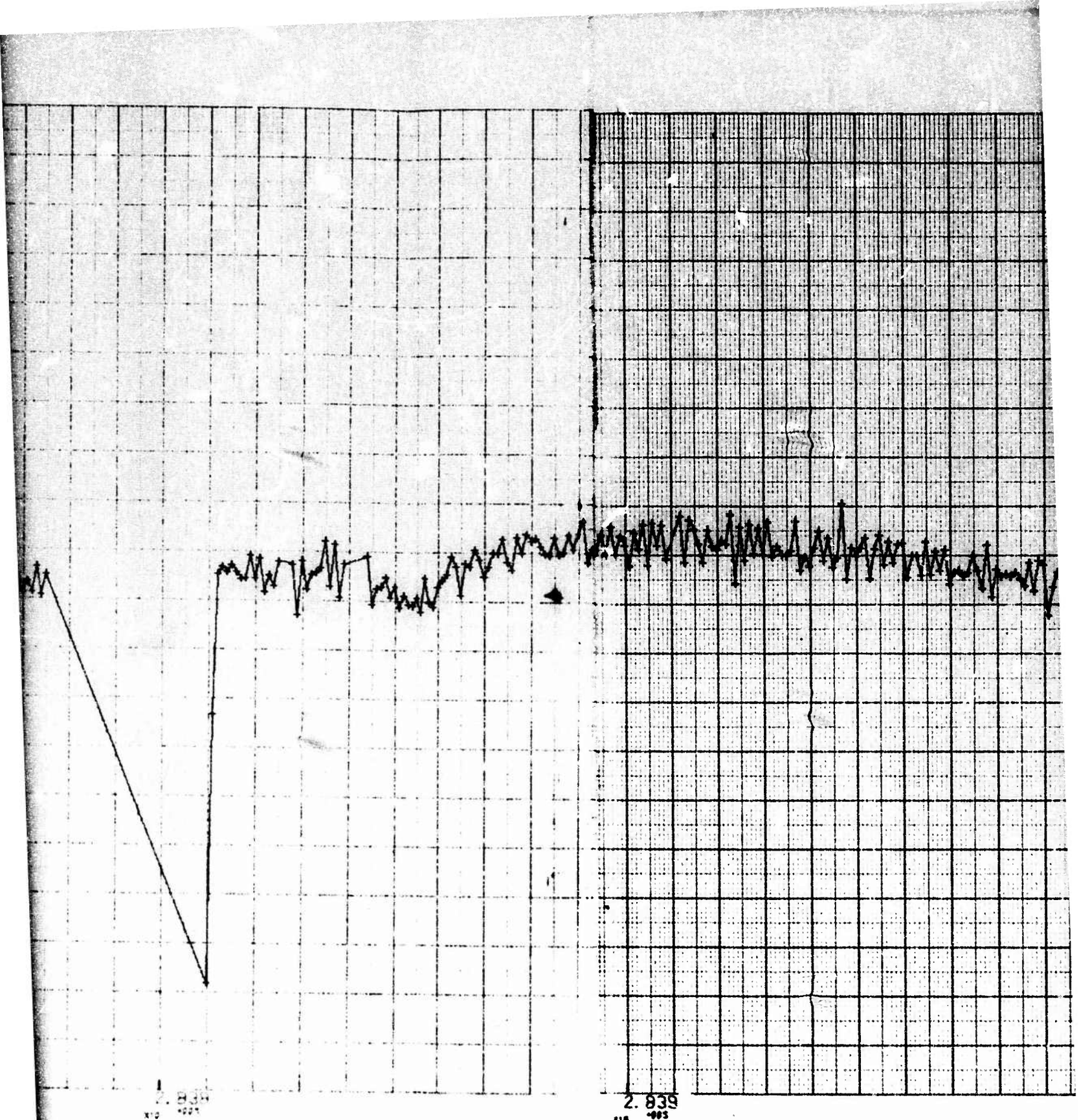
2. 839

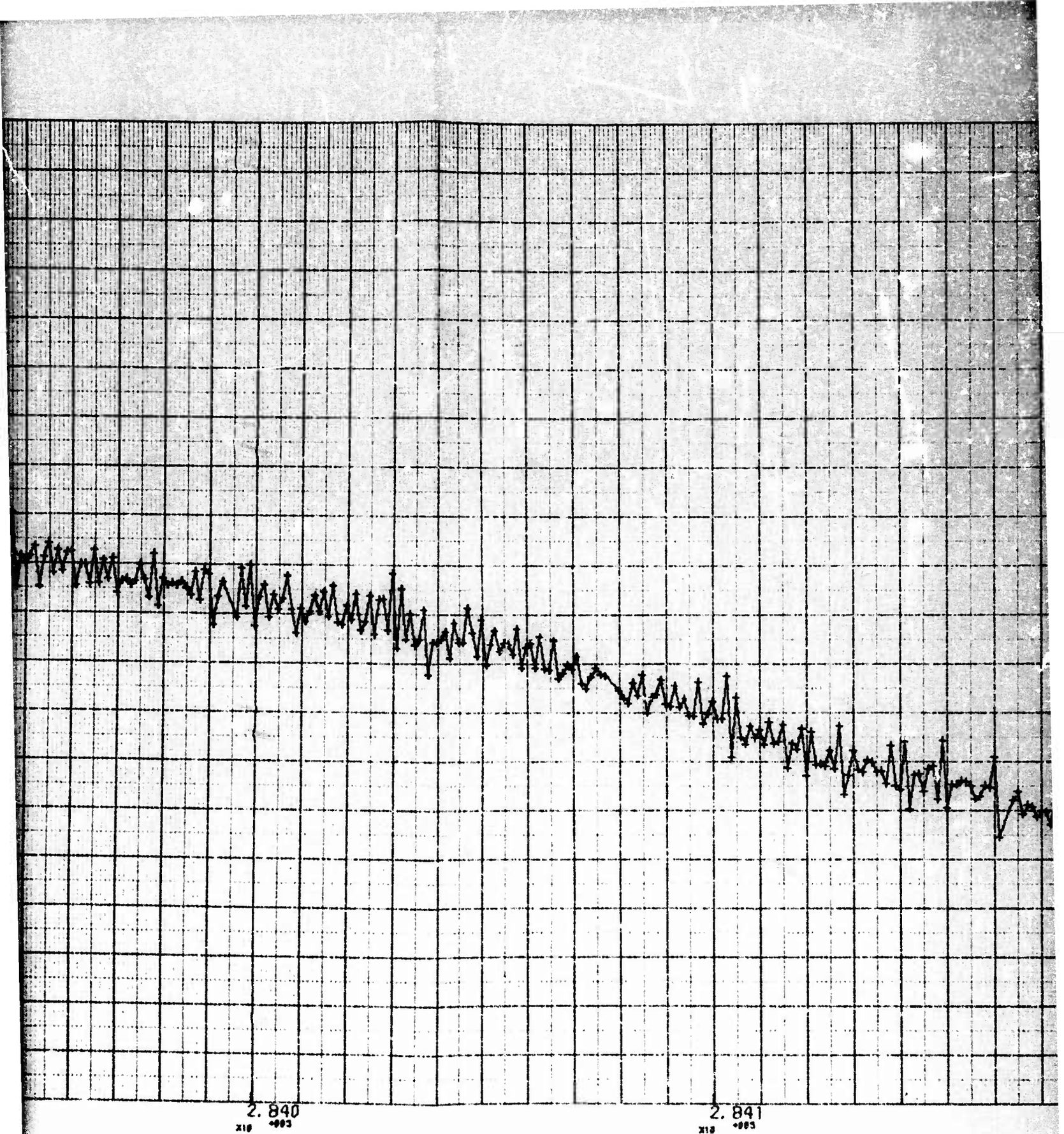
2.840
X10 +003
2.841
X10 +003

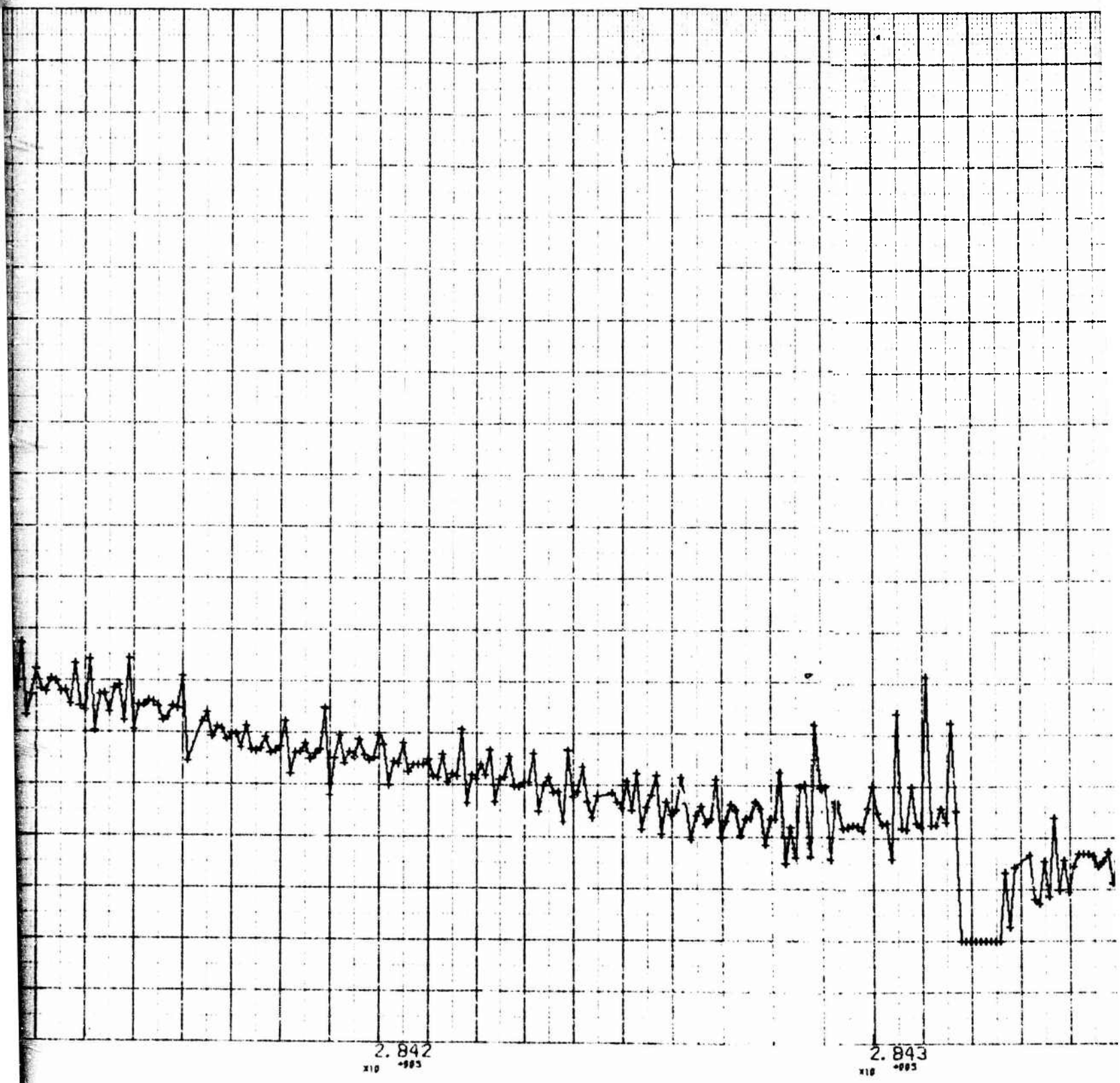

3

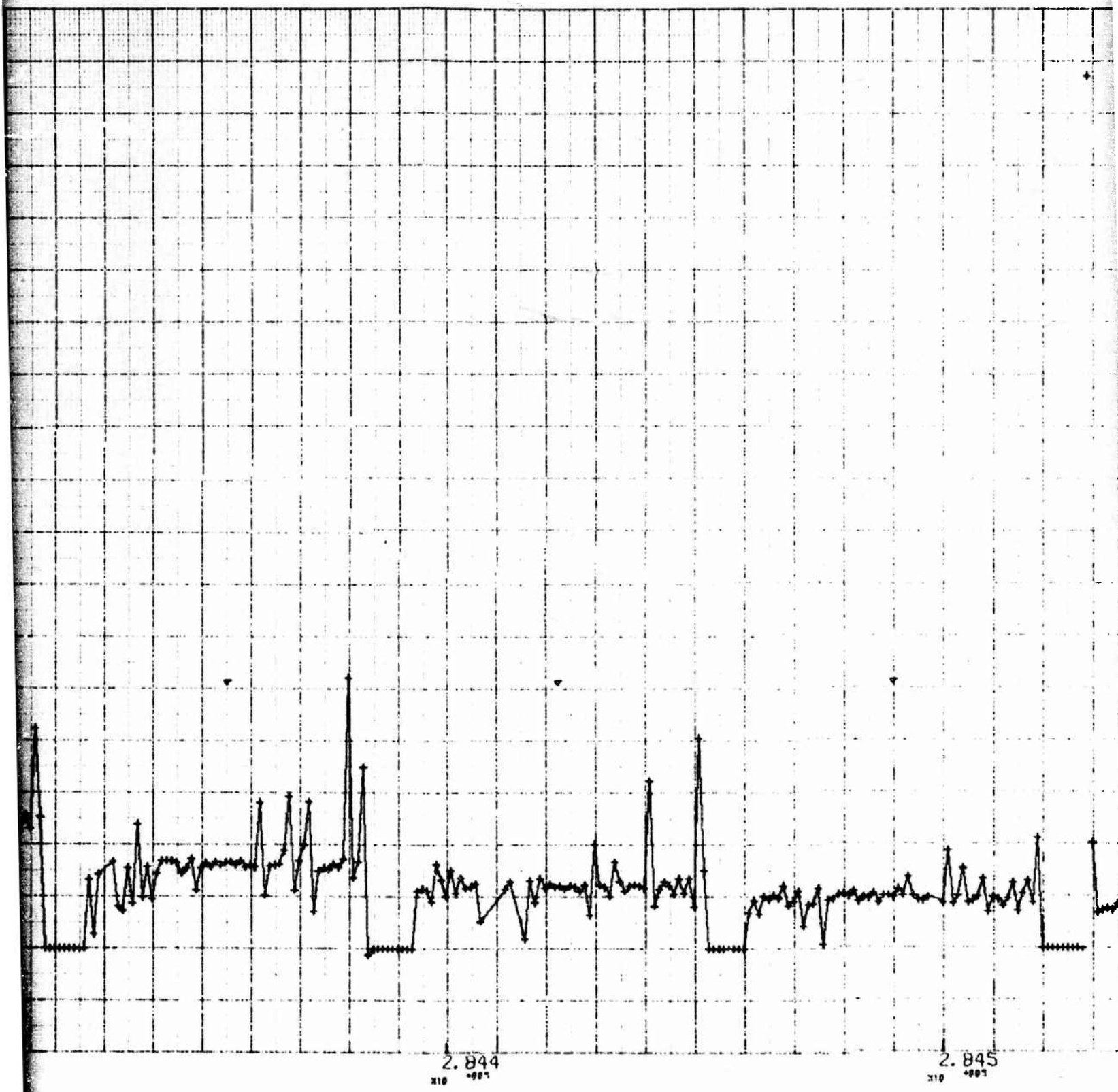

AP

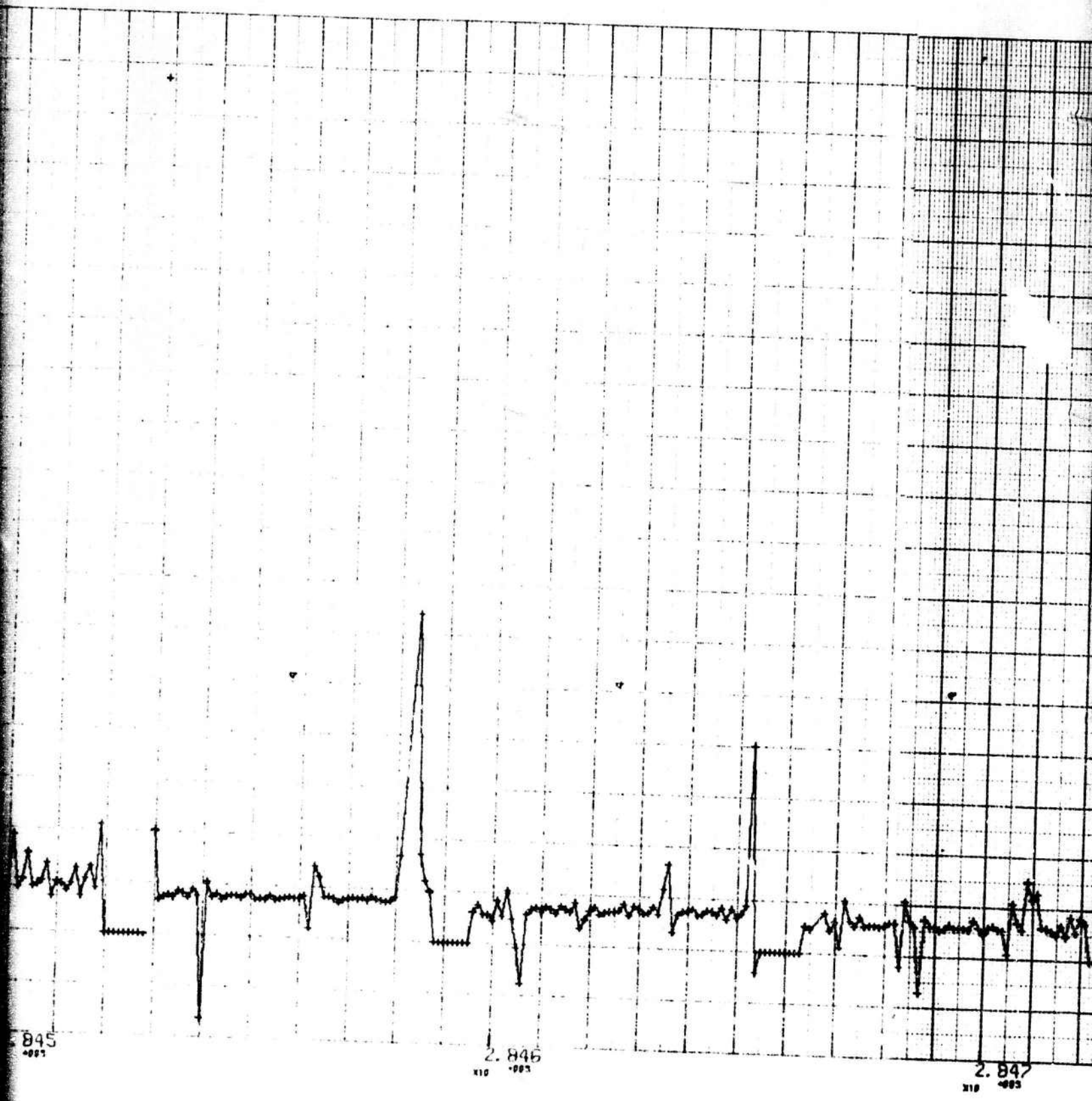

BB

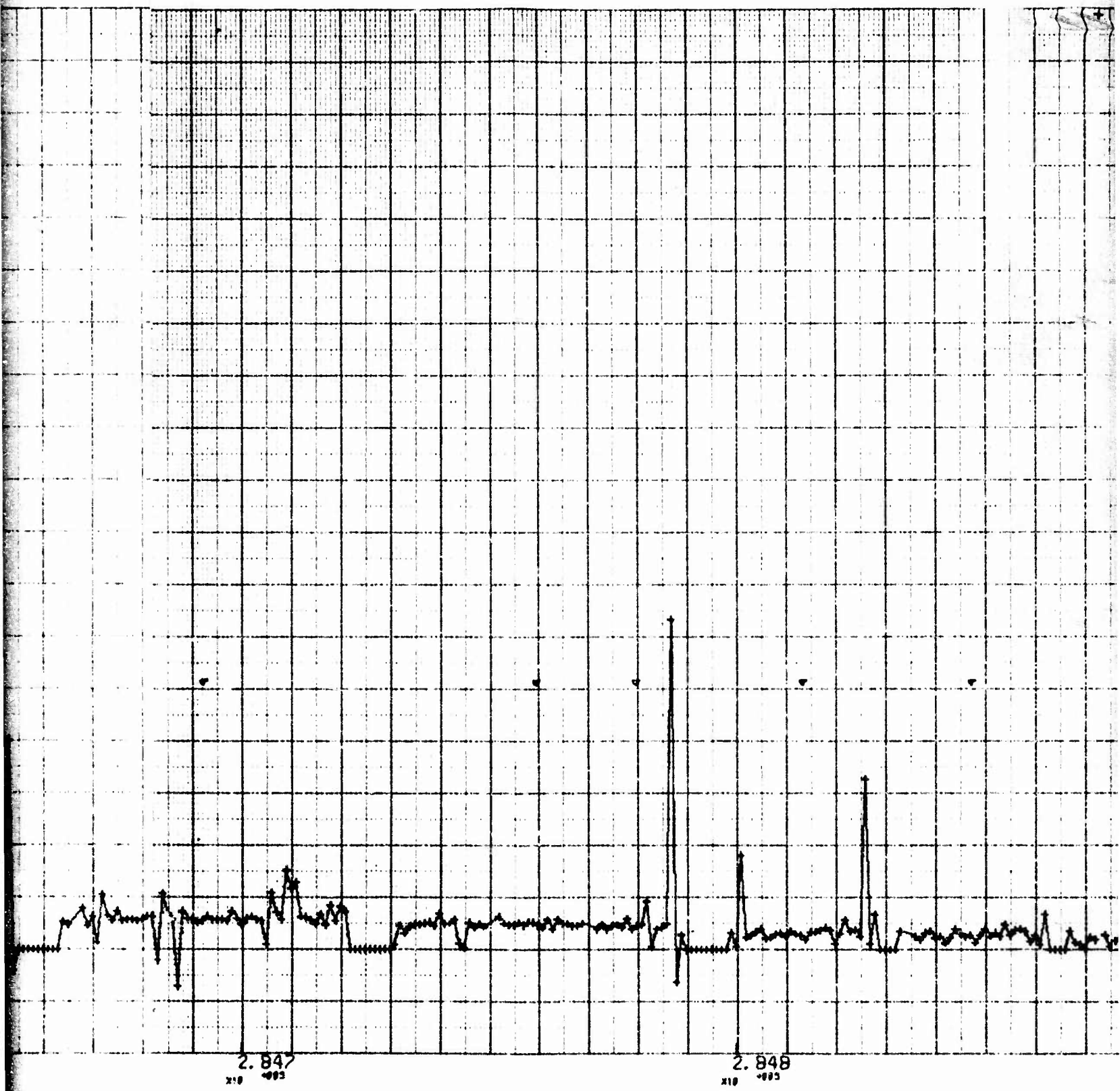

CC

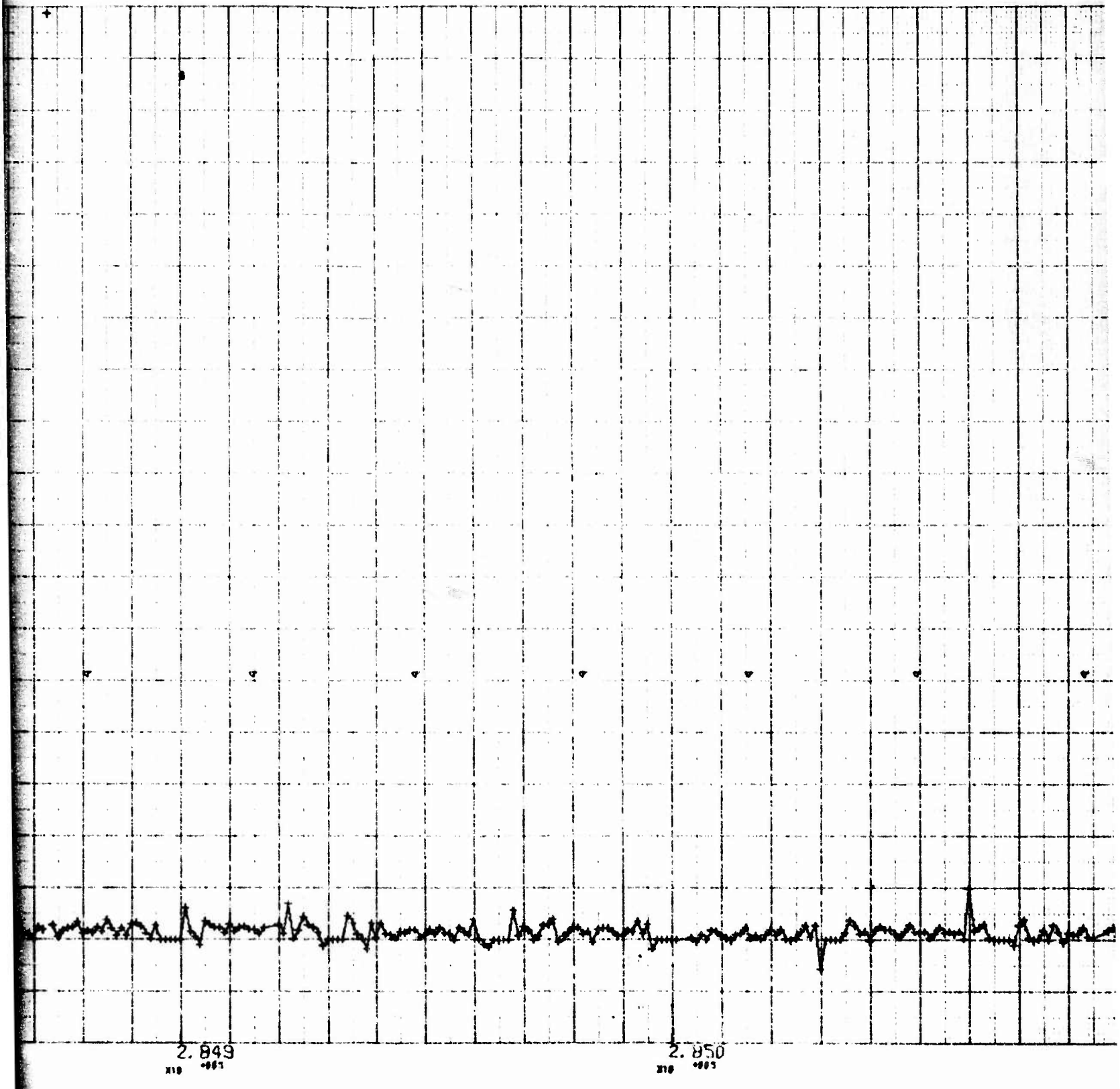
2.849
2.850

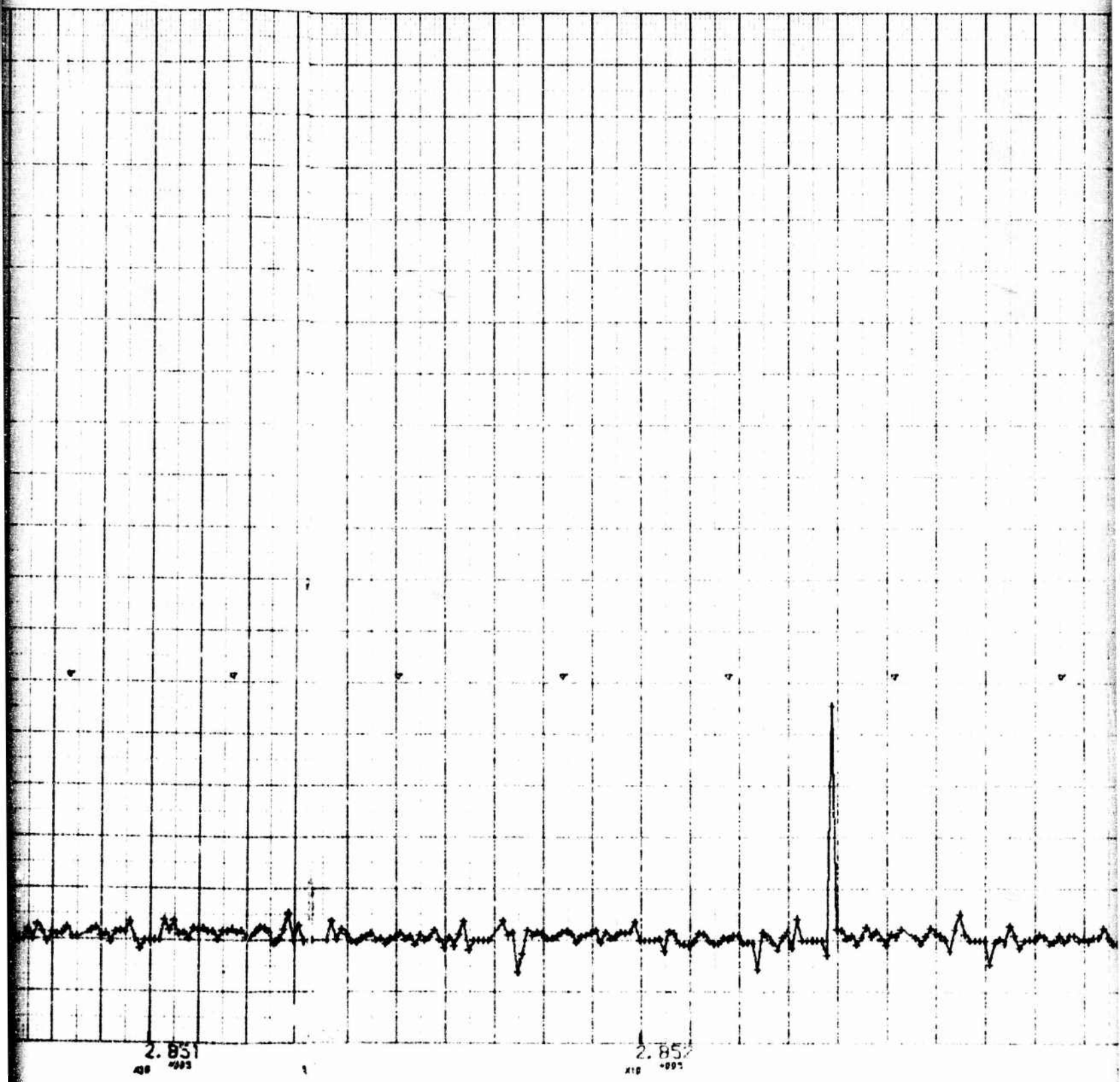
2.851
2.85

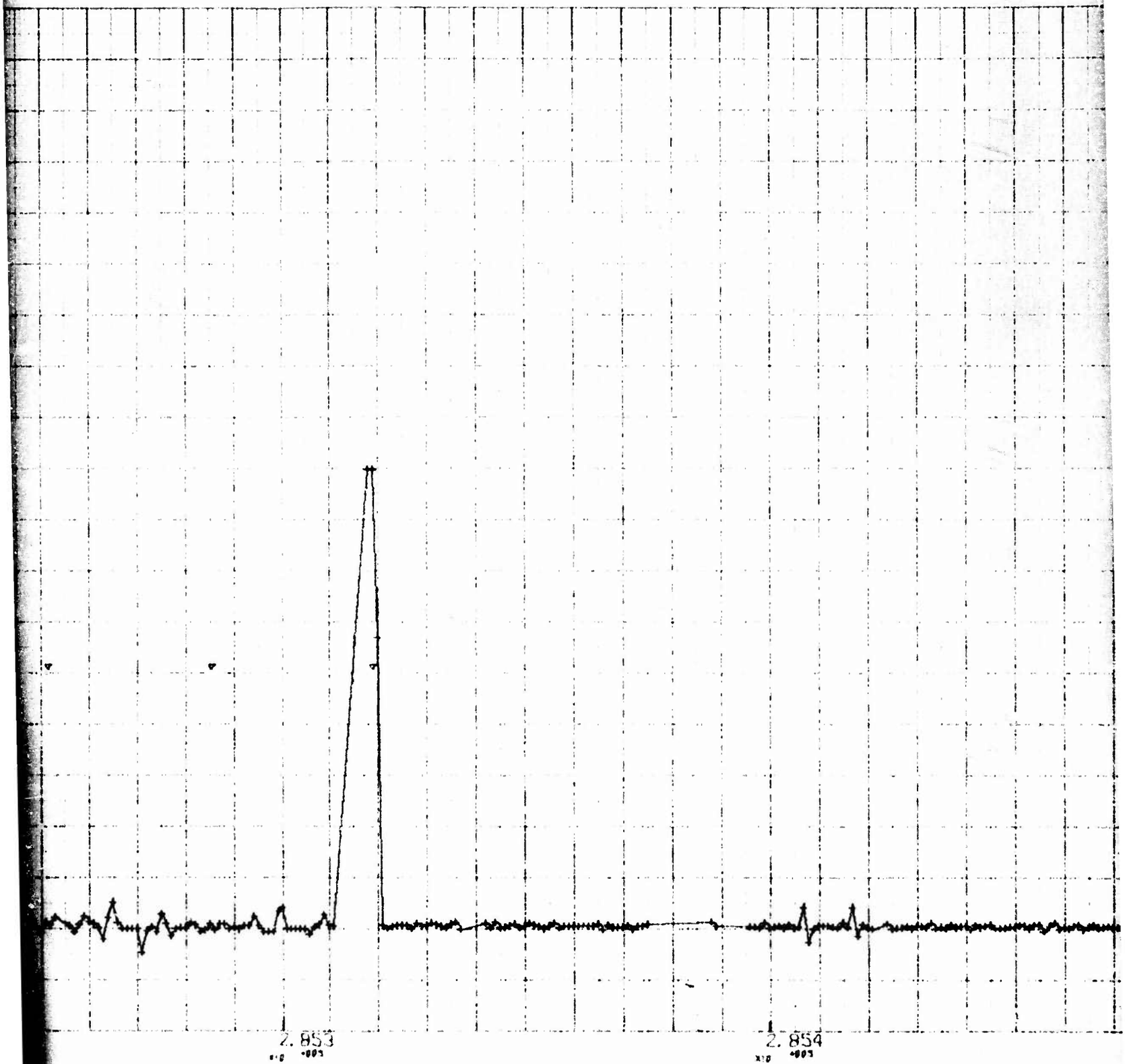
2.853
2.854

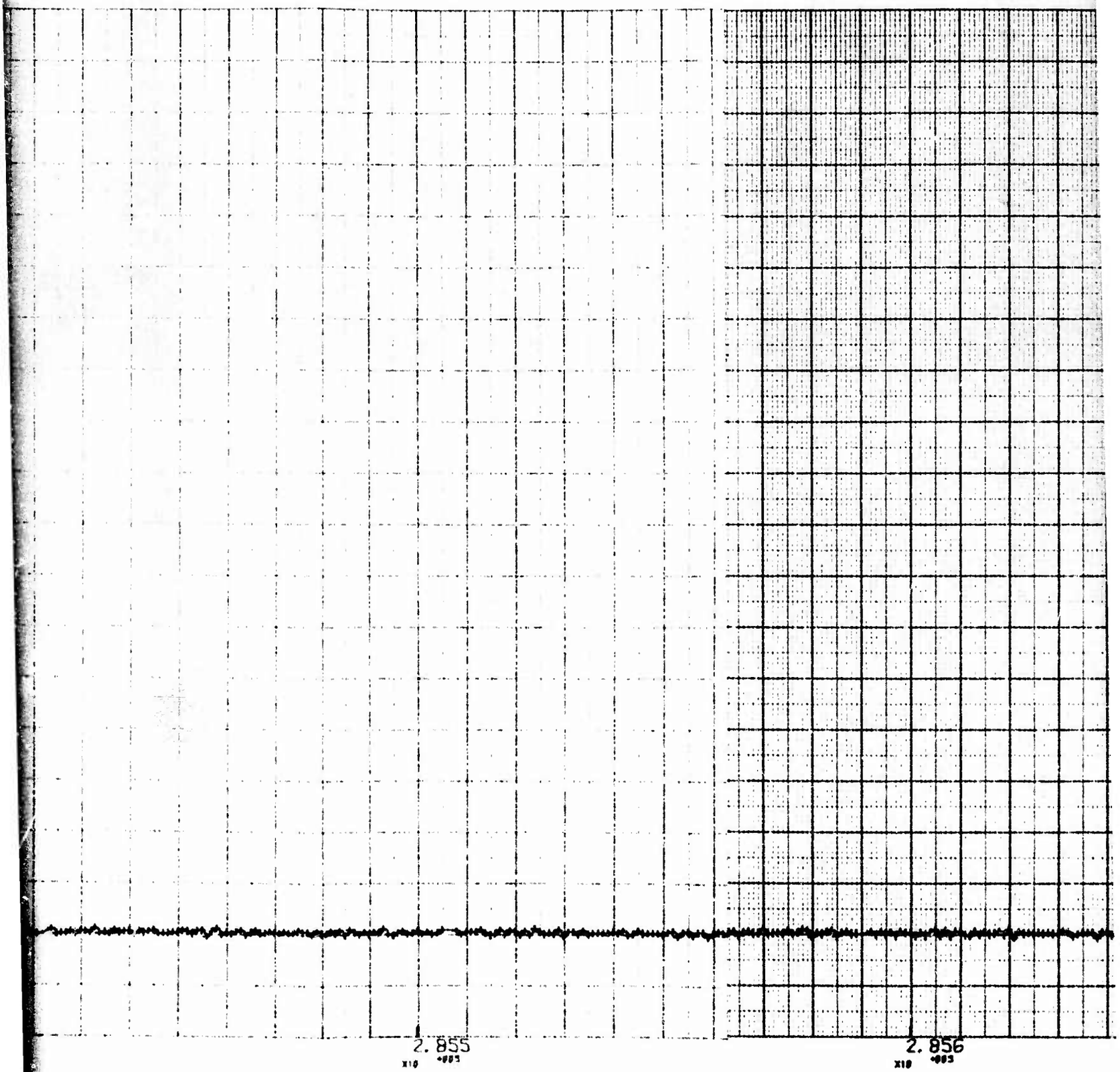
2.855
X10 +003
2.856
X10 +003

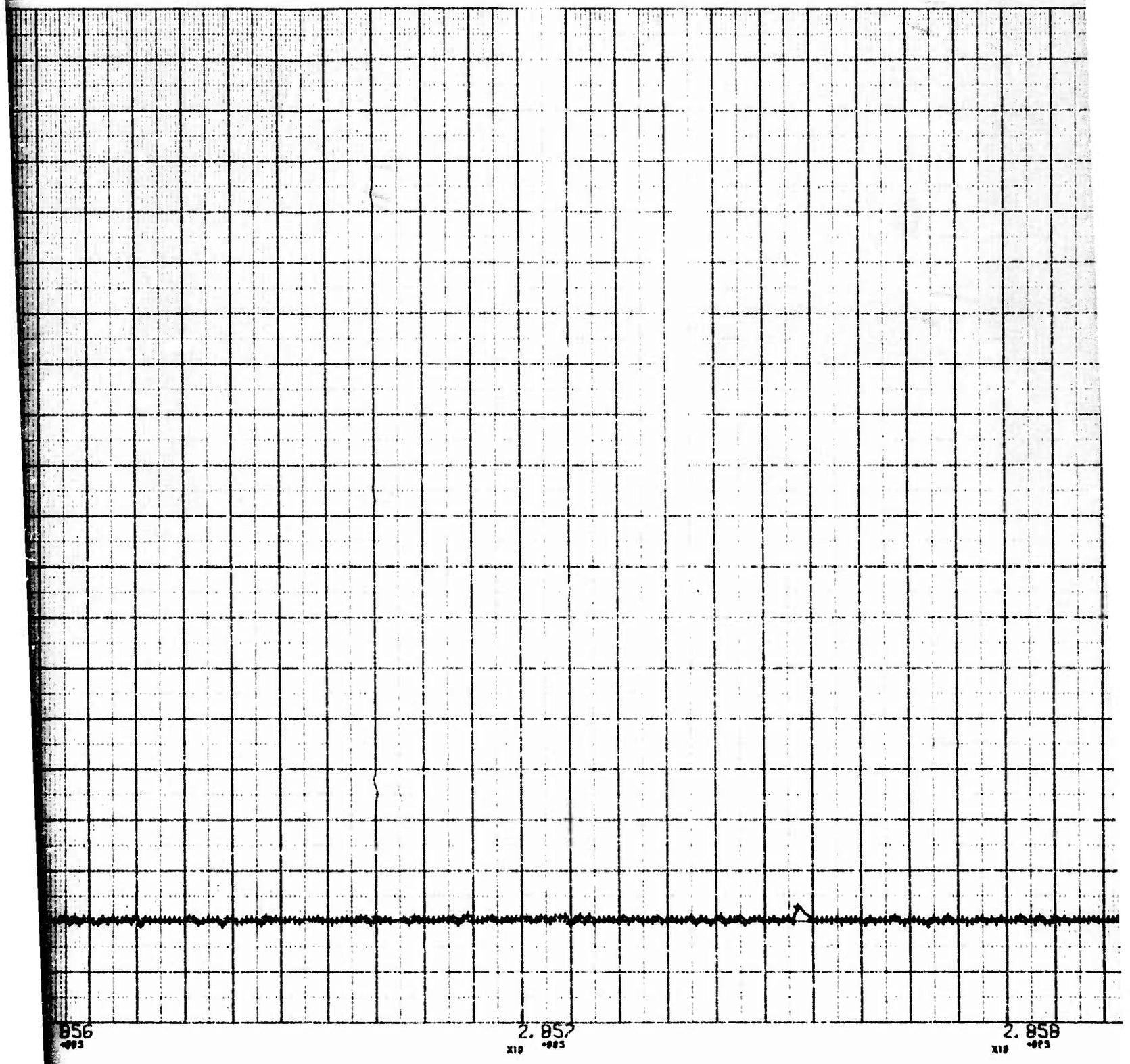

44

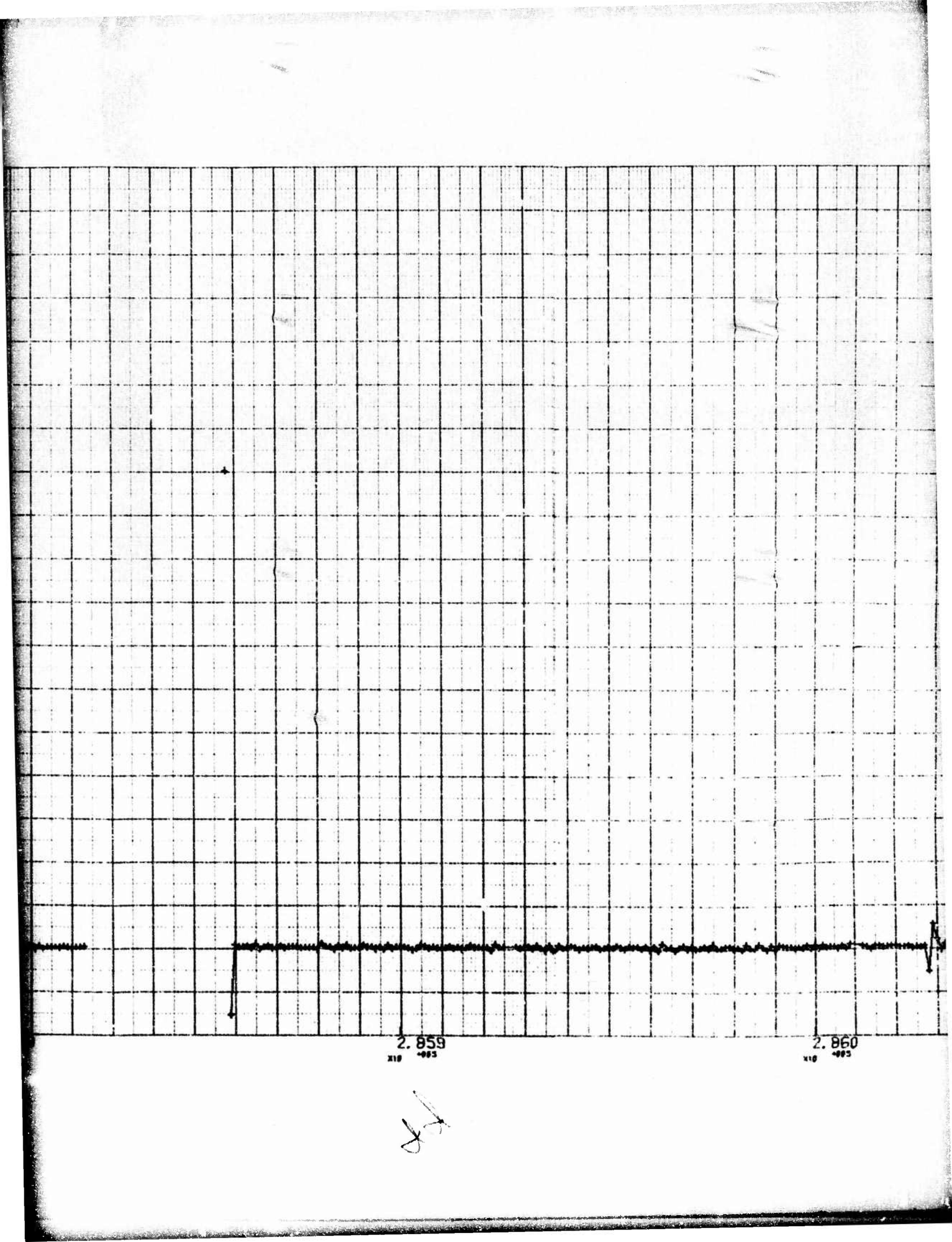
2.859
X10 +003
2.860
X10 +003

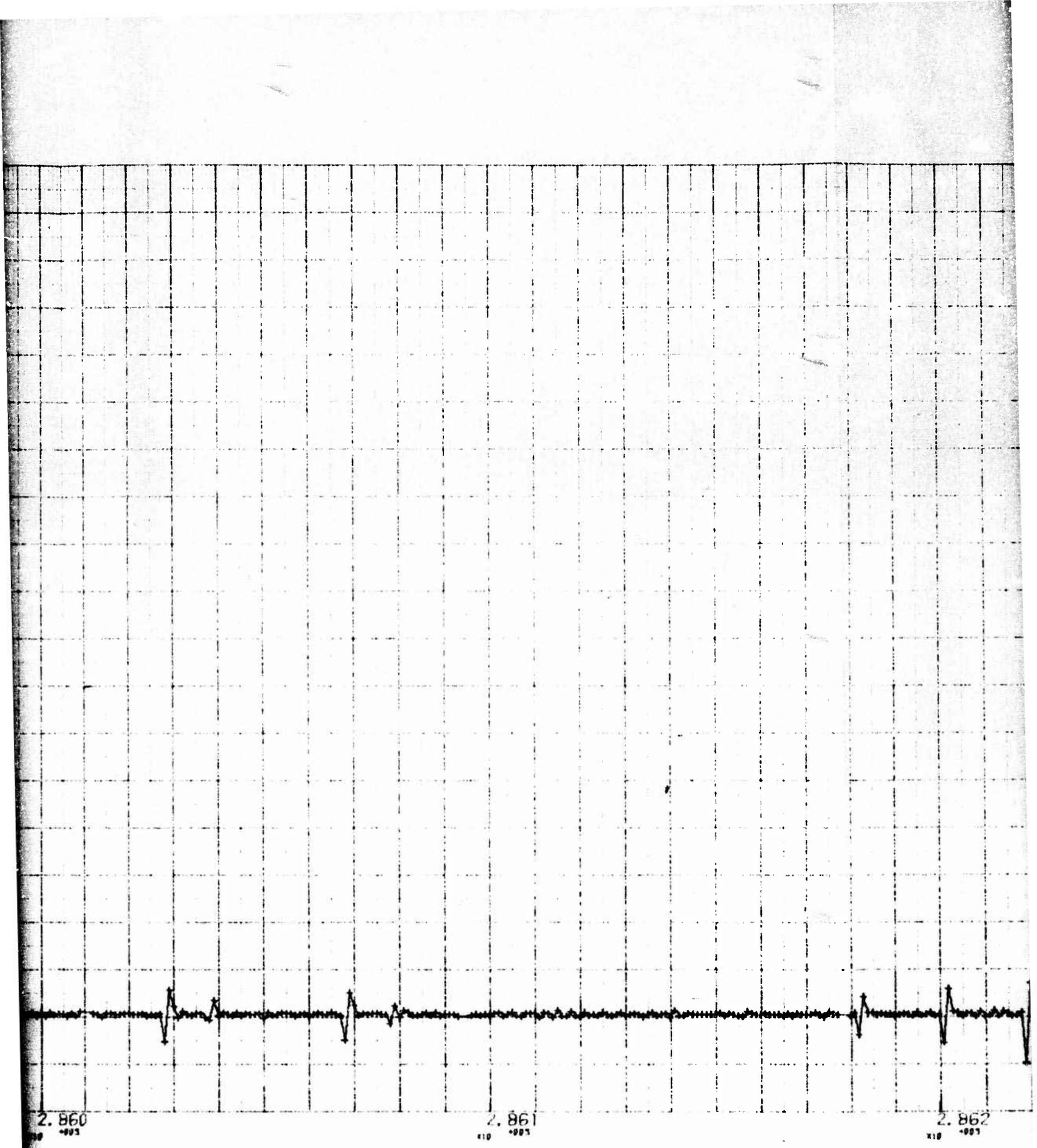

Fig. F-3. Co
(Re

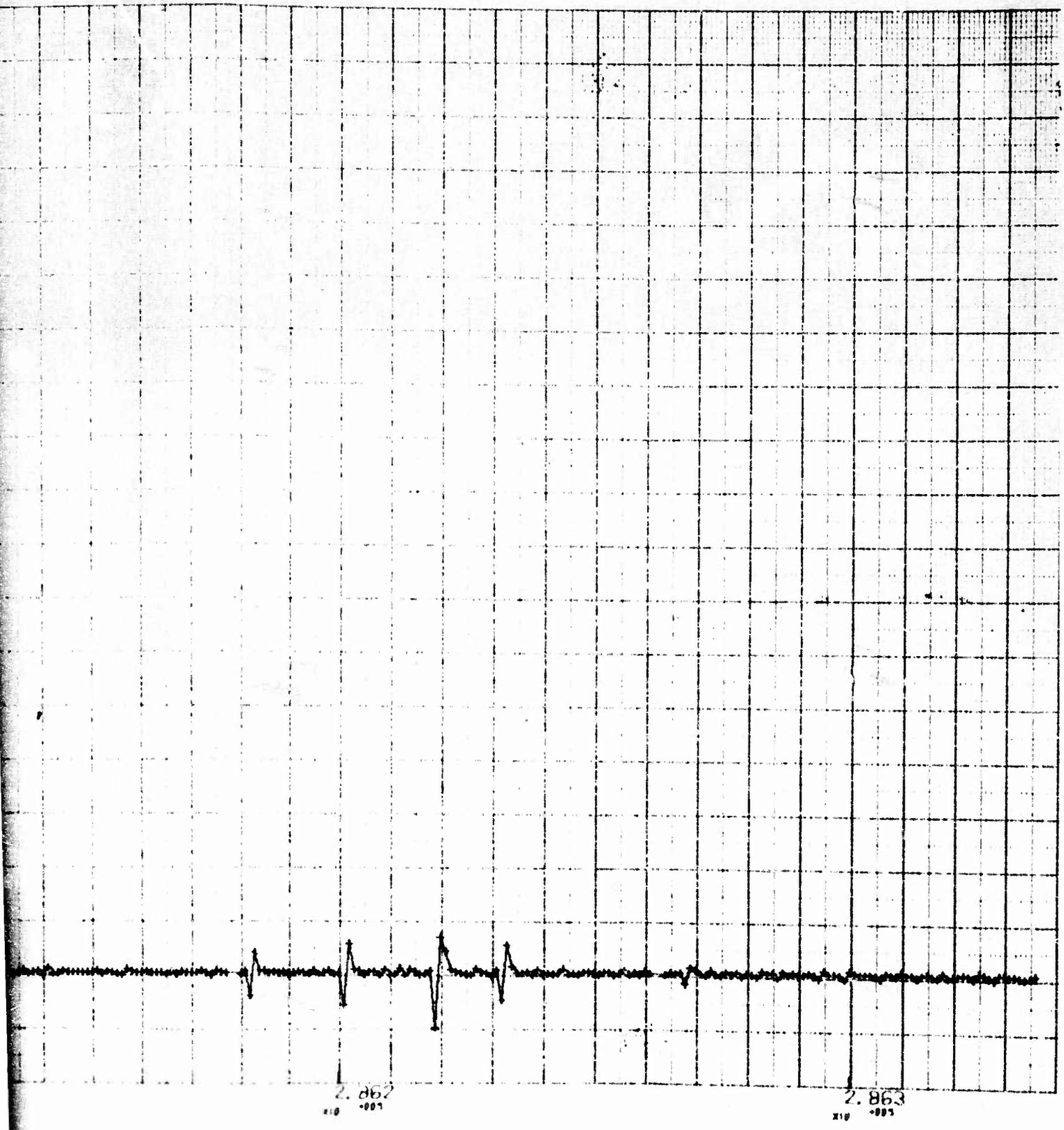

Fig. F-3. Corrected Raw Accelerometer Data
(Revolution 52.7 to 53.3)

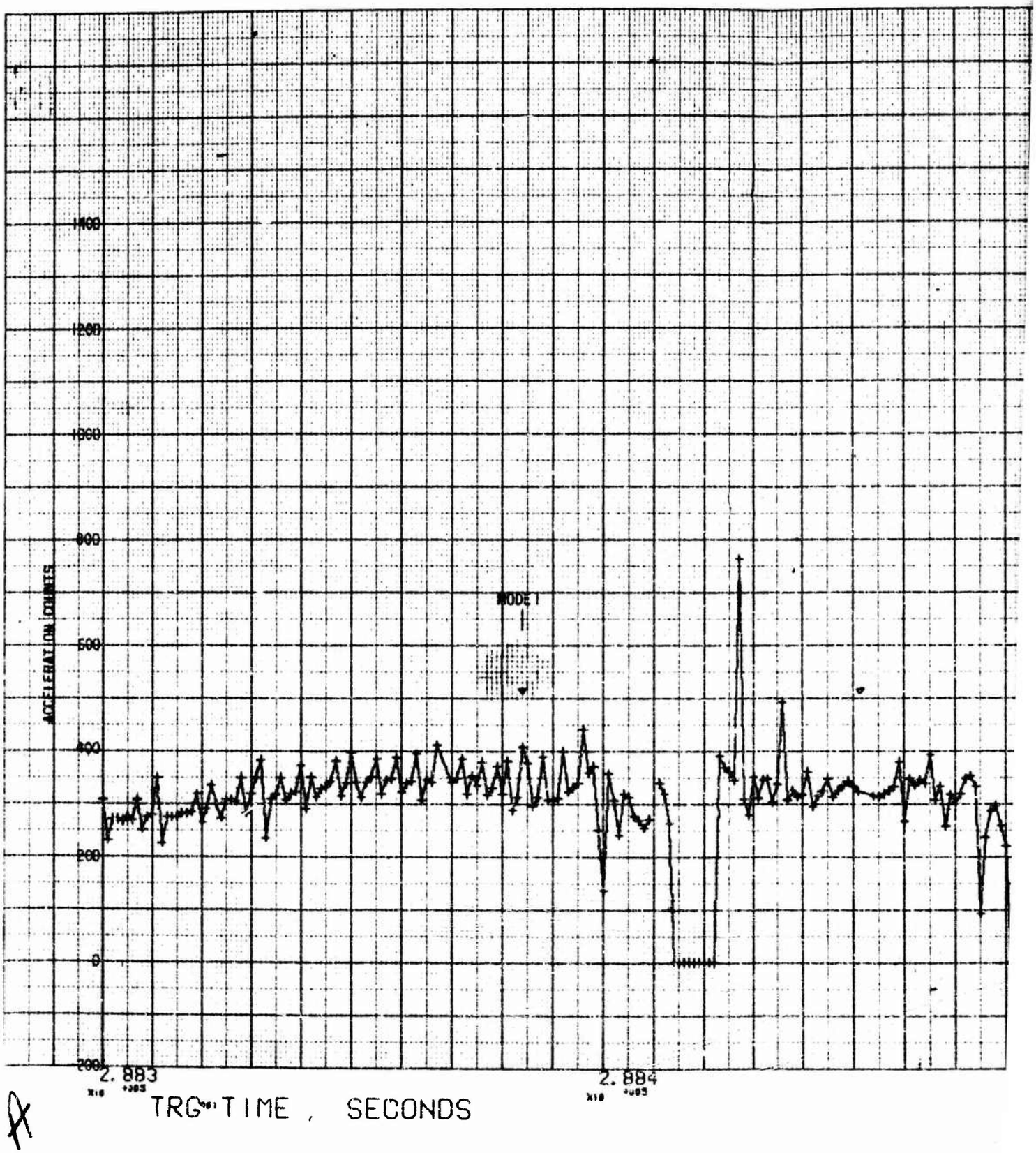
1400
1200
1000
800
600
400
200
0
-200
ACCELERATION (G'S)
MODE 1
2.883
X10 +005
2.884
X10 +005
TRG TIME , SECONDS

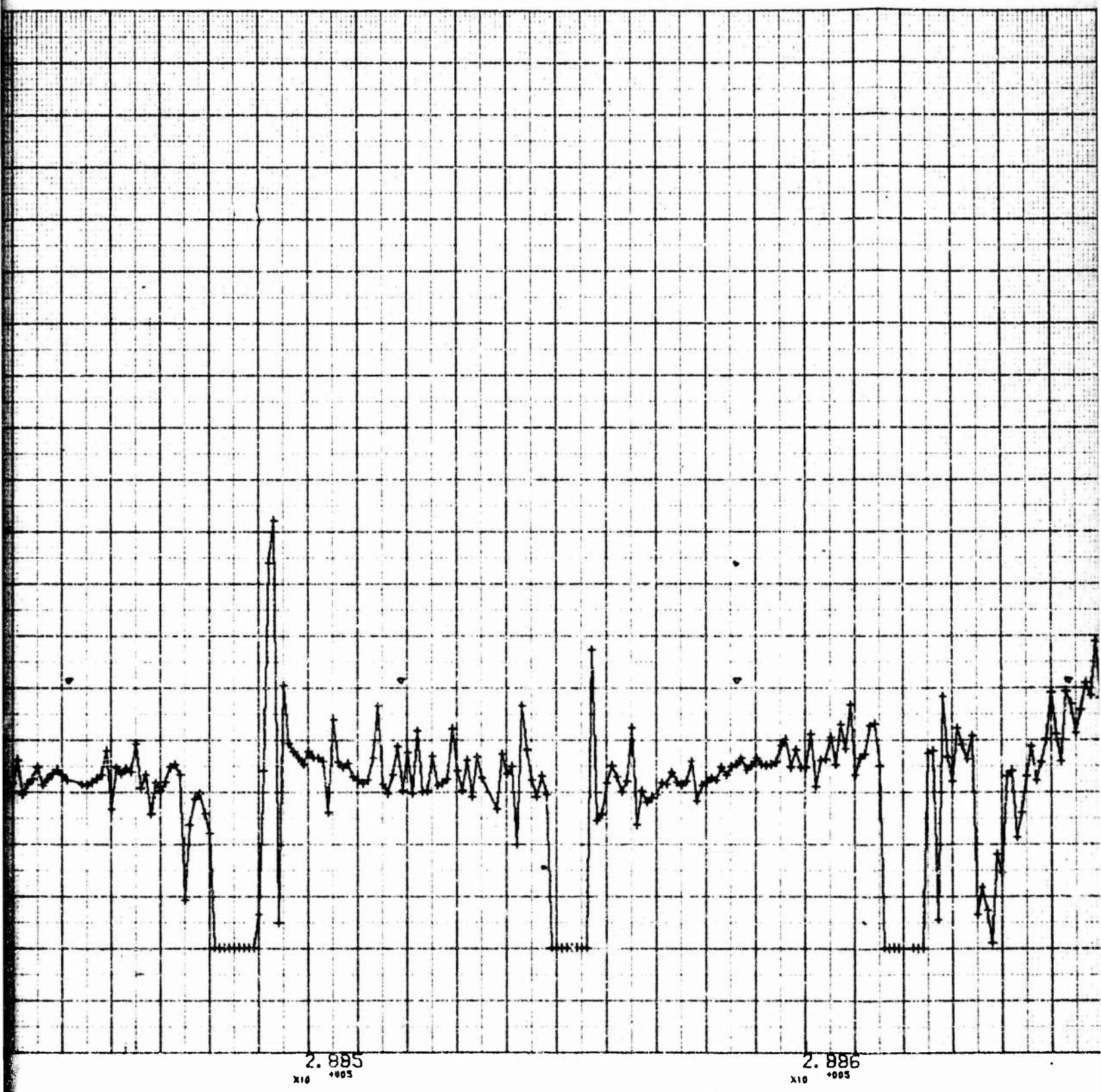

B

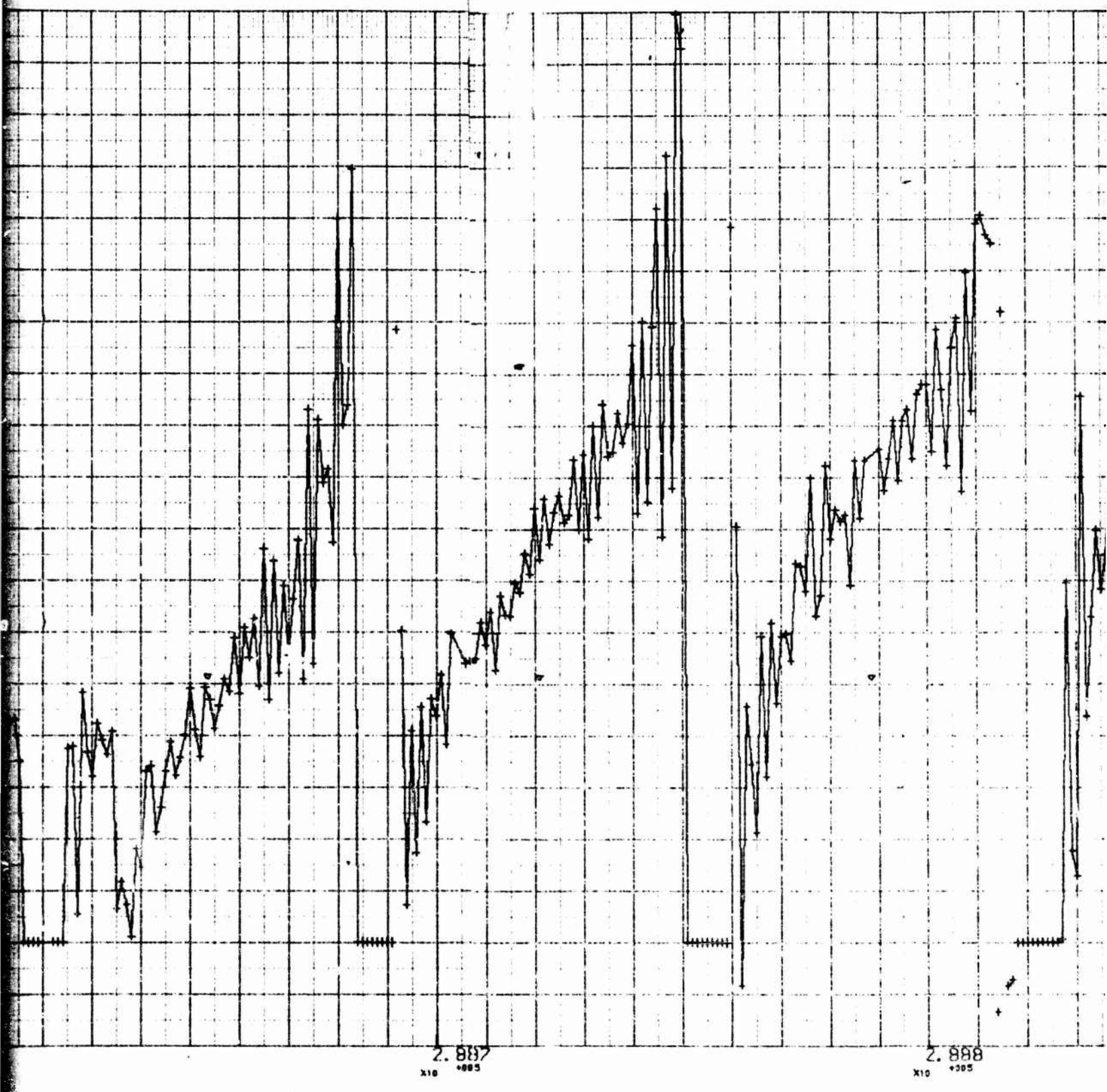
2.887
X10 +005
2.888
X10 +005

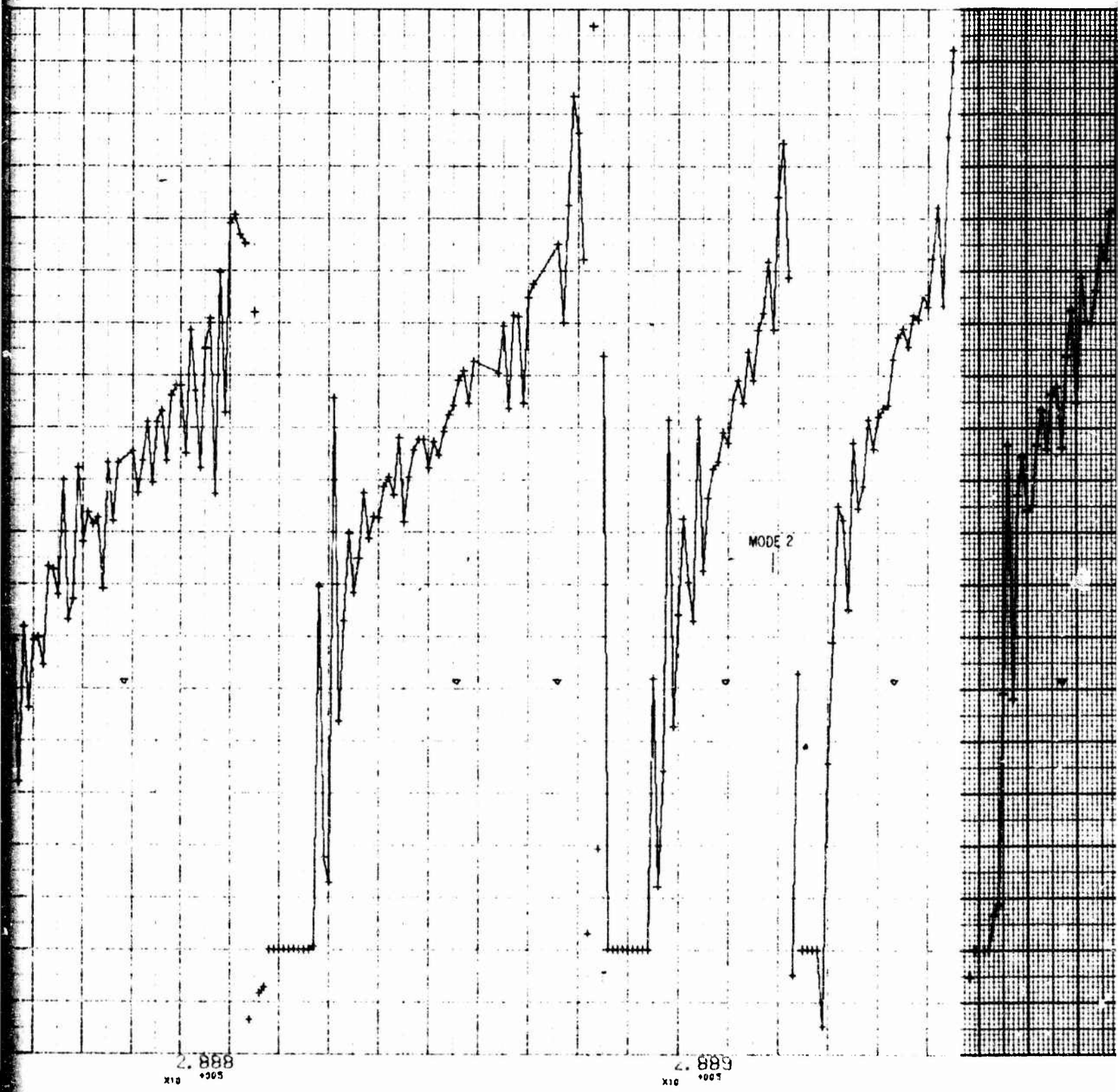

D

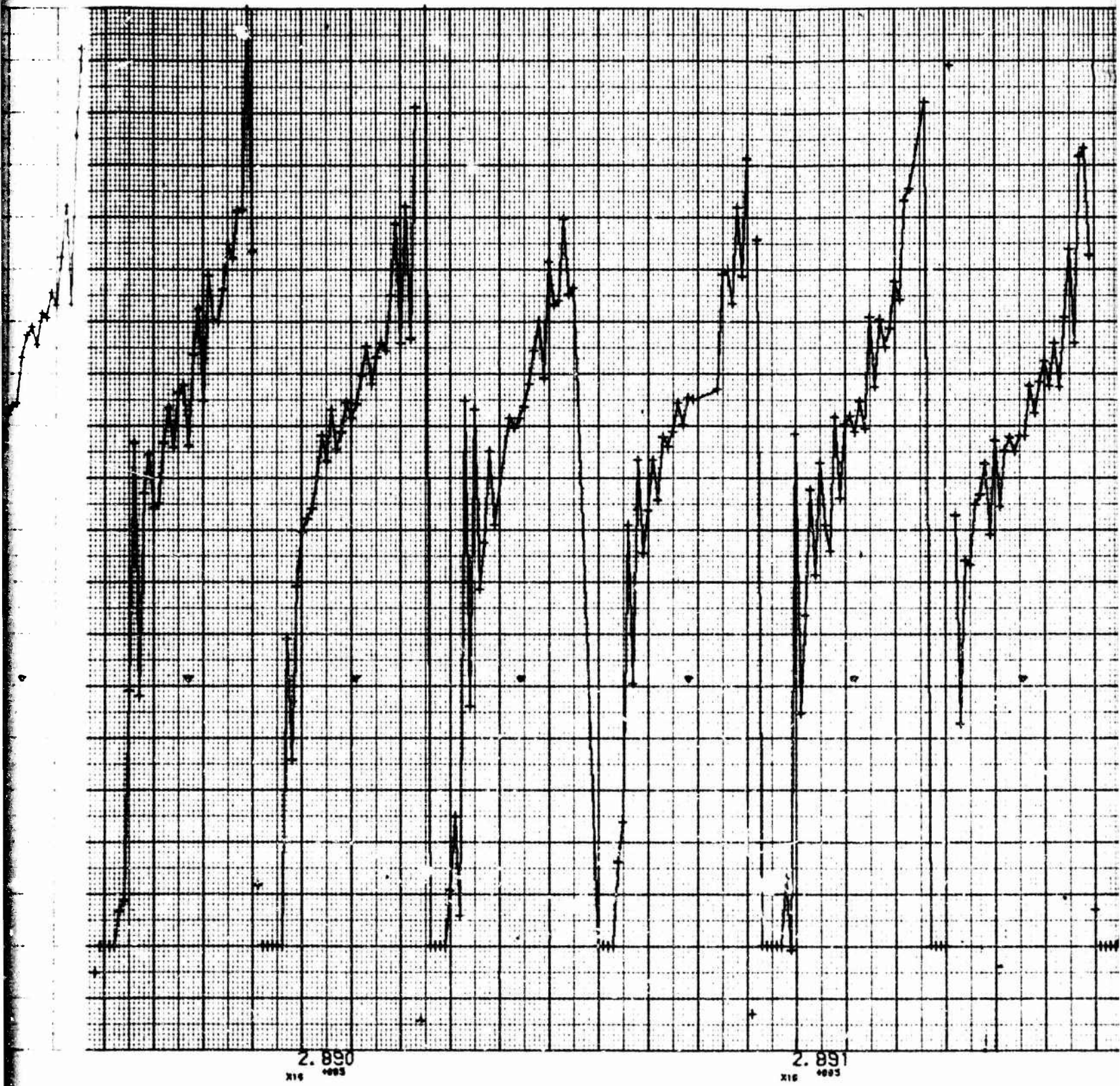
2.890
X10 +003
2.891
X10 +003

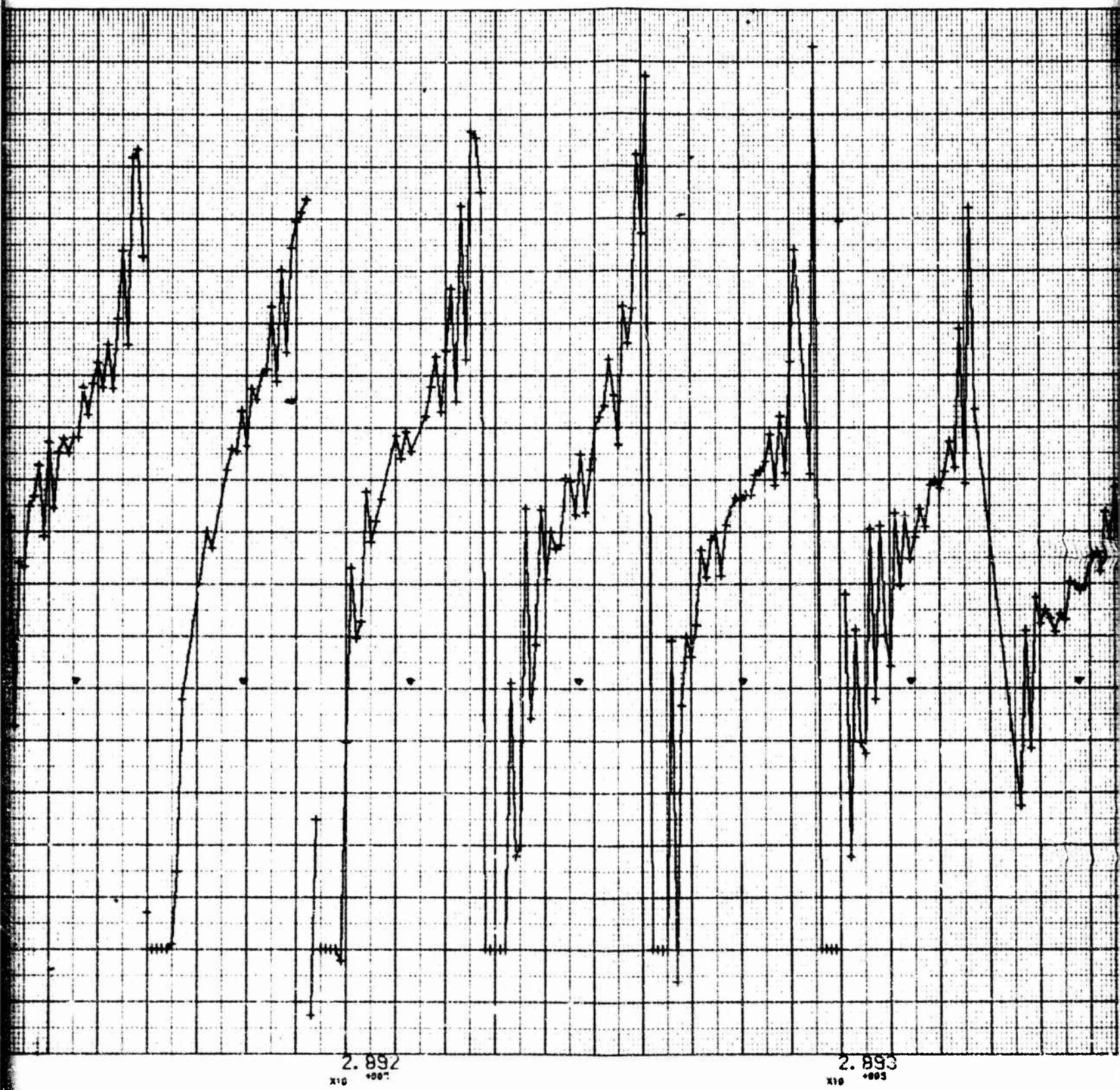

Fig. F-4. Corrected Raw Accelerometer Data
Revolution 54 Perigee)

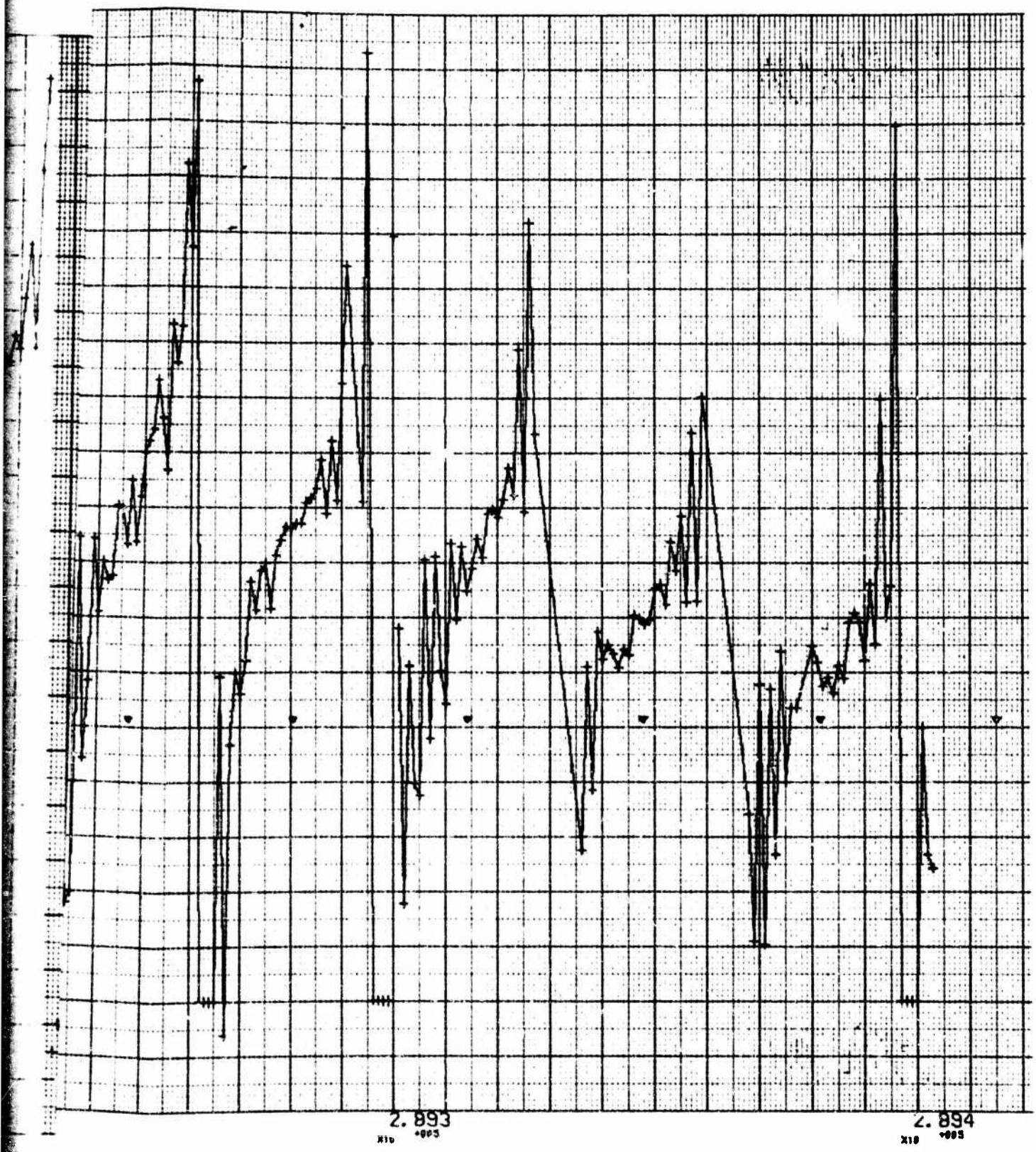

Fig. F-4. Corrected Raw Accelerometer Data (Modes 1 and 2, Revolution 54 Perigee)

APPENDIX G

REDUCED DATA PLOTS

This appendix presents the plots of reduced data from the LOGACS flight. Figure G-1 presents the drag acceleration profile reduced from the accelerometer data and the drag acceleration profile from the best-fit ephemeris. Also included are plots of latitude, longitude, and altitude from the best-fit ephemeris. The orbit rev. number is indicated near each perigee. Figure G-1 is separated into four plots, one for each day of the mission [Fig. G-1(a) is for 23 May, Fig. G-1(b) for 24 May, et .].

Figure G-2 presents information relating to the control system. The drag acceleration profiles are also included so that correlations of anomalous responses can be observed. Figure G-2 is also separated into four plots and the rev. number is indicated near perigee.

MAY 23

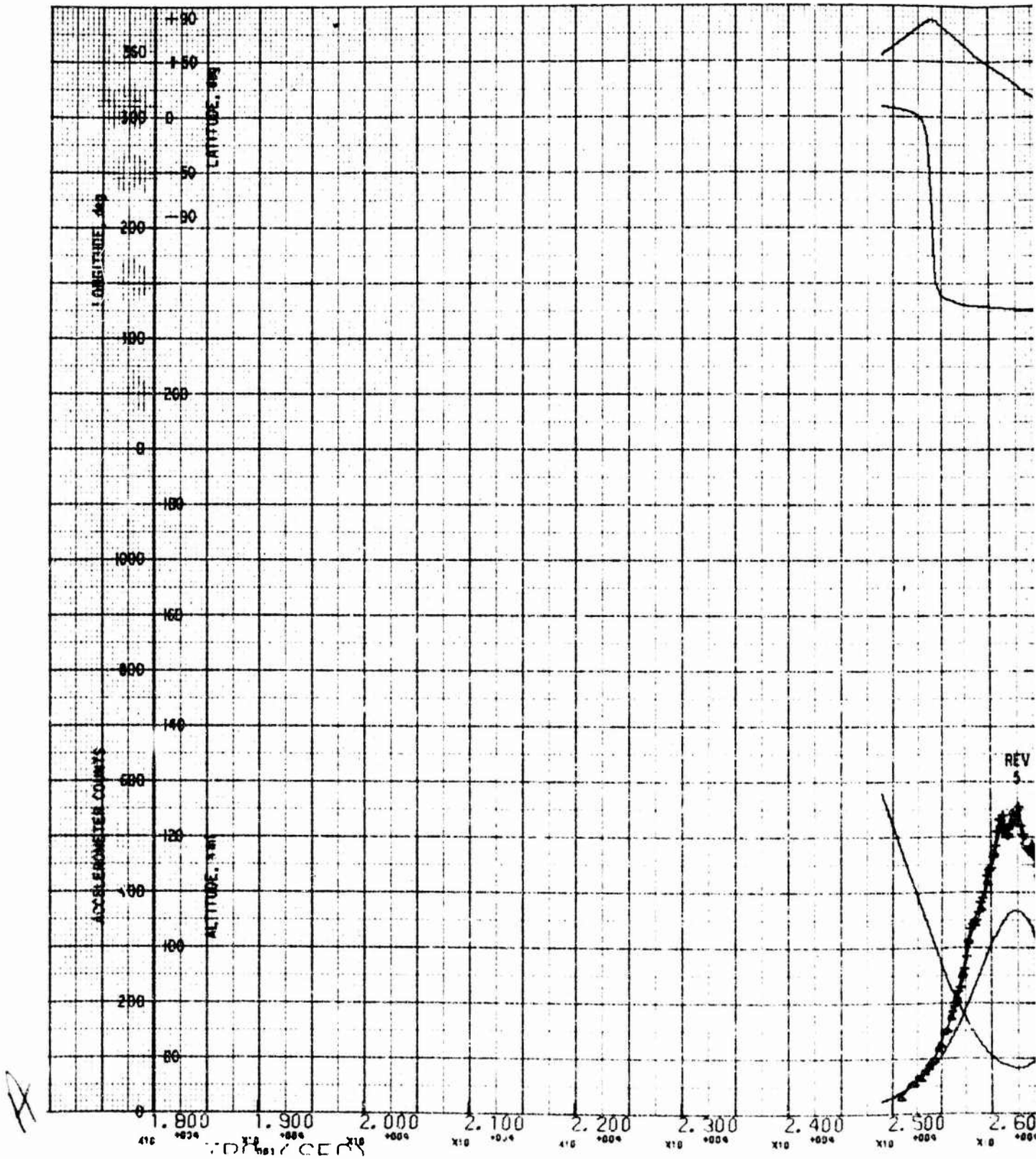
+90
+50
0
-50
-90
LATITUDE, deg
LONGITUDE, deg
ACCELEROMETER COUNTS
ALTITUDE, nmi
1.800
1.900
2.000
2.100
2.200
2.300
2.400
2.500
REV
5

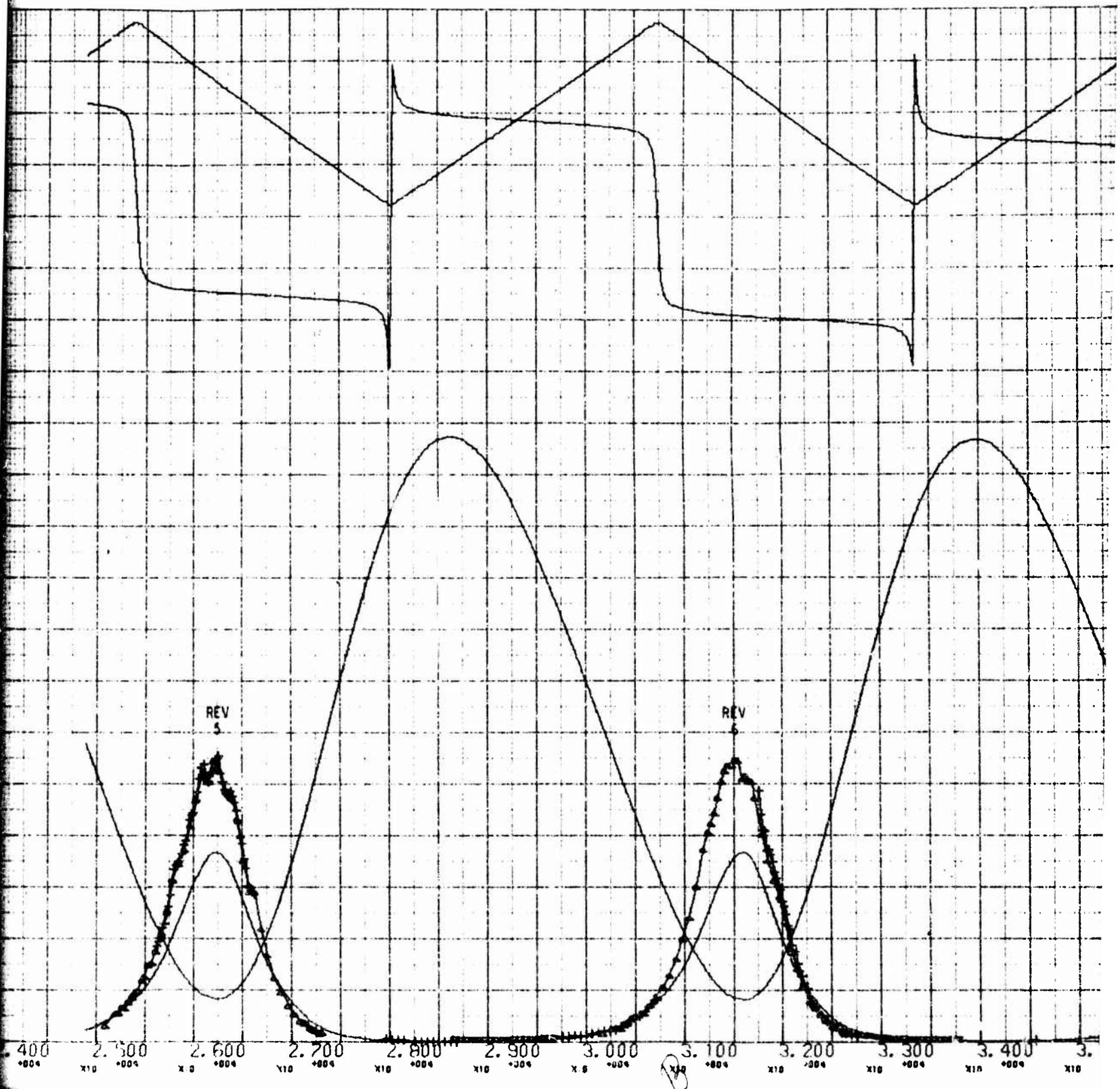
REV
5
REV
6
2.400
2.500
2.600
2.700
2.800
2.900
3.000
3.100
3.200
3.300
3.400
3.

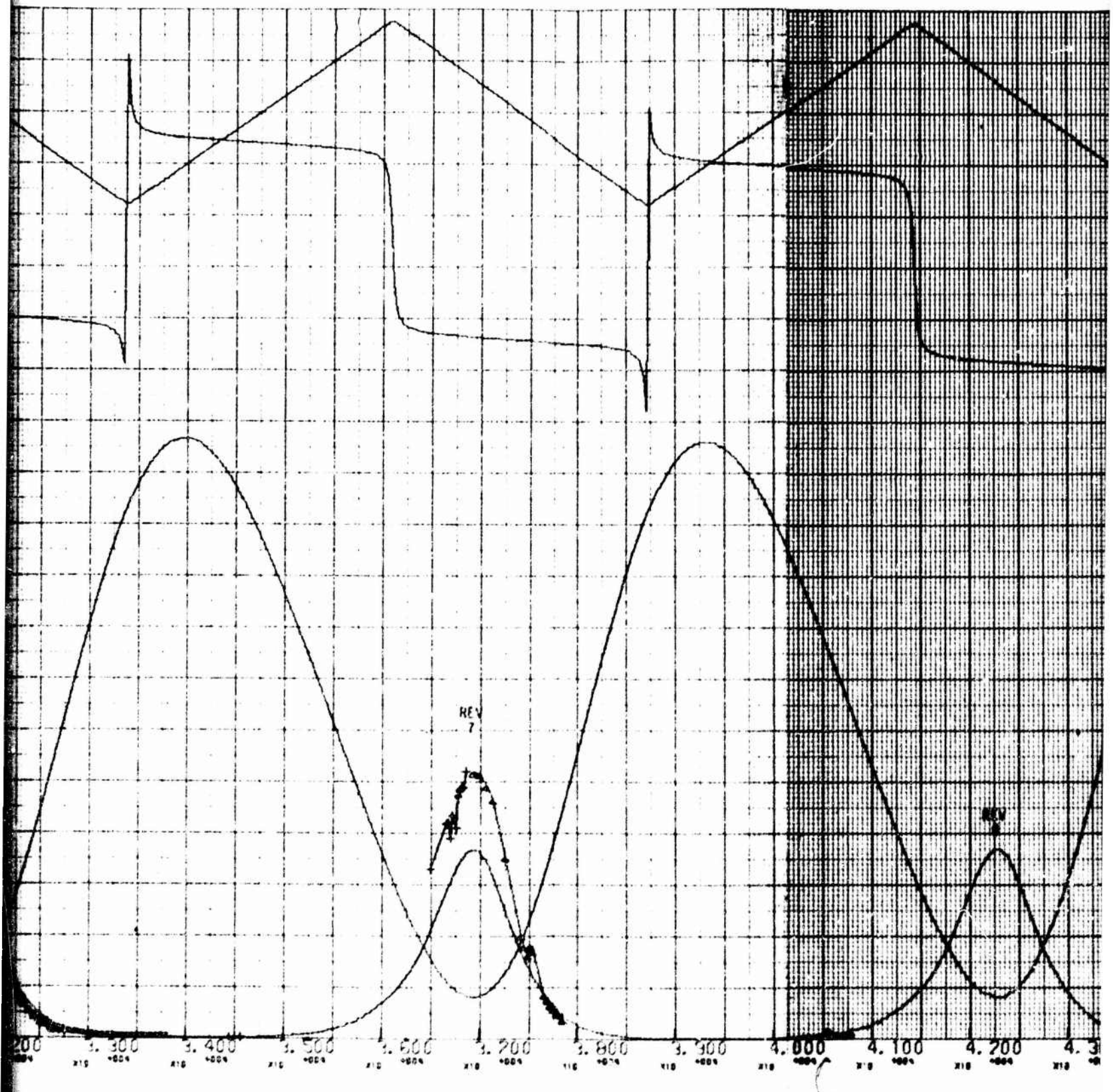
REV
7
REV
8
3.300
3.400
3.500
3.600
3.700
3.800
3.900
4.000
4.100
4.200

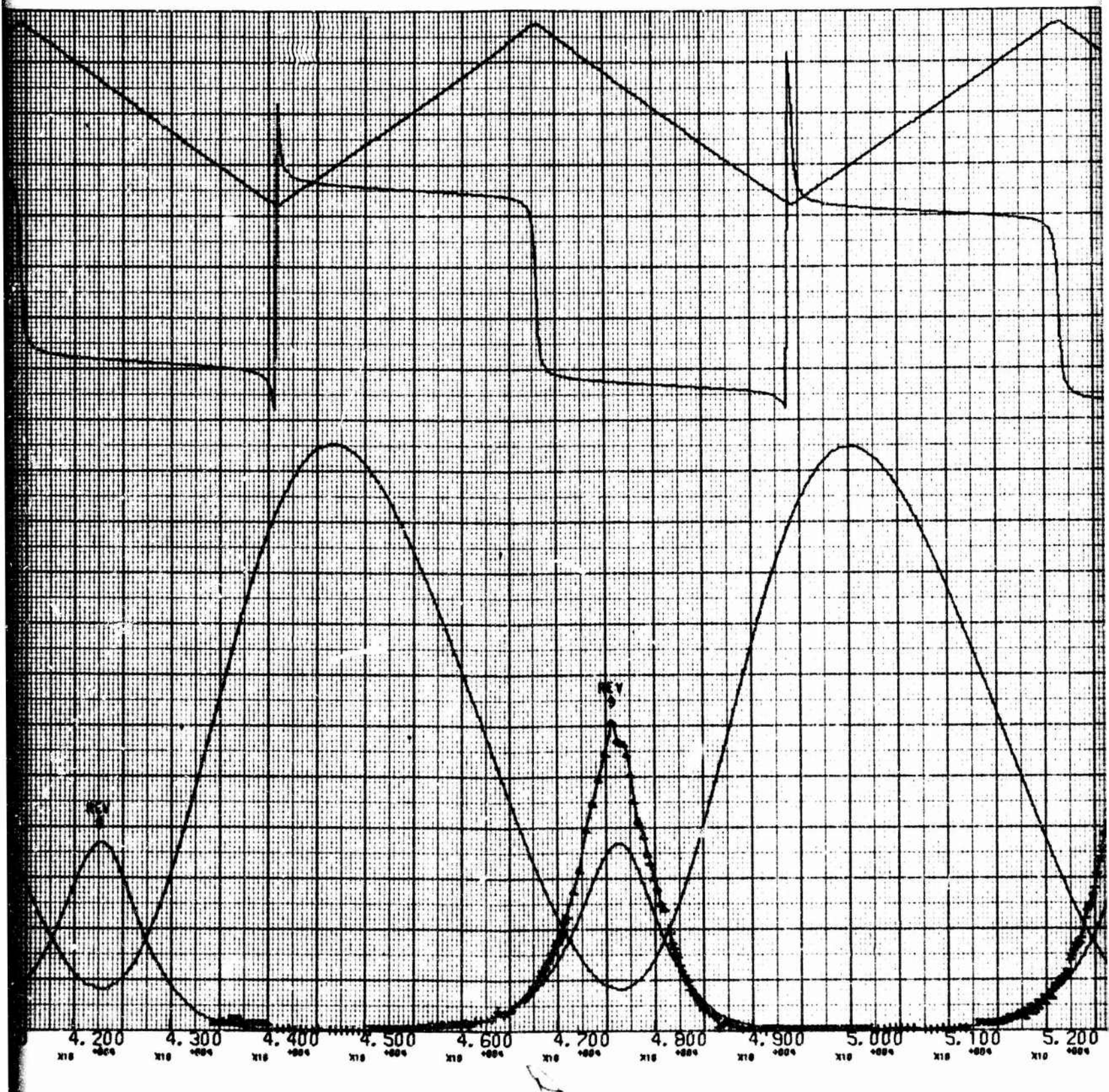
4.200
4.300
4.400
4.500
4.600
4.700
4.800
4.900
5.000
5.100
5.200

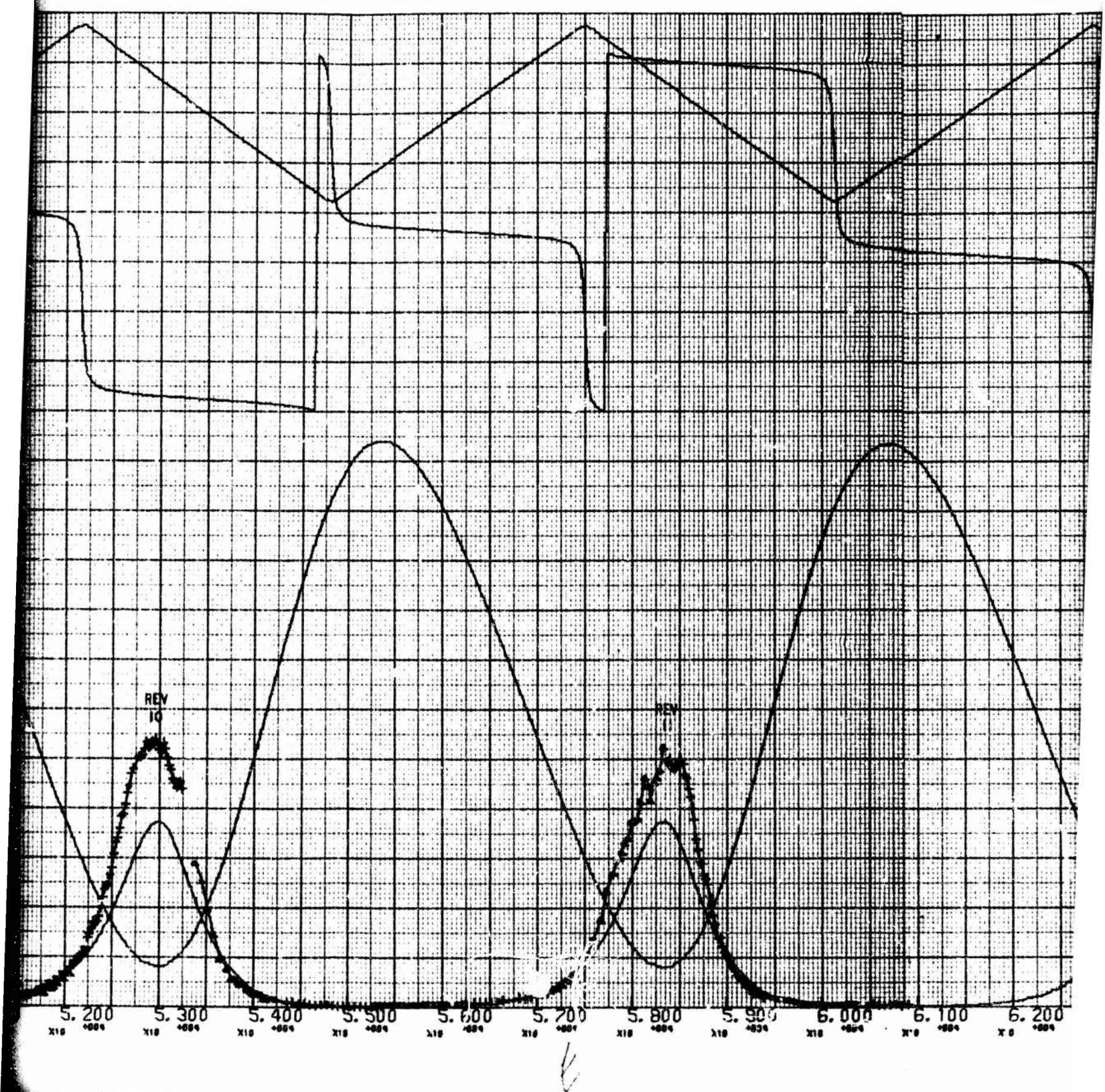
REV 10
REV 11
5. 200
5. 300
5. 400
5. 500
5. 600
5. 700
5. 800
5. 900
6. 000
6. 100
6. 200

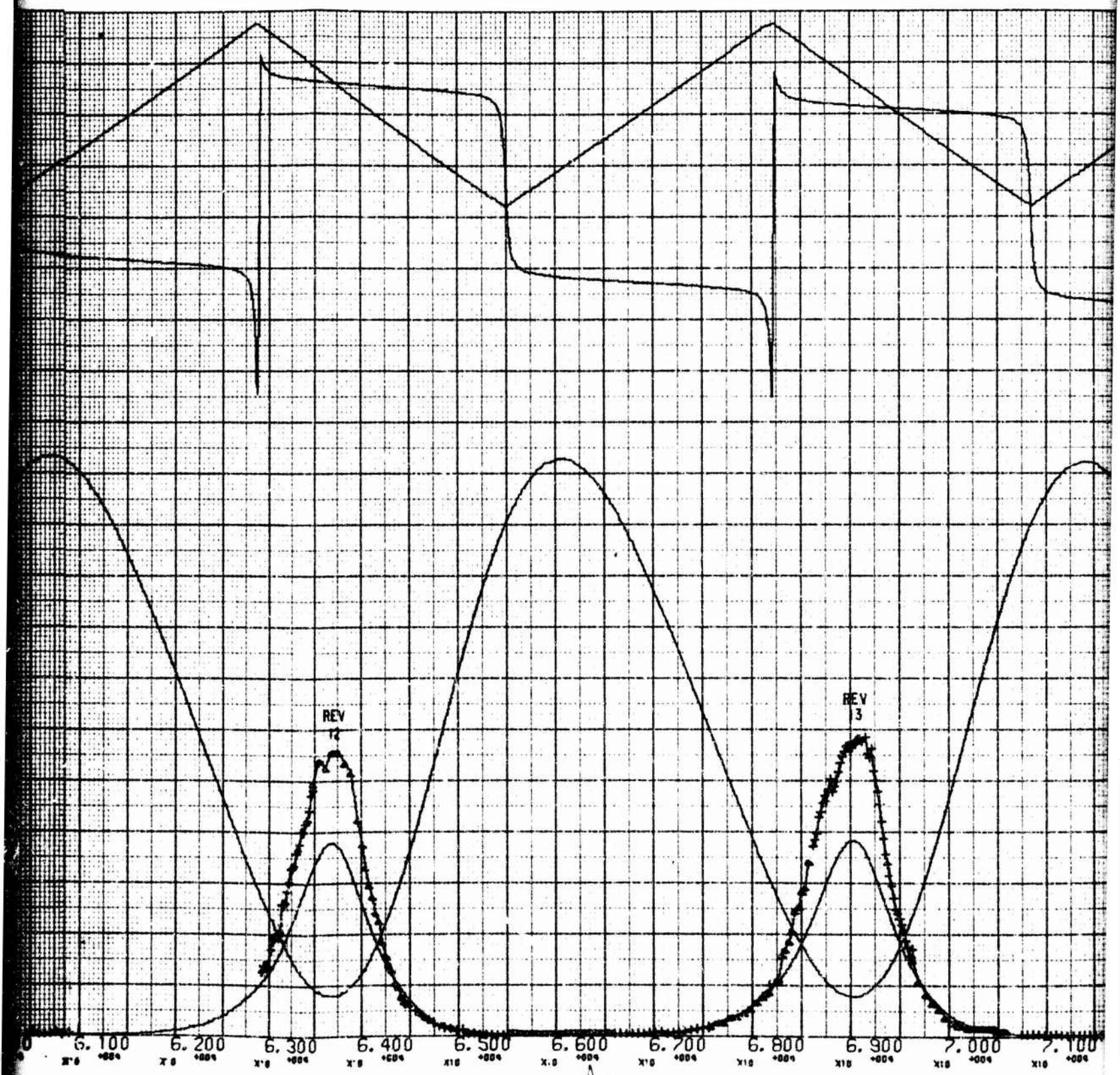
REV
12
REV
13
6.100
6.200
6.300
6.400
6.500
6.600
6.700
6.800
6.900
7.000
7.100

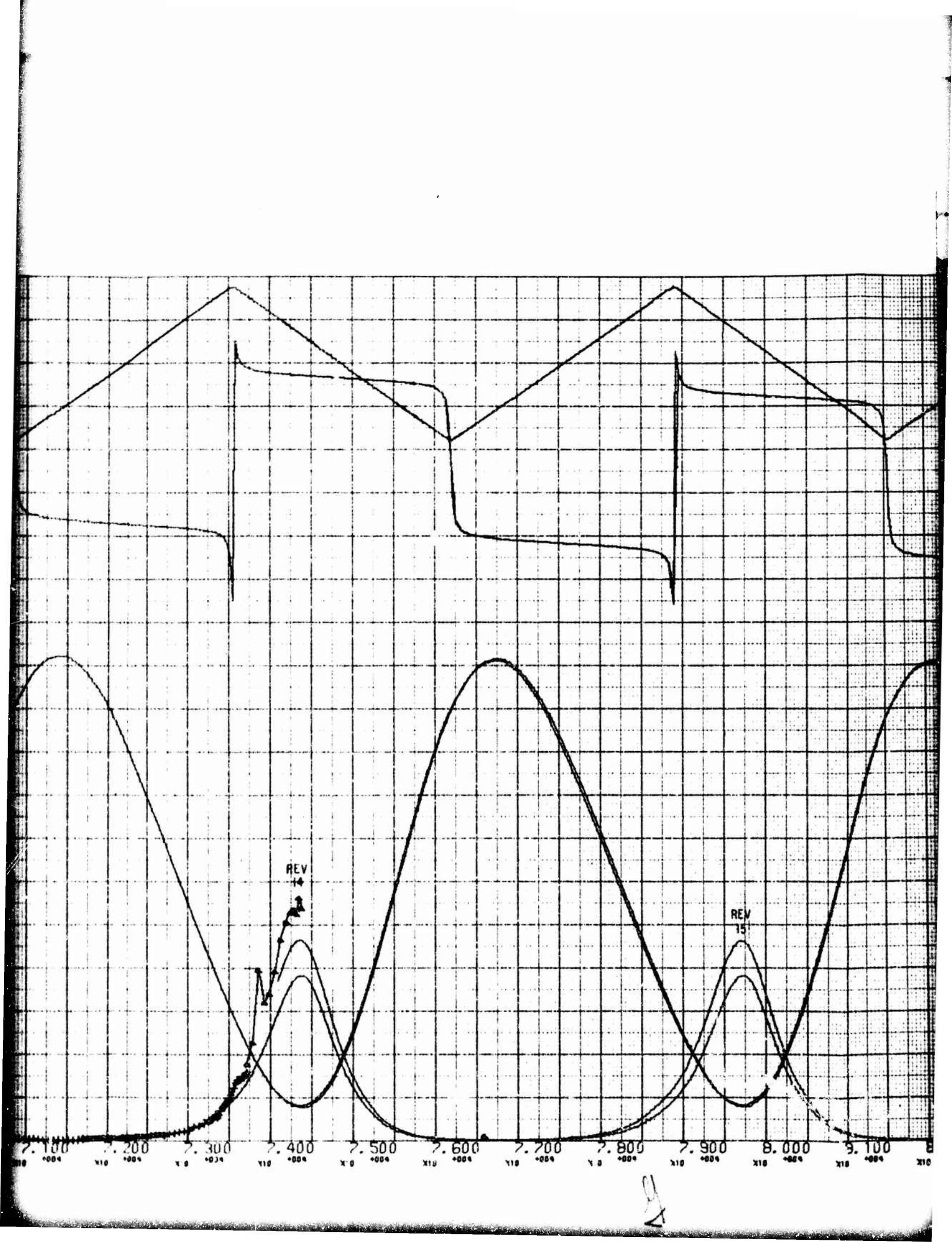
REV
14
REV
15
7.100
7.200
7.300
7.400
7.500
7.600
7.700
7.800
7.900
8.000
9.100

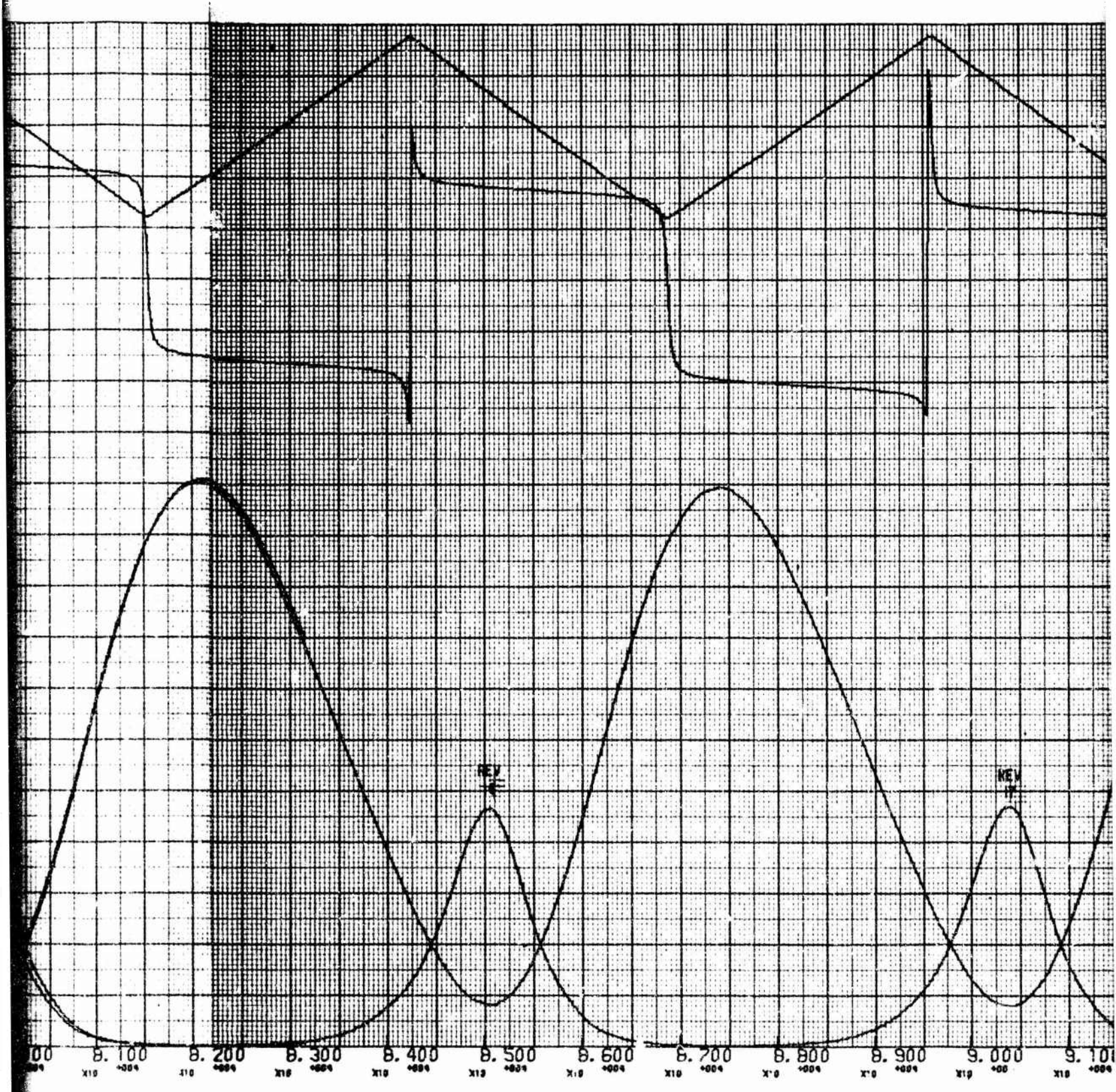
REV
REV
8.100
8.200
8.300
8.400
8.500
8.600
8.700
8.800
8.900
9.000

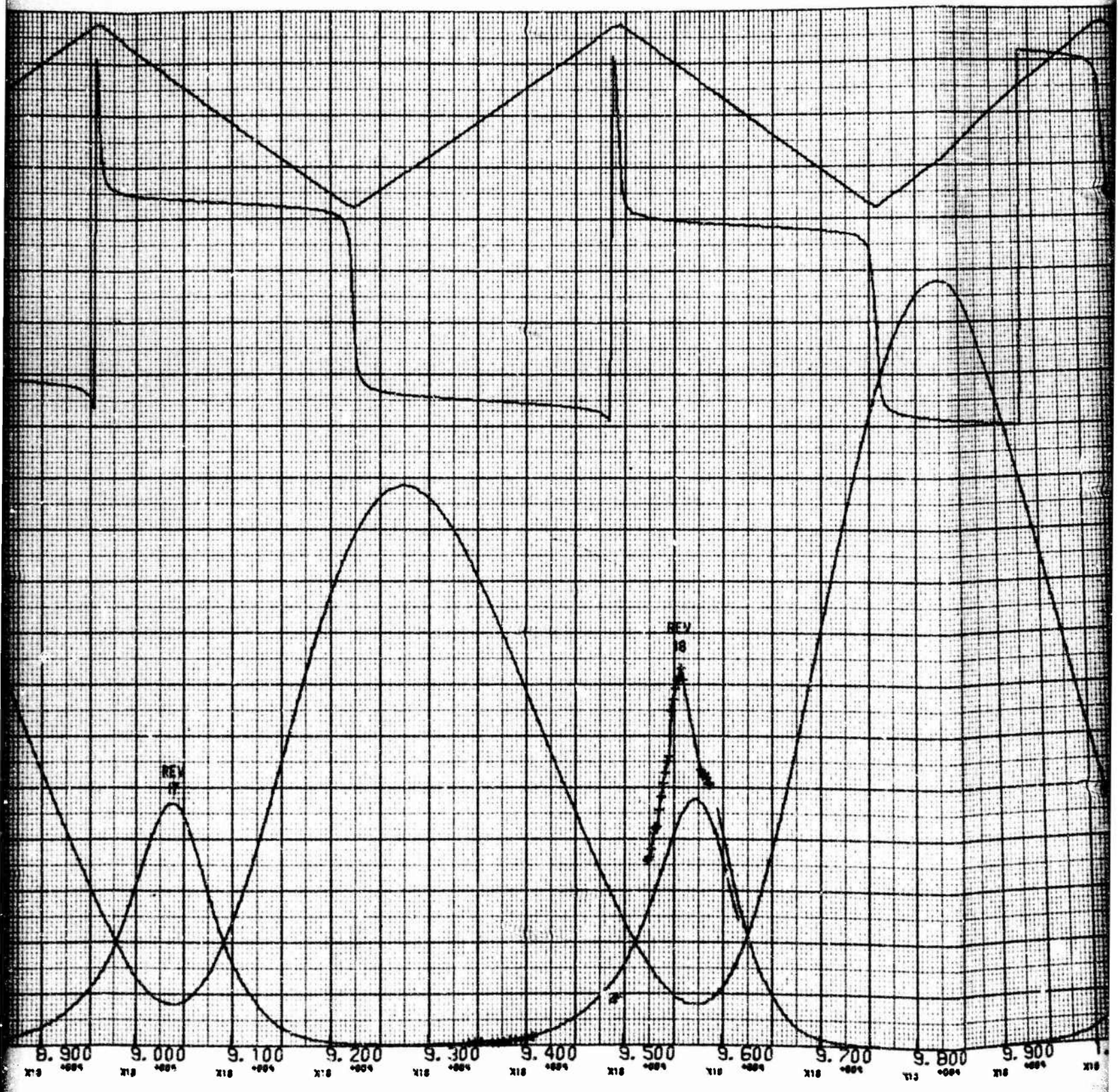

Fig. G-1. (a) Accelera

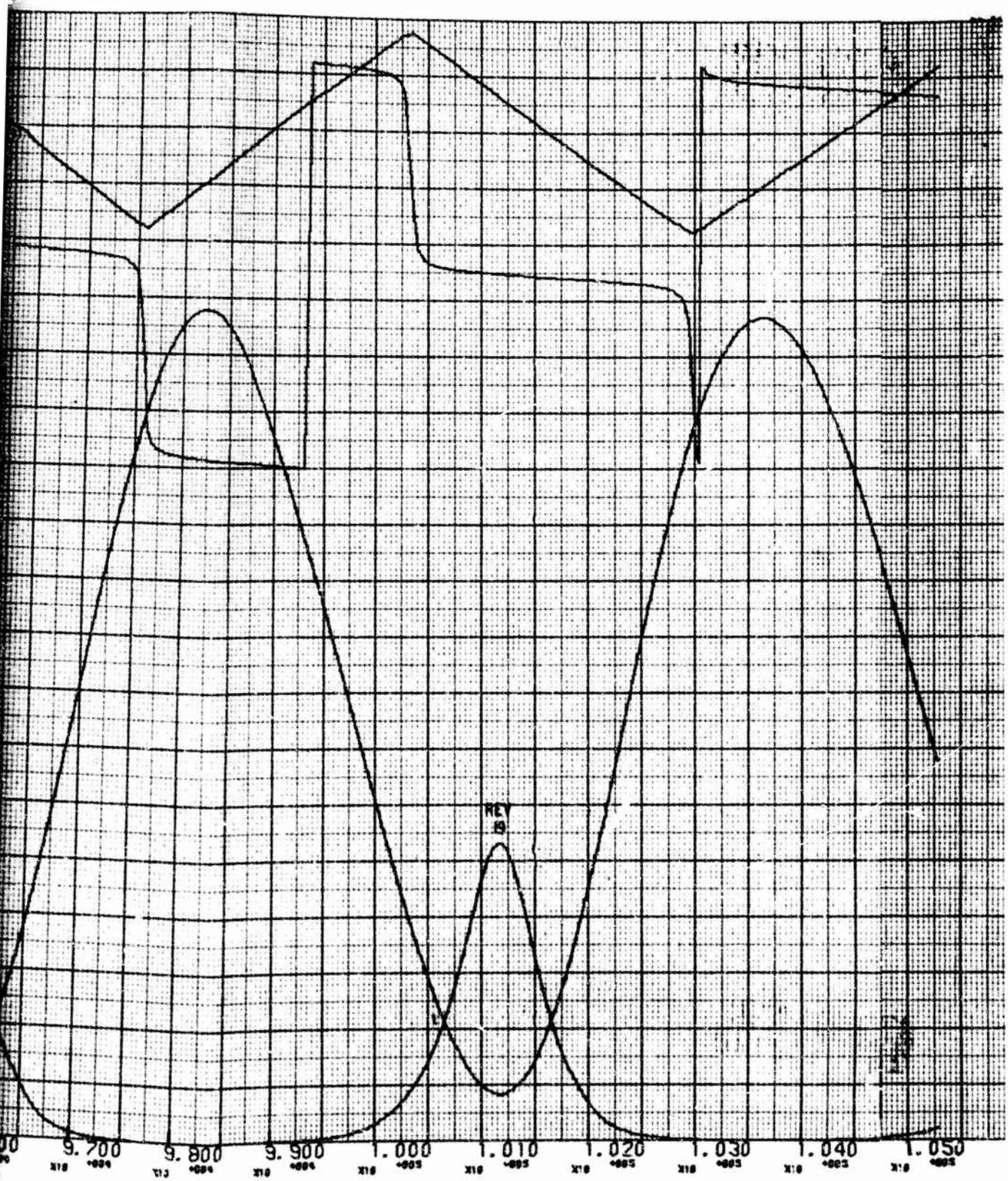

Fig. G-1. (a) Acceleration Profile and Ephemeris Data (May 23)

MAY 24

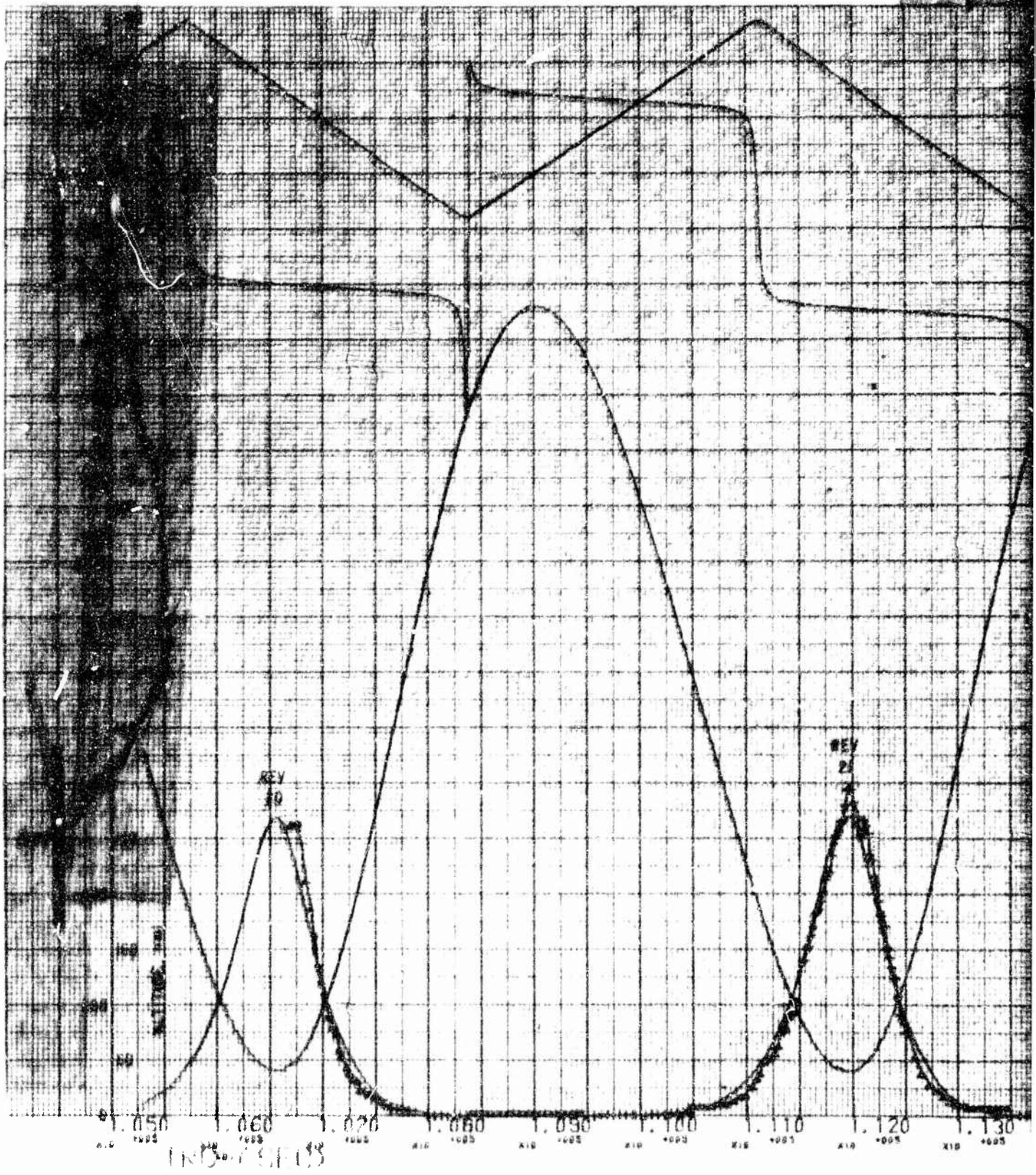

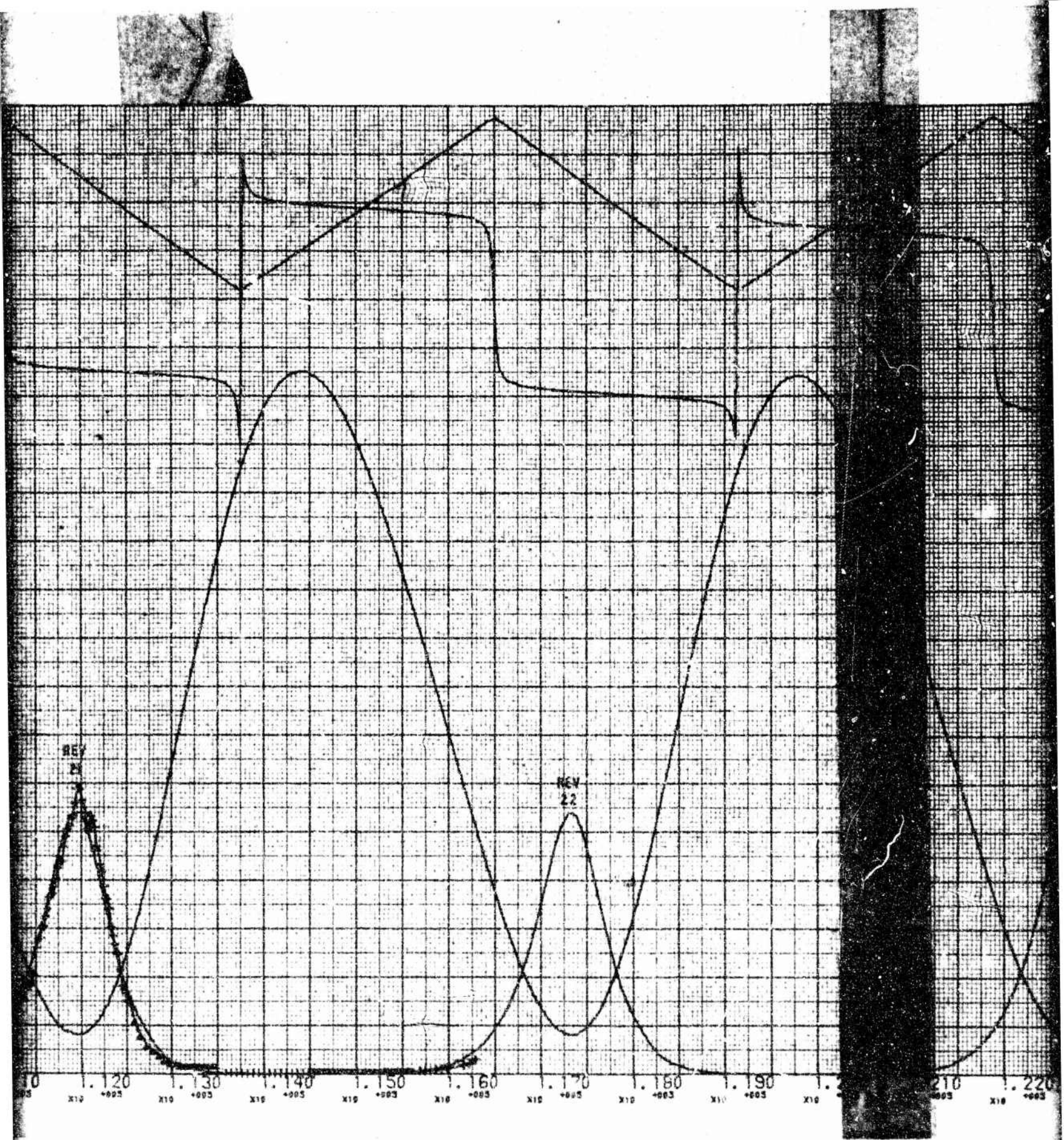
REV
21
REV
22
.120
.130
.140
.150
.160
.170
.180
.190
.220

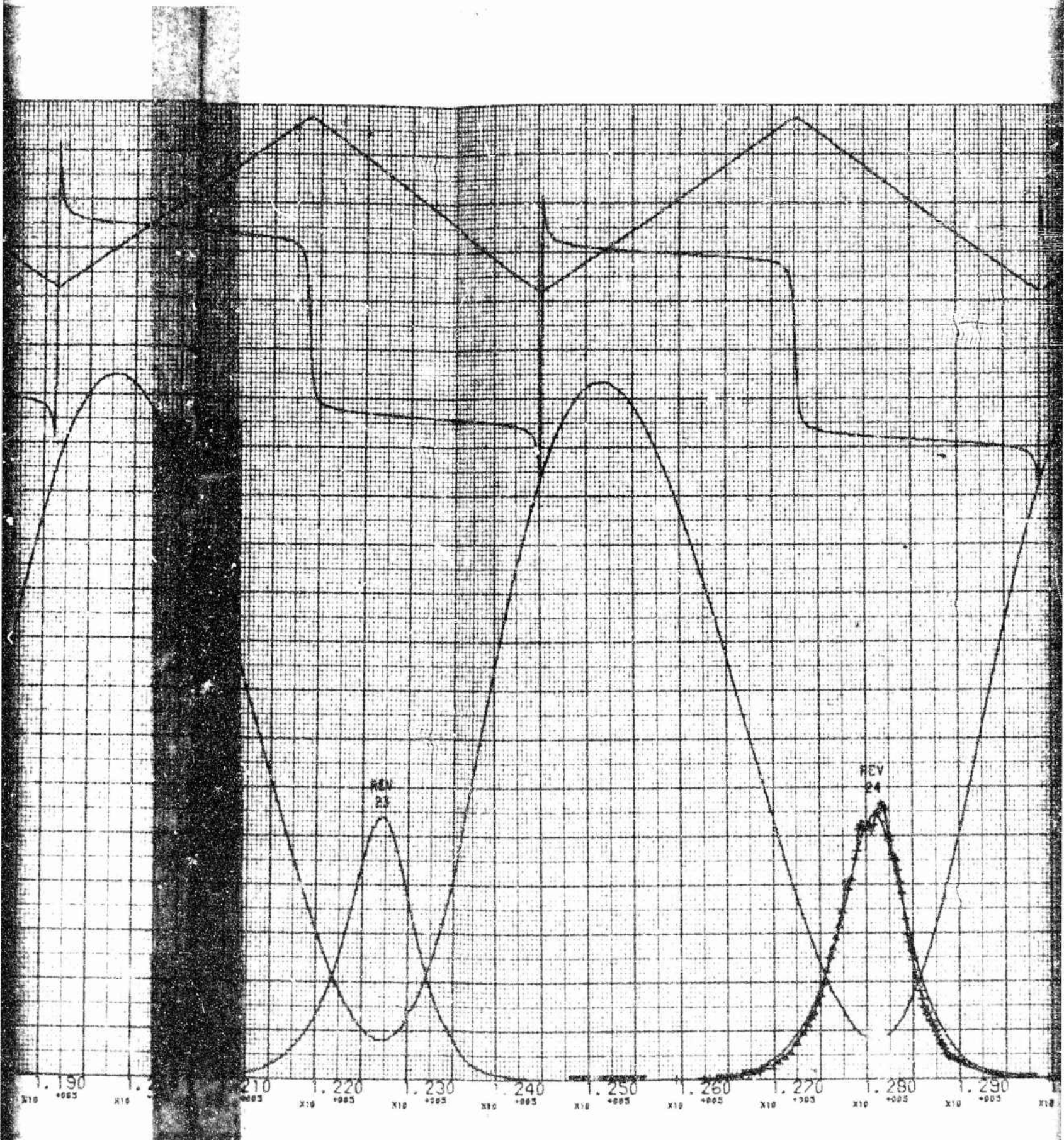
RSN
23
RCV
24
1.190
1.210
1.220
1.230
1.240
1.250
1.260
1.270
1.280
1.290

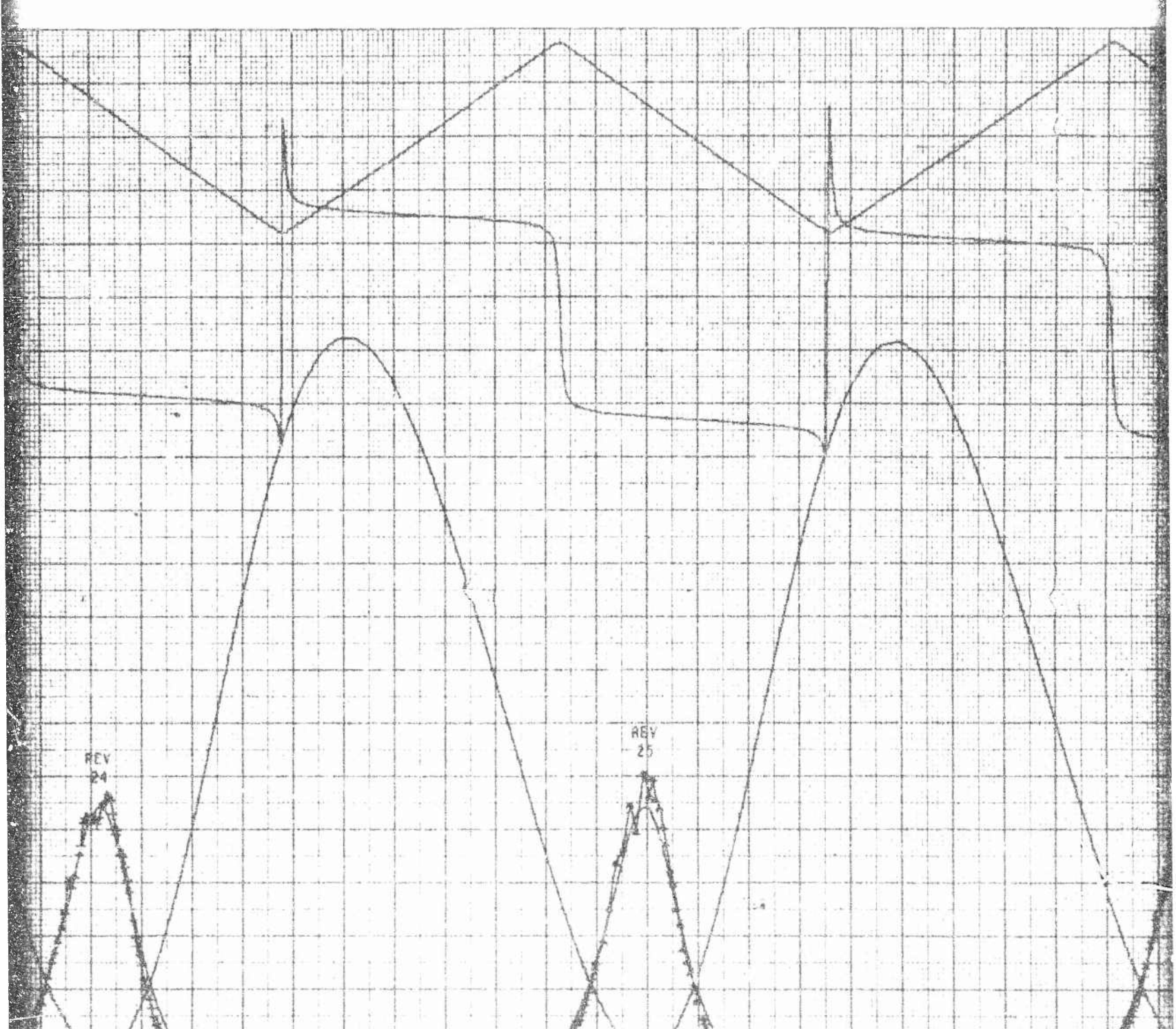
REV
24
REV
25
1.280
1.290
1.300
1.310
1.320
1.330
1.340
1.350
1.360
1.370
1.380
X10 +003

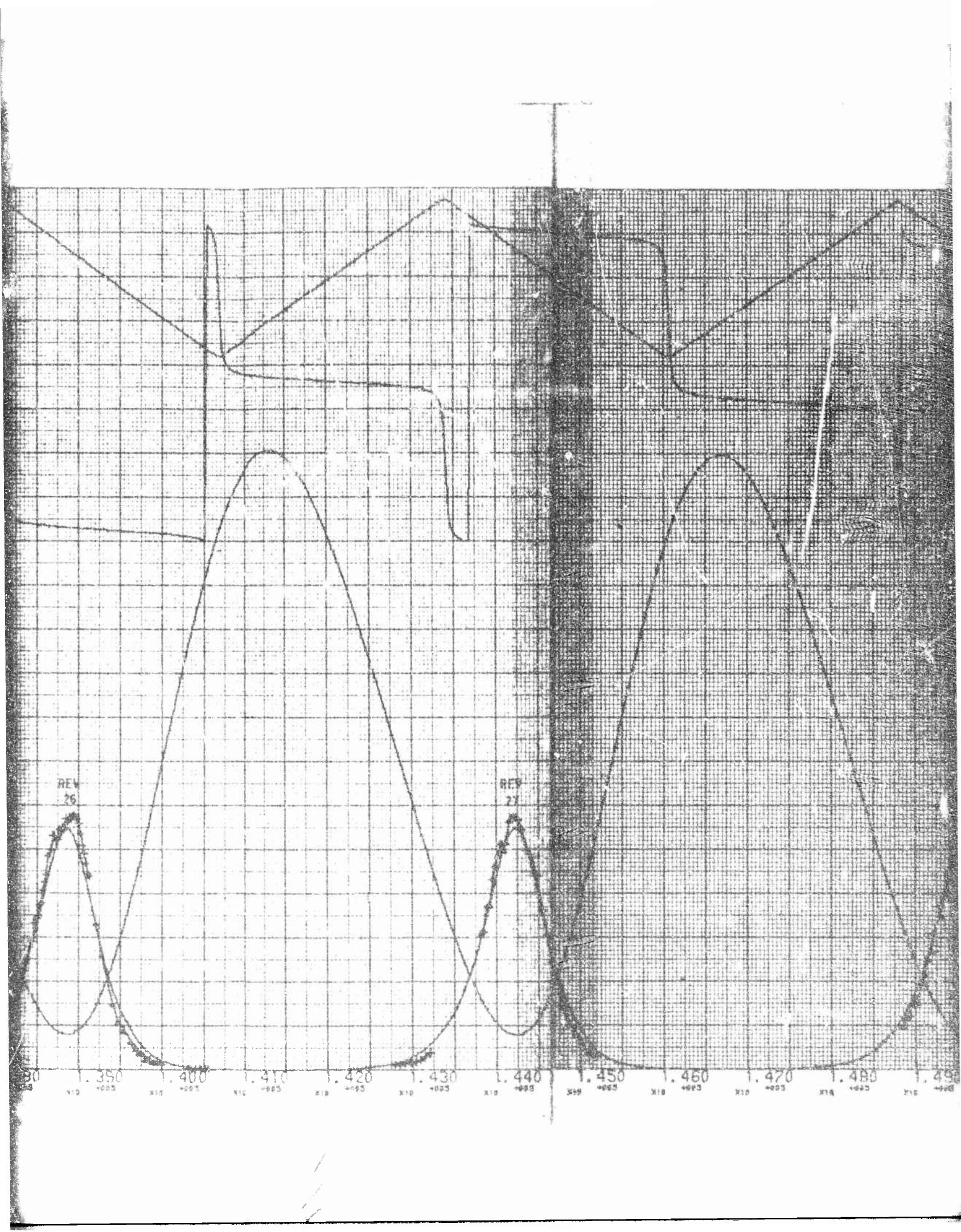
REV
26
REV
27
1.350
1.400
1.410
1.420
1.430
1.440
1.450
1.460
1.470

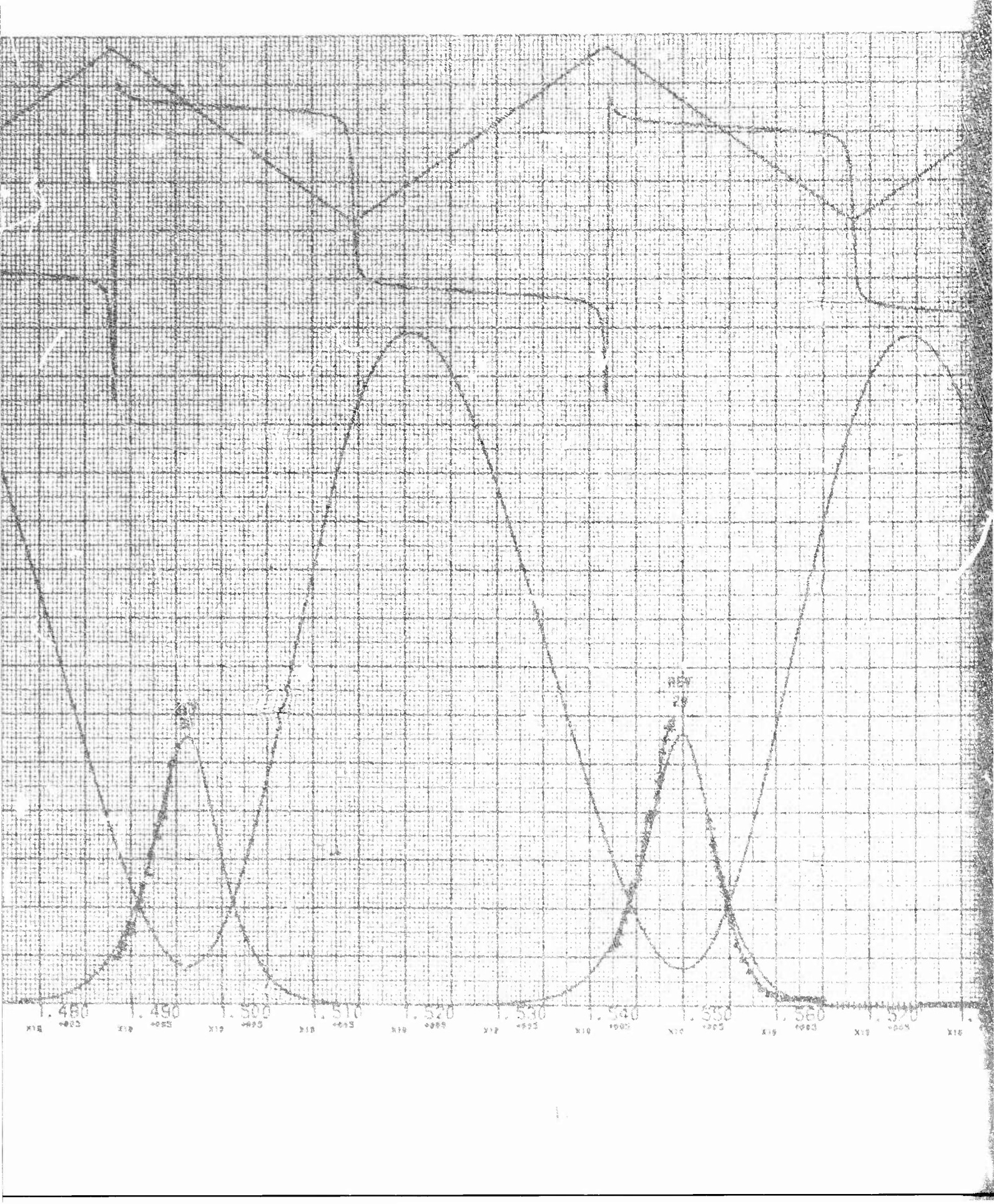
1.460
1.490
1.500
1.510
1.520
1.530
1.540
1.550
1.560
1.570

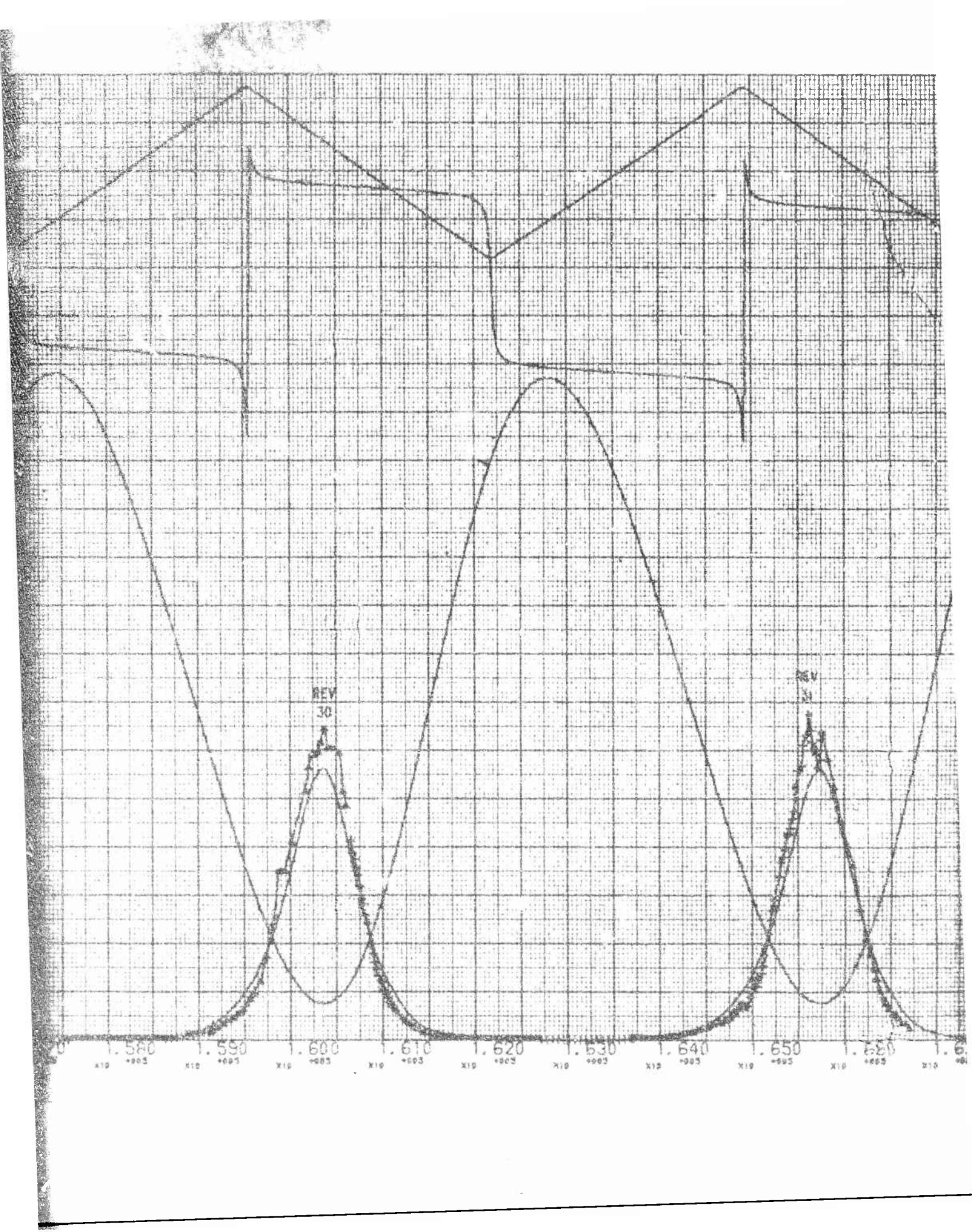
REV
30
REV
31
1.580
1.590
1.600
1.610
1.620
1.630
1.640
1.650

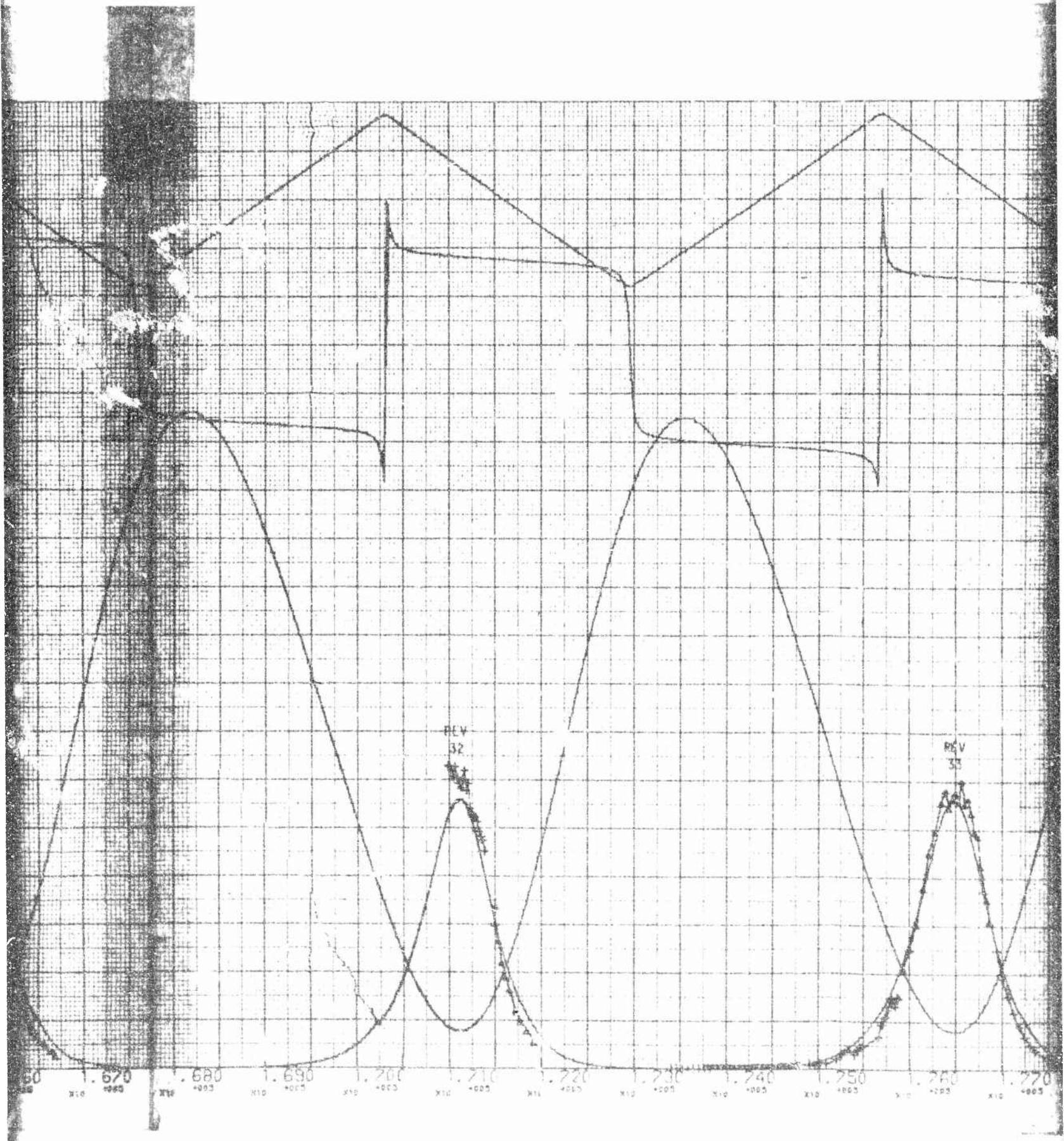
REV
32
REV
33
1.670
1.680
1.690
1.700
1.710
1.720
1.730
1.740
1.750
1.760
1.770

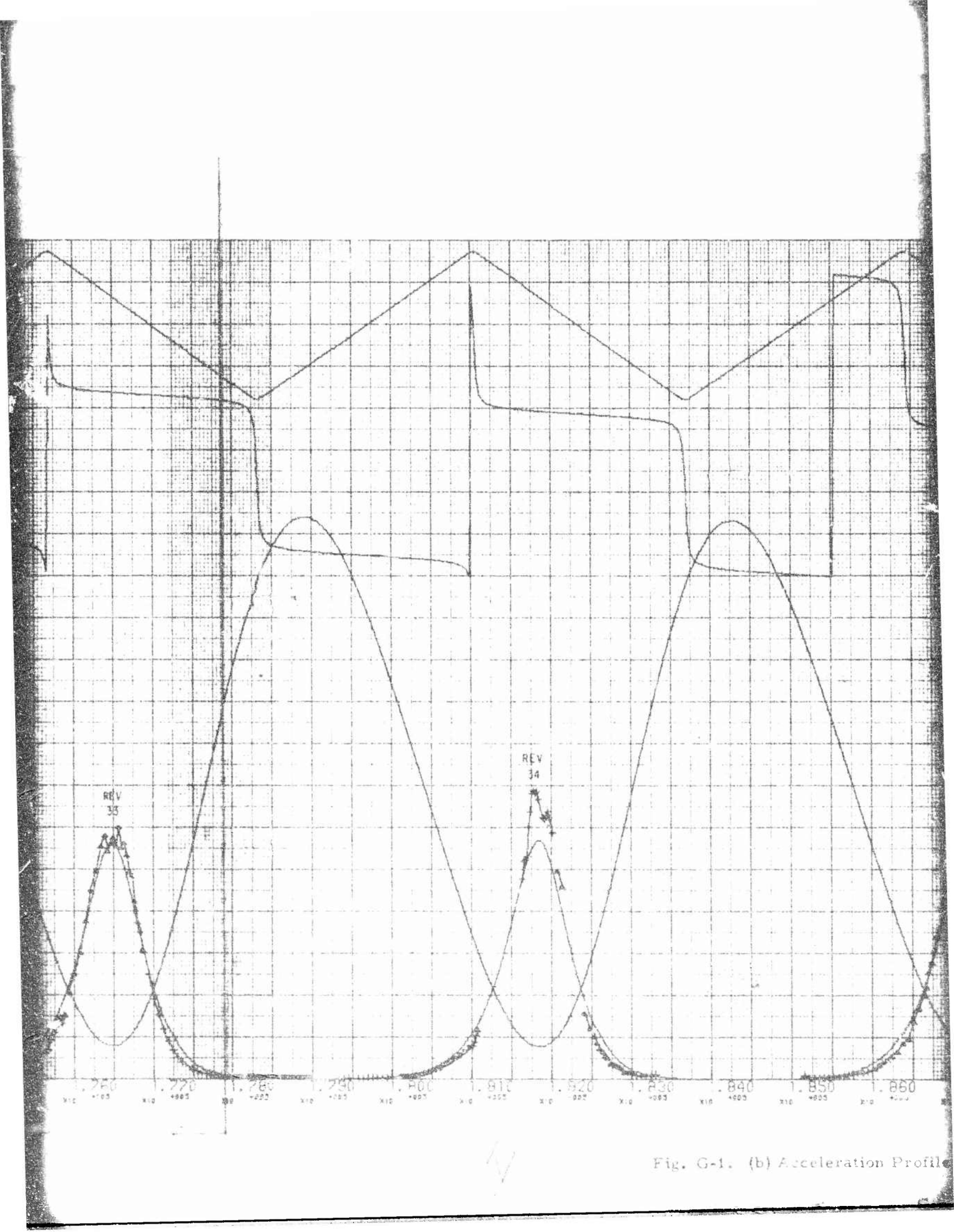

Fig. G-1. (b) Acceleration Profile

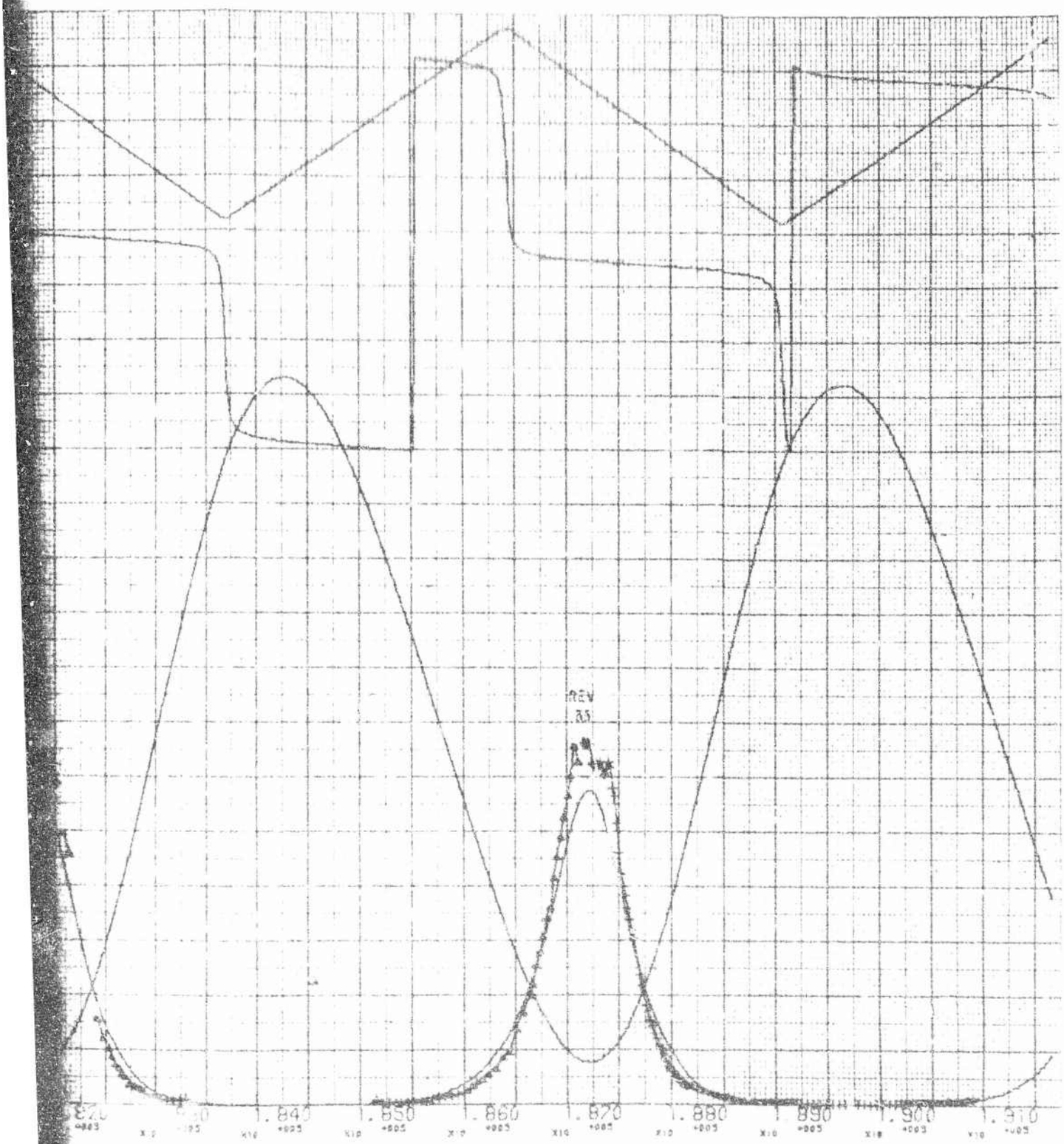

Fig. G-1. (b) Acceleration Profile and Ephemeris Data (May 24)

MAY 25

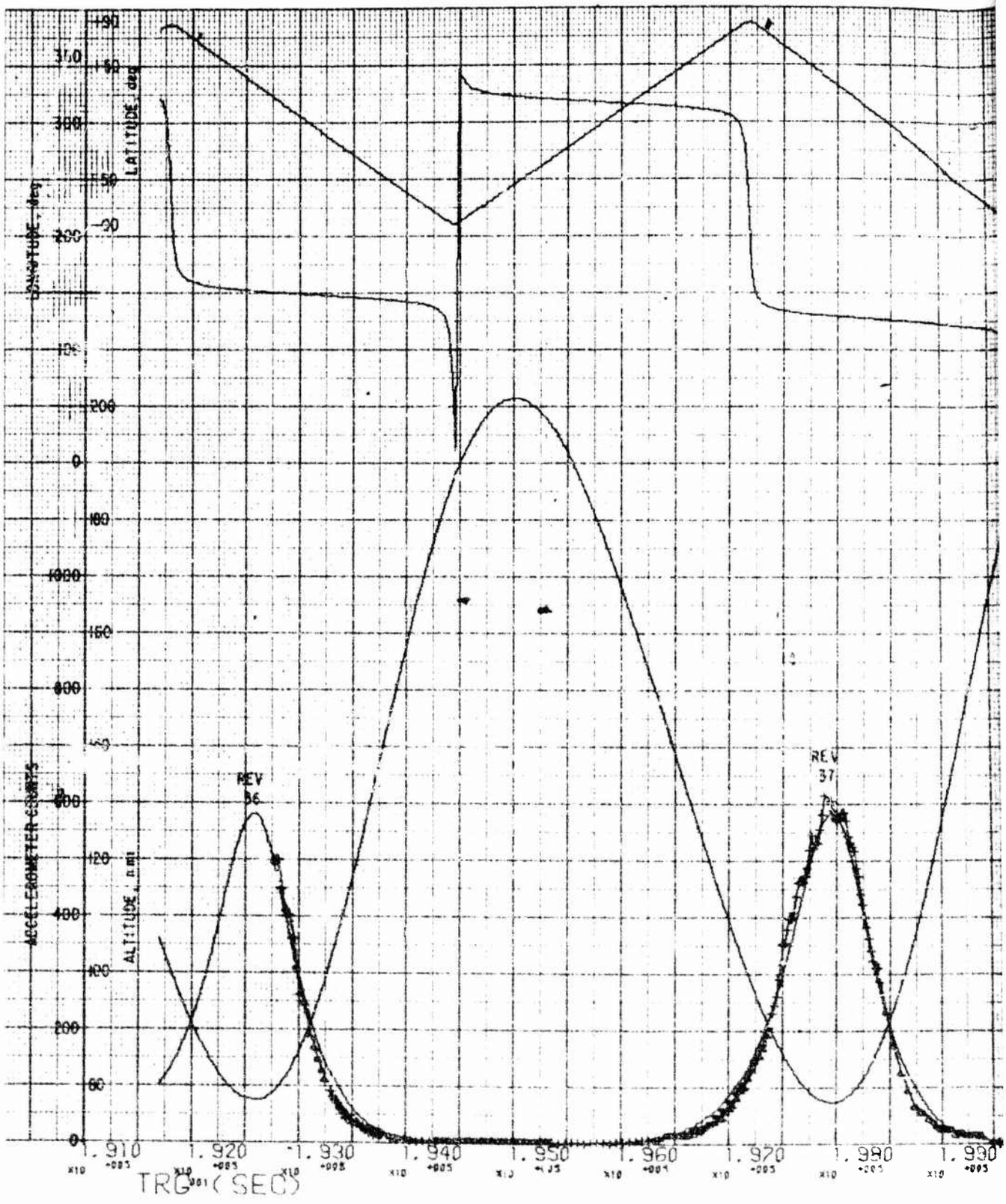
LONGITUDE, deg
LATITUDE, deg
ALTITUDE, n mi
ACCELEROMETER COUNTS
REV 36
REV 37
1.910
1.920
1.930
1.940
1.950
1.960
1.970
1.990
TRG (SEC)

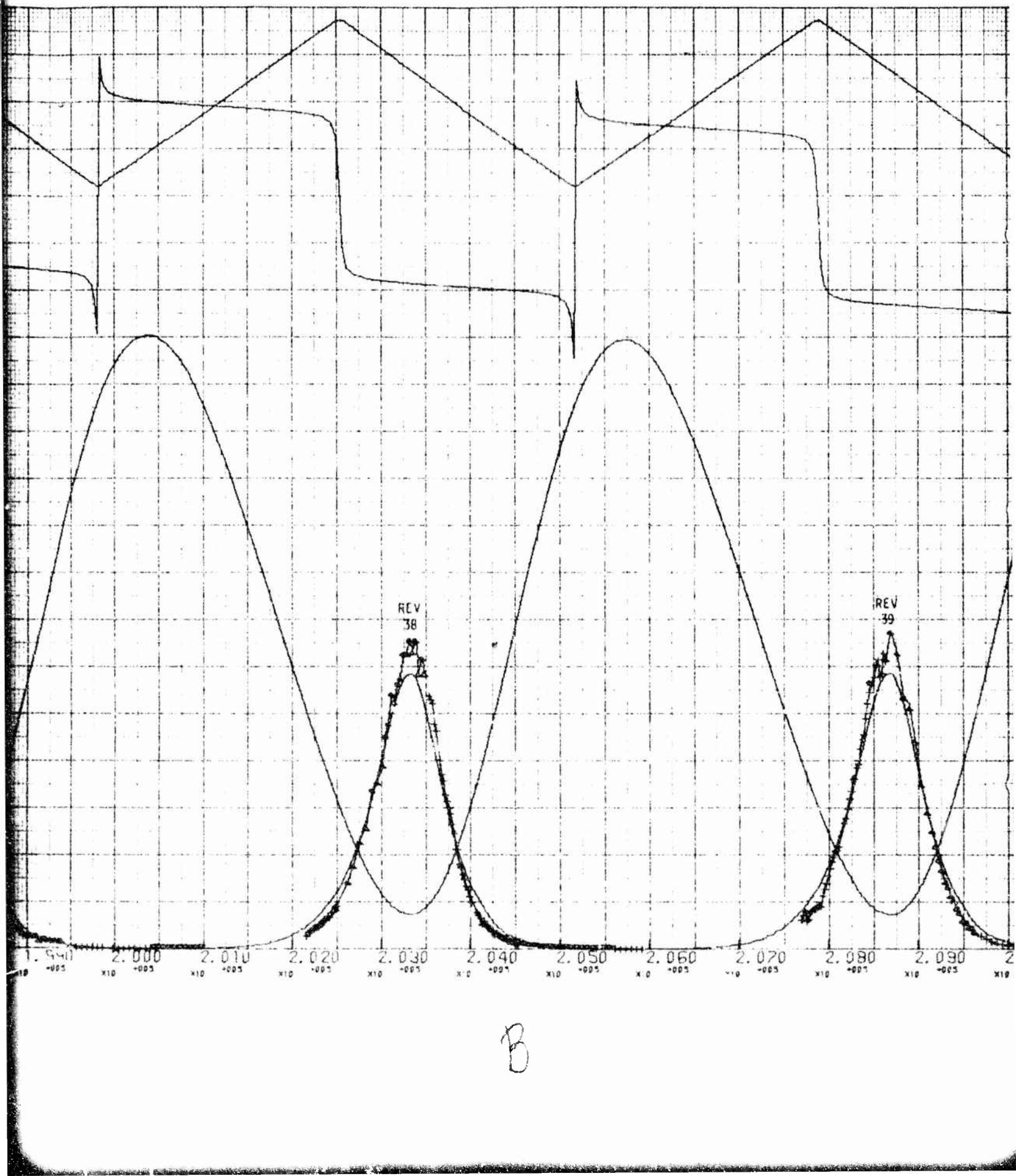
REV
38
REV
39
2.000
2.010
2.020
2.030
2.040
2.050
2.060
2.070
2.080
2.090

B

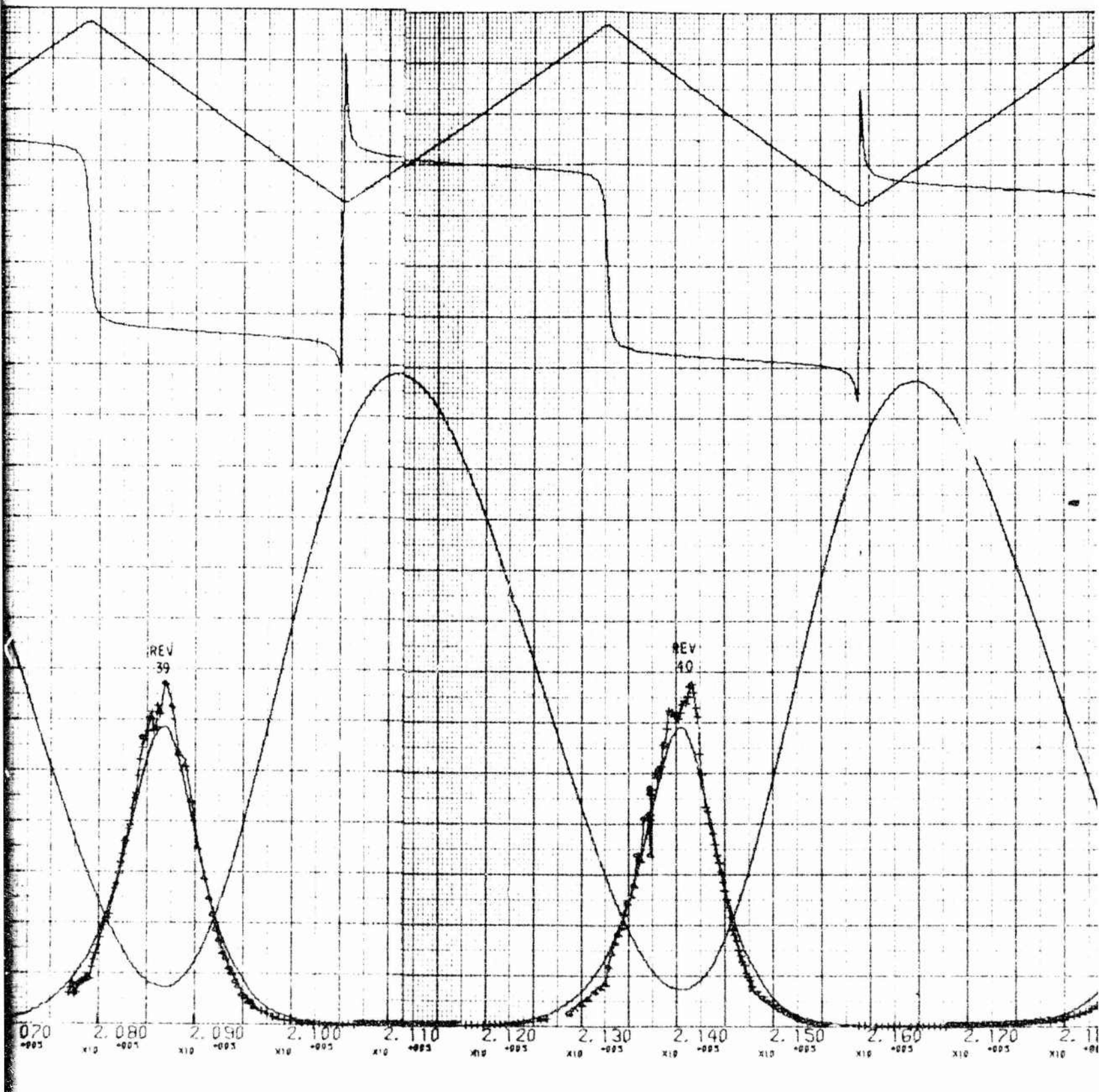
REV
39
REV
40
2.070
2.080
2.090
2.100
2.110
2.120
2.130
2.140
2.150
2.160
2.170

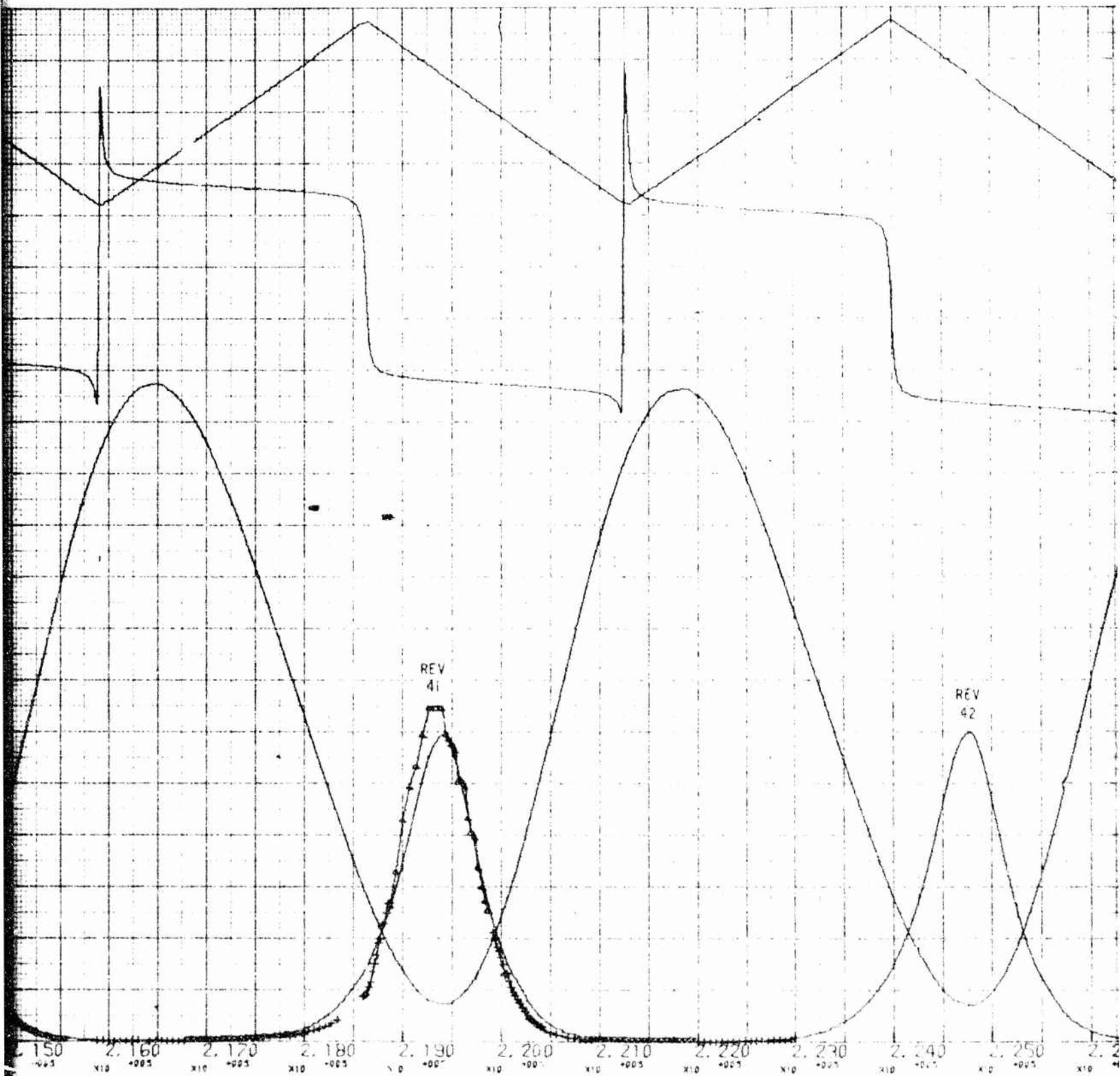
REV
41
REV
42
2.150
2.160
2.170
2.180
2.190
2.200
2.210
2.220
2.230
2.240
2.250

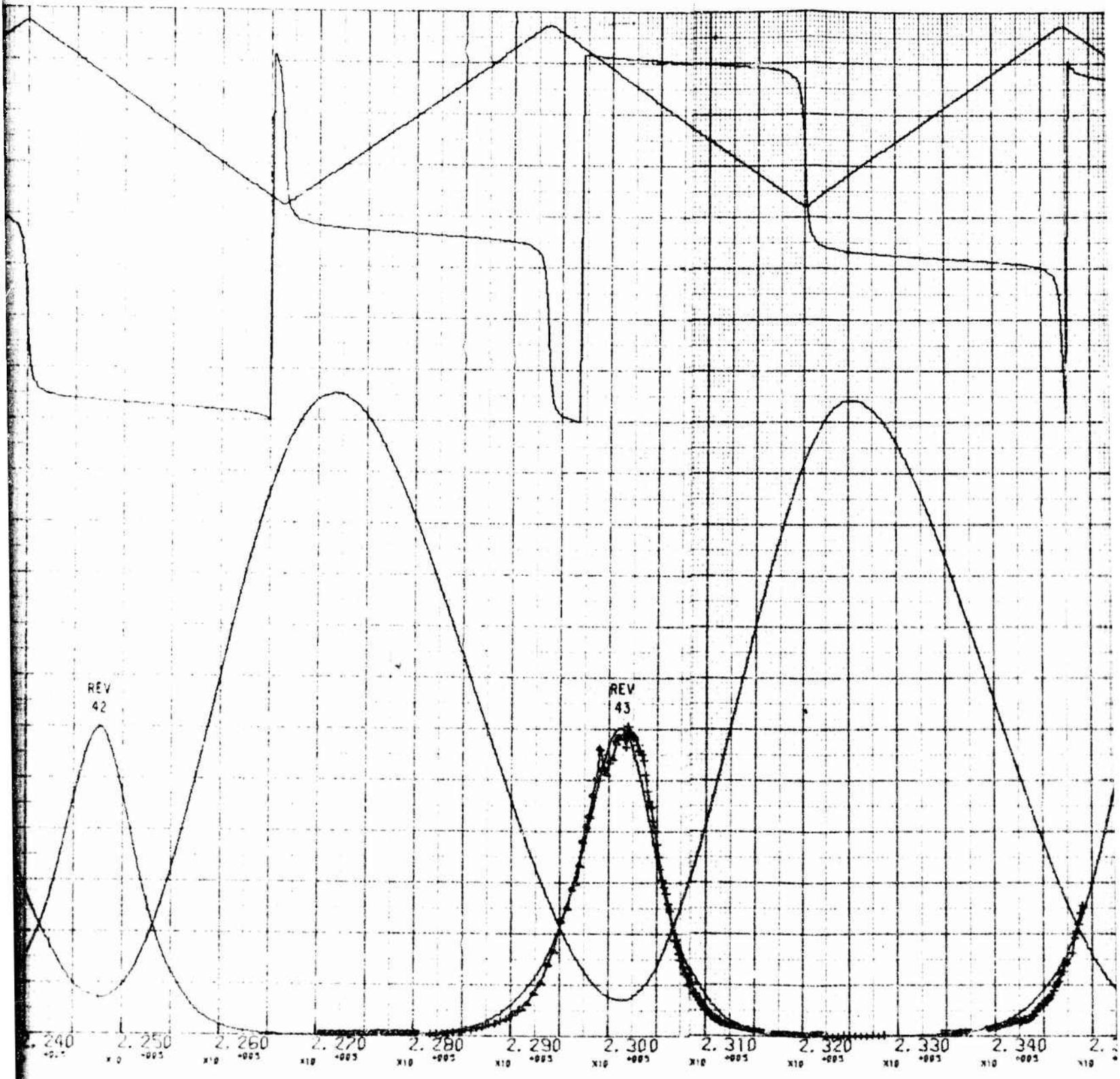
REV
42
REV
43
2.240
2.250
2.260
2.270
2.280
2.290
2.300
2.310
2.320
2.330
2.340

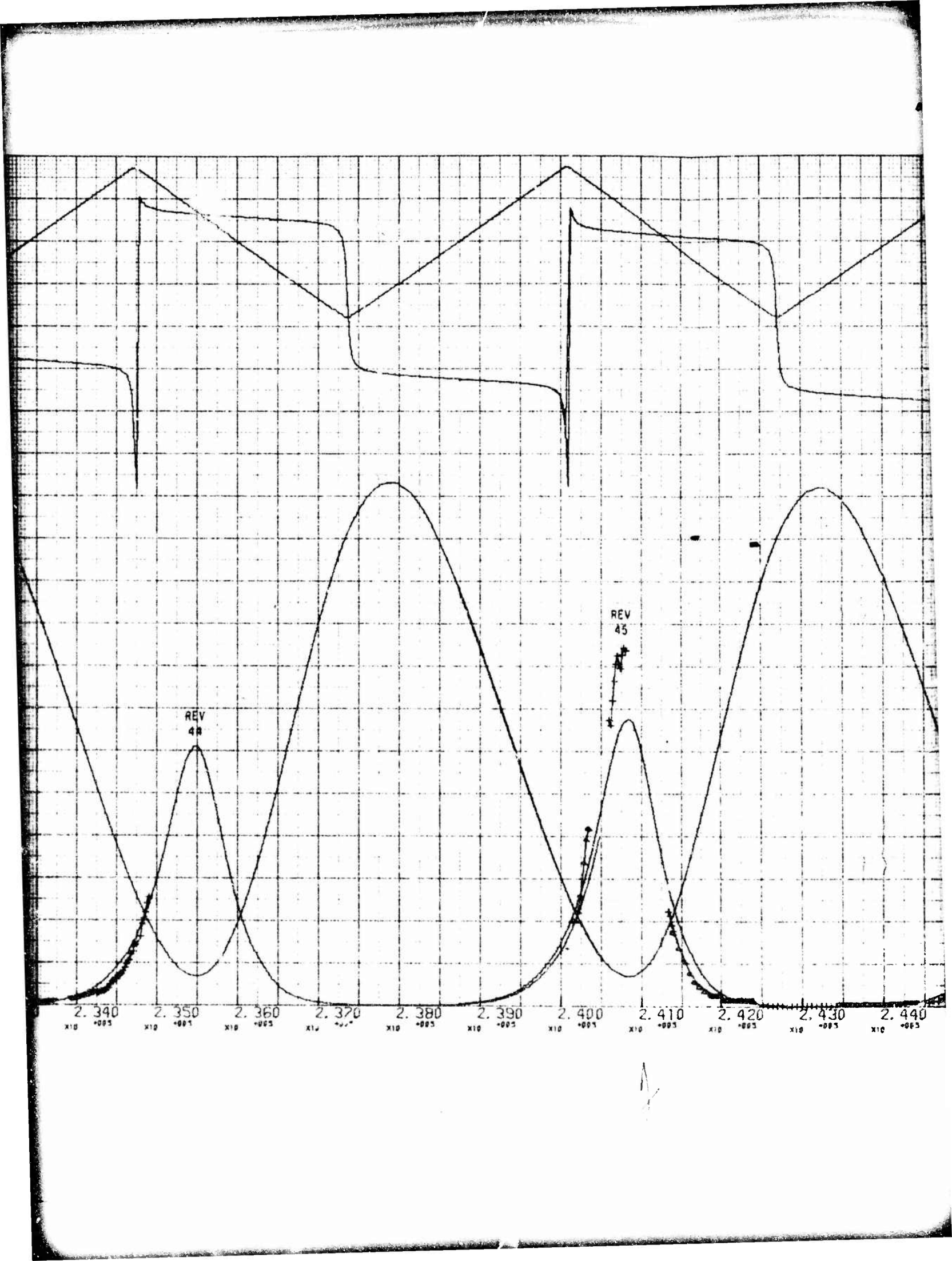
REV
48
REV
45
2.340
2.350
2.360
2.370
2.380
2.390
2.400
2.410
2.420
2.430
2.440

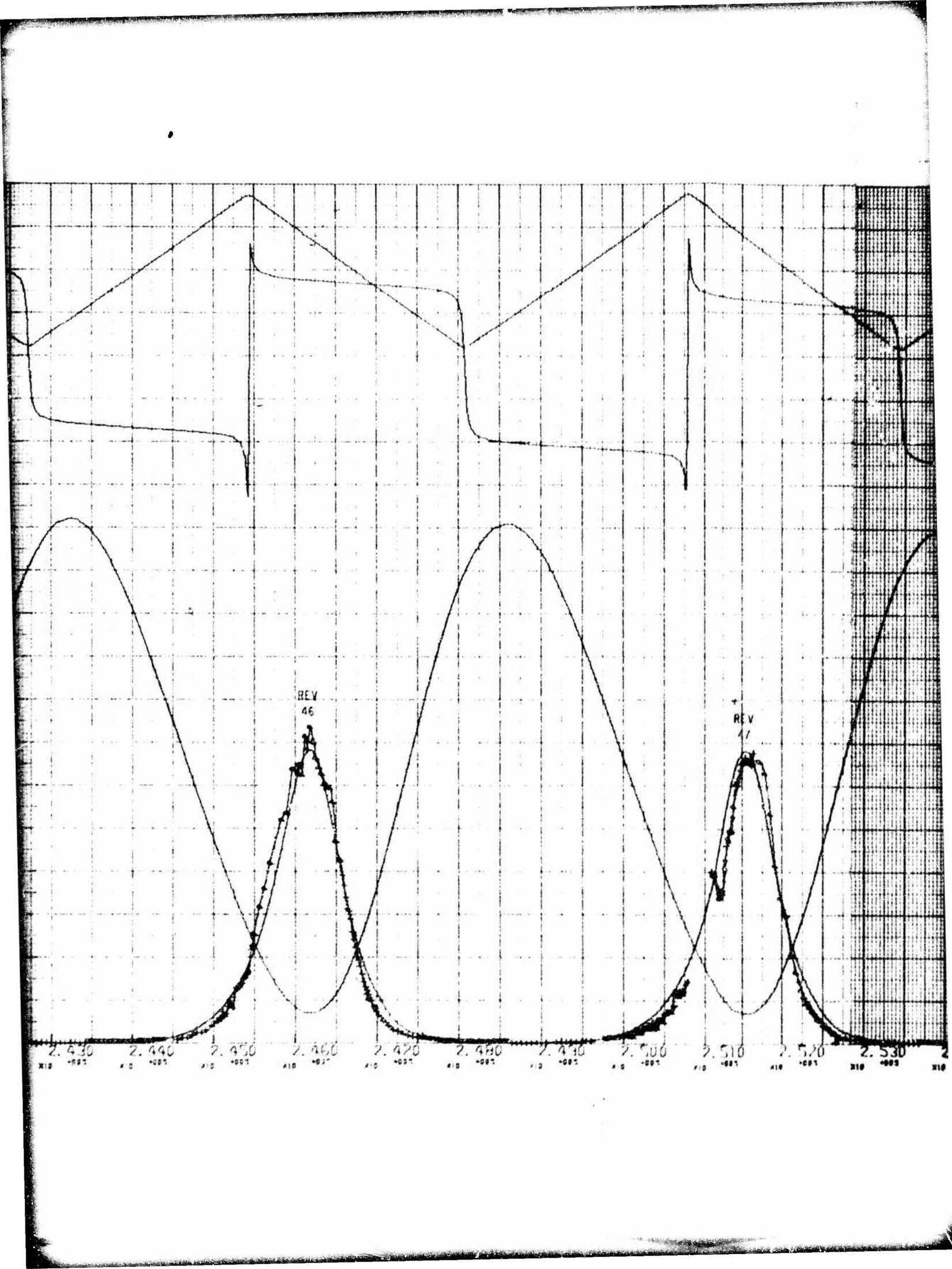
REV
46
REV
47
2.430
2.440
2.450
2.460
2.470
2.480
2.490
2.500
2.510
2.520
2.530

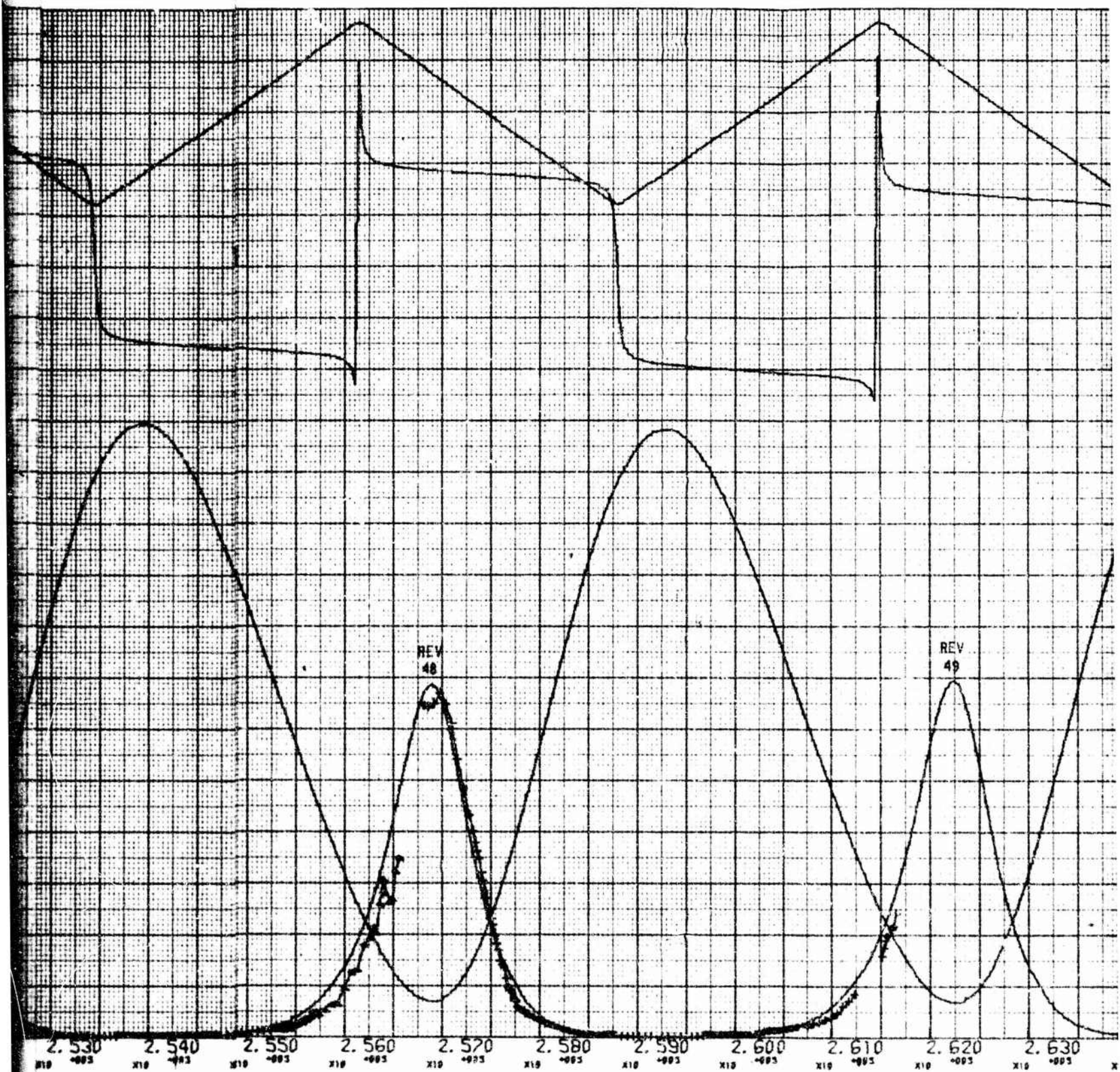
REV
48
REV
49
2.530
2.540
2.550
2.560
2.570
2.580
2.590
2.600
2.610
2.620
2.630

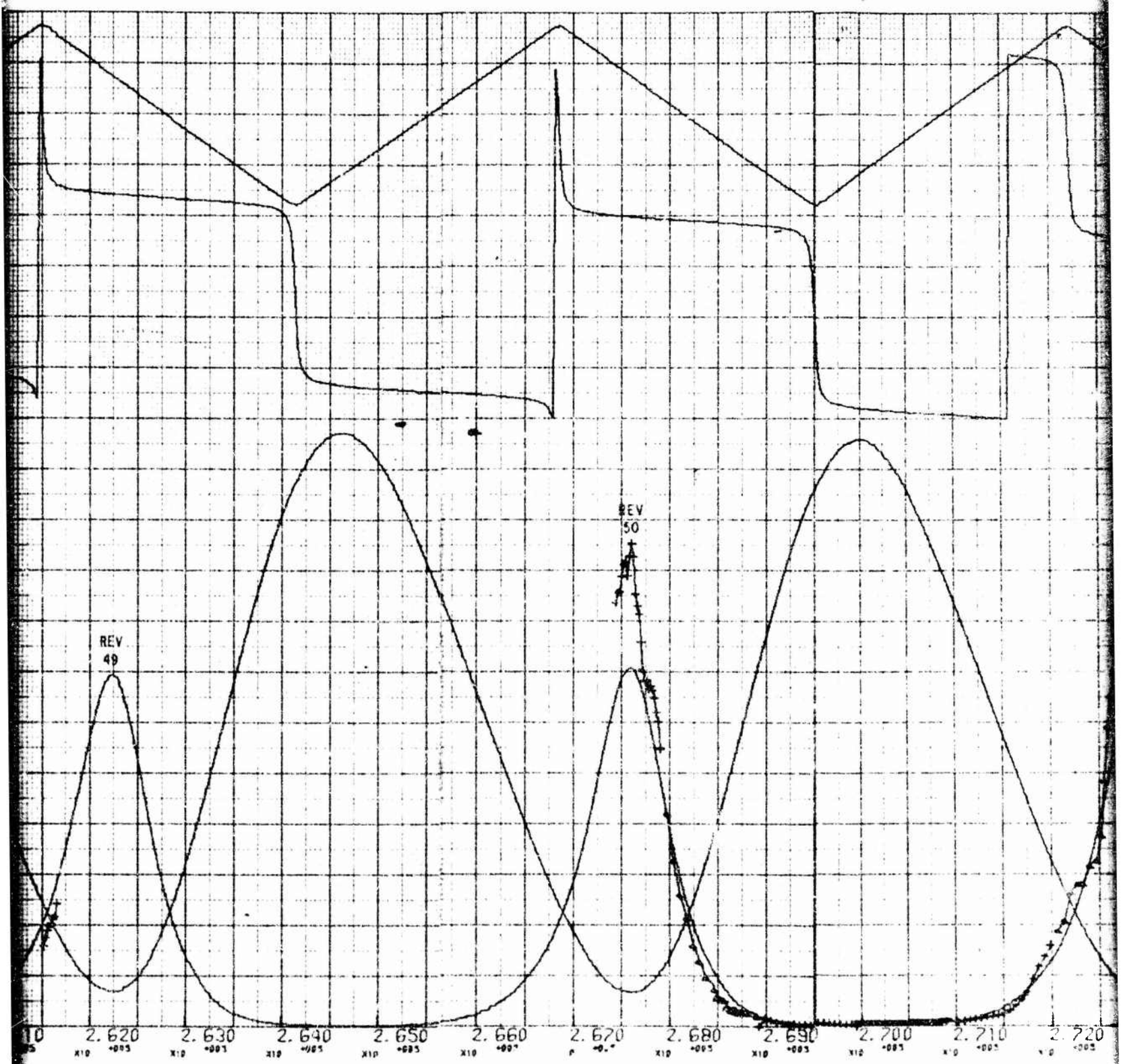

Fig. G-1. (c) Accelerati

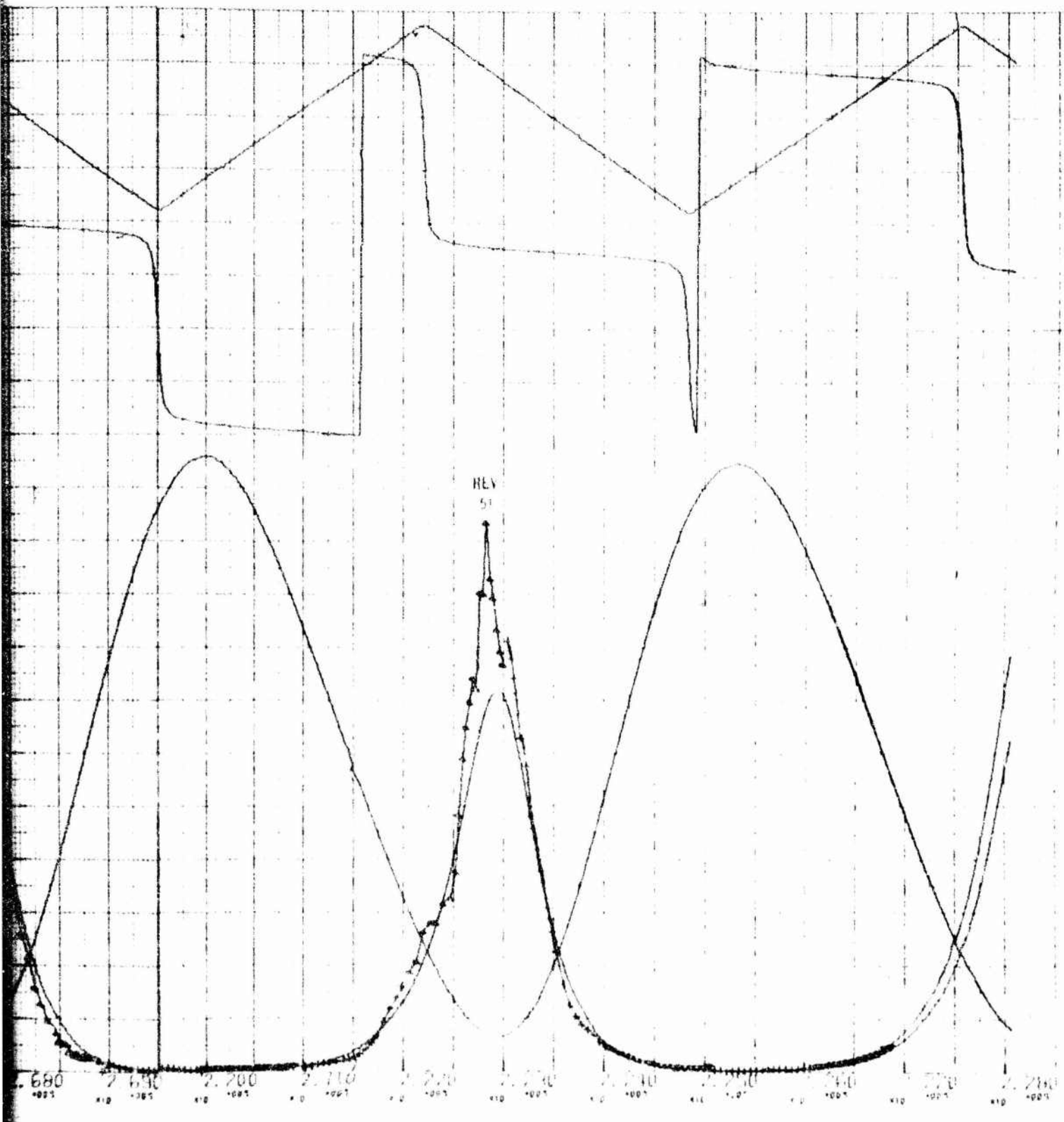

Fig. G-1. (c) Acceleration Profile and Ephemeris Data (May 25)

MAY 26

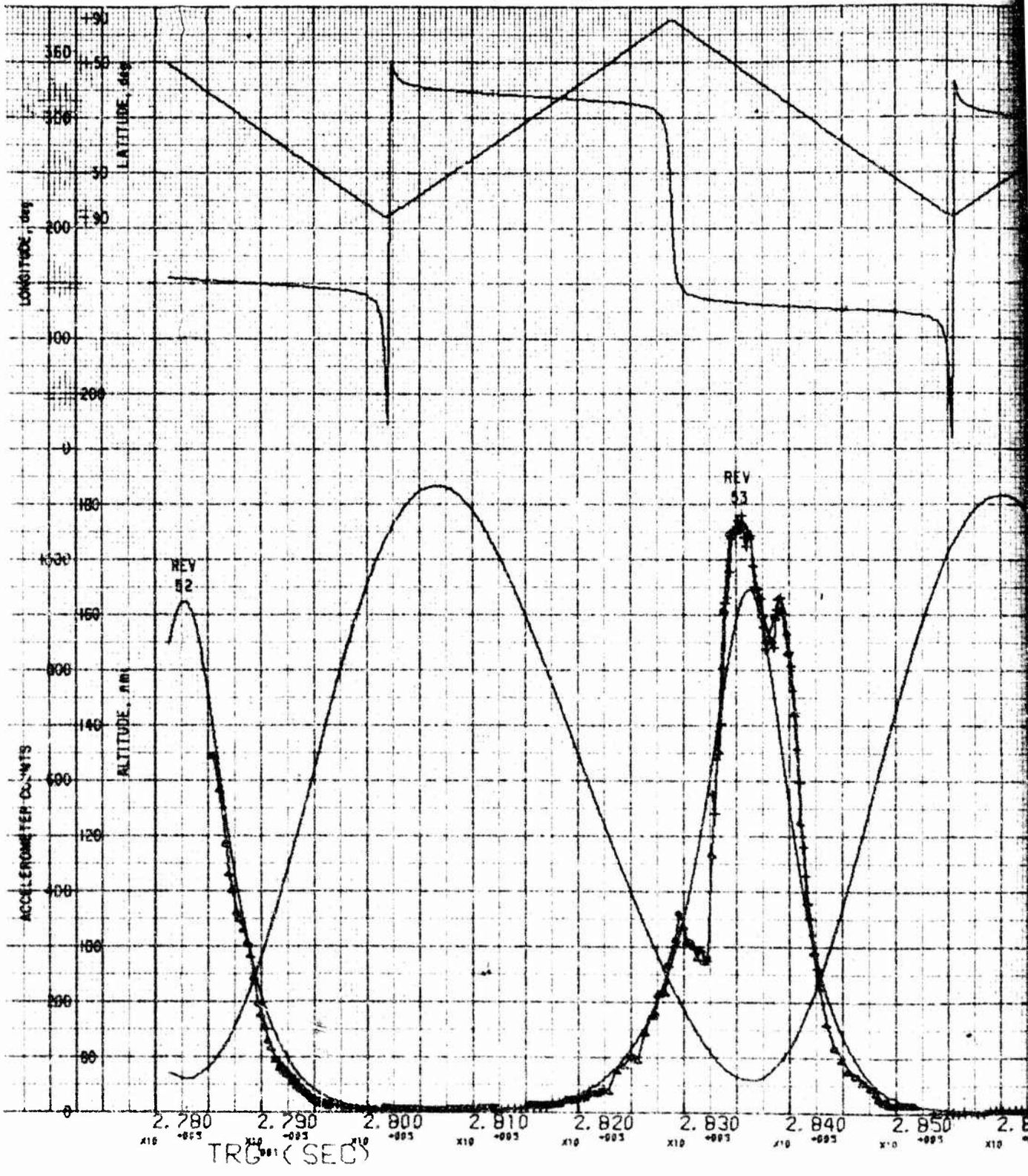
LONGITUDE, deg
LATITUDE, deg
ALTITUDE, nmi
ACCELEROMETER COUNTS
REV 52
REV 53
2.780
2.790
2.800
2.810
2.820
2.830
2.840
2.850
TRG (SECS)

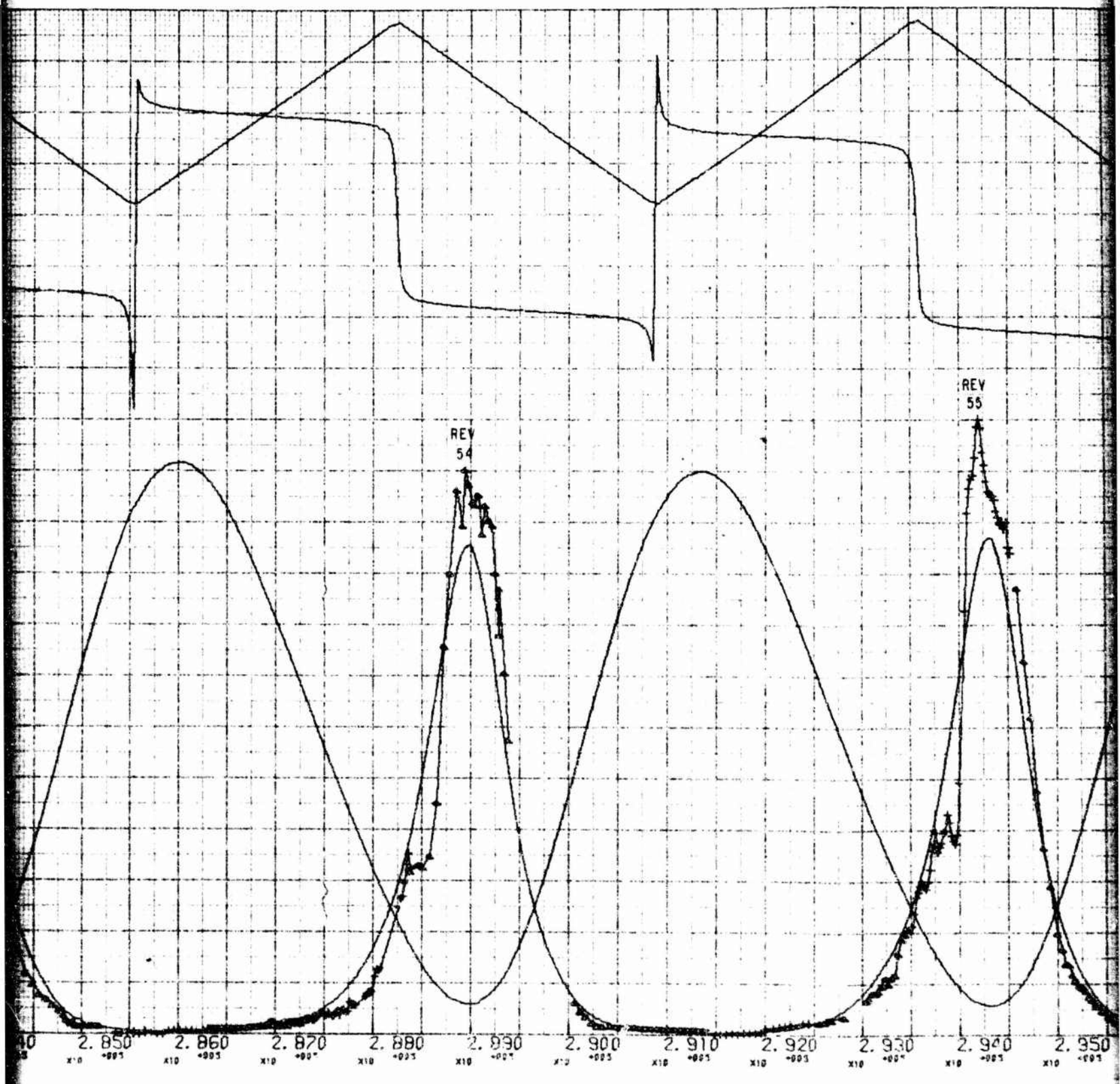
REV
54
REV
55
2.850
2.860
2.870
2.880
2.890
2.900
2.910
2.920
2.930
2.940
2.950

B

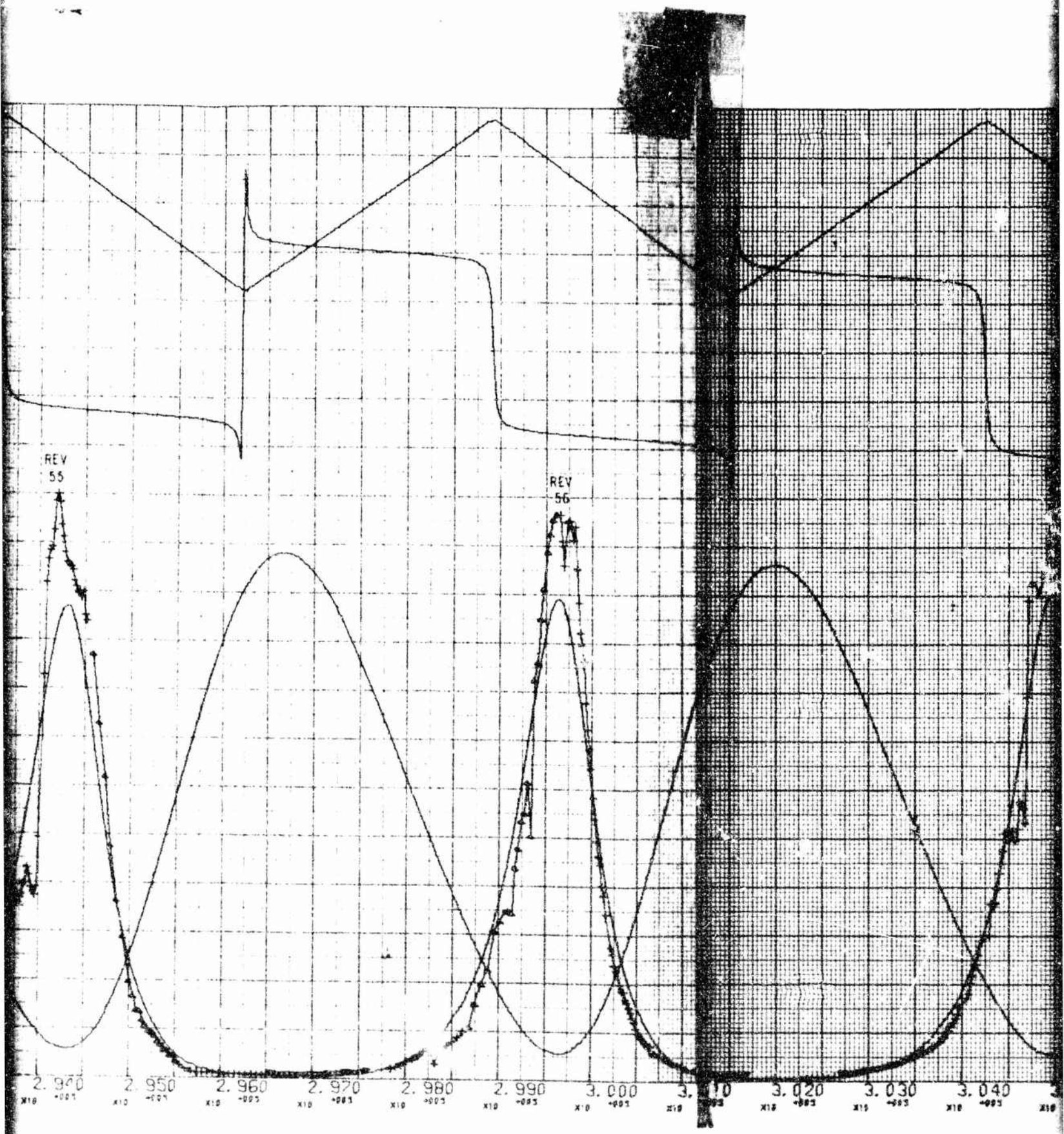
REV
55
REV
56
2.940
2.950
2.960
2.970
2.980
2.990
3.000
3.020
3.030
3.040

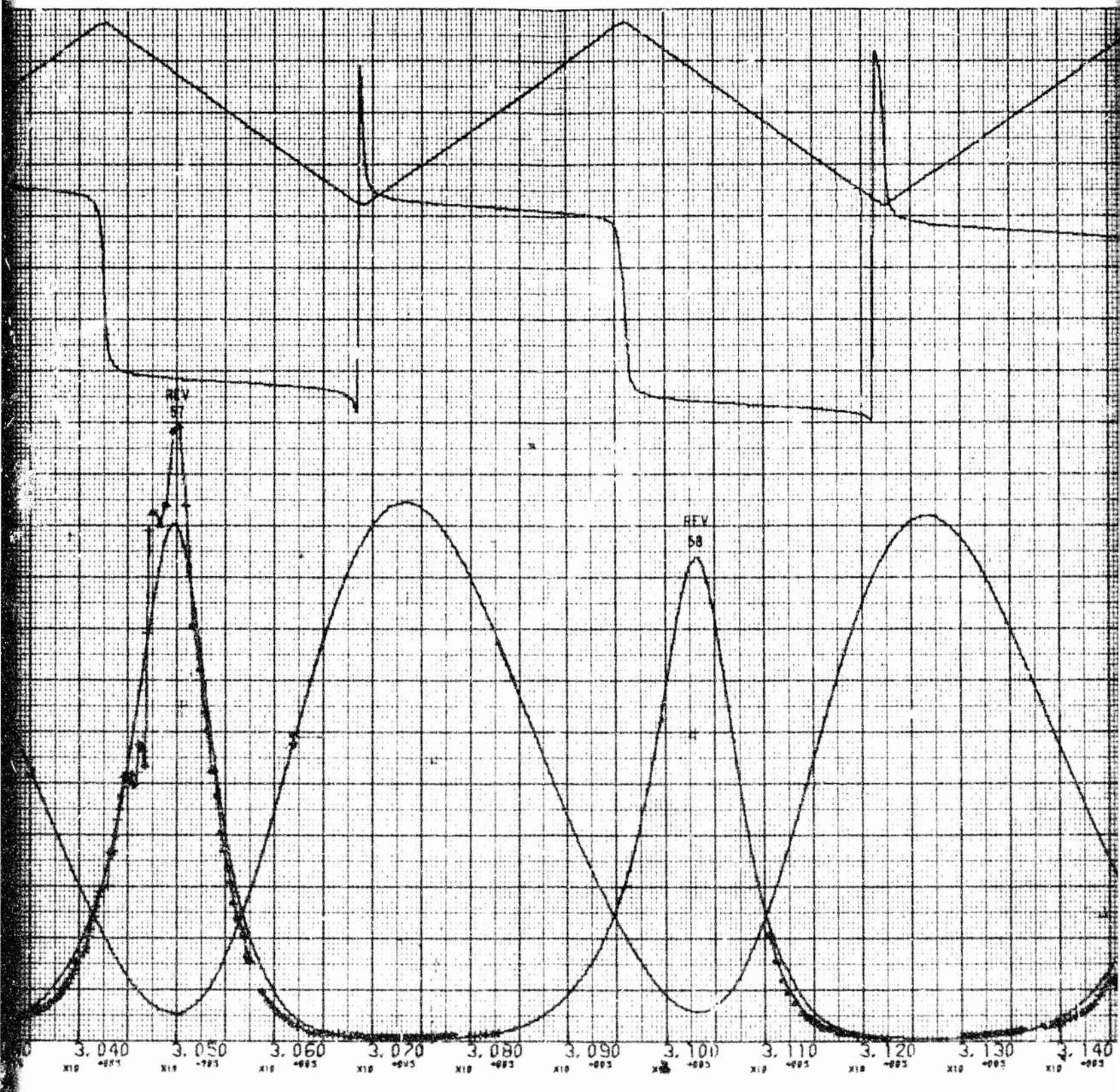
REV
57
REV
58
3.040
3.050
3.060
3.070
3.080
3.090
3.100
3.110
3.120
3.130
3.140

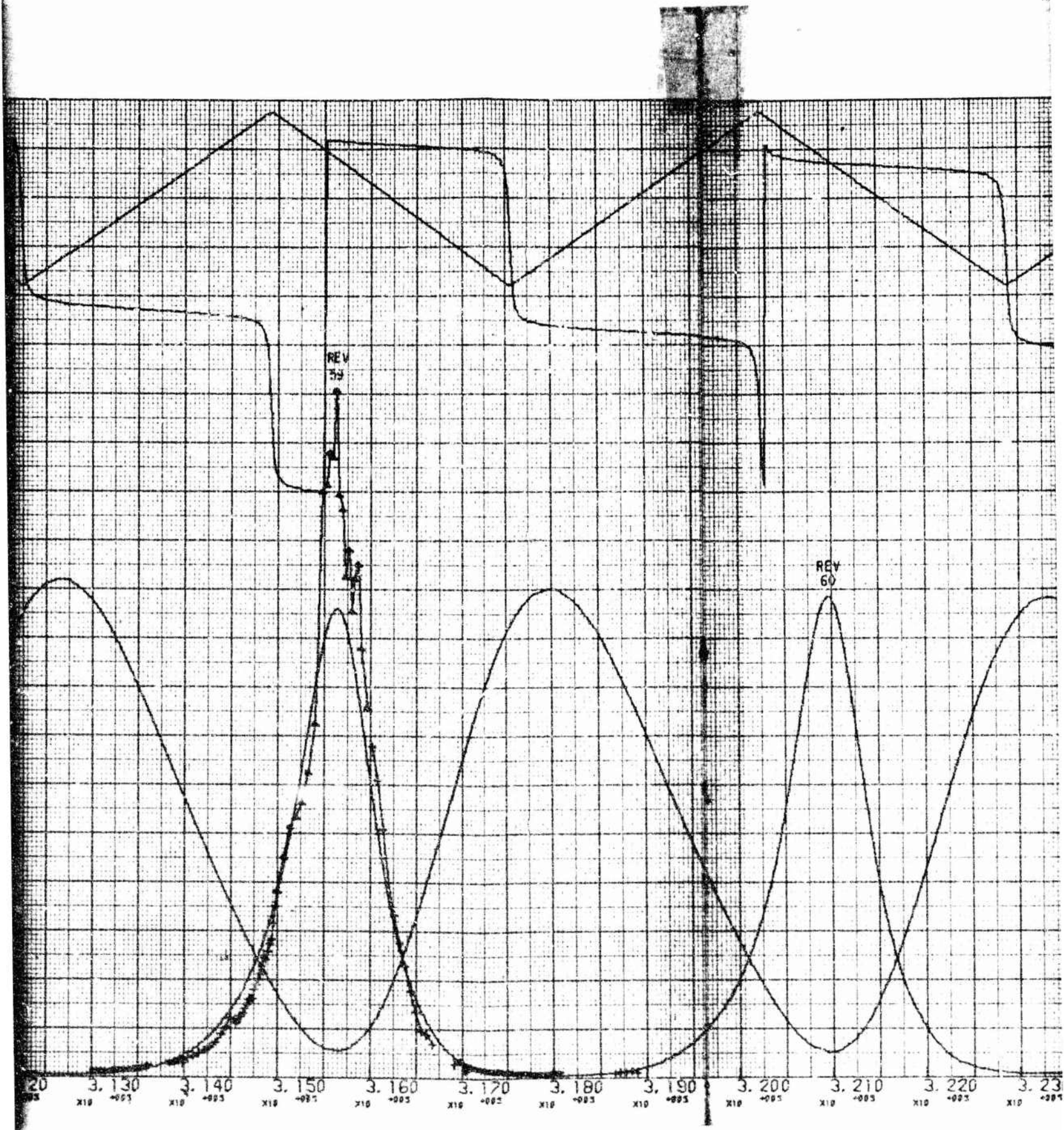
REV
59
REV
60
3.130
3.140
3.150
3.160
3.170
3.180
3.190
3.200
3.210
3.220

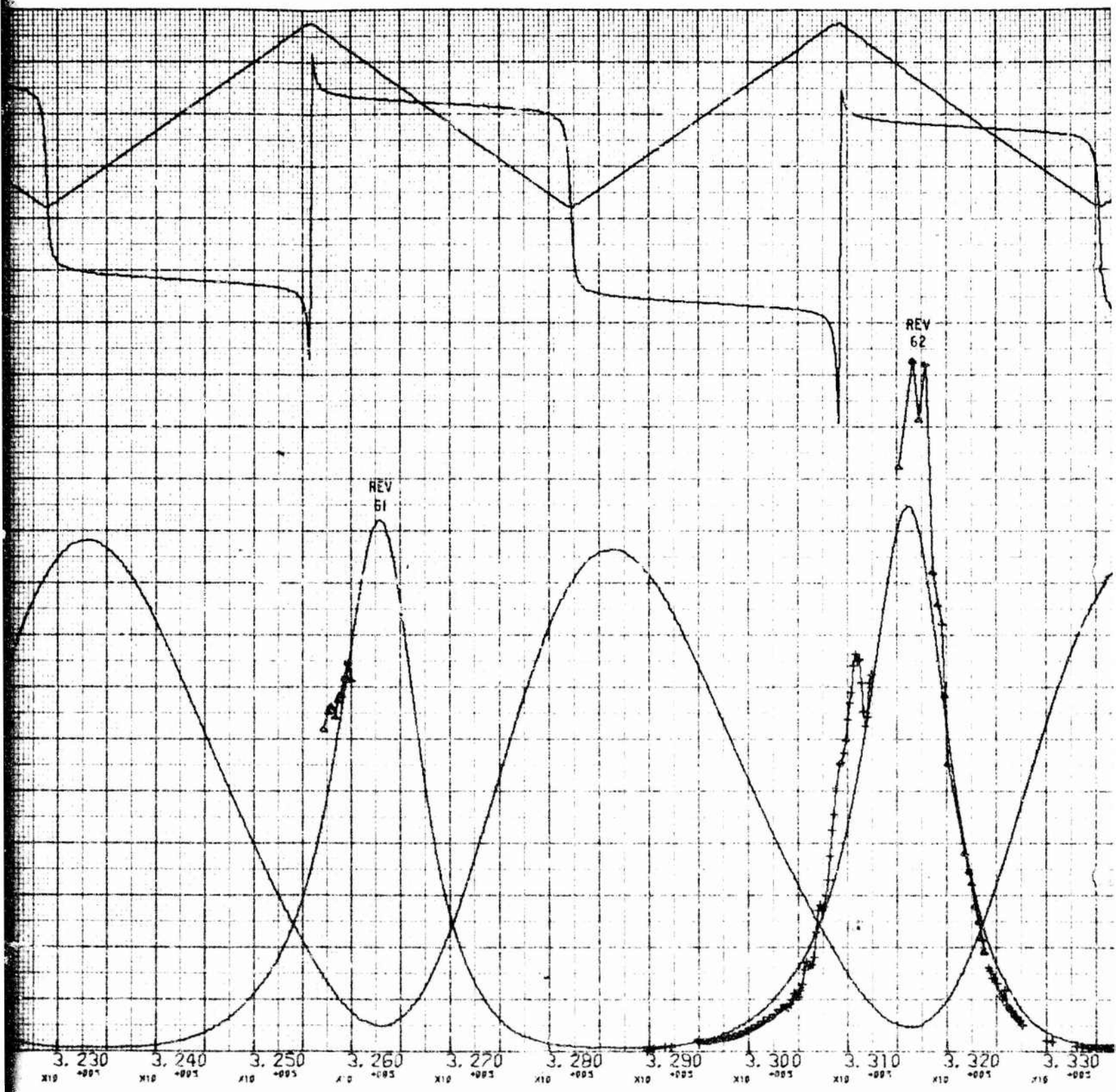
REV
61
REV
62
3. 230
3. 240
3. 250
3. 260
3. 270
3. 280
3. 290
3. 300
3. 310
3. 320
3. 330

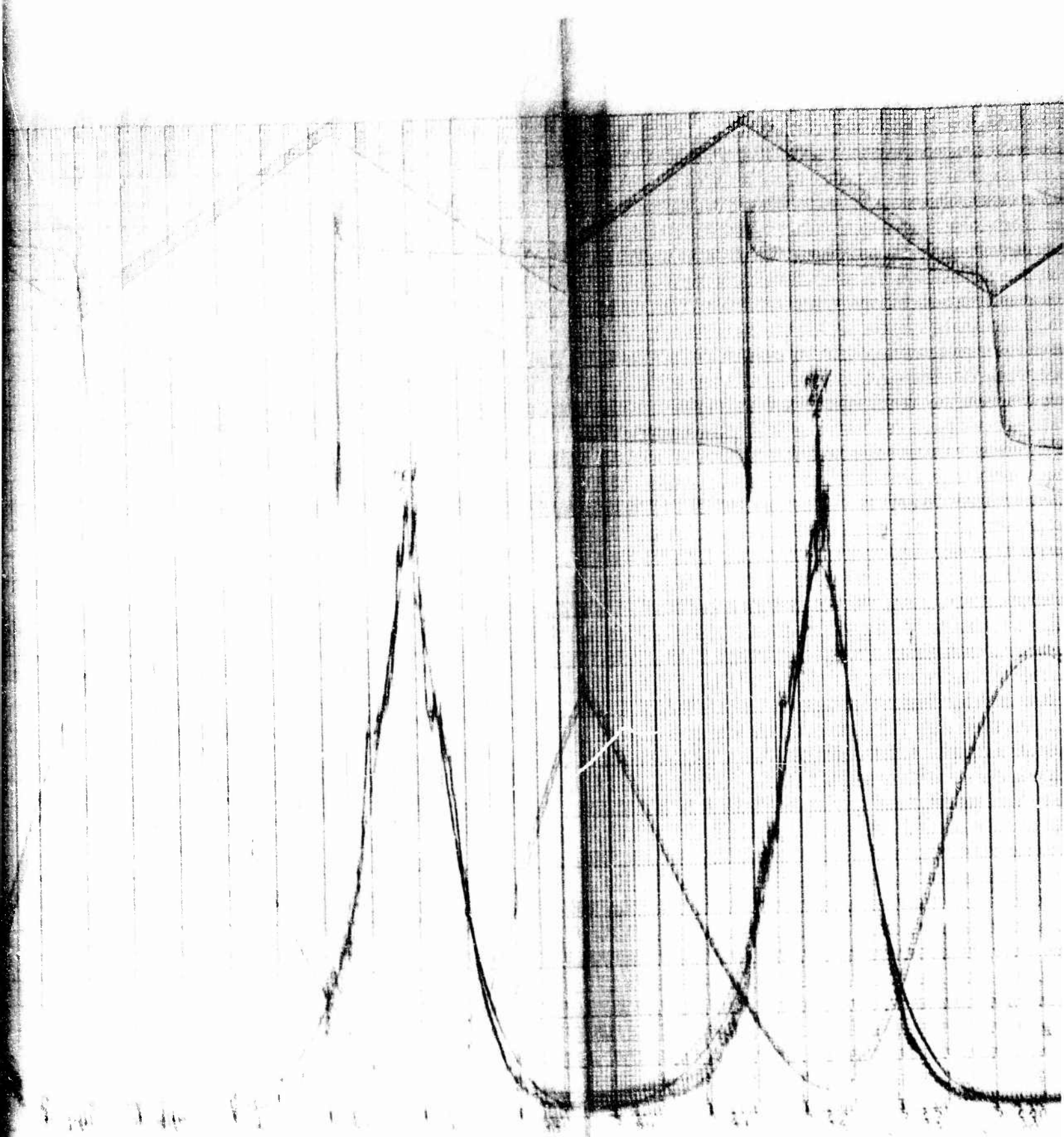

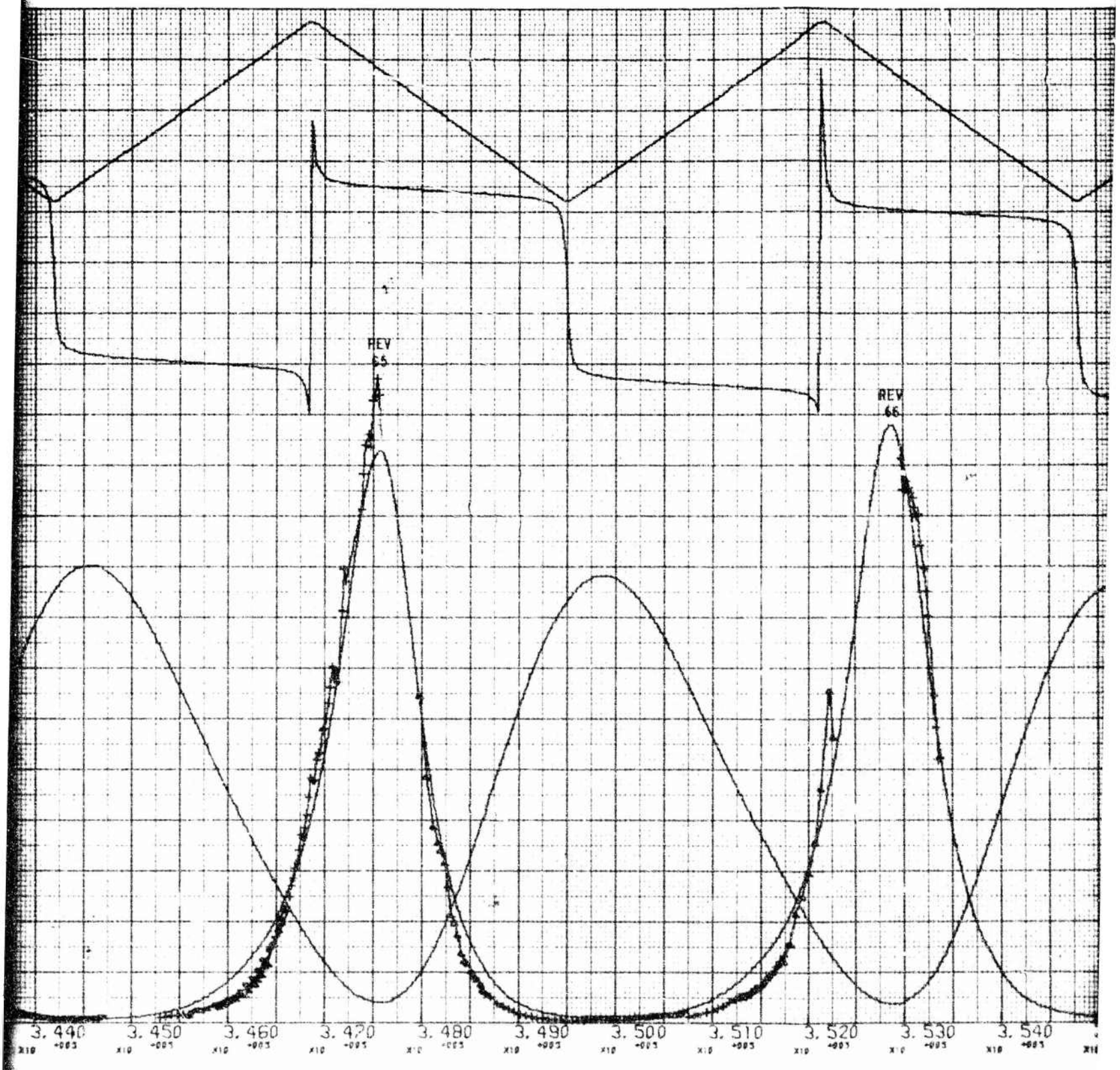

Fig. G-1. (d) Acceleration Prof

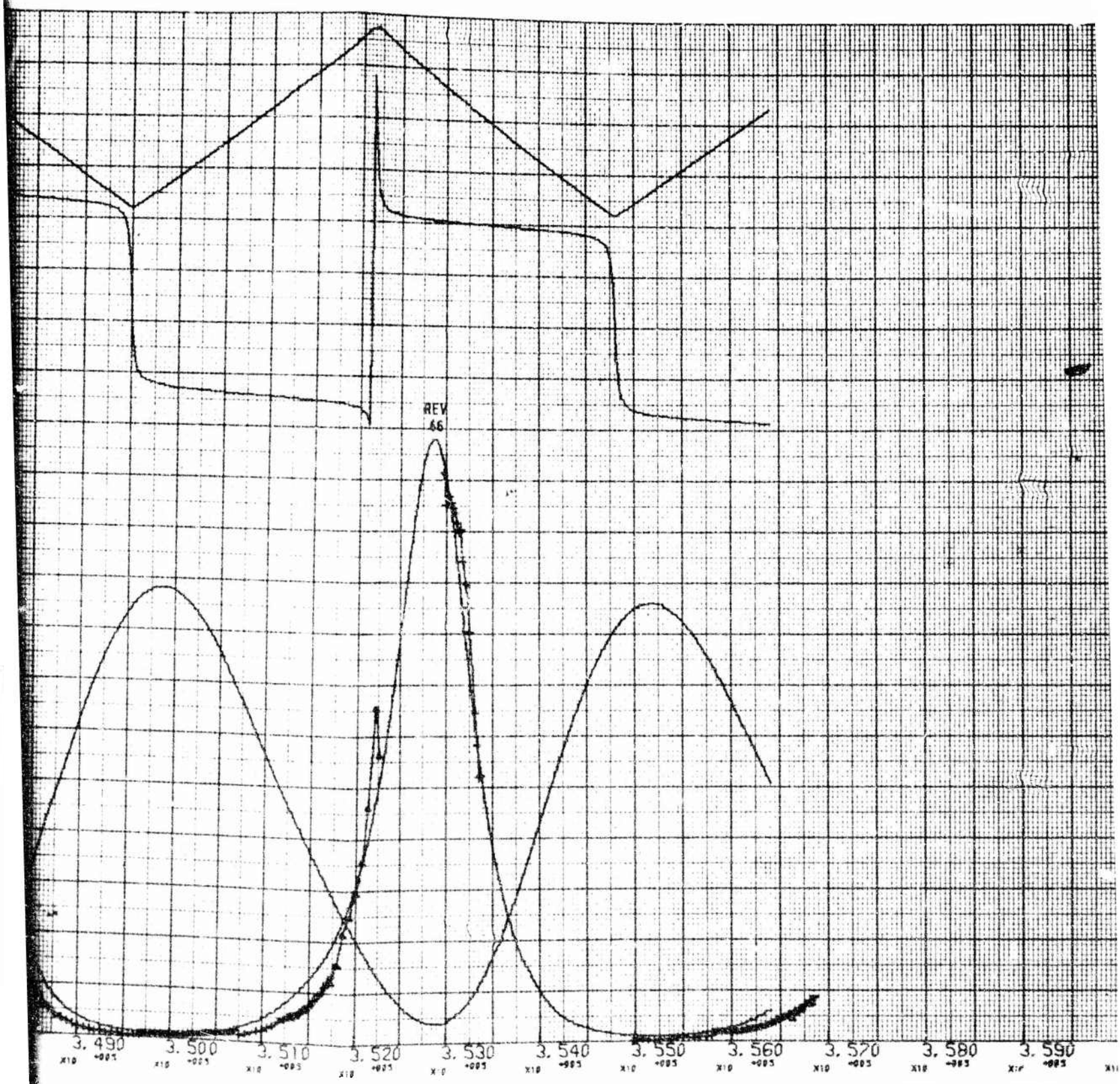

Reproduced from
best available copy.

Fig. G-1. (d) Acceleration Profile and Ephemeris Data (May 26)

MAY 23

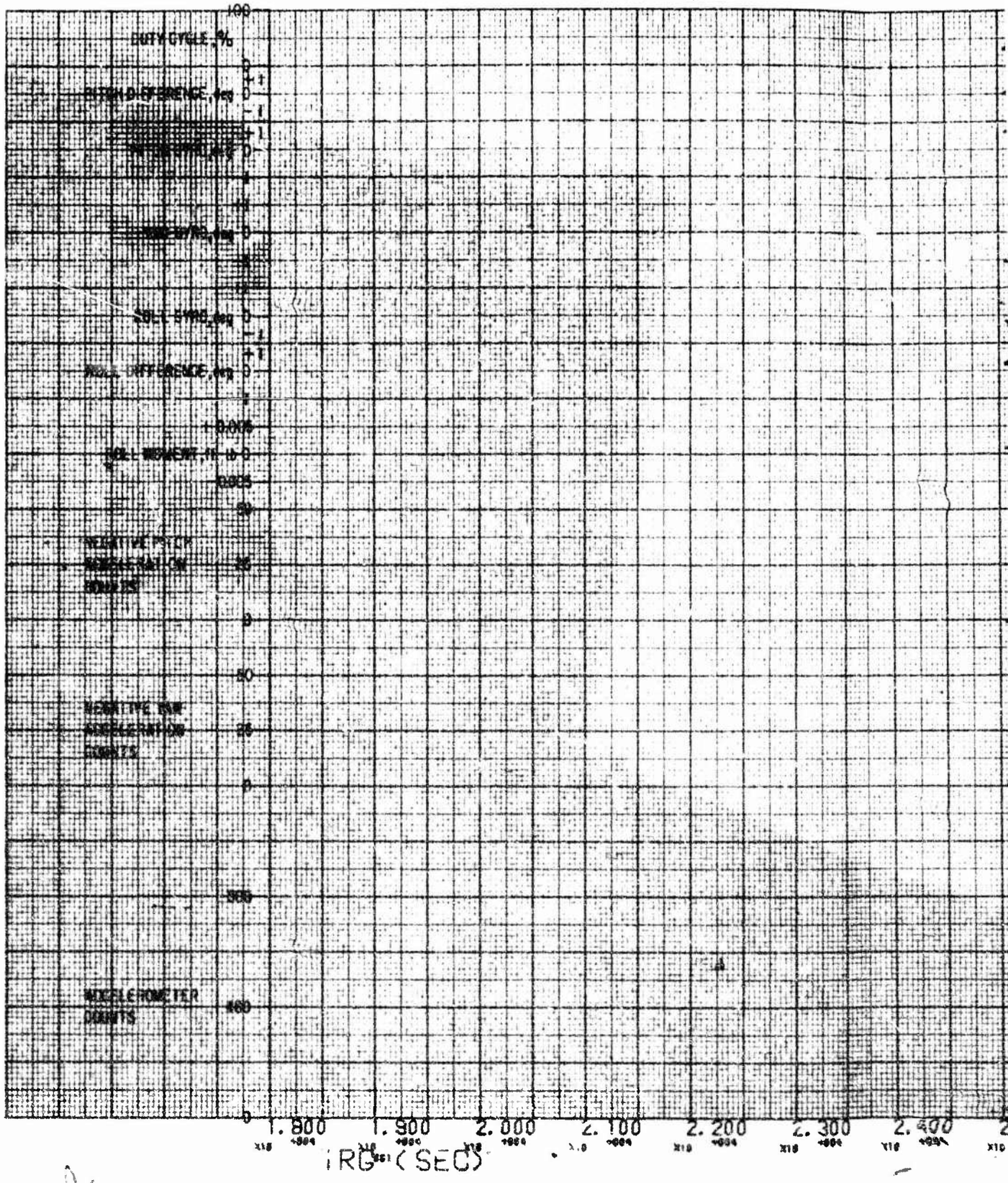
DUTY CYCLE, %
100
0
PITCH DIFFERENCE, deg
+1
0
-1
ROLL DIFFERENCE, deg
+1
0
-1
+0.005
0
-0.005
50
0
-50
460
0
1.800
1.900
2.000
2.100
2.200
2.300
2.400
TIME (SECS)

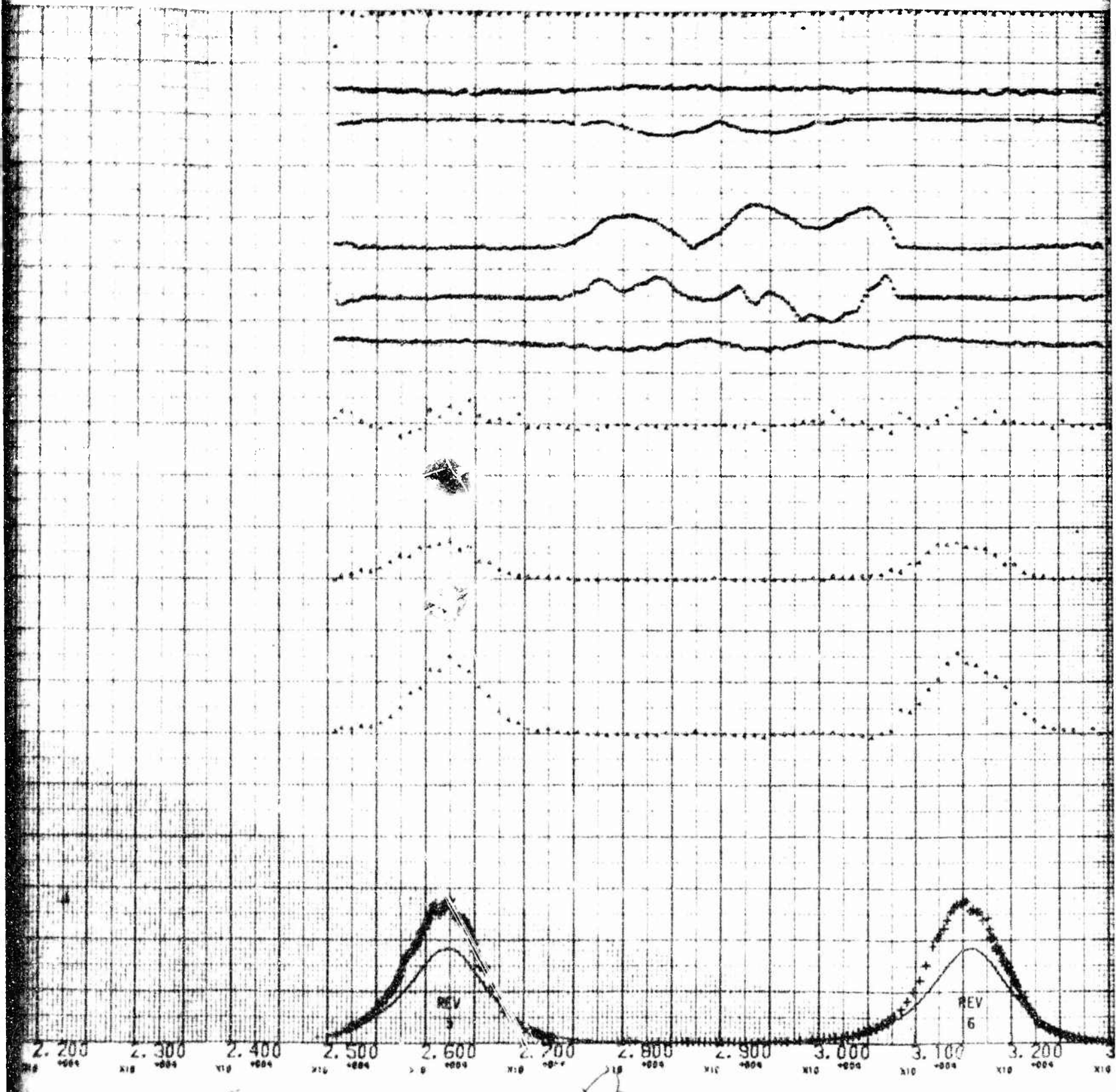
REV
3
REV
6
2.200
2.300
2.400
2.500
2.600
2.700
2.800
2.900
3.000
3.100
3.200

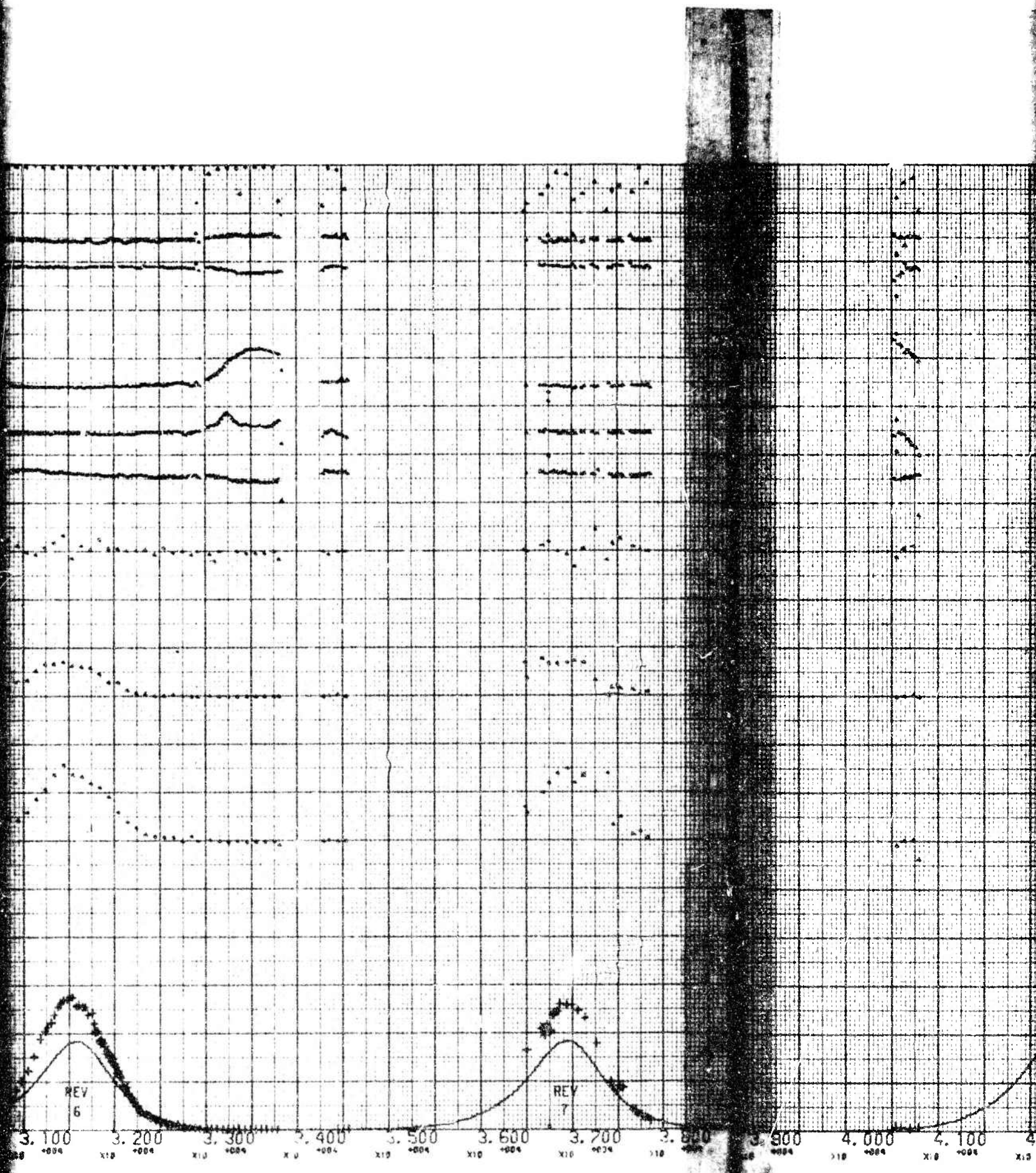
REV
6
REV
7
3.100
3.200
3.300
3.400
3.500
3.600
3.700
3.900
4.000
4.100

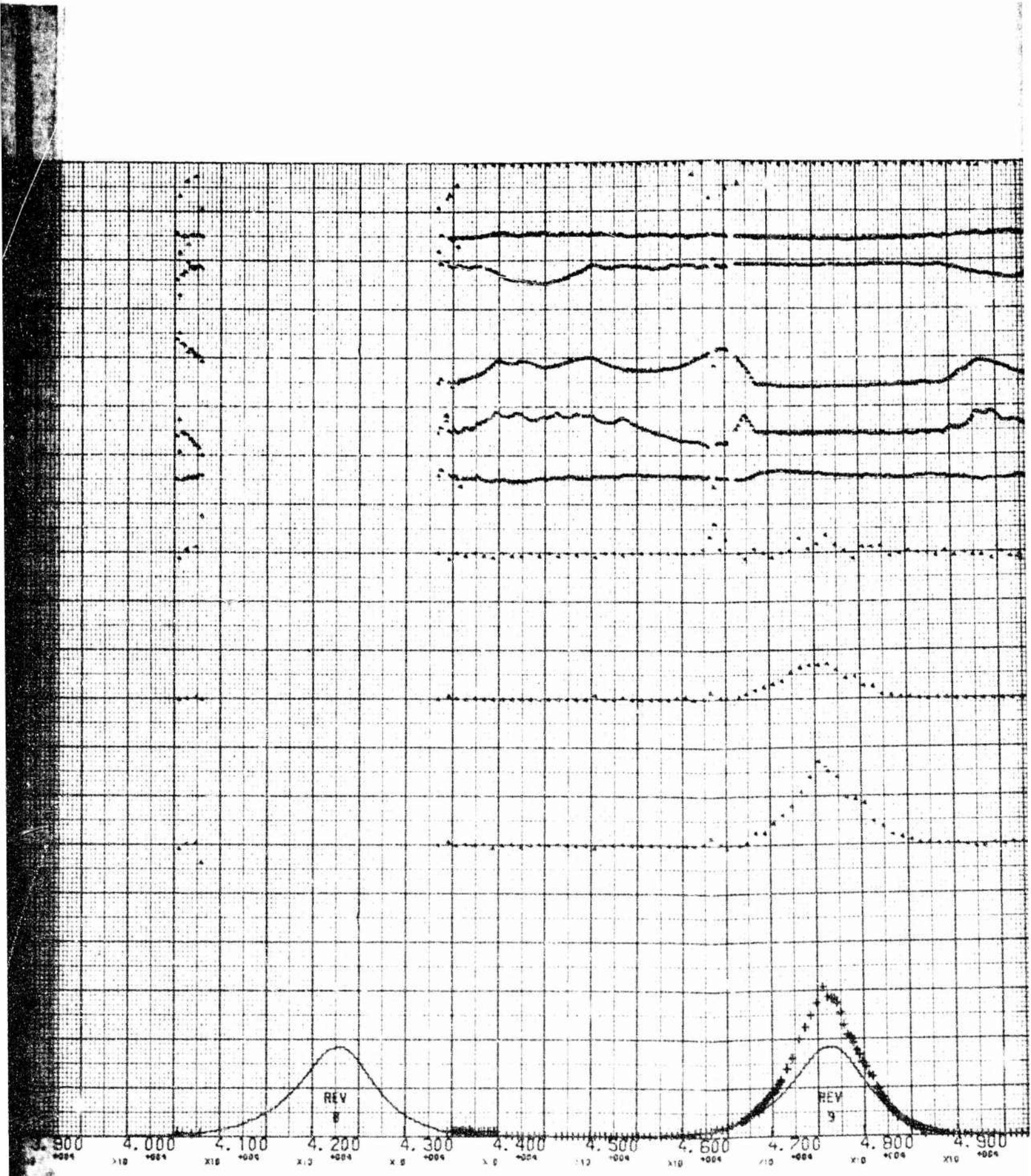
REV
8
REV
9
3.900
4.000
4.100
4.200
4.300
4.400
4.500
4.600
4.700
4.800
4.900

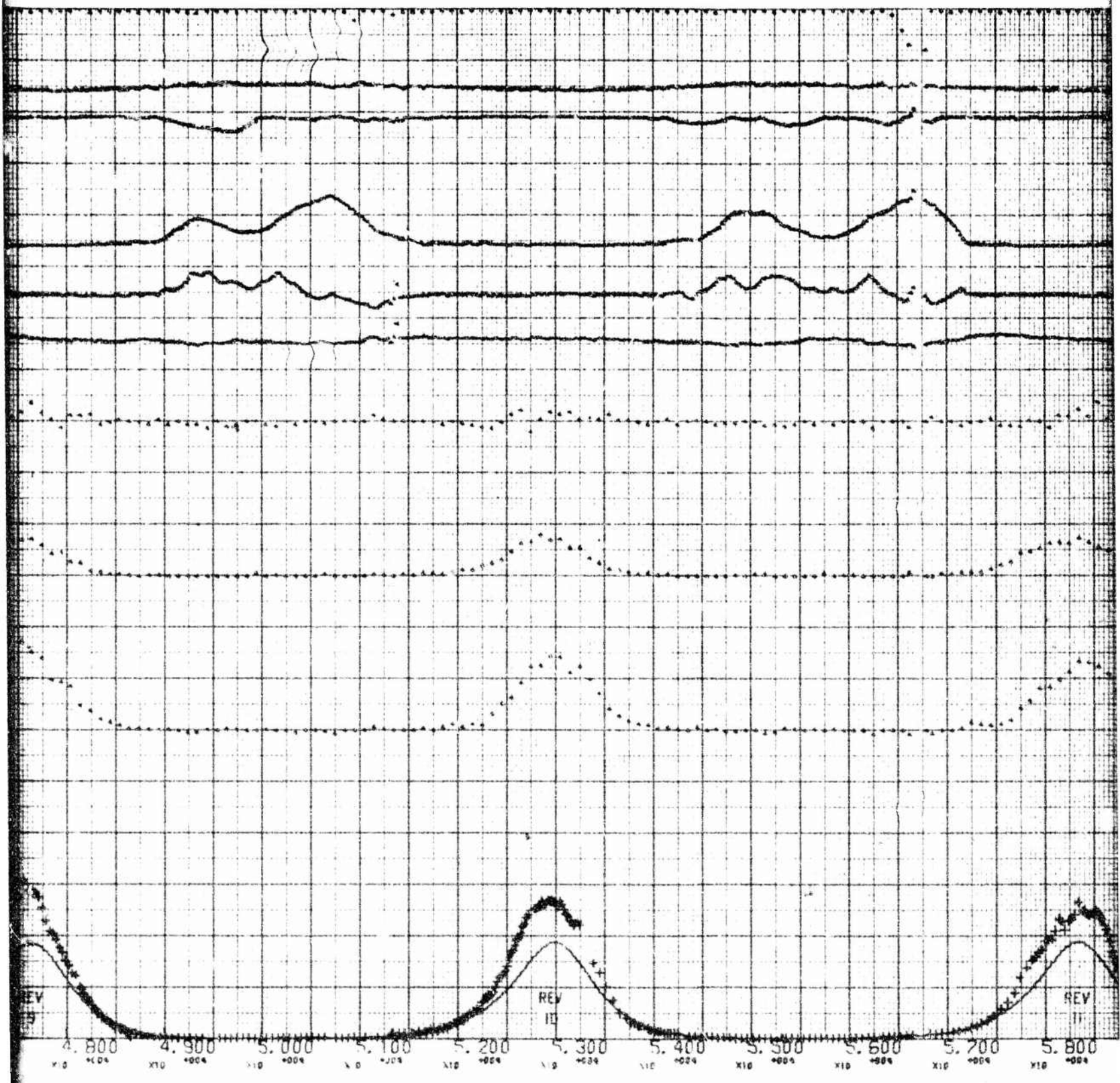
REV
9
REV
10
REV
11
4.800
4.900
5.000
5.100
5.200
5.300
5.400
5.500
5.600
5.700
5.800

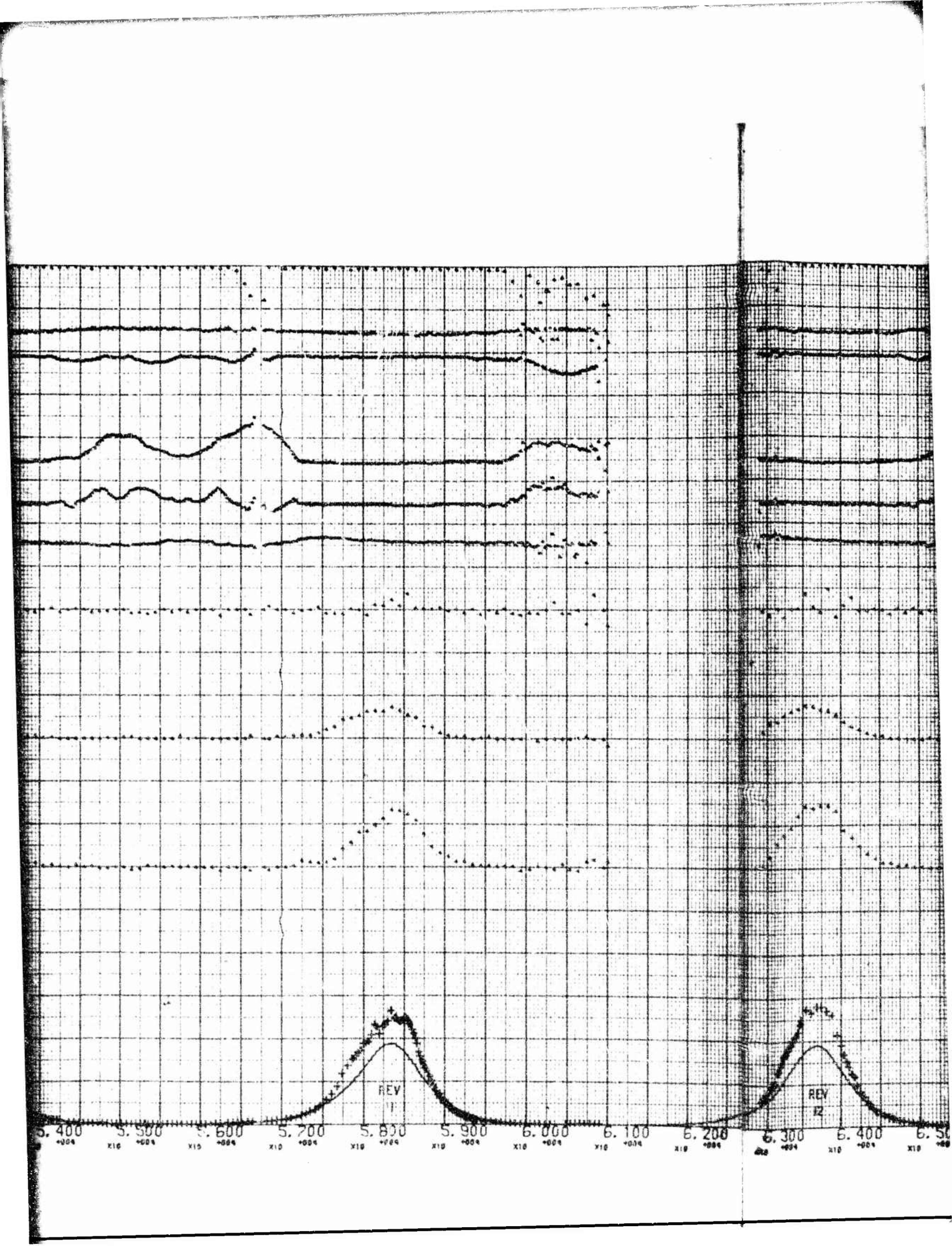
REV
11
REV
12
5.400
5.500
5.600
5.700
5.800
5.900
6.000
6.100
6.200
6.300
6.400

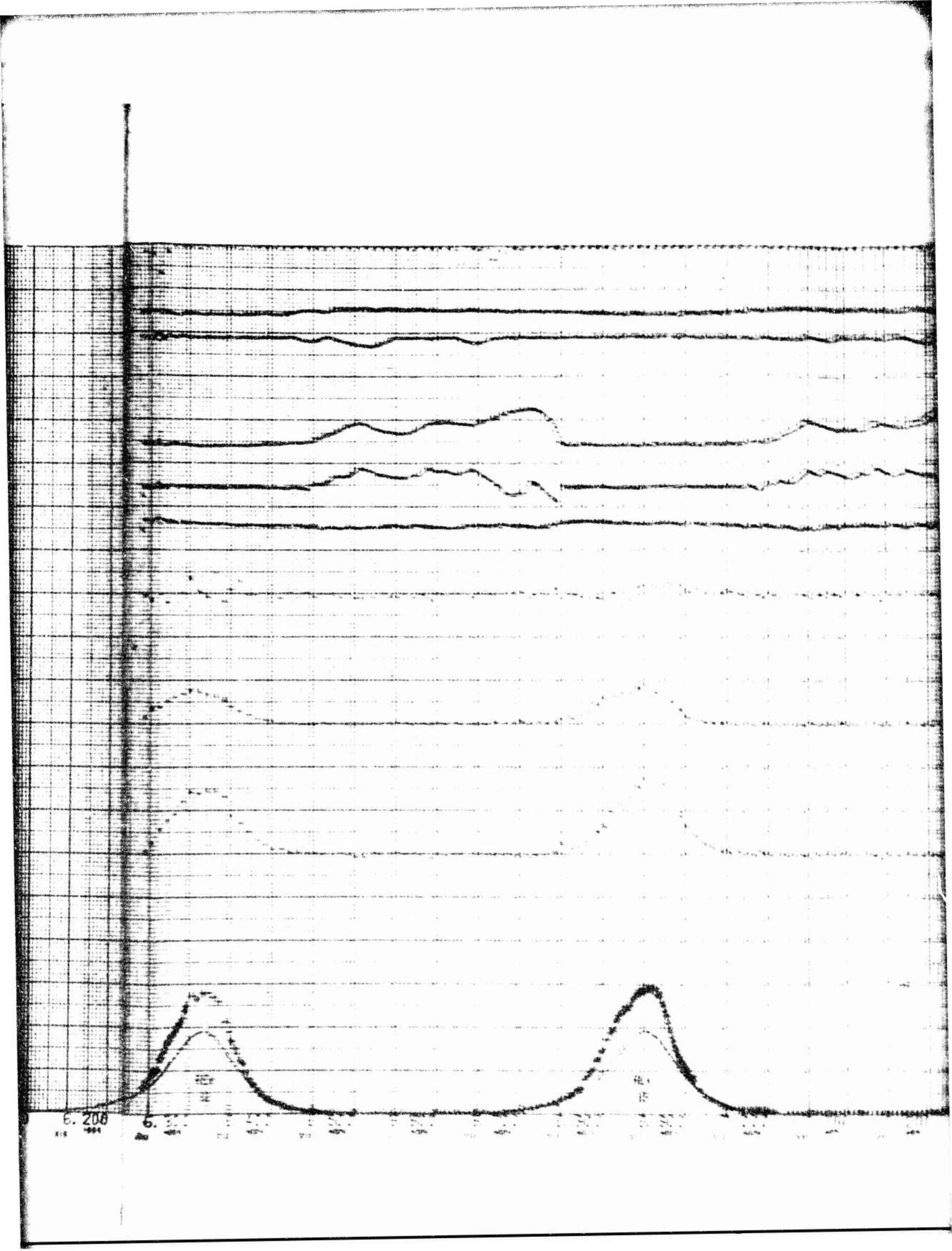
6. 208
6.

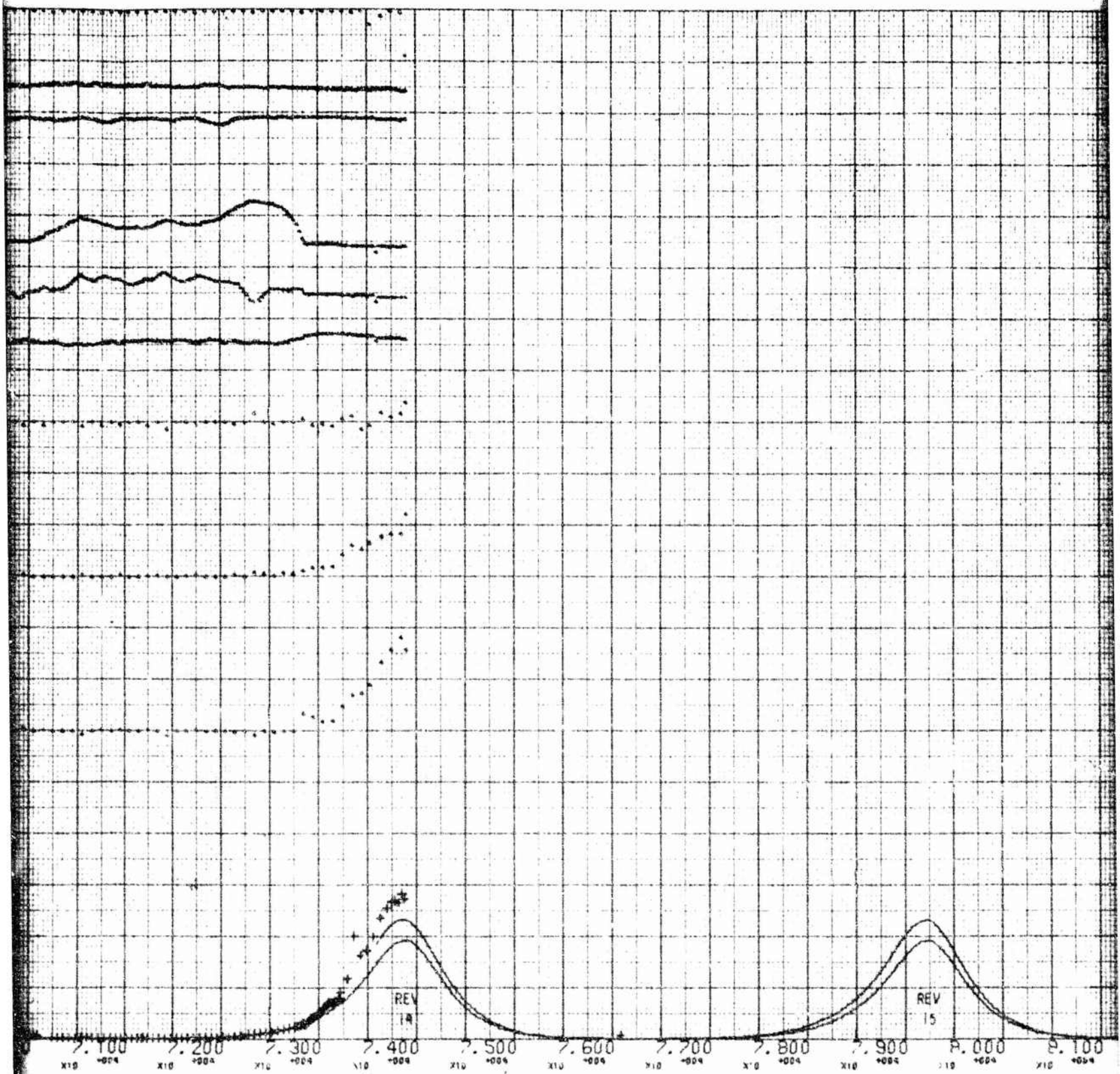
REV
14
REV
15
7.100
7.200
7.300
7.400
7.500
7.600
7.700
7.800
7.900
8.000
8.100

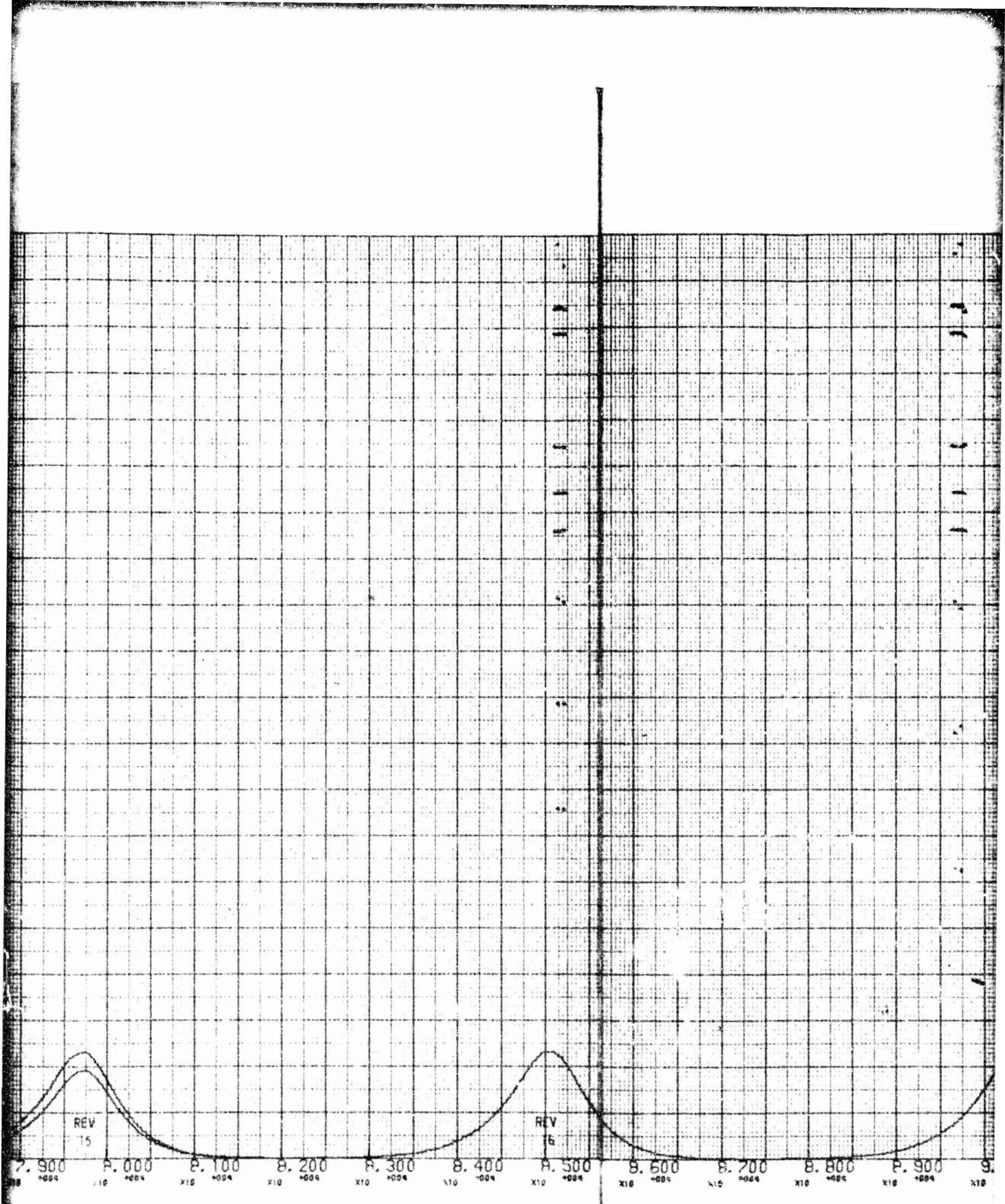
REV
15
REV
16
7.900
8.000
8.100
8.200
8.300
8.400
8.500
8.600
8.700
8.800
8.900
9.

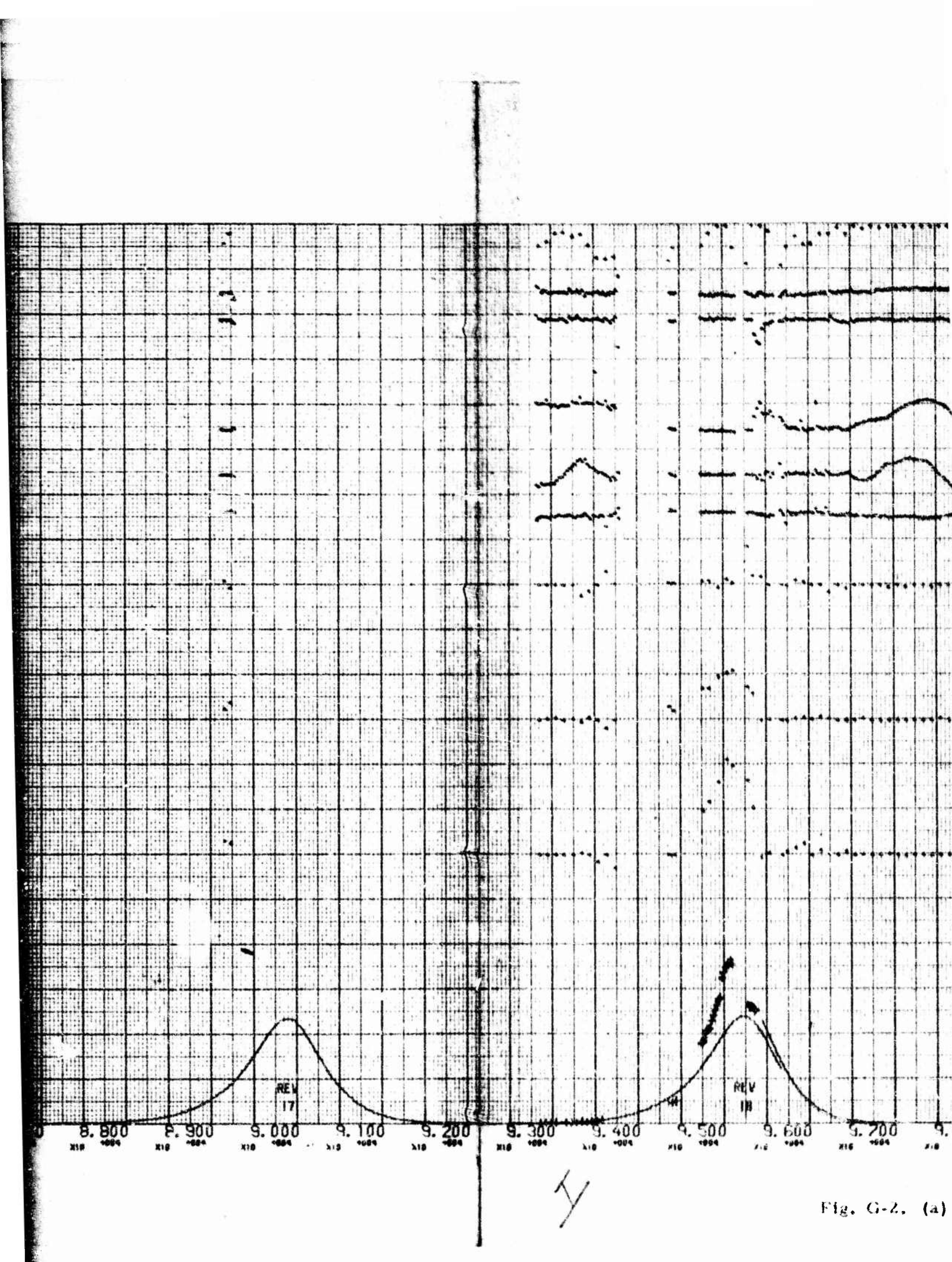
REV 17
REV 18
8.800
8.900
9.000
9.100
9.200
9.300
9.400
9.500
9.600
9.700

Fig. G-2. (a) A

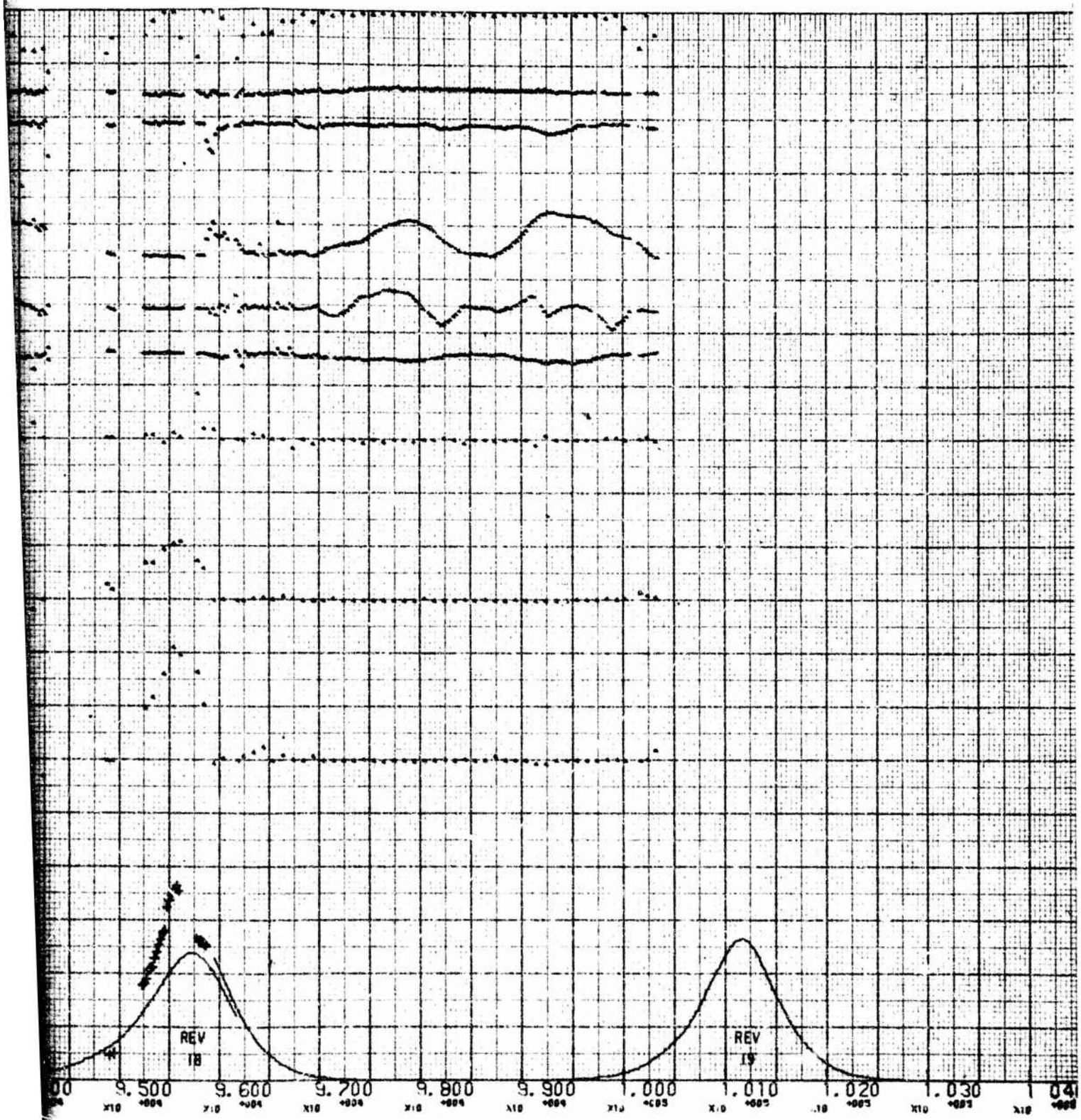

Fig. G-2. (a) Agena Control System Functions (May 23)

MAY 24

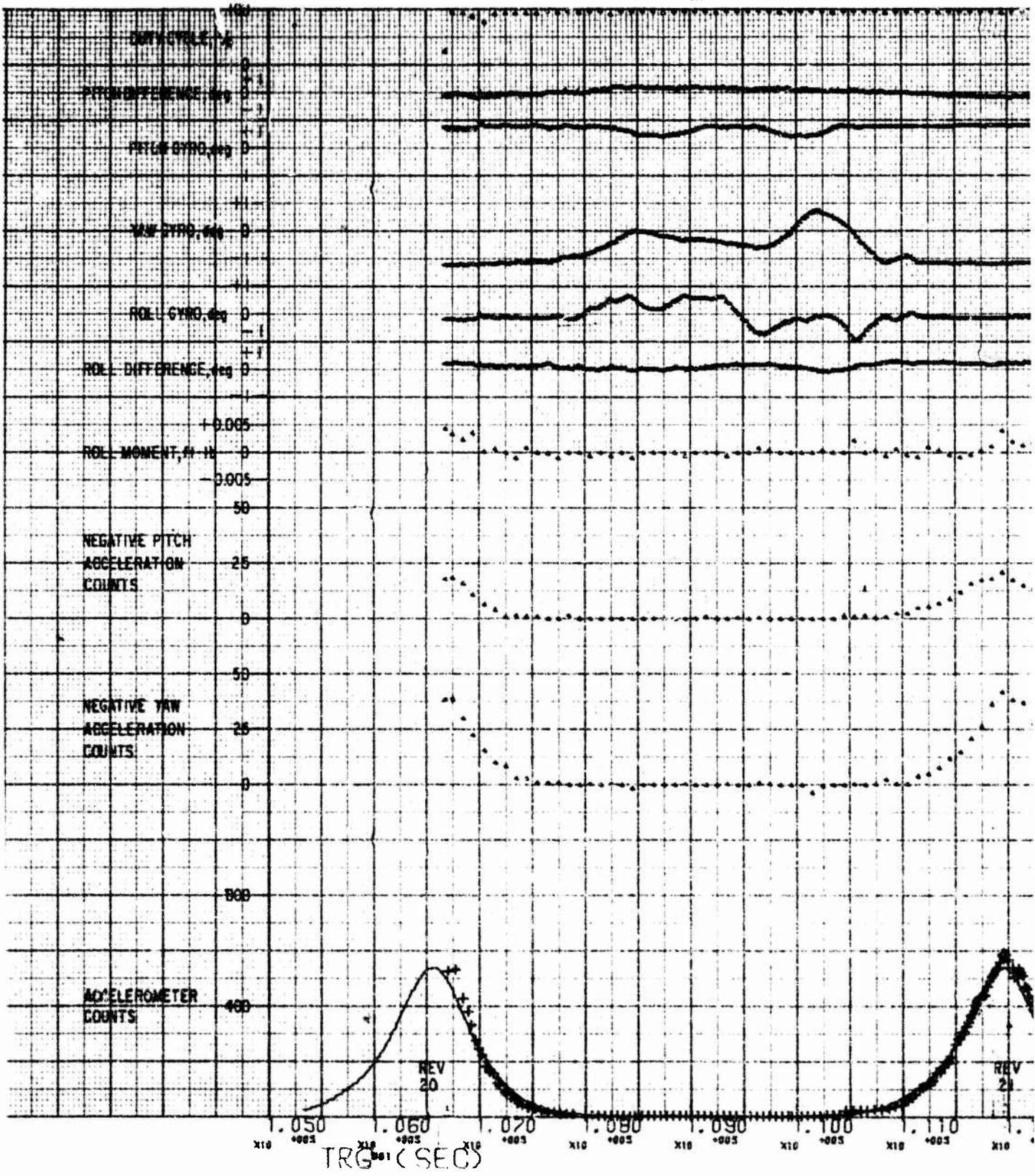
DUTY CYCLE, %
PITCH DIFFERENCE, deg
PITCH GYRO, deg
YAW GYRO, deg
ROLL GYRO, deg
ROLL DIFFERENCE, deg
+0.005
ROLL MOMENT, ft-lb
-0.005
50
NEGATIVE PITCH ACCELERATION COUNTS
25
0
50
NEGATIVE YAW ACCELERATION COUNTS
25
0
800
ACCELEROMETER COUNTS
400
REV 20
REV 21
1.050
1.060
1.070
1.080
1.090
1.100
1.110
TRG (SEC)

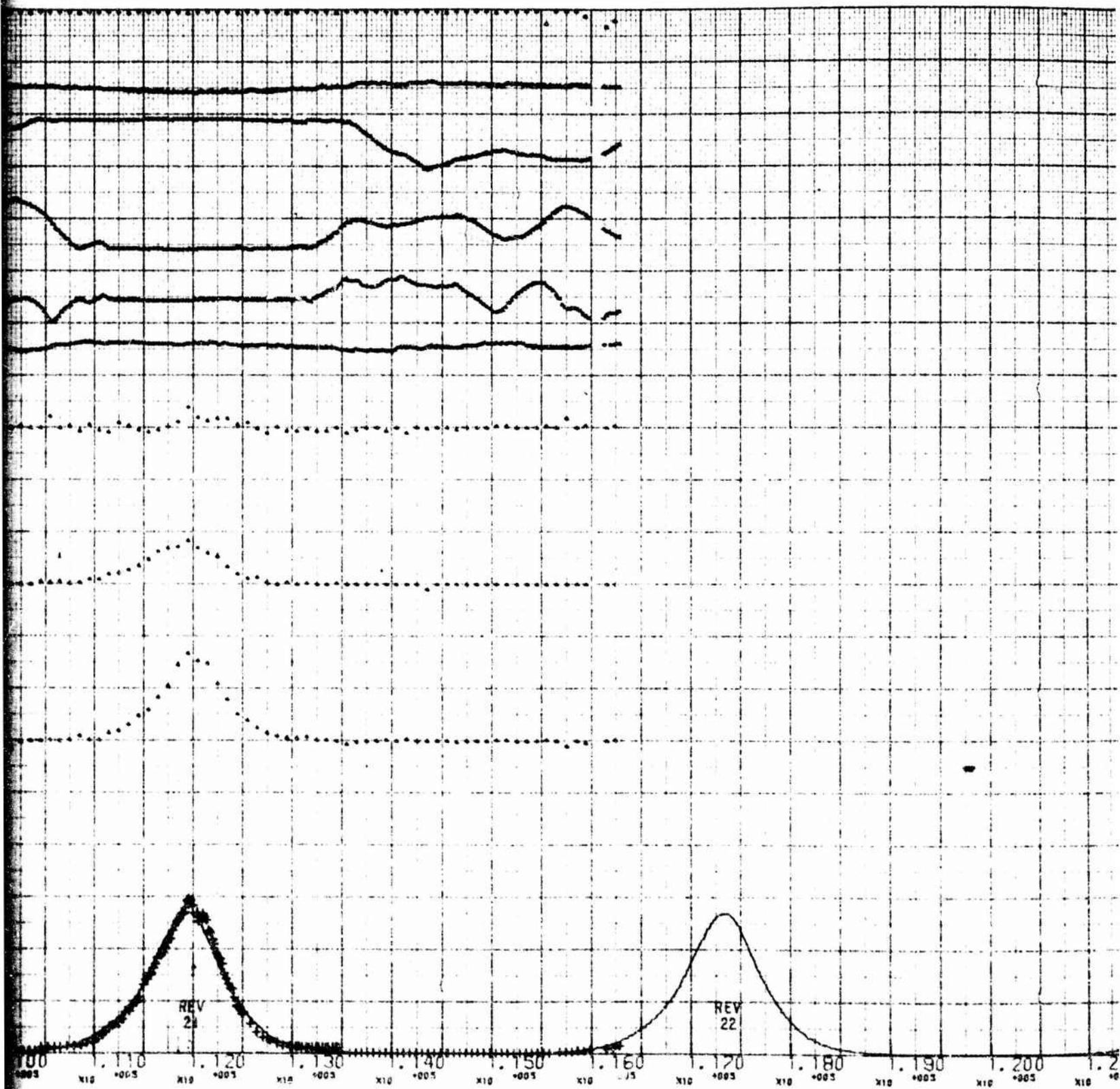

B

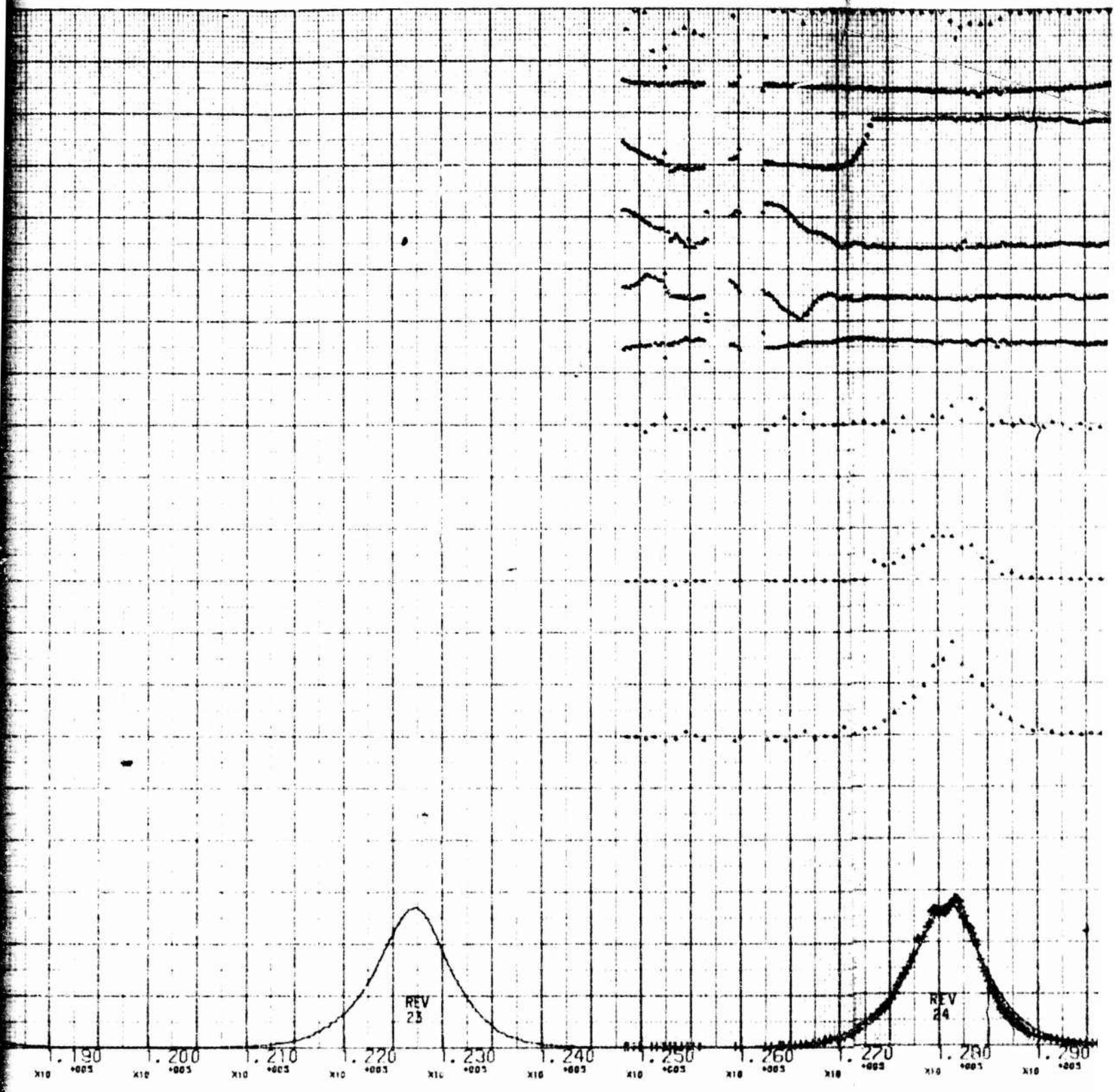

C

REV
24
REV
25
1.280
1.290
1.300
1.310
1.320
1.330
1.340
1.350
1.360
1.370
1.380
X10
+003

D

REV
26
REV
27
.360
.370
.380
.390
.400
.410
.420
.430
.440
.450
.460

1.460
1.470
1.480
1.490
1.500
1.510
1.520
1.530
1.540
1.550
1.560

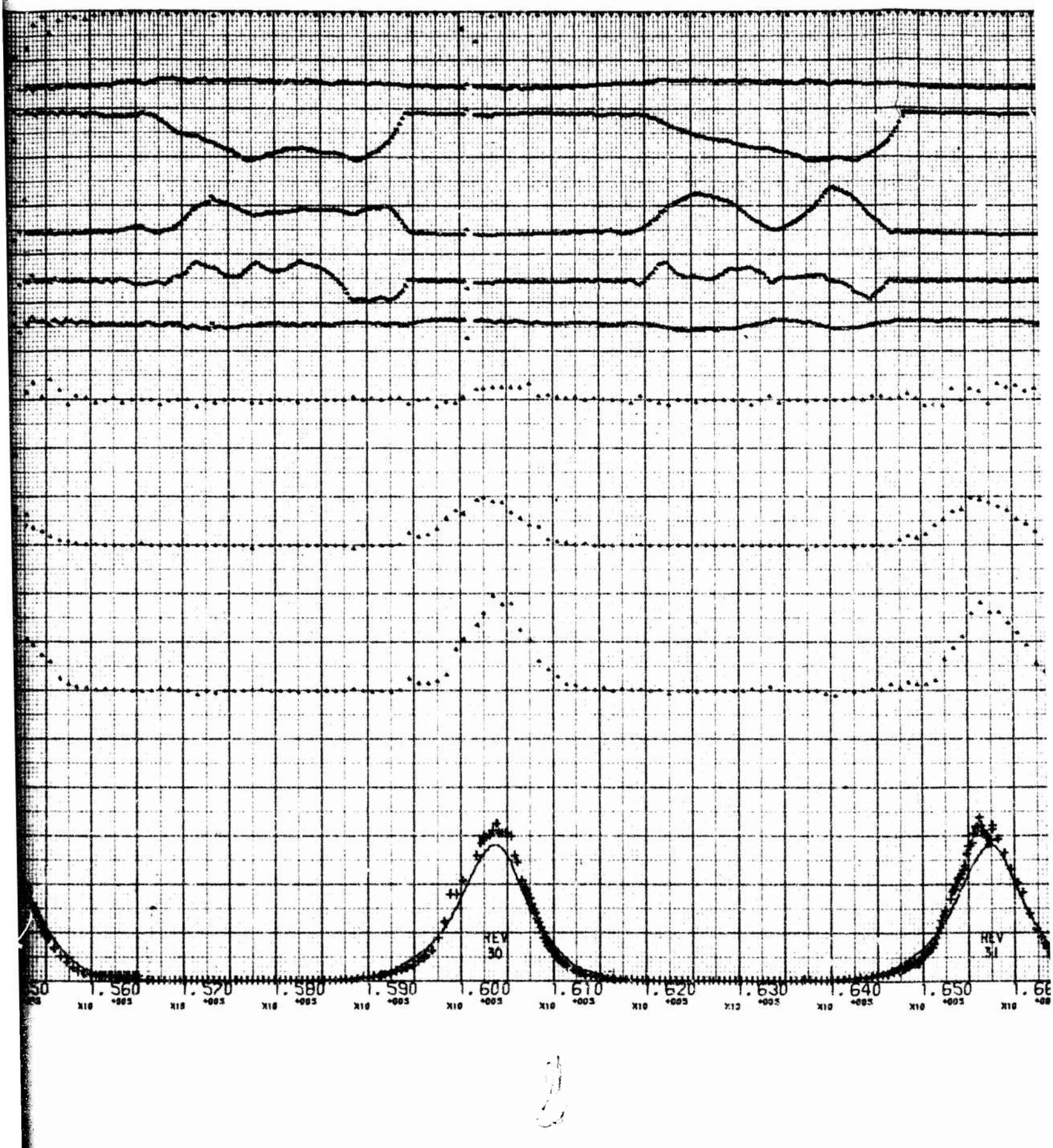
REV
30
REV
31
1.560
1.570
1.580
1.590
1.600
1.610
1.620
1.630
1.640
1.650

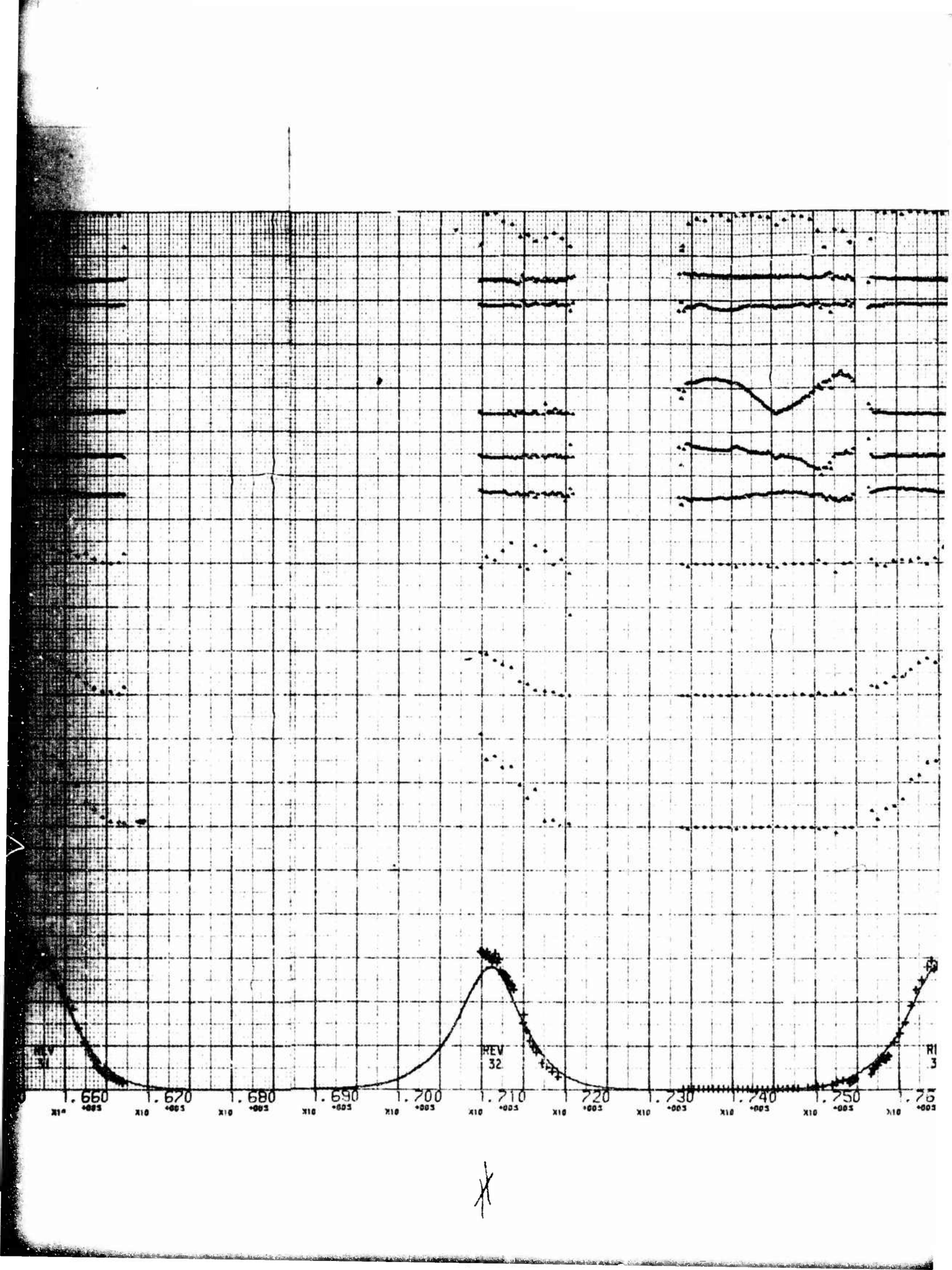
REV
32
1.660
1.670
1.680
1.690
1.700
1.710
1.720
1.730
1.740
1.750
1.75

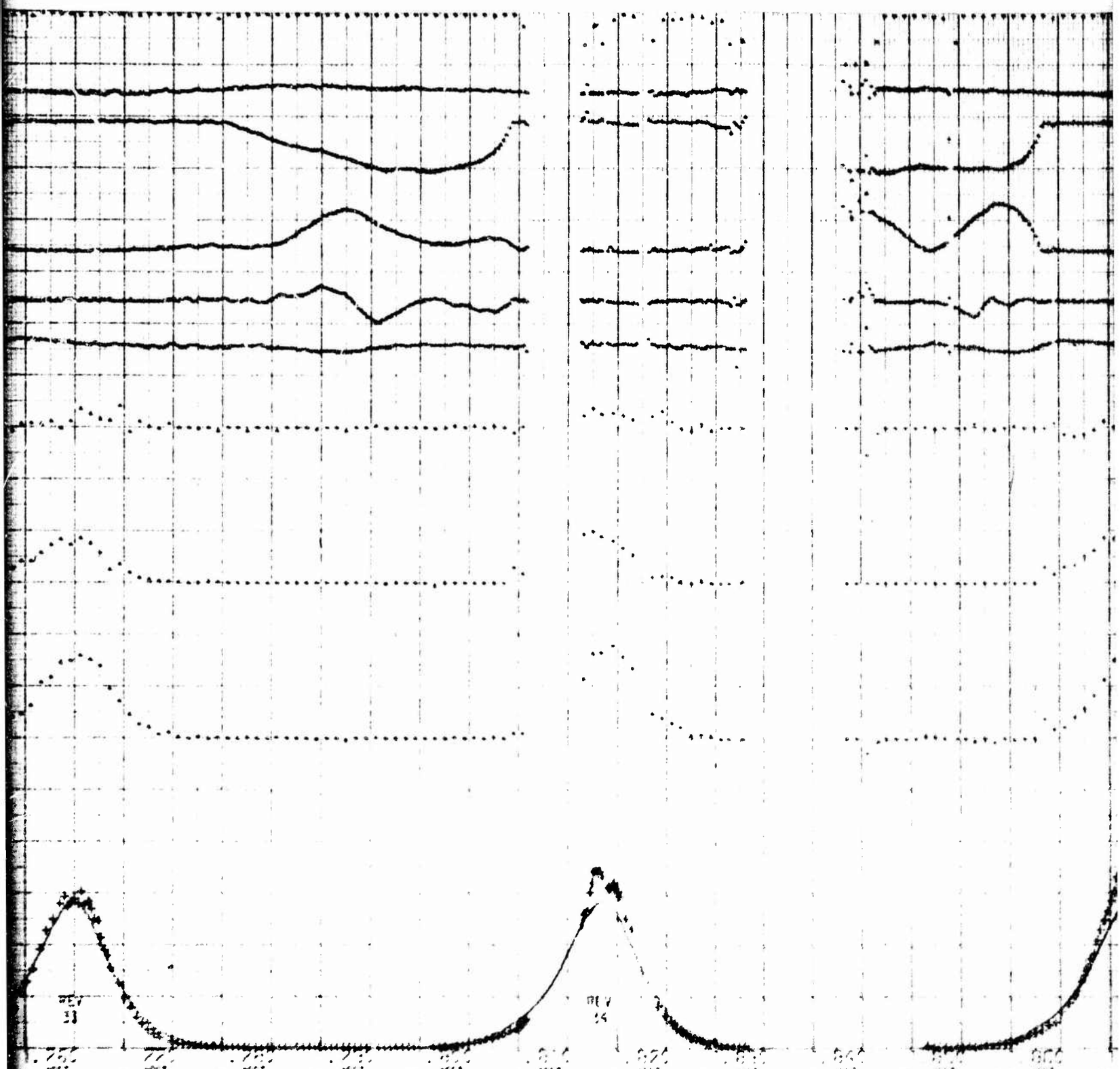

Fig. 6-22. (b) Agena Control

Fig. G-2. (b) Agena Control System Functions (May 24)

MAY 25

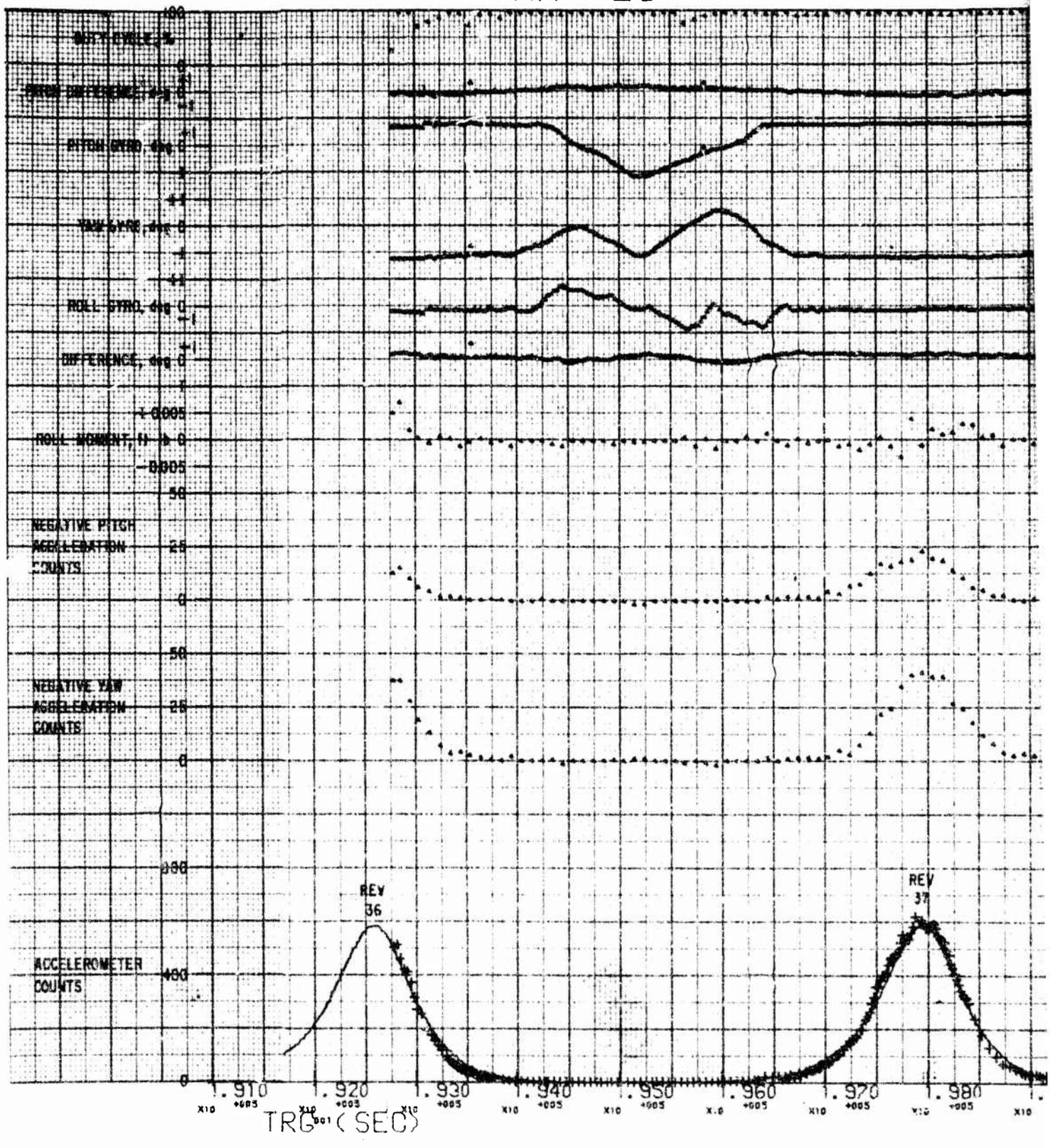
DUTY CYCLE, %
PITCH DIFFERENCE, deg
PITCH GYRO, deg
YAW GYRO, deg
ROLL GYRO, deg
DIFFERENCE, deg
ROLL MOMENT, ft-lb
NEGATIVE PITCH ACCELERATION COUNTS
NEGATIVE YAW ACCELERATION COUNTS
ACCELEROMETER COUNTS
REV 36
REV 37
1.910
1.920
1.930
1.940
1.950
1.960
1.970
1.980
TRG (SEC)

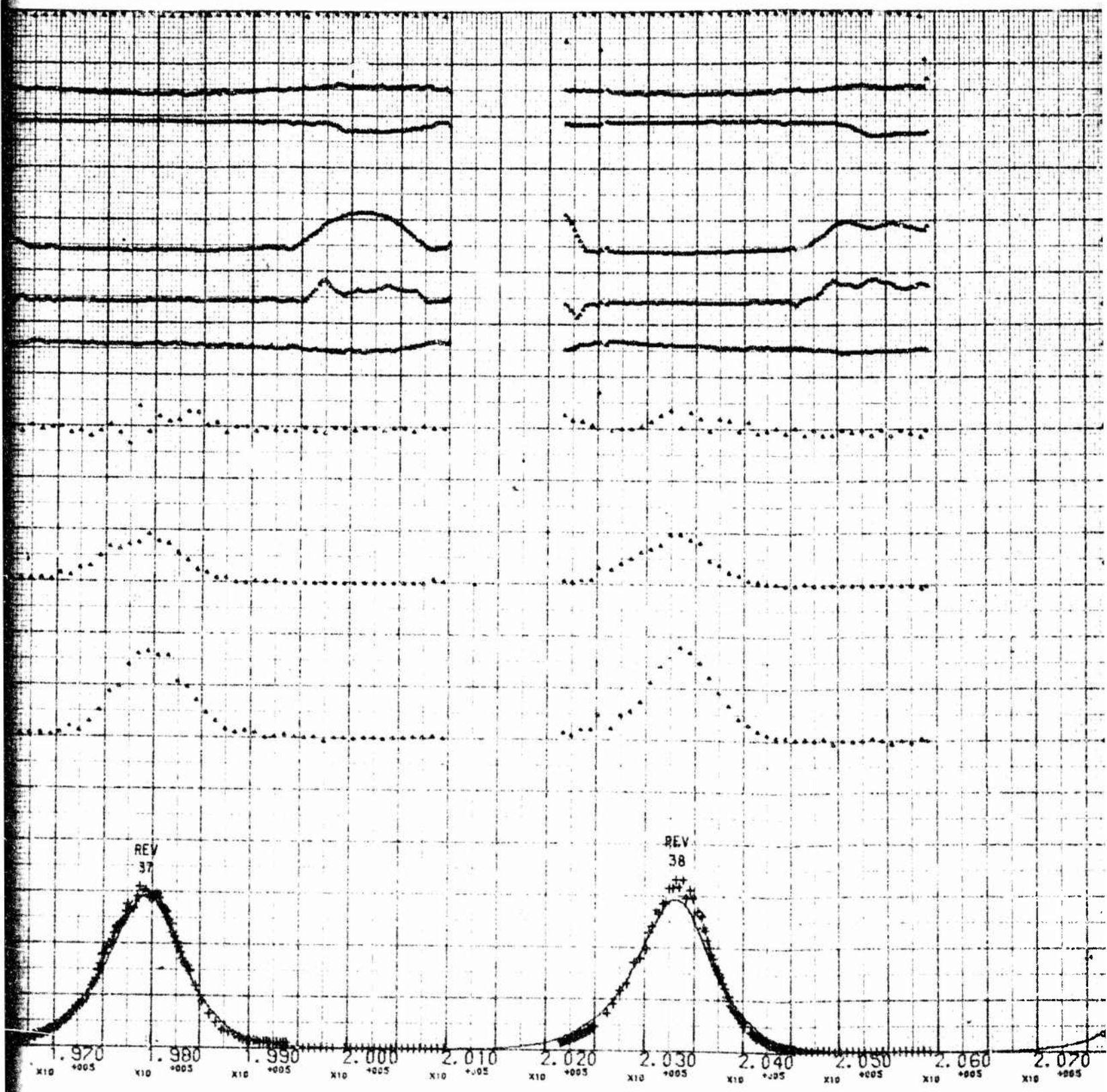
REV
37
REV
38
1.970
1.980
1.990
2.000
2.010
2.020
2.030
2.040
2.050
2.060
2.070
X10
+005

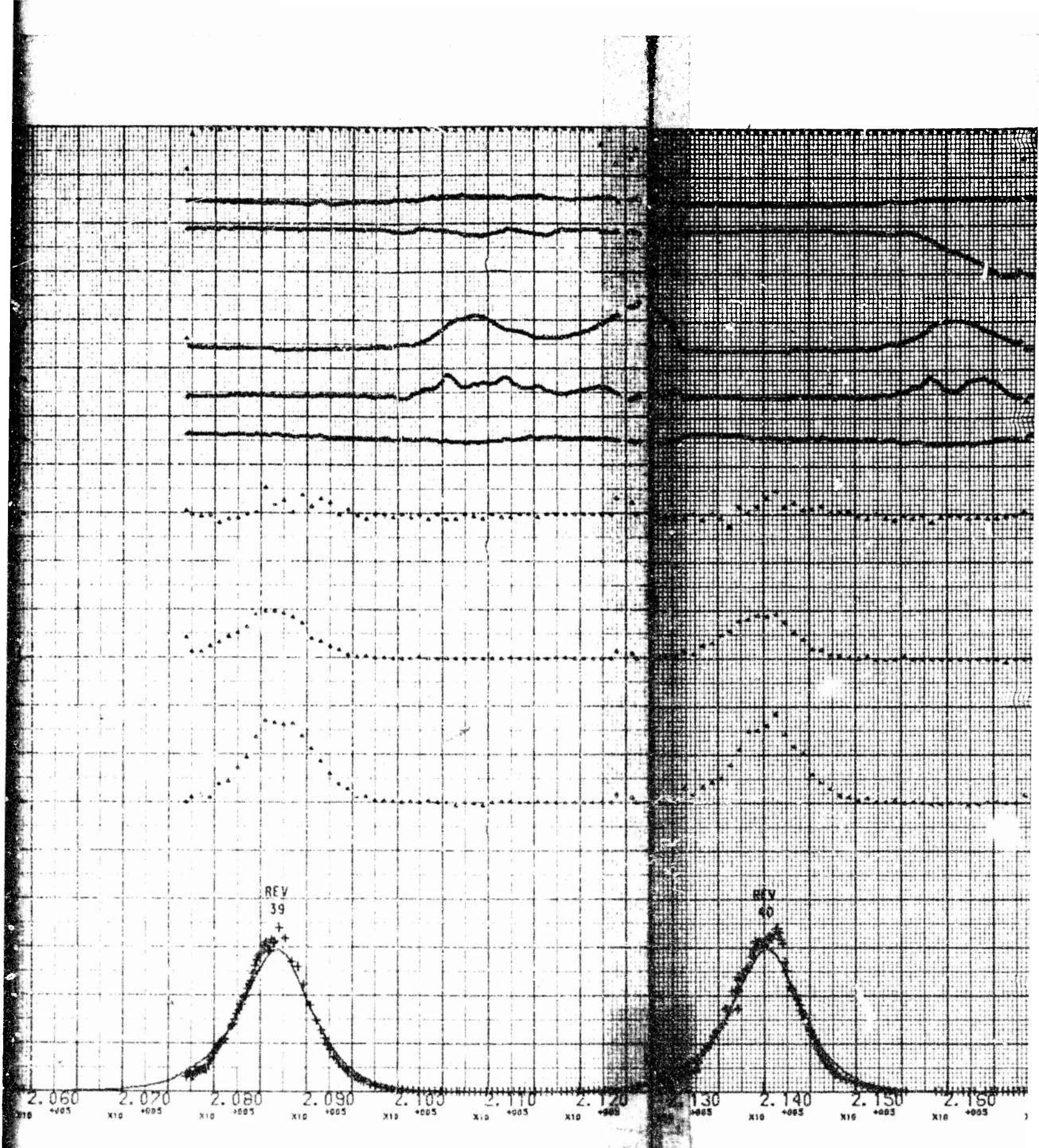
REV
39
REV
40
2.060
2.070
2.080
2.090
2.100
2.110
2.120
2.130
2.140
2.150
2.160

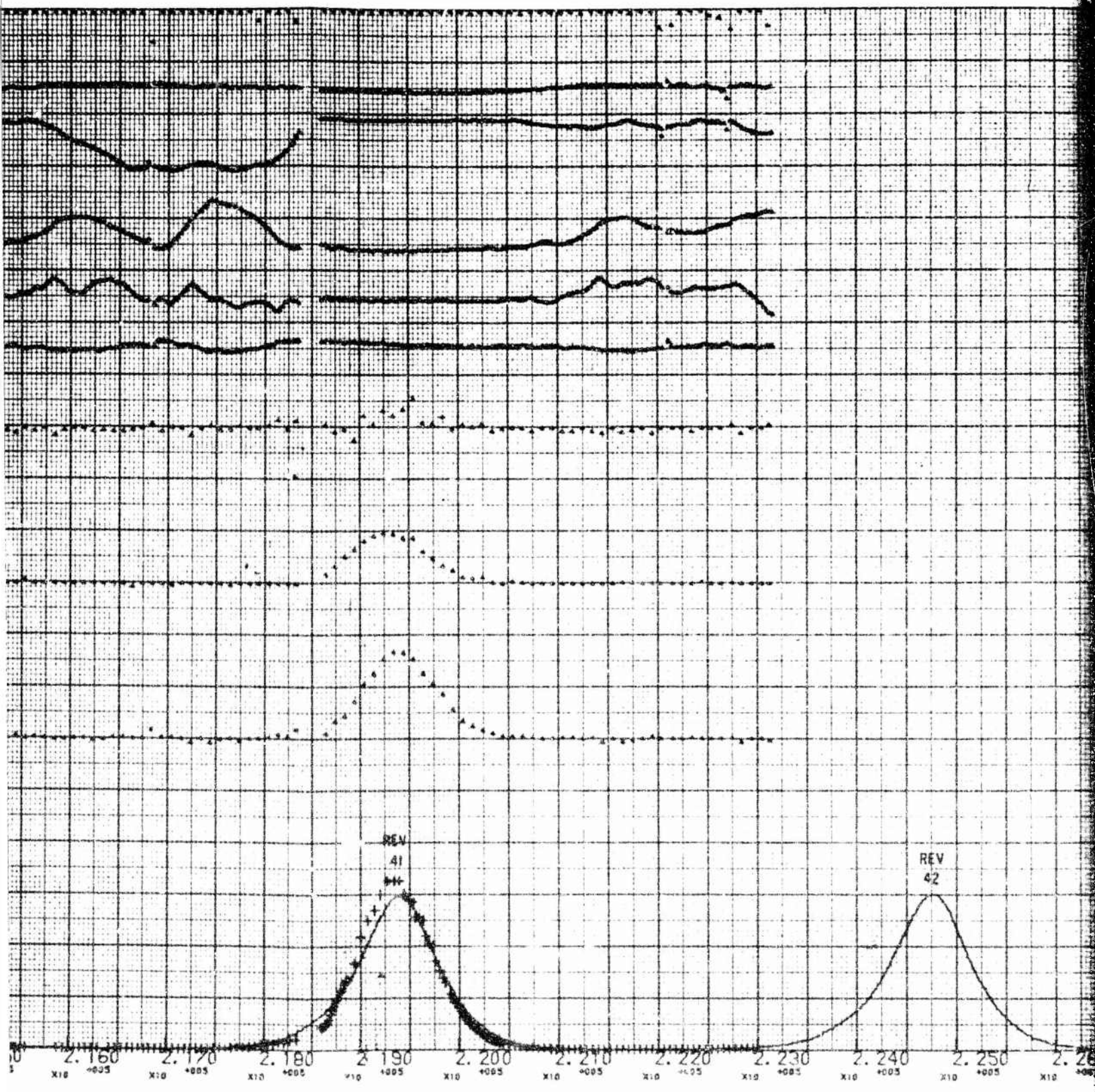
REV
41
REV
42
2.160
2.170
2.180
2.190
2.200
2.210
2.220
2.230
2.240
2.250

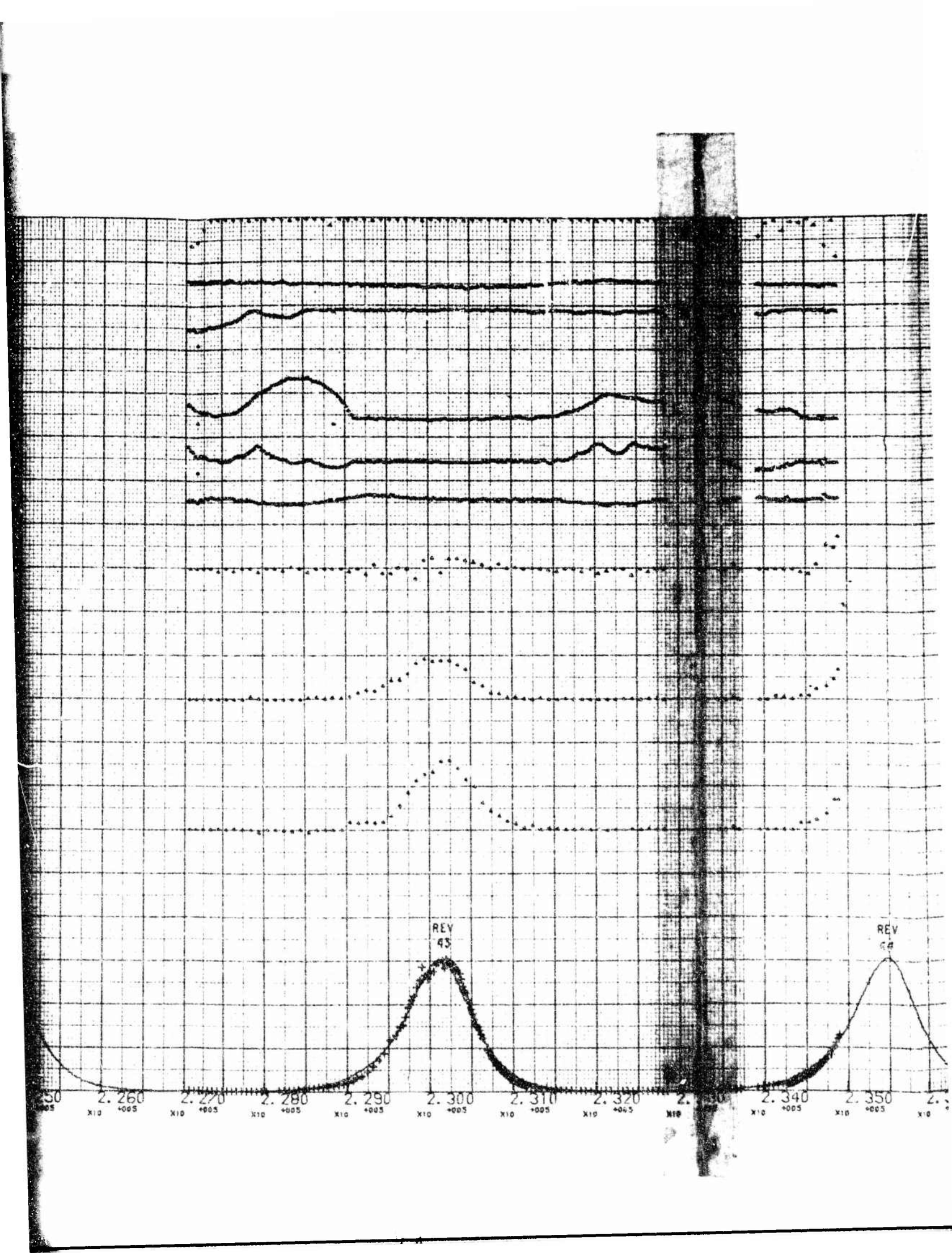
REV
43
REV
64
2.260
2.270
2.280
2.290
2.300
2.310
2.320
2.340
2.350

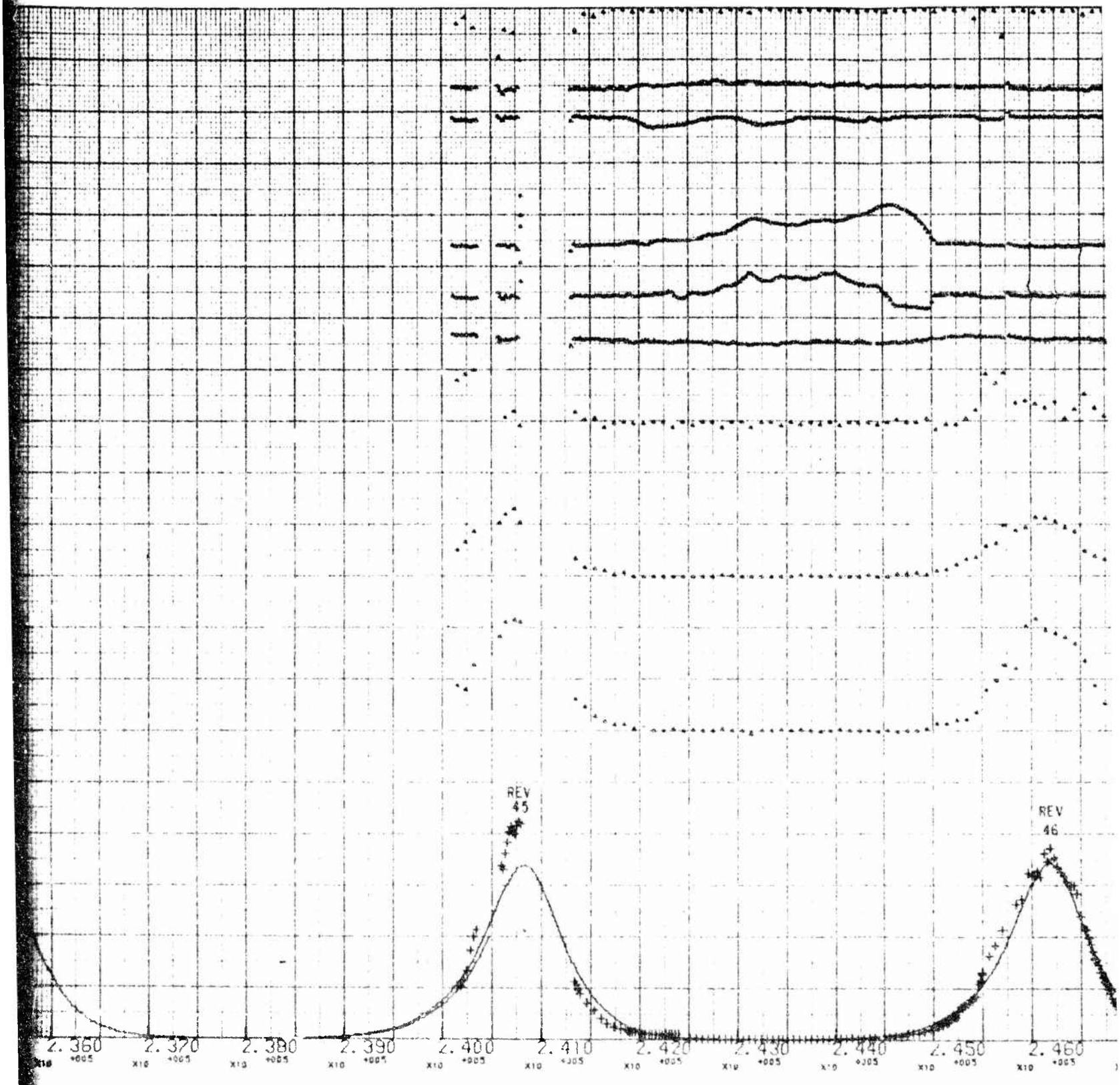
REV
45
REV
46
2.360
2.370
2.380
2.390
2.400
2.410
2.420
2.430
2.440
2.450
2.460

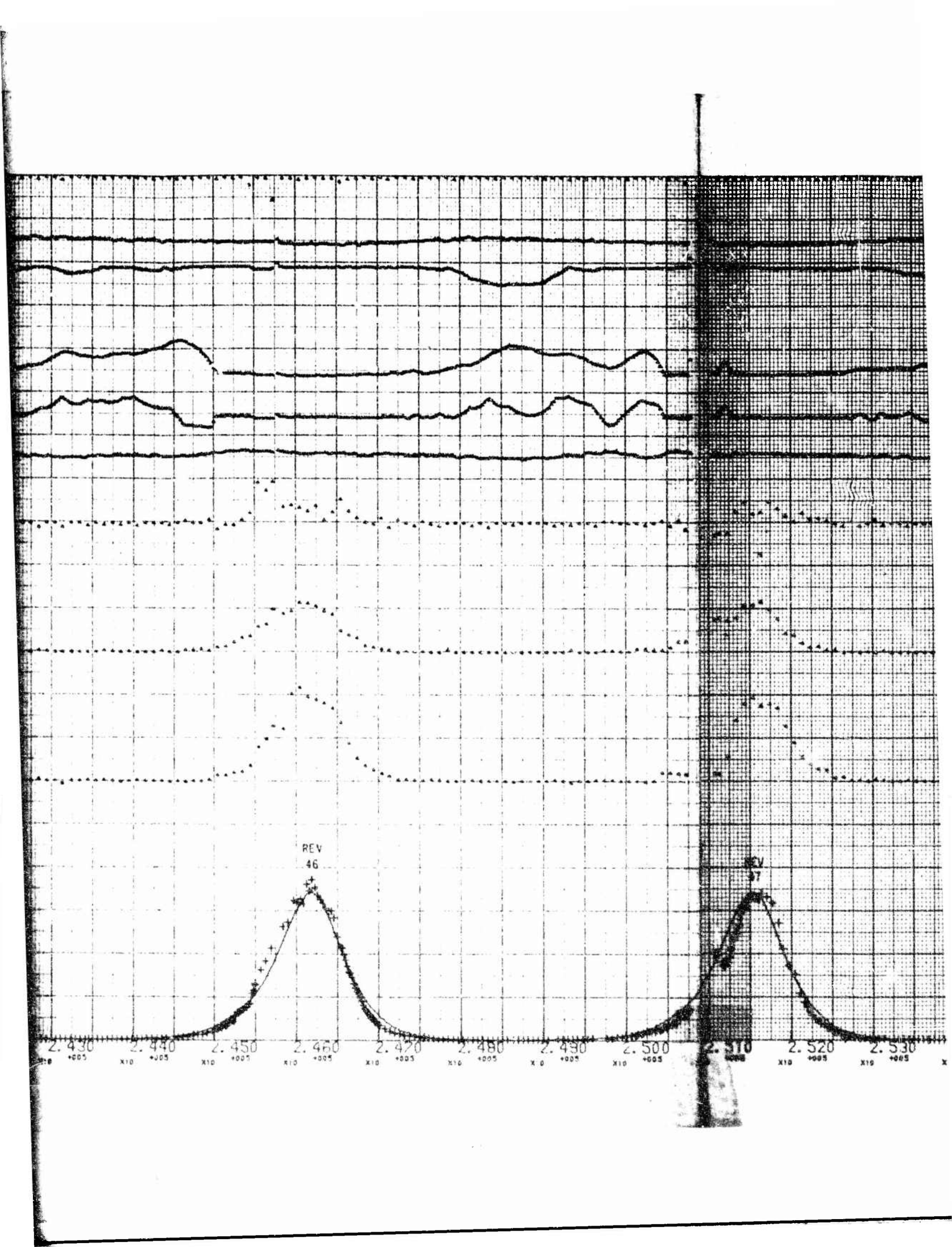
REV
46
REV
47
2.430
2.440
2.450
2.460
2.470
2.480
2.490
2.500
2.510
2.520
2.530

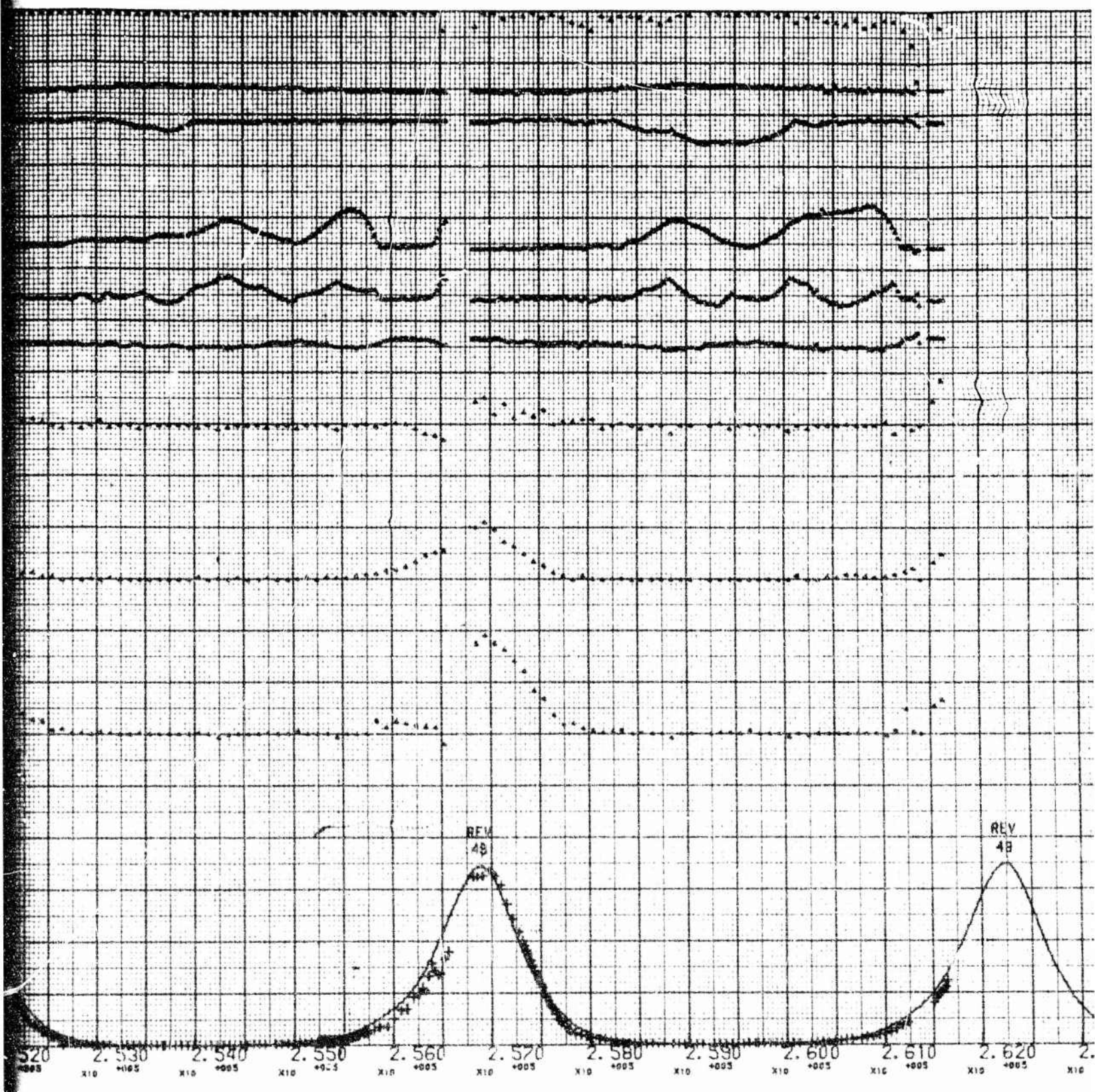
REV
48
REV
48
2.530
2.540
2.550
2.560
2.570
2.580
2.590
2.600
2.610
2.620

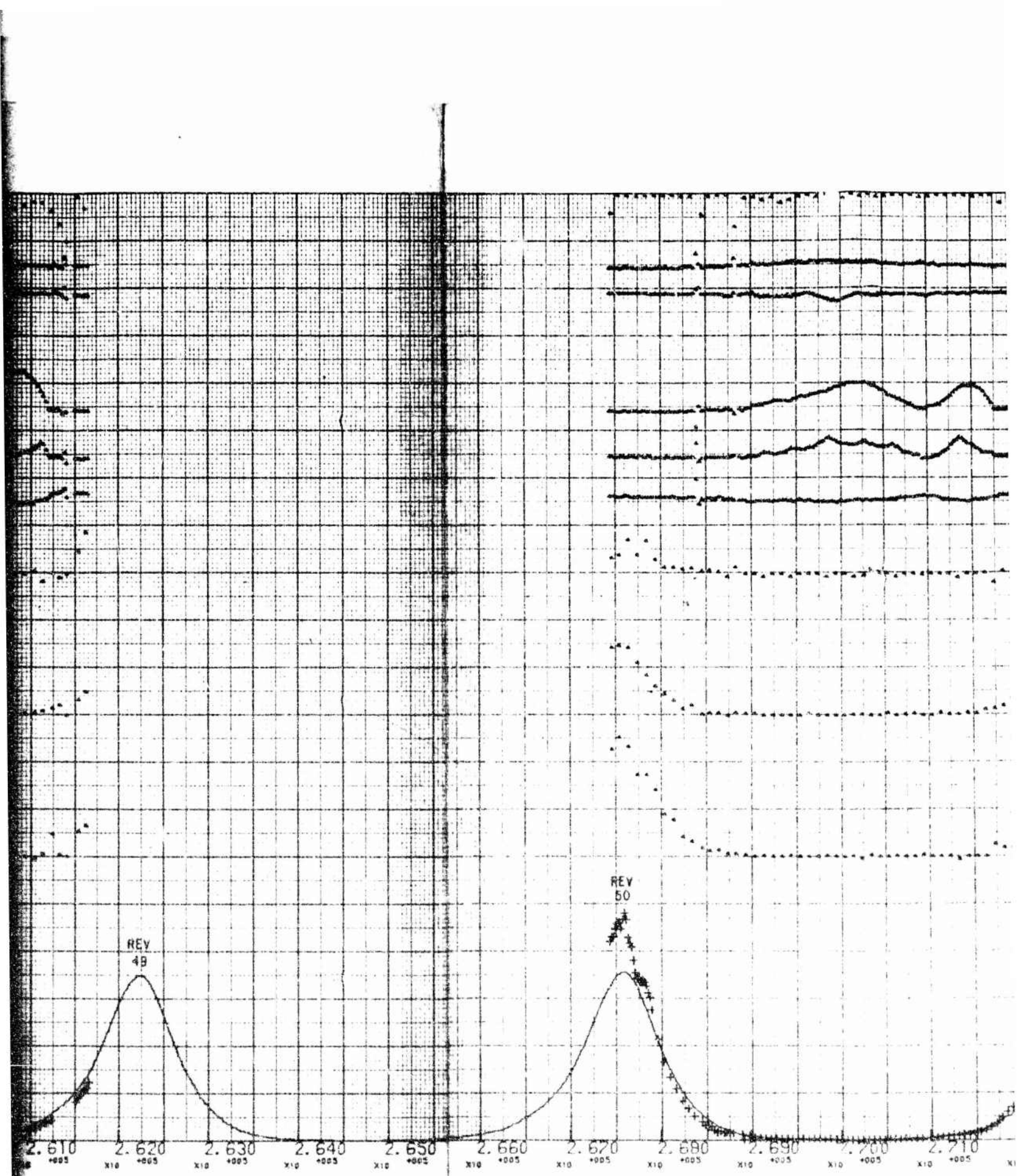
REV
48
REV
50
2.610
+005
2.620
X10
+005
2.630
X10
+005
2.640
X10
+005
2.650
X10
+005
2.660
X10
+005
2.670
X10
+005
2.680
X10
+005
2.690
X10
+005
2.700
X10
+005
2.710
X10
+005

Fig. G-2. (

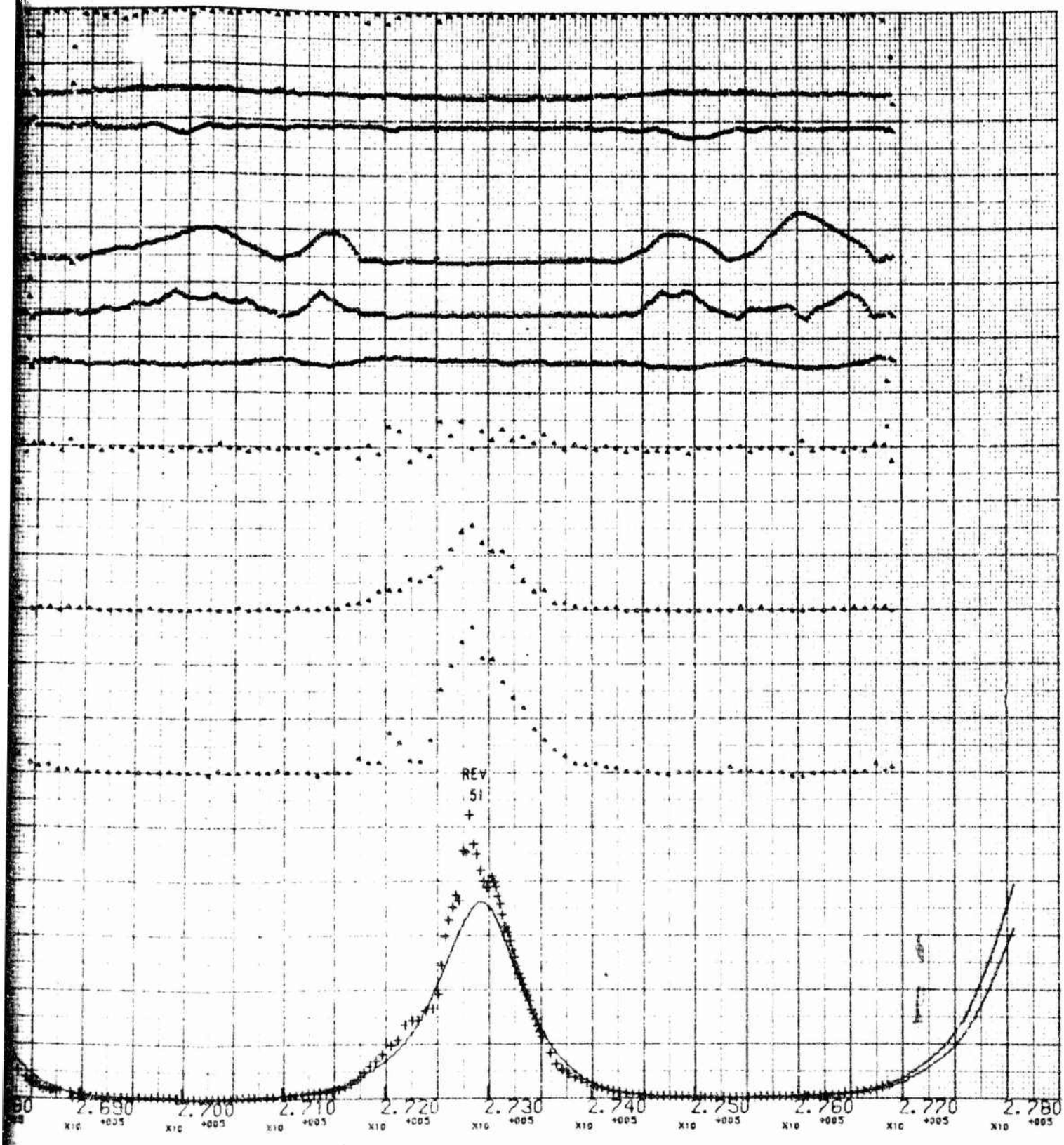

Fig. G-2. (c) Agena Control System Functions (May 25)

Reproduced from best available copy.

MAY '26

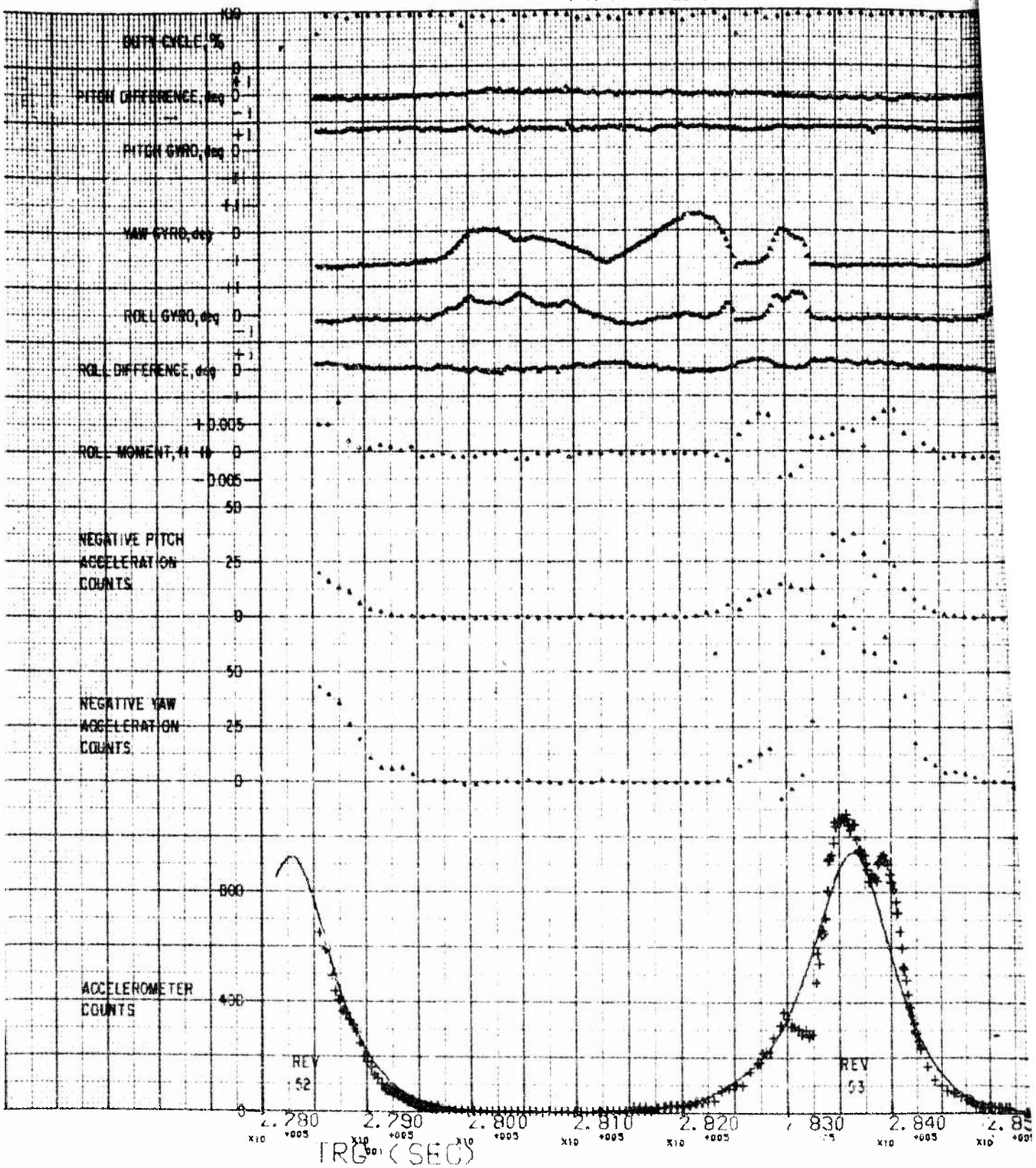
DUTY CYCLE, %
100
0
PITCH DIFFERENCE, deg
+1
0
-1
PITCH GYRO, deg
+1
0
-1
YAW GYRO, deg
+1
0
-1
ROLL GYRO, deg
+1
0
-1
ROLL DIFFERENCE, deg
+1
0
-1
+0.005
ROLL MOMENT, ft-lb
0
-0.005
50
NEGATIVE PITCH ACCELERATION COUNTS
25
0
50
NEGATIVE YAW ACCELERATION COUNTS
25
0
800
ACCELEROMETER COUNTS
400
0
REV 52
REV 53
2.780 +005 X10
2.790 +005 X10
2.800 +005 X10
2.810 +005 X10
2.820 +005 X10
2.830 +005 X10
2.840 +005 X10
TRG (SEC)

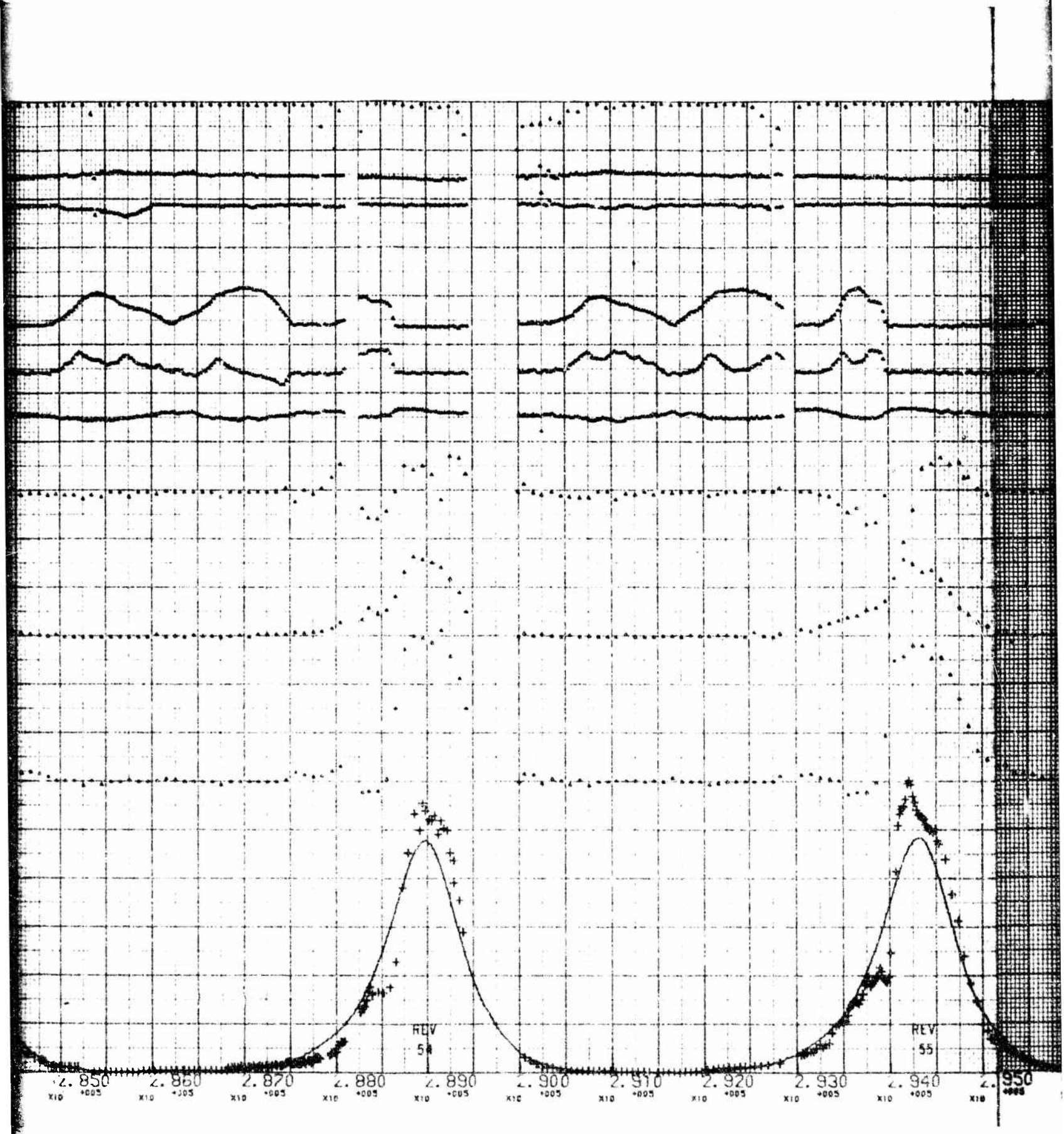
REV
58
REV
55
2.850
2.860
2.870
2.880
2.890
2.900
2.910
2.920
2.930
2.940
2.950

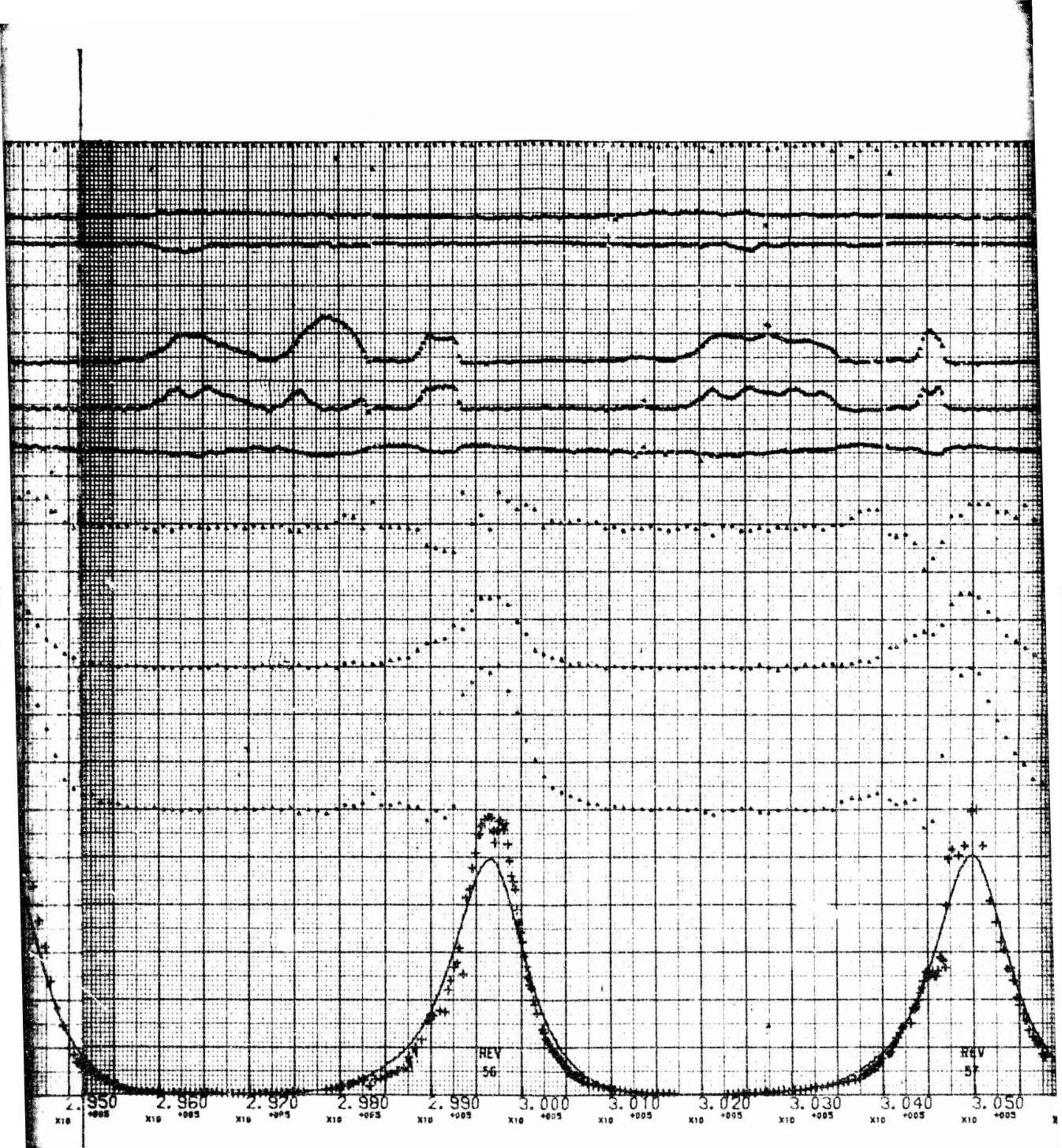
REV
56
REV
57
2.950
2.960
2.970
2.980
2.990
3.000
3.010
3.020
3.030
3.040
3.050

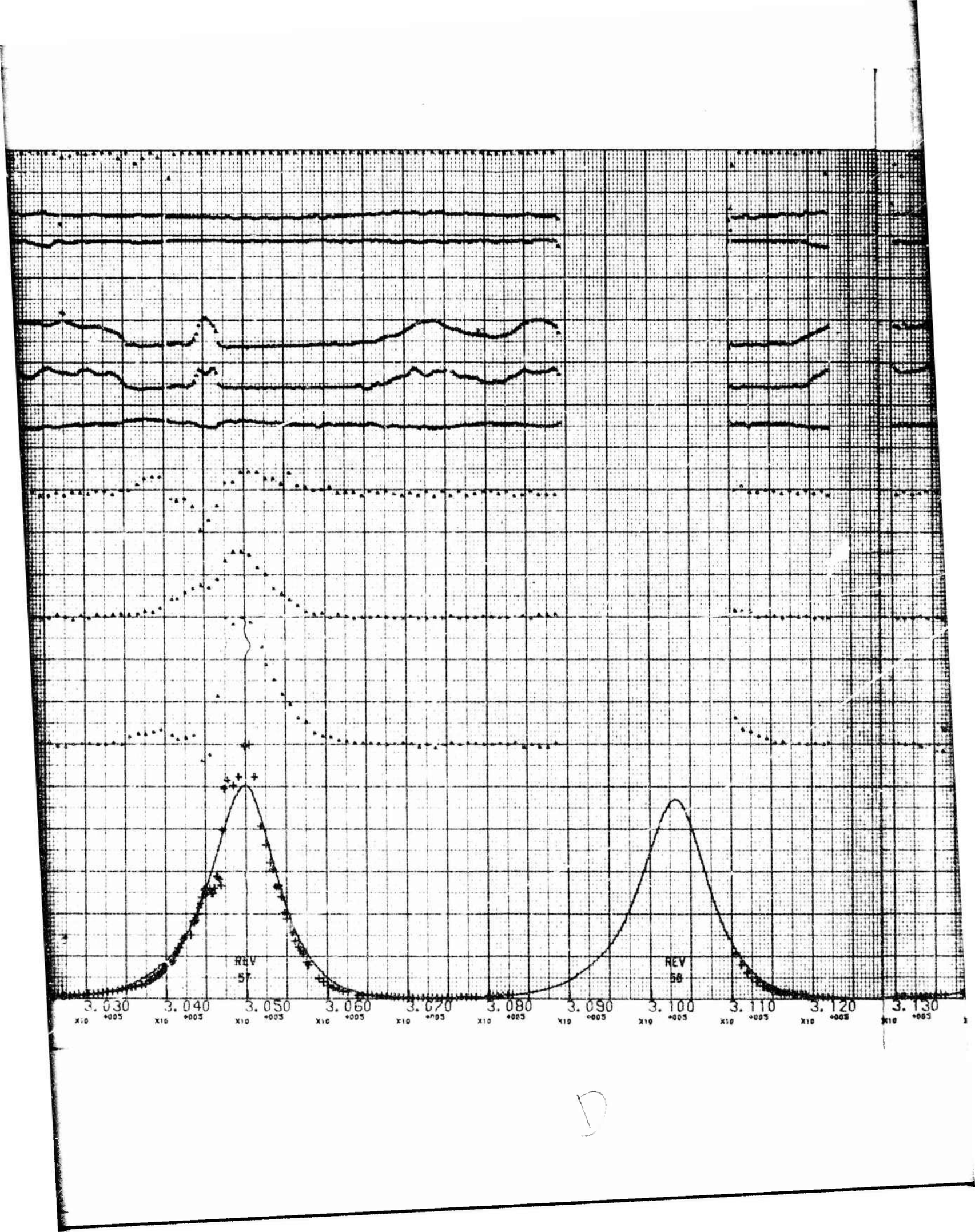
REV
57
REV
58
3.030
3.040
3.050
3.060
3.070
3.080
3.090
3.100
3.110
3.120
3.130

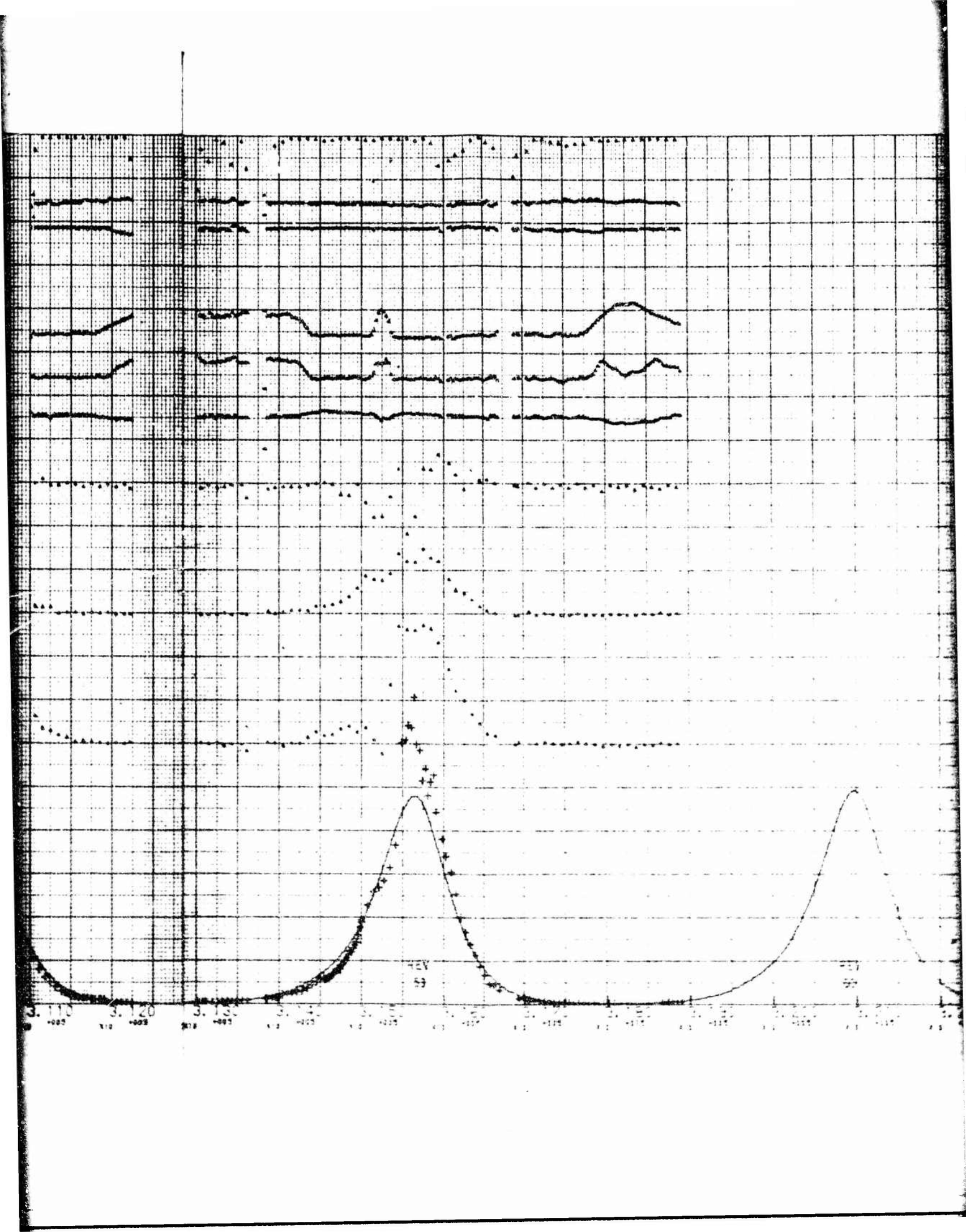

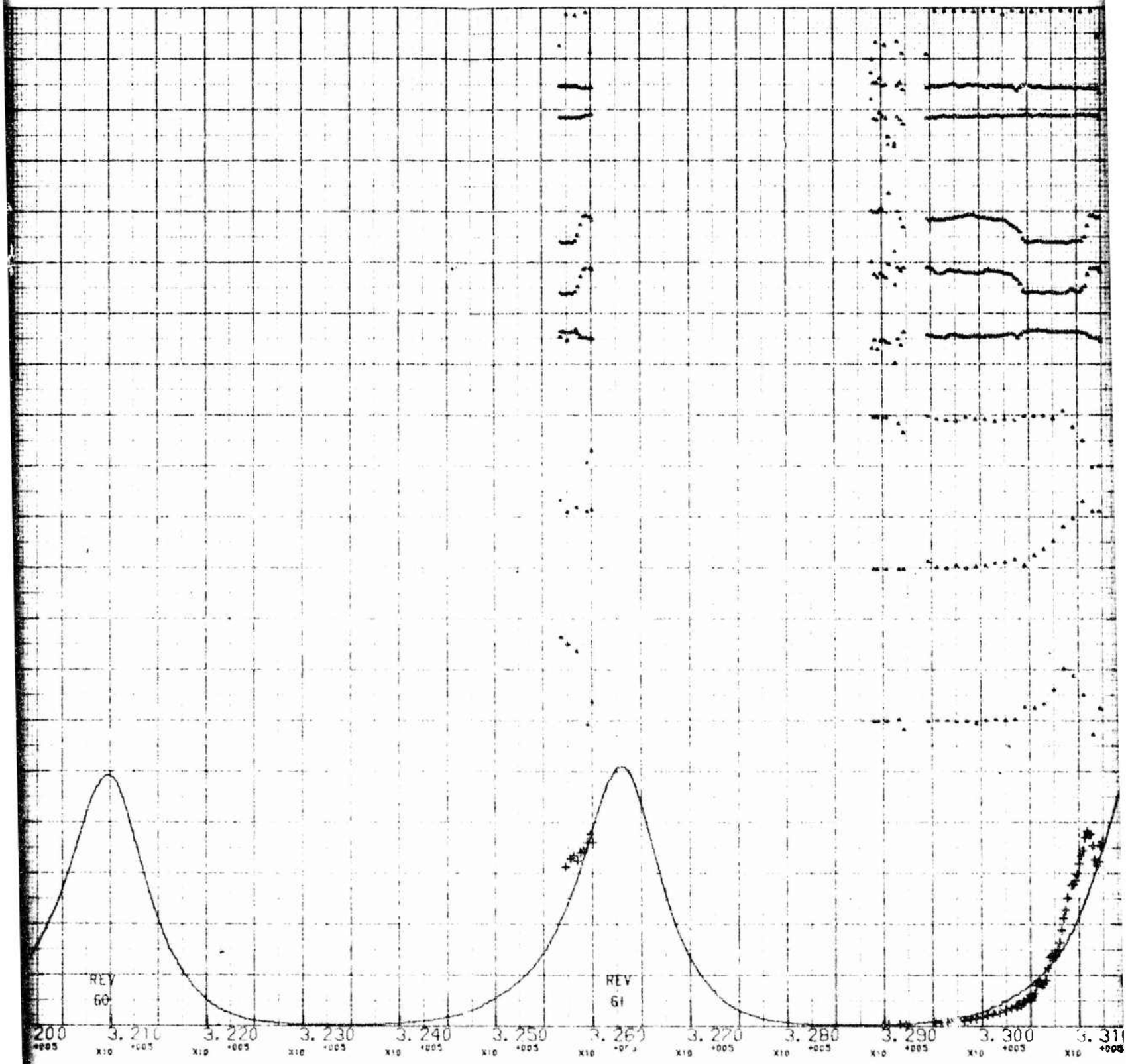
REV
60
REV
61
3.200
3.210
3.220
3.230
3.240
3.250
3.260
3.270
3.280
3.290
3.300
3.310

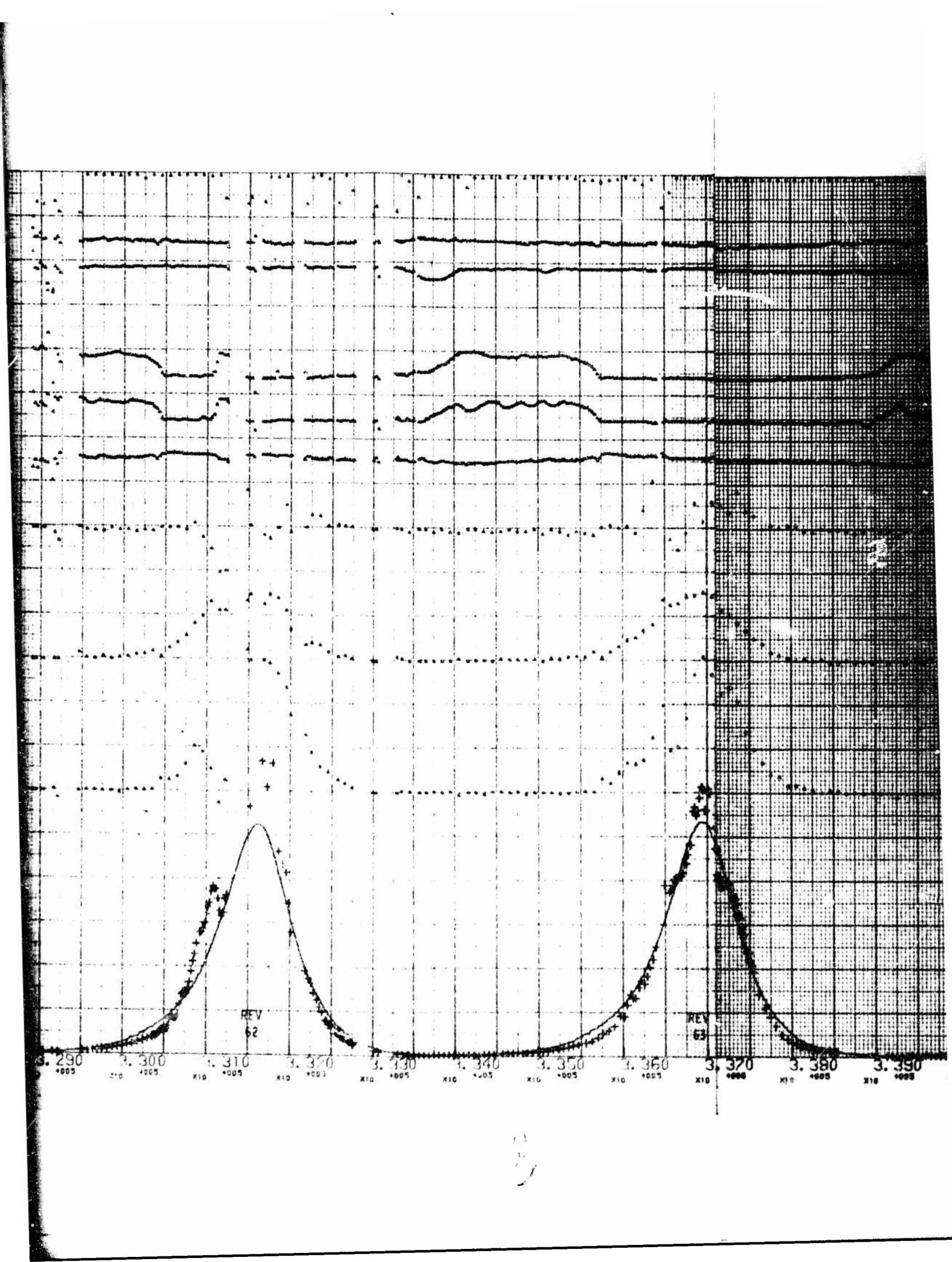
REV
62
REV
63
3. 290
3. 300
3. 310
3. 320
3. 330
3. 340
3. 350
3. 360
3. 370
3. 380
3. 390

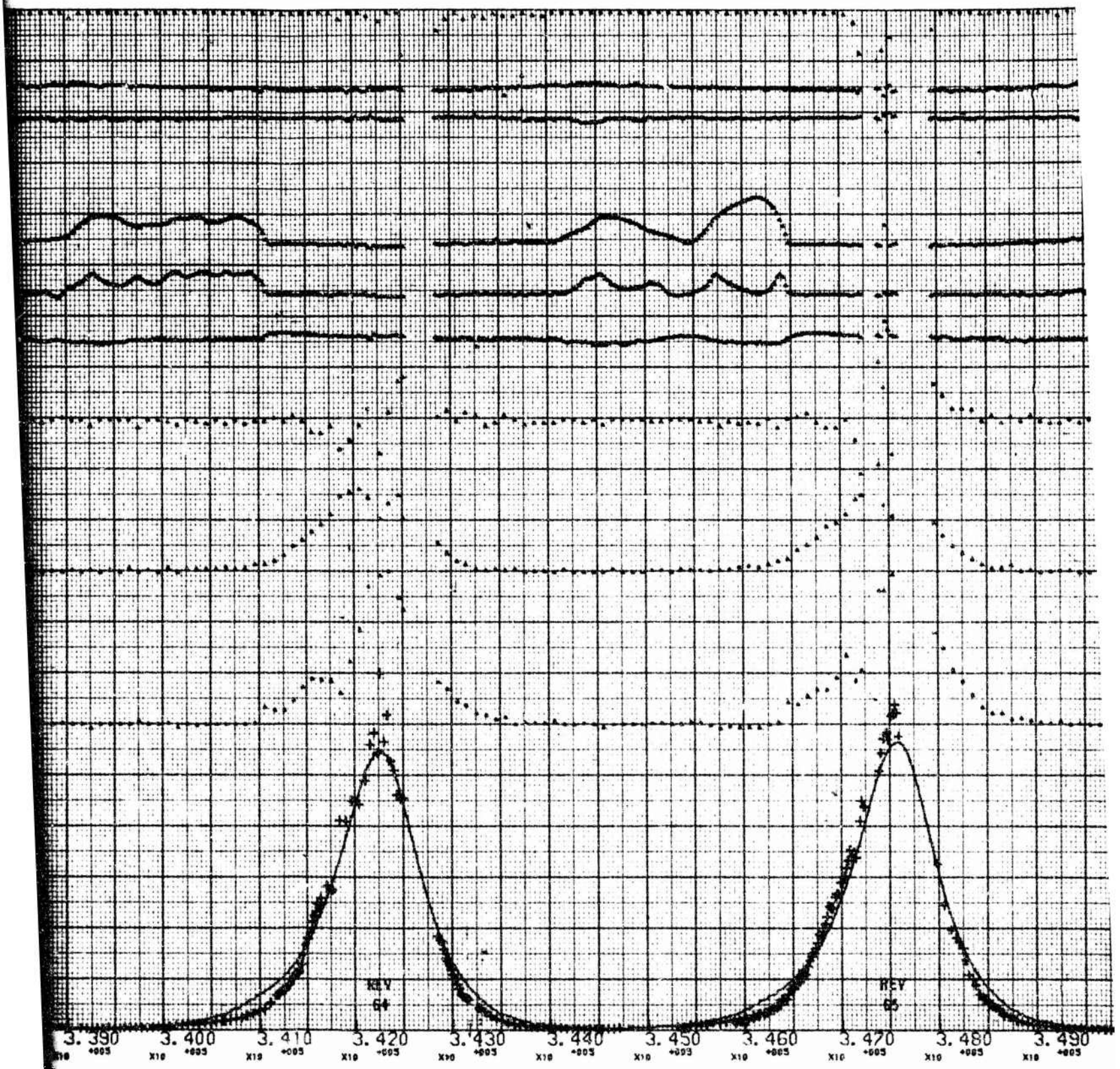
REV
64
REV
65
3. 390
3. 400
3. 410
3. 420
3. 430
3. 440
3. 450
3. 460
3. 470
3. 480
3. 490
+005
X10

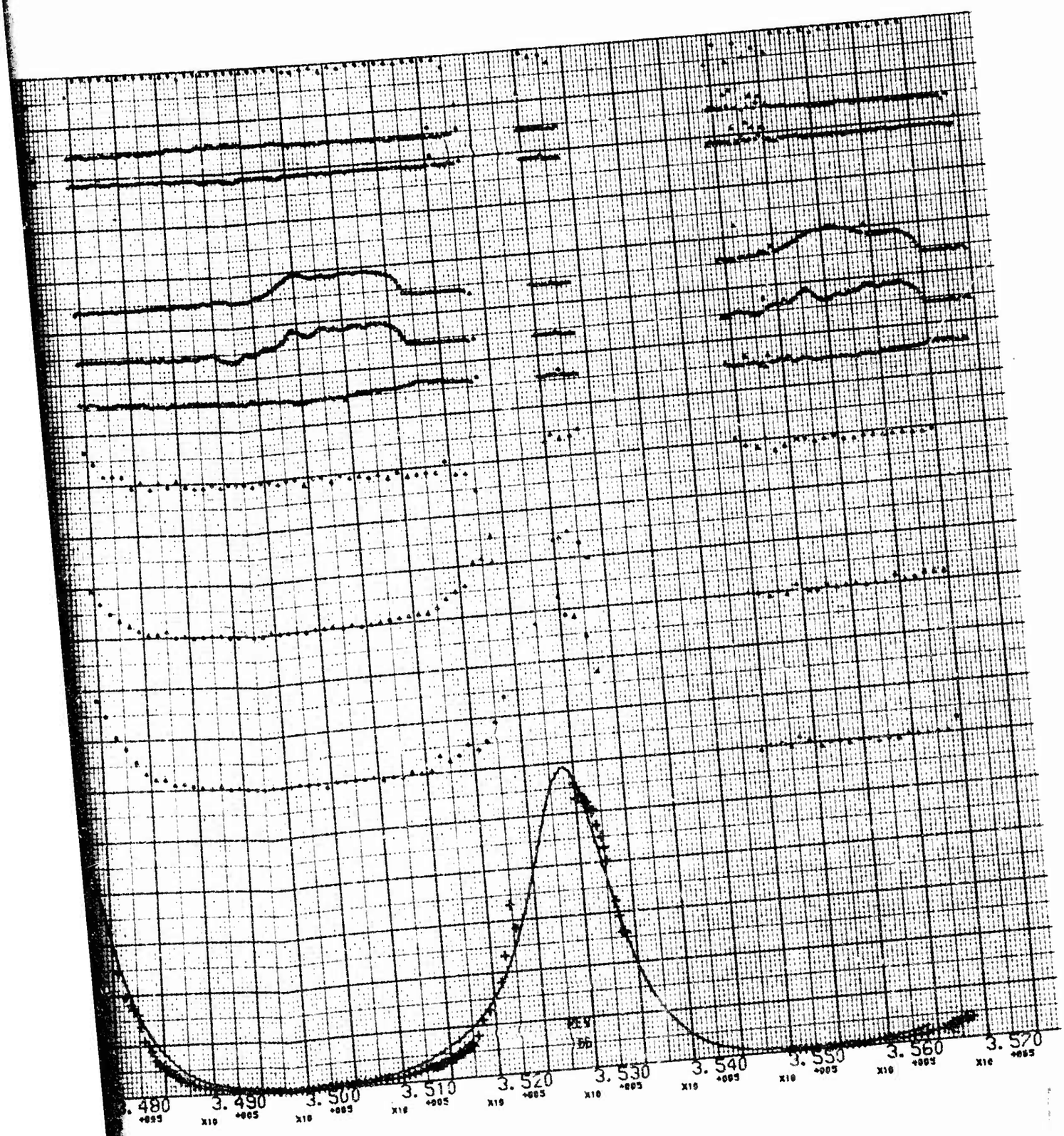

Fig. G-2. (d) Agena Control System Functions (May 26)